

# 7<sup>th</sup> International Conference of Nitride Semiconductors

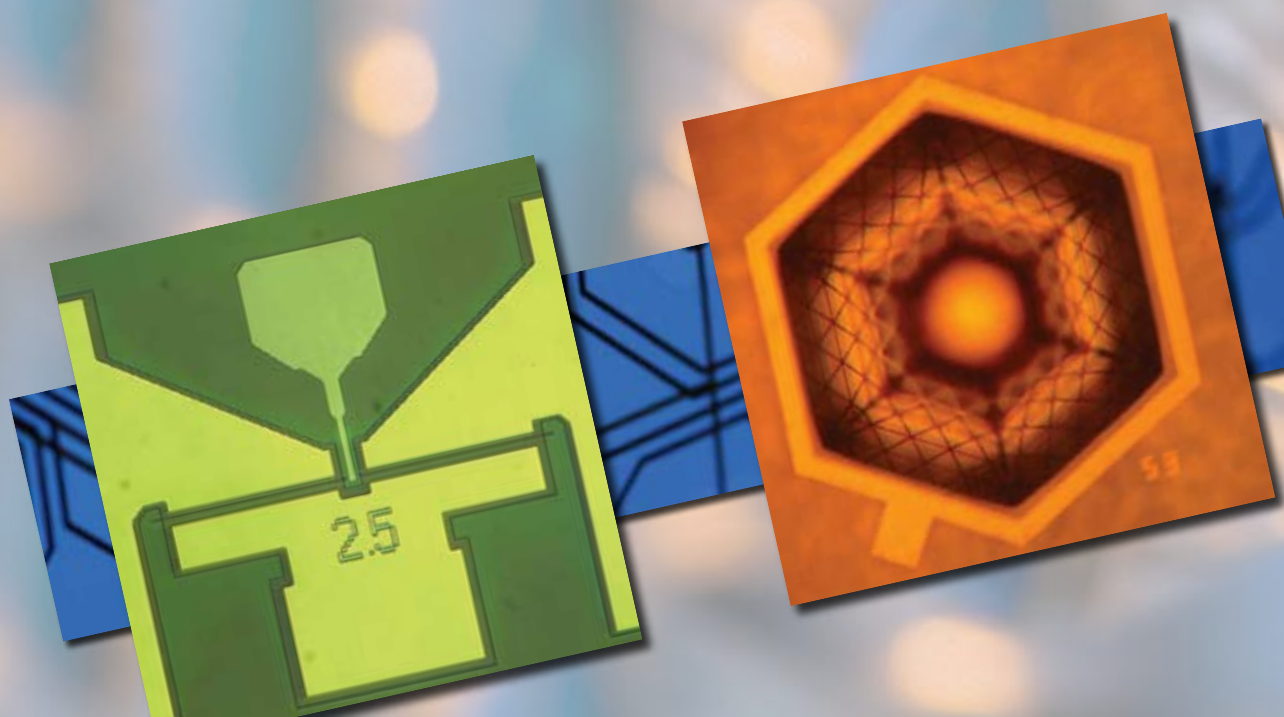
September 16-21, 2007 • MGM Grand Hotel • Las Vegas, Nevada, USA



Sponsored by

# TMS

## FINAL PROGRAM



**Welcome to**

## **7<sup>th</sup> International Conference of Nitride Semiconductors**

September 16-21, 2007 • MGM Grand Hotel • Las Vegas, Nevada, USA



*This conference follows the tradition of the previous conferences held at Bremen, Germany in 2005; Nara, Japan in 2003; Denver, Colorado, United States in 2001; Montpellier, France in 1999; Tokushima, Japan in 1997; and Nagoya, Japan in 1995.*

### **You will hear from these respected speakers:**

- Hiroshi Amano, Meijo University
- Oliver Ambacher, TU Ilmenau
- J.W. Ager, LBL
- Jeremy Baumberg, Southampton
- S.F. Chichibu, Tohoku University
- Bruno Daudin, CEA Grenoble
- Eric Feltin, EPFL
- Kenji Fujita, Mitsubishi Chemical
- Mark Galtry, Cambridge University
- Werner Goetz, Philips Lumileds
- Jung Han, Yale
- Volker Härle, Osram Opto Semiconductors GmbH
- Colin Humphreys, Cambridge University
- Y. Kawakami, Kyoto University
- M. Asif Khan, University of South Carolina
- Kevin Linthicum, Nitronex Corporation
- Miro Micovic, HRL
- Daisuke Muto, Ritsumeikan University
- Y. Narukawa, Nichia Corporation
- K. Okamoto, Rohm & Haas Electronic Materials LLC
- Yuichi Oshima, Hitachi Cable
- Bill Pribble, Cree-GaN
- Bill Schaff, Cornell
- Tom Veal, University Warwick
- Claude Weisbuch, Ecole Polytechnique-Paris
- Peidong Yang, University of California, Berkeley

### **Support for ICNS-7 is provided in part by:**

- Air Force Office of Scientific Research
- Office of Naval Research
- Defense Advanced Research Projects Agency (DARPA)

### **Table of Contents**

- 3** Networking and Social Events
- 4** Exhibition
- 5** About Your Registration
- 6** About the Location
- 8** Proceedings
- 8** Organizers
- 10** Technical Program

## Networking and Social Events

As a full conference registrant, you have the opportunity to network with your colleagues at these events!

### Sunday

#### Welcome Reception

*sponsored by Seoul Semiconductor Co. Ltd.*

5 to 7 p.m.

3<sup>rd</sup> Floor Prefunction Area

### Monday

#### All Conference Luncheon

*sponsored by RFMD*

12:30 to 2 p.m.

Rooms 115-117

#### Poster Session Reception

5:30 to 7 p.m.

3<sup>rd</sup> Floor Prefunction Area and Rooms 318-320

### Tuesday

#### Poster Session Reception

*sponsored by Nitronex Corporation*

5:30 to 7 p.m.

3<sup>rd</sup> Floor Prefunction Area and Rooms 318-320

#### Rump Session Reception

*Sponsored by Taiyo Nippon Sanso Corporation*

7 to 8:30 p.m.

Rooms 314/315 and 312/317

### Wednesday

#### Poster Session Reception

*sponsored by Cree Inc. and IQE*

1:30 to 2:30 p.m.

3<sup>rd</sup> Floor Prefunction Area and Rooms 318-320

### Thursday

#### All Conference Luncheon

*sponsored by Akzo Nobel High Purity Metalorganics*

1 to 2:30 p.m.

Rooms 309-311

#### Conference Banquet

*sponsored by Aixtron AG, and Rohm &*

*Haas Electronic Materials LLC*

6 to 10 p.m.

Prefunction Area

#### Poster Session Reception

*sponsored by Toyoda-Gosei Co. Ltd*

5 to 6 p.m.

3<sup>rd</sup> Floor Prefunction Area and Rooms 318-320

### During the Week

Morning and afternoon coffee breaks will be available in the exhibit hall and near the poster session.

*Tuesday morning coffee break is sponsored by Veeco Instruments Inc.*

## Exhibition

Visit the ICNS-7 exhibition during these hours to find the products and services you are looking for:

Monday ..... 3 to 7 p.m.  
Tuesday.....9:30 a.m. to noon / 3 to 7 p.m.  
Wednesday ..... 9:30 a.m. to noon  
Thursday ..... 9:30 a.m. to noon

### **Exhibiting Companies (as of 8/21/07)**

Air Products and Chemicals Inc.	NTT Advanced Technology Corporation
Aixtron AG	PANalytical
Akzo Nobel High Purity Metalorganics	Photon Systems Inc.
Bruker AXS Inc.	Power + Energy Inc.
Cree Inc.	Riber
Crosslight Software Inc.	Rohm & Haas Electronic Materials LLC
Crysbond Co. Ltd.	SAFC Hitech
Crystal IS Inc.	Semiconductor Technology Research Inc.
Evans Analytical Group	sp3 Diamond Technologies Inc.
Fujikin Inc.	Structured Materials Inc. Ltd.
Johnson Matthey	SVT Associates Inc.
k-Space Associates Inc.	Taiyo Nippon Sanso Corporation
LayTec GmbH	Technologies & Devices International Inc.
Leighton Electronics Inc.	The Fox Group Inc. & Nitride Crystals Ltd.
Monocrystal PLC	Veeco Instruments Inc.
Nanometrics Inc.	WEP - Dage
NOVASiC	Yole Developpement

### **Sponsors (as of 8/21/07)**

#### **Platinum Sponsors**

Aixtron AG ..... Banquet/Reception  
Rohm & Haas Electronic Materials LLC ..... Banquet/Reception

#### **Gold Sponsors**

Akzo Nobel High Purity Metalorganics ..... Thursday Luncheon  
Cree Inc..... Wednesday Poster Session Reception  
IQE ..... Wednesday Poster Session Reception  
Nitronex ..... Tuesday Poster Session Reception  
RFMD ..... Monday Luncheon  
Seoul Semiconductor Co. Ltd ..... Welcome Reception  
Sony Corporation  
Toyoda-Gosei Co. Ltd..... Thursday Poster Session Reception

#### **Silver Sponsors**

Kopin Corporation  
Mitsubishi Chemical Corporation  
Nichia Corporation  
Taiyo Nippon Sanso Corporation ..... Rump Sessions  
Veeco Instruments Inc..... Coffee Break Tuesday Morning and Lanyards

#### **Bronze Sponsors**

Air Products and Chemicals Inc.  
Osram Opto Semiconductors GmbH  
SAFC Hitech

## About Your Registration

Your full conference registration fee includes:

- Technical Sessions
- Proceedings on CD-ROM
- Conference Banquet
- Sunday Evening Refreshments
- Coffee Breaks
- Monday and Thursday Luncheons

(Student registration fee includes technical sessions, conference banquet, Sunday evening refreshments, coffee breaks, and Monday and Thursday luncheons.)



### **Badges**

Badges must be worn to gain access to the technical sessions and social functions.

### **Refund**

The deadline for refunds was August 27, 2007. No refunds are issued at the meeting.

### **Audio/Video Recording Policy**

TMS reserves the right to all audio and video reproductions of presentations at TMS sponsored meetings. Recording of sessions (audio, video, still photography, etc.) intended for personal use, distribution, publication, or copyright without the express written consent of TMS and the individual authors is strictly prohibited.

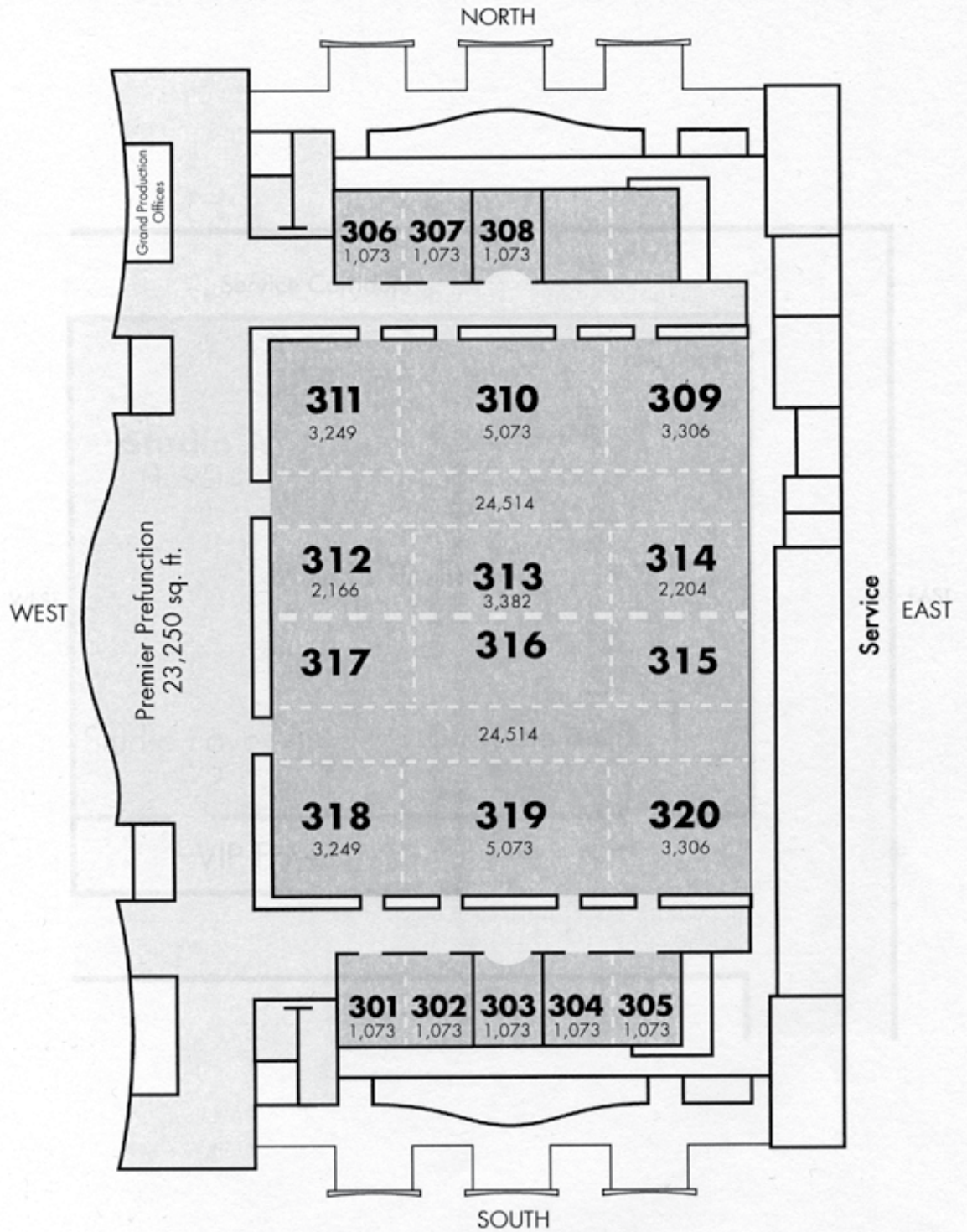
### **Americans With Disabilities Act**



TMS strongly supports the federal Americans with Disabilities Act (ADA) which prohibits discrimination against, and promotes public accessibility for, those with disabilities. In support of, and in compliance with, ADA, we ask those requiring specific equipment or services to speak with a TMS representative at the registration desk.

## About the Location

### ST LEVEL THREE MGM GRAND HOTEL CONFERENCE CENTER



## About the Location

### **Concierge**

The Concierge at the MGM Grand Hotel can assist with dining reservations at many award-winning restaurants; offer information on the availability of the hotel's pool, golf and spa; provide directions; and help to locate any service desired.

### **Transportation**

#### ***Airport Shuttle Service***

Individual shuttle and porter service is available and may be booked from 9 a.m. to 5 p.m. daily. One-way transportation with porter service is \$9.75, and transportation without porter service is \$5.

#### ***Las Vegas Monorail***

The newest attraction on the famous Las Vegas skyline is the monorail. Above traffic at speeds reaching 50 miles per hour, the monorail covers the four-mile route in approximately 14 minutes for as little as \$5. Hours of operation are 7 a.m. to 2 a.m.

Travel time from MGM Grand Station to:

- Sahara Station – 12.8 minutes
- Las Vegas Hilton Station – 11.3 minutes
- Las Vegas Convention Center Station – 9.12 minutes
- Harrah's/Imperial Palace Station – 4.95 minutes
- Flamingo/Caesars Palace Station – 3.7 minutes
- Bally's & Paris Las Vegas Station – 2.06 minutes

### **Shopping**

Stroll the shops along Studio Walk, visit Star Lane Shops on the lower level of the main lobby, or explore the shopping outlets located throughout the MGM Grand.



## Proceedings and Organizers

ICNS-7 proceedings are being published as an edition of *Physica Status Solidi* (PSS) in CD-ROM format. One copy of the CD will be shipped to each full registrant when available. Additional proceedings CD-ROMs can be purchased at the TMS registration desk. The cost is \$60 each; shipping and handling are included. The proceedings are also being published as a hard-copy volume of *Physica Status Solidi*. This version may also be purchased at the registration desk. The cost is \$160 each; shipping and handling are included.

### Organizing Committee

Shuji Nakamura, Honorary Chair  
Umesh Mishra, Conference Chair  
Steven DenBaars, Conference Co-chair  
James S. Speck, General Program Chair  
Mike Wraback, Program Vice Chair  
Yasuhiko Arakawa, Asia Program Chair  
Andrew Allerman, Americas Program Chair  
Nicholas Grandjean, Europe Program Chair  
Jeff Shealy and Mike Krames, Industrial Liaisons  
Tomas Palacios and Debdeep Jena, Publication Co-chairs

### International Advisory Committee

Chair: Bernard Gil Universite de Montpellier II, France	Katsumi Kishino Sophia University, Japan
Isamu Akasaki* Meijo University, Japan	Robert Martin University of Strathclyde, United Kingdom
Jacques I. Pankove* Astalux Inc., United States	Elias Mūnos Merino Polytechnical University of Madrid, Spain
Jürgen Christen University of Magdeburg, Germany	Suk-ki Min Korea University, Korea
Steven P. DenBaars University of California at Santa Barbara, United States	Bo Monemar Linkoping University, Sweden
Russel Dupuis Georgia Institute of Technology, United States	Theodore Moustakas Boston University, United States
Werner Goetz Philips Lumileds, United States	Yasushi Nanishi Ritsumeikan University, Japan
Volker Härle Osram Opto Semiconductors, Germany	Kentaro Onabe University of Tokyo, Japan
Fumio Hasegawa Kogakuin University, Japan	Fernando A. Ponce Arizona State University, United States
Yoichi Kawakami Kyoto University, Japan	Tadeus Suski Unipress, Poland
M. Asif Khan University of South Carolina, United States	Akihiko Yoshikawa Chiba University, Japan

\*Honorary Member

## Organizers Cont.

### Program Committee

James S. Speck, Program General Chair  
University of California at Santa Barbara

Mike Wraback, Program Vice Chair  
Army Research Laboratory

Andy Allerman, Americas Chair  
Sandia National Laboratory

Nicolas Grandjean, Europe Chair  
EPFL

Yasuhiko Arakawa, Asia-Pacific Chair  
University of Tokyo

Hiroshi Amano  
Meijo University

Oliver Ambacher  
TU Ilmenau

Jacek Baranowski  
Warsaw

Enrique Calleja  
Polytechnical University of Madrid

Shigefusa Chichibu  
Tohoku University

Robert Coffe  
Northrup-Grumman

Jean Yves Duboz  
Valbonne

Russell Dupuis  
Georgia Institute of Technology

Randy Feenstra  
Carnegie Mellon University

Shizuo Fujita  
Kyoto University

Jonathan Heffernan  
Sharp

Francois Julien  
University of Paris-Sud

M. Asif Khan  
University of South Carolina

T. Kikkawa  
Fujitsu

Mike Krames  
Philips Lumileds

Martin Kuball  
University of Bristol

Kei May Lau  
Hong Kong University of Science & Technology

Kou Matsumoto  
Taiyo Nippon Sanso Corporation

Takashi Mukai  
Nichia Corporation

Joerg Neugebauer  
MPI Dusseldorf

Joan Redwing  
The Pennsylvania State University

Steve Ringel  
The Ohio State University

Ferdinand Scholz  
University of Ulm

Martin Stutzmann  
Walter Schottky Institute

Yifeng Wu  
Cree-GaN

Euijoon Yoon  
Seoul National University

Ed Yu  
University of California at San Diego

Arturas Zukauskas  
Vilnius University

# Session Listing

## Monday, September 17

Opening Ceremony and Plenary Session.....	312/313/316/317.....	9:00AM-10:30AM.....	12
Session A: LED and Laser I.....	313/316.....	11:00AM-12:30PM.....	12
Session B: Microwave Devices I.....	314/315.....	11:00AM-12:30PM.....	12
Session C: Bulk Growth and HVPE I.....	312/317.....	11:00AM-12:30PM.....	13
Session D: LED and Laser II.....	313/316.....	2:00PM-3:30PM.....	14
Session E: Microwave Devices II.....	314/315.....	2:00PM-3:30PM.....	15
Session F: Bulk Growth and HVPE II.....	312/317.....	2:00PM-3:30PM.....	15
Session G: Quantum Dots: Growth.....	313/316.....	4:00PM-5:30PM.....	16
Session H: Epitaxial Growth for Electronic Devices.....	314/315.....	4:00PM-5:30PM.....	17
Session I: Optical Characterization of Bulk Materials and Microcavities.....	312/317.....	4:00PM-5:30PM.....	18
Poster Session I: MP: Bulk Growth and HVPE.....	Prefunction Area.....	5:30PM-7:00PM.....	19
Poster Session I: MP: Defects.....	Prefunction Area.....	5:30PM-7:00PM.....	21
Poster Session I: MP: Nanostructures: Characterization.....	Prefunction Area.....	5:30PM-7:00PM.....	23
Poster Session I: MP: Nanostructures: Growth.....	Prefunction Area.....	5:30PM-7:00PM.....	24
Poster Session I: MP: Structural Analysis.....	Prefunction Area.....	5:30PM-7:00PM.....	26
Poster Session I: MP: Structure.....	Prefunction Area.....	5:30PM-7:00PM.....	29
Poster Session I: MP: Theory.....	Prefunction Area.....	5:30PM-7:00PM.....	31

## Tuesday, September 18

Session J: Deep UV LEDs and Lasers.....	313/316.....	9:00AM-10:30AM.....	35
Session K: Microwave Devices III.....	314/315.....	9:00AM-10:30AM.....	35
Session L: Sensors and Characterization I.....	312/317.....	9:00AM-10:30AM.....	36
Session M: MOVPE Growth of AlGaIn Alloys I.....	313/316.....	11:00AM-12:30PM.....	37
Session N: High Voltage and Advanced Device Structures I.....	314/315.....	11:00AM-12:30PM.....	38
Session O: Sensors and Characterization II.....	312/317.....	11:00AM-12:30PM.....	39
Session P: MOVPE Growth of AlGaIn Alloys II.....	314/315.....	2:00PM-3:30PM.....	40
Session Q: High Voltage and Advanced Device Structures II.....	313/316.....	2:00PM-3:30PM.....	41
Session R: Optical Characterization of Lasers.....	312/317.....	2:00PM-3:30PM.....	42
Session S: Quantum Dots: Characterization.....	314/315.....	4:00PM-5:30PM.....	43
Session T: Nonpolar and Semipolar Materials and Devices I.....	313/316.....	4:00PM-5:30PM.....	44
Session U: Optical Characterization of LEDs.....	312/317.....	4:00PM-5:30PM.....	45
Poster Session II: TP: E-Devices: Device Characterization.....	Prefunction Area.....	5:30PM-7:00PM.....	46
Poster Session II: TP: E-Devices: High k and Advanced Devices.....	Prefunction Area.....	5:30PM-7:00PM.....	47
Poster Session II: TP: E-Devices: High Voltage Devices.....	Prefunction Area.....	5:30PM-7:00PM.....	49
Poster Session II: TP: E-Devices: Microwave Devices.....	Prefunction Area.....	5:30PM-7:00PM.....	49
Poster Session II: TP: E-Devices: Sensors and MEMS.....	Prefunction Area.....	5:30PM-7:00PM.....	51
Poster Session II: TP: Epitaxial.....	Prefunction Area.....	5:30PM-7:00PM.....	51
Poster Session II: TP: Epitaxy.....	Prefunction Area.....	5:30PM-7:00PM.....	52
Poster Session II: TP: Heterostructures.....	Prefunction Area.....	5:30PM-7:00PM.....	53
Poster Session II: TP: Nanostructures: Devices.....	Prefunction Area.....	5:30PM-7:00PM.....	58
Poster Session II: TP: Quantum Dots: Characterization.....	Prefunction Area.....	5:30PM-7:00PM.....	59
Rump Session I.....	314/315.....	7:30PM-9:00PM.....	60
Rump Session II.....	312/317.....	7:30PM-9:00PM.....	60

# Session Listing

## Wednesday, September 19

Session V: Solid State Lighting and LEDs .....	313/316.....	9:00AM-11:00AM.....	61
Session W: Nonpolar and Semipolar Materials and Devices II.....	314/315.....	9:00AM-11:00AM.....	62
Session X: Growth of Novel Nitride Semiconductors.....	312/317.....	9:00AM-11:00AM.....	63
Session Y: Optical and Structural Characterization and Related Topics .....	313/316.....	11:30AM-1:30PM .....	64
Session Z: Nonpolar and Semipolar Materials and Devices III.....	314/315.....	11:30AM-1:30PM .....	65
Session AA: Optoelectronic Devices.....	312/317.....	11:30AM-1:30PM .....	66
Poster Session III: WP: Characterization.....	Prefunction Area.....	1:30PM-2:30PM.....	67
Poster Session III: WP: Materials Integration.....	Prefunction Area.....	1:30PM-2:30PM.....	69
Poster Session III: WP: Materials Issues .....	Prefunction Area.....	1:30PM-2:30PM.....	76
Poster Session III: WP: Optical Characterization.....	Prefunction Area.....	1:30PM-2:30PM.....	76
Poster Session III: WP: Optical Characterization of Nonpolar and Semipolar Materials ..	Prefunction Area.....	1:30PM-2:30PM.....	81

## Thursday, September 20

Session BB: InN Growth .....	312/317.....	8:30AM-10:30AM.....	83
Session CC: Nonpolar and Semipolar Materials and Devices IV.....	313/316.....	8:30AM-10:30AM.....	84
Session DD: Engineered Properties of GaN by MOVPE Growth.....	314/315.....	8:30AM-10:30AM.....	85
Session EE: InN Heterostructures and Quantum Wells.....	312/317.....	11:00AM-1:00PM .....	86
Session FF: Nanostructures: Devices.....	313/316.....	11:00AM-1:00PM .....	87
Session GG: Optical and Structural Characterization II.....	314/315.....	11:00AM-1:00PM .....	88
Session HH: InN: Surface and Electronic Properties .....	312/317.....	2:30PM-4:30PM.....	89
Session II: Nanostructures: Characterization.....	314/315.....	2:30PM-4:30PM.....	90
Session JJ: Optical Characterization of Alloys and MQWs.....	313/316.....	2:30PM-4:30PM.....	91
Poster Session IV: ThP: Devices.....	Prefunction Area.....	5:00PM-6:00PM.....	93
Poster Session IV: ThP: LED.....	Prefunction Area.....	5:00PM-6:00PM.....	97
Poster Session IV: ThP: Other Topics.....	Prefunction Area.....	5:00PM-6:00PM.....	105

## Friday, September 21

Session KK: P-Type InN.....	312/317.....	8:30AM-10:30AM.....	109
Session LL: Nanostructures: Growth I .....	313/316.....	8:30AM-10:30AM.....	110
Session MM: Defects and Structural Characterization.....	314/315.....	8:30AM-10:30AM.....	110
Session NN: Molecular Beam Epitaxy of Nitride Semiconductors.....	312/317.....	11:00AM-12:30PM .....	111
Session OO: Nanostructures: Growth II .....	313/316.....	11:00AM-12:30PM .....	112
Session PP: MOVPE Growth of InGaN Alloys for Optoelectronics.....	314/315.....	11:00AM-12:30PM .....	113
Session QQ: Special LED Session: High Efficiency Solid State Lighting: Solutions for Global Warming .....	312/313/316/317.....	2:00PM-4:05PM.....	114
Closing Ceremony .....	312/313/316/317.....	4:05PM-5:00PM.....	114

# Technical Program

## Opening Ceremony and Plenary

Monday AM Room: 312/313/316/317  
September 17, 2007 Location: MGM Grand Hotel Conference Center

### 9:00 AM Opening Ceremony

### 9:30 AM Plenary

**III-Nitrides Seem to Be Good for Everything:** *Klaus H. Ploog*<sup>1</sup>; <sup>1</sup>Paul Drude Institute

### 10:30 AM Break

## Session A: LED and Laser I

Monday AM Room: 313/316  
September 17, 2007 Location: MGM Grand Hotel Conference Center

*Session Chairs:* Shigefusa Chichibu, Tohoku University; Ferdinand Scholz, University Ulm

### 11:00 AM Invited

**A1, High-Power III-Nitride Based Light Emitting Diodes: Progress and Challenges:** *Werner Goetz*<sup>1</sup>; <sup>1</sup>Philips Lumileds Lighting Company

After almost 20 years of intense research, III-nitride based light emitting diodes (LEDs) have now reached performance levels that rival and in many cases exceed the capabilities of existing light sources utilized for illumination or display backlighting. Especially high-power LEDs ( $P_{IN} > 0.5$  W) have recently exhibited efficacies that surpass high quality fluorescent lamps. For example, cool-white phosphor-conversion LEDs with luminous efficacy in the 100 lm/W regime (350 mA) have been reported. However, significant challenges still exist that today delay LEDs from being the light source of choice for general lighting applications. Paramount is production cost, but also issues such as the relatively low external quantum efficiency of green LEDs, the ubiquitous high drive current efficiency reduction, and the inability to precisely target the “white-point” of phosphor conversion LEDs with today’s production technology remain on the forefront of III-N LED focused research and development.

### 11:30 AM Invited

**A2, Gross Well-Width Fluctuations in InGaN Quantum Wells:** Rachel Oliver<sup>1</sup>; Nicole van der Laak<sup>1</sup>; Menno Kappers<sup>1</sup>; *Colin Humphreys*<sup>1</sup>; <sup>1</sup>University of Cambridge

Gross fluctuations in quantum well (QW) width have been observed in commercially-available green light emitting diodes. Such fluctuations are found in green-emitting quantum wells which are subjected to an anneal or temperature ramp prior to capping. Atomic force microscopy and transmission electron microscopy (TEM) studies of epilayers and QWs reveal that these fluctuations arise from a network of interlinking InGaN strips, which are found (using TEM) to be indium-rich at their centres. Plan-view TEM indicates that ~90% of all threading dislocations (TDs) intersect the QW plane between the InGaN strips. Excitons may be localised at the strips’ centres, preventing non-radiative recombination at TDs. The orientation of strips in the network is found to be strongly anisotropic and this anisotropy correlates with the alignment of step-edges in the underlying GaN. It is hence suggested that the network structure forms via the decomposition of In-rich regions arising at or near step-edges.

### 12:00 PM

**A3, Hexagonal Truncated Pyramidal LEDs through Wafer Bonding of ZnO to GaN and Laser Lift Off:** *Daniel Thompson*<sup>1</sup>; Akihiko Murai<sup>1</sup>; Steve DenBaars<sup>1</sup>; Umesh Mishra<sup>1</sup>; Shuji Nakamura<sup>1</sup>; <sup>1</sup>University of California, Santa Barbara

We report on a hexagonal pyramid LED produced by direct wafer bonding of a MOCVD grown GaN LED on sapphire to a n-type ZnO wafer, and laser lift off. Laser lift off was used to remove the sapphire of the GaN wafer, allowing creation of contacts to the n face of the GaN LED. Contacts to the ZnO allow for the creation of a vertical current path. Selective etching was used to form truncated hexagonal pyramids of the ZnO. We report on a comparison of the output power and efficiency to a GaN LED with truncated ZnO pyramid on sapphire. Both samples were packaged on silver headers with a silicone dome. We report that there is an increase of 11% output power under 20mA pulsed measurements between this laser lift off structure and a GaN LED and ZnO wafer bonded structure with no sapphire removal.

### 12:15 PM

**A4, Optical Properties of Nitride Laser Structures Grown along a Non-Polar Crystallographic Direction:** *Henryk Teisseyre*<sup>1</sup>; I. Grzegory<sup>1</sup>; C. Skierbiszewski<sup>1</sup>; A. Khachapuridze<sup>1</sup>; A. Feduniewicz-Zmuda<sup>1</sup>; M. Siekacz<sup>1</sup>; B. Lucznik<sup>1</sup>; G. Kamler<sup>1</sup>; M. Krysko<sup>1</sup>; T. Suski<sup>1</sup>; P. Perlin<sup>1</sup>; S. Porowski<sup>1</sup>; <sup>1</sup>Polish Academy of Sciences, Institute of High Pressure Physics

Due to their undesirable spontaneous and piezoelectric polarizations, nitride structures grown along polar direction are subject to high built-in electric fields. A promising means of overcoming the effects related to built-in electric fields and, thereby, obtaining higher quantum efficiencies is to grow nitrides along a non-polar direction. It is our intention to report our recent progress on non-polar homo-epitaxial structures grown by PAMBE along the non-polar direction. As a substrate we used GaN bulk crystals grown by the High Pressure Solution method and overgrown by HVPE. As has been previously reported, non-polar AlGaIn/GaN quantum wells possess sharp excitonic lines. We present optically pumped laser action on separate confinement heterostructures. Laser action is clearly proved by spontaneous emission saturation, abrupt line narrowing, and the strong TE polarization of output light. We also performed a comparison between the optical properties of polar and non-polar laser structures.

## Session B: Microwave Devices I

Monday AM Room: 314/315  
September 17, 2007 Location: MGM Grand Hotel Conference Center

*Session Chairs:* Miro Micovic, HRL Laboratories LLC; Jae-Hyun Ryou, Georgia Institute of Technology

### 11:00 AM Invited

**B1, GaN-on-Silicon RF Power Devices—Current State and Future Directions:** *Kevin Linthicum*<sup>1</sup>; <sup>1</sup>Nitronex Corporation

A GaN-on-silicon platform technology has been developed to provide the performance advantages of GaN combined with the manufacturing advantages of silicon. The NRF1 process technology has been formally qualified for 28V operation and released for production. Extensive reliability studies have been performed yielding demonstrated  $E_A = 2.0$ eV predicting an MTTF of  $10^7$  hours at 200°C junction temperatures. Air cavity and plastic over-mold assembly techniques are used for 7 product offerings available today. The NRF1 process technology is currently undergoing 48V qualification and will support the production release of a family of high power transistors for WiMAX, Cellular and Broadband market applications.

## 11:30 AM Invited

### B2, Applications of the GaN HEMT in DoD and Commercial Wireless Infrastructure: *Bill Pribble*<sup>1</sup>; <sup>1</sup>Cree, Inc.

Gallium Nitride HEMTs are well suited for applications that require high power and high operating frequencies. GaN devices exhibit high breakdown voltage (in excess of 100 volts) and can also supply up to 1 Amp per millimeter of gate periphery. Sub-micron gate lengths allow operation GaN HEMTs to Ka-band and beyond. The unique combination of high current and breakdown voltage, as well as low parasitic capacitance, enables design and fabrication of power amplifiers up to 20 GHz as well as switching circuits operating up to 900 volts at 100MHz. Applications utilizing these devices include military communication, radar systems and wireless base-stations for existing cellular infrastructure as well as emerging systems such as WiMAX.

## 12:00 PM

### B3, High-Efficiency GaN HEMTs on 3-Inch Semi-Insulating SiC Substrates: *Patrick Waltereit*<sup>1</sup>; Wolfgang Bronner<sup>1</sup>; Rüdiger Quay<sup>1</sup>; Michael Dammann<sup>1</sup>; Stefan Müller<sup>1</sup>; Rudolf Kiefer<sup>1</sup>; Brian Raynor<sup>1</sup>; Michael Mikulla<sup>1</sup>; Günther Weimann<sup>1</sup>; <sup>1</sup>Fraunhofer Institute for Applied Solid State Physics

AlGaIn/GaN HEMT structures are grown on semi-insulating SiC substrates by metal-organic-chemical-vapour-deposition with sheet resistance non-uniformities better than 2%. Device fabrication is performed using standard processing techniques involving both e-beam and stepper lithography. HEMTs demonstrate excellent high-voltage stability and large efficiencies. Devices with 0.5 $\mu$ m gate length exhibit two-terminal gate-drain breakdown voltages in excess of 160V across the entire 3-inch wafer with parasitic gate/drain currents in the low  $\mu$ A/mm range when biased at 120V drain bias under pinch-off conditions. Load-Pull measurements (800 $\mu$ m gate periphery, 2GHz) return both a linear relationship between bias-voltage and output-power as well as power-added-efficiencies >55% up to  $U_{DS}=72$ V for which an output-power-density of 9W/mm with 25dB linear gain is obtained. Initial reliability tests indicate a promising device stability after 1000h. Less than 20% drain current degradation under different DC-stress conditions ( $U_{DS}=50$ V,  $P_{DC}=2.5$ W/mm,  $T_{CHANNEL}=90$ °C and  $U_{DS}=10$ V,  $P_{DC}=7$ W/mm,  $T_{CHANNEL}=275$ °C) as well as less than 0.2dB gain reduction under RF-stress (2GHz,  $U_{DS}=50$ V,  $P_{DC}=5.5$ W/mm, 3dB compression,  $T_{CHANNEL}=160$ °C) are obtained.

## 12:15 PM

### B4, Power Performance of AlGaIn/GaN HEMTs Grown on SiC by Ammonia MBE: *Christiane Poblenz*<sup>1</sup>; Andrea Corrión<sup>1</sup>; Felix Recht<sup>1</sup>; Chang Soo Suh<sup>1</sup>; Rongming Chu<sup>1</sup>; Likun Shen<sup>1</sup>; James Speck<sup>1</sup>; Umesh Mishra<sup>1</sup>; <sup>1</sup>University of California, Santa Barbara

We report on AlGaIn/GaN high electron mobility transistor (HEMT) structures grown by ammonia MBE on semi-insulating 4H-SiC(0001) substrates with excellent power and efficiency performance. A standard HEMT with a 30 nm UID  $Al_{0.30}Ga_{0.70}N$  cap and a dislocation density of  $\sim 10^{10}$  cm<sup>-2</sup> exhibited a Hall mobility of 1643 cm<sup>2</sup>/Vs and a sheet charge density of  $1.0 \times 10^{13}$  cm<sup>-2</sup>. A maximum drain current density of 1.05 A/mm,  $f_t$  of 24 GHz and  $f_{max}$  of 54 GHz were measured for 0.7  $\mu$ m gate length devices. At 4 GHz, an output power density of > 10 W/mm with an associated PAE of 63% at  $V_{DS} = 48$  V was achieved. Gate leakage was reduced in these structures through use of a fluorine plasma surface treatment. These results are the highest reported for ammonia MBE on SiC at 4 GHz and demonstrate the potential of ammonia MBE to produce high quality AlGaIn/GaN HEMT devices.

## Session C: Bulk Growth and HVPE I

Monday AM  
September 17, 2007

Room: 312/317  
Location: MGM Grand Hotel Conference Center

*Session Chairs:* Tadeusz Suski, Unipress, Polish Academy of Sciences; Fumio Orito, Mitsubishi Chemical

## 11:00 AM Invited

### C1, Preparation of 3-Inch Freestanding GaN Substrates by Hydride Vapor Phase Epitaxy with Void-Assisted Separation: *Yuichi Oshima*<sup>1</sup>; Takehiro Yoshida<sup>1</sup>; Takeshi Eri<sup>1</sup>; Kazutoshi Watababe<sup>1</sup>; Masatomo Shibata<sup>1</sup>; Tomoyoshi Mishima<sup>1</sup>; <sup>1</sup>Hitachi-cable, Ltd.

Manufacture of 3-inch GaN substrates was attempted. Hydride vapor phase epitaxy and void-assisted separation (VAS [1]) were utilized for fabrication of freestanding GaN substrates. This study used 3.4-inch-diameter (0001) sapphire as base substrate. HVPE growth was performed on a 3.2-inch-diameter area of the base substrate. After HVPE growth, the thick GaN layer was spontaneously separated from the base substrate due to thermal stress. As a result, a GaN substrate with a diameter of approximately 3.2 inches was obtained. No cracks were generated during repetition of the same process several times. There was no additional difficulty in the separation process compared to 2-inch substrates. Therefore, further enlargement of the diameter is likely possible using the VAS method. This result greatly contributes to the potential for high-performance, low-cost nitride devices. [1] Y. Oshima et al.: Jpn. J. Appl. Phys. 42 (2003) L1.

## 11:30 AM

### C2, Lateral Epitaxial Overgrowth of AlN by Hydride Vapor Phase Epitaxy: *Derrick Kamber*<sup>1</sup>; Scott Newman<sup>1</sup>; Yuan Wu<sup>1</sup>; Steven DenBaars<sup>1</sup>; James Speck<sup>1</sup>; Shuji Nakamura<sup>1</sup>; <sup>1</sup>University of California Santa Barbara

The threading dislocation densities of AlN films were substantially reduced via lateral epitaxial overgrowth (LEO) by hydride vapor phase epitaxy (HVPE). The AlN films were grown on patterned 6H-SiC substrates containing elevated mesas separated by trench regions. A variety of different stripe patterns were used to produce fully coalesced AlN films. Transmission electron microscopy (TEM) was used to assess the structural quality of these films. TEM analysis determined that the dislocation density in the laterally grown wing regions was less than  $8.3 \times 10^6$  cm<sup>-2</sup> as compared to  $1.8 \times 10^9$  cm<sup>-2</sup> in the seed regions. Atomic force microscopy revealed that the films have a smooth surface morphology with a rms roughness of 0.71 nm over  $10 \times 10$   $\mu$ m<sup>2</sup> sampling areas. These results represent the first reported AlN LEO by HVPE. Moreover, we have achieved the lowest dislocation density for HVPE growth of AlN, and the results are comparable to the best MOCVD growth results.

## 11:45 AM

### C3, Growth of the Full-Scale GaN Single Crystal Substrate Using Na Flux Method: *Fumio Kawamura*<sup>1</sup>; Yoshihiro Kitano<sup>1</sup>; Masaki Tanpo<sup>1</sup>; Naoya Miyoshi<sup>1</sup>; Mamoru Imade<sup>1</sup>; Masashi Yoshimura<sup>1</sup>; Yasuo Kitaoka<sup>1</sup>; Takatomo Sasaki<sup>1</sup>; Yusuke Mori<sup>1</sup>; <sup>1</sup>Osaka University

We succeeded in growing a GaN single crystal substrate with diameter of about two inches using the Na flux method. Our success is due to the development of a new apparatus for growing large GaN single crystals. The crystal grown in this study has a low dislocation density of  $2.3 \times 10^5$  (cm<sup>-2</sup>). The secondary ion mass spectrometry (SIMS) technique demonstrates that the Na element is difficult to be taken in the crystal in both the + and - c directions, resulting in a Na concentration of an order of  $10^{14}$  (cm<sup>-3</sup>) in the crystal. Our success in growing a two-inch GaN substrate with a low impurity content and low dislocation density should pave the way for the Na flux method to become a practical application.

# Technical Program

12:00 PM

**C4, Free-Standing Zinc-Blende (Cubic) GaN Substrates Grown by Modified Molecular Beam Epitaxy Process:** *C. Thomas Foxon*<sup>1</sup>; Sergei Novikov<sup>1</sup>; Nicola Stanton<sup>1</sup>; Richard Campion<sup>1</sup>; Anthony Kent<sup>1</sup>; <sup>1</sup>University of Nottingham

We demonstrate bulk, free-standing, zinc-blende (cubic) GaN substrates grown by a modified molecular beam epitaxy process. We have grown free-standing cubic GaN layers up to 60 microns in thickness. Even though our growth rate is currently not particularly fast, it is already comparable with the growth rate for bulk wurtzite GaN crystals from the liquid Ga at high pressure. We present measurements, which confirm the cubic nature of the GaN wafers and show that the hexagonal content of the material is less than 10%. Cubic (001) GaN does not exhibit the spontaneous and piezoelectric polarization effects associated with (0001) c-axis wurtzite GaN, therefore, our free standing GaN wafers make ideal lattice-matched substrates for the growth of cubic GaN-based structures for blue and ultraviolet optoelectronic devices, and high power and high frequency electronic applications.

12:15 PM

**C5, Growth of Thin Protective AlN Layers on Sapphire Substrates at 1065°C for Hydride Vapor Phase Epitaxy of AlN above 1300°C:** *Junpei Tajima*<sup>1</sup>; Yuki Kubota<sup>1</sup>; Rie Togashi<sup>1</sup>; Hisashi Murakami<sup>1</sup>; Yoshinao Kumagai<sup>1</sup>; Akinori Koukita<sup>1</sup>; <sup>1</sup>Tokyo University of Agriculture and Technology

Hydride vapor phase epitaxy (HVPE) of a thick AlN layer on a foreign substrate is one of a promising method for preparation of a freestanding AlN substrate. Recently, our group has succeeded in HVPE of AlN layers on sapphire substrate above 1200°C with an aid of a resistance heating susceptor. However, the crystalline quality of the AlN layers was not necessarily good due to surface decomposition of sapphire substrate at this temperature. In this paper, effects of thin protective AlN layer growth at 1065°C on main AlN layer growth at high temperatures above 1300°C are investigated. It was clearly confirmed that FWHM values of X-ray diffraction rocking curves for symmetric (0002) and asymmetric (10-10) AlN, as well as surface morphology, was greatly improved by the protective layer growth. Concentration of oxygen impurity in the grown layer was also reduced owing to the protection of sapphire substrate.

---

## Session D: LED and Laser II

Monday PM Room: 313/316  
September 17, 2007 Location: MGM Grand Hotel Conference Center

*Session Chairs:* Yasuhiko Arakawa, University of Tokyo; Martin Kuball, University of Bristol

---

2:00 PM Invited

**D1, ThinGaN Power-LED Demonstrates 100 lm at 527 nm:** *Matthias Peter*<sup>1</sup>; P. Stauss<sup>2</sup>; A. Walter<sup>2</sup>; J. Baur<sup>2</sup>; B. Hahn<sup>2</sup>; <sup>1</sup>OSRAM Opto Semiconductors GmbH; <sup>2</sup>OSRAM Opto-Semiconductors GmbH

Recent progress in the epitaxy of green InGaN LEDs in combination with an improved 1 mm<sup>2</sup> chip design leads to a significant improvement of output power for green LEDs: 99.1 lm at 350 mA were demonstrated for a 1 mm<sup>2</sup> ThinGaN Chip at 527 nm, mounted in a Dragon package with spherical lens. Efficacies of 113 lm/W at 100 mA and 73 lm/W at 350 mA have been achieved.

2:30 PM Invited

**D2, Blue Lasing at Room-Temperature in a Lattice-Matched AlInN/GaN Vertical Cavity Surface Emitting Laser:** *Eric Feltin*<sup>1</sup>; Gabriel Christmann<sup>1</sup>; Julien Dorsaz<sup>1</sup>; Antonino Castiglia<sup>1</sup>; Anas Mouti<sup>1</sup>; Pierre Stadelmann<sup>1</sup>; Jean-François Carlin<sup>1</sup>; Raphael Butté<sup>1</sup>; Nicolas Grandjean<sup>1</sup>; Stavros Christopoulos<sup>2</sup>; Giorgio Baldassarri<sup>2</sup>; Alastair Grundy<sup>2</sup>; Pavlos Lagoudakis<sup>2</sup>; Jeremy Baumberg<sup>2</sup>; <sup>1</sup>EPFL; <sup>2</sup>University of Southampton

III-nitride optoelectronic devices have recently undergone a tremendous development with the commercialisation of white light emitting diodes and UV edge-emitting lasers. However, electrically driven compact laser sources such as vertical cavity surface emitting lasers (VCSELs) have not been demonstrated so far. We now report on the lasing action at 422nm under optical pumping of a crack-free hybrid microcavity with a bottom lattice-matched AlInN/GaN Bragg mirror and a top SiO<sub>2</sub>/Si<sub>3</sub>N<sub>4</sub> Bragg mirror. The maximum peak reflectivity of both mirrors exceeds 99% and the quality factor of the microcavity reaches 2800. The cavity is formed by *n* and *p*-type regions, an AlGaIn electron blocking layer and only three InGaIn/GaN quantum wells. Such a design is identical to that of an electrically driven VCSEL. The high finesse of the microcavity leads to lasing at room temperature for a power density of only 200 μJ/cm<sup>2</sup>, the lowest threshold reported so far for a nitride VCSEL.

3:00 PM

**D3, Low Noise Characteristics of AlGaInN-Based Self-Pulsating Laser Diodes:** *Toshiyuki Obata*<sup>1</sup>; Nobuyoshi Kitajima<sup>1</sup>; Makoto Ohta<sup>1</sup>; Hiroyasu Ichinokura<sup>1</sup>; Masaru Kuramoto<sup>1</sup>; <sup>1</sup>Sony Shiroishi Semiconductor Inc

We have successfully produced practical self-pulsating AlGaInN-based laser diodes (SP-LDs) that have low noise characteristics even with an optical feedback of 1% at a high temperature of 75°C. Our fabricated SP-LD is using a saturable absorber layer (SAL). We intentionally introduced reactive ion etching (RIE) damage to the SAL in order to reduce the carrier lifetime in the SAL by controlling the distance between the SAL and the dry-etched surface. The threshold currents of a fabricated SP-LD at 25 and 75°C were 38.8 and 54.4 mA, respectively. We also demonstrated that it is possible to suppress the relative intensity noise (RIN) even under the conditions of high temperature (75°C) and an optical feedback of 1% (RIN < -125 dB/Hz). These results indicate that practical SP-LDs for use in optical storage devices can be produced by inducing dry etching damage in the SAL.

3:15 PM

**D4, Beam Quality of Blue InGaN Laser for Projection:** *Uwe Strauss*<sup>1</sup>; Christian Rumbolz<sup>1</sup>; Christoph Eichler<sup>1</sup>; Alfred Lell<sup>1</sup>; Stephan Lutgen<sup>1</sup>; Soenke Tautz<sup>1</sup>; Marc Schillgalies<sup>1</sup>; Stefanie Brüningshoff<sup>1</sup>; <sup>1</sup>OSRAM Opto Semiconductors

The light source of choice for laser projection will be a long wavelength nitride laser because of its high wall plug efficiency and because of the small size compared to blue light by second harmonic generation. High quality of the far field is required for laser projection. However, optical confinement by GaN/AlGaIn structures becomes increasingly difficult if wavelengths shift from 405nm to the true blue spectrum. We will show excellent far fields by suppression of higher laser modes and by improved waveguiding, respectively. We present simulations of laser modes as a function of ridge widths. The slow axis far field is improved by absorber layers to guarantee M<sup>2</sup><1.5. Sufficient vertical confinement of the laser light by thick cladding layers is necessary to suppress laser modes guided inside the substrate. We present 440nm lasers for projection with threshold densities as low as 2kA/cm<sup>2</sup> and slope efficiencies of 1W/A.

3:30 PM Break

---

## Session E: Microwave Devices II

Monday PM                      Room: 314/315  
September 17, 2007            Location: MGM Grand Hotel Conference Center

*Session Chairs:* Stacia Keller, University of California; Bill Pribble, Cree, Inc.

---

### 2:00 PM Invited

**E1, GaN MMICs for RF Power Applications in the 50 GHz to 110 GHz Frequency Range:** *Miro Micovic*<sup>1</sup>; Ara Kurdoghlian<sup>1</sup>; Ivan Milosavljevic<sup>1</sup>; Paul Hashimoto<sup>1</sup>; M. Hu<sup>1</sup>; M. Antcliffe<sup>1</sup>; P. Willadsen<sup>1</sup>; W. Wong<sup>1</sup>; Adele Schmitz<sup>1</sup>; R. Bowen<sup>1</sup>; David Chow<sup>1</sup>; <sup>1</sup>HRL Laboratories LLC

Solid state RF power sources for frequencies exceeding 50 GHz are currently realized almost exclusively in GaAs and InP material systems. Until recently GaN-based devices were not seriously considered for power applications at frequencies that are higher than 50 GHz, due to difficulty with material processing. In 2006 we reported at IEDM outstanding potential of GaN MMIC technology for RF power applications at frequencies exceeding 80 GHz. The first reported W-band GaN power MMIC had over 16 dB of saturated power gain in a frequency range between 78 GHz and 88 GHz and produced almost the same output power at this frequency band as the state of the art InP HEMT MMICs with 10 times larger output device periphery. In this presentation we will report the latest advances in our W-band GaN MMIC technology and discuss the impact of GaN technology on the development of high frequency millimeter-wave power modules.

### 2:30 PM

**E2, Deep Submicron AlGaIn/GaN HEMT with Ion Implanted Source/Drain Regions and Nonalloyed Ohmic Contacts:** *Yi Pei*<sup>1</sup>; F. Recht<sup>1</sup>; Nicholas Fichtenbaum<sup>1</sup>; Stacia Keller<sup>1</sup>; Steven DenBaars<sup>1</sup>; Umesh Mishra<sup>1</sup>; <sup>1</sup>University of California, Santa Barbara

We have demonstrated the first deep submicron AlGaIn/GaN HEMTs with nonalloyed ohmic contacts by ion implantation, which show an excellent high frequency performance that is comparable to state of the art AlGaIn/GaN HEMTs with alloyed contacts. Nonalloyed ohmic contacts with 0.2  $\Omega$ •mm were achieved by Si implantation into source/drain regions with a dose of  $5 \times 10^{15}$  cm<sup>-2</sup>, energy of 50 keV and  $\pm 40^\circ$  incident angle, followed by 1280°C MOCVD annealing. For a  $L_g=150$  nm,  $W_g=2 \times 75$   $\mu$ m HEMT, a peak gm of 490 ms/mm was achieved.  $f_T$  was 91 GHz and  $f_{MAX}$  was 136 GHz at  $V_{DS}=6$ V. Increasing  $V_{DS}$  to 12 V resulted in a  $f_T$  of 81 GHz, and  $f_{MAX}$  of 149 GHz. For a  $L_g=150$  nm,  $W_g=2 \times 50$   $\mu$ m HEMT,  $f_T$  was 69 GHz and  $f_{MAX}$  was 167 GHz at a  $V_{DS}$  of 16 V. These results show implantation very promising for improving device high frequency performance.

### 2:45 PM

**E3, Ultra-Shallow Channel AlN/GaN FETs for Future High-Speed and High-Transconductance Applications:** *David Deen*<sup>1</sup>; Tom Zimmermann<sup>1</sup>; Yu Cao<sup>1</sup>; Debdeep Jena<sup>1</sup>; Huili (Grace) Xing<sup>1</sup>; <sup>1</sup>University of Notre Dame

While the AlGaIn/GaN HEMTs have been scaled down for higher speed (>200 GHz), it is clear that a thin AlN could serve well as gate barrier due to its large bandgap (6.2 eV) and high permittivity (~ 8.5). AlN/GaN based HEMTs have been demonstrated by several groups to date, however, they all seemed to be limited by the relatively poor AlN, manifested by the channel 2DEG low mobility (< 400 cm<sup>2</sup>/Vs). Recently in our lab, high quality AlN up to 5 nm have been grown on GaN without cracks, exhibiting 2DEG density as high as  $4 \times 10^{13}$  cm<sup>-2</sup> and mobility as high as 1200 cm<sup>2</sup>/Vs. HEMTs have been fabricated on these heterostructures with various AlN barrier thicknesses: 2.3, 3.5 and 5 nm. E.g. the 5 nm AlN/GaN HEMT ( $L_g=3$   $\mu$ m) showed an output current of 800 mA/mm and a transconductance of about 180 mS/mm. Our detailed findings will be then presented.

### 3:00 PM

**E4, Deeply Recessed AlGaIn/GaN HEMTs with Deep Submicron Gates:** *Rongming Chu*<sup>1</sup>; Yi Pei<sup>1</sup>; Likun Shen<sup>1</sup>; Christiane Poblenz<sup>1</sup>; James Speck<sup>1</sup>; Umesh Mishra<sup>1</sup>; <sup>1</sup>University of California, Santa Barbara

For applications at K-band and beyond, it is attractive to develop dispersion free AlGaIn/GaN HEMTs without using the field-plate. By having the device surface far from the 2DEG, and thereby minimizing the dispersion, we have developed deeply recessed AlGaIn/GaN HEMTs with exceptional performance at C- and X-band. In this report, we present our recent work on scaling the gate length of the deeply recessed HEMTs. The fabricated device has a saturation current of 0.75 A/mm, and a gate-drain breakdown of around 50 V. The extrinsic  $f_T$  is 65 GHz and the extrinsic  $f_{max}$  is 136 GHz. Preliminary microwave power measurements at 30 GHz show that when biased at 25 V, the un-passivated deep submicron HEMT has an output power density 3 W/mm with the associated PAE of 38%. These results suggest that the deep submicron deep recess technology is very promising for achieving high power performance at higher frequencies.

### 3:15 PM

**E5, Laterally Engineered Field-Plate GaN HEMTs for mmWave Applications:** *Karim Boutros*<sup>1</sup>; Keisuke Shinohara<sup>1</sup>; Andres Paniagua<sup>1</sup>; Berinder Brar<sup>1</sup>; <sup>1</sup>Teledyne Scientific

A laterally Engineered Field Plate (EFP) design is implemented to obtain a field-plated, 30nm gate structure with a minimum added capacitance due to the presence of the field plate. By reducing the field plate length, and simultaneously placing it away from the gate, we are able to reduce the field plate capacitance while maintaining its effectiveness in reducing the peak electric field at the gate edge. GaN HEMT EFP devices were fabricated with 30nm gate lengths, and 70nm field plates. A three-terminal breakdown voltage (VBD) of 63V was measured for the 30nm EFP device. This VBD represents a 2x improvement over the breakdown of 100nm T-gate devices fabricated on the same wafer. The device had an extrinsic  $f_T$  of 65GHz and an  $f_{MAX}$  of 95GHz. These results are very encouraging because they indicate we can simultaneously achieve high frequency operation and high breakdown in 30nm devices using this gate structure.

### 3:30 PM Break

---

## Session F: Bulk Growth and HVPE II

Monday PM                      Room: 312/317  
September 17, 2007            Location: MGM Grand Hotel Conference Center

*Session Chairs:* Ben Haskell, Inlustra, Inc; M. Heuken, Aixtron AG

---

### 2:00 PM

**F1, Chemical Lift-Off of GaN Epitaxial Films Grown on c-Plane Sapphire Substrates with CrN Buffer Layers by Hydride Vapor Phase Epitaxy:** *Hiroki Goto*<sup>1</sup>; Seogwoo Lee<sup>1</sup>; Hyunjae Lee<sup>1</sup>; Hyo-Jong Lee<sup>1</sup>; Junseok Ha<sup>1</sup>; Meoungwhan Cho<sup>1</sup>; Takafumi Yao<sup>1</sup>; Soonku Hong<sup>1</sup>; <sup>1</sup>Tohoku University

We propose CrN as a novel buffer for GaN growth. Rock-salt structured CrN(111) has an intermediate bond distance ( $a=2.927\text{\AA}$ ) between sapphire(0001) ( $a=2.747\text{\AA}$ ) and GaN(0001) ( $a=3.188\text{\AA}$ ). Moreover the thermal expansion coefficients of CrN ( $a=6.00 \times 10^{-6}/K$ ) lies in between those of sapphire ( $a=6.66 \times 10^{-6}/K$ ) and GaN ( $a=5.59 \times 10^{-6}/K$ ). It is expected that these material properties suppress the generation of cracks and bending in thick GaN layers on sapphire substrates. We note that CrN can be selectively etched-off by chemical solution, which can be used to realize freestanding substrates. High quality thick GaN layers were successfully grown on c-plane sapphire substrates with CrN buffers by HVPE without generation of cracks. FWHMs of X-ray rocking curve and low temperature PL show essentially identical behaviors with those of HVPE GaNs grown on LT-GaN buffer. We also confirm epitaxial growth directions of the samples as GaN(0001)/

# Technical Program

CrN(111)/sapphire(0001) as expected. Chemical lift-off of GaN thick films will be presented.

**2:15 PM**

**F2, Characterization of a Freestanding AlN Substrate Prepared by Hydride Vapor Phase Epitaxy:** *Yoshinao Kumagai*<sup>1</sup>; Toru Nagashima<sup>2</sup>; Hisashi Murakami<sup>1</sup>; Kazuya Takada<sup>2</sup>; Akinori Koukutu<sup>1</sup>; <sup>1</sup>Tokyo University of Agriculture and Technology; <sup>2</sup>Tokuyama Corporation

High-speed growth of a thick AlN layer by hydride vapor phase epitaxy (HVPE) is a promising approach for preparation of a freestanding AlN substrate. In this paper, preparation and characterization of a freestanding AlN substrate by HVPE using (111)Si as a starting substrate are investigated. A newly developed hybrid HVPE system consisted of a conventional electric furnace and a resistance heating susceptor for direct heating of the substrate was used. After AlN nucleation layer growth at 1140°C, the main AlN layer was grown at 1230°C. A 112- $\mu\text{m}$ -thick freestanding AlN substrate with a dislocation density of  $3 \times 10^9 \text{ cm}^{-2}$  was successfully obtained after the removal of the Si substrate by a chemical etchant. The AlN substrate was transparent, free of cracks, and had a smooth (0001) surface with Al polarity. Autodoping of Si from the Si substrate, and photoluminescence properties of the AlN substrate were also investigated.

**2:30 PM**

**F3, Fabrication of GaN Boules by Vertical-HVPE:** B. Schineller<sup>1</sup>; J. Kaeppler<sup>1</sup>; M. Heuken<sup>1</sup>; <sup>1</sup>AIXTRON AG

We developed a Vertical Hydride Vapor Phase Epitaxy tool for the growth of up to 7 cm long GaN boules of 2 inch size. Prototypes were built and optimized with respect to total growth rate, parasitic ammonium chloride deposition and growth uniformity of the boule. A sheath flow between the reactive species GaCl and  $\text{NH}_3$  provides separation and, thus, avoids pre-reactions. Special attention was paid to the avoidance of cold spots along the way from the growth zone into the particle trap outside of the reactor chamber. In AFM measurements a 250  $\mu\text{m}$  thin layer features parallel steps of 10-15 nm height spaced at 5 nm. For a 2 mm thick layer the surface becomes irregular with pits of about the same depth. The RMS roughness was measured to be 3 nm for a  $10 \times 10 \mu\text{m}^2$  scan field in both cases. Additional results on EPD and photoluminescence will be presented.

**2:45 PM**

**F4, Characterization of Low Defect Density Non-Polar Native GaN Substrates:** *K.-Y. Lai*<sup>1</sup>; V. D. Wheeler<sup>1</sup>; J. A. Grenko<sup>1</sup>; M. A. L. Johnson<sup>1</sup>; A. D. Hanser<sup>2</sup>; Keith Evans<sup>2</sup>; <sup>1</sup>North Carolina State University; <sup>2</sup>Kyma Technologies, Inc.

Non-polar GaN's predicted potential to improve the efficiency of LEDs was recently corroborated by researchers using a low-defect-density non-polar "native" GaN substrate. Prior attempts by others to fabricate efficient non-polar GaN LEDs appear to be stacking-fault defect-limited due to prior use of non-polar "template" GaN substrates. We report on the structural characterization, using cathodoluminescence spectroscopy and secondary electron microscopy, of low-defect-density non-polar native GaN substrates which were produced by transverse wafering of low-defect density c-plane GaN boules grown by hydride vapor phase epitaxy (HVPE). Very low non-radiative recombination center densities of  $10^6 \text{ cm}^{-2}$  and lower were observed, consistent with very low concentrations of extended defects. Results of GaN HVPE regrowth experiments will also be presented showing appreciable anisotropy in growth rate and consistent with no appreciable extended defect generation in the epilayers.

**3:00 PM**

**F5, Self-Separation Mechanism of AlN Thick Layers Grown on SiC:** *G. Reza Yazdi*<sup>1</sup>; Finn Giuliani<sup>1</sup>; Mikael Syvajarvi<sup>1</sup>; Lars Hultman<sup>1</sup>; Rositza Yakimova<sup>1</sup>; <sup>1</sup>Linköping University

This paper presents a new way to fabricate freestanding AlN wafers by physical vapor transport technique. We will report the morphological evolution from discontinuous growth, resulting in arrays of AlN microrods, to a continuous layer and will describe the different steps of AlN layer formation on 4H-SiC substrates that serve as templates for initial nucleation. By merging microrods to form a continuous layer, freestanding AlN of about

10 mm in diameter and 150  $\mu\text{m}$  thick, without cracks, was fabricated. The microrods are crucial for allowing easy separation from the substrate. We have studied conditions at which the dislocation density in the grown AlN can be reduced compared to the SiC substrates. Finally the self-separation mechanism will be discussed. The AlN surface morphology was characterized by optical microscopy, SEM, and AFM. TEM, X-ray diffraction and Cathodoluminescence were used to examine the composition and crystalline quality of the grown crystals.

**3:15 PM**

**F6, Homo Epitaxial Seeding and Grain Evolution of AlN Bulk Crystals:** *Carsten Hartmann*<sup>1</sup>; Juergen Wollweber<sup>1</sup>; Christoph Seitz<sup>1</sup>; Martin Albrecht<sup>1</sup>; Roberto Fornari<sup>1</sup>; <sup>1</sup>Institute for Crystal Growth

PVT growth, the most accepted technique to grow AlN single crystals, is performed. A precondition for sizeable and low defect crystals is homo-epitaxial seeding. The grain evolution described in this paper is considered as an effective method to develop monocrystalline seeds by using an iterative procedure. Supported by temperature field calculations a special crucible design and substrate holder geometry is developed. First AlN boules, 35 mm in diameter and 15 mm long, were grown in an inductively heated reactor on TaC crucible lids. The largest grains (4-5 mm diameter) were separated, cut in wafers, polished and used for the subsequent growth runs. Successful and reproducible epitaxial seeding is demonstrated and proved by EBSD measurements. A pre-treatment process, a deoxidizing ambience and an adapted temperature-gradient-control inhibit impurity deposition on the seed. Longitudinal cuts show the grain evolution with coarsening angles of  $10 - 15^\circ$ . The crystals are 8-10 mm in diameter.

**3:30 PM Break**

---

## Session G: Quantum Dots: Growth

Monday PM  
September 17, 2007

Room: 313/316  
Location: MGM Grand Hotel Conference Center

*Session Chairs:* Nicolas Grandjean, Federal Polytechnic School of Lausanne; Eva Monroy, Atomic Energy Commission-Grenoble

---

**4:00 PM Invited**

**G1, [0001], [11-20] and [1-100] GaN Quantum Dots: Growth and Optical Properties:** *Bruno Daudin*<sup>1</sup>; <sup>1</sup>CEA/Grenoble

Quantum dots (QDs) are of particular interest in highly defective nitride materials and are possible candidates to form active layers of a new generation of light emitting diodes. In particular, growth of nonpolar QDs is especially attractive to face the issue of internal electric field present in [0001] heterostructures, detrimental to radiative recombination efficiency. Along these lines molecular beam epitaxy growth of non polar [11-20] and [1-100] GaN QDs using [11-20] and [1-100] SiC substrates will be described. Their structural properties will be discussed. In particular, it will be shown that a wide variety of morphological shapes, ranging from quantum wells to QDs and quantum wires, can be obtained depending on growth conditions. The optical properties of non polar [11-20] and [1-100] single dots will be presented and compared to that of their polar [0001] counterparts. As expected, it is found that luminescence decay time is shorter (around 200 ps) in non polar QDs than in polar ones (in the 10 ns - 100 ms range), due to electric field reduction.

**4:30 PM**

**G2, Investigations of InN Quantum Dot Growth by Metal Organic Vapor Phase Epitaxy:** Bernard Gil<sup>1</sup>; *Olivier Briot*<sup>1</sup>; Mathieu Morret<sup>1</sup>; Sandra Ruffenach<sup>1</sup>; <sup>1</sup>CNRS

We investigate the growth of InN quantum dots by MOVPE on different foreign substrates and using different gas vectors.

4:45 PM

**G3, Mechanisms of Quantum Dot Formation in InGaN Layers Grown by MOVPE:** *André Strittmatter*<sup>1</sup>; Til Bartel<sup>1</sup>; Lars Reißmann<sup>2</sup>; Robert Seguin<sup>1</sup>; Axel Hoffmann<sup>1</sup>; Dieter Bimberg<sup>1</sup>; <sup>1</sup>Technische Universität Berlin; <sup>2</sup>Otto-von-Guericke Universität Magdeburg

Quantum dot formation in InGaN layers grown by MOVPE on Si(111) substrates was investigated by transmission electron microscopy as well as by cathodoluminescence. Two sets of samples grown either with varying In content (10%-25%) or with varying thickness (0.5 - 4 nm) of the InGaN layers were studied. Thereby, the impact of both parameters on the QD formation can be distinguished. In fact, QDs are evidenced in all layers either via locally via XTEM images or by narrow lines (FWHM < 1 meV) in the cathodoluminescence spectra recorded from sub-micron size apertures formed in metal masks. All InGaN layers are characterized by local In clustering. The In distribution functions determined from the HRTEM cross sections show identical halfwidths independent of growth parameters.

5:00 PM

**G4, Optical Properties of Single and Multi-Layer InGaN Quantum Dots:** Kathrin Sebald<sup>1</sup>; Joachim Kalden<sup>1</sup>; *Henning Lohmeyer*<sup>1</sup>; Sandra Herlufsen<sup>1</sup>; Jürgen Gutowski<sup>1</sup>; Tomohiro Yamaguchi<sup>2</sup>; Christian Tessarek<sup>2</sup>; Detlef Hommel<sup>2</sup>; <sup>1</sup>University of Bremen, Semiconductor Optics, Institute of Solid State Physics; <sup>2</sup>University of Bremen, Semiconductor Epitaxy, Institute of Solid State Physics

In the last years much effort was spent in the realization for InGaN quantum dots (QDs) in order to achieve efficient devices emitting in the UV-blue spectral region. In this contribution we will present the optical properties of single InGaN QDs grown by MOVPE. The samples were structured into mesas by focused-ion-beam etching and investigated by micro-photoluminescence measurements. The QDs are characterized by a high temperature stability of their emission up to 150 K as well as spectral diffusion effects occurring only at high excitation densities. Furthermore, the polarization of individual QD emission lines was analyzed giving an insight into their geometrical shape. Additionally, the optical properties of mesa structured InGaN QD stacks were investigated up to room temperature in order to get information on the influence of the stacking on the properties of the QDs as well as indications for coupling effects between the QDs.

5:15 PM

**G5, Spectral Linewidth Control of Hexagonal Gallium Nitride Quantum Dots:** *Takeshi Kawano*<sup>1</sup>; Satoshi Kako<sup>2</sup>; Christian Kindel<sup>3</sup>; Yasuhiko Arakawa<sup>4</sup>; <sup>1</sup>Institute of Industrial Science; <sup>2</sup>Collaborative Institute for Nano Quantum Information Electronics; <sup>3</sup>Research Center for Advanced Science and Technology; <sup>4</sup>University of Tokyo

Epitaxially grown GaN QDs embedded in AlN have attracted much attention for single-photon source (SPS) operating at room temperatures because of strong confinement effect, large optical phonon energies, and large biexciton binding energy. So far, we have demonstrated triggered single-photon generation from a single GaN QD at temperatures up to 200K. One of the obstacles to realize SPS operating at room temperatures is spectral-diffusion processes which cause the linewidth broadening due to the defects in the vicinity of GaN QDs. By means of annealing at temperatures of 1180°C for 10min and improving AlN buffer layer by inserting alternative providing growth where the material sources of Al and N are provided alternatively, an average of spectral linewidth of GaN QDs became reduced from 13.5 meV to 8.8 meV and from 13.3 meV to 11.1 meV, respectively. We believe that spectral linewidth will become much reduced by combining these two methods.

## Session H:

### Epitaxial Growth for Electronic Devices

Monday PM  
September 17, 2007

Room: 314/315  
Location: MGM Grand Hotel Conference Center

*Session Chairs:* Toshihide Kikkawa, Fujitsu Laboratories; Robert Coffie, Northrup-Gruman

4:00 PM

**H1, High Quality N-Rich GaN Growth by Plasma-Assisted Molecular Beam Epitaxy for Electronic Devices:** *Gregor Koblmüller*<sup>1</sup>; Rong Ming Chu<sup>1</sup>; Feng Wu<sup>1</sup>; Christiane Poblenz<sup>1</sup>; Andrea Corrión<sup>1</sup>; Umesh Mishra<sup>1</sup>; James Speck<sup>1</sup>; <sup>1</sup>University of California, Santa Barbara

Exploitation of N-rich growth conditions at temperatures of thermal decomposition was demonstrated to yield a layer-by-layer growth mode during the PAMBE growth of (0001) GaN. Consequently, smooth surface morphologies were achieved for thick GaN films with rms roughness < 1 nm and no new dislocations generated. The capacity of these novel growth conditions were also reflected by record RT electron mobilities greater than 980 cm<sup>2</sup>/Vs at carrier densities in the low-1E16 cm<sup>-3</sup> region, surpassing the commonly insulating nature of GaN grown under N-rich conditions at lower temperatures due to reduced impurity incorporation. Utilizing the N-rich/high-T conditions for the growth of AlGaIn/GaN HEMTs on 4H-SiC, we observed a clear trend for dislocation reduction while maintaining smooth surfaces. Non-optimized transistor structures exhibited very low buffer leakage, 2DEG mobilities and drain currents in excess of 1150 cm<sup>2</sup>/Vs and 1.2 A/mm respectively, comparing very well with state-of-the-art grown devices by MOCVD and MBE.

4:15 PM

**H2, Optimization of Regrowth Interface in III-Nitride-Based Heterostructure Field Effect Transistors Grown by MOCVD:** Jianping Liu<sup>1</sup>; Jae-Hyun Ryou<sup>1</sup>; Wonseok Lee<sup>1</sup>; Yun Zhang<sup>1</sup>; Shyh-Chiang Shen<sup>1</sup>; *Russell Dupuis*<sup>1</sup>; <sup>1</sup>Georgia Institute of Technology

For III-nitride based HFETs, the semi-insulating property of the layer including the buffer layer and the substrate underneath the channel is required in order to achieve a sharp current pinch-off and high-frequency device operation. For the case of the growth on GaN template and GaN substrates, the growth interface between the epitaxial layer and the GaN substrate/template is a critical region of the device. In order to remove the interface charged layer that is inevitably introduced during the substrate preparation and/or epitaxial growth, we studied three effects on charged layer on GaN templates and free-standing substrates: (1) Fe doping near the interface, (2) chemical cleaning, and (3) PEC (photoelectrochemical) etching. We will report in detail on the interface charge behavior depending on Fe doping scheme and surface treatment and propose the mechanism of interface charge removal. Also, performance characteristics of HFETs with and without interface charge will be analyzed.

4:30 PM

**H3, Ammonia Molecular Beam Epitaxy of AlGaIn/GaN High Electron Mobility Transistors on 6H-SiC:** *Andrea Corrión*<sup>1</sup>; Christiane Poblenz<sup>1</sup>; Feng Wu<sup>1</sup>; Likun Shen<sup>2</sup>; Felix Recht<sup>2</sup>; Rongming Chu<sup>2</sup>; Chang Soo Suh<sup>2</sup>; Umesh Mishra<sup>2</sup>; James Speck<sup>1</sup>; <sup>1</sup>Materials Department, University of California, Santa Barbara; <sup>2</sup>Electrical and Computer Engineering Department, University of California, Santa Barbara

The growth conditions for ammonia MBE of AlGaIn/GaN HEMTs on 6H-SiC were optimized for surface morphology and dislocation density, and excellent RF performance was demonstrated. It was found that decreasing growth rates and increasing V/III ratios resulted in decreasing surface roughness. The TD density decreased with decreasing V/III ratio, which resulted in enhanced surface roughness and a transition from a two- to a three-dimensional growth mode. A two-step buffer was developed in which the first step was grown under low V/III ratio conditions to achieve low

# Technical Program

dislocation density, resulting in 25% reduction in dislocation density. A three micron sample with the two-step buffer had a dislocation density of  $3 \times 10^9$  cm<sup>-2</sup>, among the lowest values ever reported for MBE GaN growth on SiC. Ammonia MBE AlGaIn/GaN HEMTs were fabricated, and an output power of >10 W/mm with a PAE of 63% was achieved at 4 GHz.

#### 4:45 PM

**H4, AlGaIn/GaN HEMTs Grown by Molecular Beam Epitaxy on 3C-SiC/Si(111):** *Yvon Cordier*<sup>1</sup>; Marc Portail<sup>1</sup>; Sébastien Chenot<sup>1</sup>; Oliver Tottereau<sup>1</sup>; Marcin Zielinski<sup>2</sup>; Thierry Chassagne<sup>2</sup>; <sup>1</sup>CRHEA-CNRS; <sup>2</sup>NOVASIC

Cubic SiC/Si(111) substrate is an interesting alternative for growing GaN. As compared with silicon, this substrate allows reducing the stress in GaN films due to both lower lattice and thermal expansion coefficient mismatch, and can provide better heat dissipation. In this work, we developed the epitaxial growth of 3C-SiC films on Si(111) by hot wall CVD. AlGaIn/GaN HEMT heterostructures were subsequently grown by MBE. Surface roughness and dislocation density (<5E9 cm<sup>-2</sup>) are at least at the same level as the ones of layers grown on bulk substrates while X-ray diffraction shows a single in-plane orientation for both GaN and 3C-SiC with respect to Si(111). Transistors and Hall effect devices were realized. GaN buffer layers are highly resistive and a 2D electron gas with a carrier density of 7E12 cm<sup>-2</sup> and mobility of 1500 cm<sup>2</sup>/V.s has been obtained for a structure with an Al content x=25% in the AlGaIn barrier.

#### 5:00 PM

**H5, Fe-Doped GaN below and above the Solubility Limit: Growth and Characterization:** *Martin Quast*<sup>1</sup>; Michal Kiecana<sup>2</sup>; Clemes Simbrunner<sup>1</sup>; Tian Li<sup>1</sup>; Andrea Navarro-Quezada<sup>1</sup>; Matthias Wegscheider<sup>1</sup>; Maciej Sawicki<sup>2</sup>; Tomasz Dietl<sup>2</sup>; Alberta Bonanni<sup>1</sup>; <sup>1</sup>Johannes Kepler Universität Linz; <sup>2</sup>Polish Academy of Sciences

In order to shed light on the origin of high temperature ferromagnetism observed in magnetically doped semiconductors and oxides, we have undertaken comprehensive studies of MOVPE grown (Ga,Fe)N, which combine a detailed space-resolved chemical analysis by transmission electron microscopy and energy dispersive X-ray spectroscopy with a thorough magnetic, optical and electric characterization. Our investigations reveal the presence of coherent nanocrystals, presumably Fe<sub>x</sub>N, with the composition and lattice parameter imposed by the GaN host. Their presence and their non-uniform distribution over the film volume affect in a decisive way the magnetic and optical properties of the films. We find, in particular, ferromagnetic signatures such as spontaneous magnetization, which persist well above room temperature and whose magnitude increase with the Fe concentration above the solubility limit. We explain these observations in terms of a high critical temperature associated with magnetic- and shape anisotropy of the Fe<sub>x</sub>N nanocrystals.

#### 5:15 PM

**H6, Inhibition of Regrowth Interface Contamination with New Fe Doped Templates for AlGaIn/GaN HEMT Applications:** *Yvon Cordier*<sup>1</sup>; Nicolas Baron<sup>2</sup>; Mohamed Azize<sup>1</sup>; Sébastien Chenot<sup>1</sup>; Olivier Tottereau<sup>1</sup>; Jean Massies<sup>1</sup>; <sup>1</sup>CRHEA-CNRS; <sup>2</sup>Picogiga International

Semi-insulating behaviour of GaN templates is required for high-frequency devices such as AlGaIn/GaN high electron mobility transistors (HEMTs). To obtain such SI templates, two ways have proven to be efficient: the self-compensation by a huge amount of defects as dislocations and Fe modulation doping for a better crystalline quality (dislocation density < 1E9 cm<sup>-2</sup>). In this work, we show that by carefully designing the Fe doping profile into SI-GaN templates grown by MOVPE and by optimizing the MBE regrowth conditions, highly-resistive GaN buffer can be achieved on these epi-ready GaN-on-Sapphire templates without any addition of acceptors during the regrowth. As a result, high-quality high electron mobility transistors can be realized. Furthermore, we report on the excellent properties of two-dimensional electron gas and device performances with electron mobility superior to 2000 cm<sup>2</sup>/V.s at room temperature and off-state leakage current as low as 5 μA/mm at 100V.

## Session I: Optical Characterization of Bulk Materials and Microcavities

Monday PM

September 17, 2007

Room: 312/317

Location: MGM Grand Hotel Conference Center

*Session Chairs:* Claude Weisbuch, University of California at Santa Barbara; Ulrich Schwarz, University Regensburg

#### 4:00 PM Invited

**I1, High-Quality Nonpolar m-Plane GaN Substrate Grown by HVPE:** *Kenji Fujito*<sup>1</sup>; Kazumasa Kiyomi<sup>1</sup>; Tae Mochizuki<sup>1</sup>; Hiroataka Oota<sup>1</sup>; Hideo Namita<sup>2</sup>; Satoru Nagao<sup>2</sup>; Isao Fujimura<sup>1</sup>; <sup>1</sup>Mitsubishi Chemical Corporation; <sup>2</sup>Mitsubishi Chemical Group Science and Technology Research Center, Inc.

We have obtained relatively large size (about 10mm X 10mm) m-plane GaN substrates grown by HVPE. Typical values for the full widths at half maximum (FWHM) of x-ray rocking curves measured for the (10-10) and (10-12) reflections were 25-35arcsec and 30-40arcsec, respectively. The dislocation distribution was observed from the [10-10] direction by cathodeluminescence method. The dark spots density was less than 2.5X10<sup>5</sup>cm<sup>-2</sup>. The surface roughness after the lapping and polishing was measured by atomic force microscopy and the RMS was less than 0.1nm. More detailed characteristics of our substrates will be presented in the conference. High-quality large size m-plane GaN substrate will enable to realize commercial production of nonpolar devices.

#### 4:30 PM

**I2, Dephasing Studies of Exciton Fine Structure in Uniaxially-Strained GaN:** *Tetsuro Ishiguro*<sup>1</sup>; Yasunori Toda<sup>1</sup>; Satoru Adachi<sup>1</sup>; Katsuyuki Hoshino<sup>2</sup>; Yasuhiko Arakawa<sup>3</sup>; <sup>1</sup>Hokkaido University; <sup>2</sup>Yamaguchi University; <sup>3</sup>University of Tokyo

Dephasing dynamics of exciton fine structure (EFS) in a GaN film on a-plane sapphire was observed and studied by utilizing a spectrally-resolved four-wave-mixing (SR-FWM) spectroscopy. In the sample, degenerate exciton states are split into their fine structures due to the exchange interaction induced by the anisotropic strain field of the substrate. Since the each exciton of FS is also highly polarized, the polarization dependent SRFWM spectra successfully resolve the dephasing dynamics in the individual resonances. The result shows a significant difference in the dephasing time between the A-exciton EFS (X<sub>Ax</sub> and X<sub>Ay</sub>), suggesting that exchange interaction is effective in the dephasing of excitonic polarization in GaN.

#### 4:45 PM

**I3, Radiative Decay Times of Free and Bound Excitons in Bulk GaN:** *Bo Monemar*<sup>1</sup>; Plamen Paskov<sup>1</sup>; Peder Bergman<sup>1</sup>; Alexey Toropov<sup>2</sup>; Tatiana Shubina<sup>2</sup>; Akira Usui<sup>3</sup>; <sup>1</sup>Linköping University; <sup>2</sup>Ioffe Physico-Technical Institute; <sup>3</sup>Furukawa Company Ltd

Transient photoluminescence (TRPL) for high quality HVPE bulk GaN crystals are reported for temperatures 2 K to 300 K. The decay of the free exciton no-phonon (NP) line is short at 2 K, about 100 ps. The FE LO phonon replicas have a longer decay time, about 1400 ps at 2 K. The donor bound exciton (DBE) NP lines have an initial short (non-exponential) decay of 300 ps at 2 K, while the LO replicas have a decay about 1300 ps. The DBE two-electron transitions (TETs) exhibit a decay above 1 ns. We suggest a nonradiative surface recombination is important for the FE NP line, but not for the FE replicas, due to reabsorption. The DBEs NP line decay is masked by strong resonant light scattering. The real radiative bulk decay times for FEs and DBEs are approximately obtained from the LO replicas.

5:00 PM

## 14, Observation of Well-Resolved Bound, Free, and Higher Order Excitons in AlN Epilayers Grown by Metalorganic Vapor Phase Epitaxy:

*Takeyoshi Onuma*<sup>1</sup>; Takahiro Koyama<sup>2</sup>; Kei Kosaka<sup>3</sup>; Keiichi Asai<sup>3</sup>; Shigeaki Sumiya<sup>3</sup>; Tomohiko Shibata<sup>3</sup>; Mitsuhiro Tanaka<sup>3</sup>; Takayuki Sota<sup>4</sup>; Akira Uedono<sup>5</sup>; Shigefusa Chichibu<sup>1</sup>; <sup>1</sup>Tohoku University; <sup>2</sup>Japan Science and Technology Agency; <sup>3</sup>NGK Insulators, Ltd.; <sup>4</sup>Waseda University; <sup>5</sup>University of Tsukuba

Distinct four bound exciton lines as well as ground-state and excited-state free exciton lines are clearly resolved in the low-temperature cathodoluminescence (CL) spectra of approximately 2- $\mu\text{m}$ -thick AlN epilayers grown on (0001) Al<sub>2</sub>O<sub>3</sub> substrates by metalorganic vapor phase epitaxy at NGK Insulators. With the decrease in the threading dislocation density from  $1 \times 10^{10}$  to  $2 \times 10^8 \text{ cm}^{-2}$ , relative intensities of characteristic deep CL bands at 4.6, 3.8, and 3.1 eV to the near-band-edge peak around 6 eV significantly decrease. Since the concentration of Al vacancies simultaneously decreases, which was confirmed by the positron annihilation measurement, those deep bands are correlated with the point defects associated with Al vacancies. From the energy difference between the ground and the first excited states, the A-exciton binding energy is determined to be 51.3 meV.

5:15 PM

15, Late News

## MP: Poster Session I

Monday, 5:30-7:00 PM  
September 17, 2007

Room: Prefunction Area  
Location: MGM Grand Hotel Conference Center

## MP: Bulk Growth and HVPE

**MP1, Cathodoluminescence Microscopy of High Quality Bulk-Like GaN ELOG Structures:** *Barbara Bastek*<sup>1</sup>; Frank Bertram<sup>1</sup>; Juergen Christen<sup>1</sup>; Christian Hennig<sup>2</sup>; Eberhard Richter<sup>2</sup>; Markus Weyers<sup>2</sup>; Günther Tränkle<sup>2</sup>; <sup>1</sup>Otto-von-Guericke-University Magdeburg; <sup>2</sup>Ferdinand-Braun-Institut für Höchstfrequenztechnik

We present cathodoluminescence microscopy characterization of bulk-like c-axis grown GaN HVPE-layers. The up to 900 $\mu\text{m}$  thick layers were grown on patterned GaN/sapphire templates (MOVPE). Epitaxial lateral overgrowth (ELOG) was performed by HVPE over WSiN-masks consisting of a hexagonal lattice of circular openings. These layers separate from the template. CL-mappings of the bottom side of the delaminated layers show a low CL-intensity from the openings where coherent c-axis growth took place. In the immediate vicinity of the openings the CL-intensity shoots up rapidly resulting in a hexagonal glowing frame of electron-hole-plasmas-luminescence. Outside these hexagons only ( $D_1^0, X_A$ ) emission is found. The evolution and termination of the characteristic ELOG growth domains are directly visualized in cross-sectional-CL-imaging. All layer top-side-surfaces are smooth and exhibit a sharp and bright ( $D_1^0, X_A$ ) luminescence at 3.472eV (FWHM=2.2meV) evidencing that the layers are completely strain free. This emission from the top is very homogeneous showing lateral fluctuation  $\sigma_E < 0.3\text{meV}$ .

**MP2, Direct Growth of InN and InGaN on Sapphire Substrates by HVPE:** *Jai Weon Jean*<sup>1</sup>; Sanghwa Lee<sup>1</sup>; Taegeon Oh<sup>1</sup>; Hyeokmin Choe<sup>1</sup>; Yuri Sohn<sup>1</sup>; Chinkyoo Kim<sup>1</sup>; <sup>1</sup>Kyunghee University

InN and InGaN were directly grown on 0.3°-miscut (toward M-plane) c-plane sapphire substrates by hydride vapor phase epitaxy (HVPE) and their growth characteristics were investigated by utilizing x-ray scattering. Depending on the various growth parameters, the formation of InN and InGaN was sensitively influenced. Six samples were grown by changing HCl flow rate, the substrate temperature and Ga and In source temperature and all the samples were pretreated with NH<sub>3</sub> for 23 seconds. By increasing the flow rate from 10 sccm to 20 sccm, InGaN phase as well as InN was observed. On the other hand, when the substrate temperature was raised from 680 to 760°C,

the increased substrate temperature dramatically suppressed the formation of InN. A similar behavior was observed for the samples grown with different source zone temperatures. By decreasing the source zone temperature from 450 to 420°C, InGaN instead of InN was preferentially grown.

**MP3, Growth of Single Crystalline GaN from Chlorine-Free Gas Phase:** *Hans-Joachim Rost*<sup>1</sup>; Dietmar Siche<sup>1</sup>; Klaus Böttcher<sup>1</sup>; Daniela Gogova<sup>1</sup>; Roberto Fornari<sup>1</sup>; <sup>1</sup>Institute for Crystal Growth

This work is focused on the development of GaN bulk growth to overcome restrictions of the established HVPE method. Evaporated Ga is transported by carrier gas to the substrate where it reacts with atomic nitrogen from the thermal ammonia decomposition to form GaN at temperatures of 1000 – 1300°C and pressures of 200 – 800 hPa. To prove the methods potential, 1 mm thick polycrystalline layers were deposited on the seed holder with rates up to 50  $\mu\text{m/h}$ . Numerical simulations of temperature-, flow- and concentration field of the gas species were used to optimize crucible geometry and growth regime. It was found experimentally that in addition to temperature, total pressure and ammonia flow other parameters like source composition, crucible material and flow conditions near the substrate may affect seeding, growth rate and layer quality. First epitaxial layers up to 250 $\mu\text{m}$  thickness were successfully grown on different bulk and template substrates.

**MP4, Growth Optimization of Thin GaN Layer Grown by HVPE:** *Denis Martin*<sup>1</sup>; Tiankai Zhu<sup>1</sup>; Nicolas Grandjean<sup>1</sup>; <sup>1</sup>Ecole Polytechnique Fédérale de Lausanne

Thin GaN layers grown by hydride vapor phase epitaxy (HVPE) are attractive for the use as templates and for the growth of single run GaN quasi-substrates. In this work, we investigate two important steps used for the growth of thin GaN layers directly on sapphire. First is the temperature ramping rate during the nucleation layer recrystallization in a horizontal HVPE reactor and second is the planarization process for the development of a fully coalesced layer less than 10 $\mu\text{m}$ . We found that the temperature ramping rate applied during the nucleation layer recrystallization step does not limit the structural quality of the GaN material and can be as low as 10°C/min. Furthermore, fast planarization of the high temperature GaN layer is obtained by inserting a low-pressure growth step. Dislocation density can be reduced in the low 10<sup>8</sup>cm<sup>-2</sup> by controlling this step while maintaining a crack free layer.

**MP5, Increase in the Growth Rate of GaN Single Crystals Grown by Gallium Hydride Vapor Phase Epitaxy Method:** *Mamoru Imade*<sup>1</sup>; Norihide Yamada<sup>1</sup>; Yoshihiro Kitano<sup>1</sup>; Fumio Kawamura<sup>1</sup>; Masashi Yoshimura<sup>1</sup>; Yasuo Kitaoka<sup>1</sup>; Yusuke Mori<sup>1</sup>; Takatomo Sasaki<sup>1</sup>; <sup>1</sup>Osaka University

A dependence of Gallium hydride (GaH<sub>x</sub>: x=1, 2, 3) production on the growth rate of GaN crystals grown by the gallium hydride vapor phase epitaxy (GaH-VPE) method was investigated. By this method, GaN crystals are synthesized in a reaction between GaH<sub>x</sub> and NH<sub>3</sub>. The growth rate of GaN crystals has been as low as 20  $\mu\text{m/h}$  at a maximum because the poor reactivity of H<sub>2</sub> gas with Ga metal limits the production of GaH<sub>x</sub>. In this study, the interfacial area between Ga metal and H<sub>2</sub> gas was enlarged to increase the GaH<sub>x</sub> synthesis, which thereby enabled an increase in the growth rate to 68  $\mu\text{m/h}$ . We showed clearly that the growth rate of GaN by the GaH-VPE method is limited by the efficiency of the reaction between the Ga metal and H<sub>2</sub> gas.

**MP6, Lattice Parameters of Bulk GaN: A Comparative Analysis:** *V. Darakchieva*<sup>1</sup>; A. Usui<sup>2</sup>; B. Monemar<sup>1</sup>; <sup>1</sup>Linkoping University; <sup>2</sup>Research and Development Division, Furukawa Co. Ltd.

Knowledge of material lattice parameters is essential both from a physical point of view and for device engineering. The lattice parameters of GaN reported in the literature show unusually large fluctuations and it is difficult to determine the intrinsic unstrained values. In this work we report on the precise determination of the lattice parameters of a high-quality undoped bulk GaN fabricated by hydride vapor phase (HVPE). The obtained values are compared with the lattice parameters of HVPE GaN bulk materials from different sources and found to be representative for state-of-the-art undoped HVPE bulk GaN. Further, a comparison with bulk GaN crystals fabricated by the high-pressure method and homoepitaxial GaN is made and significant

# Technical Program

differences in the lattice parameters are found. The observed differences will be discussed and concluding remarks on the strain-free lattice parameters will be drawn.

**MP7, Liquid Phase Epitaxy of GaN on MOCVD GaN/Sapphire and HVPE Free-Standing Substrates under High Nitrogen Pressure:** *Michal Bockowski*<sup>1</sup>; <sup>1</sup>Institute of High Pressure Physics

The liquid phase epitaxy of GaN on one- and two-inch MOCVD sapphire/GaN templates and HVPE free-standing substrates by high pressure solution method will be presented. The crystallization on patterned substrates with variety of TiN masks will be reported in details. The growth modes in normal and lateral directions will be analyzed. The defect selective etching will be used to state the average dislocation density on the surface of laterally overgrown material. The finite element calculation will be implemented for modeling the convective transport in liquid gallium. The stream lines, convectional flow velocity vectors and isotherm lines in liquid metal will be determined based on experimentally measured temperatures. The effect of seed, crucible wall and baffle for convection in liquid metal will be analyzed. It will be shown the baffle plate allows reducing the convectional flow close to the seed and obtaining macroscopically flat growth of GaN from the liquid phase.

**MP8, Migration-Enhanced-Hydride-Vapor-Phase-Epitaxy of GaN on Sapphire Substrates:** *Sanghwa Lee*<sup>1</sup>; Hyeokmin Choel<sup>1</sup>; Taegeon Oh<sup>1</sup>; Jai Weon Jean<sup>1</sup>; Yuri Sohn<sup>1</sup>; Chinkyoo Kim<sup>1</sup>; <sup>1</sup>Department of Physics, Kyunghee University

One of the promising methods to fabricate a free-standing GaN substrate is hydride vapor phase epitaxy, but its fast growth rate is not very advantageous during nucleation process. In order to reliably control the size and density of the nucleated islands migration-enhancement method was applied to HVPE. GaN films were directly grown on c-plane sapphire substrates at 1050°C without any low-temperature nucleation layers. To investigate the effect of migration, the nucleation layers of GaN were grown with different duration of growth interruptions. HCl and NH<sub>3</sub> gases were simultaneously introduced into the reactor for 5 sec and gas supply was interrupted for 30 sec, 60 sec and 120 sec, respectively. These growth and migration processes were repeated 5 times. The increased migration time decreased the density of nucleated islands and improved the surface morphology dramatically. Our results suggest that the nucleation characteristics of GaN could be controlled by altering migration time.

**MP9, Modeling of III-Nitride Bulk Crystal Growth from the Vapor Phase:** *Mark Ramm*<sup>1</sup>; Maxim Bogdanov<sup>2</sup>; Sergey Karpov<sup>1</sup>; Alexey Kulik<sup>2</sup>; <sup>1</sup>Semiconductor Technology Research, Inc.; <sup>2</sup>Soft-Impact, Ltd.

Simulation of PVT growth of AlN and HVPE growth of GaN bulk crystals has been performed by the software "Virtual Reactor" provided by STR, Inc. The heat transfer, reactive species transport, and their chemical interaction at the reactive surfaces are considered self-consistently. The major focus of the study is made on a high growth rate maintaining, V/III ratio control, parasitic deposition on the reactor walls, and crystal shape evolution. Intentional variation of the growth parameters, like temperature, precursor flow rates, and the seed-source gap, provides an effective way for stabilization and optimization of the long-term growth conditions. Special attention is given to predict the thermoelastic stress and threading dislocation density in the growing crystals, as the factors largely affecting the crystal quality. Specific features of AlN and GaN crystal growth in vertical reactors are discussed in detail in terms of simulation.

**MP10, Structural Properties of Aluminum Nitride Bulk Single Crystals Grown by PVT:** *Matthias Bickermann*<sup>1</sup>; Boris Epelbaum<sup>1</sup>; Octavian Filip<sup>1</sup>; Paul Heimann<sup>1</sup>; Shunro Nagata<sup>2</sup>; Sabine Schmidt<sup>1</sup>; Albrecht Winnacker<sup>1</sup>; <sup>1</sup>University of Erlangen; <sup>2</sup>JFE Mineral Company, Ltd.

Bulk single crystals were grown by physical vapor transport (PVT) on single-crystalline AlN seeds by directional sublimation, yielding AlN single crystals up to 1.2 inch in diameter and 12 mm in height. Polished wafers cut from such crystals were investigated by wet chemical etching and X-ray transmission rocking curve measurements in order to assess distribution and density of dislocations as well as mosaicity. We found average dislocation

densities of 10<sup>4</sup>...10<sup>7</sup> cm<sup>-2</sup>. In some areas, clearly cellular patterns were observed, which was approved by broad (0.1...1.5°) X-ray rocking curves. Overall crystalline quality is still sufficiently lower compared to smaller, spontaneously nucleated, virtually unstressed AlN crystals. As it stands, mosaicity is a challenging problem in directional sublimation; both growth conditions and seed quality have to be improved to ensure AlN bulk growth with low dislocation density.

**MP11, Sublimation Growth of 2 Inch Diameter Bulk AlN Crystals:** *Yuri Makarov*<sup>1</sup>; Tatyana Chemekova<sup>1</sup>; Oleg Avdeev<sup>1</sup>; Iosif Barash<sup>1</sup>; Eugeny Mokhov<sup>1</sup>; Sergey Nagalyuk<sup>1</sup>; Alexander Roenkov<sup>1</sup>; Alexander Segal<sup>1</sup>; Yuri Vodakov<sup>1</sup>; Heikki Helava<sup>2</sup>; Mark Ramm<sup>2</sup>; <sup>1</sup>N-Crystals, Ltd; <sup>2</sup>The Fox Group, Inc.

Sublimation growth of 15 mm diameter bulk single AlN crystals is scaled to grow 2 inch crystals. Two approaches are used to provide such scaling, one employs seeding on AlN plates of a smaller diameter followed by lateral overgrowth, the other uses seeding on 2 inch diameter SiC plates. The former technique provides good purity of the crystals but requires a number of repeated runs to reach the desired diameter. The latter technique is implemented in two stages. Initially 2-3 mm thick AlN layer is grown on SiC seed in pre-carbonised tantalum crucible in a RF heated graphite furnace. Then the AlN layer is separated from the SiC seed and used as a seed to grow bulk AlN crystal in tungsten crucible in resistively heated tungsten furnace. The second stage results in rapid reduction of impurities with length, so that no Si impurities are found at 5 mm.

**MP12, Suppression of Surface Reaction in HVPE of GaN on 6H-SiC Substrates by Insertion of CrN Buffer Layers:** *Jun Seok Ha*<sup>1</sup>; Hyo-Jong Lee<sup>1</sup>; S. Nagata<sup>1</sup>; S.W. Lee<sup>1</sup>; H.J. Lee<sup>1</sup>; H. Goto<sup>1</sup>; S.H. Lee<sup>1</sup>; M.W. Cho<sup>1</sup>; T. Yao<sup>1</sup>; <sup>1</sup>Tohoku University

6H-SiC is favorable as substrate for GaN growth in terms of lattice matching and crystal structure. However, when GaN is directly grown on SiC, it is difficult to obtain high quality GaN due to reactions between Ga and SiC. Therefore, AlN buffer layer has been used to suppress surface reactions. In this study, we deposit CrN buffer layer on SiC substrates for suppression of surface reactions. Cr layers are deposited on 6H-SiC substrates, followed by nitridation to form CrN prior to HVPE growth of GaN. The formation of CrN results in different features for Si- and C-terminated surfaces. CrN shows trigonal morphology on Si-terminated SiC, which indicates growth direction along <111> axis, while CrC<sub>x</sub> is formed on C-terminated SiC as indicated by ion-beam analysis. Consequently, GaN HVPE growth on CrN/C-terminated SiC results in grain growth indicative of deteriorated crystallinity, while high quality GaN layers are successfully grown on CrN/Si-terminated SiC.

**MP13, Synthesis of Highly Luminescent, Ge-Mg Co-Doped GaN Powders:** *Rafael Garcia*<sup>1</sup>; Alan Thomas<sup>2</sup>; Fernando Ponce<sup>1</sup>; <sup>1</sup>Arizona State University; <sup>2</sup>Rogers Corporation

GaN microcrystallites co-doped with germanium and magnesium have been grown by reacting Ga and diluted alloys (Ga-Mg-Ge) with ammonia in a horizontal quartz-tube reactor at temperatures between 1000 and 1100°C. An initial low-temperature treatment to dissolve ammonia into the Ga melt produces doped GaN powders with high conversion efficiency. The optoelectronic properties of these materials are comparable or superior to the best epitaxial films. Doping was achieved by dissolving doping impurities into the liquid Ga before reacting the alloy with ammonia. The powders synthesized by this method consist mostly of two differently shaped crystallites: large irregular particles with lengths of around 30 μm and hexagonal platelets with diameter between 2 and 5 μm. These crystallites have the hexagonal wurtzite structure and exhibit strong room-temperature luminescence with the characteristic GaN-band edge as well as Ge- and Mg-related emissions. These characteristics make these materials strong candidates for optoelectronic applications.

**MP14, The Effect of Additive of Carbon into the Na Flux on the Growth of GaN Single Crystals:** *Masaki Tanpo*<sup>1</sup>; Yoshihiro Kitano<sup>1</sup>; Fumio Kawamura<sup>1</sup>; Masashi Yoshimura<sup>1</sup>; Yasuo Kitaoka<sup>1</sup>; Yusuke Mori<sup>1</sup>; Takatomo Sasaki<sup>1</sup>; <sup>1</sup>Osaka University

We attempted an increase in the growth rate of bulk GaN single crystals in Na flux method. We have already reported some disadvantages in this method including a low growth rate. A generation of poly-crystals near gas-liquid interface lowers the growth rate because nitrogen prefers to be consumed by the growth of poly-crystals rather than the liquid phase epitaxy (LPE). In order to improve the growth rate, some attempts can be nominated: applying a thermal convection, addition of specific impurity and so on. In this study, we examined the addition of carbon into the Ga-Na mixed melt for the purpose of preventing generation of poly-crystals. Remarkable effect of the carbon on suppression of poly-crystals could be confirmed, which enabled to increase the growth rate drastically. Over 20  $\mu\text{m}/\text{h}$  which could be attained in this study is considered enough for an industrial applications.

**MP15, The Effects of Growth Temperature on the Crystallinity of GaN in Gallium Hydride Vapor Phase Epitaxy Method:** *Norihide Yamada*<sup>1</sup>; Mamoru Imade<sup>1</sup>; Yoshihiro Kitano<sup>1</sup>; Fumio Kawamura<sup>1</sup>; Masashi Yoshimura<sup>1</sup>; Yasuo Kitaoka<sup>1</sup>; Yusuke Mori<sup>1</sup>; Takatomo Sasaki<sup>1</sup>; <sup>1</sup>Osaka University

High temperature growth was examined for improving the crystallinity and the surface morphology in gallium hydride vapor phase epitaxy (GaH-VPE) method. In this method, GaN crystals are synthesized using gallium hydride ( $\text{GaH}_x$ ;  $x=1,2,3$ ) as a Ga source. We had already confirmed that the growth rate of GaN increased with  $\text{GaH}_x$  supply and reached 68  $\mu\text{m}/\text{h}$ . However, improvement of a surface morphology and crystallinity of the GaN crystal has been required. In this study, the dependence of growth temperature on the crystallinity and the surface morphology of grown crystals was investigated, resulting in achievement of the flat surface at the temperature higher than 1,150 degree. In addition, improvement of crystallinity was also realized by decreasing an impurity level in the apparatus.

**MP16, Thick a-Plane GaN Epitaxial Films by HVPE on Patterned Sapphire Substrates:** *Ying Gao*<sup>1</sup>; Rakesh Jain<sup>1</sup>; Jianping Zhang<sup>1</sup>; Jinwei Yang<sup>1</sup>; Remis Gaska<sup>1</sup>; Kai Liu<sup>2</sup>; Michael Shur<sup>2</sup>; <sup>1</sup>Sensor Electronic Technology, Inc.; <sup>2</sup>Rensselaer Polytechnic Institute

Thick a-plane GaN films have been grown on r-plane sapphire substrates by Hydride Vapor Phase Epitaxy. Maximum thickness of 50  $\mu\text{m}$  a-plane GaN films with no cracks was obtained. When film thickness is more than 50  $\mu\text{m}$ , large stress causes conventional sapphire substrates and epilayer to crack. Patterned sapphire substrates were used to effectively manage built-in strain in the epitaxial layer and to suppress cracking. Using this approach, crack-free layers up to 300  $\mu\text{m}$  thick were grown. Wafers have been fully characterized using photoluminescence, SEM and XRD. The characterization data clearly showed higher material quality of thick layers with much stronger photoluminescence intensity. SEM showed that a-plane GaN grew in different orientations with preferred facets. For optimized growth conditions the facet growth can be suppressed and surface morphology can be improved. Detailed characterization results including carrier lifetime data will be presented.

## MP: Defects

**MP17, Comparison of Deep Level Incorporation and Current-Voltage Characteristics in Ammonia and rf-Plasma Molecular Beam Epitaxy n-GaN Films:** *Aaron Arehart*<sup>1</sup>; C. Poblenz<sup>2</sup>; Andrea Corrion<sup>2</sup>; J. Speck<sup>2</sup>; U. Mishra<sup>2</sup>; S. DenBaars<sup>2</sup>; Steven Ringel<sup>1</sup>; <sup>1</sup>Ohio State University; <sup>2</sup>University of California

The use of rf-plasma and ammonia nitrogen sources for growth of molecular beam epitaxy (MBE) n-type GaN films are compared in terms of defect incorporation and Schottky barrier height characteristics using deep level optical spectroscopy (DLOS), deep level transient spectroscopy (DLTS), forward biased current-voltage-temperature (IVT) and internal photoemission (IPE) measurements. The DLTS results show traps at  $E_c-0.73$ ,  $E_c-0.57$ ,  $E_c-0.16$ , and  $E_c-0.15$  in the ammonia sample and traps at  $E_c-0.73$  and  $E_c-0.56$  for the rf-plasma sample. The DLOS spectra are quite similar with onset energies at  $E_c-3.28$ ,  $E_c-2.62$ , and  $E_c-1.28$ ; however, the

rf-plasma sample shows an additional level near  $E_c-2.04$  eV. Additionally, IVT and IPE measurements reveal nearly identical barrier heights of 1.10 eV and near-ideal room temperature ideality factors between 1.02-1.08. A full analysis of the IVT characteristics will be discussed including an enhanced thermionic-field emission characteristic energy, which we speculate could be due to donor-like surface defects.

**MP18, Correlation between the Violet Luminescence Intensity and Defect Density in AlN Epilayers Grown by Ammonia-Source Molecular Beam Epitaxy:** *Takahiro Koyama*<sup>1</sup>; Mariko Sugawara<sup>2</sup>; Takuya Hoshi<sup>3</sup>; John Kaeding<sup>4</sup>; Rajat Sharma<sup>4</sup>; Shuji Nakamura<sup>4</sup>; Akira Uedono<sup>2</sup>; Shigefusa Chichibu<sup>1</sup>; <sup>1</sup>Japan Science and Technology Agency; <sup>2</sup>University of Tsukuba; <sup>3</sup>Tohoku University; <sup>4</sup>University of California

The intensity ratios of characteristic deep cathodoluminescence (CL) bands at 4.6, 3.8, and 3.1 eV to the near-band-edge emission at 11 K of AlN epilayers grown by ammonia-source molecular beam epitaxy are correlated with the change in  $S$  parameter of positron annihilation measurement, which represents the concentration (or size) of Al vacancies ( $V_{\text{Al}}$ ). Since the relative intensities of 3.1 eV and 3.8 eV bands increase remarkably with lowering supply ratio of ammonia to Al ( $V/\text{III}$  ratio) and growth temperature ( $T_g$ ), they are assigned to donor-acceptor-pair recombination associated with  $V_{\text{Al}}$  and/or  $V_{\text{Al}}\text{-O}$  complexes. The  $V_{\text{Al}}$  concentration can be decreased by adjusting  $V/\text{III}$  ratio and  $T_g$ . As a result, the AlN epilayers exhibiting negligible deep level emissions show fine excitonic features in the CL spectra. Since defect complexes composed of cation vacancies ( $V_{\text{III-X}}$ ) act as nonradiative recombination centers (NRCs) in GaN and AlGaIn,  $V_{\text{Al-X}}$  may act as NRCs in AlN.

**MP19, Dislocation Related Defect States in GaN Irradiated with 1 MeV Electron-Beam:** *Dong Uk Lee*<sup>1</sup>; Lim-Kyoung Ha<sup>1</sup>; Jin Soak Kim<sup>1</sup>; Eun Kyu Kim<sup>1</sup>; Eui Kwan Koh<sup>2</sup>; Il Ki Han<sup>3</sup>; <sup>1</sup>Hanyang University; <sup>2</sup>Korea Basic Science and Institute; <sup>3</sup>Korea Institute of Science and Technology

We have studied defect states in GaN bulk material grown by hydride vapor phase epitaxy method. The undoped GaN layers were grown with different threading dislocation densities (TDDs). The A and B samples with thickness of 278  $\mu\text{m}$  showed TDD of  $9.0 \times 10^6 \text{ cm}^{-2}$  and  $7.2 \times 10^6 \text{ cm}^{-2}$ , respectively, while the C sample had thickness and TDD of 257  $\mu\text{m}$  and  $3.4 \times 10^6 \text{ cm}^{-2}$ , respectively. The typical defect states were measured at the activation energy of  $E_c-0.34$  eV,  $E_c-0.89$  eV,  $E_c-1.06$  eV, respectively. Especially, the energy state of  $E_c-0.89$  eV was considered as a dislocation related defect, because its density tended to increase as increasing TDD. These GaN samples were irradiated by electron beam with the energy of 1 MeV and dose ranges of  $1 \times 10^{14} \sim 10^{15} \text{ cm}^{-2}$ . The defect states in electron beam irradiated samples were characterized by capacitance-voltage and deep level transient spectroscopy measurements.

**MP20, Effects of Ultraviolet Light and Visible Laser Illumination on the Charge Status of the Surface States in a AlGaIn/GaN Heterostructure:** *Yun-Chong Chang*<sup>1</sup>; Yun-Li Li<sup>2</sup>; Jinn-Kong Sheu<sup>1</sup>; <sup>1</sup>National Cheng Kung University; <sup>2</sup>National Taiwan University

Variations of the channel resistance of a AlGaIn/GaN heterostructure with a green laser and ultraviolet (UV) illuminations were observed. The phenomena are proposed to be related to the surface states. The subsequently green laser causes the UV-generated excess electrons to leave the AlGaIn/GaN interface region and injected into the surface region. These injected electrons passivate the positively-charged surface states, which results in a higher channel resistance. This proposed model is consistent with the results from the voltage evolutions under different UV intensities, which reveals that the time constant is proportional to the UV intensities. Activation energy of 0.342 eV is extracted from the results of temperature-dependent voltage evolutions measurements. The similar value between the activation energy and the valence band discontinuity at the AlGaIn/GaN interface also supports our hypothesis about the surface states. Further experiments will be conducted to help us understand role of surface states of a AlGaIn/GaN interfaces.

# Technical Program

**MP21, Electrical Properties and Deep Centers in Semi-Insulating Fe-Doped Native GaN Substrates Grown by Hydride Vapor Phase Epitaxy:** B. Clafin<sup>1</sup>; D. Look<sup>1</sup>; H. Smith<sup>1</sup>; Z. Fang<sup>1</sup>; William Mitchell<sup>1</sup>; D. Hanser<sup>2</sup>; E. Preble<sup>2</sup>; K. Evans<sup>2</sup>; <sup>1</sup>Air Force Research Laboratory; <sup>2</sup>Kyma Technologies, Inc.

Electrical properties and deep centers in semi-insulating Fe-doped GaN substrates grown by hydride vapor phase epitaxy were characterized by thermally stimulated current (TSC) spectroscopy. Five samples from a low-Fe wafer displayed very high 300 K resistivity ( $>1011$  ohm-cm), dominated by a center at 0.94 eV. Five traps were observed in the samples by TSC, with trap B (0.56-0.60 eV) being dominant. Some variations in both peak temperature and peak amplitude of trap B were observed. A metastable trap A1 at  $\sim 0.82$  eV appeared after white-light illumination at 300 K. A sample with higher Fe displayed a lower 300 K resistivity ( $4 \times 10^9$  ohm-cm), dominated by a center at 0.58 eV. The largest TSC peak in this sample was trap A1, although trap B also appeared. These TSC traps are compared with deep-level-transient-spectroscopy traps reported in conductive epitaxial and bulk GaN.

**MP22, High Quality, High Efficiency and Ultrahigh In-Content InGaN QWs - The Problem of Thermal Stability:** Daniel Fuhrmann<sup>1</sup>; Holger Jönen<sup>1</sup>; Lars Hoffmann<sup>1</sup>; Heiko Bremers<sup>1</sup>; Uwe Rossow<sup>1</sup>; Andreas Hangleiter<sup>1</sup>; <sup>1</sup>Technical University Braunschweig

InGaN/GaN quantum well structures with Indium concentrations above 30% suited for light emitters in the green and beyond have been investigated. A homogeneous indium distribution and abrupt interfaces yield very high internal quantum efficiencies of 80% and 70% for 460nm and 510nm emission wavelength, respectively. However, for high In concentrations the heterostructures are thermally less stable. This is evident from systematic studies including varied GaN cap temperatures and different post annealing procedures. For elevated temperatures we observe a reduction of the PL intensity, a broadening and a shift to higher energies of the PL lines without indication of phase separation. The reason is the soft indium-nitrogen bond, the degradation likely occurs by In interdiffusion via defects in the structures. The critical temperatures are well below those typical for p-GaN contact layer growth and thus need to be considered in device applications.

**MP23, High Resolution Laplace Deep Level Transient Spectroscopy Studies of Electron and Hole Traps in n-Type GaN:** Jan Evans-Freeman<sup>1</sup>; Deniz Emiroglu<sup>1</sup>; Menno Kappers<sup>2</sup>; Clifford McAleese<sup>2</sup>; Colin Humphreys<sup>2</sup>; <sup>1</sup>Sheffield Hallam University; <sup>2</sup>University of Cambridge

Deep Level Transient Spectroscopy (DLTS) and Laplace DLTS (LDLTS) have been applied to MOCVD-grown n-type GaN, grown at 1020°C on c-plane sapphire. DLTS, measured up to 600K, initially recorded three peaks due to electron emission. When the next DLTS rate window was sampled immediately afterwards, a different spectrum was obtained. A large negative peak dominated at 400K, due to hole emission. An electron trap initially present at 400K in the DLTS spectrum gradually disappeared up to a measurement temperature of 520K; beyond this the hole trap was observed. It then remained detectable by DLTS for up to one week, although cooling under bias decreased its intensity severely. LDLTS reveals that this hole trap is not a simple point defect, and it is discussed in the context of the  $V_{Ga}-O_N$  defect. The electron traps have also been characterised by LDLTS and some are found to have complex capture kinetics.

**MP24, Improved Performance and Reliability of GaN Devices via Pendeo-Epitaxy:** Tsvetanka Zheleva<sup>1</sup>; Michael Derenge<sup>1</sup>; Daniel Ewing<sup>1</sup>; Pankaj Shah<sup>1</sup>; Ken Jones<sup>1</sup>; David Stepp<sup>1</sup>; Unchul Lee<sup>1</sup>; Lawrence Robins<sup>1</sup>; <sup>1</sup>Army Research Laboratory

Pendeo-epitaxy as a technology is known to enable drastic reduction of the densities of structural defects in GaN over three orders of magnitude. We have used metal organic chemical vapor deposition (MOCVD) technique to grow pendeo-epitaxial (PE)-GaN, performed analysis of the morphology, structure, and electrical properties via numerous characterization techniques, and correlated the materials and electrical characteristics with the growth and processing conditions. Further, we designed and fabricated test device structures in order to investigate the improved electronic performance of the Schottky contacts and high electron mobility transistors (HEMTs) and correlate the improved devices performance with improved structural quality of the GaN material.

**MP25, Insights into the Origin of Threading Dislocations in GaN/Al<sub>2</sub>O<sub>3</sub> from Atomic Force Microscopy:** Rachel Oliver<sup>1</sup>; Menno Kappers<sup>1</sup>; Colin Humphreys<sup>1</sup>; <sup>1</sup>University of Cambridge

Threading dislocations (TDs) in GaN/Al<sub>2</sub>O<sub>3</sub> are widely assumed to arise at the coalescence boundaries of misoriented islands. Using atomic force microscopy and employing an in situ SiH<sub>4</sub>-treatment to enlarge the TD pits, we have examined GaN/Al<sub>2</sub>O<sub>3</sub> samples at various stages of the coalescence of the GaN film. Prior to coalescence, the morphology is dominated by large ( $\sim 2$   $\mu$ m high) islands, with smaller (50 – 500 nm high) islands observed between them. Considering the (0001) surfaces of the large islands, we find no significant difference between the TD density in the boundary regions and the overall density, suggesting that TDs do not originate at coalescence boundaries. However, a TD density  $\sim 20$  times higher is observed on the surfaces of the smaller islands. When these small structures are overgrown by large islands, these TDs are incorporated into the film, resulting in TD clusters, and a rise in the overall TD density.

**MP26, Microscopic Lateral Overgrowth of GaN on Diamond like Carbon Masks by Physical Vapour Transport:** Daniela Gogova<sup>1</sup>; Martin Albrecht<sup>1</sup>; Matthias Rossberg<sup>1</sup>; Hans-Joachim Rost<sup>1</sup>; Dietmar Siche<sup>1</sup>; Roberto Fornari<sup>1</sup>; <sup>1</sup>Institut für Kristallzüchtung

In this paper results on microscopic lateral overgrowth by physical vapour transport will be presented. A diamond like carbon layer is deposited on a GaN/sapphire template prior to the growth of GaN layer by physical vapour transport. For deposition of the carbon layer a solid phase carbon source and NH<sub>3</sub> were used. The diamond like carbon layer has random opening sizes that act as windows for epitaxial overgrowth in the following step. The mask is stable even at elevated temperatures. Lateral overgrowth is done by physical vapour transport of Ga, using NH<sub>3</sub> as a nitrogen source. Layers as thick as 280  $\mu$ m are obtained. Overgrowth results in a significant decrease of the threading dislocation density compared to that of the GaN/sapphire templates. Optical properties of the resulting layer are dominated by excitonic transitions.

**MP27, Microstructure of Threading Dislocations Caused by Grain Boundaries in AlN on Sapphire Substrate:** Masataka Imura<sup>1</sup>; Hiroki Sugimura<sup>1</sup>; Narihito Okada<sup>1</sup>; Motoaki Iwaya<sup>1</sup>; Satoshi Kamiyama<sup>1</sup>; Hiroshi Amano<sup>1</sup>; Isamu Akasaki<sup>1</sup>; Tadashi Noro<sup>2</sup>; Takashi Takagi<sup>2</sup>; Akira Bandoh<sup>3</sup>; <sup>1</sup>Meijo University; <sup>2</sup>Ibiden Company, Ltd.; <sup>3</sup>Showa-Denko K.K.

Taniyasu et al. reported AlN-based light emitting diodes (LED) with peak wavelength of 210 nm by current injection. As the next step, high-power and high-efficiency deep-ultraviolet (DUV) LED has been requested. However, it is difficult to fabricate high performance DUV-LED, because the performance of the current AlGaN-based DUV-LED is strongly affected by the threading dislocations due to large lattice mismatch. Transmission electron microscopy (TEM) is generally reliable technique for analyzing threading dislocations in the layers. Hence, threading dislocations in AlN analyzed by TEM is the key issues for improving device performance of AlGaN-based DUV-LED by feedback to AlN growth from TEM analysis. As a first step, we investigated the microstructure of threading dislocations, and correlations between X-ray diffraction (XRD) peak width and threading dislocation density in detail. In addition, core structure and lattice image around them were also revealed by high-resolution (HR) TEM.

**MP28, Optical Signatures and Metastability of Magnesium Related Acceptors in GaN:** Bo Monemar<sup>1</sup>; Plamen Paskov<sup>1</sup>; Galia Pozina<sup>1</sup>; Peder Bergman<sup>1</sup>; Carl Hemmingsson<sup>1</sup>; Hiroshi Amano<sup>2</sup>; Isamu Akasaki<sup>2</sup>; Stephan Figge<sup>3</sup>; Detlef Hommel<sup>3</sup>; Akira Usui<sup>4</sup>; <sup>1</sup>Linköping University; <sup>2</sup>Meijo University; <sup>3</sup>University of Bremen; <sup>4</sup>Furukawa Company Ltd

We have studied MOVPE grown GaN:Mg layers prepared on HVPE grown bulk GaN substrates, in order to reduce the density of dislocations to below  $10^7$  cm<sup>-2</sup>. The Mg concentration was varied up to mid  $10^{19}$  cm<sup>-2</sup>. There is clear evidence of two sets of acceptors in optical spectra, both for bound excitons (BEs) and donor-acceptor pair (DAP) spectra. In p-type layers the main PL spectra (3.466 eV BE and 3.27 eV DAP) exhibit metastability. They disappear with time of excitation, in favour of deeper peaks at 3.455 eV and 3.1 eV respectively. The possible relation of these optical signatures to the Mg acceptor will be discussed. CL spectra also show evidence of the pyramidal defects in highly Mg doped GaN.

**MP29, Reduction of Threading Dislocations in AlGaIn/AlN/SiC Epitaxial Layers by Tensile Strain in a-Axis Induced with the (AlN/GaN) Multi-Buffer-Layer:** Kouichi Murakawa<sup>1</sup>; Fumio Hasegawa<sup>1</sup>; Hideo Kawanishi<sup>1</sup>; <sup>1</sup>Kogakuin University

Control of crystal quality of AlN and AlGaIn is very important for development of UV and deep-UV LEDs and LDs. We have found that FWHM of XRC of the AlN template and AlGaIn clad layers can be improved by tensile strain in a-axis introduced by the (AlN/GaN) multi-buffer layer (MBL). Furthermore, we confirmed reduction of the threading dislocations by the tensile strain directly by the TEM observation. AlN and AlGaIn epitaxial layers with Al composition of 0.6-0.8 were grown by LP-MOVPE on a 6H-SiC substrate. The tensile strain in a-axis was controlled by thickness of AlN and GaN of the MBL. Edge dislocation density was one order higher than the screw dislocation density. Some of the dislocations in the AlN template make loop to terminate each other, and the dislocation density decreases with distance from the SiC substrate. It decreases more steeply for the more strained sample.

**MP30, The Reduction of Threading Dislocations in GaN Using a GaN Nanocolumn Interlayer:** David Cherns<sup>1</sup>; Louisa Meshi<sup>1</sup>; Somboon Khongphetsak<sup>1</sup>; Ian Griffiths<sup>1</sup>; Alan Gott<sup>2</sup>; Chaowang Liu<sup>2</sup>; Philip Shields<sup>2</sup>; Wang Wang<sup>2</sup>; Richard Champion<sup>3</sup>; Sergey Novikov<sup>3</sup>; Tom Foxon<sup>3</sup>; <sup>1</sup>University of Bristol; <sup>2</sup>University of Bath; <sup>3</sup>University of Nottingham

Epitaxial lateral overgrowth (ELO) has reduced dislocation densities in GaN. We have investigated ELO on GaN nanocolumns produced either during growth or by self-organised patterning. We have grown GaN nanocolumns by MBE on AlN/(0001)sapphire substrates under nitrogen-rich conditions. The nanocolumns were then overgrown by MOCVD under conditions favouring ELO, and TEM used to examine the resulting films. Isolated nanocolumns grew without threading dislocations, but some threading dislocations formed when nanocolumns coalesced. Although some threading dislocations extended through the overlayer, extensive lateral migration of others, depending on the dislocation type, led to dislocation annihilation, lowering the threading dislocation density. In another approach, self-organised deposits of Ni islands on a GaN/(0001) sapphire substrate by MOCVD were chemically etched to leave GaN nanocolumns around 0.5  $\mu\text{m}$  apart. The Ni was removed, and MOCVD growth under ELO conditions led to a continuous GaN overlayer with dislocation densities less than  $10^8 \text{ cm}^{-2}$ .

**MP31, Theoretical Study of Rare Earth Point Defects in GaN:** Simone Sanna<sup>1</sup>; Uwe Gerstmann<sup>2</sup>; Benjamin Hourahine<sup>3</sup>; Thomas Frauenheim<sup>1</sup>; <sup>1</sup>Universität Bremen; <sup>2</sup>Université Pierre et Marie Curie, Paris; <sup>3</sup>University of Strathclyde

In the framework of the European union network Rare Earth doped Nitrides for high Brightness Electroluminescent emitters (RENiBEI), we have developed and applied theoretical techniques to simulate the behaviour of rare earth dopants in nitride materials. The Density Functional based Tight-Binding method, developed at the University of Paderborn, has been extended to include orbital dependent potentials (LDA+U and SIC-like) in attempt to model the 4f states of lanthanide impurities within a realistic crystal model. We present results of an investigation into the structural and energetic properties of rare earth point defects in GaN, considering a selection of lanthanides which are of technological relevance as phosphors for full colour displays. Rare earth substitutionals and complexes formed by substitutionals and N-vacancies are examined in some detail, discussing their possible role in the luminescence process. Differences in the behaviour of the single lanthanide ions are explained in terms of different 4f-shell occupation.

**MP32, What Kind of Crystal Quality of AlGaIn is Improved by an Alternate-Source-Feeding MOVPE or ME-MOVPE?:** Eiichiro Niikura<sup>1</sup>; Koichi Murakawa<sup>1</sup>; Shoichiro Takeda<sup>1</sup>; Fumio Hasegawa<sup>1</sup>; Hideo Kawanishi<sup>1</sup>; <sup>1</sup>Kogakuin University

The crystal quality of AlN and AlGaIn layers was improved, and optical threshold pumping power of deep UV lasers was drastically reduced, by alternate-source-feeding epitaxy (ASFE) in LP-MOVPE. FWHM of XRC and TEM observation indicated that dislocation density was not changed at all by ASFE. On the other hand, blue emission of PL from the AlGaIn clad

layer was decreased, indicating that point defects such as Ga or Al vacancy are reduced by the ASFE or ME-MOVPE. Furthermore, the yellow emission from GaN/AlGaIn MQW grown by conventional simultaneous source feeding epitaxy (SSFE) on the ASFE AlGaIn clad layer was also reduced. This fact indicates that point defects of MQW on the AlGaIn clad layer with less point defects is less than that on the AlGaIn clad layer with more point defects. As a result, deep UV lasing at 240nm could be achieved in our group.

## MP: Nanostructures: Characterization

**MP33, Energy Level Properties of InGaIn/GaN Quantum Well and Quantum Dots:** Jin Soak Kim<sup>1</sup>; Y.-I. Lee<sup>1</sup>; L. Ha<sup>1</sup>; Eun Kyu Kim<sup>1</sup>; H.J. Kim<sup>2</sup>; E. Yoon<sup>2</sup>; Y. Shon<sup>3</sup>; <sup>1</sup>Hanyang University; <sup>2</sup>Seoul National University; <sup>3</sup>Dongguk University

The III-nitride based materials have been very interesting topics of optical device technologies for several years. Nowadays, the III-nitride technologies are going to toward the nanostructures such as quantum well (QW) and quantum dots (QDs) to improve efficiency of the optical devices. In addition to these nanostructures are more applicable to electronic and information devices due to their quantum effects. Confined energy levels of carriers are most important physical properties of the QW and QD structures. Thus, characterization of these confined energy levels of the nanostructures is very important. In this study, we characterized the energy level properties of the InGaIn/GaN nanostructures by using electrical measurements such as C-V, I-V, and deep level transient spectroscopy. These methods can clarify offset of the ground state energy levels in band structure, number of confined carriers, etc. From the results, we will compare energy level properties of the QW and QDs.

**MP34, Growth and Magnetization Study of Transition Metal Doped GaN Nanostructures:** Shalini Gupta<sup>1</sup>; Hun Kang<sup>1</sup>; Matthew Kane<sup>1</sup>; Eun-Hyun Park<sup>1</sup>; Ian Ferguson<sup>1</sup>; <sup>1</sup>Georgia Institute of Technology

III-V dilute magnetic semiconductors (DMS) have attracted attention in recent years as they offer the potential to fabricate room temperature spintronic devices. Several studies have been performed on bulk GaN doped with transition metals such as manganese. However, the potential of these transition metals in GaN nanostructures has yet to be explored. This work presents the MOCVD growth and characterization of optically active GaN nanostructures which have been doped with the transition metals manganese and iron for potential spintronic applications. Introduction of both these transition metals in GaN nanostructures enhanced the nucleation of the nanostructures resulting in reduced lateral dimensions and increased nanostructure density. Both  $\text{Ga}_{1-x}\text{Mn}_x\text{N}$  and  $\text{Ga}_{1-x}\text{Fe}_x\text{N}$  nanostructures showed hysteresis behavior at 5K. Further SQUID measurements on  $\text{Ga}_{1-x}\text{Fe}_x\text{N}$  nanostructures at 300K showed a hysteresis curve with a reduced coercive field and displayed superparamagnetic behavior. These magnetically active nanostructures provide a promising avenue for future spintronic applications.

**MP35, InN Nanorods and Nanowires Grown on Different Substrates:** Zuzanna Liliental-Weber<sup>1</sup>; M. Hawkrige<sup>1</sup>; J. Mangum<sup>1</sup>; O. Kryliouk<sup>1</sup>; <sup>1</sup>Lawrence Berkeley National Laboratory

TEM was applied to study InN nanorods grown on different planes of Al<sub>2</sub>O<sub>3</sub>, GaN, and (001) Si substrates by non-catalytic, template-free H-MOVPE. Single crystal nanorod growth was obtained on all substrates. The majority of them are of a high structural perfection and exhibit abrupt side walls. The nanorods grown on c-plane sapphire have N-growth polarity. InN nanowires grown on (001) Si and (0002) GaN in a RF heated, horizontal cold-wall MOVPE reactor. Growth parameters such as V/III ratio, flow velocity, and surface pretreatments were investigated with respect to the NW nucleation structure and morphology. Most of them had a triangular shape with decreasing diameter toward the tip, but with a constant composition of hexagonal InN. Application of a two-step growth method (low V/III ratio followed by a higher V/III ratio) led to very long wires (up to 100  $\mu\text{m}$ ) with practically constant diameter and composition.

# Technical Program

**MP36, Luminescence Properties of  $\text{Al}_x\text{Ga}_{1-x}\text{N}$  ( $0.4 \leq x \leq 0.5$ )/ $\text{Al}_y\text{Ga}_{1-y}\text{N}$  ( $0.6 \leq y \leq 1$ ) Quantum Structures Grown by Gas Source Molecular Beam Epitaxy:** Sergey Nikishin<sup>1</sup>; Boris Borisov<sup>1</sup>; Vladimir Kuryatkov<sup>1</sup>; Daoying Song<sup>1</sup>; Mark Holtz<sup>1</sup>; Gregory Garrett<sup>2</sup>; Wendy Sarney<sup>2</sup>; Anand Sampath<sup>2</sup>; Hongen Shen<sup>2</sup>; Michael Wraback<sup>2</sup>; <sup>1</sup>Texas Tech University; <sup>2</sup>Army Research Laboratory

We report structural and optical properties of  $\text{Al}_x\text{Ga}_{1-x}\text{N}$  ( $0.4 < x < 0.5$ )/ $\text{Al}_y\text{Ga}_{1-y}\text{N}$  ( $0.6 < y < 1$ ) quantum structures. The structures are designed for light emission in the range from 270 to 300 nm. The well material was grown under 2D, 3D and (2D+3D) conditions by the varying group-III/ammonia ratio. The formation of nanoscale islands, or quantum dots (QDs), in the wells grown in 3D and (2D+3D) modes was observed using transmission electron microscopy. The embedded dots do not appear to generate dislocations in the surrounding wells and barriers. The room temperature cathodoluminescence (CL) and photoluminescence intensities show a maximum when wells are grown in pure 3D mode. Time-resolved photoluminescence was studied with varying excitation powers. We will describe changes observed (from ~30 ps to ~530 ps) in the decay time as the barrier (well) composition and thickness are varied. TTU acknowledges support from NSF (ECS-0304224, ECS-0609416), THECB-ARP-003644-0014-2006, and the J. F. Maddox Foundation.

**MP37, Persistent Photoconductivity Studies of C-Axis GaN Nanowires Grown by MBE:** Norman Sanford<sup>1</sup>; Paul Blanchard<sup>1</sup>; Kris Bertness<sup>1</sup>; Alexana Roshko<sup>1</sup>; Beau Burton<sup>2</sup>; Lorelle Mansfield<sup>1</sup>; John Schlager<sup>1</sup>; Steven George<sup>2</sup>; Aric Sanders<sup>1</sup>; <sup>1</sup>National Institute of Standards and Technology; <sup>2</sup>University of Colorado at Boulder

Persistent photoconductivity was measured on unintentionally doped, n-type, c-axis, GaN nanowires grown by MBE. Nanowires were composed of single wires with diameters in the range of 50-300 nm, and clusters of wires grown together. Test structures on fused quartz plates were fabricated from 2-terminal electrically contacted nanowires. Electrode gaps were roughly 3 micrometers. Depending on growth conditions, single wires biased at 1-4 V under flood-illumination at 360 nm ( $3 \text{ mW/cm}^2$ ) typically produced photocurrents of 1-300 nA that persisted from several seconds to several minutes in the dark. Multi-wire clusters often yielded 10 times greater photocurrent that could persist for many hours in the dark. The nanowire clusters also displayed sub-gap photoconductivity. Wires encased by 10 nm of conformal ALD alumina displayed persistent current that could continue more than 20 h in the dark. However, conformal ALD TaN films did not substantially increase the decay time of the persistent current.

**MP38, Raman Scattering by Coupled Plasmon-LO Phonons in InN Nanocolumns:** Snezana Lazic<sup>1</sup>; Eva Gallardo<sup>1</sup>; José Manuel Calleja<sup>1</sup>; Fernando Agulló-Rueda<sup>2</sup>; Javier Grandal<sup>3</sup>; Miguel Ángel Sánchez-García<sup>3</sup>; Enrique Calleja<sup>3</sup>; Achim Trampert<sup>4</sup>; Esperanza Luna<sup>4</sup>; <sup>1</sup>Universidad Autónoma de Madrid, Departamento de Física de Materiales; <sup>2</sup>Materials Science Institute of Madrid, CSIC; <sup>3</sup>Universidad Politécnica de Madrid, ISOM and Departamento de Ingeniería Electrónica, ETSIT; <sup>4</sup>Paul-Drude-Institut für Festkörperelektronik

Micro-Raman scattering measurements on high quality, relaxed InN nanocolumns and compact layers grown on Si(001) and Si(111) substrates by plasma-assisted molecular beam epitaxy are reported. A coupled LO phonon-plasmon mode around  $430 \text{ cm}^{-1}$ , together with the uncoupled LO phonon appears in the nanocolumnar sample. The coupled mode is attributed to spontaneous accumulation of electrons at the lateral surfaces of the nanocolumns, while the uncoupled phonon originates from the inner part. Infrared reflectance measurements confirm the presence of electrons in the nanocolumns. Our results indicate that accumulation of intrinsic electrons does not only occur on polar surfaces of InN, but also on non-polar lateral surfaces of the nanocolumns. The intensities of Raman modes measured in different scattering configurations on the columnar samples do not obey conventional selection rules. This deviation is discussed in terms of the geometrical restrictions imposed by the nanocolumn morphology on the vibration modes.

**MP39, Spatially and Spectrally Resolved Cathodoluminescence Measurements of Single GaN Nanowires and Related Nanostructures Grown by Catalyst-Free MBE:** Lawrence Robins<sup>1</sup>; Kris Bertness<sup>1</sup>; Paul Blanchard<sup>1</sup>; Norman Sanford<sup>1</sup>; John Schlager<sup>1</sup>; Mark Vaudin<sup>1</sup>; <sup>1</sup>National Institute of Standards and Technology

Cathodoluminescence (CL) scanning electron microscopy measurements were performed on c-axis oriented, single GaN nanowires, approximately 5  $\mu\text{m}$  in length and 100 to 500 nm in diameter, grown by catalyst-free molecular beam epitaxy. Features identified in low-temperature CL spectra were the excitonic peak at 3.47 eV to 3.48 eV; one- and two-phonon replica peaks at  $\approx 3.39 \text{ eV}$  and  $\approx 3.30 \text{ eV}$ ; and the broad "blue" band centered at 2.8 eV to 3.0 eV. The excitonic peak was the most intense spectral feature in all cases. Spectrally resolved CL imaging confirmed that single wires gave rise to the "blue" band. In polarization-resolved measurements, the  $\pi$ -polarized (perpendicular to c-axis) component of the excitonic peak was observed to lie 5 meV to 10 meV lower in energy than the  $\sigma$ -polarized (parallel to c-axis) component. The polarization-resolved excitonic lineshapes showed large linewidths (20 meV to 30 meV) and also large wire-to-wire variations.

**MP40, Synthesis and Characterization of InN Nanowires:** ZiLi Xie<sup>1</sup>; Rong Zhang<sup>1</sup>; Chao Nie<sup>1</sup>; Xiangqian Xiu<sup>1</sup>; Ping Han<sup>1</sup>; RuoLian Jiang<sup>1</sup>; YouDou Zheng<sup>1</sup>; <sup>1</sup>Nanjing University

Indium nitrides (InN) is a promising but challenging semiconductor, which has the smallest effective electron mass and direct bandgap (0.6-0.7eV), the highest mobility and saturation velocity, and the largest drift velocity at room temperature compared with all other III-nitrides. The novel properties make InN a promising material for photonic devices such as lasers, high efficiency solar cells, LEDs in the infrared light region, and so on. Many searches have been made in synthesis and property of 2D InN, but only a few works have been reported so far on 1D InN structures due to the synthesis difficulties. Indium nitride (InN) nanowires were synthesized by chemical vapor deposition (CVD) method on sapphire substrates with the aurum spots. The structure of the products was characterized by XRD. We also have studied the crystal structures and morphologies by HRTEM equipped with selected area electron diffraction (SAED) analysis.

## MP: Nanostructures: Growth

**MP41, Coalescence Overgrowth with Metalorganic Chemical Vapor Deposition on Molecular Beam Epitaxy Grown GaN Nano-Columns:** Tsung-Yi Tang<sup>1</sup>; Yung-Sheng Chen<sup>1</sup>; Wen-Yu Shiao<sup>1</sup>; Jeng-Jie Huang<sup>1</sup>; Chi-Feng Huang<sup>1</sup>; Tzu-Chi Liu<sup>1</sup>; Kent Averett<sup>2</sup>; John Albrecht<sup>2</sup>; C. C. Yang<sup>1</sup>; <sup>1</sup>National Taiwan University; <sup>2</sup>Air Force Research Laboratory

GaN nano-column growth can lead to threading-dislocation free epitaxial structures. However, the subsequent coalescence growth for connecting the GaN nano-columns is needed for practical device fabrication. In this paper, we report the coalescence overgrowth with metalorganic chemical vapor deposition of GaN nano-columns, which are grown with molecular beam epitaxy. After 700-nm overgrowth of GaN on the nano-column sample, the nano-columns are essentially well connected although some regions of poor atomic arrangement can be observed. Also, the top surface is not so smooth, with an island pattern of hundred microns in scale. Based on the transmission electron microscopy (TEM) study, the overgrown GaN is also threading dislocation free. High-resolution TEM images show a thin layer of poor crystalline structure existing between the nano-columns and the overgrown layer. X-ray diffraction and photoluminescence measurements show that the crystalline quality and optical property of the overgrown layer are superior to those of the nano-columns.

**MP42, Effect of the Pretreatment on the Preferred Growth Direction of GaN Nanorods:** Yuri Sohn<sup>1</sup>; Sanghwa Lee<sup>1</sup>; Jai Weon Jean<sup>1</sup>; Taegeon Oh<sup>1</sup>; Hyeokmin Choe<sup>1</sup>; Chinkyo Kim<sup>1</sup>; <sup>1</sup>Kyunghee University

The effect of  $\text{NH}_3$  or Ga pretreatment on the preferred growth direction of GaN nanorods was investigated. GaN nanorods were directly grown on c-plane sapphire substrates ( $0.3^\circ$ -miscut toward M-plane (10-10)) by HVPE at the temperature of  $530^\circ\text{C}$  for 10 minutes. Different pretreatment conditions gave rise to distinct preferred growth-directions of GaN nanorods.

By controlling the valve operation,  $\text{NH}_3$  or Ga pretreatment was selectively carried out. When the substrate was pretreated either  $\text{NH}_3$  or Ga for 23 seconds, randomly oriented GaN nanorods were observed. Not like those cases, when  $\text{NH}_3$  and HCl were simultaneously supplied to the substrate, i.e., no pretreatment of  $\text{NH}_3$  or Ga, vertically oriented GaN nanorods were observed. These results revealed that the preferred growth direction of GaN nanorods was sensitively influenced by  $\text{NH}_3$  or Ga pretreatment.

**MP43, Fabrication and Optical Properties of Nano-Structured Semipolar InGaN/GaN Multiple Quantum Wells on C-Plane GaN Template:** *Hongbo Yu<sup>1</sup>*; Taeil Jung<sup>1</sup>; P. C. Ku<sup>1</sup>; <sup>1</sup>University of Michigan

Reduction of the internal electric field (IEF) in III-nitride quantum wells (QWs) can improve the radiative recombination efficiency [1]. It is typically achieved by growing QWs on semi-polar [2] or non-polar planes. We report a novel approach to fabricate nano-structured semi-polar (NSSP) DHs. NSSP GaN are first fabricated on a planar c-plane GaN template using in situ silane and annealing treatment (Fig. 1). InGaN/GaN multiple quantum wells (MQWs) are subsequently grown on the NSSP GaN. Excitation power dependant PL shows that the IEF is remarkably reduced (Fig. 2). From temperature dependant PL, we estimate the internal quantum efficiency (IQE) to be 30%. We expect the IQE to be improved after optimization of growth conditions. Advantages of the reported fabrication include: i) the suppression of IEF using NSSP MQWs on c-plane GaN; ii) the enhancement of the active layer area by a factor of 2 in comparison to planar MQWs.

**MP44, Formation Process of the InN Nanotips:** Kwang-Ru Wang<sup>1</sup>; Su-Jien Lin<sup>1</sup>; C. H. Chen<sup>1</sup>; Zhi-Wei Jiang<sup>2</sup>; *Li-Wei Tu<sup>2</sup>*; Y. L. Chen<sup>1</sup>; Chia-Hsiu Tsai<sup>2</sup>; Li-Kuang Wang<sup>2</sup>; Min Chen<sup>2</sup>; Quark Y. S. Chen<sup>2</sup>; Jien-Wei Yeh<sup>1</sup>; T. T. Tsai<sup>1</sup>; Nyan-Hwa Tai<sup>1</sup>; <sup>1</sup>National Tsing Hua University; <sup>2</sup>National Sun Yat-Sen University

InN nanotips have been successfully fabricated on Si substrate using high quality InN/AlN/Si template grown by molecular beam epitaxy (MBE). The shape of the InN nanotip is quite similar to the bamboo shoots examined with scanning electron microscopy (SEM). According to the field-emission measurement, these nanotips have shown excellent properties that could be turned on under very low field condition. The lowest turn-on field measured in our system is only 1.35 V/ $\mu\text{m}$  and the average result is 2.05 $\pm$ 0.5 V/ $\mu\text{m}$  based on the condition of 10 $\mu\text{A}/\text{cm}^2$  in the vacuum level of around 5 $\times 10^{-6}$  torr. In-situ monitor of the formation of the nanotip has been recorded and can be clearly shown how these InN nanotips formed during the process.

**MP45, Growth and Characterization of In<sub>x</sub>Ga<sub>1-x</sub>N Nanowires by MOVPE:** *Josh Mangum<sup>1</sup>*; Olga Kryliouk<sup>1</sup>; Albert Davydov<sup>2</sup>; Zuzanna Liliental-Weber<sup>3</sup>; Tim Anderson<sup>1</sup>; <sup>1</sup>University of Florida; <sup>2</sup>National Institute of Standards and Technology; <sup>3</sup>Lawrence Berkeley National Laboratory

In<sub>x</sub>Ga<sub>1-x</sub>N nanowires (NWs) were grown on Si(100) and GaN(0002) substrates by MOVPE without using catalysts or templates. The nucleation density of the NWs can be controlled by applying various surface treatments, such as substrate nitridation and/or low temperature buffer layers. NW dimensions vary depending on the surface treatments used, however, average diameters of 100-300 nm were noticed with growth rates from 10 to 40  $\mu\text{m}/\text{hr}$ . A vapor-liquid-solid (VLS) growth mechanism is proposed due to presence of In droplets at the tip of the NWs, which act as native catalysts for 1D growth. NWs were characterized by XRD, SEM, and TEM which reveals a core-shell structure grown at low V/III ratio. An oxide shell is formed on the outside of the NW after growth due to excess In on the NW walls. A sufficiently high V/III ratio prevents the oxide shell from forming.

**MP46, Improved Optical Properties of AlGaIn Using Periodic Structures:** *Hideto Miyake<sup>1</sup>*; Takeharu Ishii<sup>1</sup>; Kazumasa Hiramatsu<sup>1</sup>; Atsushi Motogaito<sup>1</sup>; <sup>1</sup>Mie University

Al<sub>0.4</sub>Ga<sub>0.6</sub>N periodic structures were fabricated on Al<sub>0.4</sub>Ga<sub>0.6</sub>N epilayers grown on AlN/sapphire templates by electron-beam (EB) lithography and by reactive ion etching (RIE) using chlorine plasma. The effects of etching depth, dot size and lattice constant on the emission intensity were investigated. It was found that for the AlGaIn periodic structures with triangular lattice patterns, which have a lattice constant of 300 nm and a dot size of 150 nm, antireflection and enhanced transmission were obtained from the deep-

ultraviolet region to the visible region (240~700 nm). The emission intensity of the periodic structure also increased to about 3 times that of the structure with a smooth surface. The excellent optical properties of the periodic structure are expected to improve the performance of photo-detectors.

**MP47, Metalorganic Chemical Vapor Deposition of InGaIn Layers on ZnO Substrates:** Shen-Jie Wang<sup>1</sup>; Nola Li<sup>1</sup>; Eun-Hyun Park<sup>2</sup>; Zhe Feng<sup>2</sup>; Adriana Valencia<sup>3</sup>; Jeff Nause<sup>3</sup>; Matthew Kane<sup>1</sup>; *Ian Ferguson<sup>1</sup>*; <sup>1</sup>Georgia Institute of Technology; <sup>2</sup>National Taiwan University; <sup>3</sup>Cermet, Inc.

Epitaxial InGaIn layers have been successfully grown on ZnO substrates by metalorganic chemical vapor deposition. The grown materials were characterized by a series of techniques, including high-resolution X-ray diffraction, atomic force microscopy, scanning electron microscopy, secondary ion mass spectrometry, optical transmission, and room temperature and temperature-dependent photoluminescence. All results showed good quality InGaIn films with a wide range of In composition, without In droplets. The variation of In incorporation in the InGaIn layers were adjustable by changing growth temperature. AFM revealed the microstructure of the InGaIn surface. SIMS indicated the Zn and O diffusion occurring at the interface. The mechanisms of epitaxial growth and the inter-diffusion between InGaIn and ZnO substrates are discussed. Furthermore, the phase separation suppression in InGaIn layers grown on ZnO substrates with high In content is studied.

**MP48, Nanopatterning GaN with Microspheres:** W.N. Ng<sup>1</sup>; X.H. Wang<sup>1</sup>; C.H. Leung<sup>1</sup>; P.T. Lai<sup>1</sup>; *Hoi Wai Choi<sup>1</sup>*; <sup>1</sup>University of Hong Kong

We demonstrate the simple and economical solution of microsphere lithography to create nanopores and nano-islands on GaN substrates. Self-assembled hexagonal SiO<sub>2</sub> microsphere arrays are formed on SiO<sub>2</sub>-coated GaN substrates by spreading the 500 nm particles uniformly across the wafer as a monolayer, acting as a hard-mask. The wafer is subsequently dry-etched, so that triangular nano-pores are created on the oxide layer. The pattern is finally transferred onto GaN by ICP etching. The resultant triangular nanopores, of approximately 100 nm, are laid out in an orderly fashion over regions of 500 x 500  $\mu\text{m}$ . Similarly, nano-island arrays can readily be formed using a slightly modified process flow, by depositing metal through the microsphere void regions. Due to the low-dimension, strain-relaxation occurs in the heavily strained InGaIn/GaN MQW. The characterization of the GaN nanopores and nano-islands will be reported in full in the complete paper, including structural and optical properties.

**MP49, Nucleation of Nanorods and the Density Control by NH<sub>3</sub> Flow Rate:** *Taegeon Oh<sup>1</sup>*; Yuri Sohn<sup>1</sup>; Hyeokmin Choe<sup>1</sup>; Sanghwa Lee<sup>1</sup>; Jai Weon Jean<sup>1</sup>; Chinkyoo Kim<sup>1</sup>; <sup>1</sup>Kyunghee University

Nucleation characteristics and density dependence of GaN nanorods on the NH<sub>3</sub> flow rate were investigated. The GaN nanorods were grown on c-plane (0001) sapphire substrates by using hydride vapor phase epitaxy (HVPE). The growth temperature was about 500°C. HCl flow rate over Ga boat was 40 sccm and NH<sub>3</sub> flow rates were 2000 sccm, respectively. Nitrogen was used as carrier gas. With increasing growth time, the density of nucleated islands increased and individual nanorods started to form. Then, the growth time was fixed to 10 min and the NH<sub>3</sub> flow rates were varied. The sample grown with the NH<sub>3</sub> flow rate of 5000 sccm had the similar surface morphology as the one grown with the NH<sub>3</sub> flow rate of 2000 sccm, but with the NH<sub>3</sub> flow rate of 7500 sccm the diameter became two times larger and individual nanorods were clearly distinguishable.

**MP50, Optical Properties of In-Rich InAlN Nanocolumns:** *Jumpei Kamimura<sup>1</sup>*; Shunsuke Ishizawa<sup>1</sup>; Akihiko Kikuchi<sup>1</sup>; Katsumi Kishino<sup>1</sup>; <sup>1</sup>Sophia University

Optical properties of the In-rich InAlN nanocolumns were investigated. The room-temperature PL peak wavelengths of In<sub>x</sub>Al<sub>1-x</sub>N nanocolumns (xIn=0.71-1.00) ranged from 0.95 to 1.94  $\mu\text{m}$ . The full-width at half-maximum of the In<sub>0.92</sub>Al<sub>0.08</sub>N spectrum was 107 meV. The Stokes-type shifts between the emission energy and the absorption edge increased linearly with increasing the In-composition and became over 400 meV at xIn=0.71. This phenomenon can relate to spatial In-fluctuation, which is brought about due to the immiscibility between AlN and InN. The temperature dependency of the PL intensity was evaluated for the In<sub>0.92</sub>Al<sub>0.08</sub>N nanocolumns.

# Technical Program

The intensity ratio between integrated PL intensities at 300 K and 7 K, IPL(300K)/IPL(7K) was 46%, possibly showing a high internal efficiency. And it could show that In-rich InAlN possesses short effective radiative and long non-radiative lifetimes due to localized radiative recombination centers as reported in lower In-content In<sub>x</sub>Al<sub>1-x</sub>N (xIn=0.25, 0.44).

**MP51, Selective Area Heteroepitaxy of Low Dimensional a-Plane and c-Plane InGaN Nanostructures by Using Pulsed MOCVD:** *Vibhu Jindal*<sup>1</sup>; James Grandusky<sup>1</sup>; Neeraj Tripathi<sup>1</sup>; Mihir Tungare<sup>1</sup>; Odysseas Paschos<sup>1</sup>; Pradeep Haldar<sup>1</sup>; Fatemeh Shahedipour-Sandvik<sup>1</sup>; <sup>1</sup>CNSE

High density a-plane and c-plane InGaN nanostructures have been developed by nanoscale selective area epitaxial growth using pulsed MOCVD. SiO<sub>2</sub> was used as a mask with nano-patterning through anodic aluminum oxide template. The lateral dimensions of the pattern were controlled and varied between 20 nm to 150 nm by changing the anodization voltage and the electrolyte used. Different substrates such as a-plane GaN, c-plane GaN, r-plane Sapphire and c-plane Sapphire were utilized as template to develop InGaN nanostructures in a- and c- crystallographic directions. Under identical growth conditions, nanostructures on different templates have revealed different shapes of the nanostructures. The shape of the nanostructures on different templates is discussed with respect to the stability and growth rates of different planes. Low-temperature photoluminescence was used to determine the optical properties of the nanostructures while HR-TEM was employed to develop understanding on structural properties of InGaN nanostructures.

**MP52, Surface-Morphology Evolution of GaN Nanorods Grown by HVPE:** *Hyeokmin Choe*<sup>1</sup>; Yuri Sohn<sup>1</sup>; Sanghwa Lee<sup>1</sup>; Jai Weon Jean<sup>1</sup>; Taegeon Oh<sup>1</sup>; Chinkyoo Kim<sup>1</sup>; <sup>1</sup>Kyunghee University

Surface-morphology evolution of GaN nanorods grown by hydride vapor phase epitaxy (HVPE) was investigated. GaN nanorods were grown on c-plane sapphire substrates with a 0.3°-miscut toward m-plane (10-10). The growth time of these samples was set to be 10 sec, 15 sec, 1 min, 2 min, 7 min, and 15min, respectively. The growth temperature of these samples was 510°C and the surface morphology was characterized by SEM. During the initial stage of nucleation a small density of GaN grains was formed. Up to the growth time of 1 min the grain density increased a lot, but vertically grown nanorods were not observable. By increasing growth time, the density of the grains became larger and the vertical growth rate was visibly increased. Further increase of the growth time resulted in increase in diameter and individual rods merged decreasing the overall density of the rods.

**MP53, Terahertz Spectroscopy of Vertically Aligned InN Nanorod Arrays:** *Hyeyoung Ahn*<sup>1</sup>; Yun-Pu Ku<sup>1</sup>; Chun-Hao Chuang<sup>1</sup>; Ci-Ling Pan<sup>1</sup>; Shangji Gwo<sup>2</sup>; <sup>1</sup>National Chiao Tung University; <sup>2</sup>National Tsing Hua University

Terahertz time-domain spectroscopy (THz-TDS) and time-resolved THz spectroscopy is used to investigate THz conductivity and ultrafast carrier dynamics of vertically aligned indium nitride (InN) nanorod arrays and the InN film grown by nitrogen-plasma-assisted molecular-beam epitaxy on Si(111) substrates. The static THz conductivity of InN film obtained from THz-TDS is well fitted by the simple-Drude model, while negative imaginary conductivity of InN nanorods is reproduced better using the Drude-Smith model. The plasma frequency and the carrier relaxation time, that determine the free carrier dynamics, are obtained to be 49.7 THz and 70 fs, respectively for InN film. For the effective electron mass of 0.077m<sub>0</sub> of InN, the Hall mobility of the InN film is extracted to be 1624 cm<sup>2</sup>/Vs, while that of the InN nanorods is 71 cm<sup>2</sup>/Vs. Time-resolved THz spectroscopy shows that the decay time constant of the photoconductivity in film is = 15-fold longer than that in nanorods.

## MP: Structural Analysis

**MP54, A Comparative Study on Single and Double Channel AlGaIn/GaN High Electron Mobility Transistors:** *Jing Yao Zheng*<sup>1</sup>; Der Yuh Lin<sup>1</sup>; Hong Ji Lin<sup>1</sup>; <sup>1</sup>National Changhua University of Education

We present a numerical investigation on the DC and AC characteristics of AlGaIn/GaN single (SCHEMT) and double channel high electron

mobility transistors (DCHEMT) using the APSYS simulation program. The performance of DCHEMT and SCHEMT is simulated and compared. The influence of polarization charge induced by spontaneous and piezopolarization charges is considered in the simulation model. The simulation results, such as the capacitance-voltage characteristic, DC current-voltage characteristic, cutoff frequency, maximum frequency and transconductance, match well with the experimental data that have been reported. The simulation results indicate that the DCHEMT has better performance than SCHEMT. The effect of the barrier layer thicknesses between the two channels on the transconductance has been studied. We find that a flatter profile of the transconductance and a widened operation range can be achieved by optimizing the barrier layer thicknesses. A comprehensive simulation and an optimizing design for DCHEMTs is presented and discussed.

**MP55, Anomalous X-Ray Reflectivity Study of InGaN/GaN Multi-Quantum Well Structure:** *Sung Pyo Lee*<sup>1</sup>; Do Young Noh<sup>1</sup>; Sang Won Kang<sup>2</sup>; Hyo Jung Kim<sup>2</sup>; Yon-Chun Kim<sup>2</sup>; <sup>1</sup>Gwangju Institute of Science and Technology; <sup>2</sup>Samsung Electro-Mechanics

We present an anomalous x-ray reflectivity study to characterize the interfacial structure of InGaN/GaN multiple quantum well (MQW) structure. Using synchrotron radiation, the specular x-ray reflectivity(SXR) and the longitudinal diffuse reflectivity(LDR) are measured at various x-ray energies across the Ga absorption edge, 10.373 keV. At small angles, the total reflection from MQWs was dominated by the diffuse intensity, and the SXR component was hidden under the LDR component. Characteristic Bragg reflections corresponding the well-barrier period of the MQW are clearly observed in the LDR, which indicates that the MQW interfaces are very well correlated. In addition, the anomalous x-ray reflectivity(AXR), the energy dependence of x-ray reflectivity curve, was measured to determine the exact chemical profiles as well as the layer thickness of each well and barrier.

**MP56, Assessment of Scanning Spreading Resistance Microscopy for Application to n-Type GaN:** *Joy Sumner*<sup>1</sup>; Rachel Oliver<sup>1</sup>; Menno Kappers<sup>1</sup>; Colin Humphreys<sup>1</sup>; <sup>1</sup>University of Cambridge

Scanning spreading resistance microscopy (SSRM) can be used to study carrier concentrations in GaN-based semiconductors. However, the basic principles underpinning its responses are not yet fully understood. Thus we have grown appropriate Si-doped multilayers to test SSRM's spatial resolution and carrier concentration sensitivity. For samples with no undoped regions, layers with dopant concentrations from 1×10<sup>19</sup>cm<sup>-3</sup> to 2.5×10<sup>18</sup>cm<sup>-3</sup> may be distinguished, but the relationship between SSRM signal, applied bias and dopant level is complex. However, in samples with undoped layers it is very difficult to obtain any SSRM signal. SSRM is only able to distinguish between different dopant levels for biases in the range of ~2 to 7V, above which damage to the sample occurs. In terms of resolution, feature sizes down to 50nm were routinely resolved and SSRM sometimes had the ability to resolve features down to 10nm with the observed performance being strongly dependent on the probe used.

**MP57, Comparison between Extended Microtunnels along Different Crystal Orientations in GaN:** *Hsin-Hsiung Huang*<sup>1</sup>; Pei-Lun Wu<sup>1</sup>; Hung-Yu Zeng<sup>1</sup>; Feng-Ke Hsiao<sup>1</sup>; Po-Chun Liu<sup>2</sup>; Tung-Wei Chi<sup>2</sup>; Jenq-Dar Tsay<sup>2</sup>; Wei-I Lee<sup>1</sup>; <sup>1</sup>National Chiao Tung University; <sup>2</sup>Industrial Technology Research Institute

It has been demonstrated before that extended microtunnels (EMT) extending beyond hundreds of microns with triangular cross sections in thick GaN films can be easily fabricated using wet chemical etch on specially designed epitaxially lateral overgrowth (ELOG) structures. In the present study, extended microtunnels (EMTs) along the <1-100> direction and along the <11-20> direction were fabricated and compared. For tunnels along the <1-100> direction, the {11-22} family of planes were the etch stop planes, while for tunnels along the <11-20> direction, the {10-11} family of planes were the more stable planes. The activation energies of wet chemical etch for the {11-22} family of planes and the {10-11} planes were determined to be 13.8 and 3.9 kcal mol<sup>-1</sup>, respectively. As a result, the depths of the tunnels along the <1-100> direction were more than twice the depths of the tunnels along the <11-20> direction. The highest etch rate of the tunnels along the

axial direction can reach 1000  $\mu\text{m/hr}$ , which is believed to be the highest etch rate of GaN ever reported.

**MP58, Dislocation Reduction in an AlGaIn Layer Grown Using a GaN Interlayer on a High Temperature AlN Buffer:** *Jie Bai*<sup>1</sup>; T. Wang<sup>1</sup>; K. B. Lee<sup>1</sup>; P. J. Parbrook<sup>1</sup>; A. G. Cullis<sup>1</sup>; <sup>1</sup>University of Sheffield

A significant dislocation reduction is achieved in an AlGaIn layer grown on an AlN buffer by introducing a thin GaN interlayer. The mechanisms for the dislocation reduction are explored by transmission electron microscopy, energy-dispersive x-ray spectroscopy, atomic force microscopy and micro-Raman spectroscopy. The GaN interlayer takes the form of platelets on the AlN. The mechanisms of dislocation reduction in the platelet area and the area between the platelets are different. In the GaN platelets, due to the large misfit strain, the threading dislocations (TDs) in the AlN layer migrate into the interface and annihilate with each other. However, the GaN between the platelets is highly strained so that a higher density of TDs from AlN is incorporated into the upper layer. The coalescing of the platelets induced by the AlGaIn growth makes the TDs in the areas between the platelets assemble and annihilate, resulting in additional dislocation reduction.

**MP59, Electronic and Chemical Properties of Strained GaN /InGaIn Heterostructure:** *Seong Ran Jeon*<sup>1</sup>; Jong Hyub Baek<sup>1</sup>; Ja Soon Jang<sup>2</sup>; <sup>1</sup>Korea Photonics Technology Institute; <sup>2</sup>State University of New Jersey, Department of Electrical and Computer Engineering

Strain-induced spontaneous polarization and external dopant-induced piezoelectric polarization in strained layers give rise to an increase of the sheet carrier concentration for ohmic contact and an enhancement of Schottky barrier height for Schottky one. Although strained InGaIn/GaN layers have been extensively studied to obtain good contact layer in the light emitting diodes, only a few studies on electrical and electronic energy band characteristics of strained u-GaN/InGaIn layers have been reported so far. In this study, we have been investigated polarization field effect on the electrical and spectroscopic characteristics at strained u-GaN/u(n)-InGaIn layer before and after Si doping. It is shown that polarization charges originated from two dimensional electron gas sheet concentration is considerably dependent on the growth temperature, and surface Fermi level is pinned irrespective of growth conditions due to highly accumulated surface defects.

**MP60, High-Resolution Rutherford Backscattering Spectrometry for InAlGaIn/AlGaIn Single Quantum Well Structure:** *Hiroaki Sakuta*<sup>1</sup>; Takeshi Fukui<sup>1</sup>; Tsutomu Miyachi<sup>1</sup>; Satoshi Kurai<sup>1</sup>; Tsunemasa Taguchi<sup>1</sup>; <sup>1</sup>Yamaguchi University

InAlGaIn/AlGaIn single quantum well structure has been studied by means of high-resolution Rutherford backscattering spectrometry (HRBS). The composition of each layer has been estimated to be  $\text{In}_{0.02}\text{Al}_{0.17}\text{Ga}_{0.81}\text{N}/\text{Al}_{0.28}\text{Ga}_{0.72}\text{N}$  from HRBS measurement. The channeling measurements show the high degree of the crystalline perfection that can be achieved in such epitaxial layers from the normalized yield of 3.3% in the direction of the  $\langle 1-102 \rangle$  axis. The channeling spectrum also shows atomic order differences between InAlGaIn epitaxial layer and AlGaIn epitaxial layer from comparing the aluminum and gallium minimum yields of each layer, respectively. Furthermore aluminum minimum yields are larger than indium minimum yields in the InAlGaIn layer. It is indicated that the difference of the lattice displacement by the thermal vibration or the atomic displacement. In this conference, we will present the original issues on subjects, which the atomic order evaluation of each atom in InAlGaIn/AlGaIn SQW structure by the HRBS channeling.

**MP61, Inclusions in InN Imaged by HRTEM:** *Til Bartel*<sup>1</sup>; Petra Specht<sup>2</sup>; Christian Kisielowski<sup>2</sup>; <sup>1</sup>TU Berlin; <sup>2</sup>Lawrence Berkeley National Laboratory

The bandgap of InN is the subject of intense controversy ever since evidence of a transition around 0.7-0.9 eV was found in luminescence and absorption measurements a few years ago. However several groups pointed out, that these measurements could be explained by defect states or inclusions in the material. In particular, it has been shown theoretically, that metallic Indium inclusions can cause Mie resonances that could cause the observed infrared transition. We present HRTEM images of hexagonal InN layers that

show inclusions of a few nanometers in size that could cause such resonance. These inclusions are unstable under electron beam exposure, which leads to the dilution of the cluster and to a reconstruction of the InN lattice. Interestingly, InN does not show beam damage after prolonged irradiation, but locally reconstructs into a cubic lattice. Strain relaxation and inclusion of Indium is proposed as an explanation for this effect.

**MP62, Interfacet Migration in Selective Area Grown Multi-Facet Ridges with InGaIn/GaN Multiple Quantum Wells Studied by Microbeam X-Ray Diffraction:** *Andrei Sirenko*<sup>1</sup>; P. Bonanno<sup>1</sup>; S. O'Malley<sup>1</sup>; A. Kazimirov<sup>2</sup>; Z.-H. Cai<sup>3</sup>; T. Wunderer<sup>4</sup>; B. Neubert<sup>4</sup>; P. Brückner<sup>4</sup>; F. Scholz<sup>4</sup>; <sup>1</sup>New Jersey Institute of Technology; <sup>2</sup>Cornell High Energy Synchrotron Source; <sup>3</sup>Advanced Photon Source; <sup>4</sup>University of Ulm

Structural properties of multi-facet ridges with InGaIn/GaN multiple quantum wells (MQW) produced by MOVPE in the regime of selective area growth have been studied using x-ray diffraction and interpreted in terms of the interfacet migration of precursors. Samples consisted of arrays of GaN-based triangular and trapezoidal ridges with the lateral size of 4, 6, and 8 microns and the sidewalls terminated by  $\{11.2\}$  or  $\{1-1.1\}$  facets. Microbeam synchrotron radiation at CHESS and APS has been utilized for high-resolution x-ray diffraction measurements and reciprocal space mapping (RSM) of MQW structures grown both at the top  $\{00.1\}$  and sidewall facets of the ridges. Using focused synchrotron radiation with the beam size of 250 nm, we observed a few degree tilt of the  $\{00.1\}$  crystallographic planes for the GaN cap layers grown on the sidewalls of trapezoidal ridges and variation of the global strain and MQW period along the sidewalls of the triangular ridges.

**MP63, Investigation of Bonds Length in Uncapped and Capped InGaIn/GaN Quantum Dots by EXAFS:** *Edyta Piskorska-Hommel*<sup>1</sup>; Michael Siebert<sup>2</sup>; Thomas Schmidt<sup>2</sup>; Julie Cross<sup>3</sup>; Tomohiro Yamaguchi<sup>2</sup>; Jens Falta<sup>2</sup>; Detlef Hommel<sup>2</sup>; <sup>1</sup>Polish Academy of Science, Institute of Physics; <sup>2</sup>University of Bremen, Institute of Solid State Physics; <sup>3</sup>Advanced Photon Source

The investigated InGaIn quantum dots have the wurtzite structure. The cation sites are randomly occupied by In and Ga atoms and all the anion sites by N atoms. Due to the large difference between the Ga-N and In-N bond lengths, the atom positions are considered to fluctuate from the perfect lattice sites, leaving a bond-length distortion and causing a high degree of atomic ordering. Moreover, the GaN cap layer of InGaIn quantum dots introduce changes in chemical compositions of dots and introduce additional strain. The capping process can also lead to a dissolution of the dots and form a more or less homogeneous layer with properties of a quantum well. Therefore the extended x-ray absorption fine structure (EXAFS) due to a precision in the determination of interatomic distances was used to obtain an information on the bond length In-N, In-Ga and In-In in InGaIn quantum dots.

**MP64, Mechanisms of Strain Accommodation and Defect Generation in Thin GaN/AlN Heterostructures:** *Nikolai Faleev*<sup>1</sup>; Igor Levin<sup>2</sup>; Tommas Dillon<sup>1</sup>; Dennis Prather<sup>1</sup>; <sup>1</sup>University of Delaware; <sup>2</sup>National Institute of Standards and Technology

In this study, high-resolution x-ray diffraction (rocking curves and reciprocal space mapping) was used to compare strain relaxation and defect populations in thin GaN/AlN heterostructures (total thickness  $\sim 460$  nm) grown on (0001) SiC using MOCVD and HVPE, respectively. The results of XRD measurements were corroborated using transmission electron microscopy. Differently-grown films exhibited dissimilar strain relaxations and defect populations that were interpreted in terms of distinct deviations from stoichiometry under specific growth conditions. In the MOCVD film, the strains in both AlN and GaN were only partly relaxed yielding similar densities of threading dislocations (TD) in the two layers. In contrast, in the HVPE film, both layers were relaxed completely and the density of TD in the GaN layer was significantly larger than that in AlN. The principal features of epitaxial growth of GaN/AlN heterostructures along with the mechanisms of strain relaxation and defect generation will be discussed.

# Technical Program

**MP65, Microstructural Characterization of Epitaxial Lateral Overgrown (11-22) Semi-Polar GaN on (10-10) m-Plane Sapphire:** *Lin Zhou*<sup>1</sup>; David Smith<sup>1</sup>; X. Ni<sup>2</sup>; A. Baski<sup>2</sup>; H. Morkoç<sup>2</sup>; <sup>1</sup>Arizona State University, Department of Physics and School of Materials; <sup>2</sup>Virginia Commonwealth University, Department of Electrical and Computer Engineering and Department of Physics

Semi-polar (11-22) GaN films were grown by chemical vapor deposition (CVD) on (10-10) m-plane sapphire substrates. X-ray diffraction and transmission electron microscopy (TEM) analysis suggested that the epitaxial relationships for GaN on m-plane sapphire are: (11-20)GaN//[10-10]sapphire, [10-10]GaN//[11-20]sapphire, [1-211]GaN//[0001]sapphire. High-resolution cross-sectional TEM images showed that the GaN and sapphire interface is abrupt. High density of basal plane stacking faults (BSFs) was observed inside the semi-polar (11-22) GaN epilayer. Epitaxial lateral overgrowth (ELO) of GaN was also carried out on the (11-22) GaN template, with the stripes aligned along [11-20] or the [0001] directions of sapphire. TEM analysis indicated significant improvement in the crystalline quality by ELO when the mask stripes were aligned along [11-20]sapphire. However, when the growth mask stripes were aligned along [0001] direction of sapphire, TEM analysis showed no significant improvement in the crystalline quality by ELO.

**MP66, Microstructural Study of (11-20) Non-Polar III-Nitrides Films Grown by Plasma-Assisted Molecular Beam Epitaxy on (11-20) 6H SiC Substrates:** *Philippe Vennégues*<sup>1</sup>; Sebastien Founta<sup>2</sup>; Henry Mariette<sup>3</sup>; Bruno Daudin<sup>2</sup>; <sup>1</sup>National Center of Scientific Research/Research Center on the Hétéro-Epitaxy and Its Applications; <sup>2</sup>Atomic Energy Commission/Department of Fundamental Research on Condensed Matter; <sup>3</sup>National Center of Scientific Research

Transmission electron microscopy is used to study the microstructure of non-polar GaN and AlN films deposited on (11-20) 6H SiC substrates by plasma-assisted molecular beam epitaxy. Convergent beam electron diffraction shows that the polar c axis has the same sense in SiC and in the III-nitrides films. Whereas GaN films are partially relaxed thanks to the presence of misfit dislocations at the interface, AlN films are grown coherently and cracking of these films occurs for thicknesses as low as 150 nm. Both GaN and AlN structures partially replicate the 6H structure of the SiC substrate. The density of stacking faults is therefore very high. The density of partial dislocations which terminate these stacking faults reach  $10^{11}\text{cm}^{-2}$  in GaN but is below  $2.10^9\text{cm}^{-2}$  in AlN. GaN quantum wells and quantum dots grown on such AlN non-polar templates are observed by high-resolution transmission microscopy.

**MP67, Morphological Study of Non-Polar (11-20) GaN Grown on r-Plane (1-102) Sapphire:** *Carol Johnston*<sup>1</sup>; Menno Kappers<sup>1</sup>; Jonathan Barnard<sup>1</sup>; Colin Humphreys<sup>1</sup>; <sup>1</sup>Cambridge University

In order to grow high quality non-polar GaN-based LED structures it is important to understand the mechanism of GaN growth by MOVPE on r-plane i.e. (1-102) sapphire. In this work, (11-20) GaN epilayers have been characterised at three stages of growth using HRXRD, TEM and AFM. The growth conditions were such that 3D islands formed initially then coalesced to form a smooth film. XRD omega scans revealed an anisotropy in the layers with respect to the [1-100] and [0001] axes. AFM scans show that the islands are elongated along the c-axis. TEM has been used to analyse the layers further. A high density of stacking faults ( $5 \times 10^5\text{ cm}^{-1}$ ) and threading dislocations ( $4 \times 10^{10}\text{ cm}^{-2}$ ) was found. In island samples, defects run perpendicular and at  $\sim 60^\circ$  to the sapphire interface. Methods to reduce this defect density and improve the quality of these non-polar layers will be discussed.

**MP68, Plastic Strain Relaxation in Wurtzite InGaN/GaN Heteroepitaxial Systems:** *Jin Mei*<sup>1</sup>; Rong Liu<sup>1</sup>; Sridhar Srinivanson<sup>1</sup>; Fernando Ponce<sup>1</sup>; Hiromasa Omiya<sup>2</sup>; Takeshi Mukai<sup>2</sup>; <sup>1</sup>Arizona State University; <sup>2</sup>Nichia Corporation

Different plastic relaxation processes of InGaN/GaN heteroepitaxial systems occur depending on the surface geometry and threading dislocation density of underlying templates. Generation of misfit dislocation arrays via slip on the secondary  $\{11\bar{2}2\}\langle 11\bar{2}3\rangle$  slip system happens in  $\text{In}_x\text{Ga}_{1-x}\text{N}$  epilayers ( $x > 0.11$ ) on low-dislocation-density free-standing GaN substrates but not on high-dislocation-density sapphire substrates. This slip process is

also found to induce a cross-hatch pattern on the InGaN surface. On the other hand, presence of surface indentations intercepting the InGaN/GaN interface leads to almost complete strain relaxation via slip on the main  $(0001)\langle 11\bar{2}0\rangle$  slip system, regardless of the threading dislocation density in the substrates. This is observed in  $\text{In}_x\text{Ga}_{1-x}\text{N}$  films on free-standing GaN substrates with deep surface pits ( $x > 0.07$ ) as well as on high-dislocation-density GaN/sapphire templates ( $x > 0.2$ ) with mesa structures formed in GaN layer. Understanding the strain relaxation mechanisms in InGaN heteroepitaxy is helpful for growth of high-quality, fully-relaxed, InGaN films for longer-wavelength applications.

**MP69, Structural Characterisation of GaN Directly Grown on a Ge-(111) Substrate:** *Yucheng Zhang*<sup>1</sup>; Clifford McAleese<sup>1</sup>; Huixian Xiu<sup>1</sup>; Colin Humphreys<sup>1</sup>; Ruben Lieten<sup>2</sup>; S. Degroote<sup>2</sup>; G. Borghs<sup>2</sup>; <sup>1</sup>University of Cambridge; <sup>2</sup>Interuniversity Microelectronics Center

GaN epilayers have recently been grown directly on a Ge-(111) substrate. Despite the large lattice mismatch, the initial results are very encouraging. This paper presents the work on characterisation of the GaN structure using a combination of techniques including optical microscopy (OM), X-ray diffraction (XRD), atomic force microscopy (AFM) and transmission electron microscopy (TEM). Two features have been identified and investigated. One feature has a triangle shape, as observed in OM plan-view imaging, and is essentially a faceted void in Ge extending from the interface into the substrate. Another feature is the formation of domains due to the misorientation of GaN relative to the Ge substrate with a twist of  $\pm 4^\circ$  around the GaN-[0002] axis. Growth mechanisms based on these observations will be discussed.

**MP70, Structural Defects in Eu Doped GaN Observed by Transmission Electron Microscope:** *Jongwon Seo*<sup>1</sup>; Junji Sawahata<sup>1</sup>; Masaharu Mitome<sup>2</sup>; Katsuhiko Akimoto<sup>1</sup>; <sup>1</sup>University of Tsukuba; <sup>2</sup>National Institute for Materials Science

Structural properties of Eu doped GaN grown by molecular beam epitaxy on sapphire(0001) substrates with the Eu concentration from 0.5 at% to 7.5 at% were studied by transmission electron microscope (TEM). A conversion from hexagonal single crystal to polycrystalline structure was observed at the Eu concentration of about 3 at%, at which strongest Eu-related luminescence was obtained. At the Eu concentration of about 3 at%, high density of stacking fault and cubic phase were observed. The formation of the stacking fault and cubic phase may be due to the strain relaxation caused by the incorporation of Eu whose ionic radius is 1.5 times larger than that of Ga. The formation of the stacking fault and cubic phase may be responsible for the conversion from single crystal to polycrystalline structure of Eu doped GaN.

**MP71, Unintentional Doping in GaN Assessed by Scanning Capacitance Microscopy:** *Joy Sumner*<sup>1</sup>; Subhankar Das Bakshi<sup>1</sup>; Rachel Oliver<sup>1</sup>; Menno Kappers<sup>1</sup>; Colin Humphreys<sup>1</sup>; <sup>1</sup>University of Cambridge

Scanning Capacitance Microscopy (SCM), a carrier concentration sensitive atomic force microscopy technique, provides an ideal means to locate unintentionally-doped material within GaN structures, for example at GaN/sapphire interfaces and in Epitaxial Lateral Overgrowth (ELOG) samples. Using SCM we observe a region of unintentional n-type conductivity in the GaN adjacent to the GaN/sapphire interface. The variation in the width of this region and its carrier concentration with the coalescence time during GaN epilayer growth may be assessed. Quantification of carrier concentrations may be achieved by comparison with a calibration structure grown on the top GaN surface. Various doped regions are also observed in ELOG samples. GaN initially grows through the mask forming faceted stripes, which exhibit n-type conductivity. Magnesium is used to enhance coalescence, resulting in p-type regions. The top layer, grown following coalescence, appears non-conducting. Details of the carrier concentration may again be quantified using a calibration structure.

**MP72, X-Ray Diffraction Study on GaN Nano-Column Overgrowth with Molecular Beam Epitaxy:** *Wen-Yu Shiao*<sup>1</sup>; Jeng-Jie Huang<sup>1</sup>; Tsung-Yi Tang<sup>1</sup>; Yung-Sheng Chen<sup>1</sup>; Kent Averett<sup>2</sup>; John Albrecht<sup>2</sup>; C. C. Yang<sup>1</sup>; <sup>1</sup>National Taiwan University; <sup>2</sup>Air Force Research Laboratory

Reciprocal space mapping (RSM) on the (105) plane of threading-dislocation free GaN nano-columns and their overgrowth layers was

performed to compare the tilt, twist, and strain distributions of the samples grown with molecular beam epitaxy (MBE) of different conditions on sapphire and silicon substrates. From the features of RSM, it is found that the crystalline tilt is stronger in the nano-columns grown on sapphire while those grown on silicon have stronger twists. After the overgrowth with MBE, more features appear in RSM indicating that strain distribution in the overgrown layer is quite non-uniform. Comparisons of the X-ray diffraction results between the overgrown samples of the GaN nano-columns with MBE and metalorganic chemical vapor deposition (MOCVD) are made. Based on the measurements, the overgrown layer with MOCVD has a slightly higher crystalline quality when compared with that with MBE. Also, the overgrown layer generally has a higher quality than the nano-columns.

## MP: Structure

**MP73, AlN Thin Film Prepared by Sapphire Nitridation Method:** *Hiroyuki Fukuyama*<sup>1</sup>; *Katsuhito Nakamura*<sup>1</sup>; *Hidekazu Kobatake*<sup>1</sup>; *Akira Hakomori*<sup>2</sup>; *Kenji Hiraga*<sup>1</sup>; <sup>1</sup>Tohoku University; <sup>2</sup>Tokuyama Corporation

In the present study, high-quality single crystalline AlN films have been fabricated by nitriding sapphire by N<sub>2</sub>-CO gas mixtures with a precise control of driving force of the nitridation reaction based on the chemical potential diagram of the AlN-Al<sub>2</sub>O<sub>3</sub>-C-N<sub>2</sub>-CO system at elevated temperatures. The driving force of the nitridation reaction can be easily and precisely controlled by choosing a suitable composition of N<sub>2</sub>-CO gas mixture and temperature. This process provides the <0001>-axis oriented AlN film as large as 2 inch in diameter on a (11-20) plane sapphire substrate. The crystalline quality of the AlN film has the values of full-width at half-maximum (FWHM) of rocking curves using (0002) and (1-100) planes of AlN for tilt and twist components as follows; Tilt = 216 arcsec and twist = 292 arcsec. More details will be presented at the conference.

**MP74, AlN/GaN Superlattice Quality Improvement by Using Multiple Superlattice Structure:** *Martin Veis*<sup>1</sup>; *Kazuki Hagihara*<sup>1</sup>; *Shinya Nakagawa*<sup>1</sup>; *Yoku Inoue*<sup>1</sup>; *Akihiro Ishida*<sup>1</sup>; <sup>1</sup>Shizuoka University

We report on an improvement of structural and morphological quality of AlN/GaN superlattices when the multiple superlattice structure (MSL) is used. Such a structure contains a few of AlN/GaN simple superlattices with a small number of periods separated by thick GaN layer. Hot wall epitaxy technique (HWE) was used to grow these structures and atomic force microscopy (AFM) as well as X-ray diffraction measurements were used to obtain the information about their structural and morphological properties. According to AFM measurements, the number of threading dislocations and the surface roughness were decreased compare to the simple superlattice. X-ray rocking curve (XRC) measurements exhibit narrower peaks, so the full width at half maximum (FWHM) of the 0th superlattice peak was decreased by 37%.

**MP75, Control of Polarity and Reduction of Threading Dislocation Density (TDD) of AlN/AlGaIn Buffer on Sapphire by Using TMAI Pulse Supply Method:** *Norimichi Noguchi*<sup>1</sup>; *Tomoaki Ohashi*<sup>1</sup>; *Norihiko Kamata*<sup>2</sup>; *Hideki Hirayama*<sup>1</sup>; <sup>1</sup>RIKEN; <sup>2</sup>Saitama University

We fabricated high-quality AlN/AlGaIn buffers for ultraviolet (UV) light-emitting diodes (LEDs) on sapphire using TMAI pulse supply method. We succeeded in the control of polarity and obtained stable Ga (+c) polarity using this method, which was confirmed by observing the change of surface morphology. We also demonstrated this method is very effective for reducing threading dislocation density (TDD). TDD was reduced to be approximately 1/3, and the minimum TDD estimated from the surface pit density was approximately  $1 \times 10^6 \text{ cm}^{-2}$ . We observed TDs are bended and disappeared in the AlGaIn & TMAI pulse supply layer from the cross-sectional transmission electron microscope (TEM) image. We fabricated 350 nm-band InAlGaIn multi-quantum well (MQW) UV-LED on the high-quality template using TMAI pulse supply method. Output power of the LED was 2.0 mW under RT CW operation, which was approximately 1.7 times larger compared with the case using conventional AlN/AlGaIn template.

**MP76, Dislocation Generation at the Coalescence of Aluminum Nitride Lateral Epitaxy on Shallow-Grooved Sapphire Substrates:** *Jin Mei*<sup>1</sup>; *Fernando Ponce*<sup>1</sup>; *R. S. Qhalid-Fareed*<sup>2</sup>; *Asif Khan*<sup>2</sup>; <sup>1</sup>Arizona State University; <sup>2</sup>University of South Carolina

The joining of defect-free AlN stripes has been observed to trigger the generation of a large density of threading dislocations in the vicinity of the coalescence point. The AlN structure was grown by pulsed lateral epitaxy on shallow-grooved sapphire substrates. In the pre-coalescence stage, the dislocation density in the lateral epitaxial region ( $<10^8 \text{ cm}^{-2}$ ) is over two orders of magnitude less than in standard c-plane epitaxy. Basal-plane dislocations ( $b=a/3 <11-20>$ ) are generated at the coalescence point as a result of relaxation of compressive stress that develops due to temperature gradients during growth. They bend toward the surface during the post-coalescence growth stage, leading to a high density of pure-edge threading dislocations in the lateral growth regions. Some threading dislocations form loops on prismatic planes in the crystal and the basal segments are observed to glide in the [0001] direction under the electron beam in the microscope.

**MP77, Effects of Patterned Ion Implanted Sapphire Substrate for LED:** *Junggeun Jhin*<sup>1</sup>; <sup>1</sup>KOPTI

Light-emitting diodes (LEDs) were fabricated on patterned ion implanted sapphire substrates using metal organic chemical vapor deposition. The crystal qualities of the u-GaN and n-GaN epilayers grown on the patterned N<sup>+</sup>-ion implanted sapphire substrate were improved compared to that of the u-GaN and n-GaN epilayers grown on a conventional sapphire substrate. The optical properties of the u-GaN and n-GaN epilayers grown on the patterned ion implanted sapphire substrate were also improved. The light intensity of the LED at 100mA on the patterned ion implanted sapphire substrate chip was up to 78% higher than that of the conventional LED chip according to the quick test on the wafer. The increase in the light intensity is due to the relaxation of the misfit strain at high temperature and the contribution of the internal free energies to the enhancement of structural and optical properties.

**MP78, Epitaxial Growth of GaN on Lattice-Matched ZrN Buffers Prepared by Pulsed Sputtering Deposition:** *Akira Aoyama*<sup>1</sup>; *Yasuhiro Goto*<sup>1</sup>; *Shigeru Inoue*<sup>1</sup>; *Takayuki Nakano*<sup>2</sup>; *Hiroshi Fujioka*<sup>1</sup>; <sup>1</sup>University of Tokyo; <sup>2</sup>Kanagawa Academy of Science and Technology

We have demonstrated that a ZrN film prepared by pulsed sputtering deposition (PSD) works as an excellent conductive buffer layer with high light reflectivity for GaN (0001) on various substrates. We have found that high quality ZrN (111) films grow epitaxially on MgO (111) and Al<sub>2</sub>O<sub>3</sub> (0001) with flat surfaces. We have also found that GaN (0001) can be grown on these buffer layers. In-plane epitaxial relationship is GaN [11-20]//ZrN [1-10]//MgO [1-10] and GaN [11-20]//ZrN [1-10]//Al<sub>2</sub>O<sub>3</sub> [10-10] for MgO and Al<sub>2</sub>O<sub>3</sub>, respectively. FWHM values for the crystal orientation distribution of GaN measured by EBSD have been 0.16°C and 0.33°C in the [0001] direction and [10-10] direction, respectively. These results indicate that PSD-ZrN is quite attractive as a buffer layer for growth of GaN because of its small lattice mismatch of 1.3%, high conductivity, and high light reflectivity.

**MP79, Epitaxial Growth of Group III Nitrides on Rh(111) UV Mirrors:** *Shigeru Inoue*<sup>1</sup>; *Koichiro Okamoto*<sup>1</sup>; *Takayuki Nakano*<sup>2</sup>; *Jitsuo Ohta*<sup>1</sup>; *Hiroshi Fujioka*<sup>1</sup>; <sup>1</sup>University of Tokyo; <sup>2</sup>Kanagawa Academy of Science and Technology

We have succeeded in epitaxial growth of group III nitrides on mirror polished single crystalline Rh(111) substrates using a low temperature growth technique by pulsed laser deposition (PLD). Although growth of AlN films on Rh at 750°C results in formation of poly-crystalline materials, reduction in growth temperature down to 450°C makes it possible to grow high quality AlN with an in-plane epitaxial relationship of AlN[11-20]//Rh[1-10]. This success can be attributed to the suppression of the interfacial reactions between AlN and Rh. We have also confirmed that high quality GaN can be grown on the AlN/Rh structure. Since Rh exhibits the high thermal conductivity and high reflectivity even in the ultraviolet region (~70% at 300 nm), this technique makes Rh(111) quite promising for heat-dissipative substrates of future UV LEDs.

# Technical Program

**MP80, Epitaxial Growth of High Quality AlN by Pulsed Sputtering Deposition:** *Takayuki Nakano*<sup>1</sup>; Akira Aoyama<sup>2</sup>; Yasuhiro Goto<sup>2</sup>; Kouichiro Okamoto<sup>2</sup>; Sigeru Inoue<sup>2</sup>; Hiroshi Fujioka<sup>2</sup>; <sup>1</sup>Kanagawa Academy of Science and Technology; <sup>2</sup>University of Tokyo

We have grown AlN films on Al<sub>2</sub>O<sub>3</sub> (0001) and ZnO (000-1) substrates by pulsed sputtering deposition (PSD) and investigated their structural properties. We have found that crystalline quality of epitaxial AlN films can be dramatically improved by the reduction in the pulse width and pulse frequency, which is probably attributed to the enhanced migration of Al atoms on the surface. FWHM values of X-ray rocking curves for AlN grown directly on sapphire are 78 arcsec and 1314 arcsec for 0002 and 10-12 diffractions, respectively. We have also found that high quality AlN can be grown even at room temperature with this technique. These results indicate that the use of PSD is quite promising for large-area low-cost preparation of high quality AlN for future UV LEDs.

**MP81, III-Nitride Device Growth: Quantitative Analysis of In-Situ Wafer Bowing:** *Arne Knauer*<sup>1</sup>; Frank Brunner<sup>1</sup>; Thobias Schenk<sup>2</sup>; M. Borasio<sup>2</sup>; Elisabeth Steinmetz<sup>2</sup>; Markus Weyers<sup>1</sup>; Thomas Zettler<sup>2</sup>; <sup>1</sup>Ferdinand-Braun-Institut für Höchstfrequenztechnik; <sup>2</sup>LayTec GmbH

Wafer bowing measurements in combination with temperature and reflectance measurements have been recently developed into an efficient tool for empirical III-Nitride epitaxial growth optimization. This paper is going beyond: we focus on a quantitative analysis of wafer bowing throughout the full (Al,In,Ga)N based LED or laser epitaxial process. Starting from the basic models of film stress causing wafer bowing we describe the physical effects and models to be included for a quantitative analysis. The contributions of vertical temperature gradients, composition dependent lattice constants and thermal expansion coefficients will be separated. It will be shown that for (Al,In,Ga)N growth on sapphire the lattice-mismatch induced stress can be described accurately by combining the simple Stoney equation with the concept of a GaN-sapphire coincidence lattice. This enables an accurate determination of AlGaIn and InGaIn lattice constants of bulk layers and AlxGa1-xN/GaN super-lattices already during growth in MOVPE.

**MP82, Improvement of GaN Quality Prepared by Hydride Vapor Phase Epitaxy Using Air-Bridged Growth Technique:** *Hsin-Hsiung Huang*<sup>1</sup>; Po-Chun Liu<sup>2</sup>; Tung-Wei Chi<sup>2</sup>; Ming-Zheng Hsu<sup>3</sup>; Yu-Lin Chang<sup>3</sup>; Li-Wei Tu<sup>3</sup>; Jenq-Dar Tsay<sup>2</sup>; Wei-I Lee<sup>1</sup>; <sup>1</sup>National Chiao Tung University; <sup>2</sup>Industrial Technology Research Institute; <sup>3</sup>Department of Physics and Center for Nanoscience and Nanotechnology, National Sun Yat-Sen University

In the present study, a specially designed pendeo epitaxial lateral overgrowth process, called air-bridged growth, has been developed to grow thick GaN layers using hydride vapor phase epitaxy technique (HVPE). The quality of the GaN layers grown by this technique has been compared to GaN layers prepared by a more conventional pendeo growth process. The quality of GaN layers prepared by both techniques were examined by scanning electron microscopy (SEM), cathodoluminescence (CL) spectra and images, x-ray diffraction (XRD), and etch pit density (EPD) measurements. It is shown that the air-bridged growth process can effectively reduce the dislocation density from 10<sup>8</sup> cm<sup>-2</sup> to 10<sup>7</sup> cm<sup>-2</sup>. Other characterizations also indicate superior quality of the air-bridged structure over the more conventional pendeo structure.

**MP83, InN Layers Grown by the HVPE:** *Alexander Syrkin*<sup>1</sup>; Vladimir Ivantsov<sup>1</sup>; Alexander Usikov<sup>1</sup>; Vladimir Dmitriev<sup>1</sup>; Gaetan Chambard<sup>2</sup>; Pierre Ruterana<sup>2</sup>; Albert Davydov<sup>3</sup>; Siddarth Sundaresan<sup>4</sup>; Evgenii Lutsenko<sup>5</sup>; A. Mudryi<sup>6</sup>; <sup>1</sup>TDI, Inc.; <sup>2</sup>CNRS-ENSICAEN; <sup>3</sup>National Institute of Standards and Technology; <sup>4</sup>George Mason University; <sup>5</sup>Institute of Physics, National Academy of Science of Belarus; <sup>6</sup>Joint Institute of Solid State and Semiconductor Physics, National Academy of Science of Belarus

InN has attracted great interest as a promising material for THz emission, high frequency electronics and various sensors. Although high quality InN layers can be grown by molecular beam epitaxy, this material is not commercialized. Hydride Vapor Phase Epitaxy (HVPE) is known to produce high quality nitride materials with high throughput. Results on HVPE of InN are limited and the quality of reported material is low. We report the first time demonstration and properties of high quality HVPE InN. Layers are grown

on GaN/sapphire. The (00.2) XRD rocking curves (RC) had the FWHM of about 510 arc sec, being the narrowest RCs ever reported for HVPE InN. Photoluminescence showed edge emission around 0.8 eV. Hall measured free electron concentration is in the range of 10<sup>19</sup>-10<sup>20</sup> cm<sup>-3</sup> and electron mobility is ~200 cm<sup>2</sup>/V s. For the first time high quality HVPE InN is grown opening new ways for this material.

**MP84, MIS Structures with Low Interface States Density: Sc2O3/GaN, MgO/GaN, and MgScO/GaN:** *Alexander Polyakov*<sup>1</sup>; Nikolai Smirnov<sup>1</sup>; Brent Gila<sup>2</sup>; Mark Hlad<sup>2</sup>; Andrew Gerger<sup>2</sup>; Cammy Abernathy<sup>2</sup>; Lars Voss<sup>2</sup>; Stephen Pearton<sup>2</sup>; <sup>1</sup>Institute of Rare Metals; <sup>2</sup>University of Florida

Interface trap densities were measured in Sc2O3/n-GaN, MgO/n-GaN, and MgScO/n-GaN MIS structures using conductance and DLTS methods. Both techniques give for energies deeper than 0.3 eV from the conduction band edge the interface trap density on the order of 10<sup>11</sup> cm<sup>-2</sup>eV<sup>-1</sup>. DLTS measurements show that the interface trap density has a peak near 0.6-0.7 eV from the bottom of conduction band. The interface trap density measured both by conductance and DLTS methods increases in the order Sc2O3, MgO, MgScO which most likely reflects the improved lattice match of corresponding oxides with GaN. For MgScO/n-GaN structures we also observed generation of additional interface traps by the application of high positive bias. The effect could be reversed after a high negative bias was applied while annealing the sample.

**MP85, New Results on HVPE Growth of AlN, GaN, InN and Their Alloys:** *Alexander Usikov*<sup>1</sup>; Vitaliy Soukhoveev<sup>1</sup>; Liza Shapovalova<sup>1</sup>; Alexander Syrkin<sup>1</sup>; Oleg Kovalenkov<sup>1</sup>; Anna Volkova<sup>1</sup>; Vladimir Sizov<sup>1</sup>; Vladimir Ivantsov<sup>1</sup>; Vladimir Dmitriev<sup>1</sup>; <sup>1</sup>TDI, Inc.

We describe new results on HVPE growth of group III nitride layers and heterostructures including AlN, GaN, InN and their alloys. AlN, GaN, and AlGaIn were grown on sapphire and SiC. Stress control HVPE was explored to grow crack-free 4-inch AlN(20 μm)/SiC structures with zero bow and improved crystal quality and surface morphology. GaN growth rate ranged from 1 to 1,000 microns per hour. Low growth rates resulted in HVPE-first GaN/AlGaIn quantum wells. P-type as-grown GaN<Mg> layers with hole concentration in the E18 cm<sup>-3</sup> range were obtained. P-type GaN layers and AlGaIn/GaN structures with two dimensional hole gas were grown using Zn doping. InGaIn layers from 0.002 to 2 microns thick with InN content from 0 to 100 mole % were grown on GaN/sapphire substrates. Blue and green all-HVPE LEDs were made based on InGaIn/InGaIn multi-layered structures, for the first time. New directions of HVPE development will be discussed.

**MP86, Pulsed Layer Growth of AlInGaIn Nanostructures:** *Michael Jetter*<sup>1</sup>; Peter Michler<sup>1</sup>; <sup>1</sup>Universitaet Stuttgart, Institut fuer Halbleitertechnik und Funktionelle Grenzflaechen

In this contribution we report on the growth and characterization of AlGaIn nanostructures fabricated with a pulsed layer growth method with metal-organic vapour-phase epitaxy (MOVPE). The amount of material was varied, resulting in AlGaIn layer thicknesses between 1.5 nm and 6 nm, respectively. We have analyzed the material properties by x-ray diffraction (XRD) as well as photoluminescence (PL) spectroscopy. The observed XRD-spectra and the PL intensity show us the high quality of the deposited material. From the analysis of the PL spectra we have found an energetic shift of the resonance lines from 2.65 eV to 3.33 eV with decreasing well thickness. With power-, temperature-dependent and time-resolved PL experiments we have monitored the energetic levels and the carrier dynamics inside the structures to reveal the character of the observed emission. Additionally Cr-shadow masks were processed on the sample to get insight into the local material distribution, respectively luminescence behaviour.

**MP87, Room Temperature Epitaxial Growth of GaN on β-Ga<sub>2</sub>O<sub>3</sub>(100) Substrates:** *Jitsuo Ohta*<sup>1</sup>; Atsushi Kobayashi<sup>1</sup>; Satoshi Kawano<sup>1</sup>; Hiroshi Fujioka<sup>1</sup>; Shigeo Ohira<sup>2</sup>; <sup>1</sup>University of Tokyo; <sup>2</sup>Nippon Light Metal Company

We have investigated characteristics of GaN films grown on β-Ga<sub>2</sub>O<sub>3</sub>(100) substrates at room temperature (RT) by pulsed laser deposition (PLD). Growth of GaN films at 750°C has resulted in the formation of polycrystalline materials with both zincblende and wurtzite phases, which is probably due

to the intermixing reactions at the GaN/Ga<sub>2</sub>O<sub>3</sub> hetero-interface. On the other hand, pure wurtzite GaN films with high crystallinity grow epitaxially at RT with an in-plane epitaxial relationship of [11-20]GaN//[010]Ga<sub>2</sub>O<sub>3</sub>. This success can be attributed to the suppression of the interface reactions by the reduction in the growth temperature. We have also found that the heterointerfaces prepared at RT are thermally quite stable and we can grow GaN films at 750°C using the RT GaN films as buffer layers. These results indicate that RT-growth technique enables us to improve crystalline quality of GaN on Ga<sub>2</sub>O<sub>3</sub> and is quite promising for fabrication of future UV LEDs.

**MP88, Strains and Stresses in Nitride Growth: On the Limits of Stoney's Equation:** Reiner Clos<sup>1</sup>; Armin Dadgar<sup>1</sup>; Fabian Schulze<sup>1</sup>; Alois Krost<sup>1</sup>; <sup>1</sup>Otto V. Guericke University

In last years in-situ curvature measurements have become a standard tool for monitoring strains and stresses during epitaxy. This technique is based on the measurement of the substrate curvature  $k$  usually in the center of the wafer. The method always requires an equation, which correlates the curvature with the incompatibility strain arising from lattice mismatch, thermal mismatch, growth-induced mismatch etc. Usually, the data are interpreted in terms of the classical Stoney equation which is, however, limited to thin films and homogeneous stresses. We have developed general expressions for the curvature-incompatibility strain relationship in the case of large bending and arbitrary thickness ratios between film and substrate, which can be solved to a large extent analytically in the case of cylindrical symmetry. It is shown that the limits of Stoney's formula are easily reached in the case of, e.g., GaN on Si, large diameter wafers, thick layers, or temperature gradients.

**MP89, Structural Properties of AlN Grown on Sapphire at Plasma Self-Heating Condition Using Ultrahigh-Vacuum Unbalanced Magnetron Sputtering:** Huichan Seo<sup>1</sup>; Ivan Petrov<sup>1</sup>; Kyekyoon Kim<sup>1</sup>; <sup>1</sup>University of Illinois at Urbana-Champaign

AlN films were grown on sapphire substrate by ultrahigh-vacuum unbalanced magnetron sputtering in N<sub>2</sub> discharges at growth temperature as low as 94°C. The structural properties with different substrate bias and growth pressure were investigated by atomic force microscopy and X-ray diffraction measurements. At 20 mTorr there were AlN (0002) and (10-11) peaks and with increasing substrate bias the X-ray peak intensity of AlN (0002) increased with enhanced film quality and at higher bias ( $V_s > 25$  V) the film began to degrade. With decreasing growth pressure AlN (10-11) peak disappeared and the crystallinity of AlN was improved with relaxed single AlN crystal. The measured lattice parameter  $a$  was 0.49753 nm which was 0.084 % smaller than that of bulk. The epitaxial relationship of single crystal AlN film was found by pole figure and cross sectional transmission electron microscopy : (001)AlN / (001) Sap, [1-100]AlN / [11-20]Sap.

**MP90, Study of Interface Properties of III-Nitrides on Lithium Niobate for Multifunctional Optoelectronic-Acoustic-Electronic Applications:** Kyoung-Keun Lee<sup>1</sup>; Gon Namkoong<sup>2</sup>; William Doolittle<sup>1</sup>; Maria Losurdo<sup>3</sup>; Giovanni Bruno<sup>3</sup>; Hyung Koun Cho<sup>4</sup>; <sup>1</sup>Georgia Institute of Technology; <sup>2</sup>Old Dominion University; <sup>3</sup>Institute of Inorganic Methodologies and of Plasmas IMIP-CNR; <sup>4</sup>Sung Kyun Kwan University

This work presents a solution to the problem of ferroelectric repolarization on congruent lithium-niobate (CLN) for use in the epitaxy of III-Nitride multifunctional optoelectronic-acoustic-electronic applications. By lowering the annealing temperature, repolarization is eliminated at the expense of surface smoothness. The annealed CLN substrates show a surface roughness from 0.2 to 5.58 nm with no ferroelectric repolarization below 1000°C. Furthermore, according to x-ray diffraction, GaN films grown on the annealed CLN below 1000°C have no significant crystallographic differences from those grown on stoichiometric LN – a more expensive and rare substrate. Also according to XRD, the hexagonal structure of GaN is rotated 30 degree relative to the LN hexagonal structure, as expected, but the GaN on LN is epitaxial. However, cross-sectional TEM images of the GaN and substrate interface shows an approximately 18 nm thick interface region with stacking faults and mixed phases of cubic and hexagonal GaN.

**MP91, Suppression of Interdiffusion at the Heterointerface of AlN/ZnO: In Ho Im<sup>1</sup>; Seog-Woo Lee<sup>2</sup>; Jin-Sub Park<sup>1</sup>; Tsutomu Minegishi<sup>1</sup>; Seung-Hwan Park<sup>1</sup>; Takashi Hanada<sup>1</sup>; Ji-Ho Chang<sup>3</sup>; Meung-whan Cho<sup>1</sup>; Takafumi Yao<sup>1</sup>; <sup>1</sup>Institute for Materials Reserach; <sup>2</sup>Center for Interdisciplinary Research, Tohoku University; <sup>3</sup>Major of Semiconductor Physics, Korea Maritime University**

Since ZnO can be both conductive and resistive, interface layers which act as a diffusion barrier in between III-nitrides and ZnO would make ZnO more attracting as a substrate for III-nitride epitaxy. This paper reports that AlN does act as a superior interface barrier for III-nitride growth. We compare two nitride layers as a diffusion barrier: GaN and AlN. Although GaN layers are grown at low temperatures below 600°C, serious interdiffusion at the GaN/ZnO is observed with the diffusion length of Ga into ZnO being 1  $\mu$ m. On the contrary, AlN layers deposited even at 1000°C show only slight diffusion with a diffusion length of Al into ZnO being 100 nm. The superior properties of AlN as a diffusion barrier arise from the strong bonding energy of AlN. We compare structural, electrical, and optical properties of free-standing GaN layers grown on low-temperature GaN buffer and AlN buffer.

**MP92, The Growth of Bulk Gallium Nitride (GaN) Using Hydride Vapor Phase Epitaxy (HVPE):** Moon Sang Lee<sup>1</sup>; <sup>1</sup>Samsung Advanced Institute of Technology(SAIT)

Because of the lack of suitable nitride substrates, films of GaN and related nitride compounds have been commonly grown on sapphire substrate. The use of this foreign substrate causes many problems in growing GaN films such as numerous threading dislocations, stress and bowing. It also complicates the processing steps such as formation of laser cavity and electrical contact and causes the degradation of the device. Therefore, it is desirable to employ the homoepitaxial growth on the GaN substrate. In this report, we report on the origin of defect and characteristics of bulk GaN grown by HVPE.

**MP93, The Passivated Pendeo Structure for the Efficient Self-Separation of the Freestanding GaN:** Po Chun Liu<sup>1</sup>; Hsin Hsieng Huang<sup>1</sup>; Jenq Dar Tsay<sup>1</sup>; Tung Wei Chi<sup>1</sup>; Yih Der Guo<sup>1</sup>; Ruey Chyn Yeh<sup>1</sup>; <sup>1</sup>Industrial Technology Research Institute (ITRI)

A self-separated freestanding Gallium Nitride grown by the Hydride Vapor Phase Epitaxy (HVPE) is obtained using the SiO<sub>x</sub> passivated straight Pendeo (Air Bridge). The GaN can be fully lifted off from the Air Bridge structure, but GaN bulk creaked into several pieces during cooling down process. However, no creaks were found on the whole 2 inch sapphire substrate. For the purpose of comparison, the conventional Pendeo structure was also carried out under identical parameters. The self-separation was not efficiently presented on the Pendeo structure. In addition to this, lots of cracks appeared on the sapphire surface and the GaN, respectively. This could be induced by the thermal expansion coefficient mismatch between the GaN layer and the sapphire. Furthermore, the GaN growing on the sapphire should be another cause of cracks formation. It shows the Air Bridge structure can sufficiently enhance the self-separation of freestanding GaN.

## MP: Theory

**MP94, Ab-Initio Study of Compositional Anti-Correlation of In and N in InGaAsN Alloys:** Hazem Abu-Farsakh<sup>1</sup>; Joerg Neugebauer<sup>1</sup>; Martin Albrecht<sup>2</sup>; <sup>1</sup>Max-Planck-Institut fuer Eisenforschung; <sup>2</sup>Institut fuer Kristallzuechtung

InGaAsN quantum wells have attracted considerable interest as potential candidates for manufacturing infrared laser diodes. Major challenges in epitaxially growing these quaternary alloys with high structural and compositional perfection are compositional fluctuations and a tendency of 3D growth at higher temperatures. A prominent example is the recently experimentally observed but hitherto not understood anti-correlation between In and N which largely affects the optical properties of these alloys. In order to identify/understand the underlying mechanisms we have employed density functional theory to analyze the thermodynamic and kinetic processes of In-N incorporation during growth. Based on these results we show that the In-N anti-correlation results from an intricate interplay between strain

# Technical Program

and chemical energy and is driven by surface kinetics. This detailed insight allows us to discuss possible strategies how to control the In-N correlation.

**MP95, Analysis of Strain and Validity of Vegard's Law in the  $\text{Al}_x\text{Ga}_{1-x}\text{N}$  Thin Films:** *Albert Davydov*<sup>1</sup>; William Boettinger<sup>1</sup>; Alexander Shapiro<sup>1</sup>; Norman Sanford<sup>1</sup>; Vitaly Soukhovoev<sup>2</sup>; Vladimir Dmitriev<sup>2</sup>; Stacia Keller<sup>3</sup>; <sup>1</sup>National Institute of Standards and Technology; <sup>2</sup>TDI, Inc; <sup>3</sup>University of California, Santa Barbara

Compositional band-gap bowing in  $\text{Al}_x\text{Ga}_{1-x}\text{N}$  alloys is a well-established effect, which needs to be taken into account for device engineering. Evaluation of the  $E_g$  vs.  $x$  bowing parameters requires accurate determination of alloy composition, which is often inferred from postulated Vegard's law for  $\text{Al}_x\text{Ga}_{1-x}\text{N}$  lattice parameters vs.  $x$ . This paper examines validity of Vegard's law in the GaN-AlN system by exploring relationship between measured (stressed), calculated (stress-free) wurtzite lattice parameters and independently determined composition  $x$  in HVPE and MOCVD grown  $\text{Al}_x\text{Ga}_{1-x}\text{N}/\text{c-sapphire}$  films. XRD, EDS and RBS measurements combined with strain-stress modeling revealed positive deviation from Vegard's law in this system with evident bowing remaining even for the stress-free  $a_0$  and  $c_0$  lattice parameters. Validated  $a_0(x)$  and  $c_0(x)$  dependencies can further be applied for evaluation of  $x$  in  $\text{Al}_x\text{Ga}_{1-x}\text{N}$  films with unknown composition. Possible origin of deviation from Vegard's law and its relation to thermodynamic properties of  $\text{Al}_x\text{Ga}_{1-x}\text{N}$  alloys is discussed.

**MP96, Band Gap of Miscible InGaAlBN for Use in Optical Communications Systems:** *Takeshi Kimura*<sup>1</sup>; Takashi Matsuoka<sup>1</sup>; <sup>1</sup>Tohoku University

The relationship between the lattice constant and energy-band gap for the InGaAlBN system was calculated for the miscible regions using Vegard's law. The InGaAlBN system, which was proposed for use in optical communications systems, has miscible regions near the InN-rich region and near the line from GaN to AlN, as calculated using the strictly regular solution approximation. Near the InN-rich region, the InGaAlBN had the same band-gap difference,  $\Delta E_g$ , between the active and cladding layers at optical communication wavelengths as InGaAsP under the condition of lattice-matching between layers. When a strained layer, which is useful for high-performance devices, is used as an active layer in the infrared region, the  $\Delta E_g$  of InGaAlBN is larger than those of InGaAsP and InGaAlN. Moreover, the InGaAlBN system enables the fabrication of optical devices under the lattice-matching condition in a much wider range, such as from green to ultraviolet, than InGaAlN.

**MP97, Binding Energies of Hydrogenic Impurity States in GaN/AlGaN Triangular Quantum Well Structure:** *Zhen Chen*<sup>1</sup>; Umesh Mishra<sup>1</sup>; Steven DenBaars<sup>1</sup>; Shuji Nakamura<sup>1</sup>; <sup>1</sup>University of California, Santa Barbara

The ground-state binding energies of a hydrogenic impurity in a triangular quantum well structure are calculated using a variational approach. This model is valid for the common heterostructures, especially materials with a large polarization field, such as GaN/AlGaN. The binding energies are calculated as a function of the slope of the triangular potential for a given position of impurity, and as a function of the position of the impurity for a given electric field.

**MP98, Current Spreading, Heat Transfer, and Light Extraction in a Multi-Pixel LED Array:** Maxim Bogdanov<sup>1</sup>; Kirill Bulashevich<sup>1</sup>; Igor Evstratov<sup>1</sup>; *Sergey Karpov*<sup>2</sup>; <sup>1</sup>Soft-Impact, Ltd.; <sup>2</sup>Semiconductor Technology Research, Inc.

We report on coupled 3D simulation of the current spreading, heat transfer, and light extraction in a conventional square light-emitting diode (LED) and a multi-pixel LED array recently suggested to improve the high-current device performance. The square LED is found to suffer from a considerable overheating that results in the emission power rollover at high currents. In contrast, the thermal effects are suppressed in a multi-pixel LED even at higher currents, providing very uniform distribution of the wavelength and light emission intensity among the individual pixels. The modeling reproduced quantitatively well the observed dramatic difference in the LED series resistance due to the die design, the current dependence of the output power, and other operational features of the LEDs. The 3D ray-tracing is

used to estimate the light ex-traction efficiency through a semitransparent p-electrode and to identify the channels of optical losses in the dice.

**MP99, Density Functional Theory Calculations of the Strain Effects on Binding Energies and Adatom Diffusion for GaN (0001) Surfaces:** *James Grandusky*<sup>1</sup>; Vibhu Jindal<sup>1</sup>; Neeraj Tripathi<sup>1</sup>; Mihir Tungare<sup>1</sup>; James Reynolds<sup>1</sup>; Fatemeh Shahedipour-Sandvik<sup>1</sup>; <sup>1</sup>University at Albany, SUNY

Density functional theory calculations were carried out to study the binding energies and diffusion barriers for adatoms on GaN. The binding energies and diffusion barriers were calculated for Ga and N adatoms on both Ga terminated and N terminated (0001) surfaces, subjected to a hydrostatic compressive and tensile strain in the range of 0 to 5%. A complete understanding of the changes in adatom binding and diffusion under differing growth conditions was obtained. For example, the diffusion barrier of a Ga adatom is maximum for a 1% compressive strain and decreases rapidly at higher strains whereas the diffusion barrier for a N adatom is lowest at a 1% tensile strain and increases as the strain increases on a N terminated surface. These changes can explain differences in optimal growth conditions on bulk III-Nitride substrates as opposed to on III-Nitride template layers on foreign substrates.

**MP100, Electronic Basic Transition of Zincblende In(x)Ga(1-x)N/In(y)Ga(1-y)N Quantum Wells:** *Heriberto Hernandez Cocoltzi*<sup>1</sup>; Jesus Madrigal-Melchor<sup>2</sup>; Stoyan Jelev-Vlaev<sup>2</sup>; I. Rodríguez-Vargas<sup>2</sup>; David Armando Contreras Solorio<sup>2</sup>; <sup>1</sup>Benemérita Universidad Autónoma de Puebla; <sup>2</sup>Universidad Autónoma de Zacatecas, Unidad Académica de Física

Generally, the principal part of LED and laser devices made of nitrides, is an InGaN quantum well. In this work, for that type of wells in cubic phase, we calculate theoretically the fundamental transition from the first energy level of holes to the first energy level of electrons, 1h-1e. For calculations, we use several values for the band offset at the In(x)Ga(1-x)N/In(y)Ga(1-y)N interface and well width, and various concentrations of In. We use the Surface Green Function Matching method and the first neighbor tight binding approximation with a  $sp^3s^*$  basis, taking into account the spin-orbit interaction. We use tight binding parameters that give a value of 0.65 eV for the InN band gap. For the InGaN alloy we use the virtual crystal approximation. We incorporate the biaxial stress in the well, due to the different values of lattice constants between the well and the barriers. Work partially supported by VIEP-BUAP.

**MP101, Electronic Spectral Densities and Spectral Line Profiles in Quantum Dots:** *Karel Kral*<sup>1</sup>; <sup>1</sup>Academy Science of Czech Republic, Institute of Physics

Spectral line profiles of luminescence transitions in individual quantum dots have been studied in recent years and shown to be quite different from the simple form the Lorentzian line shape. Here we turn the attention to earlier calculations and measurements and compare them with the electronic spectral line profiles in individual quantum dots calculated under the assumption of quantum dot electrons interacting with the longitudinal optical phonons only. The calculated luminescence spectral line profiles will be presented and compared to the calculated electronic spectral densities which develop in the course of relaxation processes or other kinetic processes in quantum dots. The spectral densities will be numerically evaluated in the self-consistent Born (SCB) approximation to the electronic self energy. We will show the agreement of the calculated spectral line profile of the lowest energy excited state with experimental data and with other calculations.

**MP102, Filling the Green Gap: A First-Principles Study of the  $\text{LiMg}_{1-x}\text{Zn}_x\text{N}$  Alloy System:** *Aron Walsh*<sup>1</sup>; Su-Huai Wei<sup>1</sup>; <sup>1</sup>National Renewable Energy Laboratory

The lack of an efficient emitter in the 500-600nm range is severely limiting the widespread adoption of light emitting diodes for indoor lighting applications. The degradation in performance of the current In and Ga nitride alloys in this range is largely due to their lattice mismatch and associated phase instabilities. We propose and investigate the electronic structure of an alternative system, which has the potential to fill this green gap. The small lattice mismatch between  $\text{LiMgN}$  and  $\text{LiZnN}$  along with their electronic bandgaps spanning the visible range, make them in principle, ideal candidates.

**MP103, First Principles Model of Bandgap Lowering in Dilute III-V-Nitrides: Beyond Band Anticrossing:** *Vincenzo Lordi*<sup>1</sup>; James Harris<sup>1</sup>; <sup>1</sup>Stanford University

The remarkable property of III-V-N compounds is the sharp band gap lowering upon incorporation of small amounts of nitrogen. A popular model based on band anticrossing (BAC) is often used to explain the effect. We present a more comprehensive physical model based on *ab initio* calculations to explain the phenomenon over a broader applicable composition range. We find that BAC is a good descriptor of the very low concentration limit, but that a crossover to a N cluster-dominated description occurs at higher concentrations. The N clusters create energy states within the host band gap near the CBM, which hybridize into a “N band.” The result is a band gap lowering that is steeper at low concentrations and begins to flatten as the interaction between N atoms increases at higher concentrations. A portion of this work was performed under the auspices of the U.S. DoE at UC/LLNL under contract no. W-7405-Eng-48.

**MP104, Ga-Frenkel Pairs in GaN Investigated via g-Tensor Calculations:** *Uwe Gerstmann*<sup>1</sup>; Francesco Mauri<sup>1</sup>; <sup>1</sup>Université Pierre et Marie Curie, Paris

In GaN, an exceptionally important role is played by Ga-interstitials being mobile at room temperature. Despite rather large formation energy, they have been observed in irradiated wurtzite-GaN: two similar ODEPR-signals L5/L6 have been identified as interstitial Ga<sup>2+</sup> in two different lattice configurations. However, judging from experimental data and total energy calculations alone, the exact microscopic configuration remained unclear. In this work, the situation is elucidated by calculating the complete set of EPR parameters, hyperfine splittings as well as g-tensors, for reasonable defect models using a gauge-including projector augmented plane wave (GI-PAW) approach. We first show that the usual inequivalent interstitial sites, the O-site and T-site, provide almost identical hyperfine splittings. The isotropy of the g-tensor turns out to be a much more rigorous criterion, ending up in a model with near and distant frenkel pairs of a Ga-interstitial at the O-site and a distant Ga-vacancy as a rather small modification.

**MP105, Lasing Threshold of 280 nm AlGaIn Lasers under High Threshold Gain Conditions:** *Weng Chow*<sup>1</sup>; Mary Crawford<sup>1</sup>; Andrew Allerman<sup>1</sup>; Michael Kneissl<sup>2</sup>; <sup>1</sup>Sandia National Laboratories; <sup>2</sup>Technical University of Berlin

This paper analyses the threshold current density versus threshold gain relationship for AlGaIn lasers operating in the deep UV. The calculations are based on the semiconductor Bloch equations, where bandstructure, internal electric field and many-body effects are treated rigorously. The results show a strong dependence of threshold current density on threshold gain, lasing polarization, barrier Al concentration and quantum well (QW) width. The QW configurations, i.e. QW widths and barrier compositions, giving the lowest threshold current densities are distinctly different for low and high threshold gains (e.g. GG<sub>th</sub> = 40cm<sup>-1</sup> and 120cm<sup>-1</sup>, respectively). We also found that laser emission switches between TE and TM mode depending on the operating conditions and QW configuration. These differences are a consequence of the intricate interactions among band structure, internal field and many-body interaction.

**MP106, Magnetic Interactions in GaN: A Comparative Investigation of Cr, Mn, Fe, and Co Impurities:** *Lucy Assali*<sup>1</sup>; Wanda Machado<sup>1</sup>; Joao Justo<sup>2</sup>; <sup>1</sup>Universidade de Sao Paulo, Instituto de Fisica; <sup>2</sup>Universidade de Sao Paulo, Escola Politecnica

Interest in magnetic semiconductors has grown considerably, as a result of a theoretical prediction that manganese doped III-V semiconductors could retain magnetic properties up to room temperature. Those properties open a wide range of potential applications, such as spintronic devices. In this work, we present an *ab initio* investigation on the structural, electronic, and magnetic properties of isolated 3d transition metal impurities (Cr, Mn, Fe, and Co) in GaN. We considered the impurities in the substitutional cation sites, and the material in both cubic and hexagonal phases. Our calculations were performed within the all-electron spin-polarized full-potential linearized augmented plane wave methodology. The calculations provided the stable configurations, symmetries, spin states, formation and transition energies,

and magnetic moments of those impurities in GaN. A comparative study on all those impurities allowed to build a microscopic model for the chemical trends of 3d transition metals in III-nitrides semiconductors.

**MP107, Ordering, Phase-Separation and Suppression of Phase Separation in InN-GaN Alloys:** *Zhe Liu*<sup>1</sup>; Giancarlo Trimarchi<sup>1</sup>; Alex Zunger<sup>1</sup>; <sup>1</sup>National Renewable Energy Laboratory

Large atomic-size mismatch (over 10%) between InN and GaN has long been known to lead to phase separation into InN-rich and GaN-rich phases at their own equilibrium lattice constants (incoherent phase separation). Such inhomogeneous mixtures can severely limit many technological applications that rely on carrier transport. We show theoretically that this size-mismatched alloy has specific coherent, three-dimensional tetrahedral networks with much lower energies than both the equivalent random alloys and coherently separated constituents (i.e., both constituents have the same lattice constant at the interface). Such homogeneous structures are predicted to order at low temperature, and are characterized by alternate atomic bi-layers along the (201) crystallographic direction, akin to the (AC)2/(BC)2 (201) chalcopyrite (CH) crystal structure. The prediction of bulk stable ordered structure provides a mechanism to understand ordered structures observed in experiments of bulk III-V zincblende semiconductor alloys.

**MP108, Polarization Fields in Wurtzite Strained Layers and Heterostructures Grown on (hkl)-Oriented Substrates:** *Bernard Gil*<sup>1</sup>; Pierre Bigenwald<sup>2</sup>; <sup>1</sup>National Center of Scientific Research; <sup>2</sup>Universite Blaise Pascal Clermont Ferrand 2

We develop the general theory of spontaneous and piezoelectric polarization fields in wurtzite crystals via utilization of crystallography considerations and elasticity theory. As an application of it, we apply our equations to GaN-GaInN quantum wells grown on (hkl) planes and we show the specific orientations that lead to a cancellation of the Quantum Confined Stark Effect in such heterostructures that are impacting for realizing blue light emitting solid state devices. We calculate the residual electric field in (10-11)-grown and (11-22)-grown epilayers, quantum wells and diodes and compare our findings with existing data.

**MP109, Quantum-Confinement Effect and Intersubband Transitions in Zinc Blend Al<sub>x</sub>Ga<sub>1-x</sub>N/AlN Quantum Cubes:** *Shih-Wei Feng*<sup>1</sup>; Kuei-Hsien Chen<sup>2</sup>; <sup>1</sup>National University of Kaohsiung; <sup>2</sup>Academia Sinica, Institute of Atomic and Molecular Sciences

In this work, by using a series expansion model to calculate the band structures of a Al<sub>x</sub>Ga<sub>1-x</sub>N/AlN quantum cube, we theoretically study the quantum-confinement effects and its impacts on the band structures and intersubband (ISB) transitions in ZB AlGaIn quantum dots. Without spontaneous and piezoelectric polarization fields, the quantum confinement effect and size-tunable emission properties of ZB Al<sub>x</sub>Ga<sub>1-x</sub>N/AlN quantum cubes can be completely explored. Simulations results show the important factors of the composition, cluster size, quantum confined potential, effective mass, and strain in determining the optical properties and band structures of such a semiconductor compound. Meanwhile, calculation results reveal that the cube sizes as well as composition contrast must be larger such that ISB transitions between electron eigen-states can be used for telecommunication devices. These simulation results of quantum-confinement effects, size-tunable emission properties, ISB transitions, and ISB absorptions can provide significant information for the devices designs and fabrications.

**MP110, Structural and Dynamical Properties of AlInGaN Alloys:** H. W. Leite Alves<sup>1</sup>; J. L. A. Alves<sup>1</sup>; *Luisa Scolfaro*<sup>2</sup>; <sup>1</sup>Universidade Federal de São João del Rei, Departamento de Ciências Naturais; <sup>2</sup>University of Sao Paulo, Physics Institute

In this work, we have calculated *ab initio*, by using the Density Functional Theory within the Local Density Approximation, gradient conjugated techniques, and the plane-wave pseudopotential method, the structural properties, the phonon frequencies (with their hydrostatic strain dependence), and the dielectric functions of AlInGaN quaternary alloys. We have used the Troullier-Martins pseudopotentials, and the phonons were obtained by means of the Density-Functional Perturbation Theory. Our preliminary results agree well (within 3% of error) with the available experimental data, whenever

# Technical Program

these comparisons were possible. We have also described the composition dependence of the lattice constants, Bulk modulus, phonon frequencies and the static dielectric constant for some fixed In contents, 0.12 and 0.06. Based on our findings, we have speculated about the nature of the observed two-mode behavior of the E(TO) vibrational modes with the increasing of the In content in the alloy.

**MP111, The Surface Magnetoplasmon Polariton in GaN (doped)-AlN (undoped) Semiconductor Superlattice:** *Saber Farjami Shayesteh*<sup>1</sup>; <sup>1</sup>University of Guilan

The effective medium dielectric tensor of a superlattice is employed to describe doped-undoped GaN-AlN semiconductor superlattice in a external magneto-static field. According to direction of magnetic field, there configuration perpendicular, Faraday and Voigt are defined. The properties of surface polariton have been consider in detail for the perpendicular (applied magnetic field perpendicular to interface) and Faraday configuration (magnetic field parallel to interface and along with propagation vector). The dispersion relation of surface magnetoplasmon polariton is calculated for GaN (doped)-AlN (undoped) multi quantum wells. Numerical exploration shows frequency of the generalized surface wave increases as  $\omega c$  increases. Also, it is seen that as the field value increases the frequency of surface mode increases. In Addition to, calculated dispersion curve shows the surface mode propagation is reciprocal,  $\omega(k) = \omega(-k)$ , for both perpendicular and Faraday configurations. Furthermore, the dispersion curve varies with the volume fraction of the doped constituent.

## NOTES

---

## Session J: Deep UV LEDs and Lasers

Tuesday AM                      Room: 313/316  
September 18, 2007              Location: MGM Grand Hotel Conference Center

*Session Chairs:* Hiroshi Amano, Meijo University; Thomas Katona, University of South Carolina

---

### 9:00 AM Invited

#### J1, Recent Progress in AlInGaN Based Deep Ultraviolet Light Emitting Diodes: *Asif Khan*<sup>1</sup>; <sup>1</sup>University of South Carolina

Several groups have reported on deep ultraviolet light emitting diodes (LEDs) for applications in air-water and food purification. The first generation devices, with emission from 340 to 280 nm typically have cw-powers as high as 1 mW (@ 20 mA) and wall-plug efficiencies of about 1%. Their average lifetimes at 20 mA are only about 500 to 1000 hours. Due to increased number of extended defects, these performance numbers drop with decreasing emission wavelength. Currently several groups including ours are exploring ways to produce more robust devices with higher emission efficiencies. In this paper we will review the issues limiting the first generation devices' performance followed by new AlGaIn lateral epitaxy approaches leading to second generation deep UV LEDs with significantly improved lifetime-efficiency values. Finally we will discuss the potential of fabricating non-polar deep UV LEDs.

### 9:30 AM

#### J2, 340nm-Band High-Power (>7mW) InAlGaIn Quantum Well UV-LED Using p-Type InAlGaIn Layers: *Sachie Fujikawa*<sup>1</sup>; Takayoshi Takano<sup>2</sup>; Yukihiko Kondo<sup>2</sup>; Hideki Hirayama<sup>1</sup>; <sup>1</sup>RIKEN; <sup>2</sup>Matsushita Electric Works, Ltd.

In order to achieve high-efficiency ultraviolet (UV) light-emitting diodes (LEDs), p-type layers with sufficient hole concentration is quite important to suppress the electron overflow. We introduced Mg-doped InAlGaIn layers for p-type layers of the UV-LEDs for the purpose of obtaining higher hole concentration, and achieved high power CW operations (>7 mW) of the UV-LEDs. 340nm-band InAlGaIn-based multi-quantum-well (MQWs) UV-LEDs with Mg-doped InAlGaIn electron-blocking layer and p-type layers were grown on the sapphire substrates by metal-organic chemical vapor deposition (MOCVD). The output power of UV-LED with p-InAlGaIn layers (6.6mW) was approximately 4.7 times larger than that with p-AlGaIn layers (1.4mW). Maximum output power and the external quantum efficiency (EQE) of the quaternary InAlGaIn based UV-LED were 7.1mW and 0.9%, respectively, at emission wavelength of 346nm under room temperature (RT) CW operation. From these results, p-InAlGaIn is shown to be quite useful for the realization of high-efficiency UV-LEDs.

### 9:45 AM

#### J3, AlGaIn Based Deep UV LEDs with Emission at 230-270 nm: *Jianping Zhang*<sup>1</sup>; Yuri Bilenko<sup>1</sup>; Xuhong Hu<sup>1</sup>; A. Lunev<sup>1</sup>; A. Sattu<sup>1</sup>; J. Deng<sup>1</sup>; M. Shatalov<sup>1</sup>; W. Sun<sup>1</sup>; J. Yang<sup>1</sup>; R. Gaska<sup>1</sup>; <sup>1</sup>Sensor Electronic Technology

We report on development of AlGaIn deep UV LED with emission wavelength from 230 nm to 270 nm. The LED structures were grown over (0001) sapphire substrates using proprietary MEMOCVD process. LEDs showed strong emissions at as short as 232 nm. The voltages at 20 mA ranged from 8 V to 6 V with the series resistances between 35  $\Omega$  and 20  $\Omega$  for 247 nm and 270 nm LEDs, respectively. At 20 mA cw the output power of 50  $\mu$ W and 1.34 mW were measured at 247 nm and 269 nm, respectively. The cw power for 269 nm LED reached 3.25 mW at 50 mA. Maximum powers of 9 mW at 1.4 A for 247 nm and 50 mW at 2 A for 269 nm emitting LEDs were measured under pulse excitation.

### 10:00 AM

#### J4, Nitride-Based Microcavities with Quantum Wells and Quantum Dots as Active Region: *Carsten Kruse*<sup>1</sup>; Stephan Figge<sup>1</sup>; Heiko Dartsch<sup>1</sup>; Timo Aschenbrenner<sup>1</sup>; Christian Tessarek<sup>1</sup>; Henning Lohmeyer<sup>1</sup>; Kathrin Sebald<sup>1</sup>; Juergen Gutowski<sup>1</sup>; Detlef Hommel<sup>1</sup>; <sup>1</sup>University of Bremen

We realized monolithic GaN/Al<sub>0.4</sub>Ga<sub>0.6</sub>N-based microcavities (MCs) with Q-values around 300 grown by MOVPE and plasma-assisted MBE. These structures are fully strained as determined by HRXRD and of good structural quality according to SEM pictures. We also fabricated hybrid microcavities having a dielectric SiO<sub>2</sub>/TiO<sub>2</sub> layer stack as the top DBR in order to have a higher flexibility for integrating temperature-sensitive active regions like InGaIn-QD sheets into the MCs. Two main applications are in focus: VCSELs with either QW and QD stacks as active region for lasing applications or MCs with single sheets of QDs with a comparatively low density in the range of 10<sup>8</sup> – 10<sup>9</sup> cm<sup>-2</sup> for use as a single-photon emitter. We will discuss growth related issues like strain engineering using suitable AlGaIn template layers and the two-step growth of InGaIn-QDs. Furthermore, optical properties of planar MCs and micropillars will be addressed.

### 10:15 AM

#### J5, Degradation of III-Nitride Laser Diodes Grown by Molecular Beam Epitaxy: *Huixin Xiu*<sup>1</sup>; Ted Thrush<sup>1</sup>; Matthias Kauer<sup>2</sup>; Tim Smeeton<sup>2</sup>; Stewart Hooper<sup>2</sup>; Jonathan Heffernan<sup>2</sup>; Colin Humphreys<sup>1</sup>; <sup>1</sup>University of Cambridge; <sup>2</sup>Sharp Laboratories of Europe Ltd

Understanding the failure and degradation mechanisms is key to improving the lifetime of III-nitride laser diodes grown by molecular beam epitaxy. This paper reports on the defects found in electrically degraded GaN-based lasers characterised by transmission electron microscopy. In a laser which had been operated until failure, defects containing contact metals were observed. Combined with data from the laser's current-voltage characteristics, this suggested that the catastrophic failure may have been caused by local heating. In partially degraded lasers, four different types of defects were observed: cracks, stacking faults, inversion domains and dislocations. Cracks, stacking faults and inversion domains were present before and after the laser failure. The dislocation network, however, was only observed in the active region of a failed laser and may have resulted from recombination enhanced defect migration. Further investigation will be carried out to determine the role of cracks and dislocation network in the degradation of lasers.

### 10:30 AM Break

---

## Session K: Microwave Devices III

Tuesday AM                      Room: 314/315  
September 18, 2007              Location: MGM Grand Hotel Conference Center

*Session Chairs:* Kevin Linthicum, Nitronex Corporation; Yvon Cordier, Research Center on the Heteroepitaxy and Its Applications, National Scientific Research Center

---

### 9:00 AM

#### K1, Nitride Based Nanotransistors as New Sources and Detectors of THz Radiations: *Frederic Teppel*<sup>1</sup>; *Bernard Gil*<sup>1</sup>; <sup>1</sup>CNRS UMR-5650

The plasma waves in gated two-dimensional electron gas have a linear dispersion law, similar to the sound waves. The transistor channel is acting as a resonator cavity for the plasma waves, which can reach frequencies in the Terahertz (THz) range for a sufficiently short gate length Field Effect Transistors (FETs). THz emission and detection by nanometer III-V transistors have been recently reported. In this work we report on THz emission and detection by nanometer GaN/AlGaIn HEMTs. In particular, we show that specific GaN properties allow to observe THz emission up to room temperature. Possible application of GaN/AlGaIn transistors as new miniature THz sources will be discussed.

# Technical Program

9:05 AM

**K2, GaN-on-Diamond High-Electron-Mobility Transistors:** *Jonathan Felbinger*<sup>1</sup>; M.V.S. Chandra<sup>1</sup>; Lester Eastman<sup>1</sup>; John Wasserbauer<sup>2</sup>; Firooz Faili<sup>2</sup>; Dubravko Babic<sup>2</sup>; Daniel Francis<sup>2</sup>; Felix Ejeckam<sup>2</sup>; <sup>1</sup>Cornell University; <sup>2</sup>Group4 Laboratories, LLC

AlGaIn/GaN high-electron-mobility transistors (HEMTs) are fabricated on diamond and SiC substrates and their performance is compared. We demonstrate GaN-on-diamond transistors, with periphery  $W_G = 250 \mu\text{m}$ , exhibiting unity-current-gain frequency  $f_t = 27.4 \text{ GHz}$  and yielding a power density of  $2.79 \text{ W/mm}$  at  $10 \text{ GHz}$ . Recently-fabricated AlGaIn/GaN HEMTs on diamond exhibit a full-channel current of  $1.03 \text{ A/mm}$  at  $V_{GS} = 0 \text{ V}$  and a peak transconductance of  $376 \text{ mS/mm}$  with  $f_t = 53.4 \text{ GHz}$ . Additionally, the temperature rise in HEMTs on diamond and SiC substrates is reported with the devices on diamond exhibiting half the temperature rise of those on SiC. Presently, multi-finger devices are being fabricated on GaN-on-diamond to achieve higher power output and lower channel-to-channel pitch, minimizing phase dispersion, than is feasible on GaN-on-SiC.

9:20 AM

**K3, Enhancement-Mode AlGaIn/GaN HEMTs with Thin InGaIn Cap Layer:** *Masaomi Ito*<sup>1</sup>; Shigeru Kishimoto<sup>2</sup>; Fumihiko Nakamura<sup>3</sup>; Takashi Mizutani<sup>1</sup>; <sup>1</sup>Nagoya University, Department of Quantum Engineering; <sup>2</sup>Nagoya University, Department of Quantum Engineering, Venture Business Laboratory; <sup>3</sup>POWDEC K.K.

AlGaIn/GaN HEMTs receive much attention for high-power and high-frequency applications. In order to apply them to the high-power switching systems, normally-off HEMTs are indispensable. In this report, we propose to introduce a thin InGaIn cap layer on a conventional AlGaIn/GaN HEMT structure to implement the normally-off HEMTs. Polarization field in the InGaIn cap layer is expected to raise the conduction band of the AlGaIn/GaN interface leading to a threshold voltage shift to positive direction. It is possible to decrease the parasitic source resistance by removing the InGaIn cap layer at the access region. Fabricated HEMT with  $5 \text{ nm}$  thick  $\text{In}_{0.2}\text{Ga}_{0.8}\text{N}$  cap layer showed normally-off operation with a threshold voltage of  $0.3 \text{ V}$  and a maximum transconductance ( $g_{m\text{max}}$ ) of  $145 \text{ mS/mm}$ . The  $g_{m\text{max}}$  was comparable with the normally-on HEMT without the InGaIn cap layer. These results confirm the validity of introducing an  $\text{In}_{0.2}\text{Ga}_{0.8}\text{N}$  cap layer to implement the normally-off HEMTs.

9:35 AM

**K4, Growth and Characterization of AlInN/GaN Field Effect Transistors:** *Jean-François Carlin*<sup>1</sup>; Farid Medjdoub<sup>2</sup>; Marcus Ganschorek<sup>1</sup>; Eric Feltn<sup>1</sup>; Marcel Py<sup>1</sup>; Christophe Gaquiere<sup>3</sup>; Nicolas Grandjean<sup>1</sup>; Erhard Kohn<sup>2</sup>; <sup>1</sup>EPFL; <sup>2</sup>University of Ulm (EBS); <sup>3</sup>IEMN/TIGER

Lattice-matched  $\text{Al}_{0.83}\text{In}_{0.17}\text{N}/\text{GaN}$  high electron mobility transistors (HEMTs) are grown by metalorganic vapor phase epitaxy. A thin AlN interlayer is inserted at the interface in order to reduce the alloy scattering. Room-temperature mobilities of  $1200 \text{ cm}^2\text{V}^{-1}\text{s}^{-1}$  are then been obtained with nS as high as  $2.6 \times 10^{13} \text{ cm}^{-2}$ . Standard structures ( $15 \text{ nm}$  barrier, lattice-matched AlInN/GaN) typically exhibit  $2 \text{ A/mm}$  drain current density. Growth optimization on various substrates (sapphire, Silicon and SiC) and characterization of AlInN materials are discussed. Transistors having a reduced barrier thickness as low as  $5 \text{ nm}$  still provide high output current density and transconductance about  $500 \text{ mS/mm}$ . A good threshold voltage scaling with the AlInN barrier thickness reduction is observed. The high potential of the AlInN/GaN system is confirmed on HEMT devices. DC measurements demonstrate an open channel drain current density of  $2.6 \text{ A/mm}$  on HEMTs with  $50 \times 0.25 \mu\text{m}^2$  gate geometry.

9:50 AM

**K5, GaN HEMT Thermal Behavior and Implications for Reliability Testing and Analysis:** *Daniel Green*<sup>1</sup>; Bharath Vembu<sup>1</sup>; David Hepper<sup>1</sup>; Shawn Gibb<sup>1</sup>; Daniel Jin<sup>1</sup>; Rama Vetury<sup>1</sup>; Jeffrey Shealy<sup>1</sup>; Thomas Beechem<sup>2</sup>; Samuel Graham<sup>2</sup>; <sup>1</sup>RFMD Infrastructure Product Group, Inc.; <sup>2</sup>Georgia Institute of Technology

GaN HEMT reliability evaluation in a typical Arrhenius manner requires establishing peak junction temperature for a particular stress condition. Several new techniques have yielded promising results toward establishing

peak temperature for these devices in combination with a detailed physical modeling, particularly micro-Raman imaging. This paper compares results from finite element modeling to measurements by infrared imaging and micro-Raman imaging. The limitations of IR imaging were confirmed similar to earlier reports. Two techniques for establishing temperature from micro-Raman measurements were used to reveal excellent correlation to the model, and also provide insight into the relationship between temperature and structural change in the device. Temperature data is reported for base plate temperature from  $85^\circ\text{C}$  to  $140^\circ\text{C}$  for practical GaN HEMT devices. Implications of the measurements for GaN HEMT reliability stress testing and analysis will be discussed.

10:05 AM

**K6, Nanosecond Thermal Transients in Pulsed High-Power AlGaIn/GaN Devices Using Time-Resolved Micro-Raman Thermography:** *Gernot Riedel*<sup>1</sup>; J. Pomeroy<sup>1</sup>; M. Kuball<sup>1</sup>; M. Uren<sup>2</sup>; T. Martin<sup>2</sup>; <sup>1</sup>University of Bristol; <sup>2</sup>QinetiQ Ltd

Microwave power transistors are typically operated pulsed for use in communications and radar applications, resulting in fast thermal transients due to self-heating and thermal diffusion. Since self-heating degrades performance and reliability, it is important to monitor the temporal evolution of device temperature on short time-scales. Transient thermal simulations, commonly used for this purpose, are strongly affected by uncertainties in input parameters in particular within the initial  $50\text{-}200\text{ns}$  of the temperature evolution, several of which, including thermal boundary resistance, are not well known. We have applied a time-resolved micro-Raman thermography technique with  $10\text{-}15\text{ns}$  temporal resolution in order to gain unprecedented insight into the fast initial thermal transients in pulsed AlGaIn/GaN devices. Different device structures and substrate materials are investigated and comparison is made to thermal simulations. We find that thermal time constants in the first  $50\text{-}100\text{ns}$  are dominated by the thermal parameters of the GaN and not the substrate.

10:20 AM Break

---

## Session L: Sensors and Characterization I

Tuesday AM Room: 312/317  
September 18, 2007 Location: MGM Grand Hotel Conference Center

*Session Chairs:* Martin Stutzmann, Technische Universität München; Misaichi Takeuchi, RIKEN

---

9:00 AM Invited

**L1, Group-III-Nitride Based Gas Detectors and Liquid Sensors:** *Oliver Ambacher*<sup>1</sup>; <sup>1</sup>Technical University Ilmenau

Optic and electronic properties of group-III-nitride based micro- and nanostructures have been proven to be extremely sensitive to any manipulation of surface charge. Exposure of unpassivated AlGaIn/GaN high electron mobility transistors to water vapor is causing a significant depletion of the polarization induced two dimensional electron gas causing unwanted variation in the electronic device performance. Electrons and ions reaching the surface of InGaIn/GaN light emitting devices can influence their band profiles changing the wavelength as well as the intensity of light emission. In order to understand these effects we have performed a systematic investigation of surface potential variation of group-III-nitride surfaces caused by polar molecules or ions provided by liquids or gases. By this approach we realized, that group-III-nitrides are very suitable to process novel gas detectors and liquid sensors with extremely high sensitivity and selectivity to molecules and atoms with industrial relevance. Further more we noticed that unintentional surface oxidation as well as intentionally deposited metal oxide nano-layers on top of group-III-nitride micro- and nanostructures can significantly influence their electronic properties. This effect can be used to tune and optimize the performance of gas detectors and liquid sensors.

Our physical model useful to explain the sensitivities of group-III-nitrides (with and without metal oxide on top) towards polar liquids and ions will be illustrated by presenting recent measurements related to the: • detection of protons in gases and liquids, • determination of viscosity and temperature of nanolitre droplets and the • monitoring of bioreactions and cell activities. Further more we will demonstrate that nano-layers of metal oxides on top of blue emitting GaN diodes can be used to realize extremely miniaturized and sensitive ozone gas sensors.

## 9:30 AM

**L2, Piezoelectric Actuation of All-Nitride MEMS:** *Katja Tonisch<sup>1</sup>; Rüdiger Goldhahn<sup>1</sup>; Carsten Buchheim<sup>1</sup>; Volker Cimalla<sup>1</sup>; Florentina Niebelschütz<sup>1</sup>; Mary Donahue<sup>1</sup>; Oliver Ambacher<sup>1</sup>;* <sup>1</sup>Technical University Ilmenau

Few attempts to realize nitride based MEMS have been reported so far, though their piezo- and pyroelectric properties makes them favourable for sophisticated solutions. We present MEMS consisting of a novel GaN/AlGaIn/GaN-heterostructure. Thereby the lower GaN layer represents the mechanical active layer, while the upper GaN and AlGaIn layers supply the piezoelectrically active layers for actuation and the confinement of a 2D electron gas (at the lower interface). The 2DEG serves as back electrode for the piezoelectric actuation and as read-out, since it is modulated by the mechanical oscillation. The upper AlGaIn and GaN layer both contribute to the total piezoelectric response, which was determined by piezoelectric force microscopy. We studied by means of capacitance-voltage, biased Hall measurements and electroreflectance the influence of the thickness and its ratio of both layers on the electrical field distribution in order to optimize geometry and layer structure for a maximum piezoelectric actuation.

## 9:45 AM

**L3, AlGaIn/GaN – Based MEMS with Two-Dimensional Electron Gas for Novel Sensor Applications:** *Florentina Niebelschütz<sup>1</sup>; Volker Cimalla<sup>1</sup>; Katja Tonisch<sup>1</sup>; Christian Haupt<sup>1</sup>; Klemens Brückner<sup>1</sup>; Ralf Stephan<sup>1</sup>; Matthias Hein<sup>1</sup>; Oliver Ambacher<sup>1</sup>;* <sup>1</sup>Institute of Micro- and Nanotechnologies, Technische Universität Ilmenau

Novel microelectromechanical resonators structures have been realized based on AlGaIn/GaN heterostructures grown on SiC substrates confining a two dimensional electron gas (2DEG), which provides a basis for sophisticated sensor structures. By means of the developed etching technology freestanding resonators were patterned without decreasing the sheet carrier concentration and electron mobility of the 2DEG inside the beams, as concluded from electrical measurements before and after the various process steps. This highly sensitive sensor system is applied for actuation as well as read out using magnetomotive and piezoelectric actuation, respectively. Due to the high sensitivity of the 2DEG and the chemical stability of the utilized materials these structures are suitable for chemical and biological sensor applications, in which the sensitivity of the 2DEG on the surrounding environment is established as additional sensing signal, for example for simultaneous measurements of the viscosity and pH – value of a nanoliter droplet.

## 10:00 AM

**L4, Chemical Functionalization of GaN Surfaces by Hemin:** *April Brown<sup>1</sup>; Maria Losurdo<sup>2</sup>; Michael Garcia<sup>1</sup>; Scott Wolter<sup>1</sup>; Tong-Ho Kim<sup>1</sup>; Maria Giangregorio<sup>2</sup>; William Lampert<sup>3</sup>; Giovanni Bruno<sup>2</sup>;* <sup>1</sup>Duke University; <sup>2</sup>IMIP-CNR; <sup>3</sup>U.S. Army Research Office

The chemisorption and formation of self-assembled monolayers (SAMs) of hemin (a metal porphyrine) on GaN surfaces for sensing applications is presented. The chemical functionalization of GaN is achieved by using hemin solutions in DMF. The chemistry of the GaN functionalization is characterized using XPS, thickness of hemin SAMs depending on experimental conditions is determined by spectroscopic ellipsometry, and AFM is used to image the hemin self-assembling on GaN surfaces. This is the first report in literature on the kinetic (effect of time) of the GaN functionalization depending on the status of GaN surface (native oxide, wet-etched, polarity, light irradiation, etc), hemin concentration, concentration of the benzoic acid added as “spacer” in order to avoid formation of hemin aggregates that are detrimental to sensor performance. The response of the GaN/hemin to sensing few ppm of NO is also demonstrated.

## 10:15 AM

**L5, GaN Quantum Dots as Optical Transducers in Field Effect Chemical Sensors:** *Olaf Weidemann<sup>1</sup>; Eva Monroy<sup>2</sup>; Gunther Jegert<sup>1</sup>; Stefan Birner<sup>1</sup>; Martin Stutzmann<sup>1</sup>; Martin Eickhoff<sup>1</sup>;* <sup>1</sup>Technische Universität München; <sup>2</sup>CEA-Grenoble

GaN-based field-effect devices have been proven useful to detect chemically induced changes of the surface potential as the physical basis for chemical sensors in liquid or gaseous environments. For some applications, an alternative to electrical readout of the sensor signal is advantageous. To this end, GaN/AlN quantum dot (QD) nanostructures, which exhibit efficient room-temperature luminescence, allow optical detection of changes in the surface potential. We demonstrate the applicability of GaN QDs as optical transducers in chemical sensors, utilizing the optical transparency of both the sapphire substrate and the AlN matrix. GaN/AlN QD stacks were grown on conductive AlGaIn:Si back-contact layers, and were equipped with catalytic Pt front-contacts. The luminescence properties of such structures and their dependence on applied electric fields have been investigated for QD ensembles with different dot sizes. The optical response of such a system towards hydrogen-containing gases is also discussed.

## 10:30 AM Break

---

### Session M: MOVPE Growth of AlGaIn Alloys I

Tuesday AM

September 18, 2007

Room: 313/316

Location: MGM Grand Hotel Conference Center

*Session Chairs:* Hideki Hirayama, RIKEN; Kei May Lau, Hong Kong University of Science and Technology

---

## 11:00 AM

**M1, Extremely Low Dislocation Content AlN Bridge Layers on Patterned 6H-SiC Substrates by High Temperature MOVPE:** *Balakrishnan Krishnan<sup>1</sup>; Hiroki Sugimura<sup>1</sup>; Akira Bandoh<sup>2</sup>; Motoaki Iwaya<sup>1</sup>; Satoshi Kamiyama<sup>1</sup>; Hiroshi Amano<sup>1</sup>; Isamu Akasaki<sup>1</sup>;* <sup>1</sup>Meijo University, Center of Excellence-Nano Factory; <sup>2</sup>Corporate Research and Development Center, Showa-Denko K.K.

High structural quality AlN bridge layers were grown on linear trench patterned 6H-SiC substrates by high temperature MOVPE technique. Growth temperature was 1500°C. The bridge layer formation was uniform and the coalescence was smooth up to a substrate trench width of 7.52 μm. A combination of high temperature and V/III ratio modification ensured a better transverse movement of Al species and better control of coalescence and hence extremely low dislocation content AlN was achieved. Growth rate was 6 μm/h. No dislocations observed on either side of the coalescence front. The XRD omega rocking curve FWHM of symmetric (0002) and asymmetric (20-24) planes were 62 arcsec and 252 arcsec, respectively. The overall dislocation density of the AlN layer was in the order of 10<sup>6</sup> cm<sup>-2</sup> or less. A smooth step flow growth was confirmed by AFM analysis and the RMS index was 0.25 nm. The layers were crack free.

## 11:15 AM

**M2, High-Quality AlN Buffer Fabricated on Sapphire by NH<sub>3</sub> Pulse-Flow Multi-Layer Growth Method for Application to Deep UV-LEDs:** *Hideki Hirayama<sup>1</sup>; Tomoaki Ohashi<sup>1</sup>; Norihiko Kamata<sup>2</sup>;* <sup>1</sup>RIKEN; <sup>2</sup>Saitama University

We demonstrated high-quality AlN buffers on sapphire using ammonia pulse-flow multi-layer growth method by metal-organic chemical-vapor deposition (MOCVD), those are necessary for the achievement of 230-350 nm band high-brightness deep ultraviolet (UV) light-emitting diodes (LEDs) or laser diodes (LDs). We achieved crack-free, thick (3.3 μm) AlN buffer with low threading dislocation density (TDD) and atomically flat surface and with stable Ga (+c) polarity. The FWHM of XRD (102) ω-scan rocking curve was reduced from 2160 to 488 arcsec by introducing this method. The edge

# Technical Program

dislocation density of AlGa<sub>x</sub>N on AlN template were  $3.2 \times 10^9$  and  $3.5 \times 10^8$  cm<sup>-2</sup>, respectively. We confirmed atomically flat surface as step-flow mode observed from AFM images. We demonstrated single peaked operation of 250 nm AlGa<sub>x</sub>N-based deep UV-LEDs fabricated on the AlN templates and confirmed this method is quite useful for the application to deep UV emitting devices.

11:30 AM

**M3, Growth of Non-Polar Al<sub>x</sub>Ga<sub>1-x</sub>N/Al<sub>y</sub>Ga<sub>1-y</sub>N Multi Quantum Well Structures over m-SiC for the Fabrication of Light Emitting Devices:** R. S. Qhalid Fareed<sup>1</sup>; Balakrishnan Krishnan<sup>1</sup>; Bin Zhang<sup>1</sup>; Vinod Adivarahan<sup>1</sup>; Thomas Katona<sup>1</sup>; Asif Khan<sup>1</sup>; <sup>1</sup>Department of Electrical Engineering, University of South Carolina

Due to the absence of piezo-electric polarization fields, non-polar deep UV LEDs based on Al<sub>x</sub>Ga<sub>1-x</sub>N are expected to have superior performance. M-plane AlN and SiC substrates are natural substrate choices for their growth. We report the fabrication and characterization of Al<sub>x</sub>Ga<sub>1-x</sub>N layers and Multiple Quantum Wells (MQWs) over m-SiC with deep UV emission from 340 to 260 nm. Initial results of a systematic study of cathodo-photoluminescence, AFM and SEM analyses of these Al<sub>x</sub>Ga<sub>1-x</sub>N layers and MQWs are used to establish the feasibility of non-polar deep UV LEDs over bulk m-SiC substrates.

11:45 AM

**M4, MOVPE Growth of High Quality AlN Layers and Effects of Si Doping:** Sarad Thapa<sup>1</sup>; Ferdinand Scholz<sup>1</sup>; Joachim Hertkorn<sup>1</sup>; Guenther M. Prinz<sup>1</sup>; Martin Feneberg<sup>1</sup>; Klaus Thonke<sup>1</sup>; Rolf Sauer<sup>1</sup>; <sup>1</sup>Ulm University

By optimizing our MOVPE growth conditions, we have grown high quality AlN layers (rms surface roughness of 0.2 nm, HRXRD FWHM of the (002) and (104) reflections of 59 and 290 arcsec, respectively, and low temperature cathodoluminescence (CL) spectra with a FWHM of 10 meV with LO phonon replica). Further on, we studied the effects of Si incorporation on the structural and spectroscopic properties of AlN layers. Although we observed a deterioration in surface quality, much narrower HRXRD FWHM of the (002) reflection of our lightly Si doped samples could be obtained. These peaks got broader with increasing Si concentrations up to  $1 \times 10^{19}$  cm<sup>-3</sup>, decreasing again for even higher concentrations accompanied by the development of cracks. HRXRD, CL, and Raman scattering measurements show that the in-plane tensile stress of our Si-doped layers increases up to Si concentrations of  $1 \times 10^{19}$  cm<sup>-3</sup>, whereas a stress release is observed for higher concentrations.

12:00 PM

**M5, In situ Stress Measurements during Si-Doping of AlGa<sub>x</sub>N Grown by MOCVD:** Jeremy Acord<sup>1</sup>; Ian Manning<sup>1</sup>; Xiaojun Weng<sup>1</sup>; Elizabeth Dickey<sup>1</sup>; David Snyder<sup>1</sup>; Joan Redwing<sup>1</sup>; <sup>1</sup>Pennsylvania State University

Direct measurements of SiH<sub>4</sub> doping induced growth stress and dislocation bending during Al<sub>x</sub>Ga<sub>1-x</sub>N growth are presented. Prior literature demonstrated that threading edge and mixed dislocations in Al<sub>x</sub>Ga<sub>1-x</sub>N films bend near the Al<sub>y</sub>Ga<sub>1-y</sub>N (x≠y) buffer interface, leading to compressive stress relaxation and eventual tensile stress generation. This study explores SiH<sub>4</sub> doping effects on stress and dislocation evolution in Al<sub>x</sub>Ga<sub>1-x</sub>N investigated by in situ Multibeam Optical Stress Sensor (MOSS) measurements and post-growth cross-section Transmission Electron Microscopy (TEM). Lattice-mismatch induced compressive growth stress was measured in Al<sub>0.28</sub>Ga<sub>0.72</sub>N deposited on a ~85 nm AlN buffer layer on 6H-SiC. The growth stress discontinuously changed from compressive to tensile upon SiH<sub>4</sub> introduction, which increased in magnitude with film thickness. The projected dislocation inclination angle within the undoped Al<sub>0.28</sub>Ga<sub>0.72</sub>N was  $8.1 \pm 5.7^\circ$ , which increased to  $17.0 \pm 4.9^\circ$  when SiH<sub>4</sub> was introduced. These results provide direct evidence that Si-doping itself can induce dislocation bending leading to tensile stress generation.

12:15 PM

**M6, Nonpolar AIBN (11-20) and (1-100) Films Grown on SiC Substrates:** Tetsuya Akasaka<sup>1</sup>; Yasuyuki Kobayashi<sup>1</sup>; Toshiki Makimoto<sup>1</sup>; <sup>1</sup>NTT Basic Research Laboratories

We report the first-ever growth of nonpolar AIBN (11-20) and (1-100) films. The films were grown on SiC substrates by flow-rate modulation epitaxy (FME), wherein metalorganics and NH<sub>3</sub> were alternately supplied, and were systematically evaluated by high-resolution X-ray diffraction (HR-XRD), secondary ion mass spectroscopy (SIMS), and transmission electron

microscopy (TEM). Incorporation of boron atoms into AlN (11-20) and (1-100) films shifted the peak positions in HR-XRD  $\omega$ -2 $\theta$  scans to higher angles, indicating the formation of wurtzite AIBN (11-20) and (1-100) films, and the estimated boron concentration (~2%) by HR-XRD agreed well with SIMS results. TEM observations showed the wurtzite structure of an AIBN (11-20) film and the stacking fault density of  $1.6 \times 10^6$ /cm. We found that the (11-20) and (1-100) faces more effectively incorporate boron atoms into the wurtzite lattice sites than the conventional (0001) face, due to their characteristic bond configurations.

## Session N:

### High Voltage and Advanced Device Structures I

Tuesday AM  
September 18, 2007

Room: 314/315  
Location: MGM Grand Hotel Conference Center

Session Chairs: Asif Khan, University of South Carolina; Steven Ringel, Ohio State University

11:00 AM

**N1, Power AlGa<sub>x</sub>N/GaN HFETs with Excellent Vb/RonQgd for High Speed Switching:** Nariaki Ikeda<sup>1</sup>; Kazuo Kato<sup>1</sup>; Jiang Li<sup>1</sup>; Syusuke Kaya<sup>1</sup>; Takehiko Nomura<sup>1</sup>; Mitsuru Masuda<sup>1</sup>; Seikoh Yoshida<sup>1</sup>; <sup>1</sup>Furukawa Electric

In this paper, in order to confirm the advantage for the high-frequency switching operation of the GaN HFETs compared with Si devices, capacitance parameters and the figure of merit (FOM) Vb/(Ron Qgd) for a switching capability were examined. We furthermore examined the switching characteristics and capacitance parameters such as an input capacitance (Ciss), a reverse transfer capacitance (Crss), a gate to a source charge (Qgs) and a gate to a drain charge (Qgd) using the GaN HFET devices with large areas with the gate width of 240  $\mu$ m using a multi-layer structure. The maximum drain current of 55A was obtained, and the minimum on-resistance was less than 70mohm. The breakdown voltage was obtained about 800V. As a result, a low Ciss, Crss, and Qg were obtained and the FOMs of GaN HFETs have one order of magnitude larger than that of Si power devices.

11:15 AM

**N2, High Drain Current and Low Loss Normally-Off Mode AlGa<sub>x</sub>N/GaN Junction HFETs with p-Type GaN Gate:** Takahiro Fujii<sup>1</sup>; Shogo Nakamura<sup>1</sup>; Katsutoshi Mizuno<sup>1</sup>; Ryota Nega<sup>1</sup>; Mototaki Iwaya<sup>1</sup>; Satoshi Kamiyama<sup>1</sup>; Hiroshi Amano<sup>1</sup>; Isamu Akasaki<sup>1</sup>; <sup>1</sup>Meijo University

Normally-off-mode junction heterostructure FETs with p-type GaN gate showing high drain current and extremely large on/off ratio was successfully fabricated by MOVPE. After growing p-GaN:Mg/u-Al<sub>0.15</sub>Ga<sub>0.85</sub>N/u-GaN/LT-buffer/c-sapphire junction heterostructure, p-GaN:Mg except at the gate region was etched by RIE to expose u-AlGa<sub>x</sub>N barrier layer. The fabricated device had a gate length of 2 $\mu$ m, a gate width of 100 $\mu$ m, and an interval of 8 $\mu$ m between the drain and the source contacts. Drain current is found to be very sensitive to surface of u-AlGa<sub>x</sub>N barrier exposed by RIE etching. Reproducible and stable high drain current was achieved by very thin SiN passivation. Maximum drain current was  $1.58 \times 10^{-1}$  [A/mm] at V<sub>GS</sub>=4 [V], while the drain current at V<sub>GS</sub>=0[V] is as small as  $1.45 \times 10^{-8}$  [A/mm]. Therefore 7th orders of on/off ratio have been achieved. The sub-threshold swing was as small as 90 [mV/dec.]. The on resistance was 3.4 [m $\Omega$ cm<sup>2</sup>] and the threshold voltage was +0.45 [V].

11:30 AM

**N3, A Normally-Off Vertical Insulated Gate AlGa<sub>x</sub>N/GaN HFET:** Masakazu Kanechika<sup>1</sup>; Masahiro Sugimoto<sup>2</sup>; Narumasa Soejima<sup>1</sup>; Hiroyuki Ueda<sup>1</sup>; Osamu Ishiguro<sup>1</sup>; Masahito Kodama<sup>1</sup>; Eiko Hayashi<sup>1</sup>; Kenji Itoh<sup>1</sup>; Tsutomu Uesugi<sup>1</sup>; Tetsu Kachi<sup>1</sup>; <sup>1</sup>Toyota Central Research and Development Laboratories, Inc.; <sup>2</sup>Toyota Motor Corporation

We fabricated a vertical insulated gate AlGa<sub>x</sub>N/GaN heterojunction field effect transistor (HFET), using a free-standing GaN substrate. i-GaN/AlN/p-GaN/n-GaN was grown on an n-GaN substrate by MOCVD. The vertical

# Technical Program

current aperture was formed by dry-etching i-GaN/AlN/p-GaN with a mask, removing the mask, and re-growing AlGaIn/n-GaN. We measured the HFET with an active area of  $56.5 \mu\text{m} \times 40 \mu\text{m}$ . We have demonstrated that the HFET vertically operated with a threshold voltage of 1 V. The specific on-resistance was about  $50 \text{ m}\Omega\text{cm}^2$ . We have reduced the specific on-resistance by two orders, compared to the previous our work on the vertical HFET. This is due to the suppression of the Mg-diffusion to the heterojunction.

## 11:45 AM

**N4, Enhancement-Mode GaN Based Trench Gate MOSFETs:** *Hirota Otake*<sup>1</sup>; Shin Egami<sup>1</sup>; Hiroaki Ohta<sup>1</sup>; Yasushi Nanishi<sup>2</sup>; Hidemi Takasu<sup>1</sup>; <sup>1</sup>Rohm Co., Ltd.; <sup>2</sup>Ritsumeikan University

Metal oxide semiconductor field effect transistors (MOSFETs) with trench gate structures based on GaN have been developed for the first time. These MOSFETs show excellent enhancement-mode operation with moderate threshold voltage of 5.1 V and extremely high channel mobilities of  $133 \text{ cm}^2/\text{Vs}$ . The vertical structure including n-GaN/p-GaN/n-GaN layers is epitaxially grown on the sapphire substrate by conventional low-pressure MOVPE. The dry etching process is used for the formation of the trench structures, and double layered structures with SixNy and SiO<sub>2</sub> are continuously deposited for the gate insulator by electron cyclotron resonance plasma-assisted sputtering. SixNy is relatively thin, but strongly affects the stabilization of GaN surface. This structure enables us to realize vertical switching devices with high breakdown voltages and highly integrated low on-resistance with the usage of excellent physical parameters of GaN.

## 12:00 PM

**N5, Power Factor Correction Circuit Application Using AlGaIn/GaN HFETs:** *Seikoh Yoshida*<sup>1</sup>; Mitsuru Masuda<sup>1</sup>; Yuki Niiyama<sup>1</sup>; Hiroshi Kambayashi<sup>1</sup>; Takehiko Nomura<sup>1</sup>; Nariaki Ikeda<sup>1</sup>; <sup>1</sup>Furukawa Electric Company, Ltd.

We demonstrate the application of a power factor correction (PFC) circuit using AlGaIn/GaN HFETs for the first time. PFC circuits are important for a high efficiency power supply of homes and industries. The AlGaIn/GaN HFET with a large current and a high breakdown voltage operation was fabricated. That is, the maximum drain current was over 50 A, and the minimum on-resistance was less than 70 mohm. The breakdown voltage was over 600 V. Using these HFETs, an AC-DC converter with a power factor correction (PFC) circuit was fabricated. Irregular input AC current and voltage were converted to very smooth input sign waves AC voltage and current. The power factor was over 99%. Using this circuit, AC 100 V was successfully converted to DC 200 V. the output conversion efficiency from AC input to DC output was 93%. We thus demonstrated a good PFC circuit using AlGaIn/GaN HFETs.

## 12:15 PM

**N6, High Breakdown Voltage AlGaIn/GaN Heterojunction Field Effect Transistors on Sapphire Substrates:** *Junxia Shi*<sup>1</sup>; Y. C. Choi<sup>1</sup>; M. Pophristic<sup>2</sup>; M. G. Spencer<sup>1</sup>; L. F. Eastman<sup>1</sup>; <sup>1</sup>Cornell University; <sup>2</sup>Velox Semiconductor Corporation

AlGaIn/GaN heterojunction field effect transistors (HFETs) on sapphire substrates for high-power switching applications were fabricated using a self-align process. Without any additional field plate design, the fabricated devices with gate-drain spacing ( $L_{gd}$ ) of  $16 \mu\text{m}$  exhibited a high breakdown voltage (BV) of 1600 V with a specific on-resistance ( $AR_{on}$ ) of  $5.8 \text{ m}\Omega\text{-cm}^2$ . This result approaches the SiC theoretical limit. The BV- $AR_{on}$  performance showed a linear trend with variations of  $L_{gd}$ , indicating a predictable performance. In addition, the effects of the source and drain contact lengths  $L_s$  and  $L_d$  on  $AR_{on}$  have also been investigated and optimized.

## Session O:

### Sensors and Characterization II

Tuesday AM

September 18, 2007

Room: 312/317

Location: MGM Grand Hotel Conference Center

*Session Chairs:* Oliver Ambacher, Technische Universität Ilmenau; Michael Kneissl, Technical University of Berlin

## 11:00 AM

**O1, Analysis of Enzymatic Activity Using Functionalized AlGaIn/GaN Field-Effect Transistors:** *Barbara Baur*<sup>1</sup>; John Howgate<sup>1</sup>; Vedran Bandalo<sup>1</sup>; Wiebke Steins<sup>1</sup>; Martin Stutzmann<sup>1</sup>; Martin Eickhoff<sup>1</sup>; <sup>1</sup>Technische Universität München

Enzyme-modified field-effect transistors (EnFETs) were prepared by immobilisation of penicillinase on AlGaIn/GaN solution gate field-effect transistors. The stability of the transistor during operation in electrolyte solution and the influence of the immobilisation process on enzyme functionality have been investigated by a direct comparison of covalent immobilisation and physisorption. Covalent immobilisation by Schiff base formation on GaN surfaces modified with an aminopropyltriethoxysilane monolayer exhibits a high reproducibility with respect to the enzyme/substrate affinity. The stability of the enzyme layer is shown to be significantly increased by reductive amination of the Schiff base bonds. Further analysis was carried out with respect to the impact of environmental parameters on the sensor response. Buffer capacitance of the analyte restricts the dynamic measurement range, whereas the immobilisation process determines the response characteristics as well as stability and reproducibility of the sensor-signal. This conclusion is supported by modelling the potentiometric response of EnFETs based on penicillinase.

## 11:15 AM

**O2, Mechanism of Surface Current in the Vicinity of Schottky Gate Formed on AlGaIn/GaN Heterostructure:** *Junji Kotani*<sup>1</sup>; Masafumi Tajima<sup>1</sup>; Seiya Kasai<sup>1</sup>; Tamotsu Hashizume<sup>1</sup>; <sup>1</sup>Hokkaido University

We systematically characterized surface current in the vicinity of Schottky gates on the AlGaIn/GaN heterostructure, separating it from the normal leakage current through the Schottky interface. The MOVPE-grown Al<sub>0.27</sub>Ga<sub>0.73</sub>N/GaN heterostructure were used. In order to detect the lateral surface current ( $I_s$ ) separately from vertical current ( $I_v$ ), an additional Schottky gate was fabricated parallel to the main Schottky gate with a distance ( $L_{GG}$ ) of  $200\text{nm} \sim 5\mu\text{m}$ . The  $I_v$  was almost independent of  $L_{GG}$ , while the  $I_s$  drastically increased with decreasing  $L_{GG}$ . No temperature dependence observed in  $I_v$  is explained by the tunneling mechanism through thin Schottky barrier. On the other hand, clear temperature dependence appeared in  $I_s$ . It is likely that other transport mechanism, e.g., a variable-range-hopping conduction, governs the surface transport. The SiN<sub>x</sub>-based surface passivation drastically suppressed the surface current, indicating the surface states can play an important role for the surface transport from the gate edge.

## 11:30 AM

**O3, Effects of Temperature on Electrical Degradation of GaN High Electron Mobility Transistors:** *Jungwoo Joh*<sup>1</sup>; Jesús del Alamo<sup>1</sup>; <sup>1</sup>Massachusetts Institute of Technology

Although GaN high electron mobility transistors (HEMT) exhibit great performance in RF power applications, reliability is still a big concern in this technology. In order to improve reliability, it is essential to understand physical mechanisms behind device degradation. We have carried out stress experiments to understand the effects of temperature on reliability. We have found out that the critical voltage beyond which a device starts to degrade is reduced at high temperature. Our OFF state step stress experiments also show that catastrophic degradation starts at lower voltage at high temperature. These results are inconsistent with hot electrons related degradation mechanisms in that there would be much less hot electrons at high temperature due to enhanced phonon scattering. However, this can be understood with our

# Technical Program

previous hypothesis that device degradation results from crystallographic defect formation due to inverse piezoelectric effect as thermal energy can enhance defect formation.

11:45 AM

**O4, Fabrication and Characterization of m-Plane (1-100) GaN Based Metal-Oxide-Semiconductor Capacitors:** *Vinayak Tilak*<sup>1</sup>; Kevin Matocha<sup>1</sup>; Greg Dunne<sup>1</sup>; Greg Dunne<sup>1</sup>; <sup>1</sup>GE Global Research

M-plane (1-100) non-polar, Gallium Nitride(GaN) based metal-oxide-semiconductor (MOS) capacitors were fabricated by depositing low pressure chemical vapor deposition silicon dioxide at 900°C. No positive shift in the flat band voltage of m- plane GaN MOS capacitors was observed versus temperature, confirming the absence of pyroelectric effects. In contrast, C-plane (0001) polar, GaN MOS capacitors, show a positive flat band voltage shift versus temperature and the pyroelectric coefficient of  $-3 \times 10^9$  q/cm<sup>2</sup>K was measured. Smaller capacitance-voltage hysteresis was measured on m-plane GaN samples as compared to c-plane GaN samples, suggesting lower interface state density. Time dependent dielectric breakdown (TDDB) measurements are being performed and the results will be presented. We will also present results of Fowler-Nordheim tunneling measurements and estimate the conduction band offset between m-plane GaN and silicon dioxide.

12:00 PM

**O5, A Novel Anti-Stokes Raman Scattering Technique for the Direct Measurement of Hot-Phonons in AlGaIn/GaN Devices:** *James Pomeroy*<sup>1</sup>; Martin Kuball<sup>1</sup>; M. Uren<sup>2</sup>; T. Martin<sup>2</sup>; <sup>1</sup>University of Bristol; <sup>2</sup>QinetiQ Ltd

GaN-based transistors are at the forefront of next-generation high-power/frequency electronic devices. However, the role that so-called "hot-phonon" effects have on limiting their saturation velocity is not yet fully understood. Hot-phonon effects have been inferred from microwave noise-power measurements, although a direct method of probing hot phonons is preferable. We have used anti Stokes Raman scattering to measure hot-phonons in the active channel of AlGaIn/GaN HFETs, enabling their localisation and temperature to be studied. Complimentary electroluminescence (EL) measurements were used to estimate a hot-electron temperature of  $T_e \sim 1000$ K at 30V<sub>sd</sub> (24W/mm), implying a hot-phonon temperature of  $T_{ph} \sim 1000$ K, significantly above the 150°C lattice temperature derived from the Raman frequency shift. The temperature determined using the LO-phonon Stokes/anti-Stokes scattering ratio, including contributions from hot-phonons and thermal equilibrium phonons in the active channel and GaN layer, respectively, is 50°C higher than the measured lattice temperature at 30V<sub>sd</sub>, consistent with the value  $T_{ph} \sim 1000$ K.

12:15 PM

**O6, A Novel GaN-Based Multiparameter Sensor System for Biochemical Analysis:** *Benedikt Luebbbers*<sup>1</sup>; Gabriel Kittler<sup>1</sup>; Peter Ort<sup>1</sup>; Stefanie Linkohr<sup>1</sup>; Dennis Wegener<sup>2</sup>; Barbara Baur<sup>3</sup>; Michael Gebinoga<sup>4</sup>; Frank Weise<sup>4</sup>; Martin Eickhoff<sup>3</sup>; Oliver Ambacher<sup>1</sup>; <sup>1</sup>Technical University Ilmenau; <sup>2</sup>Institute for Physical High Technology Jena; <sup>3</sup>Technical University of Munich; <sup>4</sup>MacroNano®, Centre for Innovation Competence Ilmenau

GaN offers several advantages for the construction of biosensors due to its chemical stability and optical transparency. We present application examples of an AlGaIn/GaN-ISFET which exhibits an inherent pH-sensitivity close to the Nernstian limit and has a very fast response time. Combined with a picoliter dosing system, an integrated micro reference electrode and an optical spectroscopy system a novel multi parameter analysis system for aqueous solutions in the micro- to nanoliter range was constructed. Titration experiments as well as the simultaneous opto-electrochemical monitoring of enzymatic reactions and measurements with functionalized enzyme-FETs in very low volumes is shown. The experimental data obtained agrees well with reference measurements performed with state-of-the-art pH-meters and spectrophotometers in 100- to 1000-fold larger volumes. These measurements show the potential of the sensor for biochemical and pharmaceutical analysis e.g. in high-throughput screening of cancer drugs.

## Session P: MOVPE Growth of AlGaIn Alloys II

Tuesday PM  
September 18, 2007

Room: 314/315  
Location: MGM Grand Hotel Conference Center

*Session Chairs:* Kentaro Onabe, University of Tokyo; Andrew Allerman, Sandia National Laboratories

2:00 PM Invited

**P1, A Novel MOVPE System for the Growth of High-Quality Al<sub>x</sub>Ga<sub>1-x</sub>N Layers for Deep UV Emitters:** *R.S. Fareed*<sup>1</sup>; K. Balakrishnan<sup>1</sup>; V. Adivarahan<sup>1</sup>; Thomas Katona<sup>1</sup>; Asif Khan<sup>1</sup>; <sup>1</sup>University of South Carolina

We present a novel metalorganic hydride vapor epitaxy (MOVPE) approach for the growth of III-Nitride semiconductors. In this method, MOCVD and HVPE are done in the same chamber either simultaneously or sequentially in a single growth without breaking vacuum. The system is used for depositing the device structures on non-polar *r*-sapphire and *m*-SiC, and polar *c*-sapphire substrates. In addition, the viability of the system for depositing m-AlN buffer layers using pulsed MOCVD over *m*-SiC followed by 1μ thick m-AlN layer using HVPE is reported. Characterization data will be presented for these.

2:30 PM

**P2, Growth of High AlN Molar Fraction AlGaIn on Selective-Area-Growth GaN:** *Hideto Miyake*<sup>1</sup>; Norihiko Masuda<sup>1</sup>; Kazumasa Hiramatsu<sup>1</sup>; <sup>1</sup>Mie University

High-AlN-molar-fraction AlGaIn with low dislocation density was fabricated on selective-area-growth (SAG) GaN by low-pressure metalorganic vapor phase epitaxy (LP-MOVPE). To reduce threading dislocation (TD) density in the AlGaIn, SAG GaN was grown on AlN/sapphire template. The structure of SAG GaN was precisely controlled by in-situ reflection monitoring. AlGaIn growth was started before the coalescence of each SAG GaN to prevent crack generation during the subsequent AlGaIn growth. The TD density in the AlGaIn layer was  $1.3 \times 10^8$  cm<sup>-2</sup>, which is two orders of magnitude lower than that of conventional AlGaIn. The reduction of TD density is due to strain relaxation and the lateral overgrowth of AlGaIn using the SAG GaN structure.

2:45 PM

**P3, MOCVD Growth and Characterization of Al<sub>x</sub>Ga<sub>1-x</sub>N on GaN Substrates for Ultraviolet Avalanche Photodiodes:** Dongwon Yoo<sup>1</sup>; Jae Boum Limb<sup>1</sup>; Yun Zhang<sup>1</sup>; Jae-Hyun Ryou<sup>1</sup>; Shyh-Chiang Shen<sup>1</sup>; Meredith Reed<sup>2</sup>; Michael Wraback<sup>2</sup>; *Russell Dupuis*<sup>1</sup>; <sup>1</sup>Georgia Institute of Technology; <sup>2</sup>US Army Research Laboratory

AlGaIn *p-i-n* diode based wide-bandgap avalanche photodetectors (APDs) are excellent candidates for short-wavelength photodetection in the ultraviolet (UV) spectral region  $\lambda < 290$  nm. In this paper, we describe the growth and characterization of Al<sub>x</sub>Ga<sub>1-x</sub>N APDs, grown on bulk GaN substrates. To achieve improved material quality of Al<sub>x</sub>Ga<sub>1-x</sub>N, various growth parameters and schemes were studied including modulated-precursor epitaxial growth. To prevent the initiation and propagation of cracks, several strain management structure between the substrate and AlGaIn layer. We also report the performance characteristics of Al<sub>x</sub>Ga<sub>1-x</sub>N ( $x \sim 0.05$ ) *p-i-n* APD including 0.25 μm-thick unintentionally doped drift region. No microplasma or side-wall breakdown luminescence was visually observed. The avalanche gain reaches a maximum value of  $\sim 50$  at a voltage of 86.75V. Detailed growth and material characterization of Al<sub>x</sub>Ga<sub>1-x</sub>N *p-i-n* structures including TEM study and the performance of these APD devices including spectral response data will be reported.

## 3:00 PM

**P4, Critical Issue in Growing High Quality Thick AlGa<sub>N</sub> by High-Temperature MOVPE:** *Naofumi Kato*<sup>1</sup>; Takafumi Sumii<sup>1</sup>; Shuuya Sato<sup>1</sup>; Hiroki Sugimura<sup>1</sup>; Narihito Okada<sup>1</sup>; Masataka Imura<sup>1</sup>; Motoaki Iwaya<sup>1</sup>; Satoshi Kamiyama<sup>1</sup>; Hiroshi Amano<sup>1</sup>; Isamu Akasaki<sup>1</sup>; Hisaaki Maruyama<sup>2</sup>; Takashi Takagi<sup>2</sup>; Akira Bandoh<sup>3</sup>; <sup>1</sup>Meijo University; <sup>2</sup>Ceramic Operation, Ibiden Company, Limited; <sup>3</sup>Corporate R&D Center, Showa Denko K.K.

Growth of thick AlGa<sub>N</sub> on c-plane sapphire substrates was conducted by high-temperature (HT-) MOVPE. Composition of AlGa<sub>N</sub> can be controlled by growth temperature and by V/III ratio. The use of HT-AIN template extremely improves crystalline quality of the thick AlGa<sub>N</sub> layer. In addition, crystalline-quality measured by X-ray diffraction and TEM showed that the FWHMs of X-ray rocking curves (XRCs) for both tilt and twist distributions and dislocation density in AlGa<sub>N</sub> are almost the same as those in the underlying HT-AIN template for Al composition from 0.3 to 1. A thick and crack-free Al<sub>0.89</sub>Ga<sub>0.11</sub>N layer with the FWHMs of XRCs for tilt and twist distributions as narrow as 177 arcsec. and 457 arcsec., respectively, were successfully grown. Extremely smooth and atomic-size step with a RMS surface roughness as small as 0.35 nm over a 5 μm × 5 μm scan was observed. The microstructure of AlGa<sub>N</sub> on AIN will be discussed.

## 3:15 PM

**P5, AlGa<sub>N</sub> Distributed Bragg Reflectors in Comparison with Rugate Reflectors – Growth, Reflectivity, and Conductivity:** *Stephan Figge*<sup>1</sup>; Timo Aschenbrenner<sup>1</sup>; Heiko Dartsch<sup>1</sup>; Detlef Hommel<sup>1</sup>; <sup>1</sup>University of Bremen

Distributed Bragg Reflectors (DBR) are essential for the design of micro-cavity optoelectronic devices. Due to the small variation of refractive index in nitride materials at visible wave length a high composition modulation is needed to achieve reflectivity above 99%. The high aluminium content results into tensile strain and cracking of such layers. As the reflectance is determined by the first component of the Fourier-transform from the refractive index in general three different approaches are feasible: Step-wise variation of the refractive index (DBR), corrugated modulation (Rugate) or pulse width modulation of binary materials (needle technique). For similar reflectivity the Rugate structure has in comparison certain advantages such as lowest strain energy, no interfaces to be optimized, and no band offsets and therefore better vertical conductivity. In this presentation we will compare AlGa<sub>N</sub> DBRs with Rugate filters grown by MOVPE concerning growth, reflectivity and conductivity.

## 3:30 PM

**P6, Epitaxial Growth of Non-Polar AIN Films on m-ZnO Substrates:** *Kohei Ueno*<sup>1</sup>; Atsushi Kobayashi<sup>1</sup>; Jitsuo Ohta<sup>1</sup>; Hiroshi Fujioka<sup>1</sup>; Hidetaka Amanai<sup>2</sup>; Satoru Nagao<sup>2</sup>; Hideyoshi Horie<sup>2</sup>; <sup>1</sup>University of Tokyo; <sup>2</sup>Mitsubishi Chemical Group Science and Technology Research Center

We have grown *m*-plane AIN layers on *m*-plane ZnO substrates by pulsed laser deposition and investigated their structural properties. The direct growth of AIN on the ZnO substrates at 750°C has resulted in formation of polycrystalline materials due to serious interfacial reactions between AIN and ZnO. On the other hand, *m*-plane AIN has been epitaxially grown on the ZnO substrates by the use of GaN buffer layer grown at room temperature (RT). The FWHM value for AIN 1-100 XRC has turned out to be 468 arcsec. Grazing incidence angle x-ray reflectivity measurements have revealed that the heterointerface between AIN and RT-GaN is quite abrupt. XRD measurements have also revealed that the in-plane epitaxial relationship is <0001><sub>AIN</sub> || <0001><sub>GaN</sub> || <0001><sub>ZnO</sub>. These results indicate that the use of RT-GaN makes it possible to take full advantage of small lattice mismatches and wurtzite structure of ZnO substrates.

## 3:45 PM Break

## Session Q:

### High Voltage and Advanced Device Structures II

Tuesday PM

September 18, 2007

Room: 313/316

Location: MGM Grand Hotel Conference Center

*Session Chairs:* Vinayak Tilak, GE Global Research; Angela Rizzi, Georg-August-University of Goettingen

## 2:00 PM

**Q1, High Power and High Gain AlGa<sub>N</sub>/Ga<sub>N</sub> MIS-HEMTs with High-k Dielectric Layer:** *Masahito Kanamura*<sup>1</sup>; Toshihiro Ohki<sup>1</sup>; Kenji Imanishi<sup>1</sup>; Kozo Makiyama<sup>1</sup>; Naoya Okamoto<sup>1</sup>; Toshihide Kikkawa<sup>1</sup>; Naoki Hara<sup>2</sup>; Kazukiyo Joshin<sup>1</sup>; <sup>1</sup>Fujitsu Laboratories Ltd. and Fujitsu Limited; <sup>2</sup>Fujitsu Laboratories Ltd.

In this paper, we report on the fabrication of the Ga<sub>N</sub> MIS-HEMTs on the SiC substrates using the high-k Ta<sub>2</sub>O<sub>5</sub> dielectric gate insulator for the first time. The fabricated MIS-HEMTs showed the small current collapse, the large transconductance of 200 mS/mm and very low gate-leakage current with a high breakdown voltage of 400 V. We carried out on-wafer load-pull measurements for the 1 mm devices. The devices showed an output power of 9.4 W/mm and a linear gain of 23.5 dB associated with a PAE of 62% at V<sub>ds</sub> of 70 V at 2 GHz. In addition, both a high output power over 100 W and a high gain of 16 dB were successfully achieved at 2.5 GHz for the large periphery MIS-HEMTs amplifier. We also investigated the RF power stability for the devices. This work is partially supported by the Ministry of Internal Affairs and Communications, Japan.

## 2:15 PM

**Q2, Normally-Off AlGa<sub>N</sub>/Ga<sub>N</sub> MOSFETs with HfO<sub>2</sub> Gate Oxide:** *Shun Sugiura*<sup>1</sup>; Shigeru Kishimoto<sup>2</sup>; Takashi Mizutani<sup>1</sup>; Masayuki Kuroda<sup>3</sup>; Tetsuzo Ueda<sup>3</sup>; Tsuyoshi Tanaka<sup>3</sup>; <sup>1</sup>Nagoya University, Department of Quantum Engineering; <sup>2</sup>Nagoya University, Department of Quantum Engineering and Venture Business Laboratory; <sup>3</sup>Semiconductor Device Research Center Semiconductor Company Matsushita Electric Industrial Company, Ltd.

Normally-off Ga<sub>N</sub> MOSFETs are expected to be suitable for high-power switching systems. However, they suffer from problems of a small drain current and a small transconductance ( $g_m$ ) because of a large parasitic resistance and a small gate input capacitance. In this report, we have fabricated normally-off AlGa<sub>N</sub>/Ga<sub>N</sub> MOSFETs with overlap gate structure using HfO<sub>2</sub> with a large dielectric constant as a gate oxide. The HfO<sub>2</sub> thickness and the channel length were 100 nm and 2.5 μm, respectively. The normally-off operation with a threshold voltage of about 3 V was confirmed. The maximum transconductance was as large as 185 mS/mm and the drain current was 730 mA/mm at a gate voltage of 10 V. These results confirm the validity of the present MOSFET structure using HfO<sub>2</sub> as a gate oxide for high-power switching systems.

## 2:30 PM

**Q3, Gate Insulation and Current Collapse Suppression in InAlN/GaN HEMTs Using High-k Dielectrics:** *Jan Kuzmik*<sup>1</sup>; G. Pozzovivo<sup>1</sup>; Stephan Abermann<sup>1</sup>; J.-F. Carlin<sup>2</sup>; M. Gonschorek<sup>2</sup>; Karol Cico<sup>3</sup>; K. Fröhlich<sup>3</sup>; N. Grandjean<sup>2</sup>; E. Bertagnolli<sup>1</sup>; G. Strasser<sup>1</sup>; D. Pogany<sup>1</sup>; <sup>1</sup>Technical University Vienna; <sup>2</sup>EPFL Lausanne; <sup>3</sup>Slovak Academy of Science, Institute of Electrical Engineering

We investigate ZrO<sub>2</sub>, HfO<sub>2</sub> and stack of ZrO<sub>2</sub>/Al<sub>2</sub>O<sub>3</sub> as high-k dielectrics for the InAlN/GaN MOS HEMT gate insulation and surface passivation. HEMT gate geometry is 2 x 100 mic<sup>2</sup>, the source-drain spacing is 8 mic. Schottky contact-based HEMTs are prepared as a reference. The current collapse phenomenon is analyzed by pulsing the gate electrode (100 ns duration of pulses) from the base level of -10 V while keeping a constant drain bias (up-to 20 V). Results show that the gate leakage current is suppressed by 4-5 orders of magnitude by inserting the high-k dielectric. The maximal drain current of MOS HEMTs is increased to 0.9 A/mm, from 0.7 A/mm for the conventional HEMT while MOS HEMT transconductance is about the same

# Technical Program

or even increased (for ZrO<sub>2</sub>) if compared with the reference sample. We demonstrate an elimination of the current collapse after applying the high-k insulation/passivation. Ultragan project no.6903 is acknowledged.

2:45 PM

**Q4, Atomic Layer Etching of AlGaIn/GaN Structures:** *Xu Zhao*<sup>1</sup>; Jinwook Chung<sup>1</sup>; Tomas Palacios<sup>1</sup>; <sup>1</sup>Massachusetts Institute of Technology

GaN is one of the best candidates for high frequency and high power electronics. However, up to now, no reliable gate recess etching techniques have been reported. With device shrinking down to nanometer scale, an etching technique with atomic depth resolution is required. In this paper, atomic layer etching (ALE) of AlGaIn/GaN structures is demonstrated for the first time. The etching cycle of this new technology is divided into three basic steps: first, Cl<sub>2</sub> is adsorbed on the nitride surface; then the excess Cl<sub>2</sub> is removed from the etching chamber; and finally the remaining Cl<sub>2</sub> is activated by a low energy Ar plasma. The etch depth of each etching cycle is exactly 1 atomic monolayer which assures an excellent uniformity and control. No increase in the surface roughness has been observed after more than 200 etching cycles. All these properties make ALE very promising as AlGaIn/GaN gate recess technology.

3:00 PM

**Q5, Operation Robustness of AlGaIn/GaN HEMTs with an Ultrathin-Al-Layer Based Surface Control:** *Masafumi Tajima*<sup>1</sup>; Alberto Basile<sup>1</sup>; Junji Kotani<sup>1</sup>; Tamotsu Hashizume<sup>1</sup>; <sup>1</sup>RCIQE, Hokkaido University

The surface control process utilizing an ultrathin Al layer was proposed for the operation robustness of AlGaIn/GaN HEMTs. The process consists of the treatment of the AlGaIn surface using rf-excited nitrogen radicals, the deposition of an ultrathin Al layer, in situ UHV anneal at 700°C and the removal of the Al layer. The Schottky gate with the surface process showed a significant reduction of leakage current and clear temperature dependence of the I-V characteristics. For the HEMT without the surface control, the bias/temperature stress under the off-state condition brought the pronounced decrease in the drain conductance. On the other hand, no degradation appeared in the DC characteristics for the HEMT with the surface process even after the stress. The surface control process may effectively suppress the VN- and/or oxygen-related electronic levels at the AlGaIn surface, thereby preventing the multiplication of surface states during the stress.

3:15 PM

**Q6, In-Situ Passivation Combined with GaN Buffer Optimization for Extremely Low Current Dispersion and Low Gate Leakage in Si<sub>3</sub>N<sub>4</sub>/AlGaIn/GaN HEMT Devices on Si(111):** *Marianne Germain*<sup>1</sup>; Stefan Degroote<sup>1</sup>; Joff Derluyn<sup>1</sup>; Maarten Leys<sup>1</sup>; Kai Cheng<sup>2</sup>; Jo Das<sup>1</sup>; Anne Lorenz<sup>2</sup>; Marleen Van Hove<sup>1</sup>; Denis Marcon<sup>1</sup>; DongPing Xiao<sup>2</sup>; Gustaav Borghs<sup>1</sup>; <sup>1</sup>IMEC; <sup>2</sup>ESAT Katholieke Universiteit Leuven

Si substrate is the sole route towards III-nitrides process on large wafer diameter: flat (R<sub>z</sub>≥90m), crack-free HEMT epiwafers have been grown by MOVPE with diameter up to 150mm, exhibiting low sheet resistivity (260Ω/sq.) and high uniformity (≤2%), thanks to in-situ Si<sub>3</sub>N<sub>4</sub> capping. We show here that simultaneous optimization of GaN growth and of device passivation, results in a drastic reduction of buffer and surface traps impact onto device performance, assessed by pulse IV measurements. Drain lag is correlated with the appearance of deep defect-related peaks in photoluminescence spectra (6K), and completely eliminated by tuning growth temperature (ρ<sub>GaN</sub>≥10<sup>6</sup>Ω.cm). Gate formation (Ni/Au) onto MOVPE-grown Si<sub>3</sub>N<sub>4</sub>, followed by cleaning and PECVD ex-situ passivation, leads to very low gate current dispersion, associated to gate leakage current in μA/mm range. Both dc and pulsed characteristics show a current density in the order of 0.8-1A/mm, whereas maximal transconductance is 250mS/mm (L<sub>g</sub>=1μm).

3:30 PM Break

## Session R:

### Optical Characterization of Lasers

Tuesday PM

September 18, 2007

Room: 312/317

Location: MGM Grand Hotel Conference Center

*Session Chairs:* Daniel Cohen, University of California, Santa Barbara; Detlef Hommel, University of Bremen

2:00 PM

**R1, Comparison of GaInN Laser Structures Grown on Different Substrates:** *Alexander Dräger*<sup>1</sup>; Daniel Fuhrmann<sup>1</sup>; Carsten Netzel<sup>1</sup>; Uwe Rossow<sup>1</sup>; David Schenk<sup>2</sup>; Andreas Hangleiter<sup>1</sup>; <sup>1</sup>TU Braunschweig; <sup>2</sup>CNRS-CRHEA

In order to get a better understanding of the influence of different substrates on nitride laser diodes we performed optical gain spectroscopy using the variable stripe length (VSL) technique on laser structures grown by MOVPE, in order to assess the effects of nonradiative recombination. We compare samples grown on sapphire, SiC, low dislocation density GaN templates, and free-standing GaN substrates. From the analysis of the gain spectra we obtain the radiative and nonradiative carrier lifetimes and find that for samples on free-standing GaN the nonradiative carrier lifetime is one order of magnitude higher than for samples grown on sapphire or SiC and even higher than the radiative carrier lifetime. Thus, the threshold current density is hardly affected by the dislocations at such low dislocation densities.

2:15 PM

**R2, Wafer-Level Far Field Measurement of Blue Nitride Lasers:** *Dmitry Sizov*<sup>1</sup>; Rajaram Bhat<sup>1</sup>; Jerome Napierala<sup>1</sup>; Jingqun Xi<sup>1</sup>; Herve LeBlanc<sup>1</sup>; Donald Allen<sup>1</sup>; Chung-En Zah<sup>1</sup>; <sup>1</sup>Corning Incorporated

We have developed a new wafer-level laser test (WLT) method to measure far field patterns (FFPs) for lasers on a transparent substrate based on the scattered light collection from the bottom of substrate. The advantage of this method is that it requires less equipment resources as compared with other WLTs and needs only a CCD camera to determine FFPs by analyzing the image formed by the scattered lasing light. This avoids the Lloyds mirror reflection effect of the wafer surface. The images are analyzed using quasi-geometrical optics and characteristic matrix approach. Horizontal FFPs of 400-440 nm InGaIn lasers were determined with angular accuracy better than 1 degree. The lateral mode structure dependence on operating current and geometrical stripe widths was revealed. This method is helpful for both crystal growth and fabrication development and could be used in any other semiconductor system where the substrate is transparent at lasing emission wavelength.

2:30 PM

**R3, Non-Radiative Recombination Centers in InGaIn Lasers:** *Marc Schillgalies*<sup>1</sup>; Ansgar Laubsch<sup>1</sup>; Stephan Lutgen<sup>1</sup>; Adrian Avramescu<sup>1</sup>; Georg Brüderl<sup>1</sup>; Desiree Queren<sup>1</sup>; Uwe Strauß<sup>1</sup>; <sup>1</sup>OSRAM Opto Semiconductors GmbH

The analysis of electroluminescence intensity as a function of current density was used as feedback tool to reduce non-radiative recombination centers (NRC) in InGaIn-lasers. The influence of indium content of InGaIn-barriers on the NRC density, as well as the influence of a contamination of the quantum well, e.g. by magnesium, was studied in detail. The reduction of non-radiative recombination led to an improvement of laser performance. We report a threshold current density of 1.4 kA/cm<sup>2</sup> and a slope efficiency of 1.1W/A for a 10μm wide ridge-waveguide (RWG)-laser at 432nm.

2:45 PM

**R4, Inhomogeneously Broadened Optical Gain Spectra of InGaIn Quantum Well Laser Diodes:** *Kazunobu Kojima*<sup>1</sup>; Mitsuru Funato<sup>1</sup>; Yoichi Kawakami<sup>1</sup>; Harald Braun<sup>2</sup>; Ulrich Schwarz<sup>2</sup>; Shinichi Nagahama<sup>2</sup>; Takashi Mukai<sup>3</sup>; <sup>1</sup>Kyoto University; <sup>2</sup>Regensburg University; <sup>3</sup>Nichia Corporation

Optical gain spectra of near-UV, violet, blue and aquamarine InGaIn laser diodes, oscillating at 375, 407, 440, and 470 nm, respectively, are

## Session S: Quantum Dots: Characterization

Tuesday PM Room: 314/315  
September 18, 2007 Location: MGM Grand Hotel Conference Center

*Session Chairs:* Bernard Gil, National Center for Scientific Research, France; Michael Wraback, U.S. Army Research Laboratory

obtained under electrically driven condition. The near-UV and violet lasers, whose inhomogeneous broadening factors are less than or comparable with homogeneous ones, show a superlinear and linear behavior for their maximum mode gains, respectively, while the blue and aquamarine diodes with high inhomogeneous values are sublinear. Furthermore, against our expectations, longer laser diodes reveal higher mode gain below 1 kA/cm<sup>2</sup> of injected current density. Explaining this fact, two different gain models are compared; one assumes globally constant carrier density in quantum well, and the other model is based on global constant quasi-Fermi levels for both electrons and holes. The latter model predicts in agreement with the higher gain at low carrier densities for laser diodes with low inhomogeneous broadening factors.

### 3:00 PM

**R5, Laser Threshold and Optical Gain of Blue Optically Pumped InGaN/GaN MQWs Grown on Si:** E.V. Lutsenko<sup>1</sup>; A.V. Danilchuk<sup>1</sup>; N.P. Tarasuk<sup>1</sup>; V.N. Pavlovskii<sup>1</sup>; A.L. Gurskii<sup>1</sup>; G.P. Yablonskii<sup>1</sup>; H. Kalisch<sup>2</sup>; R.H. Jansen<sup>2</sup>; Y. Dikme<sup>3</sup>; B. Schineller<sup>3</sup>; M. Heuken<sup>3</sup>; <sup>1</sup>National Academy of Sciences of Belarus; <sup>2</sup>RWTH Aachen; <sup>3</sup>AIXTRON AG

Optical and laser properties of a series of MQW heterostructures grown on silicon with Al predeposition were investigated. Photoluminescence (PL) band positions covered a spectral range of 430 – 460 nm under  $I_{\text{exc}}=1$  MW/cm<sup>2</sup> and 445-505 nm under  $I_{\text{exc}}=0.15$  W/cm<sup>2</sup>. Lasing was achieved under transversal optical pumping at room temperature using only cleaved lateral facets of the samples as mirrors. The laser threshold rose monotonically from 137 kW/cm<sup>2</sup> to 300 kW/cm<sup>2</sup> with a laser wavelength increase from 440 nm to 465 nm. A numerical simulation of the laser conditions shows that the minimal threshold is realized on the fifth order mode. However, the calculated value of material optical gain of InGaN at the threshold neglecting the additional internal losses increases only from 750 cm<sup>-1</sup> to 1020 cm<sup>-1</sup>, mainly due to an absorption rise in the substrate with increasing wavelength. A correlation was observed between PL characteristics and laser threshold.

### 3:15 PM

**R6, Comparison of Scanning  $\mu$ -Electro- and  $\mu$ -Photo-Luminescence Spectroscopy of Blue InGaN LEDs on Si(001) and Si(111):** Lars Reissmann<sup>1</sup>; Fabian Schulze<sup>1</sup>; Armin Dadgar<sup>1</sup>; Jürgen Christen<sup>1</sup>; Alois Krost<sup>1</sup>; <sup>1</sup>OvG University Magdeburg

We report on scanning micro-electroluminescence ( $\mu$ -EL) and micro-photoluminescence ( $\mu$ -PL) spectroscopy measurements on LEDs on Si(001) and Si(111) substrate. Both,  $\mu$ -EL and  $\mu$ -PL were performed in the same setup. For PL excitation, the 324 nm line of a He-Cd-laser was used. The LEDs were driven by constant currents of up to 200 mA. During measurements, the identical surface areas were scanned. For the LED grown on Si(001), the PL-peak wavelength is blue-shifted compared to the EL-peaks. The positions of the extrema of FP-interferences also shift, evidencing change of refractive index with injection current. With increasing currents the EL-peak further red-shifts indicating heating. While PL peak wavelength randomly fluctuates, significant large domains of identical EL peak wavelength of 30-50  $\mu$ m size appear under current injection (50mA). Obviously the effect of local In-fluctuation becomes extinguished by the high carrier densities injected. An LED on Si(111) used as reference also shows blue-shifted PL-peak wavelength.

### 3:30 PM Break

### 4:00 PM

**S1, Excitonic Structure of Single Polar Stranski-Krastanov GaN/AlN Quantum Dots:** Dobri Simeonov<sup>1</sup>; Amelie Dussaigne<sup>1</sup>; Raphael Butté<sup>1</sup>; Nicolas Grandjean<sup>1</sup>; <sup>1</sup>École Polytechnique Fédérale de Lausanne (EPFL)

The optical properties of single GaN/AlN quantum dots (QDs) have attracted much attention but thorough spectroscopic studies are usually limited by the large QD density as well as by the spectral diffusion. Here we report a study on single polar Stranski-Krastanov GaN/AlN QDs grown by molecular beam epitaxy. Growth conditions promoting low density and large dispersion size have been used. 200 nm circular mesas have been etched allowing single dot to be isolated. Low temperature microphotoluminescence studies have been performed. The typical linewidth of single dot PL peaks is around 1 meV while the narrowest is about 700  $\mu$ eV, the lowest linewidth reported so far for polar GaN/AlN QDs. Biexciton emission was equally observed with binding energy of  $\sim 3$  meV, as well as excited states. An exhaustive study of the dot behavior on temperature, power and polarization will give more insights on the physics operating in such systems.

### 4:15 PM

**S2, Linear Polarization of the Emission of a Single Polar GaN/AlN Quantum Dot:** Richard Bardoux<sup>1</sup>; Thierry Guillet<sup>1</sup>; Pierre Lefebvre<sup>1</sup>; Thierry Taliercio<sup>1</sup>; Thierry Bretagnon<sup>1</sup>; Bernard Gil<sup>1</sup>; Fabrice Semond<sup>2</sup>; <sup>1</sup>Groupe d'étude des semiconducteurs; <sup>2</sup>Centre de Recherche pour l'Hétéro-Epitaxie et ses Applications - CNRS

We report on polarization-resolved micro-photoluminescence experiments performed on a single GaN/AlN polar quantum dot (QD) grown on Si(111) substrate. We have performed a systematic study of about 50 QDs. The emission of about half of the QD excitons is strongly linearly polarized, up to 90%. Such a polarization is known to be the signature of the asymmetry of the QD shape, which lifts the degeneracy of the optically active excitons. However in the case of our GaN QDs, the polarization angles are widely distributed and do not follow the crystallographic axes, and the sharp transition lines of each QD do not appear as doublets of cross-polarized peaks. The fine structure of GaN QD excitons therefore presents strong differences with the well understood one of InAs and CdTe QDs.

### 4:30 PM

**S3, Spatially Resolved Luminescence Spectroscopy of Single GaN/(Al,Ga)N Quantum Disks:** Uwe Jahn<sup>1</sup>; Jelena Ristic<sup>2</sup>; Enrique Calleja Pardo<sup>3</sup>; <sup>1</sup>Paul-Drude-Institut für Festkörperelektronik; <sup>2</sup>EPFL-SB-IPEQ-LOEQ; <sup>3</sup>ETSI Telecomunicacion, Universidad Politecnica

Using spatially resolved cathodoluminescence, we have measured the spectral and spatial distribution of the luminescence intensity of GaN/(Al,Ga)N nanocolumns containing GaN quantum disks grown by plasma-assisted MBE on a Si(111) substrate. The full width at half maximum of the luminescence line of the quantum disks is as large as 130 meV even for single nanocolumns. This broadening, which is about four times larger as compared with corresponding quantum wells, can be partly caused by inherent optical properties of such mesoscopic structures due to a laterally inhomogeneous distribution of strain. This strain distribution depends on the geometrical conditions, in particular, on the ratio of the diameter and the thickness of the disks. Therefore, the strain distribution can counteract the advantage of a defect-free growth of nanocolumns, i. e., a proper choice of thickness and diameter of the disk is important for the employment of such columnar heterostructures in optoelectronic-device applications.

# Technical Program

4:45 PM

**S4, Spectrally Resolved Cathodoluminescence Microscopy of InGaN Nanostructures Formed on Hexagonal GaN Pyramids:** *Juergen Christen<sup>1</sup>; Frank Bertram<sup>1</sup>; Sebastian Metzner<sup>1</sup>; Barbara Bastek<sup>1</sup>; Alexander Franke<sup>1</sup>; Michael Jetter<sup>2</sup>; T. Tsiotis<sup>2</sup>; P. Michler<sup>2</sup>;* <sup>1</sup>University Magdeburg; <sup>2</sup>Institut fuer Halbleitertechnik und Funktionelle Grenzflaechen

Hexagonal GaN pyramids were selectively overgrown by an InGaN single quantum well followed by a GaN caplayer to form a quantum dot. Although the InGaN dots were grown on GaN pyramids with micrometer size, nanostructures were formed on the top. The averaged cathodoluminescence (CL) spectrum exhibits an intense (D0,X) line from the GaN and a broad luminescence band between 2.0–2.6eV from the InGaN. The spectral position of the GaN luminescence systematically blue-shifts from base to top of the pyramid by about 25meV due to strain relaxation and impurity incorporation. The CL from the InGaN nanostructures exclusively exists at the pyramids, systematically changing its spectral position along the pyramid: while at the pyramids base the emission is observed at 2.310eV, the peak monotonously shifts to higher energies eventually reaching 2.48eV at the very top of the pyramid indicating a thinner quantum well and/or lower [In] at the tip.

5:00 PM

**S5, Temperature Dependence of the E2h Phonon Mode in Wurtzite GaN/AlN Quantum Dots:** *Jorge Budagosky<sup>1</sup>; Ana Cros<sup>1</sup>; Alberto Garcia-Cristóbal<sup>1</sup>; Andrés Cantarero<sup>1</sup>; Bruno Daudin<sup>2</sup>;* <sup>1</sup>ICMUV-University of Valencia; <sup>2</sup>CEA-Grenoble

The temperature dependence of phonon frequencies in semiconductors is commonly described in terms of a combination of anharmonic processes (two and three phonon decay) and thermal expansion effects. Concerning the E2h phonon mode, anharmonic effects in bulk AlN are dominated by two phonon decay channels; in bulk GaN, interestingly, three phonon decay channels are allowed. Our goal in this work is to analyze the influence of confinement on the phonon decay channels of GaN/AlN-QDs. By means of Raman scattering, we investigate the temperature dependence of the E2h phonon mode from 88 to 650 K. For the analysis of the experimental data it is necessary to take into account the thermal mismatch between the dot and the AlN spacer, as well as phonon anharmonic effects. It is found that the changes induced by confinement in the phonon dispersion are not enough to introduce new decay channels in the phonon recombination process.

5:15 PM

S6, Late News

## Session T:

### Nonpolar and Semipolar Materials and Devices I

Tuesday PM

Room: 313/316

September 18, 2007

Location: MGM Grand Hotel Conference Center

*Session Chairs:* Paul Fini, Inlustra, Inc.; Holger Grahn, Paul Drude Institute for Solid State Electronics

4:00 PM Invited

**T1, Growth and Properties of Non-Polar Nitrides on Various Substrates:** *Hiroshi Amano<sup>1</sup>; Daisuke Iida<sup>1</sup>; Takeshi Kawashima<sup>1</sup>; Motoaki Iwaya<sup>1</sup>; Satoshi Kamiyama<sup>1</sup>; Isamu Akasaki<sup>1</sup>;* <sup>1</sup>Meijo University

Nonpolar GaN grown on lattice mismatched substrates is rich in microstructures such as dislocations, stacking faults and inversion domains. These defects induce nonradiative recombination centers thereby affecting the efficiency of the fabricated light-emitting diodes. One-sidewall-seeded epitaxial lateral overgrowth on different substrates is found to be effective to reduce the density of threading dislocations and stacking faults and to realize low cost fabrication of LEDs. The mobility of electrons in n-type GaN:Si is improved by reducing the defect density. In comparison, conductivity control of p-type nonpolar GaN is much more feasible compared with that of c-plane GaN. A GaInN/GaN multi-quantum-well structure can be successfully

grown on low-dislocation-density nonpolar GaN. The performance of the visible LEDs fabricated on nonpolar GaN was characterized. The reduction of defects is found to be essential for the improvement of the efficiency of visible nonpolar LEDs.

4:30 PM

**T2, Improved Electroluminescence on m-Plane InGaN LEDs:** *Mathew Schmidt<sup>1</sup>; Kwang-Choong Kim<sup>1</sup>; Zhongyuan Jia<sup>1</sup>; Hitoshi Sato<sup>1</sup>; Natalie Fellows<sup>1</sup>; Hisashi Masui<sup>1</sup>; Makoto Saito<sup>1</sup>; Kenji Fujito<sup>2</sup>; Shuji Nakamura<sup>1</sup>; Steven DenBaars<sup>1</sup>; James Speck<sup>1</sup>;* <sup>1</sup>University of California, Santa Barbara; <sup>2</sup>Mitsubishi Chemical Corporation

We report on the growth and fabrication of high power and high efficiency nonpolar m-plane GaN light emitting diodes (LEDs) grown by metal organic chemical vapor deposition (MOCVD) on low defect density bulk m-plane GaN substrates. Several growths were performed to optimize the multiple quantum well (MQW) structure, such as varying the number of wells, well thickness, barrier thickness, and growth temperature. The processed LEDs were diced and packaged using both a standard epoxy technique and an advanced optic for high light extraction efficiency. Both DC and pulsed testing were performed. Quantum well thicknesses of up to 20 nm showed good performance, which has never been observed on c-plane devices. Using an advanced optic and under pulsed testing (1% duty cycle), 28 mW and an external quantum efficiency (EQE) of 45.4% was achieved at 20 mA drive current and a peak emission wavelength of 402 nm.

4:45 PM

**T3, Mg Doping of m-Plane and c-Plane GaN in MOCVD Growth Conditions:** *John Northrup<sup>1</sup>;* <sup>1</sup>Palo Alto Research Center

The m-plane is now receiving attention as a possible substrate for growth of nitride-based optoelectronic devices because of the absence of polarization fields in quantum wells grown on this surface. An important question is how the doping efficiency on the m-plane compares with dopant incorporation on other surfaces, such as the c-plane. This issue has been investigated for the case of Mg, which dopes GaN p-type by substituting for Ga. First principles calculations of formation energies for Mg on these surfaces in conditions corresponding to MOCVD growth indicate that there is an advantage to growth on the m-plane: Under the same growth conditions the formation energy of surface MgGa complexes is lower on the m-plane in comparison to the c-plane. The origin of this difference in stability will be discussed.

5:00 PM

**T4, Sidewall Epitaxial Lateral Overgrowth of Nonpolar GaN by Metalorganic Vapor Phase Epitaxy:** *Daisuke Iida<sup>1</sup>; Takeshi Kawashima<sup>1</sup>; Motoaki Iwaya<sup>1</sup>; Satoshi Kamiyama<sup>1</sup>; Hiroshi Amano<sup>1</sup>; Isamu Akasaki<sup>1</sup>;* <sup>1</sup>Meijo University

Major obstacles to achieving high-performance devices using nonpolar a-plane and m-plane GaN are very high density threading dislocations and stacking faults. Low-defect-density nonpolar plane GaN films were successfully grown by sidewall epitaxial lateral overgrowth (SELO) using metalorganic vapor phase epitaxy (MOVPE). In this study, we control the growth rate ratio of Ga-polar GaN to N-polar GaN by controlling the V/III ratio and temperature during growth. Control of the V/III ratio is found to be very important in achieving the growth of GaN from only one c-plane sidewall. It was possible to grow GaN only from N-face sidewall of the grooves by maintaining a high V/III ratio, which reduces the number of coalescence regions on grooves and decreases threading dislocation density and stacking fault density. Therefore, we can achieve one-side seeded epitaxial lateral overgrowth (OSELO).

5:15 PM

**T5, Defect-Mediated Surface Morphology of Nonpolar m-Plane GaN:** *Asako Hirai<sup>1</sup>; Benjamin Haskell<sup>1</sup>; Melvin McLaurin<sup>1</sup>; Feng Wu<sup>1</sup>; Steven DenBaars<sup>1</sup>; Shuji Nakamura<sup>1</sup>; James Speck<sup>1</sup>;* <sup>1</sup>University of California, Santa Barbara

The role of extended defects in determining the atomic scale surface morphology of nonpolar {1-100} m-plane gallium nitride has been elucidated. The heteroepitaxially grown m-GaN films are commonly reported to yield striated surface morphologies (slate morphology) correlated with their high

densities of basal plane stacking faults (SF). Here, the growth window was explored to allow non-slate morphologies for hydride vapor phase epitaxy. Lateral epitaxial overgrowth with the stripe orientations parallel to the [11-20] a-direction was then utilized to produce m-GaN films with three regimes of different extended defect contents, i.e., both threading dislocations (TDs) and SFs on window regions, only SFs on N-face wing regions, and neither TDs nor SFs on Ga-face wing regions. We have found that the elimination of SFs from the m-GaN yielded step-flow features with an average step height of 4 – 7 monolayers even for slate morphology growth conditions.

---

## Session U: Optical Characterization of LEDs

Tuesday PM                      Room: 312/317  
September 18, 2007              Location: MGM Grand Hotel Conference Center

*Session Chairs:* Peter Parbrook, University of Sheffield; Michael Krames, Philips Lumileds Lighting

---

### 4:00 PM

**U1, Quantum-Confined Stark Effects in Nonpolar m-Plane In<sub>0.15</sub>Ga<sub>0.85</sub>N/GaN Multiple Quantum Well Light-Emitting Diodes Fabricated on Low Defect Density Free-Standing Substrates:** *Takeyoshi Onuma<sup>1</sup>; Hiroaki Amaike<sup>1</sup>; Masashi Kubota<sup>2</sup>; Kuniyoshi Okamoto<sup>3</sup>; Hiroaki Ohta<sup>3</sup>; Jun Ichihara<sup>3</sup>; Hidemi Takasu<sup>3</sup>; Shigefusa Chichibu<sup>1</sup>; <sup>1</sup>Tohoku University; <sup>2</sup>University of Tsukuba; <sup>3</sup>ROHM Company, Ltd.*

Quantum-confined Stark effects in polarization-free m-plane In<sub>0.15</sub>Ga<sub>0.85</sub>N/GaN MQW LEDs fabricated on low defect density free-standing m-plane GaN substrates (Mitsubishi Chemical) were investigated by means of time-resolved photoluminescence under various external biases. The GaN substrates were sliced from thick c-plane GaN substrates grown by halide vapor phase epitaxy. The LED structure was confirmed by the cross-sectional TEM image to have almost no threading dislocations or stacking faults. Steady-state EL spectra exhibited a single peak around 2.74 eV, and the peak energy little shifted to the higher energy by the increase in current density because of the absence of polarization fields. The equivalent internal quantum efficiency, which was defined by the value of EL intensity at 300 K divided by that at 125 K, was 43%. The lifetime of carriers tunneling out from the QW increased as the junction field was lowered by applying external bias.

### 4:15 PM

**U2, Strong Polarization Effects in InGaN/GaN Light Emitting Diodes Grown on Semipolar {11-22} GaN Bulk Substrates:** *Masaya Ueda<sup>1</sup>; Mitsuru Funato<sup>1</sup>; Yoichi Kawakami<sup>1</sup>; Yukio Narukawa<sup>2</sup>; Takashi Mukai<sup>2</sup>; <sup>1</sup>Kyoto University; <sup>2</sup>Nichia Corporation*

The polarization properties of semipolar {11-22} InGaN LEDs fabricated on GaN substrates were investigated. The LEDs emit 491nm, 529nm, 593nm, or 625nm at 20 mA. For all the LEDs, EL spectra obtained with E//[1-100] were located at a few tens of meV lower energy than those with E//[1-123]. The peak energy difference became larger for longer wavelength LEDs, suggesting that the difference is caused by A and B bands and is enlarged by strain. Therefore, the EL spectra were decomposed to analyze contributions from A and B bands separately. The polarization degree of A excitons in unstrained GaN was measured 0.46, while those in the LEDs were 0.71 (491nm), 0.70 (529nm), 0.96 (593nm), and 0.78 (625nm). The polarization degrees of B excitons in the LEDs were approximately -1, while 0 in unstrained GaN. These striking differences are due to strain in the InGaN wells, which is supported by theoretical calculations.

### 4:30 PM

**U3, Photon and Electron Modulated Electroluminescence of Green Light Emitting Diodes:** *Yufeng Li<sup>1</sup>; Wei Zhao<sup>1</sup>; Yong Xia<sup>1</sup>; Mingwei Zhu<sup>1</sup>; Jayantha Senawiratne<sup>1</sup>; Theeradetch Detchprohm<sup>1</sup>; Christian Wetzel<sup>1</sup>; <sup>1</sup>Future Chips Constellation, Rensselaer Polytechnic Institute*

Piezoelectric fields, charge accumulation, and defect screening are

common factors in the discussion of performance limitations in GaInN/GaN light emitting diodes (LEDs). Modulation spectroscopy therefore seeks to separate individual contributions by selective photo carrier biasing. For this, electroluminescence in green (520–545 nm) GaInN/GaN multiple quantum well LEDs was modulated with photo-, and cathodo-luminescence within a scanning electron microscope. At low diode current (10  $\mu$ A), resonant laser excitation (488 nm) is found to boost LED efficiency 3-fold in higher performing dies (A) and up to 45-fold in poor performing ones (B). Enhancement vanishes above 0.05 mA and 3 mA, respectively. This enhancement strongly supersedes the photoluminescence signal. Similar behavior is observed in commercial LEDs (Nichia) and under cathodoluminescence modulation. The effect suggests the existence of repulsive charge states that cannot be screened by regular electron and hole injection. It may also reveal the cause of low performance in certain dies.

### 4:45 PM

**U4, Enhanced Capture of Photogenerated Carriers by Optimum Forward Bias Condition in Blue and Green (In,Ga)N Single-Quantum-Well Diodes:** *Akihiro Satake<sup>1</sup>; Kenichi Soejima<sup>1</sup>; Hideyuki Aizawa<sup>1</sup>; Kenzo Fujiwara<sup>1</sup>; <sup>1</sup>Kyushu Institute of Technology*

Improvement of external quantum efficiency in (In,Ga)N based light-emitting-diodes (LEDs) has attracted much attention as an essential issue for achieving further bright LEDs. However, it has been still a problem that external quantum efficiency remarkably droops at high injection current. In this study, vertical capture processes of photogenerated carriers in the c-plane blue and green (In,Ga)N single-quantum-well LEDs have been investigated by comparing variation in photoluminescence (PL) intensity as a function of applied voltage (-10~+4.5 V) at low temperature (20 K) under direct ( $\lambda_{ex}$ =380 nm) and indirect ( $\lambda_{ex}$ =325 nm) excitation. One striking result of the bias dependence of the PL intensity is that the photogenerated carriers are effectively captured in the active layer by optimum bias condition. The optimum bias condition is caused by interplay of carrier capture and internal quantum efficiency due to the presence of polarization-induced electric fields and localization potential minima by fluctuations of the indium concentration.

### 5:00 PM

**U5, Time-Resolved Photoluminescence Studies of High-Brightness 340-nm LEDs under Current Injection:** *Gregory Garrett<sup>1</sup>; Meredith Reed<sup>1</sup>; Hongen Shen<sup>1</sup>; Michael Wraback<sup>1</sup>; Christopher Chua<sup>2</sup>; Noble Johnson<sup>2</sup>; <sup>1</sup>U.S. Army Research Laboratory; <sup>2</sup>Palo Alto Research Center*

We present time-resolved photoluminescence (TRPL) studies on high-brightness, 340-nm LEDs under current injection. Devices exhibiting 6.5mW at 100mA drive current from a 100 $\mu$ m  $\times$  100 $\mu$ m area have been fabricated. PL lifetime measurements of InAlGaN MQW active regions under current injection are correlated with device operating parameters by using a nonlinear downconversion, optical-gating technique. In wafer level measurements, a decrease in PL lifetime by ~17% from 410 to 340ps as the injection current is increased from turn-on to the onset of roll-over (~150mA) may be attributed to enhanced nonradiative recombination associated with device heating. An increase in the low-current PL lifetime relative to that measured in the unbiased device is representative of trap saturation through current injection prior to device heating. In addition, the PL lifetime was found to decrease 10% after 120 hours of operation, indicating that degradation of the active region is correlated with the drop in output power.

### 5:15 PM

**U6, Enhancement of External Quantum Efficiency in GaN-Based Light-Emitting Diodes Using a Suspended Geometry:** *Natalie Fellows<sup>1</sup>; Hisashi Masui<sup>1</sup>; Hitoshi Saito<sup>1</sup>; Hirokuni Asamizu<sup>1</sup>; Michael Iza<sup>1</sup>; Hong Zhong<sup>1</sup>; Shuji Nakamura<sup>1</sup>; Steven DenBaars<sup>1</sup>; <sup>1</sup>University of California at Santa Barbara*

Using a transparent and mirror-less chip mounting technique we have increase the total external efficiency by 16.6%. This increase in the external quantum efficiency for light-emitting diode (LED) was based on c-plane (0001) bulk GaN employing a suspended geometry. A small size LED (200 x 550  $\mu$ m<sup>2</sup>) affixed to a Ag header is compared to an LED die lifted off the header. The output power for the LED in the suspended geometry was 27.4 mW, a 16.6% increase over the conventional placement and the

# Technical Program

EQE increased from 42.5% to 49.6% at a forward current of 20 mA under pulsed conditions. The suspended die was then placed into a cone optic and its output power and EQE improved to 30.2 mW and 54.7%, respectively.

## TP: Poster Session II

Tuesday, 5:30-7:00 PM Room: Prefunction Area  
September 18, 2007 Location: MGM Grand Hotel Conference Center

### TP: E-Devices: Device Characterization

**TP1, Effects of Fluorine Bombardment on the Electrical Characteristics of AlGaIn/GaN High Electron Mobility Transistors:** *Anirban Basu*<sup>1</sup>; Vipam Kumar<sup>1</sup>; Ilesanmi Adesida<sup>1</sup>; <sup>1</sup>Micro and Nanotechnology Laboratory, University of Illinois at Urbana-Champaign

A comprehensive study on the effects of fluorine bombardment on the electrical characteristics of AlGaIn/GaN HEMTs will be presented. Prior to gate metallization, bombardment with fluorine ions in the gate region has been shown to increase the threshold voltage of the fabricated transistors to positive values thereby yielding E-mode HEMTs. Accumulation of fluorine atoms has been detected in the two-dimensional electron gas channel under certain bombardment and annealing conditions. However, a systematic study of the effects of fluorine bombardment on device characteristics is still absent. Our results, at room temperature and at 77K, show that significant amount of sheet concentration and mobility modulation is possible through fluorine bombardment, which in turn seriously affects the electrical characteristics of fabricated devices. Device-related results along with analytical data will be presented to demonstrate the effects of fluorine that is crucial to the performance of high electron mobility transistors.

**TP2, High Temperature Behavior of GaN HEMT Devices on Si(111) and Sapphire Substrates:** *Roberto Cuerdo*<sup>1</sup>; F. Calle<sup>1</sup>; A. F. Braña<sup>1</sup>; Y. Cordier<sup>2</sup>; M. Azize<sup>2</sup>; N. Baron<sup>3</sup>; S. Chenot<sup>2</sup>; E. Muñoz<sup>1</sup>; <sup>1</sup>Institute of Optoelectronic Systems and Microtechnology and Department of Electronic Engineering - Superior Technical School of Engineers of Telecommunication (Polytechnical University of Madrid); <sup>2</sup>Research Center on the Hetero-Epitaxy and its Applications-National Scientific Research Center; <sup>3</sup>Research Center on the Hetero-Epitaxy and its Applications-National Scientific Research Center, Picogiga International

The study of GaN HEMT devices at high temperatures (HT) is necessary to understand and optimize their behaviour. Drain current ( $I_D$ ) and transconductance ( $g_m$ ) measurements, on single-gate transistors on Si(111) and sapphire with different gate lengths, were carried out from room temperature (RT) up to 350°C. All devices show lower characteristics as they are heated, mainly due to the electron mobility reduction. Nevertheless, devices recover their initial properties after the thermal cycling. Near RT, HEMTs on Si(111) present better performance than transistors on sapphire, but as temperature increases differences disappear. Therefore, it seems that substrate thermal conductivity becomes irrelevant at HT. Gate lengths and drain-source distances play also a significant role in HT performance. The relative reduction in  $I_D$  and  $g_m$  with temperature is lower for compact devices; related with the operation point of the device, from the linear regime towards the saturation region as the gate length is shortened.

**TP3, Influence of Surface Preparation and i-AlGaIn Thickness on Electrical Properties of i-AlGaIn/GaN Heterostructures:** *Takayuki Sawada*<sup>1</sup>; Kensuke Takahashi<sup>1</sup>; Kazuaki Imai<sup>1</sup>; Kazuhiko Suzuki<sup>1</sup>; Naohito Kimura<sup>1</sup>; Kazutaka Kitamori<sup>1</sup>; <sup>1</sup>Hokkaido Institute of Technology

Recently, fabrication of E-mode AlGaIn/GaN HEMT is attracting much interest. For this purpose, a recess gate structure is employed. However, influence of surface preparation and AlGaIn thickness on electrical properties of 2DEG and Schottky gate leakage current has not been fully investigated. In the present work, electrical properties of bare i-AlGaIn/GaN and Ni/i-AlGaIn/GaN Schottky samples prepared by wet-etching of the AlGaIn layer have

been systematically investigated. Hall effect measurements of bare AlGaIn/GaN samples indicated that the surface oxide increases 2DEG density, while the thinner the AlGaIn layer, the lower the 2DEG density, accompanied with reduced electron mobility. Both forward and reverse currents of Ni-Schottky samples increased with reducing the AlGaIn layer, giving smaller effective SBHs. The dependence of the effective SBH on the AlGaIn thickness can be well reproduced by considering combined leakage currents due to leaky patches with a low SBH and simple tunneling through the surface barrier.

**TP4, Performance Stability of AlGaIn/GaN HFET: Effect of Plasma Processing:** *Tamara Bakshi*<sup>1</sup>; Yaron Knafo<sup>1</sup>; Lina Ortenberg<sup>1</sup>; Ilanit Yehuda<sup>1</sup>; Joseph Kaplun<sup>1</sup>; Gregory Bunin<sup>1</sup>; <sup>1</sup>Gal El

Effect of plasma processing on the performance stability of AlGaIn/GaN HFETs was systematically investigated. Fluoride-based plasma treatment have lately been used for enhancement mode GaN HFETs. Physical mechanism of fluoride plasma treatment proposed in the past to be F<sup>-</sup> ions implantation to AlGaIn layer. In this work we present that the electron damage is the primary mechanism responsible for 2DEG depletion effect after the plasma treatment. A drain current ( $I_D$ ) decrease and a threshold voltage ( $V_T$ ) positive shift was observed for both CF<sub>4</sub> and Ar plasma treatment as a function of RF bias.  $I_D$  and  $V_T$  recovery was detected after impact ionization stress. The devices subjected to high field stress do not show any  $I_D$  and  $V_T$  recovery. Physical explanation, based on hot holes recombination with the electron charge induced during the plasma treatment, is presented. Temperature dependent measurements confirm that the effect is similar to "walkout" phenomena, well-known for GaAs PHEMTs.

**TP5, Rhodium-Based Schottky Contacts on n-Doped Gallium Nitride:** *Feng Tian*<sup>1</sup>; Eng Fong Chor<sup>1</sup>; <sup>1</sup>National University of Singapore

Rhodium (Rh)-based Schottky contacts on n-doped Gallium Nitride (GaN), including Rh/Au and Ni/Rh/Au, have been fabricated, characterized, and compared with Ni/Au contact. Although the maximum Schottky barrier height (SBH) of Rh/Au, estimated as 0.72 eV by IV measurements, is 0.01 eV lower than that of Ni/Au, it can be increased to 0.80 eV with the insertion of a thin Ni layer between Rh and GaN, thus yielding the Ni/Rh/Au contact. This surpasses that of Ni/Au by 0.07 eV and leads to a reduced reverse leakage current at -1 V for Ni/Rh/Au, by 1 order of magnitude compared to Ni/Au. Capacitance voltage measurements have revealed that the improved performance of Ni/Rh/Au is related to reduced defects at the metal/GaN interface. Thermal stability study has shown that Rh-based contacts exhibit better morphological stability than Ni/Au, and the existence of an intermediate Ni layer in Rh-based contacts helps enhance the contact thermal stability.

**TP6, The Role of Setback Layers in Wafer Fused AlGaAs/GaAs/GaN HBTs:** *Chuanxin Lian*<sup>1</sup>; Huili Xing<sup>1</sup>; <sup>1</sup>University of Notre Dame

The setback layer effects on wafer fused AlGaAs/GaAs/GaN HBTs have been studied both experimentally and theoretically. HBTs without setback showed no current gain (<1); HBTs with 20 nm UID, p- or n-GaAs setback exhibited gain of ~3, ~5 and ~7, respectively; HBTs with 30 nm p-GaAs showed improved gain of ~9. Together with the small apparent Early voltage, this points out a potential barrier at the B-C interface is likely blocking the electron flow. The lightly doped setback layer mitigates the adverse effect of this barrier: the thicker the setback, the higher the gain. However, the desired high breakdown voltage decreases with increasing setback thickness. To optimize the device performance, both electron transmission probability through the GaAs/GaN interface potential barrier and the avalanche breakdown voltage are calculated with respect to the setback thickness. The device gain dependence on the setback layer doping type has also been investigated.

**TP7, Zero-Bias N<sub>2</sub>/Cl<sub>2</sub>/O<sub>2</sub> Selective Dry Etching of GaN over AlGaIn for HEMT Gate Recessing:** *Michael Schuette*<sup>1</sup>; Wu Lu<sup>1</sup>; <sup>1</sup>Ohio State University

Highly-selective, low-damage etching of GaN-over-AlGaIn is realized by zero-bias N<sub>2</sub>(70%)/Cl<sub>2</sub>(5%)/O<sub>2</sub>(25%) inductively-coupled plasma, affording sub-10 nm/min etch rates and RMS roughnesses of ~3 Å – favorable for HEMT gate recessing. Selectivity is tuned by varying the O<sub>2</sub> fraction, and no AlGaIn etching is detectable even after 30 min, so the selectivity – although

unknown – is very high. We demonstrate linear recessing of an  $n^+$ -GaN/ $\text{Al}_{0.3}\text{Ga}_{0.7}\text{N}/\text{GaN}$  device structure, which stops abruptly upon clearing the 10 nm-thick cap.  $\text{SiO}_2$  masking used in our study is compatible with HEMT processes, where a masking dielectric is used for passivation. Recessed Schottky diodes on this device structure showed breakdown voltages greater than -200 V, compared to -75 V for non-recessed diodes. Post-etch annealing had no impact on  $I$ - $V$  characteristics, suggesting minimal plasma-induced damage. Removal of the  $n^+$ -GaN layer increased the 2DEG density by 14%, likely by removing negative polarization charge which resided at the  $n^+$ -GaN/ $\text{AlGaN}$  interface.

## TP: E-Devices: High k and Advanced Devices

**TP8, AlGaN/GaN-HFET with AlOx Gate Insulator Formed by MOCVD:** *Hiroyuki Sazawa*<sup>1</sup>; Naohiro Nishikawa<sup>1</sup>; Yoshiaki Honda<sup>1</sup>; Masahiko Hata<sup>1</sup>; Mitsuo Shimizu<sup>2</sup>; Hajime Okumura<sup>2</sup>; Takeaki Sakurai<sup>3</sup>; Katsuhiko Akimoto<sup>3</sup>; <sup>1</sup>Sumitomo-Chemical Company, Ltd.; <sup>2</sup>National Institute of Advanced Industrial Science and Technology; <sup>3</sup>University of Tsukuba

We report on metal-insulator-semiconductor (MIS) heterostructure field-effect transistor (HFET) with AlOx gate insulator formed by the metal-organic chemical vapor deposition (MOCVD) method designed for achieving low gate leak current and less current collapse. The AlOx insulator was deposited successively onto the AlGaN/GaN from trimethylaluminum (TMA) and  $n$ -butyl ether. Gas flux during the AlOx/AlGaN interface formation was mainly consisted of ammonia and nitrogen with the aim of preventing nitrogen vacancy creation on the AlGaN that could lead to the gate leak and the current collapse. The fabricated devices were evaluated under direct current operation. The gate leak current of the MIS-HFET was three orders of magnitude lower than that of conventional HFET. The change in transition drain current measured as a function of time after switching drain bias was found to be smaller in the MIS-HFET than in the HFET. Advantages of the AlOx gate insulator in MIS-HFET fabrication were demonstrated.

**TP9, AlInN/GaN HEMTs on Sapphire: DC and Pulsed Characterisation:** *Michael Fieger*<sup>1</sup>; Martin Eickelkamp<sup>1</sup>; Wanjiao Zhang<sup>1</sup>; Lars Rahimzadeh Khoshroo<sup>1</sup>; Christof Mauder<sup>1</sup>; Yilmaz Dikme<sup>2</sup>; Michael Heuken<sup>2</sup>; Achim Noculak<sup>1</sup>; Holger Kalisch<sup>1</sup>; Rolf Jansen<sup>1</sup>; Andrei Vescan<sup>1</sup>; <sup>1</sup>RWTH Aachen University; <sup>2</sup>AIXTRON AG

$\text{Al}_{0.83}\text{In}_{0.17}\text{N}/\text{GaN}$  high electron mobility transistors (HEMTs) grown by MOCVD on sapphire substrates were examined regarding their electrical characteristics. A sheet carrier concentration  $n_s$  of  $1.9 \times 10^{13} \text{ cm}^{-2}$  and a peak mobility  $\mu$  of  $1410 \text{ cm}^2/(\text{Vs})$  extracted by room temperature (RT) Hall measurements indicate the good properties of the two-dimensional electron gas (2DEG) at the heterointerface. Outstanding ohmic source and drain contacts with  $R_c$  of  $0.3 \Omega \text{ mm}$  and sheet resistances  $R_s$  as low as  $235 \Omega/\text{sq}$  provide the basis for good electrical characteristics of our HEMT devices ( $L_g = 1 \mu\text{m}$ ,  $W_g = 50 \mu\text{m}$  and  $5 \mu\text{m}$  source-drain spacing). A low knee voltage  $V_{\text{knee}}$  of 5 V and a peak transconductance  $g_m$  of 243 mS/mm were achieved. At  $V_{\text{GS}} = 2 \text{ V}$  a maximum drain current density  $I_{\text{D,sat}}$  of 1.28 A/mm was measured. Without passivation, pulsed DC I-V measurements revealed reduced dispersion compared to AlGaN/GaN HEMTs.

**TP10, Close Lattice-Matched AlInN Based Heterostructures for High Power Electronics:** *Marcus Gonschorek*<sup>1</sup>; Jean-François Carlin<sup>1</sup>; Eric Feltin<sup>1</sup>; Marcel Py<sup>1</sup>; Nicolas Grandjean<sup>1</sup>; <sup>1</sup>Ecole Polytechnique Fédérale de Lausanne (EPFL), Switzerland

Owing to the possibility of growing AlInN lattice-matched on GaN for an Indium composition of  $\sim 17.5\%$  while keeping a large band-offset and discontinuity in spontaneous polarization, AlInN alloy appears to be suitable for designing high electron mobility transistors. From the differences in spontaneous polarization across the lattice-matched AlInN/GaN heterojunction one expects a polarization induced sheet charge density of  $0.416 \text{ C/m}^2$  resulting in a two dimensional electron gas (2DEG) density of  $n_s \sim 2.6 \times 10^{13} \text{ cm}^{-2}$ . This value is confirmed by capacitance-voltage and Hall measurements. Since the lateral transport is mainly limited by the poor quality of AlInN/GaN interface, a thin AlN interlayer was inserted resulting in a record mobility of  $\sim 1200 \text{ cm}^2/\text{Vs}$  at 300 K. Based on this optimized lattice-

matched heterostructure, the 2DEG transport properties are investigated in near-lattice-matched composition range from  $x=6.9\%$  to  $19.7\%$  leading to a  $n_s$  of  $\sim 4.0 \times 10^{13} \text{ cm}^{-2}$  and  $\sim 2.2 \times 10^{13} \text{ cm}^{-2}$ , respectively.

**TP11, Comparative Studies on AlGaN/GaN MOS-HEMTs with High-k HfO<sub>2</sub> or Epitaxial Sc<sub>2</sub>O<sub>3</sub> Gate Oxide:** *Chang Liu*<sup>1</sup>; *Eng Fong Chor*<sup>1</sup>; *Leng Seow Tan*<sup>1</sup>; <sup>1</sup>National University of Singapore

AlGaN/GaN metal-oxide-semiconductor high electron mobility transistors (MOS-HEMTs) with reactive-sputtered high-k HfO<sub>2</sub> or pulsed-laser-deposition-grown epitaxial Sc<sub>2</sub>O<sub>3</sub> gate oxide were investigated. The Sc<sub>2</sub>O<sub>3</sub>/HEMT system exhibited better interface properties, including larger conduction band offset (2.04 eV) and smaller effective oxide charge density ( $4E11 \text{ eV}^{-1}\text{cm}^{-2}$ ) compared to the HfO<sub>2</sub>/HEMT structure ( $1.71 \text{ eV}$ ,  $8.7E11 \text{ eV}^{-1}\text{cm}^{-2}$ ), while a smoother interface was revealed for the latter. Owing to the good oxide quality and excellent oxide/HEMT interfaces, HfO<sub>2</sub>- and Sc<sub>2</sub>O<sub>3</sub>-MOS-HEMTs outperformed HEMTs in terms of a 66% and 84% higher ID, max, and a 5 and 6 orders of magnitude lower Ig, leak, respectively. Better performances of Sc<sub>2</sub>O<sub>3</sub>-MOS-HEMT relative to the HfO<sub>2</sub> counterpart were attributed to its superior oxide and oxide/HEMT interface quality originated from the epitaxial nature of Sc<sub>2</sub>O<sub>3</sub>. On the other hand, the high-k property of HfO<sub>2</sub> rendered HfO<sub>2</sub>-MOS-HEMT a larger extrinsic transconductance and smaller threshold voltage than Sc<sub>2</sub>O<sub>3</sub>-MOS-HEMTs.

**TP12, Effectiveness of Si Delta-Doping on AlGaN/GaN HFET with p-GaN Backbarrier:** *Sun Young Hyun*<sup>1</sup>; *Ki-Won Kim*<sup>1</sup>; *Hyun-Ick Cho*<sup>1</sup>; *Hwa-Chul Lee*<sup>1</sup>; *Clemens Ostermaier*<sup>1</sup>; *Sang-Il An*<sup>1</sup>; *Jong-Bong Ha*<sup>1</sup>; *Sung-Ho Hahn*<sup>1</sup>; *Cheol-Koo Hahn*<sup>2</sup>; *Hyun-Chul Choi*<sup>1</sup>; *Jung-Hee Lee*<sup>1</sup>; <sup>1</sup>Kyungpook National University; <sup>2</sup>Korea Electronics Technology Institute

We report on the optimal device structure to increase carrier confinement and suppress the buffer leakage current by three kinds of samples. First sample, conventional HFET structure with high-resistive(HR) GaN layer was grown [sample1]. The second sample was grown by utilizing (1 $\mu\text{m}$ ) p-GaN layer instead of HR-GaN [sample2]. Third sample is exactly the same as the second sample, except that Si-delta doped layer was inserted between channel and p-GaN layer [sample3]. The drain leakage current of sample 2 was greatly reduced by adopting p-GaN backbarrier at least one order lower compared to the conventional heterostructure (sample1). The Si delta-doped layer inserted at the junction interface (sample3) can sufficiently alleviate the channel depletion from the formation of pn junction and even further it can supply extra electrons into the channel, which greatly increase drain current by a factor of 4 compared to that of sample 2.

**TP13, Effects of Surface Passivation Films on AlGaN/GaN HEMT Structure:** *Shuichi Yagi*<sup>1</sup>; *Mitsuaki Shimizu*<sup>1</sup>; *Toshihide Ide*<sup>1</sup>; *Hajime Okumura*<sup>1</sup>; *Yoshiki Yano*<sup>2</sup>; *Nakao Akutsu*<sup>2</sup>; <sup>1</sup>AIST; <sup>2</sup>Taiyo Nippon Sanso Corporation

The effect of the high-k insulator passivation on the sheet resistance of the AlGaN/GaN heterojunction structure was investigated. The sheet resistance was reduced after the deposition of the high-k insulator films. In the case of the HEMT device operation, when the high-k material is used as MIS gate insulator, we found the changes in the gate threshold voltage. With the help of the recess gate structure, the normally-off mode operation can be achieved using high-k MIS gate structure.

**TP14, High-Mobility Ultrathin AlN/GaN And AlInN/AlN/GaN Heterojunctions Grown by MBE:** *Yu Cao*<sup>1</sup>; *Kejia Wang*<sup>1</sup>; *Debdeep Jena*<sup>1</sup>; <sup>1</sup>University of Notre Dame

Due to the large polarization difference between AlN and GaN, a high 2DEG density can be achieved with a very thin AlN layer. This results in larger transconductance, and lower threshold HEMTs. A peak extrinsic transconductance of 211 mS/mm was reported when the AlN/GaN HEMT had the electron mobility of only 365 cm<sup>2</sup>/Vs, indicating that the performance can be greatly enhanced with ultrashallow AlN/GaN heterojunctions with mobilities exceeding 1000 cm<sup>2</sup>/Vs. A series of AlN/GaN heterojunctions with high electron mobilities have been grown by MBE with the AlN layer thickness varied from 1nm-8nm. The highest mobility was  $\sim 1200 \text{ cm}^2/\text{Vs}$  (300K) and  $\sim 4000\text{-}5000 \text{ cm}^2/\text{Vs}$  (77K). To reduce the gate leakage, AlInN/AlN/GaN heterojunctions was grown with the 2DEG mobility of  $\sim 1100$

# Technical Program

cm<sup>2</sup>/Vs (300K) and ~3400 cm<sup>2</sup>/Vs (77K), where the sheet charge density is ~3e12/cm<sup>2</sup>. The structural and transport characterization of the ultrashallow 2DEG heterojunctions and their device applications will be presented.

**TP15, Influence of GaN Capping on Performance of InAlN/AlN/GaN MOS-HEMTs with Al<sub>2</sub>O<sub>3</sub> Gate Insulation Prepared by CVD:** *Gianmauro Pozzovivo*<sup>1</sup>; Jan Kuzmik<sup>1</sup>; Sebastian Golka<sup>1</sup>; Karol Cico<sup>2</sup>; Karol Fröhlich<sup>2</sup>; Jean Francois Carlin<sup>3</sup>; Nicolas Grandjean<sup>3</sup>; Werner Schrenk<sup>1</sup>; Gottfried Strasser<sup>1</sup>; Dionyz Pogany<sup>1</sup>; <sup>1</sup>Technical University Vienna; <sup>2</sup>Academy of Science of Bratislava; <sup>3</sup>EPFL Ecole polytechnique Federale de Lausanne

We investigate InAlN/AlN/GaN-based MOS-HEMTs with and without a 2nm-GaN capping below an Al<sub>2</sub>O<sub>3</sub>-insulator. An excellent reduction of the leakage current, up-to 6 orders of magnitude, is observed in MOS-HEMT structures compared to Schottky-based-HEMTs, both with GaN capping. In the case of uncapped samples the reduction in the leakage current is 3 orders of magnitude. The maximal transconductance value gm<sub>max</sub> for the GaN-capped-MOS-HEMT is about 10% higher than that for the conventional Schottky-based-HEMT, while in the case of uncapped devices gm<sub>max</sub> is about the same for both Schottky and MOSHEMT. Similarly the maximal-drain-current in the case of GaN capped MOS-HEMT is 950mA/mm exhibiting increase of 170mA/mm in comparison to the corresponding conventional Schottky-based-HEMT. We demonstrate that a GaN-cap between the InAlN-barrier and the Al<sub>2</sub>O<sub>3</sub>-film leads to the additional improvement of performances in terms of gate leakage current reduction, and to the IDS and gm<sub>max</sub> increase. Ultragan-project, contract no. 6903 is acknowledged.

**TP16, Interface Characterization of ALD Deposited Al<sub>2</sub>O<sub>3</sub> on GaN by CV Method:** *Clemens Ostermaier*<sup>1</sup>; Hwa-Chul Lee<sup>1</sup>; Sun-Young Hyun<sup>1</sup>; Sang-Il An<sup>1</sup>; Ki-Won Kim<sup>1</sup>; Hyun-Ick Cho<sup>1</sup>; Jong-Bong Ha<sup>1</sup>; Jung-Hee Lee<sup>1</sup>; <sup>1</sup>Kyungpook National University

A high dielectric interface quality is the determining factor for high power GaN MOSFET devices. We characterized 100Å thick Al<sub>2</sub>O<sub>3</sub> films deposited by ALD on MOCVD grown undoped GaN on sapphire. First we measured the leakage current and densification behavior of the dielectric after annealing at different temperatures up to 900°C and determined the polycrystalline phase change to be around 800°C. Then we characterized the interface charges of both films according to the flatband shift induced by over-bandgap light, showing the lowest interface charge density of 1.27e12 cm<sup>-2</sup> after thermal treatment at 850°C. Additionally, we measured the AC conductivity from 200 Hz to 20 kHz and calculated the interface states density (Dit) of the upper half of the GaN bandgap, showing the lowest Dit of 1e10 cm<sup>-2</sup>eV<sup>-1</sup> at 2 eV above valence band, while it remains higher round the band edge at 1.1e11 cm<sup>-2</sup>eV<sup>-1</sup>, for annealing at 750°C.

**TP17, MBE Grown AlInN and AlInN/GaN FETs:** Huili (Grace) Xing<sup>1</sup>; Tom Zimmermann<sup>1</sup>; David Deen<sup>1</sup>; Yu Cao<sup>1</sup>; Debdeep Jena<sup>1</sup>; <sup>1</sup>University of Notre Dame

AlInN has been predicted to be well suited for the barrier layer in AlInGaN-based HEMTs. AlInN lattice matched to GaN might be beneficial in improving carrier confinement as well as strain induced reliability issues, and small variations in the composition ratio (In/Al) allow one to introduce compressive or tensile strain relative to GaN thus tuning the polarization induced charges without having to compromise the benefits from large bandgaps of Al-rich AlInN. Recently in our lab, various AlInN structures have been investigated by MBE growth as well as the resultant AlInN/(AlN)/GaN HEMTs. For example, an AlInN(30nm)/AlN(3nm)/GaN structure showed a sheet charge of ~ 3.2e13 cm<sup>-2</sup> and mobility of ~ 1100 cm<sup>2</sup>/Vs at RT and ~ 3e13 cm<sup>-2</sup> and mobility of ~ 3400 cm<sup>2</sup>/Vs at 77K; and the resulting HEMT showed a maximum current of ~ 1.4 A/mm. The detailed findings on material growth, quality and devices will be presented.

**TP18, New GaN-Based MOS-HEMT Structures with Record Device Performance:** *Amir Dabiran*<sup>1</sup>; Andrei Osinsky<sup>1</sup>; Andrew Wowchak<sup>1</sup>; Brian Hertog<sup>1</sup>; Junqing Xie<sup>1</sup>; Peter Chow<sup>1</sup>; <sup>1</sup>SVT Associates

AlGaIn/GaN-based high electron mobility transistor (HEMT) structures, with high (>75%) Al contents, were grown on sapphire and SiC substrates by RF plasma-assisted molecular beam epitaxy (MBE.) Using high Al compositions allowed efficient electron confinement with thin (< 10 nm)

AlGaIn barrier layers. The highly strained AlGaIn layers induced very high sheet electron densities (> 2E13 cm<sup>-2</sup>), while the controlled growth of high quality AlGaIn/GaN resulted in high room-temperature electron mobility values (> 1700 cm<sup>2</sup>/V.s.) The combination of very high values of electron sheet density and mobility resulted in record sheet resistivity values of < 180 ohm/square. We will present the DC and RF characterization of metal-oxide-semiconductor (MOS) HEMT devices, fabricated in this work, showing the state-of-the-art performance of the new GaN-based structures.

**TP19, Optimization of GaN MOS Capacitors and FETs:** *Weixiao Huang*<sup>1</sup>; Tahir Khan<sup>2</sup>; T. Paul Chow<sup>1</sup>; <sup>1</sup>Rensselaer Polytechnic Institute; <sup>2</sup>Freescale Semiconductor

In this paper, three different gate oxide processes were explored and compared. All MOS capacitors were fabricated on n-type GaN epitaxial layers grown by MOCVD on sapphire substrates. C-V measurements were performed on the three samples and their characteristics were compared. The very small interface-state density makes OX3 a very good process choice for GaN MOSFETs and the trend of decreasing interface-state density deeper into the bandgap allows the demonstration of GaN inversion-mode MOSFETs. Both accumulation and inversion-mode MOSFETs were fabricated and characterized using OX3 process conditions. Field-effect mobilities were extracted on both circular and linear devices with different channel lengths. Mobilities in two perpendicular directions in (0001)-plane show similar values. Current collapse testing was also performed on our GaN MOSFETs and no current collapse was observed. In addition, an NMOS inverter stage, utilizing an enhancement-mode MOSFET and a depletion-mode MOSFET has also been demonstrated and characterized.

**TP20, Saturation Velocity Enhancement in Al<sub>2</sub>O<sub>3</sub>/AlGaIn/GaN MOSHFETs:** *Peter Kordos*<sup>1</sup>; Roman Stoklas<sup>1</sup>; Dagmar Gregusova<sup>1</sup>; Jozef Novak<sup>1</sup>; <sup>1</sup>Academy of Sciences

Increases in the extrinsic transconductance (64%) and in the saturation drain current (40%) of the AlGaIn/GaN MOSHFET with 4-nm-thick Al<sub>2</sub>O<sub>3</sub> gate-oxide compared to the HFET were observed. An analysis of this effect yielded higher drift mobility in the MOSHFET than that in the HFET with the zero-bias values of 1950 and 1630 cm<sup>2</sup>/Vs, respectively. The extrinsic transconductance can be well fitted using measured data of  $\mu$ d and CGS and the series resistance is found to be 10 and 5.8 Wmm for the HFET and MOSHFET, respectively. From the intrinsic transconductance evaluated effective saturation velocity in the MOSHFET (1.24·10<sup>7</sup> cm/s) is two-times higher than that in the HFET (0.62·10<sup>7</sup> cm/s). Detailed analysis showed that similar vd-enhancement exists in the MOSHFETs with SiO<sub>2</sub> and thicker Al<sub>2</sub>O<sub>3</sub> gate-oxides. Different electric-field distribution due to the deposited gate-oxide is considered to describe these features.

**TP21, Utilizing High-k GdScO<sub>3</sub> for AlGaIn/GaN-Based MOSHFETs:** Gero Heidelberger<sup>1</sup>; Martin Roeckerath<sup>1</sup>; Alfred Fox<sup>1</sup>; Michael Willemann<sup>1</sup>; Roger Steins<sup>1</sup>; Hilde Hardtdegen<sup>1</sup>; *Michel Marso*<sup>1</sup>; Hans Lüth<sup>1</sup>; <sup>1</sup>Research Centre Jülich GmbH

GaN/AlGaIn-based metal-oxide-semiconductor heterojunction field-effect transistors (MOSHFET) exhibit lower leakage currents, improved drain currents, higher positive operational voltages and better rf-properties than HFETs. On the other hand, they suffer from a loss in channel control due to the additional oxide-capacitance. As a solution, we utilized the rare-earth scandate GdScO<sub>3</sub> to isolate the gate. Due to its high dielectric constant (>20), the control of the MOSHFETs can be enhanced. For our experiments, 1.5µm GaN- and 30nm Al<sub>0.28</sub>Ga<sub>0.72</sub>N were grown on sapphire by MOCVD. Diodes and transistors were fabricated using standard technology for mesa, ohmic contact, and gate processing. For MOS devices, GdScO<sub>3</sub> was deposited by electron beam evaporation and subsequently annealed. Dc- and rf-measurements showed that by incorporating GdScO<sub>3</sub> channel control is improved. The leakage current can be reduced by seven orders of magnitude and rf-performance can be improved significantly. Therefore, we consider GdScO<sub>3</sub> as a promising dielectric for future GaN/AlGaIn-based MOSHFETs.

## TP: E-Devices: High Voltage Devices

**TP22, Fabrication of Normally-Off Mode AlGaIn/GaN HEMTs and Its Importance for GaN Electronics:** *Stephan Maroldt*<sup>1</sup>; Christian Haupt<sup>1</sup>; Katja Tonisch<sup>1</sup>; Oliver Ambacher<sup>1</sup>; <sup>1</sup>TU Ilmenau

Normally-off mode AlGaIn/GaN HEMTs fabricated by a gate recess technology offer potentially a high transconductance due to a very thin AlGaIn barrier thickness. Therefore a low maximum gate voltage is needed for turning this HEMT into an on-state, while simultaneously enables operating at high output currents and high output voltage. This property is making them an ideal on chip interface stage between external controller circuits and GaN power devices, which especially is required in high efficiency switched microwave amplifiers. In this work different technologies for obtaining normally-off behavior in AlGaIn/GaN HEMTs are investigated and compared i.e. fluorine and ozone plasma based surface modification, a passivation layer as well as a low damage chlorine plasma gate recess etching. Besides being compatible with self aligned, short gate length fabrication using different passivation layers these technologies offer the possibility of integrating normally-off and normally-on mode HEMTs on one chip.

**TP23, GaN High-Voltage Devices on Si:** *O. Schulz*<sup>1</sup>; A. Dadgar<sup>1</sup>; U. Heinle<sup>2</sup>; J. Blaesing<sup>3</sup>; A. Krtschil<sup>3</sup>; T. Hempel<sup>3</sup>; A. Diez<sup>3</sup>; I. Daumiller<sup>2</sup>; M. Kunze<sup>2</sup>; J. Christen<sup>3</sup>; A. Krost<sup>3</sup>; <sup>1</sup>AZZURRO Semiconductor AG; <sup>2</sup>MicroGaN GmbH; <sup>3</sup>Otto-von-Guericke-Universitaet Magdeburg

Having high breakdown field strengths the wide band-gap materials GaN and AlN are predestined for high voltage applications. However, the lack of homosubstrates and problems with the availability of large diameter substrates (SiC) and growth on them (sapphire) hampers a breakthrough of these materials due to high device cost. With silicon a low-cost large diameter material is available and growth on 150 mm diameter substrates has been already demonstrated. The problem using Si is the comparably high conductivity, low breakdown field strength and the difficulty to grow sufficiently thick and crack-free GaN layers to achieve high breakdown voltages. We have solved these problems and will present GaN-on-Si based FET devices for high-voltage switching applications above 1000 V.

**TP24, Investigation on Conductivity at the GaN/AlN/SiC Substrate Interface for Vertical Nitride Power FETs:** *Yuu Wakamiya*<sup>1</sup>; Fumio Hasegawa<sup>1</sup>; Hideo Kawanishi<sup>1</sup>; <sup>1</sup>Kogakuin University

Power FETs are the next promising application of AlGaIn/GaN heterostructures. In order to reduce the device size and thermal conductivity, power nitride FETs should be a vertical structure on a conductive SiC or Si substrate. An AlN or/and AlN/GaN multi-buffer layer is inevitable to grow GaN on a SiC or Si substrate by MOVPE, therefore, current flow at the GaN/AlN/SiC interface is one of the important issues to be investigated. 17 to 350 nm AlN layers were grown on 80 off n—epitaxial 4H-SiC substrates and on a GaN/AlN/SiC structure by alternate-source-feeding MOVPE. Ni/AlN/n—epi-4H-SiC sample showed Schottky characteristics except 350nm thick AlN sample, indicating that the AlN was not working as an insulator. On the other hand, Ni/AlN/GaN/n—epi-4H-SiC sample turned out MIS characteristics for the same AlN thickness. This difference can be explained by the heterovalent atomic structure at the interface between AlN(III-V) and SiC(IV-IV).

**TP25, Switching Transients in AlGaIn/GaN HEMTs Operated under High Power:** *Pankaj Shah*<sup>1</sup>; Ben Huebschman<sup>1</sup>; Edward Viveiros<sup>1</sup>; Khamsook Kingkeo<sup>1</sup>; Alfred Hung<sup>1</sup>; Ken Jones<sup>1</sup>; <sup>1</sup>US Army Research Laboratory

Communication and Radar applications place great demands on high power, high frequency AlGaIn/GaN HEMTs. Current transients originating from material properties can drain power from the source, degrade transmitted information, and contribute to lifetime reduction of a system. Drain-lag and gate-lag measurements are used to observe and interpret physically the transients during the HEMT operation and to develop models for use in ADS harmonic balance power amplifier simulation. Measurement results indicate that SiN passivated devices not exhibiting drain lag transients when operated under low stress will exhibit drain lag as the device temperature increases. Therefore, realistic operating conditions considering the modulation the device will experience in actual operation should be considered when

evaluating a device. Measured results lead to AlGaIn HEMT models based on a combination of HEMT and FET models available in ADS to accurately represent the physics in real devices.

## TP: E-Devices: Microwave Devices

**TP26, 0.15  $\mu\text{m}$  Self-Aligned AlGaIn/GaN High Electron Mobility Transistors:** *Vipan Kumar*<sup>1</sup>; Dong-Hyun Kim<sup>1</sup>; Anirban Basu<sup>1</sup>; Ilesanmi Adesida<sup>1</sup>; <sup>1</sup>University of Illinois

The high frequency response of AlGaIn/GaN high electron mobility transistors (HEMTs) is still limited by the high access resistance. In order to reduce access resistance self-aligned devices with gate-length down to 0.15  $\mu\text{m}$  have been fabricated on 6H-SiC substrates using a single step ohmic process. Our recently developed Mo/Al/Mo/Au-based ohmic contact requiring annealing temperatures between 500 and 600°C was utilized. Ohmic contact resistances between 0.3 - 0.5 ohm-mm have been achieved. These 0.15  $\mu\text{m}$  devices exhibited maximum drain current density of 985 mA/mm at a gate bias of 0 V and a drain bias of 10 V. The knee voltage was less than 2 V showing the excellent nature of the ohmic contact. A peak extrinsic transconductance (gm) of 297 mS/mm was measured at  $V_{gs} = -2.6$  V. Also, a unity gain cut-off frequency ( $f_T$ ) of 98 GHz was measured on these devices.

**TP27, Cryogenic Characteristics of Sub-100-nm-Gate AlGaIn/GaN MIS-HEMTs:** *Akira Endoh*<sup>1</sup>; Issei Watanabe<sup>1</sup>; Yoshimi Yamashita<sup>2</sup>; Takashi Mimura<sup>1</sup>; Toshiaki Matsui<sup>1</sup>; <sup>1</sup>National Institute of Information and Communications Technology; <sup>2</sup>Fujitsu Laboratories Ltd.

We fabricated AlGaIn/GaN metal-insulator-semiconductor (MIS) high electron mobility transistors (HEMTs) using SiN/SiO<sub>2</sub>/SiN triple-layer insulators, and measured their DC and RF characteristics at 300 and 16 K. The maximum drain-source current at a drain-source voltage of 5 V and a gate-source voltage of 0 V increased from 0.966 A/mm at 300 K to 1.075 A/mm at 16 K. There was no current collapse at either 300 or 16 K in the measured bias range. The cutoff frequency  $f_T$  at 16 K was 18-26% greater than that at 300 K. At a gate length  $L_g$  of 45 nm,  $f_T$  had a maximum value of 168 GHz at 16 K and 134 GHz at 300 K. The increase in  $f_T$  may result from a reduction in access resistances and an increase in electron velocity.

**TP28, DC and Microwave Performance of Recessed Gate III-N HFETs with InGaIn Etch-Stop Layer:** *Zijiang Yang*<sup>1</sup>; Nezhil Pala<sup>1</sup>; Jiayu Deng<sup>2</sup>; Xuhong Hu<sup>2</sup>; Alexei Kudymov<sup>1</sup>; Grigory Simin<sup>3</sup>; Jinwei Yang<sup>2</sup>; Remis Gaska<sup>2</sup>; Michael Shur<sup>1</sup>; <sup>1</sup>Rensselaer Polytechnic Institute; <sup>2</sup>Sensor Electronic Technology; <sup>3</sup>University of South Carolina

Recessed and double recessed gate techniques have been employed in GaN HFET technology to increase the breakdown voltage without compromising the high frequency performance. However, conventional recessed-gate processes introduce damage and traps to the active region and are not able to selectively etch epitaxial layers. In this work, we present experimental studies of a novel AlGaIn/GaN HFET structure with recessed gates fabricated by selective etching of textured AlGaIn with etch-stop InGaIn layers. Devices with 0.5 $\mu\text{m}$  long recessed gate showed the breakdown voltage increase from 40 V to 130V. The threshold voltage was independent on drain bias, which indicates the reduced short channel effects. Cut-off frequency and maximum oscillation frequency were 29.4GHz and 39.7GHz, respectively. A non-field-plated passivated device delivered 6.5 W/mm power, with 45% PAE at 40V drain bias independent of UV illumination, indicating the high material quality and process maturity.

**TP29, DC Performance of High-Power GaN FET Devices with Non-Alloyed Ohmic Contacts Fabricated by PAMBE-Based Selective-Area Growth:** *Huichan Seo*<sup>1</sup>; Patrick Chapman<sup>1</sup>; Philip Krein<sup>1</sup>; Jung-Hee Lee<sup>2</sup>; Kyekyoon Kim<sup>1</sup>; <sup>1</sup>University of Illinois at Urbana-Champaign; <sup>2</sup>Kyungpook National University

We previously reported on the metal-semiconductor field-effect transistors (MESFETs) fabricated by selective-area-growth (SAG) using plasma-assisted molecular beam epitaxy (PAMBE), which showed high peak drain current and transconductance. The SAG technique enabled selective growth

# Technical Program

of a heavily doped n<sup>-</sup>GaN layer ( $1.0 \times 10^{19} \text{ cm}^{-3}$ ) solely for the source/drain regions, giving rise to an extremely low contact resistivity ( $1.8 \times 10^{-8} \Omega \cdot \text{cm}^2$ ) for the MESFETs. In this study, we extend the same SAG technique to non-alloyed ohmic contacts. The specific contact resistances of Ti and Ti/Al with SAG were  $3.5 \times 10^{-5}$  and  $5.1 \times 10^{-5} \Omega \cdot \text{cm}^2$ , respectively, demonstrating that the SAG technique can be gainfully employed to fabricate a variety of metal contacts. The DC performance of MESFETs and HEMTs will be investigated. The interface reaction between metal contact and GaN surface will be examined by X-ray photoemission spectroscopy (XPS) and secondary ion mass spectrometry (SIMS).

**TP30, Effect of Image Charges in the Drain Delay of AlGaN/GaN HEMTs:** *Jinwook Chung*<sup>1</sup>; Xu Zhao<sup>1</sup>; Tomas Palacios<sup>1</sup>; <sup>1</sup>Massachusetts Institute of Technology

This work studies the origin of drain delay in AlGaN/GaN High Electron Mobility Transistors (HEMTs). This delay, equals to the transit time of a carrier through the depletion region at the drain side of the gate in a HEMT, accounts for almost 25% of the total delay in deep submicron devices, significantly limiting their maximum frequency performance. The drain delay is inversely proportional to  $\alpha$ , a parameter related to how injected electrons image at different metal contacts in a HEMT.  $\alpha$  can be engineered by artificially redistributing the image charges. By adding an additional metal contact in the HEMT structure ("mirror contact metal"), and varying its length and position, our simulation predicted at least a 2-fold improvement in the value of  $\alpha$  therefore significantly improving the high frequency performance and linearity of these devices. A new equivalent circuit model that takes into account all these effects will also be presented.

**TP31, Effect of Silicon Nitride Passivation on Microwave Noise Characteristics in AlGaN/GaN HEMTs on Silicon Substrate:** *Zhihong Liu*<sup>1</sup>; Subramaniam Arulkumaran<sup>1</sup>; Chee How Lee<sup>1</sup>; Geok Ing Ng<sup>1</sup>; Tao Xu<sup>2</sup>; <sup>1</sup>MMIC Design Center, Temasek Laboratories, Nanyang Technological University; <sup>2</sup>School of Electrical and Electronic Engineering, Nanyang Technological University

Effect of silicon nitride (SiN) surface passivation by Plasma Enhanced Chemical Vapor Deposition (PECVD) on microwave noise characteristics of AlGaN/GaN High Electron Mobility Transistors (HEMTs) on high-resistivity (HR) silicon substrate has been investigated. After passivation, improved DC and microwave noise performance was observed. At 10GHz, the minimum noise figure ( $NF_{\min}$ ) decreased by 25% (0.5 dB) and associate gain ( $G_a$ ) increased by 10% (1.0dB) at  $V_d=12\text{V}$  and  $I_d=50\text{mA/mm}$ . The decreased value of  $NF_{\min}$  and increased value of  $G_a$  by surface passivation is due to the increase of extrinsic transconductance ( $g_m$ ) and decrease of source resistance ( $R_s$ ), which resulted from the increase of 2DEG sheet carrier density by suppression of surface traps. The value of  $NF_{\min}$  and  $G_a$  for SiN passivated devices becomes less dependent on frequency, gate and drain bias, which shows the higher linearity and capability of being used in high drain voltage-based low noise applications.

**TP32, Field Engineering Using Drain Field Controlling Electrode for Ultra High Frequency GaN-Based Power HEMTs:** *Alexei Koudymov*<sup>1</sup>; Nezhil Pala<sup>2</sup>; Zijiang Yang<sup>1</sup>; Xuhong Hu<sup>3</sup>; Jianyu Deng<sup>3</sup>; Jinwei Yang<sup>3</sup>; Remis Gaska<sup>3</sup>; Grigory Simin<sup>4</sup>; Michael Shur<sup>1</sup>; <sup>1</sup>Rensselaer Polytechnic Institute; <sup>2</sup>Rensselaer Polytechnic Institute and SET; <sup>3</sup>SET; <sup>4</sup>University of South Carolina

GaN HEMTs applications for ultra high frequency high power rely on their ability to operate under high bias. However, as the bias increases, the high-frequency performance of HEMT degrades due to high field region extension beyond the gate increasing the effective gate length. Therefore, the field engineering at the gate edges is very important for high frequency, high power applications. In this work, we present both experimental and numerical studies of GaN HEMT utilizing the Drain Field Controlling Electrode (DFCE) to reduce the electric field spread in the device gate-to-drain opening. The simulations are performed based on experimentally validated velocity-field dependence and, hence, are valid for gate length scaling down to deep submicron. It is shown that the use of the DFCE reduces the response delay due to high field region extension more than a factor of two thus allowing for ultra-high frequency operation at high drain bias.

**TP33, Gate Recess Technology on AlGaN/GaN HFET with InGaN as Etch-Stop Layer:** *Xuhong Hu*<sup>1</sup>; Nezhil Pala<sup>2</sup>; Jianyu Deng<sup>1</sup>; Zijiang Yang<sup>2</sup>; Grigory Simin<sup>3</sup>; Jinwei Yang<sup>1</sup>; Remis Gaska<sup>1</sup>; Michael Shur<sup>2</sup>; <sup>1</sup>Sensor Electronic Technology; <sup>2</sup>Rensselaer Polytechnic Institute; <sup>3</sup>University of South Carolina

Combination of novel epitaxial growth and gate etching technology enabled us to successfully fabricate a high-power high-frequency recessed-gate AlGaN/GaN HFET. We incorporated InGaN layer in the MOCVD grown epi-structure as an etch-stop layer to precisely control the recess depth. For the RIE etching, the InGaN layer etch rate has been found to be us to be more than ten times lower than that of the AlGaN barrier layer. After the RIE etching, the InGaN layer is easily removed using wet chemical etching. We show that the quality of 2DEG at the AlGaN/GaN interface does not degrade during the gate recess process. Novel technology results in high device uniformity as confirmed by testing the maximum transconductance distribution over the 2 inches wafer. The devices with 0.5  $\mu\text{m}$  long gate have the cutoff frequency close to 30GHz and the breakdown voltage of 130V without employing the field-plating technique.

**TP34, High-Electron-Mobility AlGaN/GaN Heterostructures Grown on Si(001) by Molecular Beam Epitaxy for Microwave Application:** *Sylvain Joblot*<sup>1</sup>; Yvon Cordier<sup>2</sup>; Fabrice Semond<sup>2</sup>; Philippe Venneguès<sup>2</sup>; Sebastien Chenot<sup>2</sup>; Philippe Lorenzini<sup>2</sup>; Marc Portal<sup>2</sup>; Jean Massies<sup>2</sup>; Sanae Boulay<sup>3</sup>; S. Touati<sup>3</sup>; A. A. Sar<sup>3</sup>; V. Hoel<sup>3</sup>; C. Gaquiere<sup>3</sup>; J.C. De Jaeger<sup>3</sup>; <sup>1</sup>STMicroelectronics; <sup>2</sup>CRHEA-CNRS; <sup>3</sup>IEMN-CNRS

In this communication, we will describe the growth which allowed us to obtain hexagonal c-axis GaN layer with Ga-polarity and a single domain orientation on Si(001) substrates by using MBE. The crystal quality and electrical properties of AlGaN/GaN and 2D electron gas realized on Si(001) substrate misoriented by 6° towards the [110] direction are close to those obtained on Si(111). Furthermore, transistors with a 0.1  $\mu\text{m}$  gamma shaped recessed gate have been fabricated to confirm the feasibility and the capability of these devices for microwave power applications. Output current densities of 420mA/mm and extrinsic transconductance (gm) of 228mS/mm are measured on 300 $\mu\text{m}$  gate periphery devices. Extrinsic cut-off frequency (ft) of 28GHz and maximum oscillations frequency (fmax) of 46GHz are deduced from S-parameters measurements. At 2.15GHz, an output power density of 1W/mm associated to a PAE of 17% and a linear gain of 24dB are achieved at  $V_{DS}=30\text{V}$  and  $V_{GS}=-1.2\text{V}$ .

**TP35, High Temperature Power Performance of AlGaN/GaN HEMTs on High-Resistivity Silicon:** *Arulkumaran Subramaniam*<sup>1</sup>; Liu Zhi Hong<sup>1</sup>; Lee Chee How<sup>1</sup>; Ng Geok Ing<sup>1</sup>; <sup>1</sup>Temasek Laboratories, Nanyang Technological University

We investigated for the first time, the effect of high temperature in the microwave power performance of AlGaN/GaN high-electron-mobility transistor (HEMTs) on high-resistivity Silicon (HR-Si) for different microwave frequencies of 3 GHz, 6 GHz and 8 GHz. Due to the smaller thermal conductivity of Si substrate, very little higher rate of decrease in device output power density ( $P_{\text{out}}$ ) was observed. We can claim that the  $P_{\text{out}}$  reduction with temperature from Si-based AlGaN/GaN HEMTs is almost similar to the  $P_{\text{out}}$  reduction with temperature from Si-SiC substrate based AlGaN/GaN HEMTs. After high temperature stress, very small degradation was observed in the power performance of the device at 3 GHz. Moreover, the rate of decrease in  $P_{\text{out}}$  with temperature is not much affected by measurement frequency. The AlGaN/GaN HEMTs on HR-Si can also be used for high-power and high-frequency applications at elevated temperatures.

**TP36, Increase of Electron Velocity in GaN HEMTs by Electric Field Engineering:** *Xu Zhao*<sup>1</sup>; Jinwook Chung<sup>1</sup>; Tomas Palacios<sup>1</sup>; <sup>1</sup>Massachusetts Institute of Technology

Electron velocity influences both the intrinsic delay and drain delay of AlGaN/GaN High Electron Mobility Transistors (HEMTs). The electron velocity in AlGaN/GaN structures reaches a maximum value of  $2.5 \times 10^7 \text{ cm/s}$  at an electric field of 150 kV/cm. However, the electron velocity decreases very rapidly for electric field in excess of the optimal value. In standard GaN HEMT devices, the average electric field in the gate modulated region of the channel far exceeds the optimal value, which results in an effective electron

velocity well below the peak electron velocity. In this paper, we proposed a new GaN HEMT structure with a recessed drain access region to tailor the electric field in the drain access region of these transistors. As a result of the smoothed electric field, our device simulations predict an increase of 50% in the effective electron velocity in the new devices.

**TP37, Phonon-Engineered Reduction of Intrinsic Delay in Nitride HEMTs for mm-Wave Operation:** *Debdeep Jena*<sup>1</sup>; Jacob Khurgin<sup>2</sup>; Yujie Ding<sup>3</sup>; <sup>1</sup>University of Notre Dame; <sup>2</sup>John Hopkins University; <sup>3</sup>Lehigh University

The fT of a nitride HEMT is limited by three delays: the charging delay for the source access region (~0.5ps), the drain delay (~0.5ps), and the intrinsic delay for electrons to traverse the channel (~1ps for a ~160 nm gate HEMT), indicating a saturation velocity of ~1.6e7 cm/s for a ~70 GHz fT device.<sup>1</sup> By direct PL<sup>2</sup> and time-dependent Raman measurements of III-V nitride HEMT structures, LO phonon lifetimes have been measured to be of the order of a few ps, and the high-field saturation velocity of electrons is shown to depend upon the carrier density in the 2DEG channel.<sup>3</sup> A new theoretical model will be presented for high-speed transport properties that limit the intrinsic delay, and epitaxial solutions to the non-equilibrium phonon effect on HEMT speed will be presented. <sup>1</sup>IEEE EDL 27, 877 (2006). <sup>2</sup>APL, 88, 022103 (2006). <sup>3</sup>APL, 89, 202117 (2006).

**TP38, Temperature Effects on Short Gate-Length AlGaIn/GaN HEMTs:** *Guang Chen*<sup>1</sup>; Dong Kim<sup>1</sup>; Vipin Kumar<sup>1</sup>; Ilesanmi Adesida<sup>1</sup>; <sup>1</sup>University of Illinois at Urbana-Champaign

AlGaIn/GaN high electron mobility transistors (HEMTs) of two different gate-lengths were investigated at different temperatures before and after the passivation. Devices with gate-lengths of 100 nm and 250 nm were fabricated on MOCVD-grown AlGaIn/GaN on SiC. The DC results show that the trapping effect is dependent on temperature. The trapped electrons were released at specific temperatures with resulting changes in device properties. Small-signal equivalent circuits are extracted for both devices at different temperatures. The drift velocity is calculated from the equivalent circuit. The 250 nm-device has a drift velocity about 60% lower than the drift velocity of 100 nm device. After passivation, fT decreased for both devices. From the small signal equivalent circuit analysis, this decrease is due to both increase in gate capacitance and decrease in transconductance.

## TP: E-Devices: Sensors and MEMS

**TP39, GaN-Si-MEMS Structure Fabricated from Nano-Column GaN Quantum Well Crystal Grown on Si Substrate:** *Fang Ren Hu*<sup>1</sup>; R. Ito<sup>1</sup>; Y. Zhao<sup>1</sup>; Kazuhiro Hane<sup>1</sup>; <sup>1</sup>Tohoku University

Nano-column InGaIn/GaN multiple quantum-well crystals were deposited on Si (111) substrate. We propose a new light source device combined with MEMS (Micro-Electro-Mechanical Systems). The direction of the light beam emitted from an array of the light source can be changed by a light beam steering mechanism. From the Si substrate with GaN crystal, a micro-stage with comb actuators on which the InGaIn/GaN QW film is patterned has also been fabricated. The proposed device is monolithically composed of the GaN LEDs and Si MEMS structures. Basic researches on the growth of GaN crystals on Si substrate were also carried out. Due to the column structure and the buffer layer, the crystals were relaxed enough to obtain strong photoluminescence.

**TP40, Sensing and Current Transport Mechanisms of a High Performance Pd/AlGaIn/GaN Schottky Diode Hydrogen Sensor:** *Masamichi Akazawa*<sup>1</sup>; Hideki Hasegawa<sup>1</sup>; <sup>1</sup>Hokkaido University

AlGaIn/GaN system is attractive for constructing integrated wireless hydrogen sensor chips for hydrogen monitoring. This paper investigates sensing and current transport mechanisms of a Pd/AlGaIn/GaN Schottky diode hydrogen sensor. As reported recently,<sup>1</sup> reverse leakage current was very much reduced by oxygen gettering, and orders of magnitude current changes took place with hydrogen introduction in air. C-V measurements detected hydrogen-induced reduction of Schottky barrier height (SBH), indicating interface dipole formation by Pd-produced atomic hydrogen. However, I-

V derived SBH values were much smaller than C-V derived values. This discrepancy was quantitatively explained by the thin surface barrier model<sup>2</sup> involving thermionic field emission process. Computer simulation shows that dipole formation is rate-limited, not by interface adsorption, but by surface reaction, leading to a Langmuir isotherm behavior. <sup>1</sup>M.Akazawa and H.Hasegawa, presented at IWN2006, October 22-27, Kyoto. <sup>2</sup>H.Hasegawa and S.Oyama, J. Vac. Sci. Technol. B 20 (2002) 1647.

## TP: Epitaxial

**TP41, A Trade-Off Relation between Tilt and Twist Angle Fluctuations in InN Grown by RF-MBE:** *Akihiro Hashimoto*<sup>1</sup>; Akio Yamamoto<sup>1</sup>; Kosuke Iwao<sup>1</sup>; <sup>1</sup>University of Fukui

In the InN growth on sapphire substrates, it is difficult to control both of tilt and twist angle fluctuations at the same time. It is necessary to understand initial growth stage such as the role of nitridation process to improve the mosaicity. Low-temperature nitridation technique brings the drastically improvement of the tilt angle fluctuation, although the twist angle fluctuation becomes worse. Such experimental results strongly indicate that there is some trade-off relation between the tilt and the twist angle fluctuations as a function of the nitridation condition such as the nitridation time. In this paper, we discuss about such trade-off relation in the direct growth of InN on the nitridation sapphire substrates and also propose a simple model of initial nitridation process to explain it.

**TP42, Cathodoluminescence Spectroscopy and Mapping of AlInN Films in the Mid-Composition Grown by RF-MBE:** *Yu Mimura*<sup>1</sup>; Song-Bek Che<sup>1</sup>; Yoshihiro Ishitani<sup>1</sup>; Akihiko Yoshikawa<sup>1</sup>; <sup>1</sup>Chiba University

InN-based III-nitride semiconductors have attracted much attention as a promising material system for applications in infrared devices. However, AlInN ternary alloys in the mid-composition tend to have a poor crystallinity because of the phase separation arising from the large immiscibility between InN and AlN. We investigated on the detailed crystalline and optical properties of AlInN ternary alloys in the mid-composition grown by RF-MBE at the temperature in the range from 500 to 600°C using cathodoluminescence (CL) spectroscopy and mapping. The AlInN films grown at the temperature below 550°C have the CL spectra those peaks are lower in energy than their bandgaps in spite of their crystalline uniformity. On the other hand, the AlInN films grown at the temperature over 580°C have the CL spectra indicating their poor crystallinity. By raising the growth temperature, the optical property of alloys can be improved but the crystallinity is degraded.

**TP43, Growth of InAlN Thin Films on Si(111) Substrate with Ammonia-MBE:** *Shota Oishi*<sup>1</sup>; Seong-Woo Kim<sup>1</sup>; *Toshimasa Suzuki*<sup>1</sup>; <sup>1</sup>Nippon Institute of Technology

InAlN is a promising material not only for optoelectronic devices but also for new electronic devices such as InAlN/GaN-HFETs. InAlN thin films are usually grown with MOCVD or RF-MBE on a sapphire substrate. In this study, we grew InAlN thin films on Si(111) substrates with ammonia-MBE using HT-AlN buffer layer. Indium containing III-Nitride alloys require lower growth temperature and that is a disadvantage of ammonia-MBE to grow such materials. We varied growth temperature and In/Al flux ratio to control In mole fraction of InAlN. When the growth temperature was 550°C and flux of In and Al was 4.2E-8Torr and 2.0E-8Torr respectively, crack-free and 400nm-thick InAlN film with In composition of 12% was obtained. However, the InAlN film was separated into two phases. Depth profile measurement of matrix elements will be achieved to determine the structure of this sample and to obtain single phase InAlN layer with ammonia-MBE.

**TP44, Investigation into the Use of Molecular Hydrogen on the Growth of Gallium Nitride via Metal-Organic Molecular Beam Epitaxy:** *Daniel Billingsley*<sup>1</sup>; David Pritchett<sup>1</sup>; Shawn Burnham<sup>1</sup>; Walter Henderson<sup>1</sup>; W. Doolittle<sup>1</sup>; <sup>1</sup>Georgia Institute of Technology

Ammonia-based metal-organic molecular beam epitaxy (MOMBE) is a promising technique to exploit the benefits of molecular beam epitaxy (MBE) and metal-organic chemical vapor deposition (MOCVD). However, ammonia nitridation efficiency, as well as carbon contamination from

# Technical Program

metal-organic precursors must be improved. Molecular hydrogen (H<sub>2</sub>) was investigated as a simple technique to improve ammonia nitridation efficiency and to getter carbon containing species. H<sub>2</sub> pre-treatment of bare sapphire before nitridation showed a 30% decrease in x-ray diffraction rocking curve (002) full-width at half maximum of the subsequent GaN with increasing pretreatment temperature, indicating improved crystalline quality. H<sub>2</sub> introduction during GaN homoepitaxy on GaN templates resulted in an 87% reduction in carbon concentration and 20% increase in growth rate. The results demonstrate that the use of H<sub>2</sub> during substrate pretreatment and growth can improve crystalline quality and growth rate while reducing carbon contamination.

**TP45, M-Plane III-Nitride Materials for Polarization Sensitive Devices Grown by PAMBE with Real Time Analysis by Spectroscopic Ellipsometry:** *Pranob Misra*<sup>1</sup>; Chris Boney<sup>1</sup>; David Starikov<sup>1</sup>; Abdelhak Bensaoula<sup>1</sup>; <sup>1</sup>University of Houston

In this paper we present a study of the growth of M-plane GaN, InGa<sub>N</sub>, and AlGa<sub>N</sub> epilayers on LiAlO<sub>2</sub> substrates by plasma assisted molecular beam epitaxy (PAMBE) coupled with in-situ spectroscopic ellipsometry (SE). Previous studies on M-plane materials have suggested that optimum growth conditions with respect to surface morphology are those giving rise to Ga trilayer coverage at low growth temperature. We study the growth nucleation of GaN on LiAlO<sub>2</sub> substrates under Ga rich conditions and growth at Ga stable conditions. It is advantageous to use SE to study the growth regime since it gives a real time information about the metal overlayer thickness, alloy composition and surface roughness. The optical polarization properties of GaN and InGa<sub>N</sub> also have been studied using photoluminescence (PL) and ellipsometry. The resultant measured anisotropy can be employed for fabrication of ultraviolet (UV) and visible photodetectors sensitive to polarization of the incident light.

**TP46, Mosaicity Control of In-Rich InGa<sub>N</sub> in RF-MBE Growth by Template Technique:** *Kosuke Iwao*<sup>1</sup>; Yoshinori Yamada<sup>1</sup>; Akio Yamamoto<sup>1</sup>; Akihiro Hashimoto<sup>1</sup>; <sup>1</sup>University of Fukui

Mosaicity control of InN and In-rich InGa<sub>N</sub> layers are very interesting to improve the crystal quality. However, it has not been few reports on the InN and the In-rich InGa<sub>N</sub> layers growth using the GaN template by RF-MBE. In this paper, the tilt and the twist angle fluctuations of InN and InGa<sub>N</sub> using the GaN templates grown by RF-MBE have been investigated to reveal the key factor for the high quality InN and/or InGa<sub>N</sub> layers. The results strongly indicate that the key factor in determining of the twist angle fluctuation is not only the lattice-mismatch simply, but also the growth mode affected by the alloy formation and that the mosaicity is very sensitive to the structural quality of the GaN template and, therefore, it is expected that the mosaicity of InN may be improved to the similar degree of the mosaicity of the GaN template.

**TP47, New Nitridation Technique for Mosaicity Control in RF-MBE InN Growth:** *Kosuke Iwao*<sup>1</sup>; Akio Yamamoto<sup>1</sup>; Akihiro Hashimoto<sup>1</sup>; <sup>1</sup>University of Fukui

Mosaicity control is necessary for improvement of crystal quality of III-V nitride semiconductor materials, especially for InN. However, the mosaicity control for both of the tilt and the twist angle fluctuations has not been achieved still now in the direct growth of InN on the sapphire substrate by nitridation. Moreover, the role of nitridation process has not been so much clear from the view point of the mosaicity control. In this paper, we propose a new nitridation technique, two-step nitridation combined with the high- and the low- temperature nitridation to reduce the mosaicity and also to make clear the roles of the nitridation process in the InN growth. As the result of the new nitridation technique, the considerably improvement of the tilt and the twist angle fluctuations has been successfully achieved in the direct growth of InN without any buffer layer.

**TP48, RF-MBE Growth and Characterizations of AlGa<sub>N</sub>/GaN HEMTs on Vicinal Sapphire (0001) Substrates:** *Xu-Qiang Shen*<sup>1</sup>; Hiroyuki Sazawa<sup>2</sup>; Hajime Okumura<sup>1</sup>; <sup>1</sup>National Institute of Advanced Industrial Science and Technology (AIST); <sup>2</sup>Sumitomo-Chemical Company, Ltd.

We present our recent results concerning rf-MBE growth and characterizations of AlGa<sub>N</sub>/GaN HEMTs on vicinal sapphire (0001)

substrates. High-quality AlGa<sub>N</sub>/GaN heterostructures with stepped surface were realized by MBE growth on vicinal sapphire substrates. Great improvement of the electrical property of the 2DEG mobility is achieved by using vicinal substrates in the growth. Gate-leakage current is suppressed to more than one order by the usage of vicinal substrates. Furthermore, it is found that maximum source-drain current in the HEMTs increases with the increase of the vicinal angle due to the 2DEG mobility improvement in the heterostructure.

## TP: Epitaxy

**TP49, 2D and 3D Growth Mode Coexistence during Initial Stages of GaN Nucleation on AlN(0001) Surface in Ammonia MBE:** *Andrey Nikitin*<sup>1</sup>; Vladimir Mansurov<sup>1</sup>; Yuriy Galitsyn<sup>1</sup>; Konstantin Zhuravlev<sup>1</sup>; Pierre Tronc<sup>2</sup>; <sup>1</sup>Institute of Semiconductor Physics; <sup>2</sup>Laboratoire d'Optique Physique, Ecole Supérieure de Physique et Chimie Industrielles

The purposes of the present work are investigations of relations between 2D and 3D nucleation and subsequent growth of GaN islands on the (0001) AlN surface in wide range of the growth parameters. In situ behavior of integer and fractional order 2D diffraction streaks as well as transmission 3D Bragg spots was experimentally investigated by RHEED. The coexistence of 2D streaks intensity oscillations and 3D spots intensity increasing was revealed. Usually abrupt 2D-3D transition is observed in this system that is connected with Stranskii-Krastanov growth mode. In contrast we have observed continuous increasing of intensity Bragg spots resulted from 3D GaN islands. The Bragg spot width and in-plane lattice parameter were also changed permanently. This experimental facts point to heterogeneous 3D nucleation of GaN on AlN surface. The exponential increasing of 3D GaN islands density as function of time was revealed. Experimental results are discussed in terms of scaling theory.

**TP50, Impurity Incorporation in N-Face GaN by Plasma-Assisted Molecular Beam Epitaxy:** *Man Hoi Wong*<sup>1</sup>; Tom Mates<sup>1</sup>; James Speck<sup>1</sup>; Umesh Mishra<sup>1</sup>; <sup>1</sup>University of California Santa Barbara

Unintentional impurity incorporation in N-face GaN grown on C-face SiC by plasma-assisted MBE was studied. Direct nucleation of GaN on SiC resulted in high Si and C incorporation from the substrate, with the Si causing undesirable conduction in HEMT buffers. A 50nm N-rich AlN nucleation was sufficient in suppressing Si and C concentration to 10<sup>16</sup> cm<sup>-3</sup> in the subsequent GaN layer without significant impact to structural quality. Such nucleation scheme, together with two-step GaN to reduce threading dislocation density, offers high quality insulating materials for N-face electronics. The growth and transport of Si-doped and Mg-doped GaN on these buffers were studied. Room temperature electron mobility varied with [Si], with peak value of 355 cm<sup>2</sup>/Vs at [Si]=1x10<sup>18</sup> cm<sup>-3</sup>. Mg incorporation is dependent on III/V ratio and growth temperature. Room temperature hole mobility of 6.5 cm<sup>2</sup>/Vs was measured at [Mg] = 1.2x10<sup>20</sup> cm<sup>-3</sup>. This work provides useful information for engineering N-face devices.

**TP51, Influence of the Mn Compositional Distribution on the Magnetic Order in Diluted GaMnN Layers:** *Dong-Du Mai*<sup>1</sup>; Tore Niermann<sup>1</sup>; Jan Zenneck<sup>1</sup>; Amilcar Bedoya-Pinto<sup>1</sup>; Joerg Malindretos<sup>1</sup>; Michael Seibt<sup>1</sup>; Angela Rizzi<sup>1</sup>; <sup>1</sup>Georg-August-Universitaet Goettingen

GaMnN is a prototypical GaN-based DMS and his potential as a room temperature ferromagnetic material is still a controversial question to be answered. Diluted GaMnN layers with Mn concentrations up to several percent have been grown by plasma-assisted MBE on MOVPE-GaN/Al<sub>2</sub>O<sub>3</sub> substrates under various growth conditions. None of the samples reported here show second phase precipitates in XRD or in the TEM analysis. However different composition distributions have been evidenced by EDX during the scanning TEM analysis. GaMnN grown at T<sub>s</sub>=650°C exhibits extended structural defects and strong compositional inhomogeneity. This could be indicative of spinodal decomposition due to local strain. Samples grown at T<sub>s</sub>=775°C with a Mn concentration below the yield of second phase formation show a homogeneous Mn distribution in the layer. The magnetic properties are found to vary from spin glass to ferromagnetic behaviour at room temperature among different samples.

**TP52, InGaN Compositional Control by Ultraviolet Photoexcitation during NH<sub>3</sub>-Based MOMBE – A Pathway to 3D Epitaxy:** *David Pritchett*<sup>1</sup>; Walter Henderson<sup>1</sup>; Daniel Billingsley<sup>1</sup>; William Doolittle<sup>1</sup>; <sup>1</sup>Georgia Institute of Technology

Novel device concepts integrating features such as low-dimensionality and lateral bandgap energy modulation are complicated by expensive lithography, etching, and regrowth sequences. Metal organic molecular beam epitaxy (MOMBE) is a good candidate for in-situ patterned epitaxy of such structures due to a high vacuum environment and sensitive growth mechanism. The sensitive MOMBE growth pathways may be carefully manipulated for surface selective epitaxy. Despite successful arsenide, phosphide, and antimonide based structures grown by MOMBE with patterned dielectric masks, NH<sub>3</sub>-based MOMBE of nitrides has received little attention. Herein, we report the first InGaN films by NH<sub>3</sub>-based MOMBE. We identify a III-alkyl desorption phenomena inversely related to the resultant indium mole fraction. Moreover, we report significant InGaN alloy compositional variation using in-situ micromirror-patterned ultraviolet (UV) photoexcitation. Coupled with reported UV photoexcitation effects on GaN carbon doping, the technique shows promise for dynamic manipulation of nitride growth useful for complex, 3D device structures.

**TP53, Nitrides on a-Plane LiAlO<sub>2</sub>:** *Li-Wei Tu*<sup>1</sup>; H. M. Huang<sup>1</sup>; M. Z. Hsu<sup>1</sup>; L. K. Wang<sup>1</sup>; Y. L. Cheng<sup>1</sup>; M. C. Chou<sup>1</sup>; Q. Y. Chen<sup>2</sup>; W. K. Chu<sup>2</sup>; <sup>1</sup>National Sun Yat-Sen University; <sup>2</sup>University of Houston

Gamma-phase lithium aluminate (LiAlO<sub>2</sub>) single crystal is grown by Czochralski pulling method and a-plane LiAlO<sub>2</sub> (LAO) is chosen as the substrate for subsequent nitride epitaxial growth by plasma-assisted molecular beam epitaxy (PAMBE). The lattice mismatch between the nitride and the substrate is greatly reduced due to the small lattice mismatch of ~ 0.3% between [0001]GaN and [010]LAO and of ~1.7% between [11-20]GaN and [001]LAO in the plane of the substrate LAO(100). Pure hexagonal GaN in the [10-10] direction is successfully grown directly on the LAO substrate without buffer layer. Crystal quality and properties are analyzed through a series of measurements, including reflection high-energy electron diffraction (RHEED), field-emission electron microscopy (FESEM), cathodoluminescence (CL), photoluminescence (PL), x-ray diffraction (XRD), Raman spectroscopy, etc. Nanostructures and others are also explored on top of the non-polar m-GaN layer. Electron backscatter diffraction (EBSD) is performed on the samples to determine the nanocrystal orientation and quality.

**TP54, Non-Polar a-Plane GaN Grown on r-Plane Sapphire by Ammonia Source Molecular Beam Epitaxy:** *Tiankai Zhu*<sup>1</sup>; Amélie Dussaigne<sup>1</sup>; Claire Pinquier<sup>1</sup>; Denis Martin<sup>1</sup>; Nicolas Grandjean<sup>1</sup>; <sup>1</sup>Ecole Polytechnique Fédérale de Lausanne

Thin a-plane GaN layers are grown on r-plane sapphire substrates by ammonia source molecular beam epitaxy (MBE). Optical properties are investigated by low temperature (LT) photoluminescence (PL). The LT PL spectra are dominated by near band-edge emission at ~ 3.47 eV, with full width at half maximum ≤ 20 meV, indicating the good quality of the epilayers. Both basal stacking faults related emission peak at 3.42 eV and defects-related emission peak at 3.30 eV are observed, with a much lower intensity. Besides, the surface morphology and structural properties of MBE-grown epilayers are characterized by atomic force microscopy and high resolution X-ray diffraction, respectively. Furthermore, GaN/Al<sub>0.1</sub>Ga<sub>0.9</sub>N single quantum well (well width = 8 nm) is grown on this template by MBE. Its LT PL emission peak at ~ 3.51 eV confirms the absence of internal electric field.

**TP55, Plasma Assisted Molecular Beam Epitaxy of AlGaIn/GaN High Electron Mobility Transistors:** *Rolf Aidam*<sup>1</sup>; Lutz Kirste<sup>1</sup>; Michael Kunzer<sup>1</sup>; Stefan Müller<sup>1</sup>; Patrick Waltereit<sup>1</sup>; <sup>1</sup>Fraunhofer IAF

We report on the plasma-assisted molecular beam epitaxy of AlGaIn/GaN high electron mobility transistors (HEMTs). Growth was performed on MOCVD grown GaN Templates and SiC wafers with 3" diameter. In a detailed study of GaN growth conditions the growth rate was varied between 0.18 and 0.5 μm/h. Under optimised conditions, the surface root mean square roughness was less than 0.6nm. Low temperature PL measurements in the range 1.9 to 3.8 eV showed only the exciton-emission with a FWHM of

12meV. AlGaIn-HEMT structures exhibited room temperature Hall mobilities in excess of 1600 cm<sup>2</sup>/Vs and sheet electron concentration of 7 × 10<sup>12</sup>/cm<sup>2</sup>. We will present buffer leakage data, studied by measurement of drain source IV characteristics, as well as DC, small signal and RF measurements on HEMTs.

**TP56, Properties of Fe Doped GaN Films Prepared by Molecular Beam Epitaxy:** *Alexander Polyakov*<sup>1</sup>; Nikolai Smirnov<sup>1</sup>; Anatoliy Govorkov<sup>1</sup>; Alexander Markov<sup>1</sup>; Tatyana Yugova<sup>1</sup>; Elena Petrova<sup>1</sup>; Amir Dabiran<sup>2</sup>; Andrew Wowchak<sup>2</sup>; Andrei Osinsky<sup>2</sup>; Peter Chow<sup>2</sup>; Stephen Pearton<sup>3</sup>; <sup>1</sup>Institute of Rare Metals; <sup>2</sup>SVTA Associates, Inc.; <sup>3</sup>University of Florida

Electrical properties were studied for MBE GaN(Fe) buffers with various Fe concentrations, together with the results of electrical characterization of lightly doped n-GaN films and HEMT structures prepared on such buffers. SIMS profiling shows that, in contrast MOCVD, there are no long tails of Fe concentration extending into the undoped portions of the films. The buffers are semi-insulating, with the Fermi level pinned near Ec-0.5 eV. In agreement with SIMS data, we did not detect the presence of Fe related centers in the n-type portions of the films in the concentration exceeding some 10<sup>14</sup> cm<sup>-3</sup>. HEMTs prepared on such buffers showed good pinch-off in I-V and C-V characteristics, good interdevice insulation, and high 2DEG mobility and density. All that suggests Fe doped MBE grown buffers as a good option for preparation of HEMT structures. Detailed studies point to the optimal range of Fe source temperatures for transistor applications.

**TP57, RF-MBE Growth of Cubic InN Films on YSZ(001) Vicinal Substrates:** *Teruyuki Nakamura*<sup>1</sup>; Takahiro Kataoka<sup>1</sup>; Ryuji Katayama<sup>1</sup>; Kentaro Onabe<sup>1</sup>; <sup>1</sup>University of Tokyo

The YSZ(yttria-stabilized zirconia)(001) vicinal substrates were adopted to the growth of cubic-phase InN (c-InN) films in an attempt to improve the cubic-phase purity in the film. The YSZ substrate has the advantages of the small lattice-mismatch (3%) to c-InN and the atomically flat surface with a step-and-terraced structure obtained by annealing. The hexagonal-phase incorporation (HPI) is much reduced by the growth on such a well-defined surface as shown before. In this study, the InN films were grown by RF-MBE on the YSZ(001) just and 1° misoriented (toward <110>) substrates annealed at 1250°C in air. From an analysis of the X-ray diffraction reciprocal space mapping, it is known that the HPI ratio has decreased from 16.3% to 11.7% by using the vicinal substrate, and that the hexagonal phase is generated predominantly through the stacking faults on the c-InN(111) facets which are inclined to the upward direction of the atomic steps.

**TP58, Strain Control in AlGaIn/GaN HEMT Grown on SiC by Ammonia MBE:** *Haipeng Tang*<sup>1</sup>; Stephen Rolfe<sup>1</sup>; Jean-Marc Baribeau<sup>1</sup>; Jennifer Bardwell<sup>1</sup>; <sup>1</sup>National Research Council Canada

AlGaIn/GaN HEMT structures grown by ammonia MBE on SiC substrates exhibit a biaxial tensile strain due to a large difference of the thermal expansion coefficients of the GaN material and SiC. The thermally induced tensile strain after cooling down from a growth temperature of about 900°C is in the order of 0.1%. This level of tensile strain is significant enough to cause cracking of the HEMT structure either immediately after growth or during subsequent processing steps. Here we report results of control of lattice strain during growth so that built-in compressive lattice strain offsets part of the tensile thermal strain. The role of the AlN buffer layer and the effect of its thickness were investigated. Using two AlN interlayers within the semi-insulating (carbon-doped) GaN layer was found to effectively reduce the tensile strain. The strain engineered HEMT structures were stable in all device processing procedures including the surface passivation.

## TP: Heterostructures

**TP59, AlGaIn-Based Heterostructures Grown on 4 Inch Si(111) by MOVPE:** *Kai Cheng*<sup>1</sup>; Maarten Leys<sup>1</sup>; Joff Derluyn<sup>1</sup>; Krishnan Balachander<sup>1</sup>; Stefan Degroote<sup>1</sup>; Marianne Germain<sup>1</sup>; Gustaaf Borghs<sup>1</sup>; <sup>1</sup>IMEC

AlGaIn is an important material for ultra-violet light emitters, photo detectors and high breakdown switching devices. In this work, crack-free Al<sub>x</sub>Ga<sub>1-x</sub>N (5% < x < 55%) layers up to 1.5 μm have been grown on 4 inch

# Technical Program

Si(111) using an AlN/Al<sub>0.16</sub>Ga<sub>0.84</sub>N ( $y > 70\%$ ) template. The structural quality of AlGa<sub>0.16</sub>N layers is comparable to that of GaN layers grown on silicon(111). For Al<sub>0.16</sub>Ga<sub>0.84</sub>N, the FWHM of XRD (0002) and (-1102)  $\omega$ -scans are around 650 arc sec and 1200 arc sec respectively. Based on this high quality AlGa<sub>0.16</sub>N buffer, a double heterostructure (DH) FET was demonstrated. The sheet resistance of DH-FET is  $274 \pm 4.7 \Omega/\text{ff}$  and the uniformity value of 1.7% is also excellent. Some of the wafers have been processed. Devices with a gate length of 2 $\mu\text{m}$  show current density of 500 mA/mm and transconductance of more than 200 mS/mm.

**TP60, Characterization of Mg-Doped AlInN Grown by Metalorganic Vapor Phase Epitaxy:** Yan-Kuin Su<sup>1</sup>; An-Ting Cheng<sup>1</sup>; Wei-Chi Lai<sup>2</sup>; <sup>1</sup>Advanced Optoelectronic Technology Center, Institute of Microelectronics and Department of Electrical Engineering, National Cheng Kung University; <sup>2</sup>Institute of Electro-Optical Science and Engineering, National Cheng Kung University

We report on the growth of undoped and Mg-doped AlInN by metalorganic vapor phase epitaxy. The indium content and the FWHM of undoped AlInN layer were 20.9% and 219.6 arcsec, respectively, from HRXRD measurement. It was also observed that an additional satellite peak was formed near the AlInN peak after introducing the Mg dopant. The sheet hole concentration of  $4.73 \times 10^{12} \text{ cm}^{-2}$  was achieved after performing the thermal annealing. As the flow rate of Cp<sub>2</sub>Mg source was increased, we found that both the satellite peak and the AlInN peak shifted toward higher angles. However, higher Cp<sub>2</sub>Mg flow rate would not only decrease the conductivity of AlInN layer due to the higher Al content shown in HRXRD spectrum but increase the surface roughness. Therefore, these results suggest that p-type AlInN cladding layer nearly lattice-matched to GaN will be realized with lower Cp<sub>2</sub>Mg flow rate for optical device applications.

**TP61, Comparative Studies of InGa<sub>0.5</sub>N Multiple Quantum Wells Grown on Porous and Non-Porous GaN Layers by Metal-Organic Chemical Vapor Deposition:** Yong-Hwan Kim<sup>1</sup>; Seol Back<sup>1</sup>; Ho-Sang Kwack<sup>1</sup>; Ki-Yon Park<sup>1</sup>; Yong-Hoon Cho<sup>1</sup>; <sup>1</sup>Chungbuk National University

We have investigated the structural and optical properties of InGa<sub>0.5</sub>N multiple quantum wells (MQWs) grown on porous and non-porous GaN layers by metal organic chemical vapor deposition (MOCVD). A 2  $\mu\text{m}$ -thick undoped GaN layer was grown on sapphire substrate by MOCVD technique, and then chemically etched to form porous GaN layer. After the fabrication of the porous GaN layer, an InGa<sub>0.5</sub>N MQW light emitting diode (LED) structure was grown on top of this porous GaN structure by MOCVD (sample A). For comparison, the same InGa<sub>0.5</sub>N MQWs LED structure was grown on an un-etched (non-porous) GaN layer (sample B). The PL peak wavelength of sample B was observed to be about 436 nm, while a 32-nm blueshift was observed for sample A, which can be attributed to the change in stress and related internal field effect. Detailed comparison of the structural and optical properties for these samples will be given.

**TP62, Demonstration of GaN/InGa<sub>0.5</sub>N Light Emitting Diodes on (100)  $\beta$ -Ga<sub>2</sub>O<sub>3</sub> Substrates by Metalorganic Chemical Vapor Deposition:** ZiLi Xie<sup>1</sup>; Rong Zhang<sup>1</sup>; Xiangqian Xiu<sup>1</sup>; Ping Han<sup>1</sup>; RuoLian Jiang<sup>1</sup>; YouDou Zheng<sup>1</sup>; <sup>1</sup>Nanjing University

$\beta$ -Ga<sub>2</sub>O<sub>3</sub> is a kind of transparent conductors and has n-type conductivity. It has the unique transparency from the visible into the UV region. This is an important property for the future generations of optoelectronic devices operating at shorter wavelengths.  $\beta$ -Ga<sub>2</sub>O<sub>3</sub> is a new substrate candidate for the growth of GaN related materials and devices. The GaN/InGa<sub>0.5</sub>N MQW LED was grown on the near UV transparency  $\beta$ -Ga<sub>2</sub>O<sub>3</sub> substrate by MOCVD technique. The n-type conductive GaN buffer layer was deposited under the LED structure on the substrate. The LED successfully emitted the green light after the vertical current injection. The PL emission peak is at 529nm. The green emission peak at 537nm was obtained on EL measurements with 20V voltages and 0.7mA drive currents. This result demonstrates the high potential of  $\beta$ -Ga<sub>2</sub>O<sub>3</sub> as a new near UV transparency and conductive substrate.

**TP63, Dislocation Annihilation in GaN with Multiple MgN/GaN Buffer Layer by Metalorganic Chemical Vapor Deposition:** Y. K. Fu<sup>1</sup>; C. W. Kuo<sup>1</sup>; C. J. Tun<sup>2</sup>; C. J. Pan<sup>1</sup>; Cheng-Huang Kuo<sup>1</sup>; G. C. Chi<sup>1</sup>; <sup>1</sup>National Central University; <sup>2</sup>National Synchrotron Radiation Research Center

The unintentionally doped GaN epitaxial layers with conventional single low-temperature (LT) GaN buffer layer and with multiple MgN/GaN buffer layers were grown on sapphire substrates by metalorganic chemical vapor deposition (MOCVD). It was found that multiple MgN/GaN buffer layer exhibits lower nuclei density which could increase the volume of defect-free regions and reduce the dislocations associated with the grain boundaries. Therefore, the GaN with multiple MgN/GaN buffer layers exhibits the narrow full-width at half-maximum (FWHM) of X-ray asymmetrical reflection (102), higher mobility, lower background concentration and lower etching pits density (EPD) than the GaN with LT GaN buffer layer.

**TP64, Effect of Ammonia and Silane Flow Rate on the Structural, Electrical and Optical Properties of n-Type AlGa<sub>0.7</sub>N for UV Emitter Applications:** Kaixuan Chen<sup>1</sup>; Wonseok Lee<sup>1</sup>; Qi Dai<sup>1</sup>; Frank Mont<sup>1</sup>; Jongkyu Kim<sup>1</sup>; E. Schubert<sup>1</sup>; Wayne Liu<sup>2</sup>; Shuai Wu<sup>2</sup>; Joseph Smart<sup>2</sup>; <sup>1</sup>Rensselaer Polytechnic Institute; <sup>2</sup>Crystal IS

The effect of ammonia and silane flow on the properties of n-type Al<sub>0.3</sub>Ga<sub>0.7</sub>N grown by metal-organic vapor-phase epitaxy is systematically studied. It is found that a high ammonia flow rate strongly improves the structural, electrical and optical properties of n-type Al<sub>0.3</sub>Ga<sub>0.7</sub>N. The specific effects of a high ammonia flow rate are as follows: (i) the density of hexagonal holes on the n-type Al<sub>0.3</sub>Ga<sub>0.7</sub>N surface is drastically reduced; (ii) the electron concentration and mobility increase; (iii) defect-related deep-level transitions in photoluminescence are reduced. Furthermore, the strain in the n-type Al<sub>0.3</sub>Ga<sub>0.7</sub>N is found to be sensitive to the silane flow rate. A high silane flow rate results in a crack network in the n-type Al<sub>0.3</sub>Ga<sub>0.7</sub>N.

**TP65, Effect of Dimethylhydrazine in p-Type Conductivity of as-Grown Mg-Doped GaN:** Dong Hyuk Kim<sup>1</sup>; Go Eun Lee<sup>1</sup>; Yong Seon Jeon<sup>1</sup>; Euijoon Yoon<sup>1</sup>; Do-Young Park<sup>2</sup>; Hyeonsik Cheong<sup>2</sup>; Woo Seok Choi<sup>1</sup>; Tae Won Noh<sup>1</sup>; Jin-Hyung Cho<sup>3</sup>; Joong-Seo Park<sup>3</sup>; <sup>1</sup>Seoul National University; <sup>2</sup>Sogang University; <sup>3</sup>EpiValley Company, Ltd.

The reduction of H radicals in growth ambient will be a useful method for as-grown p-type GaN because the main origin of Mg passivation in p-type GaN is the H radical from NH<sub>3</sub>. Addition of DMHy to group V source can decrease the consumption of NH<sub>3</sub> by 90 % compared with conventional GaN growth. Raman spectra confirm that H atoms are not combined with Mg atoms even in as-grown state in Mg-doped GaN using DMHy. From the SIMS analysis, the carbon concentrations in GaN using DMHy are almost an order of magnitude higher than that of GaN using NH<sub>3</sub>. Observation of three absorption peaks related to CH<sub>n</sub> complexes in FT-IR spectra shows hydrogen trapping at carbon impurities. DMHy can reduce H radical concentration in growth ambient by reduction of NH<sub>3</sub> flow rate and also by the formation of CH<sub>n</sub> complexes, resulting in p-type conductivity of as-grown Mg-doped GaN.

**TP66, Effect of Metallic Surface Coverage on Material Quality in III-Nitride MOVPE:** Alexey Kondratyev<sup>1</sup>; Roman Talalaev<sup>2</sup>; Alexander Segal<sup>1</sup>; Eugene Yakovlev<sup>1</sup>; Wsevolod Lundin<sup>3</sup>; Evgeny Zavarin<sup>3</sup>; Mikhail Sinitsyn<sup>3</sup>; Andrew Tsatsulnikov<sup>3</sup>; <sup>1</sup>Soft-Impact; <sup>2</sup>Semiconductor Technology Research GmbH; <sup>3</sup>Ioffe Physico-Technical Institute

Pinholes or V-like defects are the well known type of defects, characteristic for nitride growth by MOVPE. This paper reports on the studies of correlation between defect appearance and MOVPE growth conditions and discusses the ways to improve the material quality. Decrease of ammonia flow at constant total flow during MOVPE of GaN in hydrogen-ammonia atmosphere at moderate temperatures (750-900°C), has revealed the overgrowth of pinholes up to their almost complete disappearance. The same effect was observed at the addition of a certain amount of TMI and was accompanied by very small incorporation of indium into the crystal. In both cases the improvement in morphology was associated with accumulation of metallic (Ga and In, respectively) atoms in the adsorption layer at the growing surface. This conclusion was supported by surface kinetics model computations. The model suggests the possible strategies for growth of the pinhole-free layers for various device structures.

**TP67, Effects of Growth Temperature and Reactor Pressure on the InGaN Films Grown by Metalorganic Chemical Vapor Deposition:** *Xian Sun*<sup>1</sup>; <sup>1</sup>Institute of Semiconductors, Chinese Academy of Sciences

InGaN films have been grown on GaN template by metalorganic chemical vapor deposition with the condition of varied growth temperature and reactor pressure. The In composition is determined by  $\omega\omega - 2\theta$  scan of Double-Crystal X-ray Diffraction (DC-XRD) and room-temperature photoluminescence (PL) measurements. It was found that the In composition increases with the reactor pressure from 100Torr to 200Torr, and slightly decreases as it increases from 200Torr to 400Torr. The growth rate and In composition of InGaN films increase with decreasing growth temperature. The potential reason lies in that InN is more stable at lower temperature. Crystal quality of InGaN films degrades with the increase of In content indicated by the full width at half maximum of  $\omega$  scan of XRD. However, extremely low growth temperature and high In/Ga ratio lead to the appearance of In droplets on the surface.

**TP68, Epitaxial Lateral Overgrowth of GaN on 4" Si(111) by MOVPE:** *Kai Cheng*<sup>1</sup>; *Vasyl Motsnyi*<sup>1</sup>; *Maarten Leys*<sup>1</sup>; *Stefan Degroote*<sup>1</sup>; *Bram Sijmus*<sup>1</sup>; *Marianne Germain*<sup>1</sup>; *Gustaaf Borghs*<sup>1</sup>; <sup>1</sup>IMEC

Epitaxial Lateral Overgrowth (ELOG) of GaN on 4" silicon(111) substrates by MOVPE was investigated in this study. ELOG was performed on a GaN template with a couple of AlGaIn intermediate layers (IL) on an AlN nucleation layer. The AlGaIn ILs supply compressive stress to the top GaN template and thereafter to the ELOG layer. Consequently, layer cracking is minimized. Two masks were used in this work: a 2" wagon wheel mask and a 4" mask with parallel stripes of various filling factors and periods. The filling factor is varied from 0.3 to 0.7. The periodic spacing is in the range of 6  $\mu\text{m}$  to 20  $\mu\text{m}$ . Temperature, V/III ratio, pressure and stripe orientation, were optimized to achieve fastest lateral growth rate. The highest lateral to vertical ratio can be more than 4. A fully coalesced layer within the critical thickness was achieved on 4" silicon substrates.

**TP69, GaN Growth on Silane Exposed AlN Seed Layers:** *Francisco Ruiz*<sup>1</sup>; *Oscar Contreras*<sup>2</sup>; *Armin Dadgar*<sup>3</sup>; *Alois Krost*<sup>3</sup>; <sup>1</sup>Centro de Investigación Científica y de Educación Superior de Ensenada; <sup>2</sup>Centro de Ciencias de la Materia Condensada, UNAM; <sup>3</sup>Otto-von-Guericke Universität Magdeburg

The microstructure and surface morphology of GaN films grown on AlN seed layers exposed to silane ( $\text{SiH}_4$ ) flow, has been studied by AFM and TEM. The AlN seed layer surface was treated at different  $\text{SiH}_4$  exposure times before the growth of the GaN film by MOCVD. Radical changes are observed on the surface morphology of the GaN films as a function of the  $\text{SiH}_4$  treatment. A pit density reduction is observed at the surface of GaN as a function of the  $\text{SiH}_4$  exposure time. The surface roughness is minimized for an optimal time of 75-to-90 sec of  $\text{SiH}_4$  exposure and a step-flow growth mode is observed at this condition. A cross-sectional microstructural analysis reveals a conglomeration of threading dislocation right above the AlN seed layer, which reduces the dislocation density at the surface resulting in an improvement of the GaN surface quality.

**TP70, Growth Characteristics of AlGaIn/GaN HEMTs on Patterned Si(111) by MOCVD:** *Yong Wang*<sup>1</sup>; *Congshun Wang*<sup>2</sup>; *Kevin Chen*<sup>2</sup>; *Kei May Lau*<sup>1</sup>; <sup>1</sup>Photonics Technology Center, Electronics and Computer Engineering Department, HongKong University of Science and Technology; <sup>2</sup>Electronics and Computer Engineering Department, HongKong University of Science and Technology

Growth characteristics of AlGaIn/GaN HEMT structures on patterned Si(111) substrates are reported. The patterns on the Si substrates were fabricated by  $\text{SiO}_2$  or  $\text{SiN}$  masks and wet etching. Growth experiments were carried out in a multi-wafer MOCVD system on unpatterned, patterned without mask, and patterned with mask Si wafers. Double AlN interlayers grown at high temperature were employed to release the tensile stress from the large mismatch in the lattice constants and thermal expansion coefficients. Before achieving optimized growth conditions, more cracking lines were observed on patterns along the [1-100] orientation than along the [11-20] orientation, resulted from more stable GaN (1-100) facets than GaN (11-20) facets. It is suggested that long patterns should be made along the [11-20] orientation. Micro-Raman measurements showed that Raman shifts at the

concave corners are bigger than that at the convex corner, indicating the larger stress at the concave corners.

**TP71, Growth of Nonpolar GaN Epitaxial Film on a Lattice-Matched  $\gamma$ -LiAlO<sub>2</sub> Substrate by Chemical Vapor Deposition:** *Chenlong Chen*<sup>1</sup>; *Mitch M.C. Chou*<sup>1</sup>; *Da-Ren Hang*<sup>1</sup>; *Cheng-Hong Way*<sup>1</sup>; *Jih-Jen Wu*<sup>2</sup>; <sup>1</sup>National Sun Yat-Sen University; <sup>2</sup>National Cheng Kung University

In this report, a simple chemical vapor deposition approach to the growth of nonpolar GaN with [10-10] orientation on a (100)  $\gamma$ -LiAlO<sub>2</sub> substrate was presented. The orientation of GaN film is identified as [10-10] or m-plane by X-ray diffraction pattern (XRD). The surface morphologies of GaN film were investigated by scanning electron microscopy (SEM). The SEM image shows a high density of well-aligned GaN islands with rectangular structure. GaN hexagons lied down on the surface of LiAlO<sub>2</sub> substrate. The orientation of GaN hexagons is the same as the assumption of lattice match. The SEM image also showed that GaN has a higher growth rate in lateral (0001) direction which is parallel to LiAlO<sub>2</sub> substrate than (10-10) growth direction. Photoluminescence (PL) characteristics of the GaN films show a strong UV light emission at room temperature.

**TP72, Heteroepitaxial Growth of High Quality GaN Thin Films on Si Substrates Coated with Self-Assembled Submicron Silica Balls:** *Sung Jin An*<sup>1</sup>; *Young Joon Hong*<sup>1</sup>; *Gyu-Chul Yi*<sup>1</sup>; *Yong-Jin Kim*<sup>2</sup>; *Dong Kun Lee*<sup>2</sup>; <sup>1</sup>POSTECH; <sup>2</sup>LG Siltron

A simple maskless overgrowth technique without either lithography or interruption can simplify the growth process, which is very helpful for high yield and low cost device fabrications. Here, we present a maskless heteroepitaxial GaN growth on a Si substrate with a self-assembled submicron silica ball layer(SBS). Monodispersed submicron-size silica balls were employed as an intermediate layer for heteroepitaxial growth of GaN layers on Si(111) substrates. The GaN surfaces were fairly flat, and no pits or cracks were observed. The FWHM value of rocking curve was  $0.18^\circ$ , much smaller than that of GaN epilayer on bare Si substrates,  $0.30^\circ$ . Furthermore, TEM and AFM revealed many enhanced structural characteristics and improved crystallinity for the GaN films on SBS substrates. In particular, for the regions on or near the silica balls, no threading dislocations were observed and the total number of dislocations of the GaN on SBS substrate was smaller than  $10^8 \text{ cm}^{-2}$ .

**TP73, High Efficiency AlN Epitaxial Growth by Hot-Wall MOCVD in Nitrogen: From Experiment and Theory:** *Anelia Kakanakova*<sup>1</sup>; <sup>1</sup>Linköping University

We show the beneficial effect of nitrogen on the AlN MOCVD growth process as manifested by high AlN growth rate, 2  $\mu\text{m/h}$ , and strong cathodoluminescence AlN near band edge emission when the AlN growth was done in nitrogen carrier gas only. Comparison is done to the properties of the AlN layers when grown in hydrogen only and in mixture of hydrogen and nitrogen. The direct participation of nitrogen in the modification of gas-phase chemistry is studied via Density Functional Theory calculations by considering the stability of reaction species like adducts, corresponding transition states for methane elimination and adduct-derived chain complexes, when exposed to an ambient of hydrogen or nitrogen molecules. The growth, including on 2 inch SiC wafers, is performed in hot-wall MOCVD reactor at temperatures higher than  $1100^\circ\text{C}$  in the view of the ever anticipated understanding that elevated temperatures during AlN epitaxy promote better crystal quality.

**TP74, Highly Uniform Hot-Wall MOCVD Growth of High-Quality AlGaIn/GaN HEMT-Structures on 100 mm Semi-Insulating 4H-SiC Substrates:** *Erik Janzén*<sup>1</sup>; *Anders Lundskog*<sup>1</sup>; *Urban Forsberg*<sup>1</sup>; *Anelia Kakanakova-Georgieva*<sup>1</sup>; *Ivan Ivanov*<sup>1</sup>; <sup>1</sup>Linköping University

We have grown an AlGaIn/GaN HEMT structure on a semi-insulating 100 mm 4H-SiC substrate in a hot-wall MOCVD reactor with rotation of the wafer during growth. The epi thickness is highly uniform with an average of 1.77  $\mu\text{m}$  and a nonuniformity ( $\sigma/\text{average}$ ) of 2.8 %. The sheet resistance is highly uniform with a very low average of 268  $\Omega$  and a nonuniformity ( $\sigma/\text{average}$ ) of 2.1 %. The results from mercury probe CV-measurements are: Sheet carrier density  $9.9 \times 10^{12} \text{ cm}^{-2}$ ,  $V(\text{pinch-off}) = -5.3 \text{ V}$ , thickness of (AlGaIn + AlN) = 25 nm, no electrons in the GaN layer. From the measured

# Technical Program

sheet resistance and the measured sheet carrier density we can calculate the room temperature drift mobility to be 2360 cm<sup>2</sup>/Vs.

**TP75, Improved Surface Morphology of Flow-Modulated MOVPE Grown AlN on Sapphire Using Thin Medium-Temperature AlN Buffer Layer:** *Dabing Li*<sup>1</sup>; Masakazu Aoki<sup>1</sup>; Hideto Miyake<sup>1</sup>; Kazumasa Hiramatsu<sup>1</sup>; Mie University

High-temperature (HT) AlN films were grown on (0001) sapphire by low-pressure flow-modulated (FM) MOVPE with and without inserting a thin medium-temperature (MT) AlN layer. The AFM and SEM measurements indicated that the thin MT-AlN layer had a strong influence on the surface morphology of the HT-AlN films. The surface morphology became quite smooth by inserting the thin MT-AlN layer and surface RMS roughness values were 0.84nm and 13.4nm for the HT-AlN films with and without the thin MT-AlN buffer layer, respectively. By etching the samples in aqueous KOH solution, it was found that the polarity of AlN films was different. The full width at half maximum values of (0002) and (10-12) for HT-AlN without the MT-AlN layer are 90arcsec and 1080arcsec and for HT-AlN with the MT-AlN layer are 65arcsec and 1512arcsec. The mechanism for the origin of the different polarity of HT-AlN with and without the thin MT-AlN layer was discussed in detail.

**TP76, Isotropic Coalescence Behaviours of GaN Islands Grown by Metalorganic Chemical Vapor Deposition:** *Soo-Jin Chua*<sup>1</sup>; Hai Long Zhou<sup>2</sup>; D.J. Srolovitz<sup>3</sup>; Dan Xu Du<sup>4</sup>; <sup>1</sup>Institute of Materials Research and Engineering; <sup>2</sup>National University of Singapore; <sup>3</sup>Yeshiva University; <sup>4</sup>Princeton University

In Epitaxial Layer Overgrowth (ELO) technology, GaN is grown inside the stripe window of a SiO<sub>2</sub> mask and then grow laterally over the mask to eventually merge and form a uniform thin film. The merging behaviours of GaN islands along different directions can influence the strain and bending of dislocations. GaN islands which merge along the direction have two parallel sides of the hexagonal islands aligned parallel whereas those aligned in the direction have their tips pointed towards one another. Growth along is found to be faster than along by a ratio of 1:0.85. After merging, the island shows different shapes which affect the strain within the islands. After the growth of the stripes to form triangular ridges, the facets are formed on stripes aligned along while the facets are formed on stripes aligned along. Defects are observed on the facets but not on the facets.

**TP77, Low Temperature Growth of Nitride Films by Near-Atmospheric Plasma-Assisted Chemical Vapor Deposition:** *Takahiro Nagata*<sup>1</sup>; Yoshiki Sakuma<sup>1</sup>; Jyunichiro Anzai<sup>2</sup>; Tsuyoshi Uehara<sup>2</sup>; Syunsuke Kunugi<sup>2</sup>; Toyohiro Chikyo<sup>1</sup>; <sup>1</sup>National Institute for Materials Science; <sup>2</sup>Seikisui Chemical Company, Ltd.

We have demonstrated the growth of GaN film by near-atmospheric plasma-assisted chemical vapor deposition for the first time. Pure nitrogen plasma can be generated stably using an alternating pulsed voltage system that applies an alternating pulsed voltage between two parallel plate electrodes. The excited nitrogen species correspond to the nitrogen second positive system. Using this plasma as a nitrogen source, metalorganic chemical vapor deposition of GaN thin films were carried out under a nitrogen partial pressure of 40 kPa. GaN thin films epitaxially at 400°C, and crystallized at as low as 150°C on (0001) sapphire substrate. From the results obtained, we found that the process using near-atmospheric plasma-assisted chemical vapor deposition has major potential for use in nitride film fabrication under high-nitrogen partial pressure and at low temperatures. In the presentation, effects of metal precursors and process gas will be discussed in detail.

**TP78, Marked Improvements in Electrical and Optical Properties for MOVPE InN Annealed at a Low Temperature (-300°C) in O<sub>2</sub> Atmosphere:** Yasuhiko Nagai<sup>1</sup>; Ken-ichi Sugita<sup>1</sup>; Akihiro Hashimoto<sup>1</sup>; Akio Yamamoto<sup>1</sup>; <sup>1</sup>University of Fukui

We have found that electrical and optical properties for MOVPE InN are markedly improved when the grown samples are annealed in the air at a low temperature around 300°C. The InN films used in this study are grown on (0001) sapphire substrates using an atmospheric-pressure MOVPE system with a horizontal reactor. For the sample annealed at 300°C for 5 h in the air,

the carrier concentration is reduced to  $5 \times 10^{18}$  cm<sup>-3</sup> from  $2 \times 10^{19}$  cm<sup>-3</sup> for an as-grown sample. The reduction in carrier concentration is accompanied with the photoluminescence peak energy shift from 0.73 to 0.67 eV. The effect by the annealing in the N<sub>2</sub> atmosphere is found to be very small. These facts indicate that donor species involved in the MOVPE InN are passivated by oxygen. No structural changes such as a change in FWHM for X-ray rocking curve are found after the annealing.

**TP79, Mechanisms of AlInN Growth by MOVPE: Modeling and Experimental Study:** *Eugene Yakovlev*<sup>1</sup>; Anna Lobanova<sup>1</sup>; Roman Talalaev<sup>2</sup>; Ian Watson<sup>3</sup>; Katharine Lorenz<sup>4</sup>; E. Alves<sup>4</sup>; <sup>1</sup>Soft-Impact, Ltd.; <sup>2</sup>Semiconductor Technology Research GmbH; <sup>3</sup>Institute of Photonics, SUPA, University of Strathclyde; <sup>4</sup>Instituto Tecnológico e Nuclear

The scope for lattice matching between AlInN alloys and GaN attracts much interest for fabrication of stress-free multilayer structures for photonic and electronic applications. In this paper, the efficiency of indium incorporation into AlInN has been studied by reactor-scale computational modeling, and experimentally, for epilayers grown on GaN/sapphire substrates in an Aixtron AIX 200/4 RF-S reactor. The AlInN growth setpoint temperature ranged from 760 to 840°C, and layer compositions were measured using Rutherford backscattering. It was found that the indium content reduces with temperature, and that compositional grading occurred at the lowest growth temperature studied. Numerical modeling reproduces the experimental compositional data well, so it can be applied for further analysis of mechanisms governing AlInN deposition. For this purpose, the effects of different operating parameters on the growth rate and InN content have been modeled. From the model predictions, conditions providing a particular target layer composition can be proposed.

**TP80, MOCVD Growth and Characterization of UV-LEDs Grown Using a Thin GaN Interlayer on a High Temperature AlN Buffer:** *Tao Wang*<sup>1</sup>; <sup>1</sup>University of Sheffield

It is a great challenge to achieve high-quality AlN layer for growth of UV emitters on sapphire. Recently, we developed a so-called GaN interlayer approach, i.e., ~20nm GaN layer is deposited on the AlN buffer prior to growth of any further structure. TEM confirmed that the dislocation density of the overlying structure has been significantly reduced. Both 340 nm and 315 nm UV emitters with improved performances have been obtained. Compared to the similar structure but without the interlayer, the EL intensity of the 340 nm LED is significantly increased by a factor of 3, and the bias voltage at 20 mA was decreased from 6.5 to 5.1V and the leakage current at a reversed bias of 10 V was reduced by more than one order magnitude. The 315 nm LED showed a strong peak at 315 nm, as expected. Further pushing the UV-LEDs toward shorter wavelengths is on-going.

**TP81, MOCVD Growth of Hexagonal Nitride on Si(100):** *Qian Sun*<sup>1</sup>; Soon-Yong Kwon<sup>1</sup>; Jung Han<sup>1</sup>; <sup>1</sup>Yale University

Recently two research groups have demonstrated hexagonal GaN-based LED and HEMT on offcut Si(100). The GaN material quality on Si(100) is at present much worse than that of GaN on sapphire or Si(111). In this paper we investigated the growth of AlN and Al<sub>0.13</sub>Ga<sub>0.87</sub>N on 4-deg offcut Si(100) to achieve single crystalline hexagonal phase. It is found that an optimum Al-pre-deposition and a high growth temperature play significant roles in the morphological and structural quality. V/III ratio during subsequent AlGaIn growth is crucial in determining in-plane alignment. Al<sub>0.13</sub>Ga<sub>0.87</sub>N grown under a low V/III ratio shows a very rough surface with many misaligned grain boundaries prohibiting coalescence and gives only a broad deep level emission around 375 nm. But the room temperature photoluminescence of smooth Al<sub>0.13</sub>Ga<sub>0.87</sub>N epilayer obtained under a high V/III condition presents a strong near band-edge emission around 334 nm. Evolution of heteronucleation and AlGaIn heterostructures will be reported.

**TP82, MOCVD Growth of InGaIn/GaN MQW on ELOG GaN Facets for Monolithic White Emission:** Jin-Woo Ju<sup>1</sup>; Lee-Woon Jang<sup>1</sup>; Seung-Jae Lee<sup>2</sup>; Jong Hyeob Baek<sup>2</sup>; *In-Hwan Lee*<sup>1</sup>; <sup>1</sup>Chonbuk National University; <sup>2</sup>Korea Photonics Technology Institute

We have investigated multiwavelength emitting InGaIn/GaN quantum wells (QWs) formed on V-shaped GaN (1-101) microfacet. After a metal-

organic chemical vapor deposition of 2  $\mu\text{m}$  thick GaN, SiO<sub>2</sub> mask stripes were formed along GaN <11-20> direction by a conventional photolithography. Subsequent regrowth of GaN generated the V-shaped (1-101) microfacets along <11-20> direction. Finally, five-period InGaN/GaN multiple QWs were fabricated on these microfacets. Interestingly, cathodoluminescence (CL) spectra measured on the microfacets showed a continuous change in the luminescence peak positions. The CL peaks were shifted to a longer wavelength from 420 nm to 440 nm as the probing points went up. We found in transmission electron microscopy that the growth rate of the QWs increased as it went up (not shown). Therefore, this nonuniform color distribution is considered to be due to the source depletion at the bottom of the microfacets. fabrication of a monolithic white light emitting diode without phosphors.

**TP83, MOVPE Grown GaN on Si(110) and Higher Index Planes:** *A. Dadgar*<sup>1</sup>; M. Wieneke<sup>1</sup>; A. Gadanez<sup>2</sup>; J. Blaesing<sup>1</sup>; T. Hempel<sup>1</sup>; A. Diez<sup>1</sup>; J. Christen<sup>1</sup>; A. Krost<sup>1</sup>; <sup>1</sup>Otto-von-Guericke-Universitaet Magdeburg

GaN grown on Si(111) is already a well established commercially available product and on Si(001) devices were recently demonstrated. On both surfaces GaN grows with c-axis orientation with much inferior quality on Si(001) than on Si(111) due to a poorer matching of atomic bonds at the interface. We have investigated the growth of GaN on surfaces with a two-fold symmetry, e. g., Si(110) or Si(115). On Si(110) the c-axis oriented AlN seed layer has only a mismatch of 0.7% for AlN <1-100> || Si <100> if every second plane is taken into account and 19% for the perpendicular direction, the latter similar as for the growth on Si(111). Compared to the growth on Si(111) the tilt and twist values for GaN/Si(110) are reduced by a factor of 1.5 and 2.5, respectively for a simple structure. Moreover, the Si(110) surface is interesting for wet chemical etching, and easier cleavage.

**TP84, MOVPE Growth of GaN on LiNbO3 Substrate:** *Abdallah Ougazzaden*<sup>1</sup>; Jean Paul Salvestrini<sup>2</sup>; Thomas Aggerstam<sup>1</sup>; Simon Gautier<sup>2</sup>; <sup>1</sup>Georgia Institute of Technology; <sup>2</sup>University of Metz

Lithium Niobate (LiNbO<sub>3</sub>) has established itself as a useful material in optoelectronics and acoustic-optics due to its large piezo-electric polarization and unique optical properties. Due to its similarities in properties, such as piezo-electric polarization, wide bandgap and mechanical and chemical stability, the AlGaIn/GaN heterostructure is attractive for optical and electrical integration with LiNbO<sub>3</sub>. The LiNbO<sub>3</sub> offer a much less in-plane mismatch to GaN (6.8%) compared to Sapphire. Besides a smaller mismatch, the unique properties of LiNbO<sub>3</sub> open up for new and novel applications. In this letter we present, for the first time, the growth of monocrystal GaN on z-cut oriented LiNbO<sub>3</sub> by metal organic vapor phase epitaxy (MOVPE). Novel growth conditions have been explored. Good surface morphology and crystalline quality of GaN/ LiNbO<sub>3</sub> has been obtained. In this presentation the novel growth conditions as well as structural, electrical and optical characterization will be presented.

**TP85, MOVPE High Quality GaN Films Grown on Si (111) Using AlN Multi-Buffer Layers:** *KungLiang Lin*<sup>1</sup>; Edward Y. Chang<sup>1</sup>; Yo-Lin Hsiao<sup>1</sup>; Wei-Ching Huang<sup>1</sup>; Tingkai Li<sup>2</sup>; Teng Hsu Sheng<sup>2</sup>; <sup>1</sup>National Chiao Tung University; <sup>2</sup>Sharp Laboratories of America, Inc

High quality GaN films grown on Si (111) substrates using AlN multi-buffer layers have been studied by MOVPE processes. The GaN films with various buffer layer structures grown at different process conditions have been evaluated using XRD, OM, PL, SEM and AFM measurements. The experimental results show that the AlN film quality and film thickness are critical for growth of crack free GaN films on Si. The cracks formed in a single layer of HT AlN film on 6" Si (111) with thickness higher than 20 nm, but a 100 nm crack free AlN films with multi-layer of HT-AlN/LT-AlN/HT-AlN can be obtained. Using the AlN multi-buffer layers, 0.5 $\mu\text{m}$  crack-free GaN film can be grown on Si(111), GaN film(2 $\mu\text{m}$  thick) with GaN(004) Mosaic FWHM of 0.12° can also be achieved. The relationship between buffer layer structure, GaN film properties and process conditions are also discussed.

**TP86, Nonpolar m-Plane GaN and InGaIn/GaN Multiple Quantum Well Light Emitting Diodes Grown Directly on  $\gamma$ -LiAlO<sub>2</sub> by MOCVD:** *Han Ping*<sup>1</sup>; Xie ZiLi<sup>1</sup>; Xiu Xiangqian<sup>1</sup>; Zhang Rong<sup>1</sup>; <sup>1</sup>Nanjing University

The M-plane GaN and InGaIn/GaN multiple quantum well light emitting

diodes (LED) materials were grown on  $\gamma$ -LiAlO<sub>2</sub> (100) (LAO(100) substrate by MOCVD using TMGa, TMIn and NH<sub>3</sub> as Ga, In and N source respectively. The structure and surface properties of the epilayers were characterized by X-ray diffraction (XRD), Polarized Raman scattering and atomic force microscope (AFM). The films had a very smooth surface with a root mean square roughness as low as 2nm for a 10\*10 $\mu\text{m}^2$  square by AFM scan area. The XRD spectra show that the material grown on LAO(100) have <1-100> m plane. The EL spectra of the M-plane InGaIn/GaN multiple quantum well LED are showing. The current voltage characteristics of these LEDs showed rectifying behavior with a turn on voltage of 1-3V. Figure1 shows the EL spectra and the current voltage characteristics (I-V) of the LED.

**TP87, Optimisation of AlInN/GaN HEMT Structures Grown by MOVPE:** *Lars Rahimzadeh Khoshroo*<sup>1</sup>; Christof Mauder<sup>1</sup>; Wanjiao Zhang<sup>1</sup>; Michael Fieger<sup>1</sup>; Martin Eickelkamp<sup>1</sup>; Yilmaz Dikme<sup>2</sup>; Joachim Woitok<sup>3</sup>; Phenwisa Niyamakom<sup>1</sup>; Helge Bay<sup>4</sup>; Andrei Vescan<sup>1</sup>; Holger Kalisch<sup>1</sup>; Michael Heuken<sup>2</sup>; Rolf Jansen<sup>1</sup>; <sup>1</sup>RWTH Aachen University; <sup>2</sup>AIXTRON AG; <sup>3</sup>PANalytical B.V; <sup>4</sup>Research Center Jülich

We report on the growth and characterisation of 190 nm thick Al<sub>0.83</sub>In<sub>0.17</sub>N layers and AlInN HEMT structures on GaN/sapphire. HRXRD rocking curve measurements exhibit FWHM values of 68 and 175 arcsec for the GaN (0002) and (10-15) reflex, respectively. The corresponding AlInN reflexes yielded 321 and 582 arcsec. In reciprocal space mappings (RSM) of GaN, a mosaic spread of 70 arcsec was measured, which is an indication of a comparably low threading dislocation density. Further, no spinodal decomposition is detected for AlInN in both symmetrical and asymmetrical RSM. RBS and HRXRD measurements showed comparable In contents and matched well with simulations. Electrical characterisations of the HEMT at room temperature yielded a charge carrier density of  $n_s = 1.88 \cdot 10^{13} \text{ cm}^{-2}$  and a mobility of  $\mu = 1410 \text{ cm}^2/\text{Vs}$ . Further optimisation of the AlInN material quality by fine-tuning the deposition parameters is currently carried out.

**TP88, Photoluminescence Study of AlGaIn/AlGaIn Quantum Well Structures for Deep UV Emitters – Barrier Height and Well Width Dependence, and Growth Interruption Effect:** *Misaichi Takeuchi*<sup>1</sup>; Ryo Kajitani<sup>2</sup>; Koji Kawasaki<sup>2</sup>; Yoshinobu Aoyagi<sup>3</sup>; <sup>1</sup>RIKEN; <sup>2</sup>Tokyo Institute of Technology; <sup>3</sup>Ritsumeikan University

We are developing AlGaIn-based deep UV emitters grown by MOCVD.<sup>1</sup> Barrier-height and well-width dependence, and growth interruption effect of AlGaIn/AlGaIn quantum well (QW) structures are investigated by photoluminescence (PL) measurements. In the previously reported deep UV emitting QW heterostructures, relatively low-height barriers (about 5% Al-content difference from the wells) and wide wells (4 ~ 6 nm) were adopted.<sup>2</sup> We reconfirmed these issues to improve the emission efficiency. As results, higher-barrier and narrower-well QWs improved the PL intensities than the conventional ones. The effect of growth interruption in the AlGaIn/AlGaIn QWs, where only the III-group sourced were stopped, was also verified. Only several second interruptions made some crystalline damages at the interrupted surfaces. This may be due to the difference in desorption from the surface between Ga and Al atoms. <sup>1</sup>Kawasaki et al., APL, 89 (2006) 261114. <sup>2</sup>Kajitani et al., Physca Status Solidi (c) (to be published.).

**TP89, Semipolar GaN Grown on m-Plane Sapphire Using MOVPE:** *Tim Wernicke*<sup>1</sup>; Carsten Netzel<sup>1</sup>; Markus Weyers<sup>1</sup>; Michael Kneissl<sup>2</sup>; <sup>1</sup>Ferdinand-Braun-Institut für Höchstfrequenztechnik; <sup>2</sup>Institute for Solid State Physics, Technical University Berlin

We have investigated the MOVPE growth of semipolar GaN films on (10-10) m-plane sapphire substrates, which can significantly reduce polarisation fields compared to c-plane GaN. A nucleation layer was grown at 660°C, followed by a high temperature GaN buffer layer grown at 1210°C. Specular GaN films with a layers thickness of 1.8  $\mu\text{m}$  were obtained. Orientation relationship was determined by XRD and yielded GaN (2-1-12) parallel sapphire (10-10) and GaN [01-10] parallel sapphire [-12-10]. Due to polarity indetermination with XRD, the layers may be (2-1-1-2) GaN, too. We were also able to obtain (10-13) or (10-1-3) GaN films on m-plane sapphire with similar growth conditions. In this case the layer consisted of crystallites with different in-plane orientations: GaN [0001] parallel to sapphire [2-1-10] and GaN [0001] parallel to sapphire [11-20]. Discussion of the orientation

# Technical Program

determination with HRXRD, surface structure and photoluminescence studies will be presented.

**TP90, Strain Relaxation and Morphological Evolution of Annealed Low-Temperature-Deposited AlN Nucleation Layers:** *Rafael Dalmau*<sup>1</sup>; Ramón Collazo<sup>1</sup>; Seiji Mita<sup>1</sup>; Anthony Rice<sup>1</sup>; Zlatko Sitar<sup>1</sup>; <sup>1</sup>North Carolina State University

AlN nucleation (buffer) layers (NL), ≈7 nm thick, were grown on (0001) sapphire substrates at 500–650°C by MOVPE and subsequently annealed at high temperature (≥1000°C) under different process atmospheres (NH<sub>3</sub>, H<sub>2</sub>, N<sub>2</sub>). The NL were analyzed by high resolution x-ray diffraction (HRXRD), atomic force microscopy (AFM), and glancing angle x-ray reflectivity (XRR) to study the evolution of strain, crystallinity, morphology, and thickness as a function of annealing treatment. HRXRD indicated that NL grew under compressive strain and annealing changed the NL strain. Surface roughening of annealed NL was observed by AFM. The thermodynamic stability of AlN at annealing temperatures suggested that the driving force for roughening was strain, while differences in annealed NL thickness and morphology observed by XRR and AFM revealed the role of annealing atmosphere in NL evolution. The suitability of NL annealed under different conditions for growth of GaN and AlN epilayers will also be discussed.

**TP91, Two-Dimensional Electron Gas Formation in AlGaIn/AlGaIn Heterostructures Grown by MOCVD:** *Misaichi Takeuchi*<sup>1</sup>; Takuma Nanjo<sup>2</sup>; Muneyoshi Suita<sup>2</sup>; Yuji Abe<sup>2</sup>; Toshiyuki Oishi<sup>2</sup>; Yasunori Tokuda<sup>2</sup>; Yoshinobu Aoyagi<sup>3</sup>; <sup>1</sup>RIKEN; <sup>2</sup>Mitsubishi Electric Corporation; <sup>3</sup>Tokyo Institute of Technology

Two-dimensional electron gas formation in AlGaIn/AlGaIn heterostructures grown by MOCVD is reported. As our best knowledge, this is the first report about these structures. Due to wider bandgaps of AlGaIn layers than GaN, shift to higher Al-content structures will surely lead to higher power operation of electrical devices. To improve the AlGaIn layer quality, we adopted thin GaN buffers which were developed for our new-concept vertical-type deep-UV emitters.<sup>1</sup> On those buffers, over 1 μm-thick Al<sub>0.2</sub>Ga<sub>0.8</sub>N channel layers can be grown without any cracks. 20 nm-thick Al<sub>0.4</sub>Ga<sub>0.6</sub>N barriers were consequently stacked. Both layers were unintentionally doped. The carrier concentration profile by C-V measurements revealed clear evidence of the two-dimensional electron gas formation on the channel side near the hetero interface. The sheet carrier concentration was estimated to be  $6.9 \times 10^{12} \text{ cm}^{-2}$ . <sup>1</sup>Kawasaki et al., APL, 89 (2006) 261114.

## TP: Nanostructures: Devices

**TP92, 2D Inversion Symmetry Violation and Spin-Dependent Current States in Strained GaN Interface Nanolayers:** *Vladimir Mashkov*<sup>1</sup>; <sup>1</sup>St. Petersburg State Polytechnic University

Strong piezoelectric interface fields coupled to Rashba spin-orbit interaction in GaN nanolayers are shown to change the band structure of the material. A new type of spontaneously broken symmetry in nano-spintronics is discussed. This broken symmetry is a 2D space inversion transformation that conserves the in-plane spin components of a charge carrier and reverses its 2D momentum. The inversion symmetry breaking is specific to 2D electron or hole systems located in space-charge layers with nano-scale strains near unrelaxed interfaces in quantum wells, quantum wires, and quantum dots. It is shown that a 2D many particle system in strained and biased space-charge nanolayers demonstrates nonequilibrium spin-dependent current states. Keldysh-technique density matrix calculations have revealed the main quantum transition probabilities that govern the dynamics of the resulting spin polarization coupled to the induced currents. Conditions for observability of such a quantum object as the spin-dependent current state are established and analyzed.

**TP93, Bi-Stable Behaviour in GaN-Based Resonant Tunneling Diode Structures:** *Sylvain Leconte*<sup>1</sup>; Sebastian Golka<sup>2</sup>; Gottfried Strasser<sup>2</sup>; Eva Monroy<sup>1</sup>; <sup>1</sup>CEA-Grenoble; <sup>2</sup>Zentrum für Mikro- und Nanostrukturen, Technische Universität Wien

III-nitride semiconductors are promising candidates to develop resonant

tunneling diodes (RTDs) with high values of peak-to-valley ratio. The development of such devices requires understanding the electronic transport along the c axis, discerning between resonant tunneling and trap-related effects. In this work, we have studied AlN/GaN double barrier RTD structures with an AlN barrier thickness of 0.5 nm and various GaN well thickness. Electrical characterization confirms the ability of these thin barriers to form a 2DEG and efficiently block the current. The RTD structures show a reproducible negative differential resistance (NDR), which appears only when scanning from negative to positive bias. These results suggest that the NDR should be interpreted as a bi-stable behavior. It is possible to switch from one state to the other one by applying an absolute voltage larger than about 4V. For bias higher than this threshold, time resolved measurements reveal a random transition between both states.

**TP94, Nanostructured Two Dimensional Electron Gases:** *Christian Haupt*<sup>1</sup>; Oliver Ambacher<sup>1</sup>; Volker Cimalla<sup>1</sup>; Stephan Maroldt<sup>1</sup>; Florentina Niebelschütz<sup>1</sup>; Katja Tonisch<sup>1</sup>; <sup>1</sup>Institute of Micro- and Nanotechnologies, Technische Universität Ilmenau

Two dimensional electron gases (2DEG) based on AlGaIn/GaN heterostructures with lateral dimensions in the range of 100 nm are utilized in nano electromechanical systems and high electron mobility transistors. In these dimensions the surface potential causes a reduction of the sheet carrier concentration in the range of several orders of magnitude. In this work we investigated 2DEG-devices structured along non-polar a-, m- and intermediate planes to determine: (a) the influence of the confining planes (b) the structural limits defined by the depletion of the 2DEG concentration and (c) the influence of the initial sheet carrier concentration. Furthermore a model was developed describing the influences of surface potentials on 2DEG-devices in the range of 10-500 nm. The simulated limits of about 10 nm by c-plane and 60 nm by a-, m-plane match with our experimental results whereas variations are the result of line edge roughness or etching damages.

**TP95, Near Ultraviolet Light Emitting Diode Composed of N-GaN/ZnO Coaxial Nanorod Heterostructures on a P-GaN Layer:** *Sung Jin An*<sup>1</sup>; Gyu-Chul Yi<sup>1</sup>; <sup>1</sup>POSTECH

One-dimensional nanorod heterostructures which show compositional modulations along either axial or radial direction offer the opportunity to design numerous novel structures for optoelectronic device applications. Despite the successful demonstration of nanodevices based on the nanorod heterostructures, practical use of the nanodevices has remained out of reach since a necessary use of tedious e-beam lithography makes it difficult to manipulate nanostructures for nanodevice applications. Here, we report on fabrication and characteristics of high efficiency nanorod LEDs using n-GaN/ZnO nanorod heterostructures on p-GaN substrates. The nanorod LEDs were turned on a forward bias voltage of 5 V, and exhibited strong emission from a large light emitting area. From EL spectra, dominant emission peaks were observed at 2.96 and 3.24 eV. The strong and large area light emission at near UV may result from the enhanced carrier injection from n-GaN nanostructures to p-GaN substrates due to quantum confinement effect in the n-GaN nanostructures.

**TP96, Nonlithographic Nanopatterning of InGaIn/GaN Multiple Quantum Wells Nanopillars by Focused Ion Beam Milling:** *Tao-Hung Hsueh*<sup>1</sup>; Shang-En Wu<sup>1</sup>; Chuan-Pu Liu<sup>1</sup>; Jinn-Kong Sheu<sup>1</sup>; Wei-Chih Lai<sup>1</sup>; Shou-Jinn Chang<sup>1</sup>; <sup>1</sup>National Cheng Kung University

Site-control InGaIn/GaN multiple quantum wells (MQWs) nanopillars have been fabricated by nonlithographic nanopatterning technique of focused ion beam (FIB) milling. 30 keV Ga ions with a beam current of 300 pA have been applied to completely remove the III-V material around the pillars. Sharp-tip array and high-aspect-ratio InGaIn/GaN MQWs pillars are achieved by stigmating and defocusing the ion beam simultaneously. High-resolution scanning electron microscope and high-resolution transmission electron microscope images show that the pillars have diameters of around 100 nm to 150 nm and MQWs structures are embedded in the nanopillars. The FIB-patterned InGaIn/GaN MQWs nanopillars have an amorphous structure around the body of pillars. Emission spectra of InGaIn/GaN MQWs embedded in the pillars are observed around 2.98 eV by cathodoluminescence

measurement in room temperature which showed a blue shift of about 35 meV compared with that of the as-grown wafer.

**TP97, Photoelectrochemical Wet Etching of m-Plane GaN for Smooth, Low Damage Etching of Optical Devices:** *Adele Tamboli*<sup>1</sup>; Elaine Haberer<sup>1</sup>; Matthew Schmidt<sup>1</sup>; Kwang Choong Kim<sup>1</sup>; James Speck<sup>1</sup>; Steven DenBaars<sup>1</sup>; Shuji Nakamura<sup>1</sup>; Evelyn Hu<sup>1</sup>; <sup>1</sup>University of California, Santa Barbara

Wet etching provides many advantages for device processing, such as low-damage etching and the formation of undercut structures. Photoelectrochemical (PEC) etching is a promising technique for wet etching of nitrides. We have previously reported on the formation of high quality undercut structures including c-plane microdisk lasers with record low thresholds. However, PEC etching of c-plane GaN is complicated by the built-in polarization, which alters the bandgaps of heterostructures and can compromise etch rates and selectivity. Additionally, it has been difficult to get high quality, smooth surfaces using PEC etching of c-plane GaN on sapphire because of the high defect density and defect-selective nature of PEC etching. However, we have observed both undercut and top-down etched surfaces with unprecedented smoothness using PEC etching of m-plane GaN on bulk substrates. We will discuss applications of PEC etching to devices including microdisks, photonic crystals, and microcavity LEDs.

**TP98, Physical Properties of Nitride Nanorod Heterostructures:** *Li-Wei Tu*<sup>1</sup>; Y. T. Lin<sup>1</sup>; Y. J. Tu<sup>1</sup>; M. Chen<sup>1</sup>; C. L. Hsiao<sup>2</sup>; M. H. Tsai<sup>1</sup>; H. W. Seo<sup>3</sup>; Q. Y. Chen<sup>4</sup>; W. K. Chu<sup>4</sup>; <sup>1</sup>National Sun Yat-Sen University; <sup>2</sup>National Taiwan University; <sup>3</sup>University of Arkansas; <sup>4</sup>University of Houston

Under proper control of the growth conditions, III-V compound nitride semiconductors in nanorod structures can be obtained through the technique of molecular beam epitaxy (MBE). The MBE system uses N<sub>2</sub> plasma as the nitrogen source and solid metals for other group III elements. Substrates are mainly Si (111) wafers. Pure binary and ternary compound and various heterostructural nanorods are grown. All the nanorods line up vertically along the crystallographic c-axis of the hexagonal phase. Density of the nanorods can be varied from low 10<sup>6</sup> to 10<sup>10</sup> cm<sup>-2</sup> with different geometrical shapes. Extensive characterizations are performed, such as field-emission scanning electron microscopy (FESEM), cathodoluminescence (CL), photoluminescence (PL), x-ray diffraction (XRD), transmission electron microscopy (TEM), Raman spectroscopy, etc. Light emitting diodes (LEDs) are fabricated out of these nanorods. Visible light emission is achieved using InGaN nanodisk as the active layer sandwiched between n- and p-type GaN nanorod. Electroluminescence (EL) spectra are measured.

**TP99, Resistivity Study of Si-Doped GaN Nanowires Grown by Catalyst-Free MBE:** *Lorelle Mansfield*<sup>1</sup>; Paul Blanchard<sup>1</sup>; Aric Sanders<sup>1</sup>; Devin Rourke<sup>1</sup>; Norman Sanford<sup>1</sup>; Kris Bertness<sup>1</sup>; <sup>1</sup>National Institute of Standards and Technology

Using two-terminal devices and a simple resistivity model, we estimated the bulk resistivity and carrier concentration of silicon-doped GaN nanowires grown by catalyst-free molecular beam epitaxy. Specific contact resistivity was calculated with an uncertainty of less than 20%. Contacts were fabricated to single nanowires with a Ti/Al metallization scheme. Using current-voltage curves to determine the resistance of several wires from each growth run and SEM to measure the dimensions, we calculated a specific contact resistivity for nanowires with different doping densities. Highly doped nanowires had a specific contact resistivity of  $1.9 \times 10^{-5} \text{ } \Omega \cdot \text{cm}^2$ . We also estimated a bulk resistivity of approximately  $0.003 \text{ } \Omega \cdot \text{cm}$  and a free carrier concentration in the nanowires on the order of  $2 \times 10^{19} \text{ cm}^{-3}$ . Moderately doped nanowires had a higher specific contact resistivity of  $3.5 \times 10^{-4} \text{ } \Omega \cdot \text{cm}^2$ , an estimated bulk resistivity of  $0.01 \text{ } \Omega \cdot \text{cm}$ , and a free carrier concentration on the order of  $3.5 \times 10^{18} \text{ cm}^{-3}$ .

**TP100, Ultraviolet Light-Emitting Diodes with Self-Assembled InGaN Quantum Dots:** *Il-Kyu Park*<sup>1</sup>; Min-Ki Kwon<sup>1</sup>; Chu-Young Cho<sup>1</sup>; Ja-Yeon Kim<sup>1</sup>; Seong-Ju Park<sup>1</sup>; <sup>1</sup>Gwangju Institute of Science and Technology

A photoluminescence study showed that the self-assembled InGaN quantum dots (QDs) provide strongly localized recombination sites for carriers and that the piezoelectric field-induced quantum-confined Stark effect (QCSE) is small because the height of QDs is too small to separate the wave functions

of electrons and holes. The InGaN QD light-emitting diode (LED) showed an emission peak at 400 nm and the peak was red-shifted with increasing injection current, indicating a small QCSE in InGaN QDs. The light output power of an InGaN QD LED increased linearly with increasing injection current due to the strongly localized recombination sites of the InGaN QDs.

**TP101, Wide Bandgap Semiconductors as High-Electron Velocity Structures for Nanoelectronics:** *Mark Johnson*<sup>1</sup>; D.W. Barlage<sup>1</sup>; <sup>1</sup>North Carolina State University

Compound semiconductors have received recent attention as alternatives to silicon for aggressively nanoscaled electronics, particularly for devices with gate lengths less than 22 nm. While much of the current research focuses on high-mobility narrow bandgap semiconductors, GaN or SiC have significant potential as alternative channel materials due to their high electron velocity. Under high source-to-drain field condition, we have identified a high peak velocity, low dielectric constant and high electron velocity saturation field as important physical parameters for alternative channel selection. We report on modeling and characterization studies aimed at identifying alternative channel materials for sub-22 nm nanoelectronics. This work considers Schottky source-drain injection into semiconductor channel, with corresponding high-K gates as device structures. Relevant device metrics such as CV/I, cut-off frequency and low threshold voltage as are used to assess nanoscaled silicon. This work points to the significant potential as well as critical challenges for SiC or GaN in nanoelectronics.

## TP: Quantum Dots: Characterization

**TP102, Fabrication of GaN/AlN Bilayer Particles by a Vapor Phase Method:** *Kazuhiro Hara*<sup>1</sup>; Tatsuhiro Mori<sup>1</sup>; Hironori Komoda<sup>1</sup>; Yuuya Oogi<sup>1</sup>; Hiroko Kominami<sup>1</sup>; Yoichiro Nakanishi<sup>1</sup>; <sup>1</sup>Shizuoka University

In contrast to the conventional powder phosphors consisting of particles with a uniform material composition, we propose GaN-based nanostructure-embedded particles, which consist of GaN quantum dots or quantum wells in the AlN matrix. We can expect the novel phosphors to have higher luminescence efficiencies owing to the carrier confinement effect. As the first step for the goal, we have demonstrated the formation of AlN core particles, and the subsequent deposition of GaN on the surface of the core particle by a vapor phase method. The AlN core particles with a diameter of about 200 nm were first formed by a reaction of vaporized Al and N<sub>2</sub> gas at 1200°C, followed by the growth of about 150-nm-thick GaN on the core surface by a reaction of GaCl and NH<sub>3</sub> at 1000°C. Thus fabricated GaN/AlN bilayer particles showed cathodoluminescence dominated by the band edge emission of GaN.

**TP103, In-Situ Measurement of the Strain Relaxation of GaN Nanograins during X-Ray Irradiation:** Hyeokmin Choe<sup>1</sup>; Sanghwa Lee<sup>1</sup>; Yuri Sohn<sup>1</sup>; Taegeon Oh<sup>1</sup>; Jai Weon Jean<sup>1</sup>; *Chinkyoo Kim*<sup>1</sup>; <sup>1</sup>Kyunghee University

The absence of lattice-matched substrates for growth of GaN thin films was a major hindrance to fabricate high-performance GaN-based optoelectronic devices. On the other hand, it has been reported that lattice-mismatched layers can be grown without introducing misfit dislocations at the interfaces in nanorods and one of the issues in fabricating nanodevices is to carefully investigate their thermal stability. Due to the small volume of individual nanorods, the thermal stability of these nanostructures is of great importance in nanodevices. In this work, GaN nanograins were grown on c-plane sapphire substrates and their thermal stability was investigated by utilizing synchrotron x-ray scattering. The sample was constantly exposed to the synchrotron x-ray source and repeated  $\theta$ -2 $\theta$  scans were sensitive to the thermal stability of the nanograins under x-ray irradiation. Interestingly the peak position shifted to a higher  $l$ -value implying that the GaN nanograins in compress strain experienced strain relaxation during x-ray irradiation.

**TP104, Mobile and Immobile Photoluminescence Band from Single Hexagonal GaN Quantum Dots Formed in an AlN Matrix:** *Konstantin Zhuravlev*<sup>1</sup>; Vladimir Mansurov<sup>1</sup>; Andrei Nikitin<sup>1</sup>; Mats Larsson<sup>1</sup>; Per Olof Holtz<sup>1</sup>; <sup>1</sup>Institute of Semiconductor Physics

Screening of built-in electric field in GaN/AlN hexagonal quantum dots (QDs) by non-equilibrium carriers have been studied by micro-

# Technical Program

photoluminescence (PL) spectroscopy. The QDs were grown by a particular MBE mode without a wetting layer. Typical dot density measured by transmission electron microscopy was  $10^{11}$  cm<sup>-2</sup>. The laser spot was 1.5 mm in diameter, the maximal excitation power was 6 mW. Sharp emission bands have been found on a low energy side of a broad PL band originating from QDs. Most of these PL bands do not shift with the excitation power varied at four orders of magnitude that evidences in negligible screening effect, while few tens of electro-hole pairs can be expected in single QD at the highest excitation power. A peculiar PL band blue-shifts with increasing excitation power. The blue shift is interpreted as being due to local electric fields induced by charged defects placed in vicinity of QD.

## TP105, MOCVD Growth and Optical Properties of InGaN Quantum Dots on a Low Dislocation-Density GaN Surface Grown Using a High Temperature AlN Buffer: *Tao Wang*<sup>1</sup>; Qi Wang<sup>1</sup>; <sup>1</sup>University of Sheffield

It is extremely difficult to achieve III-nitride quantum dot with a good uniformity. We believe that the major reason is due to a high dislocation density in III-nitride layer. Recently, we developed a so-called high temperature AlN buffer layer approach for GaN growth on sapphire by MOCVD. TEM indicated that the dislocation density is significantly reduced, compared to the conventional GaN layer. X-ray diffraction showed a less than 100 arcsec of FWHM of the symmetrical rocking curve of the GaN, which is massively narrower than that of the conventional GaN. Our InGaN QDs were grown on such high-quality GaN surface, and a significant improvement in dot uniformity has been achieved, which is much better than that grown on the conventional GaN surface. Photoluminescence (PL) measurements show a strong PL emission at 510 nm observed even on the QDs without any capping layer.

## NOTES

---

### Rump Session I

Tuesday PM                      Room: 314/315  
September 18, 2007              Location: MGM Grand Hotel Conference Center

---

Program to be announced.

---

### Rump Session II

Tuesday PM                      Room: 312/317  
September 18, 2007              Location: MGM Grand Hotel Conference Center

---

Program to be announced.

# Technical Program

## Session V: Solid State Lighting and LEDs

Wednesday AM  
September 19, 2007

Room: 313/316  
Location: MGM Grand Hotel Conference Center

*Session Chairs:* Soo-Jin Chua, National University of Singapore, Institute of Materials Research and Engineering; Alois Krost, University of Magdeburg

### 9:00 AM Invited

**V1, Recent Developments of High Efficiency White Light Emitting Diodes:** *Yukio Narukawa*<sup>1</sup>; Masahiko Sano<sup>1</sup>; Takahiko Sakamoto<sup>1</sup>; Takao Yamada<sup>1</sup>; Takashi Mukai<sup>1</sup>; <sup>1</sup>Nichia Corporation

The multiple quantum well structure LED epitaxial layers were grown on the patterned sapphire substrate by MOCVD. An indium-tin oxide (ITO) contact was employed as a p-type electrode. The LED chips were mounted on a lead frame (NICHIA RIKOH) and molded in an epoxy resin. At 20 mA under DC operation, the output power, forward voltage, peak wavelength, external quantum efficiency, wall-plug efficiency of the blue LED were 42.2 mW, 3.10 V, 443 nm, 75.4%, 68.1%, respectively. The luminous flux, forward voltage, luminous efficacy, wall-plug efficiency, color temperature and CIE chromaticity coordinates of the white LED were 9.86 lm, 3.10 V, 159 lm/W, 46.2%, 4840 K, (0.352, 0.375), respectively, at DC 20 mA. This value of luminous efficacy is about two times higher than that of fluorescent tubes. The GaN-based white light source will replace conventional lamps and bring us solid-state lighting in the near future.

### 9:30 AM

**V2, Spectral and Time Resolved Scanning Near-Field Microscopy of Broad Area 405 nm InGaN Laser Diode Dynamics:** *Harald Braun*<sup>1</sup>; Tobias Meyer<sup>1</sup>; Dominik Scholz<sup>1</sup>; Ulrich Schwarz<sup>1</sup>; Stefanie Brünninghoff<sup>2</sup>; Alfred Lell<sup>2</sup>; Uwe Strauss<sup>2</sup>; <sup>1</sup>University Regensburg; <sup>2</sup>OSRAM Opto Semiconductors GmbH

Ridge widths of GaN lasers are typically in the order of few  $\mu\text{m}$ . In contrast to GaAs material systems, beam quality of GaN broad area lasers above  $10\mu\text{m}$  is still a critical point. By time resolved scanning near-field microscopy on pulsed electrically pumped LDs with different ridge widths we observe dynamic features caused by thermal and carrier induced changes of the refractive index like filamentation, lateral mode competition and beam steering, which strongly influence the far field of the LDs. Using a high spectral resolution spectrometer we can additionally resolve the individual longitudinal modes of the laser spectrum both time resolved on a 10 ns scale and correlated to the lateral position in the waveguide. Especially on samples with broad ridges we observe complex spectral and spatial dynamics of the laser mode like different filaments lasing dynamically on different longitudinal modes.

### 9:45 AM

**V3, InGaN/GaN Multi-Facet Light Emitting Diodes toward Tailor-Made Solid-State Lighting without Phosphors:** *Mitsuru Funato*<sup>1</sup>; Takeshi Kondou<sup>1</sup>; Keita Hayashi<sup>1</sup>; Masaya Ueda<sup>1</sup>; Yoichi Kawakami<sup>1</sup>; Yukio Narukawa<sup>2</sup>; Takashi Mukai<sup>2</sup>; <sup>1</sup>Kyoto University; <sup>2</sup>Nichia Corporation

InGaN/GaN light emitting diodes (LEDs) were fabricated on GaN multi-facet structures, where (0001) and {11-22} microfacets are naturally formed by a MOVPE regrowth technique using mask stripes along the [1-100] direction. Electroluminescence was achieved by optimizing Mg-doping to GaN and device processes such as photolithography on multi-facet structures. The EL colors were confirmed to be different between (0001) and {11-22} facets due to the facet dependent InGaN composition and thickness. The additive color mixture produced intermediate colors. Because changing growth conditions and mask geometries can alter the shape of the microfacet structures, the emission colors are highly tunable. Conventional techniques to control the emission color are, for example, LEDs pumping phosphors and stacked QWs emitting different colors. The multi-facet LEDs can avoid Stokes loss observed in phosphors and have much higher emission color

controllability, compared with stacked QWs. Therefore, we believe that our LEDs are suitable for tailor-made solid-state lighting.

### 10:00 AM

**V4, Improved Performance of GaInN Based Deep Green Light Emitting Diodes through V-Defect Reduction:** *Theeradetch Detchprohm*<sup>1</sup>; Mingwei Zhu<sup>1</sup>; Wei Zhao<sup>1</sup>; Yong Xia<sup>1</sup>; Yufeng Li<sup>1</sup>; Jayantha Senawiratne<sup>1</sup>; L. Liu<sup>2</sup>; D. Hanser<sup>2</sup>; Christian Wetzel<sup>1</sup>; <sup>1</sup>Rensselaer Polytechnic Institute; <sup>2</sup>Kyama Technologies, Inc.

We developed green light emitting diode (LED) dies covering the wavelength range of 525 to 570 nm (dominant). Active regions of GaInN/GaN quantum wells were grown in c-plane MOVPE GaN on sapphire and GaN substrate. Conventional epi growth is known to decorate threading dislocations in the active region with V-defects at densities of  $10^8$  to  $10^9$   $\text{cm}^{-2}$ . These defects either emanate from the GaN buffer or originate in the quantum wells. This, in particular in green and deep green emitting dies, leads to rough growth morphology, drift of well and barrier widths, emission linewidth broadening, and large color shift with current density. Our alternate approach results in virtually V-defect-free layers and so avoids those effects to a large extent. In addition, electroluminescence output power nearly doubles while a slightly shorter emission wavelength can be compensated for. Findings are substantiated in large sets of scratch diodes and individual fabricated dies.

### 10:15 AM

**V5, High Light Efficiency and Low Forward Voltage InGaN-Based Light Emitting Diode for Illumination:** *Seung Wan Chae*<sup>1</sup>; Chung Bae Jeon<sup>1</sup>; Gun Yoo Ko<sup>1</sup>; Seok Min Hwang<sup>1</sup>; Je Won Kim<sup>1</sup>; Yong Chun Kim<sup>1</sup>; Yoon Seok Han<sup>1</sup>; Jong Rak Son<sup>1</sup>; <sup>1</sup>Samsung Electro-Mechanics

In this study, in order to achieve a low-resistance and highly transparent ohmic contacts to p-GaN for high power LEDs, we focused on development of ohmic contact layer between the p-GaN and the ITO. For this purpose, we fabricated the light emitting diode by using CIO/ITO contact on p-GaN and the patterned sapphire substrate. Then, we compared the contact resistance as well as the transmittance of the ITO electrodes contact, compared to Ni/Au electrode. Among the various ohmic contact layers, the CIO/ITO contacts showed a high transmittance over 92% at 460nm and a low contact resistance lower than  $10\text{-}3\Omega\text{cm}^2$ . In addition, the fabricated InGaN LEDs showed a low forward voltage ( $V_f$ ) of 3.28V and a luminescence of 256mW at 350mA operation with the CIO/ITO transparent contacts better than  $V_f$  of 3.25V and a luminescence of 170mW with Ni/Au contact, respectively.

### 10:30 AM

**V6, New Design of GaN Vertical Light Emitting Diodes on Metal Substrate for Solid State Lighting Application:** *Chen-Fu Chu*<sup>1</sup>; Chao-Chen Cheng<sup>1</sup>; Wen-Huan Liu<sup>1</sup>; Jiunn-Yi Chu<sup>1</sup>; Feng-Hsu Fan<sup>1</sup>; Hao-Chun Cheng<sup>1</sup>; Jui-Kang Yen<sup>1</sup>; Trung Doan<sup>2</sup>; Chuong Tran<sup>2</sup>; <sup>1</sup>Semi-Photonics; <sup>2</sup>SemiLEDs

The new design of the GaN based Vertical Light Emitting Diodes on Metal Substrate (VLEDMS) for high power solid state lighting application has been investigated. The VLEDMS exhibits low operation voltage of 3.1 V at 350 mA and can sustain much higher current, up to 3A without any performance deterioration. The low operation junction temperature of VLEDMS demonstrates excellent heat dissipation capabilities. Chip scaling can be done successfully without efficiency loss up to 80 mil chip size, shows the unique property of VLEDMS. A light output efficiency of over 100 lms/watt has been achieved in 40 mil single VLEDMS chip package. Our chips showed only a small decline in light output power over time; this change can be kept below 15% under 350mA and 700mA driving current and room temperature after 3000 hours burn-in test. Coupled with mass production ability, VLEDMS is the ideal choice for solid state lighting application.

### 10:45 AM

**V7, Enhancement in Light-Extraction of GaInN Light-Emitting Diodes by Using Indium-Tin-Oxide Graded-Refractive-Index Antireflective Contacts:** *Jong Kyu Kim*<sup>1</sup>; Sameer Chhajed<sup>1</sup>; Martin Schubert<sup>1</sup>; Jaehae Cho<sup>2</sup>; Hyunsoo Kim<sup>2</sup>; Cheolsoo Sone<sup>2</sup>; E. Fred Schubert<sup>1</sup>; <sup>1</sup>Rensselaer Polytechnic Institute; <sup>2</sup>Samsung Electro-Mechanics Company Ltd

The refractive of a thin-film material, which is chosen for its desirable conductive and transparent properties, can be precisely tailored by using

# Technical Program

oblique-angle deposition technique. As an example, we demonstrate six-layer graded-refractive-index antireflection coating made entirely of indium-tin-oxide (ITO) which is chosen for its high conductivity, high optical transmittance, and low contact resistance with p-type GaN. Each ITO layer has an individually tailored thickness and refractive index ranging from 2.19 to 1.17 to follow the modified-quintic-index profile for an optimum anti-reflection performance. Blue GaInN light-emitting diodes with the ITO graded-refractive-index antireflective contacts achieve a light-extraction efficiency enhanced by 24.2% compared to LEDs with conventional ITO contacts due to a strongly reduced Fresnel reflection.

11:00 AM Break

---

## Session W: Nonpolar and Semipolar Materials and Devices II

Wednesday AM Room: 314/315  
September 19, 2007 Location: MGM Grand Hotel Conference Center

*Session Chairs:* Patrick Waltereit, Fraunhofer Institute for Applied Solid State Physics; Balakrishnan Krishnan, University of South Carolina, Photonics Microelectronics Laboratory

9:00 AM

**W1, Homoepitaxial Growth of Nearly Stacking-Fault-Free m-Plane (In,Ga)N Films by Metalorganic Vapor Phase Using Low Defect Density Free-Standing Substrates:** *Shigefusa Chichibu*<sup>1</sup>; Masashi Kubota<sup>2</sup>; Hiroshi Yamaguchi<sup>2</sup>; Lu Zhao<sup>2</sup>; Kuniyoshi Okamoto<sup>3</sup>; Hiroaki Ohta<sup>3</sup>; <sup>1</sup>Tohoku University; <sup>2</sup>University of Tsukuba; <sup>3</sup>Rohm Company Ltd.

Nearly stacking fault-free m-plane GaN and InGaIn films were grown by MOVPE on the free-standing (FS) m-plane GaN substrates, which were cut from c-plane FS GaN substrates prepared by HVPE (Mitsubishi Chemical). The threading dislocation density of the epilayers was lower than  $5 \times 10^6 \text{ cm}^{-2}$  and the surface AFM image exhibited atomically-flat morphology with well-aligned monolayer steps. The FWHM values of the x-ray rocking curves for both GaN and InGaIn were close to the values of the substrate [31 arcsec for the (0001) azimuth]. Low temperature PL spectra of GaN epilayers exhibited well-resolved bound and free exciton lines, which obeyed the polarization selection rules. PL lifetimes of GaN epilayers at room temperature, which can be a representative of nonradiative lifetime, increased with increasing V/III ratio and the values for m-plane GaN were much lower than those of c-plane GaN grown on (0001) Al<sub>2</sub>O<sub>3</sub> substrates. The InGaIn epilayers exhibited single peaked emissions.

9:15 AM

**W2, m-Plane GaN/InGaIn/AlInN on LiAlO<sub>2</sub> Grown by MOVPE:** Y. Dikme<sup>1</sup>; H. Behmenburg<sup>1</sup>; Ch. Giesen<sup>1</sup>; M. Chou<sup>2</sup>; *M. Heuken*<sup>1</sup>; <sup>1</sup>AIXTRON AG; <sup>2</sup>National Sun Yat-Sen University

The growth of non-polar material leads to a more efficient recombination across the quantum well of GaN-based light emitting diode (LED) structures. Lithium aluminate (LiAlO<sub>2</sub>) offers the possibility to grow non-polar (m-plane) GaN. The scope of this work is the growth and the investigation of m-plane GaN-based layers on LiAlO<sub>2</sub>. All growth experiments have been performed in AIXTRON metal-organic chemical vapor deposition reactors. Atomic force microscopy of the GaN surface resulted in a root mean square (rms) value of 3.49 nm. The  $\Omega$ -scan full width of half maximum (FWHM) of a 550 nm thick GaN layer revealed 670 arcsec and no c-plane GaN peak could be detected in the  $\Omega$  2 $\theta$ -scan. The room temperature photo luminescence (RT PL) FWHM measurement resulted in 14 nm. MQW LED structures based on these GaN buffer layers showed a RT PL FWHM of 35 nm at a peak wavelength of 448 nm.

9:30 AM

**W3, P-Type Conduction in Stacking-Fault-Free m-Plane GaN:** *Mel McLaurin*<sup>1</sup>; Feng Wu<sup>1</sup>; James Speck<sup>1</sup>; <sup>1</sup>University of California, Santa Barbara

We report on transport measurements of p-type m-plane GaN grown on low defect density, free-standing m-plane (10-10) GaN substrates. The measurements showed no significant anisotropy in in-plane mobility-between the [11-20] and [0001] directions-for hole concentrations between  $2.45 \times 10^{17}$  and  $8.7 \times 10^{18} \text{ 1/cc}$ . Hole mobilities were in good agreement with in-plane measurements of c-plane oriented films grown in previous studies. This is significant considering the expected anisotropy in effective hole masses for the valence bands of GaN. Since faulted m-plane films showed significant anisotropy in electron and hole mobility, basal plane stacking faults, which have an anisotropic distribution, are discussed as a possible source of anisotropic scattering in non-polar and semi-polar films. The displaced material of the basal plane stacking faults is considered to be similar to zincblende GaN, resulting in discontinuities in the conduction and valence band edges at the zincblende/wurtzite polytype interfaces and the possibility of non-uniform carrier densities.

9:45 AM

**W4, Transmission Electron Microscopy Study of Semipolar GaN Templates and Epitaxial-Lateral-Overgrown Films Deposited on m-Plane Sapphire by Metalorganic Vapor Phase Epitaxy:** *Philippe Vennéguès*<sup>1</sup>; Zahia Bougrioua<sup>2</sup>; Tobias Guehne<sup>1</sup>; <sup>1</sup>National Center of Scientific Research/Research Center on the Hétéro-Epitaxy and Its Applications; <sup>2</sup>National Center of Scientific Research/Electronics, Microelectronics and Nanotechnology Institute

The microstructure of GaN templates and epitaxial lateral overgrown (ELO) films deposited on M-plane sapphire is investigated using different transmission electron microscopy techniques. The epitaxial relationship is  $[11-20]_{\text{sapphire}}$  parallel to  $[1-100]_{\text{GaN}}$  in-plane with a growth plane close to  $(11-22)_{\text{GaN}}$ . A mechanism to explain this relationship is proposed. The microstructure of the templates is dominated by the presence of basal stacking faults with a density of around  $3 \times 10^5 \text{ cm}^{-1}$ . Basal stacking faults are either terminated by partial dislocations or connected by prismatic stacking faults. Perfect a-type dislocations are also observed. ELO films with stripes parallel to  $[1-100]_{\text{GaN}}$  allow us to reduce the density of basal stacking faults in the overgrown regions down to  $5 \times 10^3 \text{ cm}^{-1}$ . In these overgrown materials, the density of perfect dislocations is  $108 \text{ cm}^{-2}$  while neither partial dislocation nor prismatic stacking faults are observed.

10:00 AM

**W5, Microstructure of Non-Polar (11-20) and Semi-Polar (11-26) GaN Films Grown on r-Plane Sapphire by MBE:** *Lin Zhou*<sup>1</sup>; David Smith<sup>1</sup>; R. Chandrasekaran<sup>2</sup>; T. Moustakas<sup>2</sup>; <sup>1</sup>Arizona State University, School of Materials and Department of Physics; <sup>2</sup>Boston University, Department of Electrical and Computer Engineering

GaN films and GaN/AlGaIn multiple quantum wells with (11-20) and (11-26) planes parallel to the R-plane of sapphire were grown by molecular beam epitaxy under different growth conditions. Transmission electron microscopy (TEM) analysis showed that both sets of films were single crystalline. High density of basal plane stacking faults (BSFs) was observed in the non-polar (11-20) GaN (n-GaN) films. Stacking faults (SFs) lying on {11-20}, {10-10} prismatic planes and {1-102} pyramidal planes were also observed. The SFs on {10-10} and {1-102} planes generally formed closed domains. For semi-polar (11-26) GaN (s-GaN) films, threading dislocations were observed to form small angle grain boundaries. Most BSFs in the s-GaN film were propagated from the AlN buffer. SFs on {10-10} planes were also observed and formed by folding of the BSFs. SFs propagating to the top surface created some triangular and hexagonal shaped pits on the GaN surface.

10:15 AM

**W6, Fabrication and Properties of Semi-Polar (1-101) and (11-22) InGaIn/GaN MQW Light Emitting Diodes on Patterned Si Substrates:** *Toshiki Hikosaka*<sup>1</sup>; Tomoyuki Tanikawa<sup>1</sup>; Yoshio Honda<sup>1</sup>; Masahito Yamaguchi<sup>1</sup>; Nobuhiko Sawaki<sup>1</sup>; <sup>1</sup>Nagoya University

InGaIn/GaN MQW light emitting diodes (LEDs) were fabricated on semi-polar (1-101) and (11-22) GaN templates which had been grown on

# Technical Program

patterned (001) and (113)Si substrates, respectively, for the first time. The GaN templates were of  $300 \times 300 \mu\text{m}^2$  "as-grown" square discs, formed by coalescence of appropriate GaN stripe structures made by selective MOVPE method. The MQW active layer was embedded between Si-doped n-type GaN bottom layer and Mg-doped p-type GaN top layer. The n-type electrode was facilitated by depositing AuSb on the back surface of the Si substrate. The turn-on voltage of the diodes was on the order of 3 - 4 V, and the emission intensity was linearly increased as a function of the drive current. The peak wavelengths at 20 mA were 470 nm and 453 nm, respectively, which were slightly blue-shifted at high drive currents.

**10:30 AM**  
**W7, Late News**

**10:45 AM**  
**W8, Late News**

**11:00 AM Break**

---

## Session X: Growth of Novel Nitride Semiconductors

Wednesday AM                      Room: 312/317  
September 19, 2007                      Location: MGM Grand Hotel Conference Center

*Session Chairs:* Hiroyuki Yaguchi, Saitama University; Daniel Koleske, Sandia National Laboratories

---

**9:00 AM**

**X1, MOVPE Growth and Characterization of AlInN Layers on Si(111):** *Christoph Hums<sup>1</sup>; Aniko Gadanez<sup>1</sup>; Armin Dadgar<sup>1</sup>; Jürgen Blasing<sup>1</sup>; Thomas Hempel<sup>1</sup>; Harald Witte<sup>1</sup>; Frank Bertram<sup>1</sup>; Andre Krtschil<sup>1</sup>; Jürgen Christen<sup>1</sup>; Alois Krost<sup>1</sup>; <sup>1</sup>Otto-von-Guericke-Universität Magdeburg*

For the realization of a p-channel FET based on an AlInN/GaN heterostructure growth of strained AlInN on GaN with an Indium content exceeding 32% is necessary. There are three major challenges at high In-Al-ratios: Extremely different growth conditions for the binaries, the high lattice mismatch between GaN and AlInN and a theoretically proposed miscibility gap. We report on a detailed study of the growth conditions of  $\text{Al}_{1-x}\text{In}_x\text{N}$  in a wide compositional range ( $0.09 < x < 1$ ). The samples have been characterized by XRD, CL and FESEM measurements. Fully strained  $\text{Al}_{1-x}\text{In}_x\text{N}$  layers with  $x \sim 0.34$  without phase separation up to a layer thickness of 15 nm could be grown. At higher In-content phase separation occurs and the growth mode changes from a two dimensional to three dimensional growth. We will further present results from Hall-Effect and C-V measurements and discuss the possibility of obtaining a p-channel FET.

**9:15 AM**

**X2, GaN-Based Devices on 150 mm Si(001) Substrate Grown by MOVPE:** *Fabian Schulze<sup>1</sup>; A. Dadgar<sup>1</sup>; J. Blasing<sup>1</sup>; O. Kisel<sup>1</sup>; C. Hums<sup>1</sup>; T. Hempel<sup>1</sup>; A. Krtschil<sup>1</sup>; A. Diez<sup>1</sup>; J. Christen<sup>1</sup>; A. Krost<sup>1</sup>; <sup>1</sup>Otto-v.-Guericke-University*

We present structural and optical investigations on GaN layers on Si(001) grown by metalorganic vapor phase epitaxy (MOVPE). A key parameter to obtain high quality GaN layers on Si(001) is most likely the control of the surface reconstruction of the substrate, which can be influenced by changing the surface energy. The use of  $4^\circ$  off-oriented substrates prefers one type of dimer rows, and thus, the growth of c-axis oriented GaN on Si(001) with one defined in-plane alignment is possible. The crystallographic quality is investigated by x-ray diffraction measurements, Electron Back Scatter Diffraction, FE-SEM imaging, and AFM. By growing an approximately 2.8  $\mu\text{m}$  thick, crack-free GaN buffer, the achieved crystallographic quality allows for fabricating GaN-based LEDs and FET devices on Si(001). Furthermore, we will present some first blue LED samples of the up-scaling process up to 150 mm Si(001) substrates.

**9:30 AM**

**X3, Crystalline Epitaxial GaN on Refractory Metallic Substrates for Vertical Devices:** *Jaime Freitas<sup>1</sup>; Jihyun Kim<sup>2</sup>; Larry Rowland<sup>3</sup>; <sup>1</sup>Naval Research Laboratory; <sup>2</sup>Korea University; <sup>3</sup>Aymont Technologies, Inc.*

GaN films characterized by good surface morphology, high crystalline quality and relatively low-background donor concentration were deposited on refractory metal TiC. The properties of these films are similar to high-quality films deposited on sapphire, Si and SiC substrates, and far superior to films previously deposited on metals. Low-compensation and low-concentration of background carriers observed in the GaN/TiC indicates that p-type doping can be achieved at least as easily as on GaN on sapphire substrates, which will allow the fabrication of p-n and p-i-n device structures. Point probe testing showed good rectifying behavior with relatively low leakage current for the GaN/TiC structure. Additional i-V measurements using evaporated metallic contacts on the GaN film will be presented. These findings clearly confirm the feasibility of fabricating device structures on metal substrates, and the potential use of these heterostructures for advanced design and high-power and/or high-temperature device fabrication.

**9:45 AM**

**X4, Effect of Hydrogen and Silicon Co-Doping in Ferromagnetic GaGdN Grown by MBE:** *Martin Roever<sup>1</sup>; Amilcar Bedoya-Pinto<sup>1</sup>; Dong-Du Mai<sup>1</sup>; Joerg Malindretos<sup>1</sup>; Angela Rizzi<sup>1</sup>; <sup>1</sup>Georg-August-Universitaet Goettingen*

With the aim of understanding the observed room-temperature giant magnetic moment of highly diluted GaGdN reported in literature GaGdN, GaGdN:Si and GaGdN:H have been grown by molecular beam epitaxy (MBE) and the Gd concentration is between  $10^{16}$  and  $10^{21} \text{cm}^{-3}$ . All samples are ferromagnetic at 300 K as measured by SQUID and the very high saturation magnetic moment in this type of samples is confirmed by our experiments. With co-doping of hydrogen or silicon we were able to decrease or increase respectively the strength of the magnetic moments in the layers. All our findings indicate that ferromagnetism is stabilized by electrons. Electrical measurements on GaGdN layers grown on high resistive 6H-SiC(0001) show a typical temperature dependence of hopping conductivity. The overall resistance for a layer thickness of 500 nm is 2,3 to 290 M $\Omega$  in the temperature range from 60 to 10 K.

**10:00 AM**

**X5, MBE Growth of Gadolinium Nitride and Its Integration with GaN:** *Michael Scarpulla<sup>1</sup>; Chad Gallinat<sup>1</sup>; Arthur Gossard<sup>1</sup>; James Speck<sup>1</sup>; <sup>1</sup>Materials Department, University of California, Santa Barbara*

The integration of rock-salt rare earth pnictides with III-V semiconductors holds promise for enabling and enhancing devices. We have investigated the growth of gadolinium nitride and its integration with GaN using two types of molecular beam epitaxial (MBE) growth. We use nitrogen plasma assisted MBE (PAMBE) to grow GdN on (0001) Ga-face GaN and ammonia MBE (NH3-MBE) to deposit nanoislands embedded in GaN. Results from X-ray diffraction (XRD) on the GdN films demonstrate that GdN grows in the (111) || GaN (0001) orientation expected from symmetry considerations. Reflection high energy electron diffraction demonstrates that GdN nucleates and grows via a 3D mode in NH3-MBE growth. We will discuss the structural and optical properties of both films and superlattices formed by successive layers of GaN and GdN nanoislands. Finally, we will present results from efforts to enhance tunneling efficiency in GaN tunnel junctions by embedding GdN nanoislands in the junction.

**10:15 AM**

**X6, AlN Nanowire Growth by Self-Patterning on SiC Substrates:** *G. Reza Yazdi<sup>1</sup>; Mikael Syvajarvi<sup>1</sup>; Rositza Yakimova<sup>1</sup>; <sup>1</sup>Linkoping University*

Self-patterned aligned AlN nanowires with diameter and length about 100 nm and 90  $\mu\text{m}$ , respectively were grown on 4H-SiC substrate by physical vapor transport method. AlN hexagonal pyramids (HPs) were found to be nucleation sites for the evolution of the observed morphological forms. We study size reduction and limitation by choosing proper thermodynamical parameters, and converted AlN micro size crystals to the nano size. We will report different steps of AlN hexagonal hillocks formation and their evolution to HPs, on which nanowires were grown. Some nanowire properties like bending of AlN nanowires during scanning by scanning electron microscopy

# Technical Program

(SEM) will be also reported. By using optical microscopy, SEM, and atomic force microscopy we have studied the mechanism of the nanowire formation and piezoelectricity effect. Hot KOH etching confirmed that the self-patterning is initiated by dislocation etch pits in the SiC substrates.

10:30 AM

X7, Late News

10:45 AM

X8, Late News

11:00 AM Break

---

## Session Y: Optical and Structural Characterization and Related Topics

Wednesday AM

Room: 313/316

September 19, 2007

Location: MGM Grand Hotel Conference Center

*Session Chairs:* Atsushi Yamaguchi, Kanazawa Institute of Technology;  
Colin Humphreys, University of Cambridge

---

11:30 AM

**Y1, Cumulative Growth and Microstructure Studies of Nonpolar m-Plane SLEO GaN:** Kwang-Choong Kim<sup>1</sup>; Mathew Schmidt<sup>1</sup>; *Asako Hirai*<sup>1</sup>; Makoto Saito<sup>1</sup>; Feng Wu<sup>1</sup>; Melvin McLaurin<sup>1</sup>; Erin Young<sup>1</sup>; Shuji Nakamura<sup>1</sup>; Steven DenBaars<sup>1</sup>; James Speck<sup>1</sup>; <sup>1</sup>University of California, Santa Barbara

Despite the clear advantages for optoelectronic devices, nonpolar m-plane GaN heteroepitaxy typically suffer from high densities of extended defects including threading dislocations (TDs) and stacking faults (SFs). Here, the growth characteristics and the microstructure of sidewall LEO of m-plane GaN grown by MOCVD and HVPE have been investigated. The application of SLEO to m-plane GaN heteroepitaxy yielded significant reduction on  $\omega$ -rocking curve FWHMs of on-axis (1100) reflection from 0.199° ( $\phi=0^\circ$ ) and 2.589° ( $\phi=90^\circ$ ) for template to 0.137° and 0.408° for SLEO, respectively, indicating the reduction of both TDs and SFs. The XTEM images confirmed that TDs typically form only around the shoulders between masks and openings, and SFs typically form not only at the shoulders but also over N-wing regions over SiO<sub>2</sub> masks, moreover, SF annihilation by forming loops during the lateral growth was observed. Surprisingly, changing the mask geometry yielded the fast coalescence and SF-absent N-wings grown over SiC.

11:45 AM

**Y2, Design, Growth, Fabrication, and Characterization of GaN and InGaN Solar Cells:** *Xiaodong Chen*<sup>1</sup>; Kristopher Matthews<sup>1</sup>; Dong Hao<sup>1</sup>; William Schaff<sup>1</sup>; Lester Eastman<sup>1</sup>; <sup>1</sup>Cornell University

The InGaN alloy system offers a unique opportunity to develop high efficiency multi-junction solar cells. In this study, single junction solar cells made of GaN and InGaN are successfully developed. The materials are grown on sapphire substrates by MBE, consisting of a Si-doped n-type layer, an intrinsic layer and an Mg-doped p-type layer on top. The IV curves indicate that the cell made of GaN has low series resistance (0.12 ohm-cm<sup>2</sup>) and parasitic leakage is insignificant. Contact resistances of p and n contacts are 74 O-mm and 0.2 O-mm respectively. Upon illumination by a 325 nm laser, the cell shows a clear photo-response with a fill factor of 61% and Voc=2.5V. In InGaN cell with 20% In content, the photo-response is also observed when illuminated by outdoor sunlight (~600suns). But it has been dominated by a big leakage current, which might be caused by the defects.

12:00 PM

**Y3, Nitride Photocatalyst to Generate Hydrogen Gas from Water:** *Yasuhiro Iwaki*<sup>1</sup>; Kazuki Yamaguchi<sup>1</sup>; Kazuhide Kusakabe<sup>1</sup>; Katsushi Fujii<sup>2</sup>; Kazuhiro Ohkawa<sup>1</sup>; <sup>1</sup>Tokyo University of Science; <sup>2</sup>Tohoku University

We report on the great potential of nitride photocatalyst in view of external quantum efficiency (EQE), and on properties of n-n+ structure nitride

photocatalyst we proposed. EQE of a photocatalysis cell was measured by using monochromatic light. The EQE of the GaN cell was greater than 40% at <360nm. Using InGaN, the EQE value achieved 7.2% at 400nm in visible region. These EQE values are quite large compared to the conventional oxide photocatalyst. The depletion layer separate electrons and holes generated by photons. Holes move to the surface, and oxidize the electrolyte. On the other hand, electrons go to a counterelectrode for reduction through the layer. The layer should be conductive. Thus we propose a structure with an n-type layer for light absorption on a conductive n+-type layer. The n-n+ structure nitride photocatalyst improved H<sub>2</sub> generation compared to a single n-GaN layer by 1.4 times.

12:15 PM

**Y4, Very Low Dislocation Density GaN Films Obtained Using Transition Metal Nitride Interlayers:** *Michelle Moram*<sup>1</sup>; Yucheng Zhang<sup>1</sup>; Menno Kappers<sup>1</sup>; Zoe Barber<sup>1</sup>; Colin Humphreys<sup>1</sup>; <sup>1</sup>University of Cambridge

We present a simple method to reduce threading dislocation densities (TDDs) in (0001)-oriented GaN from 5 x 10<sup>9</sup> cm<sup>-2</sup> to as low as 5 x 10<sup>6</sup> cm<sup>-2</sup> in a single step, without lithography. Thin (5-25 nm) amorphous layers of Sc, Hf, Nb, Zr and Ti were deposited on GaN-on-sapphire templates and converted to nitrides by annealing in NH<sub>3</sub>. ScN layers show few cracks or pinholes after annealing, whereas other layers showed high densities of holes. GaN initially forms dislocation-free islands when grown on ScN layers. TDDs reach 1 x 10<sup>8</sup> cm<sup>-2</sup> for coalesced GaN grown on holey interlayers, but only 3 x 10<sup>7</sup> cm<sup>-2</sup> for coalesced GaN on ScN interlayers. Partially-coalesced GaN on ScN interlayers has dislocation-free regions of > 100  $\mu$ m<sup>2</sup> and a TDD of ~5 x 10<sup>6</sup> cm<sup>-2</sup>. TEM studies show that the interlayers block dislocation propagation, with some dislocations generated upon coalescence of GaN islands.

12:30 PM

**Y5, Orders of Magnitude Reduction in Dislocation Density in GaN Grown on Si (111) by Nano Lateral Epitaxial Overgrowth:** *Soo-Jin Chua*<sup>1</sup>; Ke Yan Zang<sup>1</sup>; Ya Dong Wang<sup>2</sup>; <sup>1</sup>Institute of Materials Research and Engineering; <sup>2</sup>Singapore-MIT Alliance

GaN grown on Si(111) by MOCVD has dislocation density on the order of 10<sup>9</sup> to 10<sup>10</sup> cm<sup>-2</sup>. In nanoscale lateral epitaxy overgrowth (NLEO), where the GaN is overgrown on SiO<sub>2</sub> with nanopores etched into it, forming a selective area epitaxial mask on GaN/Si, the dislocation density in the resulting GaN is found to have dislocation density reduced by about 2 orders of magnitudes. The nanopores were etched on the SiO<sub>2</sub> with anodic alumina template forming the etch mask. The mechanism of threading dislocation density reduction is due to dislocation bending and annihilation. The narrower band-edge emission in photoluminescence spectrum shows a better optical quality in the NLEO GaN film. High quality GaN nanorod arrays have also been grown through the nanopores with very low dislocation density.

12:45 PM

**Y6, Effects of Compositionally Graded Al<sub>x</sub>Ga<sub>1-x</sub>N Buffer Layers on the Evolution of Threading Dislocations in GaN Films Grown on SiC and Si Substrates:** *Xiaojun Weng*<sup>1</sup>; Jeremy Acord<sup>1</sup>; Abhishek Jain<sup>1</sup>; Elizabeth Dickey<sup>1</sup>; Joan Redwing<sup>1</sup>; <sup>1</sup>Pennsylvania State University

The effects of Al<sub>x</sub>Ga<sub>1-x</sub>N buffer layers on the evolution of threading dislocations (TDs) in GaN films grown on SiC substrates by metalorganic chemical vapor deposition were studied and compared with the films grown on (111)Si substrates. Similar to the GaN/Al<sub>x</sub>Ga<sub>1-x</sub>N/Si heterostructures, significant TD bending and annihilation was observed in the Al<sub>x</sub>Ga<sub>1-x</sub>N buffer layers on SiC substrates, which subsequently led to reduced TD densities in the overgrown GaN films compared to those grown on SiC using thin AlN buffer layers. While the TDs in GaN films on (111)Si substrates are predominantly edge dislocations, the TD types in films on SiC substrates are affected by both the SiC surface morphology and the composition gradient of the Al<sub>x</sub>Ga<sub>1-x</sub>N buffer layers. Chemi-mechanically polished flat SiC surfaces lead to an increase in screw TD density, and a steeper gradient of Al<sub>x</sub>Ga<sub>1-x</sub>N promotes the formation of edge TDs. The mechanisms of TD selection will be discussed.

# Technical Program

1:00 PM

## Y7, Origin of Additional Threading Dislocations in AlGaIn Grown on GaN Using an AlN Interlayer: *Ranjan Datta*<sup>1</sup>; <sup>1</sup>Arizona State University

Thick AlGaIn layers with high Al contents grown epitaxially on GaN crack due to tensile strain arising from the lattice parameter mismatch. AlN interlayers can be used to prevent this cracking, but there is a concomitant increase in the edge-type threading dislocation density in the AlGaIn film. In this contribution, the origin of the additional threading dislocations (TDs) is investigated. The AlN interlayer itself micro-cracks to relieve strain, and overgrowth of AlGaIn on such a relaxed/cracked AlN layer gives rise to the formation of additional edge-type threading dislocations along the crack lines. This appears to be due to terminated misfit dislocation lines at the crack facets that are replicated during subsequent growth, resulting in additional edge TDs in the upper AlGaIn layer. The contribution of cracks in generating additional edge TDs can also depend on whether the crack lines are filled or a void is created during AlGaIn growth.

1:15 PM

Y8, Late News

## Session Z:

### Nonpolar and Semipolar Materials and Devices III

Wednesday AM  
September 19, 2007

Room: 314/315  
Location: MGM Grand Hotel Conference Center

*Session Chairs:* Philippe Vennéguès, CNRS-CRHEA; Euijoon Yoon, Seoul National University

11:30 AM Invited

## Z1, Local Spectroscopic Investigations on Semipolar InGaIn-Based Nanostructures and Their Application to LEDs: *Yoichi Kawakami*<sup>1</sup>; A. Kaneta<sup>1</sup>; K. Nishizuka<sup>1</sup>; Masaya Ueda<sup>1</sup>; Kazunobu Kojima<sup>1</sup>; M. Funato<sup>1</sup>; Y. Narukawa<sup>2</sup>; T. Mukai<sup>2</sup>; <sup>1</sup>Kyoto University; <sup>2</sup>Nitride Semiconductor Research Laboratory, Nichia Corporation

Nanoscope optical characterization using scanning near-field optical microscopy (SNOM) was performed on a (11-22) microfacet quantum well (QW) fabricated by the re-growth technique. Unlike the phenomena observed in (0001) QWs, there is not a difference between the photoluminescence (PL) spectra acquired under the illumination-collection and illumination modes, which indicates that the carrier diffusion length in the (11-22) QW is less than the probing fiber aperture of 160 nm due to a much faster radiative recombination processes as a result of a well-reduction of internal electric field. The correlation between internal quantum efficiency (IQE) and emission wavelength is elucidated by comparing the PL intensity and wavelength mappings. The highest IQE is approximately 50% at 520 nm, which is about 50 nm longer than in (0001) QWs, suggesting that the (11-22) QW is a suitable green emitter as has been demonstrated in the good performance of light emitting diodes (LEDs).

12:00 PM

## Z2, High Performance Violet-Blue and Blue LEDs on Freestanding Semipolar (10-1-1) Bulk GaN Substrate: *Hong Zhong*<sup>1</sup>; Anurag Tyagi<sup>1</sup>; Natalie Fellows<sup>1</sup>; Feng Wu<sup>1</sup>; Roy Chung<sup>1</sup>; Makoto Saito<sup>1</sup>; Kenji Fujito<sup>2</sup>; James Speck<sup>1</sup>; Steven DenBaars<sup>1</sup>; Shuji Nakamura<sup>1</sup>; <sup>1</sup>University of California, Santa Barbara; <sup>2</sup>Mitsubishi Chemical Corporation

Violet-blue and Blue InGaIn/GaN multiple-quantum-well (MQW) light emitting diodes (LEDs) with peak emission wavelengths of 411nm and 444 nm were grown on low extended defect density semipolar bulk GaN substrates by conventional metal organic chemical vapor deposition (MOCVD). Under dc operations, the electroluminescence (EL) peak emission wavelength of the violet-blue LED at 1 mA and 100 mA drive currents were 411 nm and 413 nm, respectively. Under pulsed operations (10% duty cycle), the EL peak emission wavelength of the blue LED ranged from 443.9 nm at 10 mA to 443.4 nm at 100 mA. At a forward current of 20 mA, we measured an output

power of 20.58 mW and an external quantum efficiency (EQE) of 33.91% for the violet-blue LED under dc operations and an output power of 16.21 mW and an EQE of 29% for the blue LED under pulsed operations (10% duty cycle).

12:15 PM

## Z3, High Quality Nonpolar and Semipolar GaN Films Grown on Lattice Matched ZnO Substrates at Room Temperature: *Atsushi Kobayashi*<sup>1</sup>; Kohei Ueno<sup>1</sup>; Jitsuo Ohta<sup>1</sup>; Hiroshi Fujioka<sup>1</sup>; Hidetaka Amanai<sup>2</sup>; Satoru Nagao<sup>2</sup>; Hideyoshi Horie<sup>2</sup>; <sup>1</sup>University of Tokyo; <sup>2</sup>Mitsubishi Chemical Group Science and Technology Research Center, Inc.

We have grown nonpolar and semipolar GaN films on nearly lattice matched ZnO substrates at room temperature (RT) by the use of pulsed laser deposition. ZnO crystals with various nonpolar and semipolar surfaces were used as substrates in this study. Structural and optical properties of GaN films were investigated with RHEED, AFM, HRXRD, RSM, and PL. All the GaN layers have exhibited sharp streaky RHEED patterns and small FWHM values for X-ray rocking curves, indicating that high-quality GaN films with various orientations grow epitaxially even at RT. We also found that RT growth of nonpolar and semipolar GaN on these substrates proceeds in the layer-by-layer mode. TEM observations have revealed that the heterointerfaces between RT-GaN and ZnO is quite abrupt, which is inherently important to take advantages of lattice matched ZnO substrates.

12:30 PM

## Z4, A Comparative Study of Non-Polar (11-20), Semi-Polar (11-22), and Polar (0001) AlGaIn/GaN Multiple Quantum Wells: *Jonathan Hollander*<sup>1</sup>; Nicholas Hylton<sup>2</sup>; Carol Johnston<sup>1</sup>; Menno Kappers<sup>1</sup>; Clifford McAleese<sup>1</sup>; Phil Dawson<sup>2</sup>; Colin Humphreys<sup>1</sup>; <sup>1</sup>University of Cambridge; <sup>2</sup>University of Manchester

We have grown non-polar (11-20), semi-polar (11-22), and polar (0001) GaN templates on *r*-plane, *m*-plane, and *c*-plane sapphire substrates, respectively, using metal-organic vapor-phase epitaxy. The (11-20) templates were grown using three SiN<sub>x</sub> interlayers to improve the films' structural characteristics. Ten period Al<sub>0.18</sub>Ga<sub>0.82</sub>N/GaN multiple quantum wells were then grown on each film orientation with 2nm, 3nm, 4nm, 5nm, and 6nm well thicknesses, and 10nm barriers. The structures were then analyzed to determine the thicknesses of the GaN wells and AlGaIn barriers, and the Al<sub>x</sub>Ga<sub>1-x</sub>N composition using high-resolution X-ray diffraction, X-ray reflectivity, and transmission electron microscopy. The variation of 300K photoluminescence peak emission energy with quantum well width is consistent with a reduction or elimination in the quantum-confined Stark effect in wells with semi-polar (11-22) and non-polar (11-20) orientations, respectively. The results of detailed structural characterization, temperature-dependent photoluminescence, and theoretical modeling will be presented on all the structures.

12:45 PM

## Z5, InGaIn Quantum Wells on Polar vs. Semipolar GaN Orientations: Internal Fields and Their Effect on Luminescence: *Sridhar Srinivasan*<sup>1</sup>; *Zhihao Wu*<sup>1</sup>; M. Stevens<sup>1</sup>; F. Ponce<sup>1</sup>; H. Omiya<sup>2</sup>; T. Mukai<sup>2</sup>; <sup>1</sup>Arizona State University; <sup>2</sup>Nichia Corporation

Carrier dynamics of InGaIn quantum wells (QWs) grown on polar and semipolar GaN planes has been correlated with direct measurements of the electrostatic potential using electron holography. The QWs were nominally 3 nm wide and the indium compositions were varied over a wide range in order to achieve *c*-plane emission from violet to yellow wavelengths. The recombination lifetime increases from 2 ns for the violet QW to 145 ns for the yellow QW. This trend in lifetime is correlated with a monotonic increase in the internal polarization fields from 0.4 MV/cm across the violet QW to 1.6 MV/cm across the yellow QW. Semipolar QWs, grown on {11-22} GaN planes, exhibit considerably smaller lifetimes (0.4-0.7 ns), which are found to be relatively independent of well width and indium composition. Direct measurements of the electrostatic potential across these quantum wells confirm that the internal fields in this geometry are negligible.

Wednesday PM

# Technical Program

1:00 PM

**Z6, Growth of Nonpolar Cubic GaN/AlN Multiple Quantum Wells with Intersubband Transitions for 1.5  $\mu\text{m}$  Applications:** *Donat As<sup>1</sup>; Jörg Schörmann<sup>1</sup>; Klaus Lischka<sup>1</sup>; Eric DeCuir, Jr.<sup>2</sup>; M.O. Manasreh<sup>2</sup>; <sup>1</sup>University of Paderborn; <sup>2</sup>University of Arkansas*

Cubic GaN/AlN short-period multiple quantum well structures were grown at 720°C by plasma-assisted molecular beam epitaxy on free standing 3C-SiC substrates. The samples consist of 100 nm thick GaN buffer and 20 periods of GaN/AlN active regions. The thickness of the AlN barrier is 1.35 nm for all samples, while the thickness of the GaN well varies between 1.6 nm-2.10 nm depending on the samples. The periodicity of the GaN/AlN active regions was confirmed by the presence of several peaks in the high resolution x-ray diffraction (HRXRD) spectra. The thickness of the total period was estimated by fitting the HRXRD data using a dynamic scattering theory. Furthermore, the room temperature optical absorption spectra of the intersubband transitions were obtained using a Bruker IFS-125HR spectrometer. The peak position wavelengths of these transitions were observed in the spectral region of 1.5–2.0  $\mu\text{m}$  and confirmed theoretically by using a self-consistent Poisson-Schrödinger model.

1:15 PM

Z7, Late News

---

## Session AA: Optoelectronic Devices

Wednesday AM                      Room: 312/317  
September 19, 2007                  Location: MGM Grand Hotel Conference Center

*Session Chairs:* Tae-Yeon Seong, Korea University; K. Kishino, Sophia University

---

11:30 AM **Invited**

**AA1, Photonic Crystal LEDs:** *Claude Weisbuch<sup>1</sup>; <sup>1</sup>University of California at Santa Barbara*

We first discuss the various Photonic Crystal (PhC) structures proposed to control spontaneous emission, possibly enhance it. However, the funneling of emission in one or few channels has not yet been demonstrated. The simpler task of suppressing or enhancing the emission rate still appears difficult, for a variety of reasons. We will concentrate on the extraction of waveguided light which is the major channel of light emission in thin LEDs. PhCs are then used as diffracting elements for out-of plane scattering. We show recent results on GaN based PhC LEDs, where analysis of angular resolved emission patterns allows to determine the PhC dispersion curves and the extraction efficiency for the various waveguided modes. We finally discuss the optimization of PhC extractors for efficiency and brightness as it is strongly needed to make them competitive with other light extracting schemes, implying various options and technical challenges.

12:00 PM

**AA2, Investigation of the Strong Exciton Photon Coupling in Hybrid AlInN/AlGaN Microcavities with GaN/AlGaN Multiple Quantum Wells:** *Gabriel Christmann<sup>1</sup>; Raphaël Butté<sup>1</sup>; Eric Feltin<sup>1</sup>; Jean-François Carlin<sup>1</sup>; Nicolas Grandjean<sup>1</sup>; <sup>1</sup>Ecole Polytechnique Fédérale de Lausanne (EPFL)*

We report on the observation of strong exciton-photon coupling at room temperature (RT) in hybrid AlInN/AlGaN microcavities containing multiple quantum wells (MQWs) grown by metalorganic vapor phase epitaxy on c-plane sapphire substrates. The structures consist of a strain relieving template, a 40 pair  $\text{Al}_{0.85}\text{In}_{0.15}\text{N}/\text{Al}_{0.20}\text{Ga}_{0.80}\text{N}$  distributed Bragg reflector (DBR) followed by a  $3\lambda$  cavity ( $\lambda \approx 343$  nm) containing several narrow GaN/AlGaN QWs. The structures were completed by depositing a 13 pair  $\text{SiO}_2/\text{Si}_3\text{N}_4$  DBR. The interest in using GaN/AlGaN MQWs resides in their increased exciton binding energy and oscillator strength over bulk GaN layers. This ensures stronger light-matter coupling conditions as revealed by RT angle-resolved

photoluminescence and reflectivity measurements revealing a vacuum Rabi splitting in excess of 50 meV, the highest value reported so far for a QW based microcavity. The interplay between polariton branches and Bragg modes is also seen to be significant at large angles in such system.

12:15 PM

**AA3, Resonant Modes in GaN-Based Small-Volume Pillar Microcavities:** *Henning Lohmeyer<sup>1</sup>; Kathrin Sebald<sup>1</sup>; Jürgen Gutowski<sup>1</sup>; Stephan Figge<sup>1</sup>; Timo Aschenbrenner<sup>1</sup>; Heiko Dartsch<sup>1</sup>; Carsten Kruse<sup>1</sup>; Detlef Hommel<sup>1</sup>; Jan Wiersig<sup>1</sup>; Frank Jahnke<sup>1</sup>; <sup>1</sup>University of Bremen*

The fabrication and the optical properties of GaN-based pillar microcavities with small mode volumes suitable for low-threshold lasers and control of spontaneous emission are discussed. Monolithic vertical cavities grown by molecular-beam epitaxy, and hybrid cavities employing one nitride-based Bragg reflector grown by metal-organic vapor-phase epitaxy are compared. Pillar structures with diameters between 800 nm and 3  $\mu\text{m}$  have been fabricated by focused-ion-beam etching, yielding structures with smooth sidewalls and high aspect ratios.<sup>1</sup> The discrete mode spectrum of the pillars has been studied by micro-photoluminescence measurements. The measured data for different pillar diameters show good agreement with calculations of the transmission spectra of the three-dimensional pillars based on a vectorial transfer-matrix method. The optical properties of structures with InGaN/GaN multiple quantum wells embedded are discussed as prototypes for vertical-cavity lasers. Additionally, emission properties of InGaN/GaN quantum-dot pillar microcavities are presented. <sup>1</sup>H. Lohmeyer et al., Eur.Phys.J.B 48,291 (2005).

12:30 PM

**AA4, Directional Emission III-Nitride Photonic Crystal LEDs:** *Jonathan Wierer<sup>1</sup>; Aurelien David<sup>1</sup>; <sup>1</sup>Philips Lumileds Lighting*

Employing photonic crystals in light-emitting diodes (LEDs) not only increases light extraction, but is also used to control the far-field radiation pattern of the LED. With the proper design light is redirected into useful angles increasing the radiance (light directionality) of the LED; a property useful in étendue limited applications. Data are presented on electrically driven III-Nitride photonic crystal LEDs with various lattice types and constants. Wavelength resolved radiation pattern and power measurement are used to characterize the LEDs. The number of internal optical modes and how they are extracted into air are controlled by the photonic crystal and other device parameters. Modelling is used to identify the scattered modes in the far-field radiation patterns. Photonic crystal LEDs show increased light extraction and radiance compared to non-patterned controls.

12:45 PM

**AA5, Microcavity InGaN Light Emitting Diodes with a Single Fabry-Pérot Mode:** *Yong-Seok Choi<sup>1</sup>; Michael Iza<sup>1</sup>; Gregor Koblmüller<sup>1</sup>; Christophe Hurni<sup>1</sup>; James Speck<sup>1</sup>; Claude Weisbuch<sup>1</sup>; Evelyn Hu<sup>1</sup>; <sup>1</sup>University of California at Santa Barbara*

We report on InGaN microcavity light-emitting diodes supporting a single Fabry-Pérot mode with an effective thickness of 450 nm and a cavity order of 5 at the emission wavelength of 415 nm. The device is a simple asymmetric cavity structure bounded by a highly reflective mirror at the bottom and air at the top. The single Fabry-Pérot mode alters the emission pattern, so that a larger fraction of the generated light can be coupled to the light extraction cone. The device is fabricated by utilizing flip-chip bonding, laser lift-off, dry-etch thinning, mesa formation, and contact deposition processes. Of particular challenge in the processing is the high-precision control of final microcavity thickness. The control of microcavity thickness afforded by our selective dry-etch thinning method can be further complemented by photonic crystal patterning and roughening, leading to highest improvements in light extraction efficiency.

# Technical Program

1:00 PM

**AA6, GaN Ultraviolet Avalanche Photodiodes Fabricated on Free-Standing Bulk GaN Substrates:** Yun Zhang<sup>1</sup>; Dongwon Yoo<sup>1</sup>; Jae-Boum Limb<sup>1</sup>; Jae-Hyun Ryou<sup>1</sup>; Russell Dupuis<sup>1</sup>; *Shyh-Chiang Shen*<sup>1</sup>; <sup>1</sup>Georgia Institute of Technology

We report a high-performance MOCVD-grown GaN ultraviolet (UV) p-i-n avalanche photodiodes (APD) on bulk GaN substrates. The fabricated APD devices achieved avalanche gain of > 30K and low leakage current density (<10<sup>-7</sup> A/cm<sup>2</sup>) at voltages below 50% of the device avalanche breakdown voltage. Out of more than 40 randomly selected devices tested across an 8 × 8 mm<sup>2</sup> wafer piece, over 50% of them show repeated avalanche gains greater than 10<sup>4</sup>, with device mesa areas up to 4,500 μm<sup>2</sup>. To the best of our knowledge, this is the highest linear gain reported to date among III-N-based UV APDs. The robust APD fabrication processing techniques will be suitable for III-N APD sensor array fabrication. Detailed fabrication and device characterization will be presented in the conference.

1:15 PM

**AA7, Electro-Optical Intersubband Modulator Based on Electron Tunneling between GaN/AlN Coupled Quantum Wells:** Nasrin Kheirodin<sup>1</sup>; *Laurent Nevou*<sup>1</sup>; Houssaine Machhadani<sup>1</sup>; Maria Tchernycheva<sup>1</sup>; Anatole Lupu<sup>1</sup>; Francois Julien<sup>1</sup>; Paul Crozat<sup>1</sup>; Loic Meignien<sup>1</sup>; Elias Warde<sup>1</sup>; Gianmauro Pozzovivo<sup>2</sup>; Sebastian Golka<sup>2</sup>; Gottfried Strasser<sup>2</sup>; Fabien Guillot<sup>3</sup>; Eva Monroy<sup>3</sup>; Thilo Remmele<sup>4</sup>; Martin Albrecht<sup>4</sup>; <sup>1</sup>Institut d'Electronique Fondamentale; <sup>2</sup>Technische Universität Wien; <sup>3</sup>CEA-CNRS-UJF; <sup>4</sup>Institut für Kristallzüchtung

Room temperature intersubband electro-absorption modulation in GaN/AlN coupled quantum wells is demonstrated at near-infrared wavelengths, covering the fibre-optics telecommunication wavelength range. The electro-modulation originates from electron tunneling between a wide well (reservoir) and a narrow well separated by an ultrathin (1 nm) AlN barrier. Electro-absorption modulation with opposite sign is observed at  $\lambda=1.2-1.67$  μm and  $\lambda=2.1-2.4$  μm. Both the intersubband absorption and the modulation spectroscopic measurements are in good agreement with the simulations. The maximum modulation depth with 0.8 V applied across the active region is ≈44 % at  $\lambda=2.2$  μm. The -3 dB cut-off frequency limited by the RC time constant is as high as 1.4 GHz for 10x10 μm<sup>2</sup> mesas and could be further improved by reducing the access resistance of the AlGaIn contact layers.

## WP: Poster Session III

Wednesday, 1:30-2:30 PM Room: Prefunction Area  
September 19, 2007 Location: MGM Grand Hotel Conference Center

## WP: Characterization

**WP1, A Study on the Off-State Breakdown Characteristics for the GaN Buffer Layer of AlGaIn/GaN HFET Using Space-Charge-Limited Current Conduction Mechanism:** *Akihiro Hinoki*<sup>1</sup>; Junjiroh Kikawa<sup>2</sup>; Tomoyuki Yamada<sup>2</sup>; Tadayoshi Tsuchiya<sup>2</sup>; Shinichi Kamiya<sup>2</sup>; Masahito Kurouchi<sup>2</sup>; Kenichi Kosaka<sup>1</sup>; Tsutomu Araki<sup>1</sup>; Akira Suzuki<sup>1</sup>; Yasushi Nanishi<sup>1</sup>; <sup>1</sup>Ritsumeikan University; <sup>2</sup>R&D Association for Future Electron Devices

To improve the performance of AlGaIn/GaN HFETs, the reduction in buffer leakage current through the GaN buffer layer is critical, leading to the improvement in off-state breakdown voltage for high-power operation. We have studied on the correlation between the off-state breakdown voltage and the thickness of the GaN layers using space-charge-limited current conduction mechanism. We have found that the thinner GaN layers had larger off-state breakdown voltages and higher trap density. The trap density in the GaN layer was estimated from the trap filled-limit voltage which determined off-state breakdown voltage. TEM studies showed that the thinner GaN layers had higher dislocation densities. These results suggest that the trap state formed by the threading dislocations determines the off-state breakdown voltage of the GaN layer.

**WP2, Analysis of Buffer-Trapping Effects on Gate Lag, Drain Lag and Current Collapse in AlGaIn/GaN HEMTs:** *Kazushige Horio*<sup>1</sup>; Atsushi Nakajima<sup>1</sup>; <sup>1</sup>Shibaura Institute of Technology

Although many experimental results are reported on current collapse and slow current transients (gate lag and drain lag) in AlGaIn/GaN HEMTs, few theoretical works are performed. Therefore, we have made two-dimensional analysis of AlGaIn/GaN HEMTs in which a deep donor and a deep acceptor are considered in the buffer layer, and found that lag phenomena and current collapse could be reproduced. Particularly, it is shown that gate lag is correlated with relatively high source access resistance of AlGaIn/GaN HEMTs, and that drain lag could be a major cause of current collapse. It is also shown that current collapse is more pronounced when the deep-acceptor density is higher and when an off-state drain voltage is higher. It is concluded that to minimize current collapse in AlGaIn/GaN HEMTs, an acceptor density in the buffer layer should be made low, although current cutoff behavior may be degraded when the gate length is short.

**WP3, Anomalous Temperature Dependence of Photoluminescence for InN Grown by MOVPE:** *Masashi Nakao*<sup>1</sup>; Takaaki Shimada<sup>1</sup>; Masaki Wakaba<sup>1</sup>; Nobuyuki Motegi<sup>1</sup>; Akiko Gomyou<sup>2</sup>; Seiichirou Mizuno<sup>3</sup>; Takashi Matsuoka<sup>4</sup>; <sup>1</sup>Tohoku University; <sup>2</sup>NEC Corporation; <sup>3</sup>NTT-AT Corporation

Photoluminescence (PL) measurements of MOVPE-grown and air-preserved InN crystals have been carried out at the temperature between 4 K and 300 K. PL peak wavelengths are located at around 1.52 μm at room temperature. While the PL peak-intensity increases with temperature decrease, the PL peak-wavelength shows red-shift. This tendency of PL peak-wavelength shift is an opposite change as compared with that of other III-V compounds. The observed anomalous PL behavior has precisely been investigated by additional characterization techniques, such as X-ray diffraction method, TEM observation, energy dispersive X-ray spectrometer (EDX), and electron energy-loss spectroscopy (EELS). Lattice structure has clearly been observed on the TEM image for the InN layer. Oxygen incorporation has been found from the EDX analysis. The origin of anomalous PL wavelength shift may come from the difference of thermal expansion in the InN layer. The observed effects are useful to form the crystal structure with temperature-independent emission.

**WP4, Assessment of the Accuracy of Electrical Channel Temperature Determination in High Power AlGaIn/GaN Devices Using Raman Thermography:** *Richard Simms*<sup>1</sup>; James Pomeroy<sup>1</sup>; Martin Kuball<sup>1</sup>; Micheal Uren<sup>2</sup>; Trevor Martin<sup>2</sup>; <sup>1</sup>University of Bristol; <sup>2</sup>QinetiQ Ltd

GaN-based transistor devices are at the forefront of the development of high power, high-frequency micro-electronics. High power dissipation creates self-heating with implications for device degradation. An accurate method of measuring device temperatures is needed to employ effective thermal management in device design. Electrical methods are commonly used to estimate channel temperatures but their accuracy is presently unknown. Micro-Raman thermography can be used to assess the accuracy of electrical temperature measurements. We find that electrical methods underestimate channel temperatures. This is due to the fact that electrical techniques provide an averaged temperature over the entire device. We conclude that electrical techniques can be used to provide qualitative comparisons between different device designs but are unable to provide an accurate estimation of peak temperatures. This has significant implications for reliability studies based on electrical temperature measurements. Micro-Raman spectroscopy can also be used to investigate time-resolved thermal measurements not possible by electrical methods.

**WP5, Assessment of the Pendeo-Epitaxy Effect on the 2DEG Mobility in III-Nitride HEMT Heterostructures:** K. Bulashevich<sup>1</sup>; *Sergey Karpov*<sup>1</sup>; Yu. Makarov<sup>1</sup>; T. Zheleva<sup>2</sup>; P. Shah<sup>2</sup>; M. Derenge<sup>2</sup>; K. Jones<sup>2</sup>; <sup>1</sup>Semiconductor Technology Research, Inc.; <sup>2</sup>U.S. Army Research Laboratory

We have examined theoretically the electron scattering related to the interface roughness produced by threading dislocations (TDs) in the channel of an AlGaIn/GaN HEMT heterostructure. The considered mechanism is found to limit the low-temperature mobility of electrons at high 2DEG densities, while the Coulomb scattering at charged dislocation core dominates at low 2DEG concentrations. The use of the pendeo-epitaxy enables reduction

# Technical Program

of both the TD density, typically from  $\sim 10^9$  cm $^{-2}$  to  $\sim 5\text{--}7 \times 10^6$  cm $^{-2}$ , and interface roughness, resulting in the mobility improvement. The theoretical calculations of the electron mobility accounting for the above dislocation-mediated scattering mechanisms are compared with available observations. The roughness characteristics and their correlation with the TD density were estimated from the atomic-force microscopy data. The contribution of the scattering mechanisms to the room-temperature mobility is finally estimated to assess the benefit of using the pendeo-epitaxy for the HEMT fabrication.

**WP6, Carrier Dynamics of InN Thin Films Grown on Si(111):** *Der-Jun Jang*<sup>1</sup>; G.-T. Lin<sup>1</sup>; M. E. Lee<sup>2</sup>; L.-W. Tu<sup>1</sup>; <sup>1</sup>National Sun Yat-sen University, Department of Physics and Center for Nanoscience and Nanotechnology; <sup>2</sup>National Kaoshiung Normal University, Department of Physics

The carrier dynamics of InN thin films grown on Si(111) substrates were investigated with the time-resolved photoluminescence (PL) apparatus. The PL rises steeply in the first few ps and saturates later with rise time in the range of 2–10 ps for different excitation intensities when InN thin films were photoexcited with laser pulses of energies of 1.5 eV and 3.0 eV. Carrier temperatures determined from the time-dependent PL spectra reveals that the fast cooling of carrier temperature at the first 10 ps after photoexcitation is the characteristic of energy relaxation of carriers by carrier-LO-phonon interaction. From the carrier cooling curves, we found the effective LO-phonon emission time approaches the theoretical prediction of 23 fs as decreasing the photoexcitation carrier density. This study has verified that the hot phonon effect, instead of plasma screening, plays an important role in reducing the energy loss rate of carriers with excessive energy.

**WP7, Dynamic Behavior of Metal Contacts Formed on AlGaIn/GaN Heterostructure:** *Hideki Hasegawa*<sup>1</sup>; Masamichi Akazawa<sup>1</sup>; <sup>1</sup>Hokkaido University

Current collapses in AlGaIn/GaN HFETs are due to surface state filling from Schottky gates.<sup>1</sup> However, devices with smaller gate leakage exhibit larger collapse.<sup>2</sup> To resolve this discrepancy, we investigate dynamic behavior of metal contacts on AlGaIn/GaN wafers. Circular Schottky or ohmic contacts surrounded by ring-shaped ohmic contacts were used to avoid edge leakage problems. As we reported,<sup>3</sup> Schottky reverse currents decreased by 4–5 orders of magnitude after oxygen gettering which reduces near-surface oxygen donors. After gettering, Schottky samples started to show pronounced I-V hysteresis due to trapping which was absent before gettering. Computer simulation showed that gettering, which reduces oxygen donors, but not surface states, reduces vertical component of leakage, but increases field strength for lateral tunneling. Pulsed current transient measurements detected electron emission from nitrogen vacancy-related surface states. <sup>1</sup>H.Hasegawa et al J.Vac.Sci.Technol. B21 (2002) 1844. <sup>2</sup>P.Kordos et al Appl.Phys.Lett. 86(2005)253511. <sup>3</sup>J.Kotani et al J.Vac.Sci.Technol. B24 (2006) 2148.

**WP8, Electrical Characterization of AlGaIn/GaN on Bulk AlN Substrates:** *William Mitchell*<sup>1</sup>; S. Elhamri<sup>2</sup>; G. Landis<sup>1</sup>; R. Gaska<sup>3</sup>; L. Schowalter<sup>4</sup>; <sup>1</sup>Air Force Research Laboratory; <sup>2</sup>University of Dayton; <sup>3</sup>Sensor Electronic Technology, Inc.; <sup>4</sup>Crystal IS

The results of an electrical transport study of an AlGaIn/GaN heterostructure grown on a bulk AlN substrate are presented. Temperature dependent Hall effect and magnetoresistance measurements were made on the MOCVD/MEMOCVD grown heterostructure. The temperature dependences of the Hall carrier density and mobility were characteristic of a two-dimensional electron gas (2DEG). The Hall carrier density and mobility were roughly  $1.19 \times 10^{13}$  cm $^{-2}$  and 1100 cm $^2$ /Vs at 300 K, and  $1.02 \times 10^{13}$  cm $^{-2}$  and 5279 cm $^2$ /Vs at 10 K. The magnetoresistance measurements revealed the presence of Shubnikov-de Haas (SdH) oscillations. Illumination of the sample resulted in a persistent photocurrent and enhanced the amplitude of the SdH oscillations, indicating an increase in the quantum scattering time. The ratio of the classical to quantum scattering times,  $\tau_c/\tau_q$ , was determined to be 4.3, which is within the range of reported values for AlGaIn/GaN on other substrates.

**WP9, High Intensity Red Emission from Eu Doped GaN Powders:** *Junxia Shi*<sup>1</sup>; M. V. S. Chandrashekar<sup>1</sup>; Jesse Reiherzer<sup>1</sup>; William Schaff<sup>1</sup>; Jie Lu<sup>1</sup>; Francis Disalvo<sup>1</sup>; Michael Spencer<sup>1</sup>; <sup>1</sup>Cornell University

An efficient phosphor material was produced with in-situ Eu doping in GaN by a low-cost method. The effect of growth temperature on the optical properties and structure was investigated by photoluminescence, X-ray diffraction and Raman spectroscopy. Band edge and yellow emissions were completely suppressed for the best samples, with a line-width of 2.2nm. Lattice constants, luminescence intensity and hydrostatic stress increase with Eu incorporation. Analysis of these results indicates that Eu incorporation was substitutional, with a maximum concentration of 0.5at%. Red luminescence intensity of the best sample has been estimated to be about 8 times higher than our previous work.

**WP10, In-Situ Current-Voltage Characteristics of Swift Heavy Ion Irradiated Au/n-GaN Schottky Diode:** *Vikas Baranwal*<sup>1</sup>; Sandeep Kumar<sup>2</sup>; Avinash C. Pandey<sup>1</sup>; Dinakar Kanjilal<sup>2</sup>; <sup>1</sup>University of Allahabad; <sup>2</sup>Inter-University Accelerator Centre

In the present work, in situ current-voltage characterization of Au/n-GaN Schottky diode was performed to study the effect of 50 MeV Ni ion irradiation. The Schottky barrier parameters were measured as a function of irradiation fluence. The irradiation fluence was varied from  $5 \times 10^9$  ions-cm $^{-2}$  to  $5 \times 10^{11}$  ions-cm $^{-2}$ . The ideality factor for pristine diode was 4.01, which decreases to 2.2 after the irradiation with a fluence of  $5 \times 10^9$  ions-cm $^{-2}$ . At a fluence value of  $5 \times 10^{11}$  ions-cm $^{-2}$  the value of ideality factor becomes 1.7. The Schottky barrier height increases from 1.05 eV for pristine diode to 1.08eV at a fluence of  $5 \times 10^9$  ions-cm $^{-2}$ . The values of Schottky barrier height are respectively 1.03, 1.02, 1.01 with the fluence of  $1 \times 10^{10}$  ions-cm $^{-2}$ ,  $1 \times 10^{11}$  ions-cm $^{-2}$ ,  $5 \times 10^{11}$  ions-cm $^{-2}$ . These results are interpreted on the basis of energy loss mechanisms and dynamic annealing due to swift heavy ion irradiation at the metal-semiconductor interface.

**WP11, Light Emission Characteristics of GaN HEMTs and Its Implications on Device Operations:** *Hsiang Chen*<sup>1</sup>; Guann-Pyng Li<sup>1</sup>; <sup>1</sup>University of California, Irvine

The GaN HEMTs are promising for high power and high frequency applications. However, defects induced during material growth and device fabrication imposed constraints on the device performance. A hyperspectrum imaging measurement technique to characterize the electroluminescence from GaN HEMTs is developed for real time in-situ monitoring of defects in devices. While the light emission in on-state operation is continuous throughout the entire gate width, that in off-state has distinct emission spots. Among those spots, they show two separate wavelength dependences. The first type has the same spectrum shape as the one observed at on-state and shows a minor dependence on electric field. The second type depicts a similar characteristic as the yellow band electroluminescence defect in the GaN and shows a stronger dependence on the electric field than that of the first type of emission spot. This technique reveals unique properties of possible material defects and device imperfection.

**WP12, Low On-Resistance AlGaIn/GaN HEMTs by Reducing Gate Length and Source-Gate Length:** *Toshihide Ide*<sup>1</sup>; <sup>1</sup>National Institute of Advanced Industrial Science and Technology (AIST)

In this study, the AlGaIn/GaN HEMT characteristics were improved by reducing both LG and LSG, and the low specific on-resistance was achieved. The gate length LG is varied from 0.1 to 6.0  $\mu$ m. The source-gate spacing LSG is varied from 0.5 to 1.1  $\mu$ m. The maximum transconductance g<sub>max</sub> is improved by reducing LG and LSG. The g<sub>max</sub> is proportional to (LG+LSG)<sup>-0.25</sup>. The reduction of LSG is as effective as the reduction of LG for the enhancement of g<sub>max</sub>. The highest g<sub>max</sub> is 280 mS/mm at a LG of 0.1  $\mu$ m and a LSG of 0.5  $\mu$ m. At a LG of 0.1  $\mu$ m, a LSG of 0.5  $\mu$ m and a drain-gate spacing of 1.6  $\mu$ m, the specific on-resistance and breakdown voltage are 0.1 mOhm-cm $^2$  and 56V, respectively. This result shows better specific on-resistance than the numerical calculation of the lateral GaN FETs.

**WP13, Luminescence and Vibrational Properties of Erbium-Implanted Nanoporous GaN:** *Chew Beng Soh*<sup>1</sup>; *Soo Jin Chua*<sup>1</sup>; *Si Hui Sim*<sup>2</sup>; *Sudhiranjan Tripathy*<sup>1</sup>; *E. Alves*<sup>3</sup>; *Haryono Hartono*<sup>4</sup>; <sup>1</sup>Institute of Materials Research and Engineering; <sup>2</sup>National University of Singapore; <sup>3</sup>ITN; <sup>4</sup>Singapore-MIT Alliance, National University of Singapore

Implantation of Erbium (Er) into GaN is useful in creating selected areas to emit at the green, yellow and infrared wavelengths. Enhanced Erbium activation is obtained when Erbium is implanted into porous GaN formed by electrochemical etching than into as-grown GaN. This is due to the increase in surface areas for light extraction and the availability of more free surfaces to accommodate strain when it is annealed. Furnace annealing at 1100 deg for 30 mins in nitrogen gives rise to higher band-edge photoluminescence intensity. Apart from the host GaN phonon modes, we have also observed disorder-induced lattice vibrations at 170, 200 and 350-365 cm<sup>-1</sup> from Er-implanted porous GaN. The E2 (high) mode of GaN also shifts towards higher energy at higher annealing temperatures, indicative of more Erbium occupying the VGa site (ionic radii of Er > Ga) and hence increasing the compressive stress in the GaN crystal lattice.

**WP14, Micro-Raman Analysis on InN Layers Grown by HPCVD:** *Ronny Kirste*<sup>1</sup>; *Mustafa Alevli*<sup>2</sup>; *Nikolaus Dietz*<sup>2</sup>; *Axel Hoffmann*<sup>1</sup>; <sup>1</sup>Technical University Berlin; <sup>2</sup>Georgia State University

Embedding InN and indium-rich group III-nitride alloys into wide band gap Ga<sub>1-x</sub>Al<sub>x</sub>N group III-nitrides is essential for a large number of envisioned device structures, ranging from spectral tailored displays, white LED's, or detectors. To stabilize InN at processing conditions used for GaN, a novel high-pressure chemical vapor deposition (HPCVD) system was developed enabling the growth of single-crystalline InN layers at growth temperatures at 850°C for reactor pressures around 15 bar. Raman spectra were taken on samples grown with HPCVD at different ammonia/TMI ratios and on different substrates. According to the FWHM's of the E2 (high) mode, both the ammonia/TMI ratio as well as the substrate have a strong influence on the crystalline quality of the grown InN layers. Spatially resolved Raman measurement across cracks in InN layers show different degree of strain relaxations at the edges and across of such cracks.

**WP15, Microscopic Thermal Analysis of AlGaIn/GaN HFETs Using Micro-Raman Spectroscopy and Electro-Thermal Simulation:** *Kenichi Kosaka*<sup>1</sup>; *Tatsuya Fujishima*<sup>1</sup>; *Kaoru Inoue*<sup>2</sup>; *Akihiro Hinoki*<sup>1</sup>; *Tomoyuki Yamada*<sup>2</sup>; *Tadayoshi Tsuchiya*<sup>2</sup>; *Junjiro Kikawa*<sup>2</sup>; *Shinichi Kamiya*<sup>2</sup>; *Akira Suzuki*<sup>3</sup>; *Tsutomu Araki*<sup>1</sup>; *Yasushi Nanishi*<sup>1</sup>; <sup>1</sup>Ritsumeikan University; <sup>2</sup>Advanced HF Device R&D Association for Future Electron Devices; <sup>3</sup>Ritsumeikan University and Advanced HF Device R&D Center, R&D Association for Future Electron Devices

We report on investigation of self-heating effects in AlGaIn/GaN HFETs using micro-Raman spectroscopy and numerical simulations. Both AlGaIn/GaN HFETs on sapphire and SiC substrates were studied using micro-Raman for 2D (two-dimensional) mapping. In the numerical simulations, we used a temperature-dependent thermal conductivity for each constituent material. Good agreements between the simulated and measured surface temperature distributions have been obtained, which supports the validity of simulation models. The measured infinitesimal thermal temperature distribution for HFETs on SiC substrates was found to have a peakier than that on sapphire substrates. In addition, the region around the gate edge on the drain side usually showed a maximum temperature for the devices operating at drain voltages less than about 40 V, but this maximum temperature region shifted toward the drain side when the drain voltage was farther increased. These results confirm and study usefulness of micro-Raman spectroscopy for high-resolution temperature measurements of power devices.

**WP16, Negative Differential Resistance in GaN Lateral Structure Schottky Diodes:** *Wenbao Liu*<sup>1</sup>; <sup>1</sup>Institute of Semiconductors Chinese Academy of Sciences

Lateral structure Schottky diodes were fabricated on unintentional doped GaN films grown on (0001) sapphire by metalorganic chemical vapor deposition. With increasing forward biased voltage the current has been observed to decrease slightly in current-voltage measurements. For some diodes this negative differential resistance phenomenon can repeat for many

times. Two reasons are supposed. One maybe lies in the Shibuya effect. In addition because of the bad thermal conductivity of GaN Schottky diodes heat themselves under big voltage and current, consequently the mobility of electrons decreases with increasing temperature of devices. As a result the density of current decreases and negative differential resistance appears. The mechanism behind is under further research.

**WP17, SIMS and Raman Studies of Mg-Doped InN:** *Valery Davydov*<sup>1</sup>; *Albert Klochikhin*<sup>1</sup>; *Alexander Smirnov*<sup>1</sup>; *Olga Chikalova-Luzina*<sup>1</sup>; *Mikhail Smirnov*<sup>2</sup>; *Hai Lu*<sup>3</sup>; *William Schaff*<sup>3</sup>; *Hong-Mao Lee*<sup>4</sup>; *Hon-Way Lin*<sup>4</sup>; *Shangjr Gwo*<sup>4</sup>; <sup>1</sup>Ioffe Physico-Technical Institute; <sup>2</sup>Saint-Petersburg State University, Fock Institute of Physics; <sup>3</sup>Cornell University; <sup>4</sup>National Tsing-Hua University

We present results of experimental and theoretical studies of lattice dynamics of Mg-doped InN which is promising for p-type doping. The samples studied were grown by PAMBE on sapphire (0001) and silicon (111) substrates. The Mg concentrations ranged from  $N_{Mg} = 1.6 \cdot 10^{19}$  to  $2.3 \cdot 10^{21}$  cm<sup>-3</sup>, as determined by SIMS measurements. It has been found that the normalized intensity of LO-phonon Raman band strongly correlates with the Mg concentration estimated from SIMS data. Moreover, the Raman spectra appear to be identical for the samples grown on different substrates but having similar Mg contents. These findings indicate that Raman spectroscopy is a promising technique for quantitative estimation of Mg content in Mg-doped InN samples. Lattice dynamics of hexagonal InN involving substitutional impurities and vacancies was calculated in the framework of cluster approach, and energy positions of Mg local vibration modes in InN were predicted. They were found to be consistent with experimental findings.

**WP18, The Effects of Interface States on the C-V Behavior of Insulated Gates on AlGaIn/GaN Heterostructures:** *Marcin Miczek*<sup>1</sup>; *Chihoko Mizue*<sup>1</sup>; *Tamotsu Hashizume*<sup>1</sup>; <sup>1</sup>Hokkaido University

The impact of states at the insulator/AlGaIn interface on capacitance-voltage (C-V) characteristics of a metal/insulator/AlGaIn/GaN structure was examined rigorously for the first time using a numerical solver of Poisson equation taking into account the electron emission rate from the interface states. A parallel shift of the theoretical C-V curves instead of typical change in their slope was found in the Si<sub>x</sub>/Al<sub>0.26</sub>Ga<sub>0.74</sub>N/GaN structure at 300°C during increasing the Si<sub>x</sub>/AlGaIn interface state density,  $D_{it}(E)$ . This behavior was explained by the position of Fermi level at the Si<sub>x</sub>/AlGaIn interface below the valence band maximum of AlGaIn when the gate bias was near the threshold voltage. Finally, the experimental C-V characteristics measured at room temperature and 300°C from a Si<sub>x</sub>/AlGaIn/GaN structure were analyzed and a part of  $D_{it}(E)$  was extracted. A relatively low  $D_{it}$  ( $\sim 10^{11}$  eV<sup>-1</sup>cm<sup>-2</sup>) in the upper bandgap indicates that the Si<sub>x</sub> gate insulator is applicable to high-temperature and high-power AlGaIn/GaN-based devices.

## WP: Materials Integration

**WP19, Atomic and Electronic Structure of the Cleaved 6H-SiC(11-20) Surface:** *Marco Bertelli*<sup>1</sup>; *Jan Homoth*<sup>1</sup>; *Martin Wenderoth*<sup>1</sup>; *Angela Rizzi*<sup>1</sup>; *Rainer Ulbrich*<sup>1</sup>; *Maria Clelia Righi*<sup>2</sup>; *Carlo Bertoni*<sup>2</sup>; *Alessandra Catellani*<sup>3</sup>; <sup>1</sup>Georg-August-University of Goettingen; <sup>2</sup>Università di Modena e Reggio Emilia; <sup>3</sup>CNR-IMEM

The efficiency of radiative recombination in GaN-based optical devices is improved for structures grown in a direction perpendicular to *non-polar* planes. We present a combined cross-section STM and scanning tunneling spectroscopy (STS) and *ab initio* simulations study of the *non-polar* (11-20) cleaved surface of 6H-SiC. The experiments show an unreconstructed surface in agreement with theory. Upon truncation, two surface bands appear inside the semiconductor band gap: one empty band localized on the Si atoms and one filled band on the C atoms. According to the STS experiments on n-doped samples, the Fermi energy is pinned at the surface inside the band gap. By comparison of STM filled and empty states topographies we propose that on the fresh cleaved surface the Fermi level lies at the bottom of the Si-like band. The calculated STM images reproduce the experimental contrast of the 6H stacking sequence and its bias dependence very well.

# Technical Program

**WP20, Band Structure and Effective Mass of InN under Pressure:** *Iza Gorczyca*<sup>1</sup>; Leslaw Dmowski<sup>1</sup>; Jerzy Plesiewicz<sup>1</sup>; Tadeusz Suski<sup>1</sup>; Niels Christensen<sup>2</sup>; Axel Svane<sup>2</sup>; Chad Gallinat<sup>3</sup>; Gregor Koblmüller<sup>3</sup>; James Speck<sup>3</sup>; <sup>1</sup>Institute of High Pressure Physics; <sup>2</sup>Department of Physics and Astronomy, University of Aarhus; <sup>3</sup>Materials Department, University of California

Calculations of the electronic band structure and effective mass of InN are performed within the density functional theory by means of the linear muffin-tin-orbital method with adjusted band gaps. The results show a pronounced non-parabolicity of the conduction band. Calculated variations of the optical gap and electron effective mass with free electron concentration are presented and compared to available experimental data. Pressure effects are studied. Both the fundamental band gap and the electron effective mass increase with hydrostatic pressure, but due to the non-parabolic character of the conduction band of InN the pressure coefficient of the effective mass decreases with electron concentration. Experimental verification of this behavior has been performed on three n-type samples of InN with different electron concentrations. The measurements and calculations agree in the description of the dependence of effective mass and its pressure coefficient on electron concentration.

**WP21, Bulk and Surface Electron-Induced Infrared Magneto-optic Response in InN: A Possible Evidence for a New Defect-Related Doping Mechanism:** *Tino Hofmann*<sup>1</sup>; H. Lu<sup>2</sup>; W. Schaff<sup>2</sup>; V. Darakchieva<sup>3</sup>; M. Schubert<sup>1</sup>; <sup>1</sup>University of Nebraska-Lincoln; <sup>2</sup>Cornell University; <sup>3</sup>Linköping University

Measurements of free electron induced infrared magneto-optic birefringence in naturally-doped wurtzite-structure InN thin films by generalized ellipsometry reveal that both the surface and the interior (bulk) free electron densities decrease with power-law dependencies on the film thickness. We discover a significant deviation between the bulk electron and dislocation densities. We attribute this difference to the existence of surface defects with activation mechanism different from bulk dislocations, and which identifies the possible origin of the so far persistent natural n-type conductivity in InN. Our non-contact measurements may provide the missing information to understand the physical origin of the strong electron accumulation at the InN thin film surfaces<sup>1</sup> and the thickness dependence of the high natural n-type conductivity,<sup>2,3</sup> and thus likely also the answer to the unreliable p-type conductivity.<sup>4,5</sup> Furthermore, the anisotropy of the Gamma-point effective mass is quantified. <sup>1</sup>H. Lu et al., Appl. Phys. Lett. 83, 1136 (2003). <sup>2</sup>H. Lu et al., Appl. Phys. Lett. 77, 2548 (2000). <sup>3</sup>C.H. Swartz et al., *physica status solidi (c)* 2, 2250 (2005). <sup>4</sup>P.A. Anderson et al., 89, 184104 (2006). <sup>5</sup>Jones et al., Phys. Rev. Lett. 96, 125505 (2006).

**WP22, Characteristics of InGaN/GaN Films Grown on Hemispherical Patterned Sapphire (HPS):** *Jae-Hoon Lee*<sup>1</sup>; <sup>1</sup>Samsung Electro-Mechanics

We investigated the characteristics of InGaN/GaN films grown on a hemispherical patterned sapphire (HPS) substrate. A detailed analysis of X-ray diffraction patterns resulted in a shorter lattice constant *c* of 5.1877 Å for the GaN thin films grown on HPS substrate compared to the 5.1913 Å for the samples grown on conventional sapphire substrate (CSS). The corresponding PL spectral peak wavelength of the InGaN/GaN films shifted up by 3 nm from ~448 nm for CSS to ~451 nm for HPS. Surface pattern of the HPS substrate seems to be more helpful for the accommodative relaxation of compressive strain related to the lattice mismatch between the GaN and sapphire substrate.

**WP23, Characterization of GaN-Based Lateral Polarity Heterostructures:** *Stefan Krischok*<sup>1</sup>; Pierre Lorenz<sup>1</sup>; Vadim Lebedev<sup>1</sup>; Florentina Niebelschütz<sup>1</sup>; Sindy Hauguth<sup>1</sup>; Oliver Ambacher<sup>1</sup>; Juergen Schaefer<sup>1</sup>; <sup>1</sup>TU Ilmenau

Nonlinear effects in optics have attracted much interest because they offer the possibility of generating or manipulating light in almost any manner. It is now possible to produce periodically patterned lateral polarity heterostructures for nonlinear optical applications. We have studied GaN-based lateral polarity heterostructures (LPH GaN). The investigated LPH GaN structure had a periodicity between 2 μm and a few cm in order to fulfill the demands of the different experimental techniques. The periodical samples consist of N-face (000-1) and Ga-face (0001) stripes. We present the structural differences between the N- and Ga-face measured by atomic force

microscopy (AFM), X-ray diffraction (XRD) and reflection high energy electron diffraction (RHEED) as well as differences in the chemical surfaces composition and in the valence band investigated by X-ray and ultraviolet photoelectron spectroscopy. The optical characterization was accomplished by cathodoluminescence spectroscopy. Especially the inversion domain boundary region was investigated by photoelectron emission microscopy.

**WP24, Circular Photogalvanic Effect of the Two-Dimensional Electron Gas in Al<sub>x</sub>Ga<sub>1-x</sub>N/GaN Heterostructures under Uniaxial Strain:** X.W. He<sup>1</sup>; B. Shen<sup>1</sup>; Y.Q. Tang<sup>1</sup>; Ning Tang<sup>1</sup>; F.J. Xu<sup>1</sup>; Z.X. Qin<sup>1</sup>; G. Y. Zhang<sup>1</sup>; Y. Chen<sup>2</sup>; C. Tang<sup>2</sup>; Z. Wang<sup>2</sup>; <sup>1</sup>State Key Laboratory of Artificial Microstructure and Mesoscopic Physics, School of Physics, Peking University; <sup>2</sup>Laboratory of Semiconductor Materials Science, Institute of Semiconductors, Chinese Academy of Sciences

The circular photogalvanic effect (CPGE) based on the spin of the two-dimensional electron gas (2DEG) in Al<sub>0.25</sub>Ga<sub>0.75</sub>N/GaN heterostructures has been investigated using the infrared radiation under the uniaxial strain. The photogalvanic current original from the CPGE is observed up to 10<sup>-2</sup> nA at room temperature, which has the notable change under the uniaxial strain. The amplitude of the photogalvanic current increases linearly by 20% with the augment of the strain ranging from 10<sup>-4</sup> to 10<sup>-3</sup>, indicating that the k-linear spin splitting (SIA) of the subbands in the triangular quantum well at Al<sub>0.25</sub>Ga<sub>0.75</sub>N/GaN heterointerfaces is enhanced owing to the additional strain. Based on the experimental results, it is suggested that the Rashba constant in Al<sub>x</sub>Ga<sub>1-x</sub>N/GaN heterostructures can be modulated through the outer strain.

**WP25, Comparison of Transition Metal Incorporation and Phase Segregation in MOCVD-Grown Ga(Fe,Mn)N:** Matthew Kane<sup>1</sup>; Shalini Gupta<sup>1</sup>; William Fenwick<sup>1</sup>; Man Han<sup>1</sup>; Z. Zhang<sup>1</sup>; Ian Ferguson<sup>1</sup>; <sup>1</sup>Georgia Institute of Technology

Nitride-based dilute magnetic semiconductors have been of recent interest in spintronics. It is still controversial as to whether the observed room temperature magnetic hysteresis is due to transition metal agglomeration or formation of a midgap impurity band. The comparison of Mn and Fe incorporation in GaN allows for a simultaneous evaluation of these models. This study explores the magnetic properties of Ga<sub>1-x</sub>Mn<sub>x</sub>N and Ga<sub>1-x</sub>Fe<sub>x</sub>N grown by MOCVD. Magnetic hysteresis is observed at room temperature, even at dilute alloying concentrations. Competing contributions from isolated d<sup>5</sup> and d<sup>4</sup>/d<sup>6</sup> ions and a transition metal-rich phase dominate the magnetic signature. Conversion of the trivalent to divalent transition metal states has been confirmed via optical transmission. A distinct splitting is observed in the ZFC/FC magnetization curves with silicon codoping, consistent with an array of nanoscale clusters. The Ga<sub>1-x</sub>Fe<sub>x</sub>N samples exhibited a degraded crystalline quality relative to the Ga<sub>1-x</sub>Mn<sub>x</sub>N as evidenced by structural studies.

**WP26, Crystal Growth of InN by the Use of Field Effect MOCVD:** *Takashi Inushima*<sup>1</sup>; Masaaki Higo<sup>1</sup>; Ramkrishna Biswas<sup>1</sup>; <sup>1</sup>Tokai University

Thermodynamically stable wurtzite structure InN has a polar axis parallel to the *c*-direction of the crystal lattice. Electrostatically, such macroscopic lattice polarization can be controlled by external field as is in conventional ferroelectric materials. In this experiment we controlled the polarity of InN by the use of field effect MOCVD, where electric field was applied along the *c*-direction of InN, the growth direction. We set two electrodes in the horizontal MOCVD system; SUS electrode was placed 3 mm above the other electrode Mo susceptor. The effect of the electric field was evaluated by the rocking curves of InN(0002) Bragg spots, Raman spectra, band gap energy and superconductivity. The electric field improved the crystal quality when it was applied both during crystal growth and during cooling down. When the field of 1 kV/cm was applied from the substrate to SUS electrode, enhancing N-surface growth, the narrowest rocking curve was obtained.

**WP27, Development of a Procedure for MOVPE Growth of GaN on ZnO-Buffered C-Sapphire Substrates Followed by Chemical Lift-off of the GaN:** *Abdallah Ougazzaden*<sup>1</sup>; Dave Roger<sup>2</sup>; Manijhi Razeghi<sup>3</sup>; <sup>1</sup>Georgia Institute of Technology; <sup>2</sup>Nanovation SARL; <sup>3</sup>Northwestern University

The development of GaN devices has been hampered by the lack of suitable transparent, lattice- and thermal-matching substrates since good quality;

single crystal GaN substrates have not been widely available at acceptable cost levels. Hence, GaN has been grown on a variety of substrates. Most of the work has been done using c-sapphire and 6H-SiC substrates. Another alternative and promising substrate for GaN epilayers is Zinc Oxide (ZnO). It has the same wurtzite structure than GaN and a small lattice mismatch (2%). Furthermore, c-axis GaN/ZnO shows a much-reduced mismatch in thermal expansion coefficient compared with GaN/SiC or GaN/c-sapphire. In this paper, we present the development of an MOVPE growth procedure which yields high quality GaN on ZnO. SEM and AFM confirmed homogeneous ZnO and GaN films. XRD, Raman and PL studies confirmed that the layers were well-crystallised. Auger spectroscopy showed no evidence of Zn or Al at the film surface.

**WP28, Electric Field Effect Free Characteristics of Ultra-Thin In-Rich  $\text{In}_{0.7}\text{Ga}_{0.3}\text{N}/\text{GaN}$  Multiple Quantum Well Light Emitting Diodes:** *Hee Jin Kim*<sup>1</sup>; Soon-Yong Kwon<sup>1</sup>; Pilkyung Moon<sup>1</sup>; Suk Choi<sup>1</sup>; Yong Seon Jeon<sup>1</sup>; Sung Hyun Park<sup>1</sup>; Seung-Hwan Park<sup>2</sup>; Taehoon Chung<sup>3</sup>; Jong Hyeob Baek<sup>3</sup>; Yoon Soo Park<sup>4</sup>; Euijoon Yoon<sup>1</sup>; <sup>1</sup>Seoul National University; <sup>2</sup>Catholic University of Daegu; <sup>3</sup>Korea Photonics Technology Institute; <sup>4</sup>Rensselaer Polytechnic Institute

We confirmed electric field effect free property in ultra-thin In-rich (UTIR)  $\text{In}_{0.7}\text{Ga}_{0.3}\text{N}/\text{GaN}$  multiple quantum well (MQW) by fabrication of light emitting diode (LED) device. The current-voltage characteristic of this LED showed rectifying behavior with a forward voltage of 3.4 V at 20 mA. Electroluminescence (EL) peak from UTIR InGaN/GaN MQW LED was observed at 393 nm with a narrow full width at half maximum of 20 nm. Electric field effect free characteristics in UTIR InGaN/GaN MQW LEDs were revealed by negligible EL peak shift with increasing injection current as well as the energy band calculation using  $k\cdot p$  method. This electric field free UTIR InGaN/GaN MQW LEDs is expected to be a new near-ultraviolet source.

**WP29, Electrical and Optical Properties of Thick Highly Doped P-Type GaN Layers Grown by HVPE:** *Alexander Usikov*<sup>1</sup>; Oleg Kovalenkov<sup>1</sup>; Vitaliy Soukhoveev<sup>1</sup>; Vladimir Vantsov<sup>1</sup>; Alexander Syrkin<sup>1</sup>; Vladimir Dmitriev<sup>1</sup>; Alexey Nikiforov<sup>2</sup>; Siddarth Sundaresan<sup>3</sup>; Stojan Jeliazkov<sup>4</sup>; Albert Davydov<sup>4</sup>; <sup>1</sup>Technologies and Devices International, Inc.; <sup>2</sup>Boston University; <sup>3</sup>George Mason University; <sup>4</sup>National Institute of Standards and Technology

We report on p-type GaN layers and AlGaIn/GaN heterostructures grown by hydride vapor phase epitaxy. Highly doped p-GaN thick layers and structures with low electrical resistivity are attractive substrates for novel GaN-based devices. As grown GaN layers had p-type conductivity with concentration  $N_A-N_D$  up to  $1 \times 10^{19} \text{ cm}^{-3}$  and  $8 \times 10^{17} \text{ cm}^{-3}$  for Mg-doped and Zn-doped layers, respectively. Acceptor atom concentration was varied from  $10^{17}$  to  $10^{20} \text{ cm}^{-3}$ . Hydrogen concentration was about 10 times less than that for Mg, which may explain effective p-type doping for as-grown GaN layers. Electrical conductivity at 300 K for p-GaN ranged from 1 to  $50 \text{ Ohm}^{-1} \text{ cm}^{-1}$  depending on doping level. Micro cathodo luminescence revealed a columnar-like structure of the GaN layers with a non-uniform distribution of material regions having dominant 362 nm or 430 nm luminescence. Transport properties for p-doped GaN layers and relationship between impurity,  $N_A-N_D$ , and carrier concentrations will be discussed in details.

**WP30, Electrical Conduction in Cubic GaN Films Grown on GaAs(001) by RF-MBE:** Masatoshi Kohno<sup>1</sup>; Teruyuki Nakamura<sup>1</sup>; Takahiro Kataoka<sup>1</sup>; Ryuji Katayama<sup>1</sup>; *Kentaro Onabe*<sup>1</sup>; <sup>1</sup>University of Tokyo

The electrical conduction property in c-GaN films grown on GaAs(001) by RF-MBE has been studied in relation with the amount of the hexagonal phase inclusion, or cubic phase purity. In a high-phase-purity (93%) film, the electron concentration and mobility at 300 K are typically  $8 \times 10^{17} \text{ cm}^{-3}$  and  $110 \text{ cm}^2/\text{Vs}$ , respectively. It is known that a parallel conduction is occurring in which the high mobility region somewhat away from the hetero-interface dominates the conduction at higher currents. In a lower-phase-purity (75%) film, it is indicated that the low mobility region extends over the larger region of the film. Above the cubic phase purity of 90%, the electron concentration rapidly decreases and the mobility rapidly increases by one or two orders of magnitudes, suggesting that the stacking faults are the major source of the

carrier electrons and causing the scattering centers responsible for the low mobility region.

**WP31, Electrical Properties and Optical Absorption in Periodic InN:In Structures:** *Tatiana Komissarova*<sup>1</sup>; Dmitry Plotnikov<sup>2</sup>; Valentine Jmerik<sup>2</sup>; Tatiana Shubina<sup>2</sup>; Andrey Mizerov<sup>2</sup>; Alexey Semenov<sup>2</sup>; Sergey Ivanov<sup>2</sup>; Ludmila Ryabova<sup>1</sup>; Dmitry Khokhlov<sup>1</sup>; <sup>1</sup>Moscow State University; <sup>2</sup>Ioffe Physico-Technical Institute, Russian Academy of Sciences

Metallic In nanoclusters may form spontaneously in InN epitaxial films during growth process. We performed electrophysical and optical absorption measurements in conventional InN epilayers and intentionally formed InN/In composite periodical structures (PS). It was found that the intentional introduction of In metal cluster sheets in InN does not change noticeably the carrier concentration and mobility of composite InN/In PS with respect to pure InN films, while absorption spectra in PS are significantly modified. The absorption spectra have a complicated shape, which may result from superposition of Mie resonances and absorption in the semiconductor matrix. The principal absorption edge is shifted to higher energies with increasing In amount in the indium inserts. This effect is discussed in terms of variation of the Mie resonance energy in the clusters and depletion of the medium by indium due to the Lifshitz-Slezov mechanism. The relevant uncertainty in the optical gap of InN is analyzed.

**WP32, Electron Density and Electron Scattering Processes of Inside Bulk Region in InN Films:** *Yoshihiro Ishitani*<sup>1</sup>; Masayuki Fujiwara<sup>1</sup>; Xinqiang Wang<sup>1</sup>; Song-Bek Che<sup>1</sup>; Akihiko Yoshikawa<sup>1</sup>; <sup>1</sup>Chiba University

We analyzed the infrared reflectance spectra of InN down to  $200 \text{ cm}^{-1}$ . This measurement removed the barrier for the elucidation of electronic properties inside bulk region: the barrier by the surface and interface electron accumulation. It was found that the surface electrons had the mobility of the order of  $10 \text{ cm}^2/\text{Vs}$  or less, and that the electrons accumulated around the InN/GaN interface had the density of  $10^{13} \text{ cm}^{-2}$ . The value inside the bulk region was down to  $3 \times 10^{17} \text{ cm}^{-3}$  even though the average one of all the area was nearly  $10^{18} \text{ cm}^{-3}$ . These electrons showed the remarkable E1(LO) phonon-plasmon coupling (LOPC) feature just around the energy level anti-crossing region of two LOPC modes. The obtained electron scattering rate for E1 symmetry was smaller than that for A1 one reported by another group. The reduction of edge type dislocation density is important for the improvement of the electron scattering property.

**WP33, Electron Irradiation and the Equilibrium of Open Core Dislocations in Gallium Nitride:** *Michael Hawkrigde*<sup>1</sup>; David Cherns<sup>2</sup>; <sup>1</sup>Lawrence Berkeley National Laboratory; <sup>2</sup>University of Bristol

Under electron irradiation, nanopipes in GaN are found to evolve into the so-called bamboo structure and eventually into a chain of pinholes [Pailloux et al., Applied Physics Letters 86, 131908 (2005)]. Here, the driving mechanism for this morphological evolution is examined using transmission and scanning transmission electron microscopy studies of undoped GaN grown by hydride vapor phase epitaxy. Irradiation at varying beam energies shows that morphological evolution occurs below the threshold for direct knock-on damage, and that pinholes migrate towards the beam. It is proposed that these observations can be explained by the stimulated diffusion of point defects. In areas relatively unexposed to electrons, a survey of core character, diameter and depth into the layer suggests that a similar process occurs by post-growth annealing, i.e. due to point defects mobile at the growth temperature. The implications of these results for understanding dislocation core structures are assessed.

**WP34, Epitaxy of InN/In<sub>2</sub>O<sub>3</sub> Heterostructures:** *Chunyu Wang*<sup>1</sup>; Vadim Lebedev<sup>1</sup>; Volker Cimalla<sup>1</sup>; Thomas Kups<sup>1</sup>; Gernot Ecker<sup>1</sup>; Oliver Ambacher<sup>1</sup>; J. G. Lozano<sup>2</sup>; Francisco M. Morales<sup>2</sup>; R. Garcia<sup>2</sup>; D. González<sup>2</sup>; <sup>1</sup>TU Ilmenau; <sup>2</sup>Universidad de Cádiz

The heterosystem InN/In<sub>2</sub>O<sub>3</sub> is very attractive for two reasons: first, by the use of In<sub>2</sub>O<sub>3</sub> serving as a template, hexagonal(h-) and cubic(c-) phases of InN with an improved structural quality can be obtained which have the highest electron mobility among III-nitrides; second, high-quality c-In<sub>2</sub>O<sub>3</sub> films having a larger band gap (~3.7 eV) than InN can be deposited on InN which are excellent candidates as gate oxide material for InN based high-

# Technical Program

frequency field effect transistors. In this work, the epitaxial growth of the heterosystems InN/In<sub>2</sub>O<sub>3</sub> as well as In<sub>2</sub>O<sub>3</sub>/InN was investigated. High-quality c-InN(001) was deposited on (100)In<sub>2</sub>O<sub>3</sub> template with a reticular misfit of 1.6%, while single crystalline c-In<sub>2</sub>O<sub>3</sub>(111) was epitaxially grown on h-InN(0001) with an effective lattice misfit of 2.4%. The epitaxial relationship of the heterosystem In<sub>2</sub>O<sub>3</sub>/InN was determined as In<sub>2</sub>O<sub>3</sub>[111]//InN[0001] and In<sub>2</sub>O<sub>3</sub>[10-1]//InN[11-20]. Phenomenological models for the growth and interfaces of the heterosystems are proposed.

**WP35, Eu<sup>3+</sup> Doped GaN Thin Films Grown on Sapphire by Pulsed Laser Deposition:** *Nestor Perea-Lopez*<sup>1</sup>; Jonathan Tao<sup>1</sup>; Jan Talbot<sup>1</sup>; Joanna McKittrick<sup>1</sup>; Madis Raukas<sup>2</sup>; Joe Laski<sup>2</sup>; Kailash Mishra<sup>2</sup>; Gustavo Hirata<sup>3</sup>; <sup>1</sup>University of California, San Diego; <sup>2</sup>OSRAM Sylvania; <sup>3</sup>Centro de Ciencias de la Material Condensada-Universidad Nacional Autónoma de México

By means of pulsed laser deposition, Eu<sup>3+</sup> doped GaN thin films were grown on sapphire. The PLD target was formed by pressing GaN:Eu<sup>3+</sup> powder synthesized by dissolving stoichiometric amounts of Ga<sub>2</sub>O<sub>3</sub> and Eu<sub>2</sub>O<sub>3</sub> in nitric acid, which produces Ga<sub>(1-x)</sub>Eu<sub>x</sub>(NO<sub>3</sub>)<sub>3</sub>. Next, the nitrates were oxidized in a tubular furnace with O<sub>2</sub> flow forming Ga<sub>2(1-x)</sub>Eu<sub>2x</sub>O<sub>3</sub>. Finally, the oxide powder was flushed with anhydrous ammonia to produce the desired nitride product: Ga<sub>(1-x)</sub>Eu<sub>x</sub>N. The growth was done in a stainless steel vacuum chamber partially filled with N<sub>2</sub> (400 mTorr). For the deposit, the 3<sup>rd</sup> harmonic of a Nd:YAG laser ( $\lambda=355\text{nm}$ ) was focused on the surface of the target. After deposition, annealing in NH<sub>3</sub> was required to have films with pure GaN hexagonal phase. The luminescence of the film was characterized by photo and cathodoluminescence. In addition, their chemical and structural properties were analyzed with SEM, EDS, XRD, AES and ESCA.

**WP36, Experimental and Ab-Initio Studies of Temperature Dependent InN Decomposition in Various Ambient:** *Rie Togashi*<sup>1</sup>; Tomoki Kamoshita<sup>1</sup>; Yuuki Nishizawa<sup>1</sup>; Hisashi Murakami<sup>1</sup>; Yoshinao Kumagai<sup>1</sup>; Akinori Koukita<sup>1</sup>; <sup>1</sup>Tokyo University of Agriculture and Technology

Thermal stability and decomposition behaviors of InN films in various ambient are quite important issues not only for achieving InN growth with high-quality and high-growth-rates but also for revealing the growth mechanism of III-N semiconductors. In this paper, decomposition of N-polarity InN films grown on (0001) sapphire substrates by HVPE are investigated in various ambient and at various temperatures by both experimental analysis and first-principles calculation. It was found that decomposition of an InN film in flowing N<sub>2</sub> starts to occur at about 600°C, whereas that in flowing H<sub>2</sub> becomes significant at 400°C leaving In droplets on the surface as well as decrease of the film thickness. This fact means that the use of an inert carrier gas is favorable for InN growth. The decomposition mechanism including its activation energy was compared among InN, GaN, and AlN, that was also well explained by first-principles calculation.

**WP37, Growth and Characterization of InCrN and (In,Ga,Cr)N Diluted Magnetic Semiconductors:** *Shigeya Kimura*<sup>1</sup>; Shuichi Emura<sup>1</sup>; Yuki Hiromura<sup>1</sup>; Yi Kai Zhou<sup>1</sup>; Shigehiko Hasegawa<sup>1</sup>; Hajime Asahi<sup>1</sup>; <sup>1</sup>Osaka University

Diluted magnetic semiconductors (DMSs) are attractive materials for potential applications in spin-dependent photonic and electronic devices. It is reported that some III-nitride based DMSs show room-temperature ferromagnetism. GaCrN and InCrN are ones such materials. It is considered that relative location between band gap and Cr *d* level in DMSs is related to the mechanism of their ferromagnetism. Therefore, it is expected to enable to control ferromagnetic ordering of (In,Ga,Cr)N system by tuning band gap energy with changing the contents of In and Ga. GaCrN, InCrN and (In,Ga,Cr)N films were synthesized on GaN (0001) templates at 350°C using plasma-assisted molecular beam epitaxy. X-ray diffraction (XRD)  $\theta$ -2 $\theta$  curve shows that lattice constant of (In,Ga,Cr)N is systematically shifted with In and Ga content following Vegard's law. Ferromagnetic behavior is observed at room temperature for Cr doped In<sub>0.77</sub>Ga<sub>0.23</sub>N sample grown with a Cr cell temperature of 930°C.

**WP38, Growth and Characterization of InN Thin Film by Metal-Organic Vapor Phase Epitaxy (MOVPE) on Different Buffers:** *Pen-Hsiu Chang*<sup>1</sup>; C.A. Chang<sup>1</sup>; N.C. Chen<sup>1</sup>; H.C. Peng<sup>1</sup>; D.C. Lin<sup>2</sup>; <sup>1</sup>Chang-Gung University; <sup>2</sup>Tamkang University

Superconductivity and transport characteristics of In- and N-polarity InN thin film on sapphire substrate were presented in this study. Single-crystalline In- and N-polarity InN films were obtained with nitridation, AlN, In<sub>0.22</sub>Ga<sub>0.78</sub>N, In<sub>0.3</sub>Ga<sub>0.7</sub>N, GaN as buffer layer by metal-organic vapor phase epitaxy (MOVPE) respectively. The influence of buffers on the growth of InN film was characterized by their transport properties, XRD, PL (Photoluminescence), AFM and SEM. Charge accumulation of the In- and N-polarity InN films were studied. The influence of InN polarity on the superconductivity and transport property was also investigated in this work. Details are discussed in the paper.

**WP39, Growth of High Purity Cubic InN Films on MgO (100) Substrates:** *Remi Ohba*<sup>1</sup>; Kazuya Mitamura<sup>1</sup>; Satoshi Kawano<sup>1</sup>; Jitsuo Ohta<sup>1</sup>; Hiroshi Fujioka<sup>1</sup>; Masaharu Oshima<sup>1</sup>; <sup>1</sup>The University of Tokyo

We have grown cubic InN films on MgO (100) substrates by pulsed laser deposition (PLD) and have investigated their structural properties. Direct growth of InN on MgO (100) substrates results in formation of hexagonal c-plane InN films. However, the use of cubic GaN(100) buffer layers, which should alleviate the lattice mismatch between InN and MgO, enables us to grow high quality cubic InN (100). Careful data interpretation for EBSD phase mapping and x-ray reciprocal space mapping has led us to conclude that the phase purity of the cubic InN film grown with the cubic GaN buffer layer is as high as 99%. This successful crystal growth of high purity cubic InN by PLD can be attributed to the enhanced surface migration of In atoms, which is important to convey the cubic arrangement of the atoms in the MgO substrates to the InN films.

**WP40, Growth of High Purity Un-Doped and Mg-Doped GaN Thick Films by CVD:** *Rafael Garcia*<sup>1</sup>; Alan Thomas<sup>2</sup>; Fernando Ponce<sup>1</sup>; <sup>1</sup>Arizona State University; <sup>2</sup>Rogers Corporation

High-quality doped and un-doped GaN thick films have been grown on different substrates by reacting Ga and Ga-Mg alloys with ammonium chloride using ammonia as a carrier gas in a horizontal quartz tube reactor at 900°C. The un-doped films were grown by a two-step chemical vapor deposition process using Ga and NH<sub>4</sub>Cl as starting reagents. The doped films were deposited by the same method plus an intermediate step, making a diluted alloy Ga-Mg before the CVD process. These films consist of self assembled micro-columns that coalesce to form high density thick layers. They have a wurtzite structure and exhibit strong room-temperature luminescence with the characteristic GaN band edge as well as the Mg-related emissions for the doped films. The optoelectronic properties of these films are comparable to the GaN thin films grown epitaxially with other techniques. This growth technique can be used for inexpensive, large area electroluminescent devices.

**WP41, Growth of High Quality InN on Production Style PA-MBE System:** *Iulian Gherasoiu*<sup>1</sup>; Mark O'Steen<sup>1</sup>; Tom Bird<sup>1</sup>; Dave Gotthold<sup>1</sup>; A. Chandolu<sup>2</sup>; D. Y. Song<sup>2</sup>; S. X. Xu<sup>2</sup>; M. Holtz<sup>2</sup>; S. A. Nikishin<sup>2</sup>; William Schaff<sup>3</sup>; <sup>1</sup>Veeco Instruments Inc.; <sup>2</sup>Nano Tech Center at Texas Tech University; <sup>3</sup>Cornell University

We have demonstrated step-flow growth mode of InN, with monolayer height terrace steps (0.281nm), using a production-style PA-MBE system, GEN200. MOCVD GaN templates have been overgrown in a two-step process. The surface morphology exhibits the step-flow features on relatively large areas and the RMS roughness over an area of 5 x 5  $\mu\text{m}^2$  is 1.4nm. We also investigated the consequences of In droplets formation during the growth, and we have found that the VLS growth mechanism generates defective layer areas underneath the droplets. The Hall mobility of 1 $\mu\text{m}$  thick InN layers, grown in such step-flow mode is slightly higher than 1400 cm<sup>2</sup>/Vs while for other growth conditions we have obtained mobility as high as 1904 cm<sup>2</sup>/Vs at room temperature. The samples exhibit high intensity PL spectra with a band edge absorption (~0.64eV) that follows the predictions of Moss-Burstein effect.

**WP42, Growth of Nonpolar A-Plane GaN on R-Plane Sapphire:** *Matthias Wieneke*<sup>1</sup>; Armin Dadgar<sup>1</sup>; Jürgen Blasing<sup>1</sup>; Andre Krtischil<sup>1</sup>; Hartmut Witte<sup>1</sup>; Thomas Hempel<sup>1</sup>; Peter Veit<sup>1</sup>; Jürgen Christen<sup>1</sup>; Alois Krost<sup>1</sup>; <sup>1</sup>Otto-von-Guericke-University Magdeburg FNW/IEP

Nonpolar a-plane GaN films were grown on r-plane sapphire by metal-organic vapor phase epitaxy. By varying the growth-temperature and the thickness of an in-situ deposited SiN nanomask the influence on the surface morphology, the electrical and micro structural properties were studied. Optical Nomarski microscopy images showed a decrease of pit density with decreasing growth temperature and thickness of the SiN nanomask, respectively. Additionally, the surfaces were studied by scanning electron microscopy and atomic force microscopy. Investigation of the grown films by high resolution X-ray diffraction revealed anisotropic micro structural properties. In addition the growth defects of the GaN films were studied by transmission electron microscopy. Electrical properties were studied by Hall effect and CV measurements. An enhanced electron concentration is found at the substrate/GaN interface when using a SiN mask. Furthermore, in samples without a mask the high resistivity is controlled by electrically active defects.

**WP43, High-Temperature Growth of AlN in a Production Scale 11x2" MOVPE Reactor:** *Frank Brunner*<sup>1</sup>; Harry Protzmann<sup>2</sup>; Michael Heuken<sup>2</sup>; Arne Knauer<sup>1</sup>; Markus Weyers<sup>1</sup>; Michael Kneissl<sup>1</sup>; <sup>1</sup>Ferdinand-Braun-Institut für Höchstfrequenztechnik (FBH) im FVB e.V.; <sup>2</sup>AIXTRON AG

We report on the growth of high quality AlN films on sapphire by MOVPE in an AIX2400G3-HT planetary reactor. Specific reactor hardware modifications were conducted to facilitate growth temperatures of up to 1600°C and to obtain reduced parasitic gas phase reactions. Growth was optimized regarding growth rates, surface morphology as well as optical and structural properties of the AlN layers on sapphire. With increasing growth temperature we observe a transition from a 3-dimensional columnar-like AlN surface to a feature-less smooth morphology. The impact of the growth parameters and the re-designed reactor inlet configuration on the AlN properties has been investigated in detail by X-ray diffraction, AFM, photoluminescence and SIMS. The effects of residual reactor contaminants (e.g. oxygen) on the growth behaviour and the role of Ga as a possible surfactant during AlN growth will be discussed.

**WP44, Hydrostatic Pressure Coefficient of Photoluminescence in InGaN: From InN to GaN:** *Gijs Franssen*<sup>1</sup>; Tadeusz Suski<sup>1</sup>; Agata Kaminska<sup>2</sup>; Izabela Gorczyca<sup>1</sup>; Andrzej Suchocki<sup>2</sup>; H. Lu<sup>3</sup>; W. J. Schaff<sup>4</sup>; M. Kurouchi<sup>4</sup>; Y. Nanishi<sup>4</sup>; E. Iliopoulos<sup>5</sup>; A. Georgakilas<sup>5</sup>; <sup>1</sup>Polish Academy of Science, Institute of High Pressures Physics; <sup>2</sup>Polish Academy of Science, Institute of Physics; <sup>3</sup>Cornell University, Department of Electrical and Computer Engineering; <sup>4</sup>Ritsumeikan University, Department of Photonics, School of Science and Engineering; <sup>5</sup>FORTH, Institute of Electronic Structure and Lasers

The microscopic origin of (i) very efficient light emission from InGaN structures with  $x > 10\text{-}20\%$  and (ii) a strong reduction of this efficiency for  $x > 20\text{-}30\%$  are much debated. In order to understand these phenomena, accurate knowledge of the band structure of InGaN alloys is essential. Hydrostatic pressure measurements are useful for the exploration of the band structure. In this work, we present a study of the photoluminescence (PL) pressure coefficient  $dE/dp$  of InGaN alloys, which is closely related to the band gap pressure coefficient  $dE_g/dp$ . Evolution of  $dE/dp$  is studied in the entire range of ternary alloys from GaN to InN. Basing on these findings as well as on first-principle calculations we discuss the possible origin of the evolution of the band gap with In content and pressure. Special attention is paid to the large bowing in the region with low In content.

**WP45, Increase in Luminescence Efficiency of GaPN Epilayers Grown by Migration-Enhanced Epitaxy:** *Kazuyuki Umeno*<sup>1</sup>; Yuzo Furukawa<sup>1</sup>; Ryosuke Noma<sup>1</sup>; Hiroo Yonezu<sup>1</sup>; Akihiro Wakahara<sup>1</sup>; Kunio Itoh<sup>2</sup>; <sup>1</sup>Toyoashi University of Technology; <sup>2</sup>Tsuyama National College of Technology

Dilute nitrides, such as GaPN alloys, have received much attention for Si-based monolithic optoelectronic integrated circuits. However, GaPN layers grown by molecular-beam epitaxy (MBE) showed remarkable thermal quenching in photoluminescence (PL) intensity caused by non-radiative

recombination centers. In this work, migration-enhanced epitaxy (MEE) for the GaPN layers were demonstrated to improve the luminescence efficiency. 100-nm-thick GaPN layers were grown on GaP (001) substrates by low-temperature MEE (LT-MEE) at 500°C and high-temperature MBE (HT-MBE) at 580°C with an rf-MBE apparatus. The change of the surface reconstruction was clearly observed during LT-MEE growth with reflection high-energy electron diffraction (RHEED). The PL peak intensity of the LT-MEE-grown GaPN layer was about ten-time higher than that of the HT-MBE-grown layer around room-temperature in spite of the low growth temperature. This result indicates the reduction of non-radiative recombination centers in the GaPN layer by increasing the surface migration length of Ga adatoms.

**WP46, Influence of Substrate Misorientation on Properties of Nitride Epitaxial Layers and Quantum Structures Grown on Freestanding GaN:** *Gijs Franssen*<sup>1</sup>; Tadeusz Suski<sup>1</sup>; Marcin Krysko<sup>1</sup>; Boleslaw Lucznik<sup>1</sup>; Izabela Grzegory<sup>1</sup>; Stanislaw Krukowski<sup>1</sup>; Aleksander Khachapuridze<sup>1</sup>; Jerzy Plesiewicz<sup>2</sup>; Leslaw Dmowski<sup>1</sup>; Robert Czernecki<sup>2</sup>; Szymon Grzanka<sup>2</sup>; Michal Leszczynski<sup>2</sup>; Piotr Perlin<sup>2</sup>; Sylwester Porowski<sup>1</sup>; <sup>1</sup>Institute of High Pressures Physics PAS; <sup>2</sup>TopGaN Ltd.

We studied the influence of GaN substrate misorientation (up to 3 deg with respect to the c-axis) on InGaN optical properties. InGaN layers and quantum structures, and GaN:Mg layers were grown by MOVPE method. X-ray Bragg reflection, photoluminescence (PL) peak energy and PL peak width and their temperature dependences of the grown structures were analyzed. A very pronounced correlation between the substrate misorientation and the examined properties of studied InGaN samples was found. For example, a higher misorientation angles give lower In-incorporation, causing a blue shift of the PL peak energy. Strikingly, higher misorientation (i.e., lower In content) leads to higher alloy disorder related to In segregation processes, clearly seen in InGaN layers. In addition, we observe a very pronounced influence of GaN substrate misorientation on the hole concentration in GaN:Mg layers. A discussion of the microscopic origin of the observed phenomena based on substrate-morphology related effects will be given.

**WP47, Influence of the Illumination on the Spin Splitting of the Two-Dimensional Electron Gas in AlxGa1-xN/GaN Heterostructures:** *Ning Tang*<sup>1</sup>; *Bo Shen*<sup>1</sup>; Kui Han<sup>1</sup>; Zhijian Yang<sup>1</sup>; Zhixin Qin<sup>1</sup>; Guoyi Zhang<sup>1</sup>; Tie Lin<sup>2</sup>; Wenzheng Zhou<sup>2</sup>; Junhao Chu<sup>2</sup>; <sup>1</sup>State Key Laboratory of Artificial Microstructure and Mesoscopic Physics, School of Physics, Peking University; <sup>2</sup>National Laboratory for Infrared Physics, Shanghai Institute of Technical Physics, Chinese Academy of Sciences

Spin splitting of the two-dimensional electron gas (2DEG) in AlxGa1-xN/GaN heterostructures has been investigated by means of magnetotransport measurements under the illumination at low temperatures. The beating patterns in the oscillatory magnetoresistance originating from zero-field splitting and magnetointersubband scattering (MIS) effects of the 2DEG are observed in this study. Corresponding to the shift of the beating nodes originating from zero-field spin splitting, it is found that the spin splitting energy decreases after the illumination. It is also found that the illumination decreases the electric field at AlxGa1-xN/GaN heterointerfaces. Based on the experimental results, it is suggested that the zero-field spin splitting of the 2DEG in AlxGa1-xN/GaN heterostructures mainly arises from the Rashba effect.

**WP48, Infrared Microphotorefectance Spectra of InN:** *Kazutoshi Fukui*<sup>1</sup>; Kenta Kurihara<sup>1</sup>; Tooru Yanagawa<sup>1</sup>; Akio Yamamoto<sup>1</sup>; <sup>1</sup>University of Fukui

Investigations into electrical properties of InN thin films by electric measurement methods often have some discrepancies which are probably due to the existence of oxides, interface and/or surface charge accumulations, etc. The optical measurement methods, for example infrared reflectance measurements, also give some information related to charge concentrations, mobility, etc. In previous work, we derived not only TO and LO phonon frequencies, but also plasma frequencies and their damping factors from fitting infrared reflectance spectra to the theoretical formula, and we discussed the carrier concentration of InN thin films. In this work, we have carried out infrared microphotorefectance measurements to extend this method to the local electric information of thin films.

# Technical Program

**WP49, Interplay between Strain and Composition in AlInN Alloys: Effect on the Validity of Vegard's Law:** *V. Darakchieva*<sup>1</sup>; M. Beckers<sup>1</sup>; L. Hultman<sup>1</sup>; B. Monemar<sup>1</sup>; J.-F. Carlin<sup>2</sup>; N. Grandjean<sup>2</sup>; <sup>1</sup>Linköping University; <sup>2</sup>Ecole Polytechnique Federale de Lausanne

AlInN alloys have lately attracted a lot of attention due to the large energy range covered by their band gap and the possibility for lattice matching to GaN. The physical properties of ternary compounds are typically discussed based on Vegard's law. However, recent theoretical and experimental works on AlInN alloys revealed some deviations from Vegard's law for this material system. Correction factors that largely differ depending on the growth peculiarities, material properties, composition range and particular method used to extract alloy composition have been suggested and motivated the need of further investigations. In this work we present comparative study on the composition of AlInN alloys by X-ray reciprocal space mapping (RSM) and Rutherford back-scattering. The effects of strain relaxation and type of strain in the films on the extracted composition from the RSM are discussed and the implications on the validity of Vegard's law are outlined.

**WP50, Local Vibration Modes and Nitrogen Incorporation in AlGaAs: N Layers:** S. Lazic<sup>1</sup>; Eva Gallardo<sup>2</sup>; J. Calleja<sup>1</sup>; J. Miguel-Sánchez<sup>2</sup>; M. Montes<sup>3</sup>; A. Hierro<sup>3</sup>; R. Gargallo-Caballero<sup>3</sup>; A. Guzmán<sup>3</sup>; E. Muñoz<sup>3</sup>; A. M. Teweldeberhan<sup>4</sup>; S. Fahy<sup>4</sup>; <sup>1</sup>Department de Física de Materiales, Universidad Autónoma de Madrid; <sup>2</sup>Department de Física de Materiales, Universidad Autónoma de Madrid; <sup>3</sup>Instituto de Sistemas Optoelectrónicos y Microtecnología, Universidad Politécnica de Madrid; <sup>4</sup>Tyndall National Institute

Raman scattering measurements in dilute AlGaAs:N films grown by plasma-assisted molecular beam epitaxy on (100) GaAs substrates reveal strong local vibration modes (LVM) associated to N complexes. The LVM observed frequencies around 325, 385, 400, 450 and 500 cm<sup>-1</sup> are in fair agreement with density functional theory supercell calculations of Al<sub>n</sub>Ga<sub>3-n</sub>N complexes (n=1,2,3). We find that most of the observed LVM correspond to n=1 and n=2 complexes. The LVM spectra are resonant with N-related electronic transitions in the energy range from 1.75 to 1.79 eV. The values of the extended phonon frequencies reveal changes in the N distribution depending on the growth conditions: A transition from random to non-random nitrogen distribution is observed upon increasing the substrate temperature. Our results confirm the preferential bonding of N to Al in AlGaAs:N, due to the higher Al-N bond strength as compared to the Ga-N bond.

**WP51, Low-Temperature Grown Compositionally Graded InGaN Films:** *N. Miller*<sup>1</sup>; R. E. Jones<sup>1</sup>; K. M. Yu<sup>2</sup>; P. Flanigan<sup>3</sup>; J. Wu<sup>3</sup>; J. W. Ager<sup>2</sup>; Z. Liliental-Weber<sup>2</sup>; E. E. Haller<sup>1</sup>; W. Walukiewicz<sup>2</sup>; T. L. Williamson<sup>4</sup>; M. A. Hoffbauer<sup>4</sup>; <sup>1</sup>Department of Materials Science and Engineering, University of California, Berkeley and Materials Sciences Division, Lawrence Berkeley National Laboratory; <sup>2</sup>Materials Sciences Division, Lawrence Berkeley National Laboratory; <sup>3</sup>Department of Materials Science and Engineering, University of California, Berkeley; <sup>4</sup>Chemistry Division, Los Alamos National Laboratory

Energetic neutral atomic-beam lithography/epitaxy (ENABLE) provides a larger N atom flux and eliminates the need for high substrate temperatures as compared to molecular beam epitaxy making isothermal growth over the entire InGaN alloy composition range possible without phase separation. 500-800 nm thick compositionally graded InGaN films were grown by ENABLE at ~450 °C: (1) with the Ga-rich material on the surface and (2) with the In-rich material on the surface. Rutherford backscattering spectrometry (RBS), transmission electron microscopy, x-ray diffraction, absorption spectroscopy, photoluminescence, and Hall effect measurements were used to assess the thickness, composition, crystalline quality, and optical and electrical properties of the films. The RBS and Hall effect data were used to model the electrical properties and expected distribution of free electrons throughout the thickness of the films. The results establish the new ENABLE method as uniquely capable of growing compositionally graded InGaN films and possibly InN/GaN heterostructures.

**WP52, Luminescence and Vibrational Properties of Erbium-Implanted Nanoporous GaN:** *Chew Beng Soh*<sup>1</sup>; Soo Jin Chua<sup>1</sup>; Si Hui Sim<sup>2</sup>; Sudhiranjan Tripathy<sup>1</sup>; E. Alves<sup>3</sup>; <sup>1</sup>Institute of Materials Research and Engineering; <sup>2</sup>National University of Singapore; <sup>3</sup>Instituto Tecnológico e Nuclear

Implantation of Erbium (Er) into GaN is useful in creating selected areas to emit at the green, yellow and infrared wavelengths. Enhanced Erbium activation is obtained when Erbium is implanted into porous GaN formed by electrochemical etching than into as-grown GaN. This is due to the increase in surface areas for light extraction and the availability of more free surfaces to accommodate strain when it is annealed. Furnace annealing at 1100 deg for 30 mins in nitrogen gives rise to higher band-edge photoluminescence intensity. Apart from the host GaN phonon modes, we have also observed disorder-induced lattice vibrations at 170, 200 and 350-365 cm<sup>-1</sup> from Er-implanted porous GaN. The E2 (high) mode of GaN also shifts towards higher energy at higher annealing temperatures, indicative of more Erbium occupying the VGa site (ionic radii of Er > Ga) and hence increasing the compressive stress in the GaN crystal lattice.

**WP53, Luminescence Property of GaPN Layer Grown by OMVPE:** *Susumu Hatakenaka*<sup>1</sup>; Akihiro Wakahara<sup>2</sup>; Yoshiyuki Nakanishi<sup>1</sup>; Yuzo Furukawa<sup>1</sup>; Hiroshi Okada<sup>1</sup>; Hiroo Yonezu<sup>1</sup>; <sup>1</sup>Toyohashi University of Technology

GaPN is expected to realize Si-based monolithic optoelectronic integrated circuits owing to lattice-match to Si. (In)GaPN based light emitting diodes on Si have been realized by molecular beam epitaxy (MBE). However, GaPN grown by MBE showed large thermal quenching in photoluminescence (PL) intensity owing to point defects were induced by N-radical. In this work, we try to improve luminescence property of GaPN using organometallic vapor phase epitaxy (OMVPE) which is radical-free growth method. GaPN layers were grown on GaP(100) using trimethylgallium (TMGa) or triethylgallium (TEGa). Unintentional carbon incorporation in GaPN by TEG decreased by 1/4 compared with TMGa. As a result, non-radiative recombination centers decreased by about two orders of magnitude by TEGa. Compared to MBE, Full width at half maximum (FWHM) of PL peak in OMVPE-GaPN was 140meV whereas FWHM of MBE-GaPN was 200meV. PL intensity of deep level has decreased by about two orders of magnitude using OMVPE.

**WP54, MBE Growth and Characterization of Mg-Doped InGaN and InAlN:** *Kristopher Matthews*<sup>1</sup>; Xiaodong Chen<sup>1</sup>; Dong Hao<sup>1</sup>; William Schaff<sup>1</sup>; Lester Eastman<sup>1</sup>; <sup>1</sup>Cornell University

We report on the growth of Mg-doped InGaN and InAlN by molecular beam epitaxy. We successfully obtain high quality In<sub>x</sub>Ga<sub>1-x</sub>N films on (0001) sapphire substrate. Phase separation does not occur in In<sub>x</sub>Ga<sub>1-x</sub>N films with Indium content up to 0.88. Hall measurement shows that hole concentration of 7.7x10<sup>17</sup> cm<sup>-3</sup> is achieved on Mg-doped In<sub>0.04</sub>Ga<sub>0.96</sub>N. When x>0.11, the Hall samples exhibit strong n-type polarity, whereas p-type polarity is confirmed by hot probe measurement for all of Mg-doped InGaN. Ni/Au film is deposited on Mg-doped In<sub>x</sub>Ga<sub>1-x</sub>N as the contact metal. The contact resistance as high as 2700 Ω•mm is obtained when x=0.25 while it is only 0.03 Ω•mm when x=0.85. High quality crack-free InAlN film is also grown on sapphire substrate with AlN/InN quantum-well buffer layer. So far all of Mg-doped InAlN films show n-type polarity by Hall measurement, but it is promising to achieve p-polarity with varying Mg flux.

**WP55, Mg-Doped InN Epilayers and in Rich InGaN Alloys:** *Neelam Khan*<sup>1</sup>; Neeraj Nepal<sup>1</sup>; Ashok Sedhain<sup>1</sup>; Hongxing Jiang<sup>1</sup>; Jingyu Lin<sup>1</sup>; <sup>1</sup>Kansas State University

Mg-doped InN epilayers and In-rich InGaN alloys were grown on sapphire substrates by metal organic chemical vapor deposition. Effects of Mg concentration on the structural, electrical and photoluminescence (PL) emission properties of Mg-doped InN have been investigated. PL studies revealed a dominant emission line at ~ 0.76 eV in Mg-doped InN epilayers, which was absent in undoped InN epilayers and was about 60 meV below the band edge emission peak at ~ 0.82 eV. The PL peak position and the temperature dependent emission intensity corroborated each other and suggested that the Mg acceptor level in InN is about 60 meV above the valance band maximum. Mg doped InGaN epilayers have also been grown and their structural, optical, and electrical properties have been measured and

will be reported. The implications of our results on achieving p-type InGa<sub>N</sub> alloys with high In-contents will be discussed.

**WP56, MOVPE Growth and Photoluminescence Properties of InAs<sub>N</sub> QDs:** *Shigeyuki Kuboya*<sup>1</sup>; Thieu Quang Tu<sup>1</sup>; Shun Takahashi<sup>1</sup>; Fumihiro Nakajima<sup>1</sup>; Ryuji Katayama<sup>1</sup>; Kentaro Onabe<sup>1</sup>; <sup>1</sup>University of Tokyo

The self-assembled InAs<sub>N</sub> quantum dots (QDs) were grown on GaAs (001) by MOVPE. With the DMHy (N precursor) supply, the dot width decreased from 31 nm to 18 nm and the dot density increased from  $3.3 \times 10^{10} \text{ cm}^{-2}$  to  $4.1 \times 10^{10} \text{ cm}^{-2}$  at the equivalent nominal thickness of 2.6 ML. The reduction of the dot size is attributed to the increased wetting layer thickness for the QD formation. The increase of the dot density is attributed to the decreased migration lengths of the surface species. The RT-PL peak wavelengths of the 2.6 ML InAs and InAs<sub>N</sub> QDs were 1135 nm and 1159 nm, respectively. This red-shift is caused by the N-incorporation-induced bandgap reduction, which is dominant over the possible blue-shift for the reduced dot sizes (quantum size effect). The temperature dependence of PL shows that the N-related carrier localization is no significance in the QDs in contrast with the bulk InAs<sub>N</sub> films.

**WP57, Optical Gain of Eu<sup>3+</sup> Ion Implanted AlGa<sub>N</sub> and Its Al Compositional Dependence:** *Akihiro Wakahara*<sup>1</sup>; Takashi Shimojo<sup>1</sup>; Hiroaki Kawai<sup>1</sup>; Hiroshi Okada<sup>1</sup>; Takeshi Ohshima<sup>2</sup>; Shin-ichiro Sato<sup>2</sup>; <sup>1</sup>Toyoashi University of Technology; <sup>2</sup>Japan Atomic Energy Agency

Optical properties, such as optical modal gain and optical loss, of Eu implanted AlGa<sub>N</sub> with various AlN molar fractions are measured to investigate the potential application of Eu-implanted AlGa<sub>N</sub> for optical devices. The optical gain measured at 300K by using variable length stripe (VSL) method for Eu-implanted GaN is as high as  $50 \text{ cm}^{-1}$ , which is the same order of MBE-grown GaN:Eu. The optical gain increases with increasing the AlN molar fraction and shows maximum value of  $\sim 130 \text{ cm}^{-1}$  around the AlN molar fraction of 0.2. While the optical loss is of the order of  $\sim 10 \text{ cm}^{-1}$ .

**WP58, Optical Properties of Cubic InN from Mid-IR into the VUV Range:** *Pascal Schley*<sup>1</sup>; Christian Napierala<sup>1</sup>; Rüdiger Goldhahn<sup>1</sup>; Gerhard Gobsch<sup>1</sup>; Jörg Schörmann<sup>2</sup>; Donat As<sup>2</sup>; Klaus Lischka<sup>2</sup>; Martin Feneberg<sup>3</sup>; Klaus Thonke<sup>3</sup>; Frank Fuchs<sup>4</sup>; Friedhelm Bechstedt<sup>4</sup>; <sup>1</sup>TU Ilmenau; <sup>2</sup>University Paderborn; <sup>3</sup>University Ulm; <sup>4</sup>Friedrich-Schiller-University Jena

We present a comprehensive optical characterization of single crystalline cubic (c) InN films grown by MBE on c-GaN/3C-SiC pseudo-substrates. Ellipsometry was applied in order to determine the dielectric function (DF) from the mid-infrared into the VUV spectral region. All layers show strong emission around 0.5 eV at low temperature. The high electron densities cause pronounced Stokes and Burstein-Moss shifts at the gap. Taking into account carrier-induced band-gap renormalization, the non-parabolicity and the filling of the conduction band we determine a zero-density c-InN band gap of 0.61 eV which is about 70 meV lower than for hexagonal InN. In addition, the DF shows pronounced features at high photon energies. The transition energies for these Van-Hove singularities are determined. Their values as well as the shape of the DF are in excellent agreement with the results of DFT-LDA calculations for which electron-hole interaction was taken into account.

**WP59, Photoluminescence of Cubic InN Films on MgO(001) Substrates:** *Takeru Inoue*<sup>1</sup>; Youhei Iwahashi<sup>1</sup>; Shingo Oishi<sup>1</sup>; Misao Orihara<sup>1</sup>; Yasuto Hizikata<sup>1</sup>; Hiroyuki Yaguchi<sup>1</sup>; Sadafumi Yoshida<sup>1</sup>; <sup>1</sup>Saitama University

Although there have recently been a lot of reports on the growth and characterization of hexagonal InN (h-InN), the growth of cubic InN (c-InN) films has been less reported. Furthermore, the physical properties of c-InN, such as band gap energy, have been still unclear. In this study, we report on the photoluminescence (PL) from c-InN films grown on MgO substrates with a cubic GaN underlayer by RF-N<sub>2</sub> plasma molecular beam epitaxy. A single PL peak was observed at 0.47eV. By analyzing the reflectance spectra of c-InN films, we found c-InN is a direct transition type semiconductor and that the band gap energy is 0.48 eV. The difference in the PL peak energy between h- and c-InN is in good agreement with the difference predicted by ab initio calculations.

**WP60, Photoluminescence Study of Hexagonal InN/InGa<sub>N</sub> Quantum Well Structures Grown on 3C-SiC (001) Substrates by Molecular Beam Epitaxy:** *Shigeru Hirano*<sup>1</sup>; Takeru Inoue<sup>1</sup>; Go Shikata<sup>1</sup>; Misao Orihara<sup>1</sup>; Yasuto Hijikata<sup>1</sup>; *Hiroyuki Yaguchi*<sup>1</sup>; Sadafumi Yoshida<sup>1</sup>; <sup>1</sup>Saitama University

We have studied the well-width dependence of photoluminescence from hexagonal InN/InGa<sub>N</sub> multiple quantum well structures grown on 3C-SiC (001) substrates with an InGa<sub>N</sub> underlayer by plasma assisted molecular beam epitaxy. We have observed photoluminescence spectra of InN/InGa<sub>N</sub> MQWs with various well widths. The photoluminescence peak due to quantum wells was clearly observed even at room temperature and found to shift to higher energies with decreasing well width due to the quantum confinement effect. The well width dependence of the photoluminescence peak energy can be explained by assuming that the valence band offset is relatively large. We also discuss the effect of the built-in electric fields on the PL peak energy.

**WP61, Raman Study of High-N-Content GaAs<sub>N</sub> Films Grown by MOVPE:** *Fumihiro Nakajima*<sup>1</sup>; *Sakuntam Sanorpim*<sup>2</sup>; *Wataru Ono*<sup>1</sup>; *Shigeyuki Kuboya*<sup>1</sup>; *Ryuji Katayama*<sup>1</sup>; *Kentaro Onabe*<sup>1</sup>; <sup>1</sup>University of Tokyo; <sup>2</sup>Chulalongkorn University

MOVPE-grown GaAs<sub>N</sub> films with the N content up to 5.1% were studied by micro-Raman scattering spectroscopy. In the Raman spectra, besides GaAs LO(T), additional peaks including one caused by the Ga-N localized vibrational mode (LVM), have developed with increasing N content. Additional peaks except LVM are caused by the inherently forbidden modes which have appeared due to the lattice-orientation disorder caused by N incorporation. LVM is considered to cause the weaker temperature dependence of the bandgap in higher N-content films previously discussed. The N contents estimated from the relative intensities of LVM and LO(T) were identical with those determined from X-ray diffraction for lower N contents. The discrepancy for higher N contents (N>3%) suggests the significance of the point defects like N interstitials and vacancies. An improved coincidence was achieved after annealing the films, indicating that more N atoms occupy the proper lattice sites with less point defects.

**WP62, Structural and Optical Properties of In-Rich InGa<sub>N</sub> Dots Grown by Metalorganic Chemical Vapor Deposition:** *Wen-Che Tsai*<sup>1</sup>; *Hsuan Lin*<sup>1</sup>; *Wen-Chen Ke*<sup>1</sup>; *Wen-Hao Chang*<sup>1</sup>; *Wu-Ching Chou*<sup>1</sup>; *Wei-Kuo Chen*<sup>1</sup>; *Ming-Chih Lee*<sup>1</sup>; <sup>1</sup>National Chiao Tung University

Surface morphologies, alloy compositions and emission properties of In-rich In<sub>x</sub>Ga<sub>1-x</sub>N dots ( $x \geq 0.87$ ) grown by metalorganic chemical vapor deposition at various growth temperatures (550-750°C) were investigated. The nucleation of InGa<sub>N</sub> dots was found to be governed by the surface migration of In adatoms. With the increasing growth temperature, the incorporation of Ga into InN during the growth of InGa<sub>N</sub> dots is kinetically inhibited, which tends to decompose into In-rich islands and a thin Ga-rich layer. These In-rich islands exhibit PL emission in the near-infrared range. Another visible emission band was also observed for samples grown at higher temperatures. The formation of a thin Ga-rich layer is likely to be responsible for the visible emission.

**WP63, Synthesis of Rare-Earth Activated AlN and GaN Powders via a Three-Step Conversion Process:** *Jonathan Tao*<sup>1</sup>; *Nestor Perea-Lopez*<sup>1</sup>; *Joanna Mckittrick*<sup>1</sup>; *Jan Talbot*<sup>1</sup>; *Madis Raukas*<sup>2</sup>; *Joe Laski*<sup>2</sup>; *Kailash Mishra*<sup>2</sup>; *Gustavo Hirata*<sup>3</sup>; <sup>1</sup>University of California, San Diego; <sup>2</sup>Osram Sylvania; <sup>3</sup>CCMC-UNAM

Using a three-step solution method, we have successfully synthesized rare-earth activated AlN, GaN, as well as undoped GaAlN. Rare-earth activators including Eu<sup>3+</sup>, Tb<sup>3+</sup>, Dy<sup>3+</sup>, and Tm<sup>3+</sup> are first added as nitrate precursors to an aqueous Al(NO<sub>3</sub>)<sub>3</sub> precursor. Then the mixture is converted into Al(OH)<sub>3</sub> by combining with aqueous NH<sub>4</sub>OH at room temperature. The product is then mixed with aqueous NH<sub>4</sub>F to form rare-earth activated (NH<sub>4</sub>)<sub>3</sub>AlF<sub>6</sub>. The conversion process is complete when the hexafluoride compound is flushed with anhydrous ammonia to produce the final nitride product. GaN and GaAlN are synthesized similarly. Single phase AlN, GaN and GaAlN formation has been confirmed by XRD. EDS measurements indicates an oxygen concentration of approximately 4 at% in GaN powders, and slightly higher in AlN powders. Luminescence measurements show clearly

# Technical Program

observable emission from  $\text{Eu}^{3+}$  and  $\text{Tb}^{3+}$  co-activated AlN samples as well as emission from  $\text{Dy}^{3+}$  and  $\text{Tm}^{3+}$  co-activated AlN samples.

**WP64, Temperature Dependence of the Density of the Two-Dimensional Electron Gases in  $\text{Al}_x\text{Ga}_{1-x}\text{N}/\text{GaN}$  Heterostructures:** Maojun Wang<sup>1</sup>; Bo Shen<sup>1</sup>; Ning Tang<sup>1</sup>; Fujun Xu<sup>1</sup>; Sen Huang<sup>1</sup>; Jian Xu<sup>1</sup>; Zhenlin Miao<sup>1</sup>; Zhijian Yang<sup>1</sup>; Zhixin Qin<sup>1</sup>; Guoyi Zhang<sup>1</sup>; <sup>1</sup>State Key Laboratory of Artificial Microstructure and Mesoscopic Physics, School of Physics, Peking University

Temperature dependence of the density of the two-dimensional electron gas (2DEG) in  $\text{Al}_0.18\text{Ga}_{0.82}\text{N}/\text{GaN}$  heterostructures has been investigated by means of high temperature Hall measurements from room temperature to 500°C before and after  $\text{SiN}_x$  passivation. In as-grown heterostructures, the 2DEG density decreases with increasing temperature from room temperature to 250°C, and then changes to increase with increasing temperature at higher temperatures, which is suggested to be caused by the change of the conduction band offset and the increased background electron concentration in GaN layer at higher temperatures, respectively. Theoretical calculation of the 2DEG density in  $\text{Al}_x\text{Ga}_{1-x}\text{N}/\text{GaN}$  heterostructures at various temperatures is consistent with the experimental results. The 2DEG density increases much after  $\text{SiN}_x$  passivation and it is revealed that the increased 2DEG density is mainly caused by the excess Si dangling bonds at the  $\text{SiN}_x/\text{Al}_0.18\text{Ga}_{0.82}\text{N}$  interface and Si atoms incorporated into the  $\text{Al}_0.18\text{Ga}_{0.82}\text{N}$  barrier during the  $\text{SiN}_x$  growth.

**WP65, The Comparison of Structural, Optical, and Magnetic Properties of Undoped and P-Type GaN Implanted with Mn+ (1, 5 and 10 at%):** Yoon Shon<sup>1</sup>; H. Jeon<sup>1</sup>; C. Park<sup>1</sup>; S.-W. Lee<sup>1</sup>; T. Kang<sup>1</sup>; Eun Kim<sup>2</sup>; D. Fu<sup>3</sup>; J. Lee<sup>4</sup>; <sup>1</sup>Dongguk University; <sup>2</sup>Hanyang University; <sup>3</sup>Wuhan University; <sup>4</sup>Gyeongang National University

Undoped GaN epilayers were prepared by molecular beam epitaxy (MBE) and subsequently implanted with the Mn+ of 1 and 10 at%. P-type GaN epilayers were grown by metalorganic chemical vapor deposition (MOCVD) and subsequently implanted with the Mn+ of 5 and 10 at%. In relation to Mn-activation, it was confirmed that the photoluminescence peak at 2.5 eV in a donor-Mn acceptor transition (D-A pair) and the photoluminescence peak around 3.0 eV is a conduction band to Mn acceptor transition. The undoped and p-type GaMnN epilayers measured at 10 K with the Mn concentration of 10% showed clear ferromagnetic hysteresis loop with increasing annealing temperature and ferromagnetic behavior persisting up to 300 K. However, the magnetic properties of the p-type GaMnN were enhanced in comparison with those of the undoped GaMnN. And also, the p-type GaMnN epilayer with the Mn concentration of 5% showed weak and unstable ferromagnetic hysteresis loop.

**WP66, Thermal Stability, Morphological and Structural Properties of Metalorganic Vapor Phase Epitaxy Grown  $\text{AlInN}$  on  $\text{Si}(111)$ :** Aniko Gadanez<sup>1</sup>; Jürgen Bläsing<sup>1</sup>; Armin Dadgar<sup>1</sup>; Christoph Hums<sup>1</sup>; Thomas Hempel<sup>2</sup>; Jürgen Christen<sup>2</sup>; Alois Krost<sup>1</sup>; <sup>1</sup>Otto-von-Guericke Universität Magdeburg, FNW/IEP/AHE; <sup>2</sup>Otto-von-Guericke-Universität Magdeburg, FNW/IEP/AFP

$\text{AlInN}$  is an interesting compound for electronic and optoelectronic applications as high-current FETs and for unstrained Bragg mirrors lattice matched to GaN. We investigated  $\text{AlInN}$  layers on  $\text{GaN}/\text{Si}(111)$  with In concentrations between 9% < x < 36% and a maximal thickness of 100 nm grown by MOVPE. Subject to the In concentration the layers are fully pseudomorphic or exhibit both relaxed and pseudomorphic parts. The thermal stability of the layers with x < 22% was investigated between 30 and 960°C. It is considerably depending on the degree of relaxation: after different thermal treatment, the relaxed areas show decreasing quality, a well-pronounced phase separation and a loss of Indium. An additional effect under thermal treatment is an observably higher extension of relaxed regions with increasing lattice mismatch. By high-resolution X-ray diffraction and field emission scanning electron microscopy (FESEM) morphological characteristics in the alloy, as the values of twist and lattice constants, In-sublimation and relaxation were determined.

**WP67, Ultra-High Temperature Microwave Annealing of In-Situ Doped and Ion-Implanted GaN Layers Using Protective Ceramic Caps:** Siddarth Sundaresan<sup>1</sup>; Madhu Murthy<sup>1</sup>; Nadeemullah Mahadik<sup>1</sup>; Albert Davydov<sup>2</sup>; Elba Gomar-Nadal<sup>3</sup>; R. Vispute<sup>3</sup>; M. Mastro<sup>4</sup>; Charles Eddy<sup>4</sup>; R. Holm<sup>4</sup>; R. Henry<sup>4</sup>; Syed Qadri<sup>4</sup>; Yong-lai Tian<sup>5</sup>; Mulpuri Rao<sup>1</sup>; <sup>1</sup>George Mason University; <sup>2</sup>National Institute of Standards and Technology; <sup>3</sup>University of Maryland; <sup>4</sup>Naval Research Laboratory; <sup>5</sup>LT Technologies

Using a novel microwave RTA system capable of ultra-fast heating rates > 400°C/s, we were able to anneal Mg in-situ doped GaN at 1300–1500°C, when the GaN is protected by PLD AlN cap. The surface of the AlN capped GaN layer annealed at 1500°C for 5 s is very smooth (RMS roughness = 0.6 nm). An electron-beam deposited MgO cap successfully protected the GaN surface during microwave annealing only up to 1300°C, but significant GaN decomposition is observed for higher temperature anneals. PL and Hall measurements performed on the AlN capped samples indicate that the 1500°C / 5 s microwave annealing is more effective than 1300°C / 5 s microwave annealing in activating the Mg-dopants by decreasing the concentration of compensating deep donor levels. Detailed results on XRD, PL, and electrical characterization of in-situ and ion-implantation Mg-doped GaN will be presented.

## WP: Materials Issues

**WP68, Ozone and UV Assisted Oxidation of InN Surfaces:** Gernot Ecker<sup>1</sup>; Chunyu Wang<sup>1</sup>; Volker Cimalla<sup>1</sup>; Vadim Lebedev<sup>1</sup>; Oliver Ambacher<sup>1</sup>; <sup>1</sup>TU Ilmenau

High quality InN layers suffer from extremely high electron concentrations especially at surfaces and interfaces. Even if their electron mobility could be extremely high, this prevents the electron depletion and so the application of this outstanding material in field effect transistors. Surface treatments like oxidation assisted by UV irradiation under Ozone atmosphere results in a decrease of the surface electron concentration. This has been confirmed by resistance and Hall measurements. In order to investigate this mechanism and understand the band bending, laterally highly resolved Auger measurements have been carried out. As the result a correlation of the surface O content and the Auger peak shift to lower energies was found. The measurements show that the oxidation is laterally inhomogeneous and depends on the quality of the InN layer. This oxidation procedure helps to enable InN for FET device application.

**WP69, Structural and Optical Characterization of InN/InGaN Multiple Quantum Wells Grown by Plasma-Assisted MBE:** Javier Grandal<sup>1</sup>; Ana Bengoechea<sup>1</sup>; Miguel Sánchez-García<sup>1</sup>; Enrique Calleja<sup>1</sup>; Esperanza Luna<sup>2</sup>; Achim Trampert<sup>2</sup>; Snezana Lazic<sup>3</sup>; Eva Gallardo<sup>3</sup>; José Calleja<sup>3</sup>; <sup>1</sup>Instituto de Sistemas Optoelectrónicos y Microtecnología-Escuela Técnica Superior de Ingenieros de Telecomunicación-Universidad Politécnica de Madrid; <sup>2</sup>Paul Drude Institute; <sup>3</sup>Universidad Autónoma de Madrid

This work reports on the growth by PA-MBE and characterization of  $\text{InN}/\text{In}_{0.85}\text{Ga}_{0.15}\text{N}$  MQW. Samples were characterized by SEM, TEM, AFM, XRD, PL and Raman spectroscopy. Low temperature PL spectra of a 10 x  $\text{InN}/\text{In}_{0.85}\text{Ga}_{0.15}\text{N}$  MQW sample reveal an emission at 0.81 eV (1.53  $\mu\text{m}$ ) from the MQW together with an emission from the barriers modulated by Fabry-Perot oscillations. Satellite peaks up to the second order are observed at the XRD scans. XRD simulation estimates a well and barrier thicknesses of 2.4 nm and 9.1 nm, respectively. The crystal quality of the interfaces is analyzed by TEM. Raman spectroscopy will give information on the strain present in the overall structure. The growth of intermediate blocking layers to avoid the dissociation of the InN wells will be also carried out in order to perform a high temperature p-type doped GaN cap layer on top of the MQW.

## WP: Optical Characterization

**WP70, Biexciton Binding Energy of GaN Films Grown on Various Substrates:** Satoru Adachi<sup>1</sup>; Yasunori Toda<sup>1</sup>; <sup>1</sup>Hokkaido University

The optical investigation for a series of excitons such as neutral (or charged) excitons and multiexcitons has been a focus of constant attention in

semiconductors with various materials and structures. In particular, biexciton has been investigated systematically in the confined structures and Haynes rule is verified experimentally and theoretically. While the strain modifies the band structure and affects the binding energy, the influence has not been investigated so far in GaN. We report here the biexciton binding energy of GaN under biaxial and uniaxial strains investigated by spectrally-resolved four-wave mixing (FWM) technique, where wurtzite GaN with the different thickness grown on various substrates such as c-sapphire, a-sapphire, and 6H-SiC were used.

**WP71, Carrier Dynamics in Wide-Band-Gap AlGaIn/AlGaIn Quantum Wells:** *Gintautas Tamulaitis*<sup>1</sup>; Juras Mickevičius<sup>1</sup>; Edmundas Kuokstis<sup>1</sup>; Kai Liu<sup>2</sup>; Michael Shur<sup>2</sup>; Jianping Zhang<sup>3</sup>; Remis Gaska<sup>3</sup>; <sup>1</sup>Vilnius University; <sup>2</sup>Rensselaer Polytechnic Institute; <sup>3</sup>Sensor Electronic Technology, Inc.

We report on time-resolved photoluminescence (PL) spectroscopy and light-induced transient grating technique studies of carrier dynamics in wide-band-gap AlGaIn multiple quantum wells (MQWs). A set of Al<sub>0.35</sub>Ga<sub>0.65</sub>N/Al<sub>0.49</sub>Ga<sub>0.51</sub>N MQWs with fixed barrier width and well widths varying from 1.65 nm to 5.0 nm has been grown by metal-organic chemical vapor deposition. The radiative decay time, which affects the initial part of PL intensity decay after pulsed excitation, is influenced by screening of the built-in electric field, which spatially separates the electrons and holes. This fast PL decrease is more pronounced in wider quantum wells and at higher initial carrier density but saturates when the carrier density is high enough to completely screen the built-in electric field. The lifetime of nonequilibrium carriers (excitons), which is determined by nonradiative recombination, increases with decreasing the well width. The effect was interpreted by stronger localization preventing carrier migration to nonradiative recombination centers.

**WP72, Cathodoluminescence Nano-Characterization of a-Plane GaN ELOG Structures: Direct Imaging of Growth Domains, Morphological Defects, and Impurity Incorporation:** *Barbara Bastek*<sup>1</sup>; Frank Bertram<sup>1</sup>; Juergen Christen<sup>1</sup>; Tim Wernicke<sup>2</sup>; Markus Weyers<sup>2</sup>; Michael Kneissl<sup>3</sup>; <sup>1</sup>Otto-von-Guericke-University Magdeburg; <sup>2</sup>Ferdinand-Braun-Institut für Höchstfrequenztechnik, Berlin; <sup>3</sup>Ferdinand-Braun-Institut für Höchstfrequenztechnik, Berlin and Institute for Solid State Physics, Technical University Berlin

The distinctly different ELO growth regimes of a-plane GaN ELOG resulting from stripe mask orientation in [0001], [01-11], and [01-10], respectively, were directly imaged by highly spatially and spectrally resolved cathodoluminescence microscopy (CL). The characteristic basal plane stacking fault (BSF) emission at 3.41eV dominates the spatially integrated luminescence. In contrast, local spot mode CL evidences a completely different picture: striation like patterns of different CL wavelength strictly oriented in individual crystal directions and originating from either BSF, prismatic stacking fault (PSF), and/or impurity related DAP emission are clearly resolved. Preferential local impurity incorporation is evidenced. While [0001]-stripes result in symmetrical ELOG, for [01-10]-stripes almost no overgrowth in [000-1] but a strong lateral overgrowth in [0001] is found. Perfect, homogeneous and unstrained a-oriented, laterally c-direction grown GaN domains form, dominated by intense, sharp (D<sup>0</sup>,X) emission at 3.471eV (relaxed GaN). No BSF, PSF or other defect CL is found there!

**WP73, Comparative Raman Study of the Anharmonic Properties of GaN and ZnO:** *Jose Mendez*<sup>2</sup>; Lingyun Shi<sup>1</sup>; Christian Poweleit<sup>1</sup>; <sup>1</sup>Arizona State University

We report a comparative study of the temperature dependence of the frequency and linewidth of the Raman-active  $E_2$  modes in GaN and ZnO. The spectra were obtained with an ultra-high resolution Raman instrument capable of measuring linewidths as small as 0.05 cm<sup>-1</sup>. The high resolution of the spectra makes it possible to detect asymmetries not only in the ZnO spectra, as previously reported, but also in GaN. Another intriguing finding is that the temperature dependence of the high-energy  $E_2$  phonon frequency in ZnO is not monotonic: the mode frequency *increases* as a function of temperature at low temperatures, and it starts to decrease around 150 K. We use the similarity of the phonon dispersion curves in both materials to introduce a simple but realistic model of the Raman lineshape and frequency

that explains the above findings and provides a unified description of the anharmonic properties of GaN and ZnO.

**WP74, Effects of Grown-In Defects on Electron Spin Dynamics in Dilute Nitride Alloys:** X. Wang<sup>1</sup>; *Irina Buyanova*<sup>1</sup>; Weimin Chen<sup>1</sup>; Y. Hong<sup>2</sup>; Charles Tu<sup>2</sup>; <sup>1</sup>Linkoping University; <sup>2</sup>University of California

Adding to unusual electronic properties of novel dilute nitrides is strong electron spin polarization observed upon optical orientation in Ga(In)NAs, attributed to strong spin dependent recombination (SDR) facilitated by N incorporation. However, the origin of defects involved in SDR and whether it is inherent to all dilute nitrides remain unknown. This work tackle these important issues by correlating electron spin dynamics with defect properties of several dilute nitride materials, such Ga(In)NP and Ga(In)NAs alloys. Optical orientation measurements are used to evaluate presence of the SDR processes and to determine its efficiency, whereas the optically detected magnetic resonance technique is employed for chemical identification of responsible defects. Effects of defect types (e.g. As anitises vs Ga interstitials) and their concentrations are closely examined by varying conditions of the MBE growth (such as growth temperature, bombardment of impinging N ions, N content in the alloy, doping, etc.) and post-growth rapid thermal annealing.

**WP75, Enhancement of Free-Carrier Screening Due to Tunneling in Coupled Asymmetric GaN/Al<sub>0.5</sub>Ga<sub>0.5</sub>N/GaN Multiquantum Wells:** *Young Park*<sup>1</sup>; Chang Mo Park<sup>1</sup>; Bo-Ra Hwang<sup>1</sup>; Hyunsik Im<sup>1</sup>; Tae W. Kang<sup>1</sup>; Myung-Soo Han<sup>2</sup>; <sup>1</sup>Dongguk University; <sup>2</sup>Korea Photonics Technology Institute

Coupled multi-quantum well structures consisting of GaN(1 nm)/Al<sub>0.5</sub>Ga<sub>0.5</sub>N(2.2 nm)/GaN(2 nm) bounded by Al<sub>0.5</sub>Ga<sub>0.5</sub>N (10 nm) barriers were characterized by photoluminescence measurements. The recombination dynamics of carriers localized in asymmetric double quantum wells were studied by analyzing temperature-dependent and time-resolved photoluminescence spectra. We observed carrier transfer between weakly and strongly localized states which resulted in a stronger blue emission with increasing temperature and we analyzed its effects on the spectra in terms of the quantum confined screening effect. Time-resolved measurements yielded lifetimes of various transitions which had different origins ranging between ~120 ns and ~1300 ns.

**WP76, Excitonic Spin Relaxation Dynamics in GaN:** *Christelle Brimont*<sup>1</sup>; Mathieu Gallart<sup>1</sup>; Olivier Crégut<sup>1</sup>; Bernd Hönerlage<sup>1</sup>; Pierre Gilliot<sup>1</sup>; <sup>1</sup>Institute of Physics and Chemistry of Materials of Strasbourg-Group of Non-Linear Optics and Optoelectronics; University of Louis Pasteur-National Center of Scientific Research

Performing a non-degenerate pump-probe experiments, we study the relaxation dynamics of spin-polarized excitons in wurtzite epitaxial GaN. For negative time delays between pump and probe pulses, the time- and spectrally-resolved differential reflectivity (DR/R) displays a T<sub>2</sub> rise time with spectral oscillatory features in the vicinity of the excitonic resonances: These oscillations are caused by interference between the pump electric field and the probe induced polarization within the sample. For positive time delays, the analysis of DR/R of the two circular probe components allows us to extract, for each spin relaxation process, the characteristic time constants. The spin relaxation of the exciton as a whole is negligible in regard to the spin relaxation of the individual carriers. We determined T<sub>e</sub>=15 ps for the electron in the conduction band, T<sub>hh</sub>=5 ps, and T<sub>lh</sub>=1.5 ps for the heavy hole and for the light hole, respectively.

**WP77, Highly Sensitive Optical Probe for Uniaxial Strain in GaN Epitaxial Films:** *Yasunori Toda*<sup>1</sup>; Satoru Adachi<sup>1</sup>; Tetsuro Ishiguro<sup>1</sup>; Kazuyuki Tadamoto<sup>2</sup>; Katsuyuki Hoshino<sup>2</sup>; <sup>1</sup>Hokkaido University; <sup>2</sup>Yamaguchi University

We have previously demonstrated that spectrally-resolved four-wave mixing (SR-FWM) highlights the anisotropically polarized excitons in the uniaxially strained GaN films. In this work, we have applied this technique to the GaN films on isotropic substrates, and have examined the sensitivity of the technique. The measurements have been performed with the collinearly polarized two-pulse FWM in reflection geometry, in which the enhancement of sensitivity for exciton polarizations is achieved by nonlinear response of the

# Technical Program

oscillator strength. Several samples show the anti-correlated polarizations in each exciton, suggesting the existence of weak uniaxial strain. The minimum changes of the polarized FWM intensity and exchange energy splittings are found in the 2.3 $\mu$ m-thick GaN on 6H-SiC, and give a resolution of uniaxial strain of  $5.0 \times 10^{-5}$ , which is comparable with the resolution of conventional X-ray diffraction analysis.

**WP78, Internal Quantum Efficiency of Al<sub>x</sub>Ga<sub>1-x</sub>N (0<x<1) on AlN Template:** *Narihito Okada*<sup>1</sup>; Motoaki Iwaya<sup>1</sup>; Satoshi Kamiyama<sup>1</sup>; Hiroshi Amano<sup>1</sup>; Isamu Akasaki<sup>1</sup>; Hisaaki Maruyama<sup>2</sup>; Takashi Takagi<sup>2</sup>; Akira Bando<sup>3</sup>; Hideaki Murotani<sup>4</sup>; Yoichi Yamada<sup>4</sup>; <sup>1</sup>Meijo-University; <sup>2</sup>Ibiden Company, Ltd; <sup>3</sup>Showa Denko K.K.; <sup>4</sup>Yamaguchi University

High-performance UV light emitting devices are applicable in many fields including biomedical applications. To realize such novel applications, it is essential to grow high crystalline quality AlGa<sub>x</sub>N without cracks. When AlGa<sub>x</sub>N is grown on AlN, crack can be suppressed. In addition, AlN can be used as a window for the UV light because of its wide bandgap. Therefore, AlN template is ideal for the growth of AlGa<sub>x</sub>N. However, internal quantum efficiency (IQE) of AlGa<sub>x</sub>N on AlN template has not been reported so far. In this study, we performed MOVPE growth of thick AlGa<sub>x</sub>N with the whole compositional range on AlN templates. Then, the IQEs were evaluated by comparing photoluminescence peak intensity at 7K and room temperature.

**WP79, Intrinsic Electric Fields in Wide Band Gap AlGa<sub>x</sub>N Quantum Wells:** *Saulius Marcinkevicius*<sup>1</sup>; Andrea Pinos<sup>1</sup>; Kai Liu<sup>2</sup>; Dmitry Veksler<sup>2</sup>; Michael Shur<sup>2</sup>; Jianping Zhang<sup>3</sup>; Remis Gaska<sup>3</sup>; <sup>1</sup>Royal Institute of Technology; <sup>2</sup>Rensselaer Polytechnic Institute; <sup>3</sup>Sensor Electronic Technology, Inc.

Built-in electric fields are studied in Al<sub>x</sub>Ga<sub>1-x</sub>N/Al<sub>y</sub>Ga<sub>1-y</sub>N quantum wells (QWs) with different Al molar fractions and QW and barrier widths. The field magnitude is evaluated by comparing bias- and free carrier density-induced Stark shifts for QWs embedded into p-i-n structures. For lower Al content, the field is about 1 MV/cm, for Al<sub>0.35</sub>Ga<sub>0.65</sub>/Al<sub>0.5</sub>Ga<sub>0.5</sub>N QWs, the field is considerably smaller, ~0.3 MV/cm. Strong sublinear dependence of polarization on Al molar fraction is suggested as a possible reason for this observation. The Stark shift increases with increased QW and barrier width; the latter dependence agrees with the calculated distribution of the built-in field between the quantum well and barrier layers. After strong pulsed excitation, which leads to screening of the built-in fields, the field de-screening occurs with a characteristic time of 70 – 90 ps. The de-screening is faster in wider QWs because of a more efficient electron and hole separation.

**WP80, Luminescence Studies in Nitride Quaternary Alloys Double Quantum Wells:** S. C. P. Rodrigues<sup>1</sup>; *Luisa Scolfaro*<sup>2</sup>; M. N. d' Eurydice<sup>3</sup>; G. M. Sipahi<sup>3</sup>; E. F. da Silva Jr.<sup>4</sup>; <sup>1</sup>Universidade Federal Rural de Pernambuco, Departamento de Física; <sup>2</sup>University of Sao Paulo, Physics Institute; <sup>3</sup>Universidade de São Paulo, Instituto de Física de São Carlos; <sup>4</sup>Universidade Federal de Pernambuco, Departamento de Física

The quaternary AlGaInN alloy can reach shorter wavelength as compared with a single quantum well, which is important in optical communication devices, operating at wavelengths of 1.3 and 1.55  $\mu$ m, such as in optical fiber communication networks. In this work we study double quantum wells (DQWs) of nitride quaternary alloys in cubic phase. In this way it will be possible to obtain high optical gain without strain-induced piezoelectric and spontaneous polarizations effects. Quaternary derived p-doped systems are also investigated. Band structures and photoluminescence spectra calculations of Al<sub>x</sub>In<sub>y</sub>Ga<sub>1-x-y</sub>N/Al<sub>x</sub>In<sub>y</sub>Ga<sub>1-x-y</sub>N DQWs were performed by using the k $\cdot$ p theory and solving self-consistently the 8 x 8 Kane multiband effective mass/Poisson equations. We discuss the effects imposed by the Al and In molar fractions on the emission features of the systems. Our findings can be used as a guide for future experiments, helping on the design of optical communications devices.

**WP81, Micro-Raman Characterization of BGaN Growth on AlN Template Substrate:** *Sidi Ould Saad Hamady*<sup>1</sup>; Tewfik Baghdadli<sup>1</sup>; Simon Gautier<sup>1</sup>; Jérôme Martin<sup>1</sup>; Abdallah Ougazzaden<sup>2</sup>; <sup>1</sup>University Metz, Supélec; <sup>2</sup>Georgia Institute of Technology

We have investigated the Raman spectra of BGaN layers grown by MOVPE on AlN template. The boron content covered the composition range

from 0% (pure GaN) to 1.75%. The homogeneity of BGaN layers were studied by micro-Raman mapping and the phonon modes characteristics are determined as a function of boron content, according to the laser polarisation. These modes frequencies are shifted compared to that of pure GaN, and their intensities and linewidths depend on boron content. In particular the E2 and A1(LO) phonon modes shifts and linewidths strongly depend on boron composition. This behaviour is discussed according to the composition and strain effects and indicates a relaxation of the strain showing that the boron incorporation in GaN reduces the lattice mismatch with AlN substrate.

**WP82, MOVPE Growth and Investigation of AlInN/AlN Multiple Quantum Wells (MQW):** *Christof Mauder*<sup>1</sup>; Lars Rahimzadeh Khoshroo<sup>1</sup>; Vladimir I. Kozlovsky<sup>2</sup>; Gennadi P. Yablonskii<sup>3</sup>; Joachim Voitok<sup>4</sup>; Yilmaz Dikme<sup>5</sup>; Michael Heuken<sup>5</sup>; Holger Kalisch<sup>1</sup>; Rolf H. Jansen<sup>1</sup>; <sup>1</sup>RWTH Aachen University; <sup>2</sup>Lebedev Physical Institute of RAS; <sup>3</sup>National Academy of Sciences of Belarus; <sup>4</sup>PANalytical B.V.; <sup>5</sup>AIXTRON AG

We report about the growth and characterisation of thick Al<sub>0.83</sub>In<sub>0.17</sub>N layers and multi-quantum-well structures (MQW) containing 8 periods of Al<sub>0.83</sub>In<sub>0.17</sub>N/AlN quantum wells. All samples show good quality in HRXRD evaluation and were investigated by low-temperature cathodoluminescence (CL) and photoluminescence (PL) measurements. For thick Al<sub>0.83</sub>In<sub>0.17</sub>N layers, a distinct emission peak in CL at 339 nm wavelength is detected. This emission line is shifted to 326 nm for the MQW samples, which could possibly be ascribed to the quantization energy for electrons and holes. Similar results are obtained in optical investigations, where the thick layer emits at 337 nm and the superlattice structures exhibit a strong decline in transmitted intensity at approx. 320 nm. For both type of samples, a high fraction of defect-related emission is visible in the CL spectra, which saturates at higher excitation intensities. The further development of these structures with regard to highly efficient UV emitters is ongoing.

**WP83, Near-Field Optical Investigations of InGa<sub>x</sub>N Based LED with Aligned Micropit Structure:** *Ok Hwan Cha*<sup>1</sup>; Hyun Jeong<sup>1</sup>; Chang-Hee Hong<sup>1</sup>; Eun-Kyung Suh<sup>1</sup>; Mun Seok Jeong<sup>2</sup>; Hung-Seob Cheong<sup>3</sup>; <sup>1</sup>Chonbuk National University, Semiconductor Physics Research Center; <sup>2</sup>Gwangju Institute of Science and Technology, Advanced Photonics Research Institute; <sup>3</sup>LG Innotek

In this study, optical properties of InGa<sub>x</sub>N-blue-LEDs fabricated on aligned micropits grown on wet-etched patterned sapphire substrates (WPSSs) were investigated with UV near-field scanning optical microscopy (NSOM). The GaN template grown on WPSS consisted of well aligned hexagonal depressions (micropits) with small horizontal regions in between them. The WPSSs led not only for the reduction of TDs but also for the enhancement of light extraction efficiency of fabricated LEDs. The horizontal MQW regions consisted of thicker wells and barriers compared to the inclined MQWs of the hexagonal depressions. The horizontal MQW regions show bright emission in NSOM image at a relatively longer wavelength than the inclined MQWs. It indicates that the fabricated LEDs possess low (horizontal) and high (inclined) luminescence energy regions acted as potential-well and -barrier along the lateral direction. By this potential variation along the lateral direction, the excited carriers are well confined in the horizontal MQWs observed as bright regions in the NSOM-mapping.

**WP84, Nonpolar GaN Layers Grown by Sidewall Epitaxial Lateral Overgrowth: Optical Evidences for a Reduced Stacking Fault Density:** *Plamen Paskov*<sup>1</sup>; Bo Monemar<sup>1</sup>; Motoaki Iwaya<sup>2</sup>; Satoshi Kamiyama<sup>2</sup>; Hiroshi Amano<sup>2</sup>; Isamu Akasaki<sup>2</sup>; <sup>1</sup>Linköping University, Department of Physics, Chemistry and Biology; <sup>2</sup>Meijo University, Faculty of Science and Technology

Nonpolar a-plane and m-plane GaN layers grown by MOCVD employing sidewall-seeded epitaxial lateral overgrowth (SELO) were studied by photoluminescence (PL), polarization dependent PL and micro-PL. The SELO technique makes use of grooved GaN templates with SiO<sub>2</sub> masks deposited on the terraces. The effects of both the groove orientations and the groove/terrace width ratio on the emission spectra, particularly on the stacking fault (SF) related emission bands in the 3.29-3.42 eV region, were examined. The PL spectra of both types nonpolar layers reveal a significant reduction of the defect related emissions when the grooves are oriented perpendicular to

the c-axis of GaN and the groove/terrace width ratio is smaller than one. The suppression of SF formation in the areas where a lateral overgrowth along the [0001] direction occurs is confirmed by spatially resolved micro-PL showing no SF related emissions over the terrace regions.

## **WP85, Optical Transition Energy of Strained and Fully-Relaxed GaN Films:** *Seogwoo Lee*<sup>1</sup>; <sup>1</sup>Tohoku University

Most of GaN-based devices have been heteroepitaxially grown. Hence lattice strain is induced in GaN epilayers. The bandgap energy of a semiconductor changes with temperature and strain. Although the temperature dependence of optical transition energy (OTE) of a semiconductor has been well expressed by Varshni's equation, the effect of strain on this equation has not been evaluated. In order to evaluate the contribution of strain, we carried out detailed optical studies on a GaN layer grown on sapphire substrate with a CrN buffer layer. The GaN layer was partially detached from the sapphire substrate by selective chemical etching of the CrN buffer. Based on detailed micro photoluminescence and Raman scattering measurements on both etched and unetched parts of the GaN layer, we propose a new equation, which consists of temperature component and strain component. The impact of this new equation is that we can evaluate the OTE, once strain is evaluated.

## **WP86, Photoluminescence Decay Processes in AlGaIn Alloys:** *Kazutoshi Fukui*<sup>1</sup>; Naoto Nakagawa<sup>1</sup>; Tomohide Sakai<sup>1</sup>; Shun-ichi Naoe<sup>2</sup>; Hideto Miyake<sup>3</sup>; Kazumasa Hiramatsu<sup>3</sup>; <sup>1</sup>University of Fukui; <sup>2</sup>Kanazawa University; <sup>3</sup>Mie University

Ternary AlGaIn alloys are promising materials for ultraviolet (UV) optical devices. However, their low photoluminescence (PL) efficiency near band-edge excitonic PL at room temperature (RT) is one of the severe problems realizing UV emission devices. Then, it is important to study basic optical properties, such as PL decay processes. For InGaIn PL decay processes, the time resolved decay (TRD) curves can be fitted as the extended exponential decay curves, which indicate that strong indium inhomogeneity plays an important role. However, TRD curves of AlGaIn can not be fitted as extended exponential functions, and we have been reporting that three single exponential functions model is appropriate for PL decay processes of AlGaIn and InAlGaIn. In this report, we present PL and PL excitation (PLE) spectra of each decay component, and their temperature dependence to investigate decay mechanisms of AlGaIn alloys.

## **WP87, Picosecond Excitonic Spin Relaxation in Hexagonal GaN and Nanosecond Excitonic Spin Relaxation in Cubic GaN:** *Atsushi Tackuchi*<sup>1</sup>; Hirotaka Otake<sup>1</sup>; Taisuke Fujita<sup>1</sup>; Takako Chinone<sup>2</sup>; Ji-Hao Liang<sup>2</sup>; Masataka Kajikawa<sup>3</sup>; Fumiyoshi Takano<sup>3</sup>; Hiro Akinaga<sup>3</sup>; <sup>1</sup>Waseda University; <sup>2</sup>Stanley Electric Company, Ltd.; <sup>3</sup>Nanotechnology Research Institute, AIST

The excitonic spin relaxations in hexagonal GaN and cubic GaN are observed by spin-dependent pump and probe reflectance measurements with subpicosecond time resolution. The A-band free exciton in hexagonal GaN shows a sub-picosecond spin relaxation of 0.47 ps at 150 K. The acceptor-bound exciton in hexagonal GaN shows the spin relaxation times of 1.40 – 1.14 ps at 15-50 K. Meanwhile the spin relaxation times in cubic GaN at 15 – 75 K are found to be longer than 5 ns. Although these results present a striking contrast of the spin relaxation time, the long nanosecond spin relaxation time in cubic GaN is consistent with the dependence that spin relaxation time becomes longer for wider-band-gap zincblende semiconductors. The fast picosecond spin relaxations in hexagonal GaN might arise from the unique band structure.

## **WP88, Raman Scattering Analysis of GaN with Various Dislocation Densities:** *Toshio Kitamura*<sup>1</sup>; Shin-iti Nakashima<sup>1</sup>; Nayuha Nakamura<sup>2</sup>; Kei Furuta<sup>3</sup>; Hajime Okumura<sup>1</sup>; <sup>1</sup>National Institute of Advanced Industrial Science and Technology; <sup>2</sup>Nihon University; <sup>3</sup>R&D Association for Future Electron Devices International

In this paper, we characterized the GaN crystals with various dislocation densities by micro-Raman spectroscopy. Crystallinity for the GaN layer was examined through measurements of the Raman shift and the width of the  $E_2(\text{high})$ ,  $E_1(\text{TO})$ , and  $A_1(\text{TO})$  phonon bands. The Raman bands in GaN crystals broaden with increasing of dislocation density. The in-plane distribution of strain and crystallinity in epilayers with various dislocation

densities was also examined by Raman mapping measurement. The spatial fluctuation of phonon frequency and band width in samples was observed. The magnitude of fluctuation of Raman parameters became large with increase of dislocation density. The increase of dislocation density in GaN epilayers induces not only the broadening of Raman band but also increase of fluctuation.

## **WP89, Raman Scattering and Cathodoluminescence Characterization of Near Lattice-Matched In<sub>x</sub>Al<sub>1-x</sub>N Epilayers:** David Pastor<sup>1</sup>; Ramon Cusco<sup>1</sup>; Luis Artus<sup>1</sup>; Sergi Hernandez<sup>1</sup>; Oscar Martinez<sup>1</sup>; Juan Jimenez<sup>1</sup>; Robert Martin<sup>1</sup>; Kevin O'Donnell<sup>1</sup>; Ian Watson<sup>1</sup>; <sup>1</sup>Institute Jaume Almera (C.S.I.C.)

Although the InAlN alloy has great potential as efficient barrier in GaN-based devices, data on its optical properties are scarce owing to the difficulty of growing high-quality material. We present cathodoluminescence (CL) and Raman scattering measurements on a set of near lattice-matched InAlN epilayers grown by MOCVD on GaN/sapphire substrates. The Raman spectra show the  $A_1(\text{LO})$  and InN-like  $E_2$  modes of the alloy, whose frequencies are in good agreement with existing model calculations. No noticeable frequency shift of the  $E_2$  modes are observed for the In compositions studied, which suggests pseudomorphological growth of the thin films. The CL spectra exhibit a luminescence peak above the GaN band-edge emission that shifts to lower energies for increasing InN fraction is observed. For the lattice-matched composition, the peak emission is estimated to be about 3.7 eV.

## **WP90, Raman Scattering Study of B<sub>x</sub>Ga<sub>1-x</sub>N Epilayers Grown by MOVPE on GaN Substrates:** Esther Alarcon-Llado<sup>1</sup>; Ramon Cusco<sup>1</sup>; Jordi Ibanez<sup>1</sup>; Luis Artus<sup>1</sup>; Abdallah Ougazzaden<sup>2</sup>; Simon Gautier<sup>3</sup>; <sup>1</sup>Institute Jaume Almera (C.S.I.C.); <sup>2</sup>Georgia Institute of Technology; <sup>3</sup>University of Metz and SUPELEC, Laboratory Materiaux Optiques, Photonique et Systemes

The demand for ultraviolet laser devices with shorter wavelengths has prompted the investigation of alloying in the group-III nitrides to obtain materials with larger band gaps than that of the GaN. B<sub>x</sub>Ga<sub>1-x</sub>N is a potential candidate which can be lattice-matched to SiC and AlN if a sufficient amount of boron can be achieved. However, the high lattice mismatch between BN and GaN makes it difficult to obtain B<sub>x</sub>Ga<sub>1-x</sub>N with an appreciable B concentration. We present a study of a set of B<sub>x</sub>Ga<sub>1-x</sub>N thin films grown by MOPVCD with B concentration between 1.1 and 3.6%. B incorporation was checked by SIMS measurements. XRD measurements reveal an additional peak that shifts with B composition attributed to the alloy. UV Raman scattering measurements show that the  $A_1(\text{LO})$  frequency increases with increasing B composition. Strain relaxation occurs in thick samples leading to a blueshift of the  $A_1(\text{LO})$  mode.

## **WP91, Recombination Dynamics of Localized Excitons in AlGaIn-Based Quantum Wells:** *Hideaki Murotani*<sup>1</sup>; Takuya Saito<sup>1</sup>; Nobuo Kato<sup>1</sup>; Yoichi Yamada<sup>1</sup>; Tsunemasa Taguchi<sup>1</sup>; <sup>1</sup>Yamaguchi University

We have studied the effect of internal electric field on exciton localization in AlGaIn-based quantum wells (QWs) by means of time-resolved photoluminescence (PL) spectroscopy. We analyzed the observed time-dependent PL using rate equations and obtained the PL lifetime and the localization time of excitons for three QWs with different well-layer thickness. The localization time became longer with increasing well-layer thickness. This result indicates that a quantum confined Stark effect causes the reduction in transition probability of excitons from extended to localized states. In addition, the localization time decreased with increasing excitation density and the three QWs indicated almost the same localization time at higher excitation density. Since the alloy composition is the same for the three QWs, the degree of localization due to alloy disorder does not change so much. Then, we consider that the screening of the internal electric field results in the same localization time.

## **WP92, Remarkable Enhancement of 254-280 nm Deep UV Emission from AlGaIn Quantum Wells by Using High-Quality AlN Buffer on Sapphire:** *Toru Yatabe*<sup>1</sup>; Hideki Hirayama<sup>1</sup>; Tomoaki Ohashi<sup>1</sup>; Norihiko Kamata<sup>2</sup>; <sup>1</sup>RIKEN; <sup>2</sup>Saitama University

We observed remarkable enhancement of 254-280 nm deep UV emission from AlGaIn multi quantum wells (MQWs) by using low threading dislocation density (TDD) AlN templates fabricated on sapphire substrates.

# Technical Program

High-quality AlN templates were fabricated by using ammonia pulse-flow multi-layer growth method by metal-organic chemical vapor deposition (MOCVD). The screw dislocation density of AlGaN layer on AlN template were  $3.5 \times 10^8 \text{ cm}^{-2}$ . The photoluminescence (PL) intensity of 278 nm AlGaN-QW emission was increased by approximately 30 times by reducing the full width at half-maximum (FWHM) of X-ray diffraction (XRD) (102)  $\omega$ -scan rocking curve of AlGaN buffer from 1214 to 488 arcsec. The internal quantum efficiency (IQE) of the AlGaN-QW was as high as 30% from the temperature dependence of PL intensity. We also observed the PL intensity enhancement with the reduction of the XRD FWHM for QWs with peak emission wavelength of 254, 260, 270 and 280 nm.

**WP93, Scanning Near-Field Optical Microscopy of AlGaN-Based Quantum Wells:** *Hideaki Murotani*<sup>1</sup>; Nobuo Kato<sup>1</sup>; Takuya Saito<sup>1</sup>; Yoichi Yamada<sup>1</sup>; Tsunemasa Taguchi<sup>1</sup>; <sup>1</sup>Yamaguchi University

We have studied the influence of both localization and internal electric field on the microscopic photoluminescence (PL) properties of AlGaN-based quantum wells (QWs) by means of scanning near-field optical microscopy (SNOM). We measured SNOM-PL images of three QWs with different well-layer thickness under an illumination-collection (I-C) mode and observed the correlation between the PL intensity and the PL peak wavelength. The shorter-wavelength PL indicated the stronger intensity for the wider QW. We consider that the correlation is caused by the inhomogeneous screening of the internal electric field. Under the I-C mode, the screening and the resultant PL blue shift are large at localization centers (local potential minima) as compared with those at local potential maxima. Therefore, we conclude that the correlation becomes prominent when the screening of the internal electric field (blue shift) is larger than the potential fluctuation due to alloy disorder (Stokes shift).

**WP94, Strain and Defects in AlN Grown with High-Temperature MOVPE:** *Max Buegler*<sup>1</sup>; Ute Haboeck<sup>1</sup>; Ronny Kirste<sup>1</sup>; Christian Thomsen<sup>1</sup>; Frank Brunner<sup>2</sup>; Arne Knauer<sup>2</sup>; Markus Weyers<sup>2</sup>; Michael Kneissl<sup>1</sup>; Axel Hoffmann<sup>1</sup>; <sup>1</sup>TU-Berlin, Institute for Solid State Physics; <sup>2</sup>Ferdinand-Braun-Institut für Höchstfrequenztechnik

The growth of high quality AlN layers is an essential precondition for deep-UV emitters. To achieve this AlN-epilayers were investigated by means of photoluminescence (PL) and Raman spectroscopy. The samples were grown on sapphire substrates by metalorganic vapor phase epitaxy at temperatures between 1200°C and 1500°C. We observed an emission line near the bandedge at 5.95eV which can be attributed to a donor-bound exciton. Its emission energy depends on the growth temperature. Additionally, Raman spectroscopy shows a significant shift of the strain-sensitive E2(high) mode. Due to the fact that the emission of the bound exciton shows the same behavior as the E2(high), we attribute the shift of the emission to the strain state of the sample. Furthermore, we investigated deep defects in the AlN-epilayers which can also be observed in PL spectra at 3.8eV.

**WP95, The 3.3eV Band in GaN: Correlation with Defects by CL and TEM Studies:** *Martin Schirra*<sup>1</sup>; *Martin Feneberg*<sup>1</sup>; Günther Prinz<sup>2</sup>; Rolf Sauer<sup>1</sup>; Klaus Thonke<sup>1</sup>; Thomas Wunderer<sup>2</sup>; Peter Brückner<sup>2</sup>; Ferdinand Scholz<sup>2</sup>; Andrey Chuvilin<sup>3</sup>; Ute Kaiser<sup>3</sup>; Isabel Knoke<sup>4</sup>; Elke Meissner<sup>1</sup>; <sup>1</sup>Universität Ulm, Institut für Halbleiterphysik; <sup>2</sup>Universität Ulm, Institut für Optoelektronik; <sup>3</sup>Universität Ulm, Materialwissenschaftliche Elektronenmikroskopie; <sup>4</sup>Fraunhofer Institut IISB, Erlangen

Non- and semipolar GaN samples frequently exhibit emission bands at 3.3 eV and around 3.41 eV which are believed to be defect-related. We performed a systematic cathodoluminescence (CL) and transmission electron microscopy (TEM) study on selectively overgrown GaN stripes with semipolar {1-101} side facets. Under unfavorable growth conditions these also show intense defect-related bands. Spatially resolved CL spectra allow to assign distinct bands to different regions of the triangularly shaped GaN stripes. Monochromatic CL images reveal, that the 3.3 eV and the 3.41 eV emission originate from the lower part of the triangles, while the band gap related emission is found on top of the triangles. Defects are identified by TEM images and their influence on the luminescence spectra and maps is discussed in detail.

**WP96, The CL Emission Observation of the InGaN/GaN MQWs V Shaped Pits with Different Superlattices Underlayers:** *Wei-Chih Lai*<sup>1</sup>; Yu-Shing Huang<sup>1</sup>; Wei-Yu Yen<sup>1</sup>; Jinn-Kong Sheu<sup>1</sup>; Cheng-Huang Kuo<sup>2</sup>; Tao Hung Hsueh<sup>3</sup>; Shouu-Jinn Chang<sup>4</sup>; <sup>1</sup>National Cheng Kung University, Institute of Electro-Optical Science and Engineering; <sup>2</sup>National Central University, Department of Optics and Photonics; <sup>3</sup>National Cheng Kung University, Center of Micro/Nano Science and Technology; <sup>4</sup>National Cheng Kung University, Institute of Microelectronics

Bulk GaN films are known to contain a high density of defects threading dislocations. These threading dislocations caused formation of V shaped pits on the InGaN/GaN MQWs. In this study we prepared three InGaN/GaN MQWs with different SLs under layers to create different the V-shaped pits. The InGaN/GaN MQWs had got wider diameter V shaped pits and rougher surface if we introduce the SLs under layers. The V shaped pits diameter of sample with SLs under layers is around twice larger than sample without SLs under layers. The grain like emission was seen on the CL spatial images. The samples with SLs under layers showed CL intensity inhomogeneous on the CL spatial images. Moreover we found the light escaped from V shaped pits of InGaN/GaN MQWs with AlGaN/GaN SLs under layers. That might be the key issue to get better efficiency of the light emitting devices.

**WP97, Thermal Quenching of Luminescence and Isovalent Traps Model for Rare Earth Ions Doped AlN:** *Wojciech Jadwisiewicz*<sup>1</sup>; Henryk Lozykowski<sup>1</sup>; <sup>1</sup>Ohio University

Investigations of luminescent properties of rare earth implanted AlN thin films at temperature in the range 9-800 K are reported. The temperature studies of photoluminescence and cathodoluminescence spectra revealed unexpectedly weak thermal quenching of visible luminescence in Pr, Eu, Gd, Tb, Dy, Tm and Yb-doped AlN samples. Photoluminescence excitation spectra, obtained under UV excitation in the spectral range 200-400 nm, exhibit several bands. It is proposed that the RE ions exist in semiconductors as isolated ions (singlet), nearest neighbors (nn) ion pairs (dimer), and three ions (trimer). The Koster-Slater and simple spherical potential-well models for RE structured isovalent (RESI) hole trap are proposed. The exciton binding energies of RESI traps are calculated and compared with experimental thermal quenching energies. The energy transfer processes between AlN host and 4f-shell systems are emphasized as the main mechanisms for thermal quenching processes rather than nonradiative decay of 4f transitions.

**WP98, Time-Resolved Photoluminescence Studies of InGaN/GaN Quantum Wells on GaN Homo Substrates:** *Yue-Dae Han*<sup>1</sup>; J. G. Park<sup>1</sup>; D. Lee<sup>1</sup>; C. C. Kim<sup>2</sup>; C. S. Kim<sup>2</sup>; Y. H. Choi<sup>2</sup>; M. S. Noh<sup>2</sup>; <sup>1</sup>Chungnam National University; <sup>2</sup>LG Electronics Institute of Technology

Optical properties have been investigated from InGaN/GaN quantum wells (QWs) grown on GaN homo substrates. InGaN QWs are known to have a strong piezoelectric field across wells in addition to strong carrier localization in the well. However, it is difficult to separate these contributions, which is important to understand the mechanism and optimize QW structures for device applications. In order to determine the degree of localization and piezoelectric field in QWs, time-resolved photoluminescence (PL) using a streak camera or time-correlated single photon counting system with a femtosecond laser has been measured in conjunction with excitation power dependence and temperature dependence of PL spectrum. We have found that the carrier lifetime at low temperature, which gives information on the wavelength overlap between electron and hole, is very sensitive to the variation of growth condition and structural change. The results are analyzed together with continuous wave PL and room temperature time-resolved PL.

**WP99, V-Pits' Morphologies and the Related Optical Properties of InGaN/GaN Multiple Quantum Wells:** *Fen Lin*<sup>1</sup>; Ning Xiang<sup>1</sup>; Peng Chen<sup>2</sup>; Shue Yin Chow<sup>2</sup>; Soo Jin Chua<sup>1</sup>; <sup>1</sup>National University of Singapore; <sup>2</sup>Institute of Materials Research and Engineering

The V-pits' morphologies and the related optical properties of InGaN/GaN multiple quantum wells (MQWs) were studied by scanning electron microscopy (SEM), transmission electron microscopy (TEM), and photoluminescence (PL). The InGaN/GaN MQWs with high-density large V-pits were grown by metal organic chemical vapor deposition. It is found that the morphology of the V-pits affects the MQWs' morphology as well as

# Technical Program

the recombination mechanism. Three types of MQWs with different facet morphologies were studied, which contribute to three different PL emission bands: 1) the normal c-plane MQWs; 2) the MQWs grown on {10-11} faceted sidewalls, which contribute to a PL band with much higher energy than the c-plane MQW emission band; and 3) the MQWs grown on the {11-2m} ( $m \geq 2$ ) faceted sidewalls, which give a PL band with the energy in between the above two bands.

**WP100, Very Strong Nonlinear Optical Absorption in Green GaInN/GaN Multiple Quantum Well Structures:** *Wei Zhao*<sup>1</sup>; Mingwei Zhu<sup>1</sup>; Yong Xia<sup>1</sup>; Yufeng Li<sup>1</sup>; Jayantha Senawiratne<sup>1</sup>; Shi You<sup>1</sup>; Theeradetch Detchprohm<sup>1</sup>; Christian Wetzel<sup>1</sup>; <sup>1</sup>Rensselaer Polytechnic Institute

The efficiency of green GaInN/GaN light emitting diodes (LEDs) is known to drop under high current densities. To explore the reason, 535 nm emitting GaInN/GaN multiple quantum well (MQW) and GaN epilayers were characterized using z-scan techniques under comparable excitation conditions with a continuous wave laser. Two wavelengths, 514 nm and 488 nm, were selected right below and above the apparent optical absorption edge. At 514 nm, a very large nonlinear absorption coefficient  $\beta = 2.6 \text{ cm}^2/\text{W}$  was obtained. This leads to a 20% absorption at a photon flux of  $21 \text{ kW}/\text{cm}^2$ . We attribute this to nonlinear free-carrier absorption. On the other hand, at 488 nm, a nonlinear saturable absorption with  $\beta = -1.7 \text{ cm}^2/\text{W}$  was observed. This induced transparency indicates photon bleaching in the MQW. Apparently free carrier dynamics strongly affects optical nonlinearity, while nonlinear absorption provides only a small contribution to the limitations of current green LEDs.

## WP: Optical Characterization of Nonpolar and Semipolar Materials

**WP101, Anisotropic Optical Matrix Elements in Strained GaN-Quantum Wells with Various Substrate Orientations:** *Atsushi Yamaguchi*<sup>1</sup>; <sup>1</sup>Kanazawa Institute of Technology

In-plane optical anisotropies in compressively strained III-nitride quantum wells on semi-polar and non-polar substrates were calculated by using  $6 \times 6$   $k,p$  Hamiltonian. It is shown that the quantum confinement and compressive strain have the opposite effects on the anisotropy. For example, the compressive strain enhances the transition for light polarized to the c-axis in quantum wells on non-polar substrates, while the quantum confinement effect enhances the transition for light polarized to the perpendicular direction. Thus, the in-plane polarization degree is determined by the competition of these two effects. These characteristics are also verified by analytical calculations, and it is found that the signs of  $(A_x - A_y)$  and  $(D_x - D_y)$  are essential factors to determine the above-mentioned polarization properties, where  $A_x$  and  $A_y$  are valence band parameters and  $D_x$  and  $D_y$  are deformation potentials. Based on the calculated results, the structural design of laser diodes on semi-polar and non-polar substrates is also discussed.

**WP102, Energy Relaxation Processes of Photo-Generated Carriers in Mg Doped (0001)GaN and (1-101)GaN:** *Nobuhiko Sawaki*<sup>1</sup>; Jun Saida<sup>1</sup>; Eun Hee Kim<sup>1</sup>; Toshiki Hikosaka<sup>1</sup>; Yoshio Honda<sup>1</sup>; Masahito Yamaguchi<sup>1</sup>; <sup>1</sup>Nagoya University

The pico-second energy relaxation of photo-generated excess carriers in Mg doped (0001)GaN and (1-101)GaN is studied at room temperature. The samples were grown by MOVPE on a patterned Si substrate. The PL intensity correlation curves showed double exponential decay in high energies, from which we determined fast and slow decay time constants. The slow process on the order of 80-200ps was energy insensitive. At low energies, we found anti-correlation behavior, which suggests that the accumulation of carriers in the localized centers occurs as the result of the relaxation from high energy states. The fast decay process was observed over a wide energy range and the time constant around 10ps depended on the energy. The fast process was attributed to the potential fluctuation near the valence band edge in the Mg doped GaN.

**WP103, Growth and Optical Properties of a-Plane AlN and Al Rich AlN/Al<sub>1-x</sub>Ga<sub>x</sub>N Quantum Wells Grown on r-Plane Sapphire Substrate:** *Talal Al Tahtamouni*<sup>1</sup>; Ashok Sedhain<sup>1</sup>; Jingyu Lin<sup>1</sup>; Hongxing Jiang<sup>1</sup>; <sup>1</sup>Kansas State University

Deep ultraviolet (UV) emitters and detectors operating in the 200–340 nm wavelength range have many important applications, including water purification, biological/chemical agent detection and medical care. To realize deep UV emission ( $\lambda < 280 \text{ nm}$ ), Al-rich AlGaN based QWs are required. The growth of QW structures along the polar direction is characterized by the presence of polarization induced electrostatic fields, which limit the performance of optoelectronic devices that employ QWs as active regions. Growth along nonpolar directions produces nitride-based quantum structures that are unaffected by the strong electrostatic fields. We report on the growth of a-plane AlN epilayer templates and AlN/Al<sub>0.65</sub>Ga<sub>0.35</sub>N QWs on r-plane sapphire substrate by MOCVD. Deep UV photoluminescence was employed to study the optical properties of the AlN templates and QWs. A range of well widths for a- and c-plane QWs was investigated, which allows us to identify the emission characteristics that are unique to nonpolar orientations.

**WP104, High Quantum Efficiency of Semipolar GaInN/GaN Quantum Wells:** *Martin Feneberg*<sup>1</sup>; Frank Lipski<sup>1</sup>; Martin Schirra<sup>1</sup>; Rolf Sauer<sup>1</sup>; Klaus Thonke<sup>1</sup>; Thomas Wunderer<sup>2</sup>; Peter Brückner<sup>2</sup>; Ferdinand Scholz<sup>2</sup>; <sup>1</sup>Institut für Halbleiterphysik, Universität Ulm; <sup>2</sup>Institut für Optoelektronik, Universität Ulm

The development of efficient GaInN/GaN based light emitting devices is hampered by built-in electric fields. These fields, arising from piezoelectric and spontaneous polarization, separate electron and hole wavefunctions and reduce their spatial overlap. Therefore, the internal quantum efficiency is drastically reduced in the presence of built-in fields. To decrease the detrimental influence of the polarization fields on quantum efficiency, growth on non- or semipolar crystal facets is conducted. We investigate samples containing quantum wells grown on the {1-101} facet of selectively overgrown GaN stripes and compare them to samples grown on the commonly used c plane. By field-dependent photoluminescence we experimentally determined direction and strength of built-in polarization fields. A much weaker field inside the tilted semipolar quantum wells is found (-0.1 MV/cm) compared to structures grown on the polar c-plane (-1.9 MV/cm).

**WP105, Internal Quantum Efficiency (IQE) and Optical Polarization Analysis of InGaN/GaN Multiple Quantum Wells on a-Plane GaN:** *Eu-Ying Lin*<sup>1</sup>; C. Y. Chen<sup>1</sup>; *Tsong-Sheng Lay*<sup>1</sup>; T. C. Wang<sup>2</sup>; J. D. Tsay<sup>2</sup>; <sup>1</sup>National Sun Yat-Sen University; <sup>2</sup>ITRI

Internal Quantum Efficiency (IQE) and polarized light emission of non-polar InGaN/GaN MQW grown on a-plane (1120) GaN film were investigated in comparison with polar c-plane (0001) InGaN/GaN LED samples. In the temperature dependence and power dependence PL spectra, the IQE for a-plane and c-plane InGaN/GaN multiple quantum wells were carried out without the time-resolved PL experiment. The a-plane and c-plane InGaN/GaN MQW polarized phenomenon in normal-emitting and edge-emitting PL measurements were also observed and analyzed. The anisotropic structure of quantum wire in a-plane MQW was clearly observed in edge-emitting PL spectrum and TEM.

**WP106, Optical Properties in Nonpolar a-Plane Strained GaN by Native Gallium Oxide Layer Grown by Photo-Electrochemical Method:** *Han-Min Wu*<sup>1</sup>; Chih-Ming Lai<sup>2</sup>; Lung-Han Peng<sup>1</sup>; *Sung-Li Wang*<sup>1</sup>; <sup>1</sup>National Taiwan University; <sup>2</sup>Ming Chuan University

We report the observation of enhanced green emission centered at 500nm, accompanied with spectral blue shift of 4nm in the UV (360nm) bandedge emission upon a-plane GaN passivated with photo-enhanced wet chemical oxide. The a-plane GaN was grown on the r-plane of sapphire substrate by MOCVD. The polarized micro-PL study was carried out by a pulsed 266nm Nd:YAG laser. The temperature dependent luminescence data reveal an evolution of gain competition between the green and the UV emission bands and at 50K the green emission intensity is larger than that of the UV band by 50%. By dissolving the oxide we resume the emission spectrum of the grown a-GaN. These observations are ascribed to a compressively-strained a-GaN thin surface layer due to the coherently grown gallium hydroxide

# Technical Program

GaOOH atop that is responsible for the spectral blue shift and the generation of acceptor like deep-levels that result in the enhanced green emission.

**WP107, Optical Properties of GaN/AlGaIn Quantum Wells Grown by Molecular Beam Epitaxy on a-Plane GaN ELO Templates:** *Amélie Dussaigne*<sup>1</sup>; Claire Pinquier<sup>1</sup>; Tiankai Zhu<sup>1</sup>; Denis Martin<sup>1</sup>; Nicolas Grandjean<sup>1</sup>; <sup>1</sup>Ecole Polytechnique Fédérale de Lausanne

Non-polar GaN is of great interest due to the possibility of elaborating III-nitride heterostructures without internal electric field. This would allow improving the efficiency of light emitting diodes and lasers. In this work, optical properties of GaN/AlGaIn quantum wells (QWs) grown by molecular beam epitaxy (MBE) on a-plane GaN templates are presented. These templates are grown by hydride vapor phase epitaxy using epitaxial lateral overgrowth technique in order to reduce the defect density. GaN/AlGaIn single QWs are realized by MBE using ammonia as nitrogen source with various parameters: Al composition (5-20%) and well width (2-8 nm). Micro-photoluminescence (PL) and macro-PL measurements have been performed. Typical full width at half maximum of 30 meV demonstrates high optical quality. The absence of internal electric field is confirmed. Sharp transition energies on the PL peak of the 2 nm-low Al content QW are ascribed to exciton localization. Their origin will be discussed.

**WP108, Optical Properties of High Quality MOVPE Grown Non-Polar a-Plane GaN Epilayers:** *Alexander Franke*<sup>1</sup>; Barbara Bastek<sup>1</sup>; Martin Noltemeyer<sup>1</sup>; Frank Bertram<sup>1</sup>; Juergen Christen<sup>1</sup>; Matthias Wieneke<sup>1</sup>; Armin Dadgar<sup>1</sup>; Alois Krost<sup>1</sup>; Ronny Kirste<sup>2</sup>; Ute Harboeck<sup>2</sup>; Axel Hoffmann<sup>2</sup>; <sup>1</sup>Otto-von-Guericke-University Magdeburg, Institute of Experimental Physics; <sup>2</sup>Technical University Berlin, Institute of Solid State Physics

High quality MOVPE grown (11-20) a-plane GaN layers are characterized using photoluminescence (PL) and cathodoluminescence (CL) spectroscopy. The 4K PL spectra show (D<sup>0</sup>, X) emission lines at 3.495 eV as well as (A<sup>0</sup>, X) transitions at 3.482 eV, respectively. Their spectral position corresponds to a compressive stress of 0.9 GPa in quantitative agreement with 0.6 GPa obtained by Raman spectroscopy. The dominating defect emission at 3.42 eV is attributed to basal plane stacking faults (BSF). The s-shape temperature dependence of its peak energy reveals a localization energy of 25 meV. BSF CL-mappings of both, intensity and peak wavelength exhibit a striation contrast with stripes exactly oriented along the (1,-1,0,0) direction as quantified in the 2D-spectral density function of the maps. In contrast, the PSF CL-images result in a spotty pattern showing no preferential orientation. CL linescans across adjacent columns shows an alternation of the BSF energy up to 9.94 meV.

**WP109, Optically Induced Strain Relaxation in Anisotropically Strained M-Plane GaN Films:** Timur Flissikowski<sup>1</sup>; Oliver Brandt<sup>1</sup>; Pranob Misra<sup>1</sup>; *Holger Grahn*<sup>1</sup>; <sup>1</sup>Paul-Drude-Institute

Strained M-plane GaN films, where the c-axis (z-direction) lies in the film plane, can exhibit a very large in-plane polarization anisotropy. For a certain range of in-plane strain values, the wave function of the highest and the second highest valence band (VB) becomes completely  $|x\rangle$ -like and  $|z\rangle$ -like, respectively. This wavefunction symmetry can be directly observed in transmission measurements by an energy gap, which depends on the in-plane polarization directions. We demonstrate that strong optical pumping results in a permanent change of the transmission of the film. However, the change is only present for one polarization direction. By spatially resolved Raman spectroscopy, and by measuring the transition energies from the two uppermost VBs by spatially resolved photo-reflectance spectroscopy, we investigated the local strain in the film. Finally, we found that the tightly focused laser induces a relaxation of the strained film which effects only the direction perpendicular to the c-axis.

**WP110, Polarization- and Temperature Dependent Photoluminescence and Reflectivity Study of Nonpolar (11-20) GaN:** *Tobias Guehne*<sup>1</sup>; Zahia Bougrioua<sup>1</sup>; Sophie Laügt<sup>1</sup>; Mathieu Leroux<sup>1</sup>; <sup>1</sup>Centre de Recherche sur l'Hétéroépitaxie et ses Applications-CNRS

By use of R (1-102) oriented sapphire substrates, GaN can be grown along the nonpolar [11-20] direction. In these cases, the polar c-axis is not along the growth direction. As a result, QCSE in quantum heterostructures, caused

by internal fields originating from interfacial charges, can be annihilated when they are grown on (11-20) GaN templates. We investigate in this work the optical properties of laterally overgrown nonpolar GaN on partially masked (11-20) GaN templates grown by metalorganic vapor phase epitaxy. In conjunction with internal strain components deduced from HRXRD measurements, the transition energies and the oscillator strength of the free excitons are calculated in order to compare them with the experimentally obtained values.

**WP111, Stimulated Emission from Nonpolar and Polar AlN:** *Narihito Okada*<sup>1</sup>; Kentaro Nagamatsu<sup>1</sup>; Motoaki Iwaya<sup>1</sup>; Satoshi Kamiyama<sup>1</sup>; Hiroshi Amano<sup>1</sup>; Isamu Akasaki<sup>1</sup>; Hisaaki Maruyama<sup>2</sup>; Takashi Takagi<sup>2</sup>; Akira Bando<sup>3</sup>; Hideaki Murotani<sup>4</sup>; Yoichi Yamada<sup>1</sup>; <sup>1</sup>Meijo-University; <sup>2</sup>Ibiden Company, Ltd; <sup>3</sup>Showa Denko K.K.; <sup>4</sup>Yamaguchi University

Nonpolar AlN is attracted much attention to realize high-performance UV light emitting devices due to elimination of the internal electric field induced by piezoelectricity in the quantum well. However, experimental evaluation of the advantage of nonpolar plane had been still hindered because of the presence of high-density dislocations and stacking faults in nonpolar AlN layer. We have succeeded to achieve high-quality polar and nonpolar epitaxial lateral overgrown (ELO) AlN layers by high-temperature metal-organic vapor phase epitaxy (HT-MOVPE). In this letter, we report stimulated emission from nonpolar and polar AlN by optical excitation. Then, stimulated emission from nonpolar AlN was confirmed and a threshold excitation power density of nonpolar AlN is almost the same as that of polar AlN both at 8K and 100K.

**WP112, The Internal Quantum Efficiency Behavior of a-Plane and c-Plane InGaN/GaN MQWs with Different Indium Compositions:** *Te-Chung Wang*<sup>1</sup>; Tsung-Shine Ko<sup>1</sup>; Run-Ci Gao<sup>1</sup>; Tien-Chang Lu<sup>1</sup>; Hao-Chung Kuo<sup>1</sup>; Sing-Chung Wang<sup>1</sup>; Jenq-Dar Tsay<sup>2</sup>; <sup>1</sup>National Chiao Tung University; <sup>2</sup>Industrial Technology Research Institute

Despite many reports about the advantages of non-polar plane had published, it's still not clear about the IQE behavior for different indium composition/wavelength. According to the theoretical calculation, without the influence of polar effect, the spontaneous polarization field and piezoelectric field both could be eliminated. And there is highly potential to realize high bright light emitting device at blue/green wavelength. For sure the phenomenon, we prepared four groups of samples consist of a-plane and c-plane MQWs with the same geometric MQW structure and with different indium compositions to analysis the IQE behavior. And we find the localized state might enhance the performance of a-plane MQW although the TDD is quite high. This result reveals the potential of a-plane InGaIn MQW to high bright blue/green LED. On the other hand, the indium phase separation might also occur on a-plane InGaIn MQW so that the intensity decrease and spectrum bandwidth broaden.

## Session BB: InN Growth

Thursday AM Room: 312/317  
September 20, 2007 Location: MGM Grand Hotel Conference Center

*Session Chairs:* Thomas Myers, West Virginia University; Joan Redwing, Pennsylvania State University

### 8:30 AM Invited

**BB1, Electrical Properties of InGaN Grown by Molecular Beam Epitaxy:** *William Schaff*<sup>1</sup>; Xiaodong Chen<sup>1</sup>; Dong Hao<sup>1</sup>; Kris Matthews<sup>1</sup>; Les Eastman<sup>1</sup>; <sup>1</sup>Cornell University

The electrical properties of InGaN that is either undoped, or Mg doped, are compared to learn about the nature of p-type conductivity. When In alloy fraction beyond 5% is used, Hall measurements indicate a n-type polarity, even when Mg doping is employed. In contrast, hot probe measurements show that p-polarity can be measured for the entire range of Mg-doped In mole fractions. The conflicting polarity indications are the result of surface electron accumulation. Parasitic electron conductivity can further be seen in p-n homojunctions at In fractions including 20% and 30%. This has an impact on structures such as solar cells. Temperature variable conductivity and PL from different layer structures provides further understanding of the nature of InGaN:Mg. P-type InAlN is shown for In mole fractions near 50%.

### 9:00 AM

**BB2, An Experimental Real Time Study of Hydrogen Behavior in InN:** *Maria Losurdo*<sup>1</sup>; Tong-Ho Kim<sup>2</sup>; Giorgio Pettinari<sup>3</sup>; Antonio Polimeni<sup>3</sup>; Mario Capizzi<sup>3</sup>; Maria Giangregorio<sup>1</sup>; Soojeong Choi<sup>2</sup>; Giovanni Bruno<sup>1</sup>; April Brown<sup>2</sup>; <sup>1</sup>Istituto di Metodologie Inorganiche e dei Plasmi-National Research Council; <sup>2</sup>Electrical and Computer Engineering-Duke University; <sup>3</sup>Universita La Sapienza

The interaction of InN epitaxial films grown by MBE with atomic hydrogen produced by a remote H<sub>2</sub> r.f. plasma source is investigated in real time by exploiting spectroscopic ellipsometry. The dependence of InN-H reaction rate on temperature is presented. We found that a competition between hydrogen incorporation in InN and desorption as NH<sub>x</sub> exists leading to stable hydrogen inclusion at T<300°C, while hydrogen becomes unstable and desorbs as InH<sub>x</sub> at T>300°C. Real time ellipsometry data are supported by a photoluminescence study, which provides experimental evidence that hydrogen acts as a donor in InN: the electron concentration increases upon sample hydrogenation and decreases with post-hydrogenation thermal annealing at 300°C. Optical spectra as a function of annealing time and temperature indicate that hydrogen-related donors occupy two stable equilibrium sites, and diffuse out from the samples with two characteristic activation energies, whose values have been determined.

### 9:15 AM

**BB3, Improvement of the Surface Morphology of a-Plane InN Using Low-Temperature InN Buffer Layers:** *Go Shikata*<sup>1</sup>; Shigeru Hirano<sup>1</sup>; Takeru Inoue<sup>1</sup>; Misao Orihara<sup>1</sup>; Yasuto Hijikata<sup>1</sup>; Hiroyuki Yaguchi<sup>1</sup>; Sadafumi Yoshida<sup>1</sup>; <sup>1</sup>Saitama University

We report on the improvement of the surface morphology of a-plane InN films grown by RF molecular beam epitaxy using low-temperature (LT) InN buffer layers. Although the surface of InN films grown without LT-InN buffer layers was rather rough, we could successfully obtain InN films with a smooth surface by using LT-InN buffer layers. The full width at half maximum values of the X-ray diffraction (11-20) rocking curve were 2800 arcsec and 4700 arcsec for a-plane InN samples grown at 500°C with and without LT-InN buffer layers, respectively. Thus, we could improve also the crystalline quality of a-plane InN films by using LT-InN buffer layers. Strong photoluminescence was observed at ~0.63 eV, which is lower than the PL peak energy for c-plane InN films. This red shift is probably due to the Franz-Keldysh effect.

### 9:30 AM

**BB4, Real-Time Observation of Spontaneous, Cyclic Growth and Decomposition of InN during MOVPE:** *Fan Jiang*<sup>1</sup>; Anneli Munkholm<sup>2</sup>; Ruey-Ven Wang<sup>1</sup>; Kujtim Latifi<sup>3</sup>; Carol Thompson<sup>3</sup>; Ken Elder<sup>4</sup>; Paul Fuoss<sup>1</sup>; Costas Dimitropoulos<sup>2</sup>; Stephen Streiffer<sup>1</sup>; Gregory Stephenson<sup>1</sup>; <sup>1</sup>Argonne National Laboratory; <sup>2</sup>Philips Lumileds Lighting Company; <sup>3</sup>Northern Illinois University; <sup>4</sup>Oakland University

We have been using real-time synchrotron x-ray scattering and fluorescence as in situ probes to study growth of InN and InGaN by MOVPE. In this talk we report that MOVPE of InN on GaN can be inherently unstable, spontaneously cycling between growth and decomposition. Under constant input flows of NH<sub>3</sub> and trimethylindium (TMI) at temperatures in the range 550-675°C, we observe a cyclic process: epitaxial islands of crystalline InN nucleate and grow to micron size; the InN islands collectively decompose into liquid In droplets; the liquid In evaporates; and another cycle of InN growth begins. These results will be discussed in terms of a model in which the effective nitrogen activity produced by catalytic decomposition of NH<sub>3</sub> on the surface depends on the amount of InN and In liquid present.

### 9:45 AM

**BB5, Etching and Optical Deterioration of Nitrogen-Face of Wurtzite InN in NH<sub>3</sub> Ambient:** *Akio Yamamoto*<sup>1</sup>; Ken-ichi Sugita<sup>1</sup>; Yasuhiko Nagai<sup>1</sup>; Akihiro Hashimoto<sup>1</sup>; <sup>1</sup>University of Fukui

We describe the etching and optical degradation of N-face of wurtzite InN in the NH<sub>3</sub> ambient at around 600°C. Both In- and N-polar InN films with a thickness about 0.5 μm are grown on (0001) sapphire with the atmospheric-pressure MOVPE. After the growth, InN samples are annealed at 500-650°C for 2-6 h in the NH<sub>3</sub> flow (6 slm). The InN samples are etched by the annealing and the etching rate of the N-face is found to be three times higher than that of the In-face. For both In- and N-polar films, the N-face shows a larger PL peak shift to the higher energy side than the In-face, showing that a high density of donor-type defects are preferentially introduced on the N-face of InN. Such instability of N-face in the NH<sub>3</sub> ambient seems to be related to the poorer quality of MOVPE InN.

### 10:00 AM

**BB6, The Importance of Reducing Strain for the Improvement of Crystalline Quality of MOVPE InN:** *Ken-ichi Sugita*<sup>1</sup>; Akihiro Hashimoto<sup>1</sup>; Akio Yamamoto<sup>1</sup>; <sup>1</sup>University of Fukui

This paper reports the c-lattice parameter dependence of tilt and twist fluctuations for MOVPE InN. Using an atmospheric-pressure MOVPE system with a horizontal reactor, InN films are grown on GaN/α-Al<sub>2</sub>O<sub>3</sub>(0001) templates or directly on α-Al<sub>2</sub>O<sub>3</sub>(0001) using a low temperature GaN buffer. Growth temperature is varied from 450 to 65°C. The c-lattice parameter is increased with increasing growth temperature. Since the c-lattice parameter for strain-free is reported to be 5.703 Å, the result obtained here shows that, with increasing growth temperature, the strain is changed from tensile to compressive at a temperature around 550°C. A clear correlation exists between c-lattice parameter and tilt and twist fluctuations. It is found that the minimum values for both tilt and twist fluctuations are obtained for the strain-free c-lattice parameter. This means that the reduction of strain is very important to improve the crystalline quality of MOVPE InN.

### 10:15 AM

**BB7, The Growth and Characterization of InN Layers Grown by High-pressure CVD:** *Nikolaus Dietz*<sup>1</sup>; Mustafa Alevli<sup>1</sup>; Ramazan Atalay<sup>1</sup>; Goksel Durkaya<sup>1</sup>; William Fenwick<sup>2</sup>; Hun Kang<sup>2</sup>; Ian Ferguson<sup>2</sup>; <sup>1</sup>Georgia State University; <sup>2</sup>Georgia Institute of Technology

The successful integration of InN and indium-rich group III-nitride layers into wide band gap group III-nitrides, is a fundamental step enabling envisioned emerging device structures, such as high-efficient spectral agile white LED's, radiation hardened magneto/optoelectronics, spectral tailored detectors, or advanced device structures for high speed optoelectronics and optical communication. This contribution will present results on the growth and real-time characterization on InN layers grown by a novel high-pressure chemical vapor deposition (HPCVD) system, which has been developed at GSU. The HPCVD system is capable to control the vast different partial pressures of the constituents for reactor pressures up to 100bar. Single-

# Technical Program

crystalline InN layers grown at growth temperatures of 850°C and reactor pressures around 15 bar are of high structural quality with XRD FWHM better than 400 arcsec, demonstrating that the chosen HPCVD pathway works. Selected results on the structural and optical properties of grown InN films are presented.

10:30 AM Break

---

## Session CC: Nonpolar and Semipolar Materials and Devices IV

Thursday AM Room: 313/316  
September 20, 2007 Location: MGM Grand Hotel Conference Center

*Session Chairs:* Shuji Nakamura, University of California, Santa Barbara; S. Park, Gwanju Institute of Science and Technology

---

8:30 AM Invited

**CC1, Progress of Nonpolar m-Plane InGaN/GaN Laser Diodes:** *Kuniyoshi Okamoto*<sup>1</sup>; Hiroaki Ohta<sup>1</sup>; Shigefusa Chichibu<sup>2</sup>; Taketoshi Tanaka<sup>1</sup>; Testuhiro Tanabe<sup>1</sup>; Hidemi Takasu<sup>1</sup>; <sup>1</sup>ROHM Company, Ltd.; <sup>2</sup>Tohoku University

Continuous-wave operation of nonpolar m-plane violet InGaN/GaN laser diodes (LDs) has been realized by using m-plane GaN homoepitaxial substrates. The LDs had almost no stacking faults and macroscopic cracks, and their performance was already comparable to that of conventional c-plane violet LDs. A distinct characteristic of nonpolar LDs was the strong anisotropy of the photon emission, according to the polarization selection rules for anisotropically strained InGaN quantum wells. As a result, the threshold current density (4.0 kA/cm<sup>2</sup>) of the LDs whose ridge stripe was parallel to the c-axis was lower than that of a-axis stripe LDs. We will show such unique characteristics of m-plane LDs and our recent works on optimizing the device structure and the growth conditions for longer wavelength m-plane LDs.

9:00 AM

**CC2, AlGaIn-Cladding-Free Nonpolar InGaIn/GaN Laser Diodes:** *Mathew Schmidt*<sup>1</sup>; Daniel Feezell<sup>1</sup>; Robert Farrell<sup>1</sup>; Makoto Saito<sup>1</sup>; Kenji Fujito<sup>2</sup>; Daniel Cohen<sup>1</sup>; James Speck<sup>1</sup>; Shuji Nakamura<sup>1</sup>; Steven DenBaars<sup>1</sup>; <sup>1</sup>University of California, Santa Barbara; <sup>2</sup>Mitsubishi Chemical Corporation

We demonstrate a nonpolar m-plane GaN laser diode that does not contain any AlGaIn cladding layers for optical waveguiding. The ability to grow thick quantum wells ( $\approx 8$  nm) on m-plane GaN leads to sufficient optical confinement without the need for AlGaIn claddings. Broad area lasers were grown by metal organic vapor deposition (MOCVD) on bulk m-plane GaN substrates and fabricated using etched facets. Threshold current densities as low as 2.3 kA/cm<sup>2</sup> were observed. AlGaIn-cladding-free nonpolar GaN-based laser diodes offer several advantages over conventional c-plane GaN-based lasers. The presence of thick AlGaIn cladding layers can be detrimental to device performance by increasing the series resistance, operating voltage, operating temperature, and threshold current density. Thick AlGaIn layers, or high Al-content AlGaIn layers, lead to cracking issues, as well. Employing an AlGaIn-cladding-free design can have a significant impact on both improving device performance and manufacturability.

9:15 AM

**CC3, Non-Polar Al<sub>x</sub>Ga<sub>1-x</sub>N/Al<sub>y</sub>Ga<sub>1-y</sub>N Multiple Quantum Well Deep UV LEDs over Bulk m-GaN:** *Balakrishnan Krishnan*<sup>1</sup>; Vinod Adivarahan<sup>1</sup>; Thomas Katona<sup>1</sup>; R.S. Fareed<sup>2</sup>; Bin Zhang<sup>1</sup>; Asif Khan<sup>1</sup>; <sup>1</sup>University of South Carolina, Electrical Engineering; <sup>2</sup>Photonics Microelectronics Laboratory

Al<sub>x</sub>Ga<sub>1-x</sub>N non-polar LEDs are expected to be superior to their polar counterparts due to the absence of piezo-electric polarization fields. Recently, several groups have reported on very high-efficiency visible LEDs<sup>1</sup> and laser diodes<sup>2</sup> using GaN/Al<sub>x</sub>Ga<sub>1-x</sub>N layers over bulk m-plane GaN substrates. We now report the fabrication and characterization of Al<sub>x</sub>Ga<sub>1-x</sub>N/Al<sub>y</sub>Ga<sub>1-y</sub>N Multiple Quantum Wells (MQWs) over bulk m-GaN with emission at 348 nm. Initial results of a comparative study of photoluminescence

and electroluminescence are used to establish the feasibility of non-polar deep UV LEDs over bulk m-GaN substrates. <sup>1</sup>K. Okamoto, H. Ohta, S.F. Chichibu, J. Ichihara and H. Takasu, *Jap. J. App. Phys.* 46(2007)L187-L189. <sup>2</sup>M.C. Schmidt, K.C.Kim, M. Farrell, D.F.Feezell, D.A. Cohen, M. Saito, K. Fujito, J.S. Speck, S.P. DenBaars and S. Nakamura, *Jap. J. App. Phys.* 46(2007)L190-L191.

9:30 AM

**CC4, Fabrication of GaInN MQW LED with Low Defect Density on m-Plane SiC Substrate:** *Takeshi Kawashima*<sup>1</sup>; Takeshi Hayakawa<sup>1</sup>; Masako Hayashi<sup>1</sup>; Tetsuya Nagai<sup>1</sup>; Daishuke Iida<sup>1</sup>; Aya Miura<sup>1</sup>; Yoshinao Kasamatsu<sup>1</sup>; Motoaki Iwaya<sup>1</sup>; Satoshi Kamiyama<sup>1</sup>; Hiroshi Amano<sup>1</sup>; Isamu Akasaki<sup>1</sup>; <sup>1</sup>Meijo University

One of problems of realizing high-efficiency green light emitting devices is the large internal electric fields, such as the spontaneous polarization and piezo-electric field. Using a nonpolar plane, the piezoelectric field is suppressed. In this study, we report the fabrication of m-plane GaInN multiple quantum well (MQW) LED with low defect density on m-plane SiC. Low-defect-density GaN films on m-SiC was grown by the sidewall epitaxial lateral overgrowth (SELO) technique. A periodic grooved structure in which the terrace was covered with SiO<sub>2</sub> mask was fabricated by reactive ion etching and conventional photolithography. The stripe direction was  $\langle 1-100 \rangle$ . A GaN layer was grown from the sidewall of a seed GaN. As a result, we succeeded in growing low-defect-density m-plane GaN. We fabricated m-plane GaInN MQW LED on SELO-grown GaN film. The light output power of LED on SELO-grown GaN was about 50 times stronger than that on non-ELO GaN.

9:45 AM

**CC5, InGaIn/GaN Laser Diodes on Semipolar (10-1-1) Bulk GaN Substrates:** *Anurag Tyagi*<sup>1</sup>; Hong Zhong<sup>1</sup>; Roy Chung<sup>1</sup>; Daniel Feezell<sup>1</sup>; Makoto Saito<sup>1</sup>; Kenji Fujito<sup>2</sup>; James Speck<sup>1</sup>; Steven DenBaars<sup>1</sup>; Shuji Nakamura<sup>1</sup>; <sup>1</sup>University of California, Santa Barbara; <sup>2</sup>Mitsubishi Chemical Corporation

The first semipolar nitride laser diodes (LDs) have been realized on low extended defect density semipolar GaN bulk substrates. The LDs were grown by conventional metal organic chemical vapor deposition (MOCVD). Broad area lasers were fabricated and tested under pulsed conditions. Lasing was observed at a duty cycle of 0.025% with a threshold current density ( $J_{th}$ ) of 18 kA/cm<sup>2</sup>. An output power of 18 mW was measured from a single facet of the device at a drive current of 1.2 A, with the calculated differential quantum efficiency ( $\eta_{diff}$ ) being 15%. Stimulated emission was observed at 405.9 nm with a narrow full width half maximum (FWHM) of less than 0.3 nm.

10:00 AM

**CC6, InGaIn-Based LEDs Grown by Plasma-Assisted MBE on (0001) Sapphire with GaN QDs in the Nucleation Layer:** *C. Thomidis*<sup>1</sup>; A. Nikiforov<sup>1</sup>; Tao Xu<sup>1</sup>; Theodore Moustakas<sup>1</sup>; <sup>1</sup>Boston University

Blue-violet LEDs based on InGaIn MQWs were grown by RF-plasma MBE on (0001) sapphire with GaN QDs incorporated in the nucleation layer as a mechanism of dislocation filtering. Devices with dimensions 800  $\mu$ m x 800  $\mu$ m were fabricated and evaluated at a bare die configuration by measuring their EL spectra and power output. At low injection current, the EL spectra peak at 440 nm. At high injection current a second peak at 385 nm becomes the dominant one and it is attributed to tunneling of injected electrons through the electron blocking layer. The dependence of the power output as a function of the injection current was studied systematically in order to evaluate the effects of heating. Power outputs up to 9 mW were measured at the injection current of 1 A.

10:15 AM

**CC7, Growth of Non-Polar a- and m-Plane GaN by Ammonia Molecular Beam Epitaxy:** *Erin Young*<sup>1</sup>; Melvin McLaurin<sup>1</sup>; Feng Wu<sup>1</sup>; Tom Mates<sup>1</sup>; Jim Speck<sup>1</sup>; <sup>1</sup>University of California at Santa Barbara

Non-polar orientations of the III-V wurtzite nitrides are currently of interest due to their potential in eliminating polarization discontinuities and improving the efficiency of nitride-based light emitters. In this work, we demonstrate growth of non-polar a-plane (11-20) and m-plane (1-100) GaN

by ammonia molecular beam epitaxy (MBE) on *r*-plane sapphire and *m*-plane SiC, respectively. Films were determined to be of high epitaxial quality and showed anisotropic surface morphologies and structural properties consistent with a high stacking fault density. The surface morphology of *m*-plane GaN was strongly dependent on growth conditions, showing small islands at low growth temperatures and smooth, slate-like morphology with abrupt terraces at higher growth temperatures and V/III ratios. Mg incorporation at concentrations between  $8 \times 10^{18}$  and  $6 \times 10^{19}$  /cm<sup>3</sup> was also achieved for *m*-GaN films, a promising result towards achieving devices by ammonia MBE.

10:30 AM Break

---

## Session DD: Engineered Properties of GaN by MOVPE Growth

Thursday AM                      Room: 314/315  
September 20, 2007              Location: MGM Grand Hotel Conference Center

*Session Chairs:* Koh Matsumoto, Taiyo Nippon Sanso Corporation;  
Randall Feenstra, Carnegie Mellon University

---

8:30 AM

**DD1, Fabrication of a GaN p/n Lateral Polarity Junction by Polar Doping Selectivity:** *Ramon Collazo*<sup>1</sup>; Seiji Mita<sup>1</sup>; Anthony Rice<sup>1</sup>; Rafael Dalmau<sup>1</sup>; Zlatko Sitar<sup>1</sup>; <sup>1</sup>North Carolina State University

The difference in surface energy between the Ga-polar orientation and the N-polar orientation of GaN translates into a completely different behavior for the incorporation of intentional and unintentional impurities. Oxygen is found to be an impurity with higher concentration in N-polar films than in Ga-polar films and is the cause for the high carrier concentration observed in N-polar films. We fabricated a lateral p/n junction in GaN by the simultaneous growth of p- and n-type regions, utilizing the doping selectivity of the two different polar domains, which resulted in an n-type carrier concentration of  $1.7 \times 10^{19}$  cm<sup>-3</sup> with an electron hall mobility of 99 cm<sup>2</sup>/Vs in the N-polar domains, and a p-type carrier concentration of  $1.1 \times 10^{17}$  cm<sup>-3</sup> with a hole hall mobility of 12 cm<sup>2</sup>/Vs in the Ga-polar domains. These junctions showed the characteristics that define a p/n junction: current rectification, electroluminescence, and photo-effect.

8:45 AM

**DD2, Electrical Characterization of p-Type N-Polar GaN Grown by Metalorganic Chemical Vapor Deposition:** *Nicholas Fichtenbaum*<sup>1</sup>; Chris Schaake<sup>1</sup>; Tom Mates<sup>1</sup>; Christine Cobb<sup>1</sup>; Stacia Keller<sup>1</sup>; Steven DenBaars<sup>1</sup>; James Speck<sup>1</sup>; Umesh Mishra<sup>1</sup>; <sup>1</sup>University of California, Santa Barbara

We report on Mg-doped N-polar and Ga-polar GaN films grown by MOCVD. The bis-cyclopentadienyl magnesium (Cp<sub>2</sub>Mg) flow was varied between 64 and 640 nmol/min, for N-polar and Ga-polar samples, while other growth conditions were held constant. The sample surfaces were characterized by atomic force microscopy (AFM). Electrical measurements were made to determine the resistivity, specific contact resistance, carrier concentrations, mobilities, and activation energies. N-polar samples exhibited a minimum resistivity of 1.6 Ω•cm while Ga-polar samples had a minimum resistivity of 1.2 Ω•cm. Hall effect measurements revealed hole concentrations and mobilities of  $5 \times 10^{17}$  cm<sup>-3</sup> and 4 cm<sup>2</sup>/V•s for the N-polar and  $6 \times 10^{17}$  cm<sup>-3</sup> and 13 cm<sup>2</sup>/V•s for the Ga-polar. Temperature dependent measurements revealed an activation energy of 105 meV for N-polar and 108 meV for the Ga-polar. Finally, current-voltage measurements were used to characterize the properties of N-polar p-n diodes as a function of the Cp<sub>2</sub>Mg flow.

9:00 AM

**DD3, Impact of Ultra-Low Nucleation Density on GaN Film Dislocation Density:** *Daniel Koleske*<sup>1</sup>; Stephen Lee<sup>1</sup>; Michael Coltrin<sup>1</sup>; Gerald Thaler<sup>1</sup>; Karen Cross<sup>1</sup>; <sup>1</sup>Sandia National Laboratories

For improved GaN films on sapphire, GaN nucleation layers (NLs) are typically used prior to high temperature growth. Recently, a correlation between the nucleation density and the GaN film dislocation density has been

suggested. However, from the available studies it is difficult to determine the strength of this correlation and the extent that reduced nucleation density can be used to achieve lower dislocation density films. Recently, we have initiated studies of ultra-low (< 10<sup>7</sup> cm<sup>-2</sup>) nucleation densities on sapphire using multi-step NL growth and annealing schemes. We find that the nucleation density correlates directly with the thickness of the first NL and subsequent NL growth and annealing cycles only add to the nuclei volume. A simple geometric model for dislocation generation will be presented to explain the power law behavior of the dislocation density on the nucleation density for dislocation generation primarily along tilt boundaries or in random arrays.

9:15 AM

**DD4, Metal Organic Chemical Vapor Deposition of N-Polar GaN Films on Vicinal Substrates:** *Stacia Keller*<sup>1</sup>; Nicholas Fichtenbaum<sup>1</sup>; Feng Wu<sup>1</sup>; David Brown<sup>1</sup>; Angel Rosales<sup>1</sup>; Steven DenBaars<sup>1</sup>; James Speck<sup>1</sup>; Umesh Mishra<sup>1</sup>; <sup>1</sup>University of California

Smooth, high quality N-polar GaN films with treading dislocation densities comparable to Ga-polar GaN films were obtained by MOCVD on misoriented sapphire substrates. While MOCVD growth of Ga-polar (Al,Ga,In)N has been widely studied in the past, the investigation of N-polar films and heterostructures was hampered by the poor surface morphology often observed for MOCVD grown films caused by the formation of hexagonal hillocks. In this presentation we will show, that the hillock formation can be prevented through growth on vicinal sapphire substrates. With increasing misorientation angle the structural and optical quality of the N-polar GaN films significantly improved, and the properties of GaN grown on 4 deg off substrates were comparable to Ga-polar GaN films (XRD: FWHM (002) = 300 arcsec, FWHM (201) = 480 arcsec). The influence of the sapphire nitridation, the nucleation layer, and main layer growth conditions on the film properties will be discussed.

9:30 AM

**DD5, Selective Area Growth of GaN on Patterned Sapphire Substrates by Metalorganic Vapor Phase Epitaxy for Highly Efficient UV Light Emitting Diodes:** *Katsuyuki Hoshino*<sup>1</sup>; Masahiro Araki<sup>1</sup>; Kazuyuki Tadamoto<sup>1</sup>; <sup>1</sup>Yamaguchi University

We have successfully obtained high-quality GaN films on patterned sapphire substrates (PSSs) by utilizing selective area growth (SAG) and epitaxial lateral overgrowth (ELO) without any mask. The dislocation density reached a value as low as  $8 \times 10^7$  cm<sup>-2</sup>. We have also fabricated a LED. The output power and external quantum efficiency of the LED operated at 20 mA were 22.7 mW and 40.4%, respectively. GaN films were grown on PSSs having striped grooves. The growth in the ridge region was suppressed by controlling both growth temperature and H<sub>2</sub>/(H<sub>2</sub>+N<sub>2</sub>) ratio, resulting that the SAG in the groove region was performed. After the SAG, both the ridges and grooves were buried completely under the GaN layer by utilizing ELO. The growth technique developed here is very effective in reducing the dislocation density and increasing the extraction efficiency in the LEDs because of the light scattering at the patterned GaN/sapphire interface.

9:45 AM

**DD6, In-Situ X-Ray Diffraction during MOCVD of III-Nitrides:** Clemens Simbrunner<sup>1</sup>; Tian Li<sup>1</sup>; Matthias Wegscheider<sup>1</sup>; Andrea Navarro-Quezada<sup>1</sup>; *Martin Quast*<sup>1</sup>; Alberta Bonanni<sup>1</sup>; Alexander Kharchenko<sup>2</sup>; Jürgen Bethke<sup>2</sup>; Klaus Lischka<sup>3</sup>; Helmut Sitter<sup>1</sup>; <sup>1</sup>Johannes Kepler Universität Linz; <sup>2</sup>PANalytical B. V.; <sup>3</sup>University of Paderborn

We implemented, to our knowledge the first time, *in-situ* x-ray diffraction (IXRD) as a real-time process-control tool for the metalorganic chemical vapor deposition of III-nitrides using a PANalytical standard Cu x-ray source. Presently, we are able to measure *in-situ* x-ray diffraction and spectroscopic ellipsometry on rotating samples during the deposition process in our AIXTRON 200 RF-S reactor. Due to the unique geometry of the reactor, IXRD can be performed simultaneously to spectroscopic ellipsometry. In particular, we report on the potential of IXRD as an *in-situ* monitoring tool, during the deposition of III-nitride hetero- and superlattice (SL)-structures, yielding SL periodicity and composition. Furthermore, we present a kinetic analysis of the relaxation processes during the SL-deposition which is demonstrated by *in-situ* reciprocal space mapping.

# Technical Program

10:00 AM

DD7, Late News

10:15 AM

DD8, Late News

10:30 AM Break

---

## Session EE: InN Heterostructures and Quantum Wells

Thursday AM

Room: 312/317

September 20, 2007

Location: MGM Grand Hotel Conference Center

*Session Chairs:* Tim Veal, University of Warwick; Maria Losurdo, Institute of Inorganic Methodologies and Plasmas

---

11:00 AM

**EE1, Structural Quality Improvement in 1 ML InN/GaN Quantum Wells Using Bulk-GaN Substrate:** Hideyuki Saito<sup>1</sup>; Song-Bek Che<sup>1</sup>; Kazuaki Matsui<sup>1</sup>; Naoki Hashimoto<sup>1</sup>; Eun-Soon Hwang<sup>1</sup>; Xinqiang Wang<sup>1</sup>; Yoshihiro Ishitani<sup>1</sup>; Akihiko Yoshikawa<sup>1</sup>; <sup>1</sup>Chiba University

Ultrathin InN well (~1ML) insertion in GaN matrix has been demonstrated recently<sup>1</sup>. This novel InN nano-structure is potentially applicable to room-temperature operating excitonic devices. In this structure, very flat surface/interface quality is required because the quantum well thickness is only 1ML. The samples reported in Ref.1, however, had relatively high density threading dislocations (TDs) more than  $10^8\text{cm}^{-2}$ , because MOCVD-GaN templates grown on sapphire were used. Generally, in MBE-GaN growth on the templates, hexagonal growth spiral hillocks are observed on their surface and these are correlated to the TDs, which seriously affect flatness of the 1ML InN well. In this study, to improve structural perfection in the InN(1ML)/GaN QWs, low dislocation density bulk-GaN substrates (TDD~ $10^6\text{cm}^{-2}$ ) were used. Superior interface and structural quality was obtained and fine 1ML InN well formation was achieved even for a single QW structure grown on bulk-GaN. <sup>1</sup> A. Yoshikawa et. al., APL 90, 073101 (2007)

11:15 AM

**EE2, Study on "One-Monolayer InN" Epitaxy Process on Ga-Polarity GaN Template: Effects of GaN Matrix on Epitaxy Temperature and Self-Limiting Thickness of In-Polarity InN:** Naoki Hashimoto<sup>1</sup>; Song-Bek Che<sup>1</sup>; Hideyuki Saito<sup>1</sup>; Eun-Sook Hwang<sup>1</sup>; Xinqiang Wang<sup>1</sup>; Yoshihiro Ishitani<sup>1</sup>; Akihiko Yoshikawa<sup>1</sup>; <sup>1</sup>Chiba University

Recently, we have demonstrated successful fabrication of novel structure InN/GaN MQWs consisting of 1-ML-thick InN wells inserted in GaN matrix by RF-MBE<sup>1</sup>. Here, atomically flat/sharp In-polarity InN wells were coherently grown at such high temperatures up to 650°C on the basis of 1) self-ordering process arising from immiscibility-nature between InN and GaN, and 2) effectively increased In-N bonding by the GaN-matrix effect. In this paper, in order to clarify the detailed mechanism on 1-ML InN deposition on Ga-polarity GaN, in-situ and real time monitoring by both RHEED and spectroscopic ellipsometry of InN epitaxy processes on Ga-polarity GaN were performed. It was shown that the deposition of InN is self-limited so that the thickness is around 1-ML (up to a few-MLs) and following InN deposition was stopped by its reevaporation at such high temperatures of 650°C for In-polarity InN epitaxy. <sup>1</sup> A. Yoshikawa et.al., Appl. Phys. Lett. 90, 073101 (2007).

11:30 AM

**EE3, Optical Emission Properties of InN/In<sub>0.7</sub>Ga<sub>0.3</sub>N Multi-Quantum Wells on Bulk-GaN Substrates:** Songbek Che<sup>1</sup>; Xinqiang Wang<sup>2</sup>; Yoshihiro Ishitani<sup>1</sup>; Akihiko Yoshikawa<sup>1</sup>; <sup>1</sup>Graduate Course of Electrical and Electron Engineering, Venture Business Laboratory, InN-Project as a CREST-program of JST, Chiba University; <sup>2</sup>InN-Project as a CREST-program of JST, Chiba University

InN/In<sub>0.7</sub>Ga<sub>0.3</sub>N multi-quantum wells are key materials for the development of nitride-based near-infrared optical devices. In order to realize LEDs or LDs

with the MQWs, investigation of their optical properties such as light-emission efficiency is important. In this study, InN/In<sub>0.7</sub>Ga<sub>0.3</sub>N MQWs were grown on bulk-GaN substrates (TDD~ $10^6\text{cm}^{-2}$ ) because superior optical properties and clearer dependence on InN well thickness (0.5~1.5nm) compared with that on sapphire were obtained. By comparing the experimental results with theoretical calculations and considering lattice relaxation behavior in the MQW region, we found that when the InN well thickness is less than 1 nm, which corresponds to the critical thickness in the MQWs, drastic increase in PL intensity is observed. This is mainly caused by minimizing piezoelectric effect in thinner InN well samples.

11:45 AM

**EE4, Intensity-Dependent Photoluminescence Studies of the Electric Field in N-Face and In-Face InN/InGaN Multiple Quantum Wells:** Grace Chern<sup>1</sup>; Eric Readinger<sup>1</sup>; Hongen Shen<sup>1</sup>; Michael Wraback<sup>1</sup>; Gregor Koblmüller<sup>2</sup>; Chad Gallinat<sup>2</sup>; James Speck<sup>2</sup>; <sup>1</sup>US Army Research Laboratory; <sup>2</sup>University of California, Santa Barbara

We probe the electric field in In-face and N-face InN/InGaN multiple quantum wells (MQWs) using low temperature intensity-dependent photoluminescence (PL) under continuous-wave laser excitation at 900nm. The In-face structure consists of 30 periods of 2.5nm thick InN wells and 24nm thick In<sub>0.92</sub>Ga<sub>0.08</sub>N barriers. The N-face sample consists of 25 periods of 1.5nm InN wells and 15nm thick In<sub>0.88</sub>Ga<sub>0.12</sub>N barriers. At low excitation power, the PL peak energy from both In-face and N-face MQWs is redshifted relative to that from bulk InN. As excitation power increases, we observe a 50 and 44meV blueshift of the PL peak energy from the In-face and N-face MQWs, respectively. The blueshift is a result of the optically induced screening of the built-in electric field. From the measured blueshift, we calculate a minimum change of the electric field to be ~0.4MV/cm and ~0.6MV/cm in the In-face and N-face well regions, respectively.

12:00 PM

**EE5, Growth and Characterization of InN/GaN Heterojunctions by MBE:** Kejia (Albert) Wang<sup>1</sup>; Debdeep Jena<sup>1</sup>; <sup>1</sup>University of Notre Dame

In this work, the growth of InN on GaN by MBE has been studied. High quality InN was achieved by optimizing the substrate temperature and the III/V flux ratio. Structural quality was characterized by X-ray diffraction measurements, and Hall measurements of a 1.8 mm thick InN sample shows high electron concentrations (~  $3 \times 10^{18}\text{cm}^{-3}$ ) and high room-temperature mobilities (~ 1500 cm<sup>2</sup>/Vs). Optical measurements including absorption and photoluminescence show that the bandgap of grown InN is ~0.7 eV. A strong correlation is found between the structural and transport properties of the InN. The band offset of InN and GaN was measured through a C-V intercept-method measurement. Taking into account the effect of the interface polarization dipole, the conduction band offset between InN and GaN was extracted to be around 1.5 eV.

12:15 PM

**EE6, Atmospheric-Pressure MOVPE Growth of In-Rich InAlN:** Yoshinori Houchin<sup>1</sup>; Akihiro Hashimoto<sup>1</sup>; Akio Yamamoto<sup>1</sup>; <sup>1</sup>University of Fukui

We report the atmospheric-pressure MOVPE growth of In-rich InAlN. An InAlN is grown on a nitrided (0001) sapphire at 600-700°C in the pressure of 730 Torr. The incorporation of In in InAlN is increased with increasing growth temperature. An increase in In content is also observed for films grown at a position farther from the up-stream end of the susceptor. Such an increase in In, i.e., a decrease in Al incorporation can be explained by the parasitic reaction of TMA with NH<sub>3</sub>. A single-crystalline InAlN film with an In content of 1-0.55 is successfully grown by adjusting growth temperature and TMI/(TMI+TMA) molar ratio. FWHM of X-ray rocking curve for InAlN is increased with decreasing In content. The carrier concentrations in InAlN films are comparable to that in InN ( $1.5 \times 10^{19}\text{cm}^{-3}$ ). All the single-crystalline InAlN films with an In content of 1-0.7 show a photoluminescence at room temperature.

12:30 PM

EE7, Late News

12:45 PM

EE8, Late News

## Session FF: Nanostructures: Devices

Thursday AM Room: 313/316  
September 20, 2007 Location: MGM Grand Hotel Conference Center

*Session Chairs:* Tomas Palacios, Massachusetts Institute of Technology;  
Debdeep Jena, University of Notre Dame

### 11:00 AM Invited

**FF1, III-Nitride Nanowires and Networks: Growth, Heterostructures, Epitaxial Alignment, and Applications:** *Jung Han*<sup>1</sup>; Shigefusa Chichibu<sup>2</sup>; Hong Tang<sup>1</sup>; <sup>1</sup>Yale University; <sup>2</sup>Tohoku University

Most of NWs are prepared by catalytic VLS method on amorphous or polycrystalline substrates. The as-grown, hay-stack like NWs are dispersed randomly onto target wafers, where electrical contacting and/or characterizations are performed. The purpose of this paper is to demonstrate a hybrid approach toward the construction of GaN NW arrays and networks through the use of (optical) lithographically-defined selective-area growth (SAG) and bottom-up VLS synthesis. Spatially ordered and flexibly patterned NW networks are prepared, in which the stochastic nature in contemporary process of NW synthesis and fabrication is greatly mitigated. While we anticipate a new paradigm rendered by this novel and more deterministic fabrication process in pursuing NW-based electronic and photonic applications, we will focus in this talk on the nanomechanical characterizations of ordered NW arrays to demonstrate the possibility of a new direction in NW research, complementary and orthogonal to the existing nanoelectronic and nanophotonics.

### 11:30 AM

**FF2, Growth and Characterization of Vertically Aligned III-Nitride Nanowires:** *George Wang*<sup>1</sup>; Qiming Li<sup>1</sup>; A. Alec Talin<sup>1</sup>; J. Randall Creighton<sup>1</sup>; Elaine Lai<sup>1</sup>; Ilke Arslan<sup>1</sup>; Richard Anderson<sup>1</sup>; Donald Werder<sup>2</sup>; <sup>1</sup>Sandia National Laboratories; <sup>2</sup>Los Alamos National Laboratory

Nanowires based on the direct bandgap semiconductor Group III nitride (AlGaInN) materials system have attracted attention as potential building blocks in optoelectronics, sensing, and electronics. We have employed a VLS-based metal-organic chemical vapor deposition process to synthesize highly aligned arrays of single-crystalline GaN nanowires on sapphire substrates without the use of a patterned template. The effects of growth time, temperature, and catalyst preparation were found to have strong effects on the ordered growth and will be discussed. The optical and electrical properties of the nanowires were studied and show a strong correlation with the growth temperature, which we propose is due to carbon incorporation from the metal-organic source. Building on our growth technique, aligned radial heterostructure nanowire arrays were synthesized and characterized using 3D STEM imaging. Sandia is a multiprogram laboratory operated by Sandia Corporation, a Lockheed Martin Company, for the United States Department of Energy under contract DE-AC04-94AL85000.

### 11:45 AM

**FF3, Near-Infrared Intersubband Emission from GaN/AlN Quantum Dots and Quantum Wells:** Laurent Nevou<sup>1</sup>; *Francois Julien*<sup>1</sup>; Maria Tchernycheva<sup>1</sup>; Fabien Guillot<sup>2</sup>; Eva Monroy<sup>2</sup>; <sup>1</sup>Institut d'Electronique Fondamentale; <sup>2</sup>Equipe mixte CEA-CNRS-UJF Nanophysique et Semiconducteurs, DRFMC/SP2M/PSC

We report on the observation of intersubband (ISB) luminescence at 300 K from GaN/AlN quantum dots (QD) and quantum wells (QW) in the wavelength range of 1.5 to 2.3  $\mu\text{m}$ . All samples have been grown by plasma-assisted molecular beam epitaxy on AlN/c-sapphire templates. Under optical excitation at  $\lambda=1.34 \mu\text{m}$ , the GaN/AlN QD superlattice exhibits emission at  $\lambda=1.5 \mu\text{m}$  ascribed to the pz-s intraband transition of electrons. This phonon-assisted process provides room for population inversion. We next report on QW samples containing 2.1 nm thick GaN wells with 3 nm thick AlN barriers. The active region is designed to exhibit three bound states in the

conduction band. Under optical pumping resonant with the e1-e3 transition ( $\lambda=0.98 \mu\text{m}$ ), ISB emission corresponding to the e3-e2 transition is observed at  $\lambda=2.1$  (2.3)  $\mu\text{m}$  for heavily (lightly) doped QWs. Prospects for ISB lasers using nitride QWs or QDs will be discussed.

### 12:00 PM

**FF4, GaN/AlGaIn Nanocolumn Ultraviolet Light Emitting Diodes on N-(111) Si Substrates Grown by Rf-Plasma Assisted Molecular Beam Epitaxy:** *Hiroto Sekiguchi*<sup>1</sup>; Shunsuke Ishizawa<sup>1</sup>; Koki Sakamoto<sup>1</sup>; Goh Kobayashi<sup>1</sup>; Jo Tanaka<sup>1</sup>; Kei Kato<sup>1</sup>; Akihiko Kikuchi<sup>1</sup>; Katsumi Kishino<sup>1</sup>; <sup>1</sup>Sophia University

Self-organized nitride nanocolumns which has 20~200 nm in diameter have great potentiality for high performance light emitting diodes in UV to NIR region due to their dislocation-free nature and high light extraction efficiency. In this study, the room temperature operation of surface-connection type GaN/AlGaIn nanocolumn UV-LED was demonstrated for the first time. The nanocolumn UV-LED was grown on n-type (111) Si substrate by rf-plasma assisted molecular beam epitaxy as a sequence of n-GaN, n-Al<sub>0.25</sub>Ga<sub>0.75</sub>N nanocolumns, 3-periods GaN/Al<sub>0.25</sub>Ga<sub>0.75</sub>N multiple quantum disk active region, i-Al<sub>0.35</sub>Ga<sub>0.65</sub>N nanocolumn, p-Al<sub>0.25</sub>Ga<sub>0.75</sub>N and p-GaN. For the p-type region, we increased nanocolumn diameter to connect the neighboring nanocolumns, consequently surface of the nanocolumn LED became continuous film. The electroluminescence (EL) of the nanocolumn UV-LED was observed through a Ni/Au semi-transparent p-electrode (500 $\mu\text{m}$ ). The peak wavelength was 354 nm with the FWHM of 29.3 nm. But the small area observation (50 $\mu\text{m}$ ) showed narrower FWHM of 12.0 nm.

### 12:15 PM

**FF5, Optical Properties of High Quality Factor GaN/AlInN Microdisks:** *Dobri Simeonov*<sup>1</sup>; Eric Feltn<sup>1</sup>; Hans-Jörg Bühlmann<sup>1</sup>; Stephane Mattei<sup>1</sup>; Julien Dorsaz<sup>1</sup>; Jean-François Carlin<sup>1</sup>; Raphael Butté<sup>1</sup>; Nicolas Grandjean<sup>1</sup>; <sup>1</sup>École Polytechnique Fédérale de Lausanne (EPFL)

Microdisk structures attract much attention owing to their potential for fabricating low-threshold lasers and for studying cavity quantum electrodynamics phenomena such as strong light-matter coupling or the Purcell effect. We present here the fabrication of mushroom-like microdisk structures containing InGaN/GaN quantum wells (QW), using the lattice-matched GaN/AlInN system. A selective lateral wet chemical etching technique of the previously oxidized AlInN interlayer is used to optically isolate the cavity from the underlying GaN template. Whispering-gallery modes with quality factors (Q) exceeding several thousands ( $Q>3200$ ) are observed. We demonstrate that this value is absorption limited and genuine values of  $Q\sim 6000$  at QW transparency are reported. Low threshold lasing action at room temperature is equally obtained. FDTD simulations provide a detailed understanding of the microdisks' optical properties. A close comparison of these optical properties to those previously reported for inverted cone structures highlights the versatility and adaptability of such 3D microcavities.

### 12:30 PM

**FF6, C-Axis GaN Nanowires for High-Quality-Factor Mechanical Oscillators:** Shawn Tanner<sup>1</sup>; Jason Gray<sup>1</sup>; Kris Bertness<sup>2</sup>; Norman Sanford<sup>2</sup>; *Charles Rogers*<sup>1</sup>; <sup>1</sup>University of Colorado; <sup>2</sup>National Institute of Standards and Technology

We report on the electromechanical properties of c-axis GaN nanowires in high-quality-factor mechanical resonators and closed loop oscillators. The GaN nanowires are grown by catalyst-free molecular beam epitaxy, are single crystal, typically hexagonal in cross section, from 50-100 nm diameter, and 5-15 microns in length depending upon growth time. Such nanowires have masses in the picogram range. The nanowires display singly-clamped cantilever mechanical resonances above 1 MHz, with typical resonance full width at half maximum power of less than 100 Hz i.e., a mechanical quality factor, Q, well above  $10^4$ . We use piezoelectric drive and scanning electron microscope detection of nanowire motion to observe closed loop GaN nanowire oscillators with Q above  $10^6$ . We will discuss using these oscillators as sensors, demonstrating mass detection sensitivities below  $10^{-18}$  grams in a 1 second averaging time. Temperature dependencies and observed noise properties will be discussed.

# Technical Program

12:45 PM

**FF7, Electrical Defect and Transport Properties of a Single GaN Nanorod P-N Junction Diode:** *Young Park*<sup>1</sup>; Chang M. Park<sup>1</sup>; Bo Ra Hwang<sup>1</sup>; Hyunsik Im<sup>1</sup>; H. Y. Cho<sup>1</sup>; T. W. Kang<sup>1</sup>; M. S. Son<sup>2</sup>; K. H. Yoo<sup>2</sup>; <sup>1</sup>Dongguk University; <sup>2</sup>Yeonse University

The electrical properties of a single GaN nanorod p-n junction diode were characterized by the temperature-dependent current-voltage and deep level transient spectroscopy measurements. The p-n junction nanorods were patterned on a SiO<sub>2</sub> substrate by using e-beam lithography. In order to confirm the formation of p-n junction, cathodoluminescence and current-voltage measurements, as a function of temperature, were made. The current-voltage curve exhibits strong temperature dependence, suggesting that thermionic emission over a barrier dominates. This barrier most likely corresponds to emission from a deep level in the band. The deep level appears to be an electron trap at E<sub>c</sub>-0.40 eV below the conduction band with a capture cross section of 2.22x10<sup>-16</sup> cm<sup>2</sup> near the depletion region of the p-n junction.

---

## Session GG:

### Optical and Structural Characterization II

Thursday AM

Room: 314/315

September 20, 2007

Location: MGM Grand Hotel Conference Center

*Session Chairs:* Christiane Poblenz, University of California, Santa Barbara; Martin Albrecht, Institut für Kristallzüchtung

---

11:00 AM Invited

**GG1, Origin of Defect-Insensitive Emission Probability in (Al,In,Ga)N Alloy Films Containing In:** *Shigetaka Chichibu*<sup>1</sup>; <sup>1</sup>Tohoku University

Group-III nitride semiconductors (Al,In,Ga)N have shown enormous potential as light sources for full-color displays, traffic signals, and solid-state lighting. Remarkably, InGaN blue- and green-LEDs fabricated on c-plane (0001) sapphire substrates emit brilliant light although the threading dislocation density generated due to lattice mismatch is six orders of magnitude higher than that in conventional (Al,In,Ga)(As,P) amber, red, and IR LEDs. In this presentation, we explain why three-dimensional (3D) bulk (Al,In,Ga)N films containing In exhibit a defect-insensitive emission probability. From the results of time-resolved PL and positron annihilation measurements, the nonradiative recombination process in GaN will be shown to be governed by certain defects introduced with the incorporation of Ga vacancies. From the extremely short positron diffusion lengths and short radiative lifetimes of excitonic emissions, we conclude that hole capturing by localizing valence states associated with atomic condensates of In-N outrun the capturing by the nonradiative recombination centers in In-containing alloys.

11:30 AM

**GG2, Luminescence Lifetime in the Vicinity of Threading Dislocations on Bulk GaN Studied by Picosecond Time Resolved Cathodoluminescence (pTRCL):** *Samuel Sonderegger*<sup>1</sup>; Jelena Ristic<sup>1</sup>; Pierre Corfdir<sup>1</sup>; Eric Feltin<sup>1</sup>; Nicolas Grandjean<sup>1</sup>; Benoit Deveaud<sup>1</sup>; Jean-Daniel Ganière<sup>1</sup>; <sup>1</sup>EPFL

In order to enlighten the role of threading dislocations (TDs) on luminescence properties of GaN and nitride based heterostructures, radiative and non-radiative lifetimes in the vicinity of and on TDs have been studied by recently demonstrated picosecond time resolved cathodoluminescence (pTRCL) both in bulk GaN and InGaN/GaN quantum wells. The studied GaN ELOG samples comprise up to 10<sup>7</sup> TDs per cm<sup>2</sup>. Individual TDs resolved at a temperature of 100K by quasi continuous cathodoluminescence appear as correlated dark spots on the surface. First results show a 25% decrease of effective lifetime when changing the excitation spot from a dislocation free zone onto a dislocation (42 ps down to 30 ps). This variation is most probably due to the decrease of the non-radiative lifetime meaning that non-radiative recombination becomes predominant when approaching a dislocation. Ongoing studies by pTRCL on InGaN QW are aimed at quantifying the influence of TDs on luminescence properties.

11:45 AM

**GG3, The Influence of Dislocations on Optical Properties of InGaN-Cathodoluminescence and Transmission Electron Microscopy of Layers Grown on Miscut GaN Substrates:** *Martin Albrecht*<sup>1</sup>; Thilo Remmele<sup>1</sup>; Tadeusz Suski<sup>2</sup>; Gijs Franssen<sup>2</sup>; M. Krysko<sup>2</sup>; B. Lucznik<sup>2</sup>; Izabella Grzegory<sup>2</sup>; Piotr Perlin<sup>2</sup>; Sylwester Porowski<sup>2</sup>; <sup>1</sup>Institut für Kristallzüchtung; <sup>2</sup>Institute of High Pressures Physics 'Unipress', Polish Academy of Sciences

We present results from spectral cathodoluminescence mappings and Z-contrast transmission electron microscopy analysis of MOVPE grown In<sub>x</sub>Ga<sub>1-x</sub>N layers (nominally x=0.1). GaN substrates with miscut from 0.3 to 3 deg were used. CL spectral maps show a terrace structure formed of (0001) and {n1-1m} facets by distinct CL emissions. The (0001) and {n1-1m} facets show CL bands at 3.05 eV and 3.15 eV respectively. According to Z-contrast images the difference in emission is caused by different In contents. With increasing miscut the total area of (0001) facets reduces, with respect to that of {n1-1m} facets leading to a blue shift of the integral CL. Samples grown on dislocation free substrates do not show terraces and a homogeneous CL. We discuss the difference in optical properties as dependent on miscut and dislocations density in terms of dislocation induced step bunching and kinetics In incorporation kinetics into different microfacets.

12:00 PM

**GG4, Relationship between Threading Dislocation and Nonradiative Recombination Centers in Green Emitting InGaN-Based Quantum Wells Studied by Scanning Near-Field Optical Microscope:** *Akio Kaneta*<sup>1</sup>; <sup>1</sup>Kyoto University

Multi-mode scanning near-field optical microscope (SNOM) photoluminescence (PL) and atomic force microscope (AFM) measurements were performed at the same scanning area in green-light-emitting InGaN single quantum well on epitaxially laterally overgrown GaN at room temperature. As the result of AFM measurement, there is a possibility that the misfit dislocations are generated at GaN/InGaN interface, because the threading dislocation density of green sample is larger by one order magnitude than violet and blue sample. Additionally, the SNOM mapping revealed that the weak PL domains correspond to threading dislocations, where weak PL was observed in the area emitting at lower energy bands. These results indicate that the carriers are captured easily in nonradiative recombination centers originating from the threading dislocations in the green sample. Therefore, the improvement of crystal quality of InGaN quantum well is important to realize the high luminous efficiency optical devices.

12:15 PM

**GG5, Direct Correlation of Spectral Luminescence with the Spatial Distribution of Threading Dislocations in Green Light Emitting InGaN Quantum Wells:** *Jacob Brooksby*<sup>1</sup>; Jin Mei<sup>1</sup>; Fernando Ponce<sup>1</sup>; <sup>1</sup>Arizona State University

A direct correlation has been established between the spatial variation in monochromatic cathodoluminescence images and the distribution of threading dislocations for a green emitting InGaN quantum well grown on a sapphire substrate. The nature of the QW emission is influenced by the microstructure of the underlying GaN, consisting of low-angle grain boundaries with tilt and twist components surrounded by threading dislocations at the boundaries. A strong correlation is observed between this structure and the peak and low-energy portion of the emission, with threading dislocations as boundaries between bright and darker regions of luminescence. The high-energy portion of the emission is localized and generally complementary to the remaining emission. Cross-section transmission electron microscopy images show that small pits nucleate in the capping layer at threading dislocations, approximately 5-10 nm above the quantum well, and that the quantum well quality is good.

12:30 PM

**GG6, High Sensitivity of Photoluminescence-Excitation Spectroscopy for Probing Effects of Plasma-Induced Surface Damages to Carrier Transports in  $\text{Al}_x\text{Ga}_{1-x}\text{N}/\text{GaN}$  Heterostructures:** *Hideo Takeuchi*<sup>1</sup>; Takeo Shirahama<sup>1</sup>; Yoshitsugu Yamamoto<sup>1</sup>; Yoshitaka Kamo<sup>1</sup>; Tetsuo Kunii<sup>1</sup>; Tomoki Oku<sup>1</sup>; Hiroyasu Tanaka<sup>2</sup>; Masaaki Nakayama<sup>2</sup>; <sup>1</sup>Mitsubishi Electric Corporation; <sup>2</sup>Graduate School of Engineering, Osaka City University

We demonstrate that photoluminescence-excitation (PLE) spectroscopy is applicable to probe effects of plasma-induced surface damages to carrier transports in  $\text{Al}_x\text{Ga}_{1-x}\text{N}/\text{GaN}$  heterostructures, through systematic characterizations of as-grown and plasma-exposed samples. It is found from the characterization of the surface morphology that the plasma exposure remarkably modifies the atomic step boundaries and the pits in the  $\text{Al}_x\text{Ga}_{1-x}\text{N}$  surface. The PLE spectrum of the as-grown sample measured at the energy of the photoluminescence from the GaN layer shows a step rising from the  $\text{Al}_x\text{Ga}_{1-x}\text{N}$  fundamental transition energy, which reflects the photogenerated carrier transport from the  $\text{Al}_x\text{Ga}_{1-x}\text{N}$  layer to the GaN layer, while the rising step disappears in the plasma-exposed sample. In contrast, the reflectance spectra are the same in the two samples; namely, the excitonic transition itself is hardly affected by the plasma exposure. Thus, it is concluded that PLE spectroscopy is highly sensitive to probe the carrier-transport characteristics in the  $\text{Al}_x\text{Ga}_{1-x}\text{N}/\text{GaN}$  heterostructure.

12:45 PM

**GG7, Characterization of Fluorine-Plasma-Induced Deep Centers in  $\text{AlGa}/\text{GaN}$  Heterostructure by Persistent Photoconductivity:** *B.K. Li*<sup>1</sup>; K.J. Chen<sup>2</sup>; K.M. Lau<sup>2</sup>; W.K. Ge<sup>1</sup>; J.N. Wang<sup>1</sup>; <sup>1</sup>Department of Physics, Hong Kong University of Science and Technology; <sup>2</sup>Department of Electronic and Computer Engineering, Hong Kong University of Science and Technology

The fluorine (F) plasma treatment can effectively incorporate fluorine ions in  $\text{AlGa}/\text{GaN}$  heterostructures. The properties of the F-related deep centers are studied by the temperature dependent persistent photoconductivity (PPC) and Hall measurements. Electron mobility of the F-treated sample is almost temperature independent, in contrast to that of un-treated sample. This suggests a change of scattering mechanism due to fluorine induced centers. In comparison with the un-treated sample, a much more pronounced PPC effect is observed for the F-treated sample indicating that the F-related centers are electron traps. The PPC decay follows a stretched exponential function, and an energy barrier of 0.62 eV for electrons' recapture from the 2DEG channel by the F-related centers is determined from temperature dependent PPC decay behavior. Illuminated with 488nm light, the photo-ionization cross section of F-related centers is estimated around  $\sim 10\text{E}-17\text{cm}^2$  at 305K. The configuration coordinate diagram of F-related deep center is obtained.

## Session HH:

### InN: Surface and Electronic Properties

Thursday PM Room: 312/317  
September 20, 2007 Location: MGM Grand Hotel Conference Center

*Session Chairs:* Yasushi Nanishi, Ritsumeikan University; Joel Ager, Lawrence Berkeley National Laboratory

2:30 PM Invited

**HH1, Surface Properties of InN and In-Rich Alloys:** *Tim Veal*<sup>1</sup>; <sup>1</sup>University of Warwick

One of the most striking properties of InN is its extreme surface electron accumulation. Angle-resolved synchrotron radiation photoemission spectroscopy of InN surfaces has been used to map the dispersion of the quantized subbands in the surface potential well, enabling the energies of the subband minima and the subband electron effective masses to be determined. Additionally, using high-resolution x-ray photoemission spectroscopy (XPS), the surface Fermi level, and therefore the surface electron accumulation, has been found to be the same for both In- and N-polarity InN. Core-level XPS of clean InN surfaces indicates termination by In-adlayers: 3.4 ML and 2.0

ML of In on the surface of In- and N-polarity InN, respectively. Based on first principles calculations, the In-In bonds in the surface In-adlayers have recently been associated with the donor-type surface states responsible for the intrinsic electron accumulation. Studies of the surfaces of p-type InN and In-rich alloys are also reported.

3:00 PM

**HH2, Effect of Surface States on Electrical Characteristics of InN and  $\text{In}_{1-x}\text{Ga}_x\text{N}$ :** *Joanne Yim*<sup>1</sup>; R. Jones<sup>1</sup>; K. M. Yu<sup>2</sup>; J. W. Ager<sup>2</sup>; W. Walukiewicz<sup>2</sup>; J. Wu<sup>1</sup>; W. J. Schaff<sup>3</sup>; <sup>1</sup>University of California - Berkeley; <sup>2</sup>Lawrence Berkeley National Laboratory; <sup>3</sup>Cornell University

Surface states are known to pin the Fermi level in InN and  $\text{In}_{1-x}\text{Ga}_x\text{N}$ , strongly affecting charge distribution and transport on the surface and interfaces. By solving Poisson's equation in an electrolyte-based capacitance-voltage measurement configuration, we have calculated the band bending and space charge distribution in this system and developed an electronic model generally applicable to both p- and n-type nitride thin films. Both conduction band non-parabolicity and band renormalization effects due to the high surface electron concentration were included. The calculated space charge distributions, using the majority dopant concentration as a fitting parameter, are in excellent agreement with experimental data. The model quantitatively confirms increasingly strong n-type electrical characteristics on the surface due to electron accumulation in p-type  $\text{In}_{1-x}\text{Ga}_x\text{N}$  for decreasing values of x.

3:15 PM

**HH3, Study on Surface Electron Accumulation on A-Plane InN by Electrolyte-Based Capacitance-Voltage Measurements:** *Mitsuhiko Noda*<sup>1</sup>; Shinji Fukumoto<sup>1</sup>; Daisuke Muto<sup>1</sup>; Kin Man Yu<sup>2</sup>; Nate Miller<sup>2</sup>; Rebecca Jones<sup>2</sup>; Joel Ager III<sup>2</sup>; Eugene Haller<sup>2</sup>; Hiroyuki Naoi<sup>1</sup>; Tsutomu Araki<sup>1</sup>; Yasushi Nanishi<sup>1</sup>; Wladek Walukiewicz<sup>2</sup>; <sup>1</sup>Ritsumeikan University; <sup>2</sup>Lawrence Berkeley National Laboratory

InN is a promising material for applications in long wavelength optical devices and high-speed and high-frequency electrical devices owing to its outstanding material properties. In order to fully utilize the potential of InN, it is important to understand the surface and interface properties of InN. It is well known that an electron accumulation layer exists at the surface of polar C-plane InN, making it very difficult to form a Schottky junction and thus hindering the research and development of this material toward electronic device applications. On the other hand, the absence of the electron accumulation layer was theoretically predicted for non-polar InN surfaces. The experimental results we obtained from electrolyte-based capacitance-voltage (ECV) measurements, however, imply that an electron accumulation layer also exists at the surface of non-polar A-plane InN. We will report these results, and compare them to those obtained from polar C-plane InN grown by MBE under similar conditions.

3:30 PM

**HH4, Control of Electron Concentration in In-Face InN:** *Chad Gallinat*<sup>1</sup>; Gregor Koblmüller<sup>1</sup>; James Speck<sup>1</sup>; <sup>1</sup>University of California at Santa Barbara

We studied the effect of growth conditions and Si- and Mg-doping on the electrical conduction of In-face InN films grown by plasma-assisted molecular beam epitaxy. Growth temperatures in the range of 420°C – 480°C offered control over the electron concentration within the range of  $\sim 2 \times 10^{17} \text{ e/cm}^3 - 2 \times 10^{18} \text{ e/cm}^3$  while maintaining high electron mobilities and optimized structural quality. To achieve electron concentrations higher than  $2 \times 10^{18} \text{ cm}^{-3}$  Si-doping was necessary. Relatively high electron mobilities ( $>1500 \text{ cm}^2/\text{Vs}$ ) were maintained at the lowest Si concentrations while increasing the electron concentration into the low  $10^{18} \text{ cm}^{-3}$  range. To decrease electron concentrations as low as  $3 \times 10^{16} \text{ cm}^{-3}$  Mg-doping was employed to compensate the high UID electron concentrations. Through the use of Mg-doping, variable growth temperature and Si-doping the electron concentration was accurately controlled over the range  $\sim 3 \times 10^{16} \text{ cm}^{-3} - 5 \times 10^{19} \text{ cm}^{-3}$ .

# Technical Program

3:45 PM

**HH5, N-Face InN Multiple Carrier Transport:** *Tamara Fehlberg*<sup>1</sup>; Gregor Koblmüller<sup>2</sup>; Gilberto Umana-Membreno<sup>1</sup>; Chad Gallinat<sup>2</sup>; James Speck<sup>2</sup>; Brett Nener<sup>1</sup>; Giacinta Parish<sup>1</sup>; <sup>1</sup>University of Western Australia; <sup>2</sup>University of California, Santa Barbara

N-face indium nitride samples were grown on C-face SiC substrates via plasma-assisted molecular beam epitaxy using a GaN buffer layer. The temperature (20 - 300 K) and film thickness (500 - 2000 nm) dependence of multiple carrier transport has been measured via multiple magnetic field Hall measurements. Surface and bulk electron properties were extracted using a quantitative mobility spectrum analysis. Bulk electron mobility shows a clear temperature dependence, with a steep increase with temperature up to the peak mobility, a maximum well over 3000 cm<sup>2</sup>/Vs at about 100 K in the thickest samples. Bulk electron concentrations are around  $2 \times 10^{17}$  cm<sup>-3</sup>. Bulk and surface mobilities increase with sample thickness. Surface electron mobilities are over twice those of In-polar InN, with only a slight reduction in surface concentration. The temperature dependence of both bulk and surface mobilities are significantly different to that of all In-polar samples previously studied.

4:00 PM

**HH6, GaN and InN Conduction Band States Studied by Spectroscopic Ellipsometry at Finite Temperatures:** *Christoph Cobet*<sup>1</sup>; Munise Raketel<sup>1</sup>; Christoph Werner<sup>1</sup>; Rüdiger Goldhahn<sup>2</sup>; Norbert Esser<sup>1</sup>; <sup>1</sup>Institute for Analytical Sciences; <sup>2</sup>Technische Universität Ilmenau

We apply spectroscopic ellipsometry in the spectral range between 18-20eV in order to study the conduction bands in GaN and InN. In this spectral range the optical response is defined by excitations of localized core d-electrons to empty states. The imaginary part of the measured dielectric function is thus proportional to the conduction band density of states (DOS) with dominant p-symmetry. Further more, we can assign distinct maxima in dielectric function to specific transitions at high symmetry points in the Brillouin zone. In the presented work we compare e.g. the results for GaN- and InN, which reveal a surprisingly high agreement in respective DOS. A special attention is assigned to temperature effects on the DOS. By comparing the temperature evolution of excitation features measured between 18 and 20eV with those measured among the interband transitions at lower energies, we can study temperature shifts of valence and conduction band states separately.

4:15 PM

**HH7, Conduction Band Nonparabolicity and Band Filling in InN under Hydrostatic Pressure:** *Tadeusz Suski*<sup>1</sup>; Izabela Gorczyca<sup>1</sup>; Gijs Franssen<sup>1</sup>; Agata Kaminska<sup>2</sup>; N. E. Christensen<sup>3</sup>; A. Svane<sup>3</sup>; Andrzej Suchocki<sup>1</sup>; H. Lu<sup>4</sup>; W. J. Schaff<sup>5</sup>; E. Iliopoulos<sup>5</sup>; A. Georgakilas<sup>5</sup>; <sup>1</sup>Polish Academy of Science, Institute of High Pressure Physics; <sup>2</sup>Polish Academy of Science, Institute of Physics; <sup>3</sup>University of Aarhus, Department of Physics and Astronomy; <sup>4</sup>Cornell University, Department of Electrical and Computer Engineering; <sup>5</sup>FORTH, Institute of Electronic Structure and Lasers

The low value of about 0.7 eV of the InN band gap leads (via pronounced interaction between conduction band and valence band) to a low effective electron mass  $m^*$  and a nonparabolic shape of the conduction band. The external pressure causes the band gap to increase and influences the conduction band nonparabolicity. This leads to significant effects of pressure and band filling on  $m^*$  and the photoluminescence (PL) peak energy EPL. This was proved through experimental and theoretical studies. The PL peak pressure coefficient  $dEPL/dp$  is shown to depend on the electron concentration in accordance with ab-initio calculations. It decreases from about 27 meV/GPa to about 21 meV/GPa on the increase of electron concentration from  $3.6 \times 10^{17}$  to  $1.1 \times 10^{19}$  cm<sup>-3</sup>.

4:30 PM Break

## Session II:

### Nanostructures: Characterization

Thursday PM

September 20, 2007

Room: 314/315

Location: MGM Grand Hotel Conference Center

*Session Chairs:* Eun Suh, Chonbuk University; Peter Clifton, Imago Scientific Instruments

2:30 PM

**III, Photoluminescence and Raman Spectroscopy of MBE-Grown InN Nanocolumns:** *Jaime Segura Ruiz*<sup>1</sup>; Núria Garro Martínez<sup>1</sup>; Andrés Cantarero Sáez<sup>1</sup>; Christian Denker<sup>2</sup>; F. Werner<sup>2</sup>; Jörg Malindretos<sup>2</sup>; Angela Rizzi<sup>2</sup>; <sup>1</sup>Instituto de Ciencia de los Materiales. Universidad de Valencia; <sup>2</sup>IV. Physikalisches Institut, Georg-August Universität Göttingen

InN nanocolumns grown by molecular beam epitaxy on p-Si (111) substrates are studied by means of photoluminescence (PL) and micro-Raman spectroscopy. We find that slight variations in the growth conditions can modify the PL energy peak up to 100 meV. An increase in the PL energy also involves a reduction of the integrated intensity. Raman spectra show that, while the E<sub>2h</sub> mode does not change significantly, the A<sub>1</sub>(LO) mode is damped for samples with higher PL energy. Screening effects due to a high electron concentration could explain the attenuation of this polar mode. This overall phenomenology points out the existence of unintentional doping induced by local defects. The temperature and power excitation dependence observed for the PL signal shows clear signatures of localized states. The evolution of the integrated intensity with temperature is well fitted by a model assuming two activation energies, comprised in the 6-10 and 30-50 meV ranges.

2:45 PM

**II2, Time-Resolved Photoluminescence Study of GaN Nanowires Grown by Catalyst-Free MBE:** *John Schlager*<sup>1</sup>; Kris Bertness<sup>1</sup>; Paul Blanchard<sup>1</sup>; Norman Sanford<sup>1</sup>; <sup>1</sup>National Institute of Standards and Technology

We report steady-state and time-resolved photoluminescence (PL and TRPL) measurements on individual GaN nanowires (6 – 20  $\mu$ m long, 30–500 nm in diameter) dispersed onto fused quartz substrates. PL intensity for the longer and thicker wires was higher than that of the shorter wires. The longer (> 12  $\mu$ m) wires displayed a red shift of the dominant donor-bound A exciton emission attributable to the tensile strain induced by differential thermal expansion between the wires and the quartz substrates. The PL lifetimes ranged from 200 ps to over 2 ns, which compare well to those of low-defect bulk GaN. The lifetime dependence on pump intensity, emission wavelength, and temperature and the shapes of the decay curves indicated interesting exciton dynamics. Spatially resolved TRPL showed uniform temporal response across a single wire and varying response along wire complexes. Waveguiding and optically pumped laser action was observed in the longer nanowires.

3:00 PM

**III3, Photocurrent Gain Enhancement in M-Axis GaN Nanowires:** *Hsin-Yi Chen*<sup>1</sup>; Ruei-Shan Chen<sup>2</sup>; Chin-Pei Chen<sup>2</sup>; Li-Chyong Chen<sup>3</sup>; Kuei-Hsien Chen<sup>2</sup>; Ying-Jay Yang<sup>1</sup>; <sup>1</sup>Graduate Institute of Electronic Engineering, National Taiwan University; <sup>2</sup>Institute of Atomic and Molecular Sciences, Academia Sinica; <sup>3</sup>National Taiwan University Center for Condensed Matter Sciences

The photoconductivity (PC) characterization has been done for the different sized GaN nanowires with common long-axis along  $\langle 111 \rangle$  orientations (m-axis) grown by thermal chemical vapor deposition (CVD). The excellent visible-blind and ultraviolet-absorbed performances have been demonstrated for the GaN single nanowire devices. The photocurrent gain, one of the PC parameters determining the photocurrent generation efficiency of a photoconductor, has been estimated and discussed for the individual GaN nanowires. The size-dependent study shows that the GaN nanowires with smaller diameter (d = 40-100 nm) exhibit the ultrahigh gain in the range of  $10^4 - 10^5$ , which are over two orders of magnitude higher than that of the

# Technical Program

bigger nanowire ( $d = 250$  nm) and conventional thin film counterparts. The probable size effect on the photoconductivity due to the different surface band bending in m-axis GaN nanowires is also proposed and discussed as compared to the c-axis nanowires and bulks.

3:15 PM

**II4, Interface Instability in GaN/AlN Multiple Quantum Wells:** *Sylvain Nicolay*<sup>1</sup>; Eric Feltin<sup>1</sup>; Jean-François Carlin<sup>1</sup>; Laurent Nevou<sup>2</sup>; François. H. Julien<sup>2</sup>; Nicolas Grandjean<sup>1</sup>; <sup>1</sup>Ecole Polytechnique fédérale de Lausanne (EPFL), FSB, IPEQ, LASPE; <sup>2</sup>Action OptoGaN, Institut d'Electronique Fondamentale (IEF), Université Paris Sud

Special cares are taken for ultra-fast intersubband transitions (ISBT) in III-nitride semiconductors. The possibility of obtaining ISB devices operating in the telecom range is enabled thanks to the high conduction band offset of GaN/AlN quantum wells (QWs). In this work, the effect of strain on ISB transitions in III-nitride multiple (M) QWs is investigated. Strain dependence is studied by growing heterostructures on both AlN and GaN templates and by varying the overall aluminum content in the structures. We have found that short period GaN/AlN MQWs grown on GaN templates experience critical interface instability that strongly reduces ISBT energies, and even quenches ISBT absorption for ultra thin wells. Thus, we have grown GaN/AlN MQWs on AlN templates and obtained absorption at 0.78 eV, which is the shortest ISB wavelength reported so far for crack-free GaN/AlN MQW structures grown by MOVPE.

3:30 PM

**II5, Biexciton Recombination in High Quality GaN/AlGaIn Quantum Wells:** *Flavian Stokker-Cherugi*<sup>1</sup>; Anna Vinattieri<sup>1</sup>; Eric Feltin<sup>2</sup>; Dobri Simeonov<sup>2</sup>; Jean-François Carlin<sup>2</sup>; Raphaël Butté<sup>2</sup>; Nicolas Grandjean<sup>2</sup>; Massimo Gurioli<sup>1</sup>; <sup>1</sup>University of Florence; <sup>2</sup>EPFL

We report on a clear experimental demonstration of the presence of biexciton recombination in high-quality GaN/AlGaIn QWs, thus opening the way to relevant improvements of the performances of GaN based devices. The samples have been grown by metalorganic vapor phase epitaxy (MOVPE) optimizing the deposition conditions and strongly reducing the Al fluctuations in the barriers. This leads to a photoluminescence (PL) broadening of only 5 meV at  $T = 10$  K for an Al content in the barriers of 5%. The biexciton binding energy is found to be of the order of 9 meV. The recombination kinetics show that the exciton and biexciton components are not thermalized at low temperature allowing to extract the intrinsic lifetime of the two components (which is a novelty with respect to GaAs based nanostructures where biexcitons have been extensively studied).

3:45 PM

**II6, Space Charged Region in GaN and InN Nanocolumns Investigated by Atomic Force Microscopy:** *Merten Niebelschütz*<sup>1</sup>; Volker Cimalla<sup>1</sup>; Oliver Ambacher<sup>1</sup>; Torsten Machleidt<sup>2</sup>; Jelena Ristic<sup>3</sup>; Javier Grandal<sup>3</sup>; Miguel Ángel Sánchez-García<sup>3</sup>; Enrique Calleja<sup>3</sup>; <sup>1</sup>Institute of Micro- and Nanotechnologies, Technische Universität Ilmenau; <sup>2</sup>Department of Computer Graphics Program, Technische Universität Ilmenau; <sup>3</sup>ISOM-Department Ingeniería Electrónica, ETSI Telecomunicación, Universidad Politécnica

High quality InN and GaN nanocolumns of different length and diameter grown by molecular beam epitaxy (MBE) were electrically characterized directly and non-destructive by Atomic Force Microscopy (AFM) as a function of the column diameter. The "exact" column diameter was determined from AFM images by Blind Tip Estimation (BTE) and subsequent image reconstruction in order to avoid artifacts due to the finite AFM tip radius. In GaN the conductivity rise up to a "critical" diameter due to a depletion region at the surface of the nanocolumns and remains constant above. In contrast, the accumulation layer at the surface causes decreasing conductivity in InN nanocolumns with increasing diameter. Thus, the nanocolumn surface acts as the preferential conduction path. These facts prove that there is electron accumulation in as-grown non-polar InN surfaces, according to calculations of the Fermi level pinning in InN.

4:00 PM

**II7, Local Electrode Atom Probe (LEAP®) Analysis of GaN-Based Structures:** *Peter Clifton*<sup>1</sup>; Stephan Gerstl<sup>1</sup>; Mark Galtrey<sup>2</sup>; David Larson<sup>1</sup>; Diane Zhu<sup>2</sup>; Clifford McAleese<sup>2</sup>; <sup>1</sup>Imago Scientific Instruments; <sup>2</sup>University of Cambridge

The use of Atom Probe Tomography (APT) for the atomic-scale analysis of metallic alloys is well established, but the specimen shape and conductivity requirements have typically limited the application of the technique for the analysis of semiconductor materials. With the advent of commercial laser atom probe instruments and the focussed-ion-beam (FIB) lift-out techniques for specimen preparation, LEAP® has developed into a powerful technique for analysis of semiconductor nanostructures. Offering the combination of high spatial resolution (sub-nm in all three dimensions) and chemical sensitivity (~ 10 ppm detection limits), APT is the only technique that can meet the layer-morphology and interface-chemical-diffuseness characterisation requirements necessary for GaN-based quantum well (QW) type structures. The development of this application will be described, key areas such as specimen preparation will be explained and example datasets will be shown. It is found that GaN-type QW structures are well suited to atom probe analysis.

4:15 PM

**II8, Thermal Suppression of Relaxation Bottleneck in a GaN Microcavity:** *Flavian Stokker-Cherugi*<sup>1</sup>; Anna Vinattieri<sup>1</sup>; Marcello Colocci<sup>1</sup>; Fabrice Sémond<sup>2</sup>; Mathieu Leroux<sup>2</sup>; Jean Massies<sup>2</sup>; Ian R. Sellers<sup>2</sup>; Massimo Gurioli<sup>1</sup>; <sup>1</sup>University of Florence; <sup>2</sup>CRHEA-CNRS; <sup>3</sup>University of Buffalo

We present an experimental study aimed to discuss the presence of a phonon bottleneck in a  $\lambda/2$  GaN bulk microcavity at different temperatures. Time resolved measurements show a very fast lifetime (3 ps) suggesting a major role of non-radiative channels in the polariton recombination kinetics. In order to determine the presence of a relaxation bottleneck, angular photoluminescence (PL) measurements were performed at different temperatures for large negative detuning. At low T the PL shows a marked maximum, at the angle corresponding to the resonance between the exciton and the photon modes, which is an experimental demonstration of the presence of a relaxation bottleneck. Thus, a strong relaxation bottleneck is observed at low T in our microcavity. Suppression of the bottleneck is found when increasing the temperature, denoting a very strong polariton-phonon scattering, also in connection with the very short exciton lifetime.

4:30 PM Break

---

## Session JJ:

### Optical Characterization of Alloys and MQWs

Thursday PM  
September 20, 2007

Room: 313/316  
Location: MGM Grand Hotel Conference Center

*Session Chairs:* Bo Monemar, Linköping University; Shigefusa Chichibu, Tohoku University

---

2:30 PM

**JJ1, In-Situ Control of AlGaIn and InGaIn Composition by Single Beam Deflectometer:** *Mikhail Belousov*<sup>1</sup>; Steve Ting<sup>1</sup>; Aniruddh Parekh<sup>1</sup>; Alex Gurary<sup>1</sup>; William Quinn<sup>1</sup>; <sup>1</sup>Veeco TurboDisc Operations

In-situ optical deflectometry provides the ability to measure wafer curvature changes due to layer-to-layer lattice and thermal expansion mismatch, substrate temperature gradients, layer doping concentration, and nucleation conditions. We have performed a detailed in-situ stress study of InGaIn and AlGaIn bulk layers and InGaIn multiple quantum wells as a function of composition and layer thickness. Using a Veeco Single Beam Deflectometer with a curvature resolution of  $\sim 0.1$  km<sup>-1</sup> we demonstrate that InGaIn composition can be measured with accuracy up to  $\sim 0.2\%$ . Since curvature change during epilayer growth is proportional to epi-layer thickness and substrate lattice mismatch, we propose that in-situ curvature measurement

# Technical Program

may be used in lieu of ex-situ X-ray diffraction (XRD) measurement in order to improve run-to-run wavelength repeatability for the manufacture of blue and green InGaN LEDs.

**2:45 PM**

**JJ2, Direct Observation of Indium Compositional Fluctuation in GaInN/GaN Multi-Quantum Wells Using an X-Ray Micro-Beam of the 8-GeV Storage Ring:** *Takao Miyajima*<sup>1</sup>; Shigeaki Uemura<sup>1</sup>; Yoshihiro Kudo<sup>1</sup>; Yasuko Terada<sup>2</sup>; Noriyuki Fuutagawa<sup>1</sup>; <sup>1</sup>Sony Corporation; <sup>2</sup>Japan Synchrotron Radiation Institute

GaN-based optical devices demonstrate high external quantum efficiency even though there are threading dislocations with high density of  $10^8$ - $10^{10}$  cm<sup>-2</sup>. This unusual situation can be explained by a model related to indium compositional fluctuation. In this model, the indium composition at any threading dislocation is lower than in the surrounding region. Although this model is supported by time-resolved PL and SNOM results, there are few reports of the direct observation of the indium composition around threading dislocations. We succeeded to observe the amount of indium contents' fluctuation in a  $50\mu\text{m} \times 30\mu\text{m}$  region of annealed Ga<sub>0.9</sub>In<sub>0.2</sub>N/GaN MQWs by measuring the indium's fluorescent x-ray excited by a  $1.3\mu\text{m} \times 3.8\mu\text{m}$  x-ray micro-beam. In the mapping, there are the island-shaped regions which clearly coincide with the low-radiative regions observed by Hg-lamp excited fluorescent microscopy. The indium contents in the island-shaped regions are 20% less than in the surrounding region.

**3:00 PM**

**JJ3, Lattice Polarity Determination for GaN by Modulation Spectroscopy:** *Ryuji Katayama*<sup>1</sup>; Hiroyuki Yaguchi<sup>2</sup>; Kentaro Onabe<sup>1</sup>; <sup>1</sup>University of Tokyo; <sup>2</sup>Saitama University

A novel polarity-determination method for GaN using modulation spectroscopy is demonstrated, which requires only simple optical setups and is a non-destructive investigation. The method is based on the capability of modulation spectroscopy for the assignment of the electric-field direction. Under the usual case of relatively small residual strains and electron densities, a strong spontaneous polarization induces an upward band-bending toward Ga-polar surfaces, and a downward but weaker bending toward N-polar surfaces. The above difference in band profiles between Ga- and N-polarity GaN films grown by rf-MBE could be distinguished in terms of the flip of the spectral phases, utilizing the different modulation mechanisms between photoreflectance and electroreflectance. Further quantitative lineshape analysis revealed that the excitonic contribution for Ga-polar surface is much smaller than the other. It is interpreted as a field-induced exciton dissociation at a high-field region, expected from the band profile derived as a self-consistent solution of Poisson-Schrödinger equation.

**3:15 PM**

**JJ4, Characterization of Pseudomorphic Al<sub>x</sub>Ga<sub>1-x</sub>N Layers on Bulk AlN Substrates:** *Leo Schowalter*<sup>1</sup>; Joseph Smart<sup>1</sup>; Wayne Liu<sup>1</sup>; Robert Bondokov<sup>1</sup>; Ken Morgan<sup>1</sup>; Gregory Garrett<sup>2</sup>; Anand Sampath<sup>2</sup>; Hongen Shen<sup>2</sup>; Michael Wraback<sup>2</sup>; <sup>1</sup>Crystal IS, Inc.; <sup>2</sup>Army Research Laboratory

High Al-concentration Al<sub>x</sub>Ga<sub>1-x</sub>N can be grown on c-face (Al polarity) AlN substrates cut from bulk crystals with threading dislocation densities or order  $10^5$ cm<sup>-2</sup> or less. For this study,  $0.5\mu\text{m}$ -thick Al<sub>0.6</sub>Ga<sub>0.4</sub>N layers were grown on AlN substrates. The FWHM of XRD rocking curves of both the symmetric and asymmetric peaks on the epitaxial layers were typically  $60^\circ$  or less. The layers were pseudomorphically strained to the AlN substrate even though the layer thicknesses exceeded the Matthews-Blakeslee critical thickness by more than an order of magnitude. Photoluminescence showed a peak at about 250nm with a linewidth of 130meV at RT which decreased to ~80meV at 11K while the intensity increased 400 fold. The time-resolved PL showed lifetimes between 100 and 200ps. These results indicate high quality but the low threading dislocation density is not limiting the lifetime allowing other non-radiative decay mechanisms to be studied.

**3:30 PM**

**JJ5, Mechanisms for Enhanced Quantum Efficiency of InGaN Quantum Wells Grown on InGaN Underlayers:** *Mary Crawford*<sup>1</sup>; Daniel Koleske<sup>1</sup>; Nancy Missert<sup>1</sup>; Stephen Lee<sup>1</sup>; Michael Banas<sup>1</sup>; David Follstaedt<sup>1</sup>; Katherine Bogart<sup>1</sup>; Gerald Thaler<sup>1</sup>; Karen Cross<sup>1</sup>; Yong Xia<sup>2</sup>; Christian Wetzel<sup>2</sup>; E. Fred Schubert<sup>2</sup>; <sup>1</sup>Sandia National Laboratories; <sup>2</sup>Rensselaer Polytechnic Institute

Recent reports have demonstrated that the growth of InGaN quantum wells (QWs) on low-temperature InGaN underlayers enables dramatic enhancement of QW photoluminescence (PL). These underlayers (ULs) may impact a range of materials properties, including controlled nucleation of V-defects that interact with overlying InGaN QWs. We have performed spectroscopic studies to elucidate the mechanisms by which ULs enable this striking luminescence enhancement. These studies included analysis of InGaN QWs on ULs of different compositions and thicknesses, as well as different growth temperatures to control V-defect formation. Temperature-dependent and time-resolved PL and cathodoluminescence studies revealed that underlayer composition is a critical parameter, with the addition of only 2.5% indium in the UL providing > 6X enhancement of internal quantum efficiency. Study of QWs on ULs grown at various temperatures further revealed that the decoration of threading dislocations by V-defects is not the dominant mechanism for PL enhancement.

**3:45 PM**

**JJ6, Growth by MOVPE of AlGaIn/GaN Structures with Intersubband Transitions in the 1.2-1.7  $\mu\text{m}$  Region of the Spectrum:** *Matthew Halsall*<sup>1</sup>; Ben Sherliker<sup>1</sup>; Mark Sherwin<sup>2</sup>; Paul Harrison<sup>3</sup>; Peter Parbrook<sup>4</sup>; Tao Wang<sup>4</sup>; <sup>1</sup>University of Manchester; <sup>2</sup>University of California; <sup>3</sup>University of Leeds; <sup>4</sup>University of Sheffield

We report the growth of very small period superlattices of Al<sub>x</sub>Ga<sub>1-x</sub>N/GaN with high aluminium content ( $x=0.7$ ) designed to have intersubband transitions in the wavelength range 1.3-1.55  $\mu\text{m}$ . The sample parameters were calculated using a self-consistent solution, aiming to achieve an e1-e2 transition at 1.54  $\mu\text{m}$ . In order to achieve large intersubband energies via MOVPE growth a high aluminium content was adopted and very thin 1 nm-1.2 nm thick GaN layers were attempted. Infrared absorption measurements show clear intersubband transitions at 1.5  $\mu\text{m}$ . The absorption lines are significantly narrower than those reported by other groups. The improved growth quality allows the observation of the e1-e3 transition at 1.18  $\mu\text{m}$ , the shortest wavelength intersubband transition yet reported. The application of such transitions to ultra-fast communications will be discussed along with the recent improvement of nitride growth technology which makes the realization of a 1.5  $\mu\text{m}$  intersubband laser a real possibility.

**4:00 PM**

**JJ7, Optical Properties of Near Lattice-Matched GaN/AlInN Quantum Wells:** Lay Theng Tan<sup>1</sup>; *Robert Martin*<sup>1</sup>; Kevin O'Donnell<sup>1</sup>; Zhihao Wu<sup>2</sup>; Fernando Ponce<sup>2</sup>; Ian Watson<sup>1</sup>; <sup>1</sup>Strathclyde University; <sup>2</sup>Arizona State University

Al<sub>1-x</sub>In<sub>x</sub>N opens up a wide range of important applications as it covers an extremely large energy gap range and, most importantly, can be lattice-matched to GaN. This work describes a series of near lattice-matched GaN/Al<sub>1-x</sub>In<sub>x</sub>N single quantum wells, grown on both free-standing GaN and sapphire substrates by MOVPE, and studied using photoluminescence spectroscopy and transmission electron microscopy. TEM micrographs confirm the high crystalline quality and reveal the lower quantum well interface to be considerably sharper than the upper one. PL spectra show luminescence originating from the wells, barriers and underlying GaN buffer layers and highlight differences between growth on FS-GaN and sapphire. A near linear dependence of the quantum well transition energy on the well-width is demonstrated to result from intense in-built spontaneous polarisation fields, whose screening is illustrated using power dependent PL measurements. PLE data provide further information on the near lattice-matched Al<sub>1-x</sub>In<sub>x</sub>N barrier layers.

4:15 PM

**JJ8, Luminescence/Excitation Spectra of Eu-Implanted AlGa<sub>x</sub>N:** Ke Wang<sup>1</sup>; Katharina Lorenz<sup>2</sup>; Paul Edwards<sup>1</sup>; Ben Hourahine<sup>1</sup>; Ian Watson<sup>1</sup>; Eduardo Alves<sup>2</sup>; Kevin O'Donnell<sup>1</sup>; Robert Martin<sup>1</sup>; <sup>1</sup>Strathclyde University; <sup>2</sup>ITN, Sacavém, Portugal

Photoluminescence and photoluminescence excitation spectroscopy of europium-implanted Al<sub>x</sub>Ga<sub>1-x</sub>N alloys, over the full composition range from x = 0 to 1, reveal significant changes in the spectral pattern of the main <sup>5</sup>D<sub>0</sub>—<sup>7</sup>F<sub>2</sub> transition. The peak of the Eu spectral multiplet shifts from 621.7 nm for GaN:Eu to 624.4 nm for AlN:Eu. For GaN:Eu, there are two luminescent Eu centres, only one of which can be excited by a broad excitation band lying below the GaN bandgap. Above 16% AlN, the spectral pattern of Al<sub>x</sub>Ga<sub>1-x</sub>N:Eu simplifies and red-shifts. PLE spectra feature the AlGa<sub>x</sub>N band-edges and reveal broad below-gap excitation bands. The PL excited below and above gap has the same spectral pattern. We conclude that the Eu luminescence from AlGa<sub>x</sub>N:Eu is from a single Eu site, analogous to that excited in GaN:Eu by below-gap excitation. A strong influence of the AlN content on the emission intensity of AlGa<sub>x</sub>N:Eu is also described.

4:30 PM Break

## ThP: Poster Session IV

Thursday, 5:00-6:00 PM Room: Prefunction Area  
September 20, 2007 Location: MGM Grand Hotel Conference Center

### ThP: Devices

**ThP1, AlGa<sub>x</sub>N-Based Deep UV Photodiodes with 330 nm Spectral Cutoff:** Thomas Katona<sup>1</sup>; Vinod Adivarahan<sup>1</sup>; Shamima Afroz<sup>1</sup>; Bin Zhang<sup>1</sup>; Asif Khan<sup>1</sup>; <sup>1</sup>University of South Carolina

We report on AlGa<sub>x</sub>N-based deep UV photodiodes that exhibit a gain of 20 under 310 nm illumination. The photodiodes have a peak spectral response at 310 nm with a FWHM of approximately 20 nm. These devices are among the first photovoltaic photodiodes exhibiting gain to be fabricated with an AlGa<sub>x</sub>N active region. Devices were grown on sapphire substrates using pulsed atomic layer epitaxy (PALE), and conventional MOCVD growth. Pulsed AlN buffers and strain management superlattices were grown to reduce the defect density resulting from AlN/sapphire heteroepitaxy and to allow for growth of a thick buffer template of approximately 3.0 μm of Al<sub>0.5</sub>Ga<sub>0.5</sub>N. Circular mesa geometry photodiodes were fabricated with device sizes ranging from 20 μm to 100 μm in diameter. The diodes exhibited room-temperature dark currents below 0.5 picoamps at reverse bias exceeding 20 Volts. The dark current increased gradually above -20 Volts with gain observed at -140 Volts.

**ThP2, AlGa<sub>x</sub>N-Based High Power 280 nm Light Source:** Yuri Bilenko<sup>1</sup>; Alex Lunev<sup>1</sup>; Igor Shturm<sup>1</sup>; Jianping Zhang<sup>1</sup>; Xuhong Hu<sup>1</sup>; Remis Gaska<sup>1</sup>; <sup>1</sup>Sensor Electronic Technology, Inc.

We report our latest results in developing high power deep ultraviolet light sources based on AlGa<sub>x</sub>N LEDs. The sources consisted of multi-chip arrays with up to 64 LED chips integrated with high power packages for efficient heat extraction. Multi-chip arrays were mounted on top of heat sinks with built-in thermo-electrical coolers which allowed extraction of up to 3.5 W of heating power with LED temperature increase less than 40°C. Deep UV sources were tested in CW and pulse operation modes with current pulse widths of 20-40 ns. Sources with peak emission at 282 ± 2 nm wavelength delivered up to 40 mW of CW output optical power at 600 mA current. In pulsed regime the maximum output power was 290 mW at 5.5 A current. This is the highest output power reported for sub-300 nm semiconductor light sources.

**ThP3, Device Self-Heating Effects in Deep UV LEDs Studied by Systematic Variation in Pulsed Current Injection:** Meredith Reed<sup>1</sup>; Michael Wraback<sup>1</sup>; A. Lunev<sup>2</sup>; Y. Bilenko<sup>2</sup>; X. Hu<sup>2</sup>; A. Sattu<sup>2</sup>; J. Deng<sup>2</sup>; M. Shatalov<sup>2</sup>; R. Gaska<sup>2</sup>; <sup>1</sup>Army Research Laboratory; <sup>2</sup>Sensor Electronic Technology, Inc.

SET, Inc. 280nm LEDs were studied under various DC and pulse conditions to demonstrate the impact of self-heating associated with nonradiative recombination on the output power and lifetime of the devices. A reduction in output power occurs as the pulse width and duty cycle are increased. For 1μsec pulse width the output power at saturation current decreases from 30mW to 4mW as the duty cycle is increased from 1% to 50%, while for 100μsec pulse width, the output power at saturation current decreases from 10mW to 3.5mW for the same range of duty cycle. In both cases, the output power at 50% duty cycle approaches that of the DC conditions, indicating that self-heating has a significant impact on the device performance. Lifetime testing at 100mA was performed under DC and pulsed conditions of 100μsec and 1% duty cycle, with half-lives of 20 hours and 1400 hours, respectively.

**ThP4, Double Heterostructure Ultraviolet Light Emitting Diodes with Nanometer Scale Compositionally Inhomogeneous Active Regions:** Anand Sampath<sup>1</sup>; Meredith Reed<sup>1</sup>; Gregory Garrett<sup>1</sup>; Eric Readinger<sup>1</sup>; H. Shen<sup>1</sup>; Michael Wraback<sup>1</sup>; Chris Chua<sup>2</sup>; Noble Johnson<sup>2</sup>; Alexander Usikov<sup>3</sup>; Oleg Kovalenkov<sup>3</sup>; Lisa Shapovalova<sup>3</sup>; Vladimir Dimitriev<sup>3</sup>; <sup>1</sup>US Army Research Laboratory; <sup>2</sup>Palo Alto Research Center; <sup>3</sup>Technologies and Devices International

We report the growth, fabrication and evaluation of double heterostructure UVLEDs operating at wavelengths below 325nm that employ a bulk (80nm) AlGa<sub>x</sub>N active region containing nanoscale compositional inhomogeneities (NCI), deposited by plasma-assisted molecular beam epitaxy. The devices were deposited on AlGa<sub>x</sub>N templates grown by hydride vapor phase epitaxy and containing electron and hole injection layers grown by metalorganic chemical vapor deposition. Wafer level measurements of 324 nm LEDs show an output power of 0.43mW for DC drive current of 100mA, while 310nm LEDs show an output power of 0.12mW under similar bias. Time-resolved photoluminescence decays are consistent with the electroluminescence data. These results are comparable to those of conventional multiple quantum well-based devices, which indicates that polarization fields deleterious to wave function overlap in conventional double heterostructure devices of similar active layer thickness are mitigated in NCI AlGa<sub>x</sub>N.

**ThP5, Dual Band Deep Ultraviolet AlGa<sub>x</sub>N Photodetectors:** S. Aslam<sup>1</sup>; Miko<sup>1</sup>; D. E. Pugel<sup>1</sup>; D. Franz<sup>1</sup>; H. Jones<sup>1</sup>; B. Guan<sup>1</sup>; Jianping Zhang<sup>2</sup>; R. Gaska<sup>2</sup>; <sup>1</sup>NASA/Goddard Space Flight Center; <sup>2</sup>Sensor Electronic Technology

We report on the fabrication and testing of bias-controlled dual band AlGa<sub>x</sub>N-based deep UV back-illuminated photodetectors. A two-terminal n-p-n photo-transistor-like structure consisting of 47% n-AlGa<sub>x</sub>N, 20% p-AlGa<sub>x</sub>N, p-GaN and top contact layer of n-GaN was grown on sapphire substrates by MOCVD. When a forward bias is applied between the top electrode and the bottom electrode, the detectors detect light with wavelength longer than 320 nm (UV-A spectral range) and reject UV-B light with wavelengths in the range from 280 nm to 320 nm. The maximum quantum efficiency in this operation regime is in the range from 320 nm to 360 nm. Under reverse bias these devices detect UV-B and reject UV-A. The maximum quantum efficiency shifts to the spectral range from 280 nm to 320 nm. We will present detailed characterization results of the photodetectors, which can separate UV-A and UV-B using the same pixel by bias switching.

**ThP6, Electrical Properties of GaInN/Si Heterointerfaces:** Rebecca Jones<sup>1</sup>; Joel Ager<sup>2</sup>; Kin Yu<sup>2</sup>; Zuzanna Lilliental-Weber<sup>2</sup>; Darren Yamaguchi<sup>1</sup>; Leon Hsu<sup>3</sup>; Eugene Haller<sup>1</sup>; Wladek Walukiewicz<sup>2</sup>; Josh Mangum<sup>4</sup>; Olga Kryliouk<sup>4</sup>; William Schaff<sup>3</sup>; <sup>1</sup>University of California Berkeley; <sup>2</sup>Lawrence Berkeley National Laboratory; <sup>3</sup>University of Minnesota; <sup>4</sup>University of Florida; <sup>5</sup>Cornell University

Multijunction solar cells employ tunnel junctions to connect the individual cells in series, due to large band offsets. These tunnel junctions typically require formation of heavily doped regions at the heterointerfaces. Thus, there is interest in systems with simplified tunnel junctions. We have found

# Technical Program

that  $\text{Ga}_{1-y}\text{In}_y\text{N}/\text{Si}$  is one such system. With  $y = 0.46$ , there is no band offset between the n-type GaInN and the adjacent p-type Si layers. Further, a two junction GaInN/Si solar cell has a predicted maximum efficiency of 38%, compared to 26% for a single junction Si solar cell with similar assumptions. We present the calculations of the band alignment of such a two-junction solar cell, as well as the estimates of cell efficiency. We then show experimental characterization of films of n-type GaInN grown on (111) p-type Si, including I-V measurements that demonstrate ohmic contact between the layers.

**ThP7, Enhanced Light Extraction Efficiency in Flip-Chip GaN Light-Emitting Diodes with Nanotextured Indium-Tin Oxide/Ag Reflectors:** *Ja-Yeon Kim*<sup>1</sup>; *Min-Ki Kwon*<sup>1</sup>; *Il-Kyu Park*<sup>1</sup>; *Dong-Min Jeon*<sup>2</sup>; *Je Won Kim*<sup>2</sup>; *Yong-Chun Kim*<sup>2</sup>; *Seong-Ju Park*<sup>1</sup>; <sup>1</sup>Gwangju Institute of Science and Technology; <sup>2</sup>Samsung Electro-Mechanics Company

We report on the Ag reflector deposited on nanotextured indium-tin oxide (ITO) in flip-chip light emitting diodes (FCLEDs). The nanotextured ITO was fabricated by wet etching process using a buffered oxide etch (BOE) solution at various ITO etching time of 5, 7, and 10 sec. The FCLED with a nanotextured ITO/Ag reflector etched for 7sec showed an excellent adhesion, thermal property, and higher light-output power of 161.3% at an injection current of 300 mA compared to that with a flat ITO/Ag reflector. This result was attributed to an increase of surface area of nanotextured ITO and increase of probability of reflection of light on the roughened interface between Ag and nanotextured ITO layers.

**ThP8, Enhanced Performance in Ultraviolet Light-Emitting Diodes with Patterned ZnO Transparent Conducting Oxide:** *Jae-Hong Lim*<sup>1</sup>; *Min-Suk Oh*<sup>1</sup>; *Ja-Yeon Kim*<sup>1</sup>; *Dong-Min Jeon*<sup>2</sup>; *Je Won Kim*<sup>2</sup>; *Yong-Chun Kim*<sup>2</sup>; *Seong-Ju Park*<sup>1</sup>; <sup>1</sup>Gwangju Institute of Science and Technology; <sup>2</sup>Samsung Electro-Mechanics Company

The effect of patterned gallium oxide-doped ZnO (GZO) layers on the electrical and optical property of ultraviolet light-emitting diodes (LEDs) is reported. GZO films were deposited on Ni/Au p-type contact layer by pulsed laser deposition, and then the GZO layer was patterned by etching in a 1 wt% HCl aqueous solution. The GaN-based LEDs with patterned GZO layers showed forward voltages similar to Ni/Au p-contact, and this was attributed to that the ohmic contact to p-GaN is mainly formed by Ni/Au p-contact layers. The optical output power of the LED with patterned GZO layers exceeded that of an LED with Ni/Au contact to p-GaN by over 20%. The increase in optical output power of LEDs with patterned GZO layers can be attributed to a small difference of refractive indices between GaN and GZO.

**ThP9, Enhancement of Light Extraction in GaN LEDs Using Photonic Crystals and Index Guiding Layers:** *Kelly McGroddy*<sup>1</sup>; *Aurelien David*<sup>1</sup>; *Michael Iza*<sup>1</sup>; *Elison Matioli*<sup>1</sup>; *Shuji Nakamura*<sup>1</sup>; *James Speck*<sup>1</sup>; *Claude Weisbuch*<sup>1</sup>; *Evelyn Hu*<sup>1</sup>; <sup>1</sup>University of California, Santa Barbara

GaN has become the prominent material for blue-green light emitting diodes (LEDs). The limiting factor to achieving the high efficiencies needed is the external efficiency due to poor extraction of the emitted light from the device. This work has realized the importance of an integrated optimization of the device structure by using 2D photonic crystals (PCs) in-plane and index guiding layers in the vertical direction to emit most of the LED light into specific guided modes which can be efficiently extracted by the PC. To optimize this effect, PC LEDs with PC lattice constants of 185nm to 600nm and depths of 120nm and 250nm have been fabricated on material structures with various thicknesses and compositions of AlGaIn layers. The effects on the emission properties, measured experimentally by angular-resolved electroluminescence will be reported. Additionally, the various processing and design challenges will be discussed along with the electrical characteristics of the devices.

**ThP10, Fabrication and Characterization of Integrated Colloidal Quantum Dot and Porous GaN Structures:** *Seol Back*<sup>1</sup>; *Yong-Hwan Kim*<sup>1</sup>; *Yong-Hoon Cho*<sup>1</sup>; <sup>1</sup>Chungbuk National University

Colloidal quantum dots (QDs) were used on GaN based structure to fabricate white light emitting diodes (LEDs) by using color conversion technique. We investigated optical properties of QDs on different surface shape between nonporous and porous n-type and p-type GaN layers. Porous structure on n-

type and p-type GaN layers was formed by wet etching process. The QDs on each substrate were deposited by spin coating technique. For studying optical properties, photoluminescence and confocal microscope measurements were carried out. Two separated peak of GaN and QDs were clearly found in PL spectra at room temperature. The GaN emission intensity was reduced after deposition of QDs. From the confocal microscope measurement, we found that the QDs emission was uniformed on non-porous surface but the emission was concentrated only pore region on porous surface.

**ThP11, Gallium Nitride LEDs Incorporating Organic Semiconductor Heterojunctions:** *Hyunjin Kim*<sup>1</sup>; *Qiang Zhang*<sup>1</sup>; *Cuong Dang*<sup>1</sup>; *Yoon-Kyu Song*<sup>1</sup>; *Arto Nurmikko*<sup>1</sup>; <sup>1</sup>Brown University

We have investigated the physical integration of organic thin film semiconductors with GaN-based device structures, to explore new types of "hybrid" heterojunction device structures. In particular, planar hybrid nitride-organic junctions have been shown to be quite versatile in enabling charge injection and excitation transfer across the two very different electronic material constituents. In one device configuration, we have replaced the conventional thermally processed p-type metallization contact to a blue InGaIn MQW LED by an organic hole injector layer,  $\alpha$ -NPD, deposited on the nitride device structure at room temperature. The L-I-V characteristics of the LED are nearly comparable to those of a fully inorganic reference device, with current densities up to about 20 A/cm<sup>2</sup>. The rationale for these types of structures is the monolithic integration to nitride devices of complementary organic devices, such as for compact biosensors.

**ThP12, GaN Vertical n-p Junctions Prepared by Si Ion-Implantation:** *Martin Kocan*<sup>1</sup>; *Gilberto Umama-Membreno*<sup>1</sup>; *Felix Recht*<sup>2</sup>; *Azlan Baharin*<sup>1</sup>; *Nicholas Fichtenbaum*<sup>2</sup>; *Lee McCarthy*<sup>2</sup>; *Stacia Keller*<sup>2</sup>; *Roberto Menozzi*<sup>1</sup>; *Umesh Mishra*<sup>2</sup>; *Giacinta Parish*<sup>1</sup>; *Brett Nener*<sup>1</sup>; <sup>1</sup>School of Electrical, Electronic and Computer Engineering, University of Western Australia; <sup>2</sup>Department of Electrical and Computer Engineering, University of California, Santa Barbara; <sup>3</sup>Department of Information Technology, University of Parma

We report on vertical n-p junctions formed on p/p' GaN layers by silicon ion-implantation. Post-implantation damage removal was performed by annealing the samples at 1260°C in N<sub>2</sub>/NH<sub>3</sub> ambient. In devices with a vertical n-p junction topology, light emission under forward bias conditions was observed near the periphery of the n-contact region confirming existence of a n-p junction and indicating that carrier transport across the junction occurs predominantly in the vicinity of the device periphery. Thus, the rectifying behaviour observed in current-voltage measurements is associated with the n-p junctions formed by ion-implantation. The electrical-characteristics of the n-p diodes does not seem to be limited by the quality of the implanted junction but rather by the high spreading resistance of the underlying p' contact layer. The role of this layer was to facilitate contact to the buried n-p junction, however, further optimisation is obviously necessary in order to decrease the sheet resistance.

**ThP13, Improvement of GaN-Based LED with SiO<sub>2</sub> Photonic Crystal on an ITO Film by Holographic Lithography:** *Hsi-Hsuan Yen*<sup>1</sup>; *Hao-Chung Kuo*<sup>1</sup>; <sup>1</sup>National Chiao Tung University

GaN-based light-emitting diode (LED) with SiO<sub>2</sub> photonic crystal (PhC) made by holographic lithography on an indium-tin-oxide (ITO) film was fabricated. The PhC made on SiO<sub>2</sub> but an ITO film improves the light extraction efficiency of the GaN-based LED and prevents from increasing the resistance of the ITO film. Fig. 1 shows the schematic diagram of the GaN-based LED structure with SiO<sub>2</sub> PhC on an ITO film and Fig. 2 shows the SEM photograph of the SiO<sub>2</sub> PhC. It was found that the forward voltage at 20 mA of the GaN-based LED with SiO<sub>2</sub> PhC on an ITO film was 1.9% higher than the GaN-based LED with an ITO film only. In Fig. 3, it was found that the output power of GaN-based LED with SiO<sub>2</sub> PhC on an ITO films was 26.5% and 125.3% higher than GaN-based LED with an ITO or Ni/Au film only, respectively.

**ThP14, Improvement of Light Extraction Efficiency in GaN-Based LED by Patterning p-GaN Using Silica Colloid Mask:** Jeong Woo Park<sup>1</sup>; Jeong-Ho Park<sup>1</sup>; Hye-Yeong Koo<sup>1</sup>; Ja-Yeon Kim<sup>1</sup>; Dong-Yu Kim<sup>1</sup>; Ho-Young Song<sup>2</sup>; Je Won Kim<sup>2</sup>; Yon-Chun Kim<sup>2</sup>; <sup>1</sup>Gwangju Institute of Science and Technology; <sup>2</sup>Samsung Electro-Mechanics Company, Ltd.

Two-dimensional silica colloidal mask was used to etch p-GaN surface to improve the light extraction efficiency of GaN LEDs by randomly patterning p-GaN surface. By treating the p-GaN surface with polyelectrolyte, mono layer silica colloids with 500nm in diameter could be uniformly distributed on the 2-inch p-GaN wafer. The patterns were produced on the p-GaN by using a plasma etching process with Ar/Cl<sub>2</sub>/He plasma source gases. LED samples with etching depth of 150nm and 230nm were fabricated on p-GaN and output power was measured with chip-probing. The increase of optical output power of 3% and 7% was observed for etching depth of 150nm and 230nm, respectively compared to a reference sample without patterns on p-GaN surface. These results show that the two-dimensional silica colloidal template can be used to provide random patterns on p-GaN for high-efficiency GaN-based LEDs.

**ThP15, InGaN-Based LED with Low Efficiency Droop at High Operation Current Density:** Yun-Li Li<sup>1</sup>; Yi-Ru Huang<sup>1</sup>; <sup>1</sup>National Taiwan University

For last few years, there have been a lot of progresses on nitride based light-emitting diodes (LEDs), especially InGaN/GaN LEDs with multiple-quantum-well (MQW) structures as active region emitting visible spectrum. However, for InGaN/GaN LEDs, there is a very well-known fundamental problem of efficiency “droop” - the reduction in an LED’s efficiency as its drive current is increased. In this research, InGaN-based blue light-emitting diodes (LEDs) with different multiple quantum well (MQW) structures and growth conditions on c-plane sapphire substrates are investigated. It is observed that the droop effect can be drastically reduced with design of MQW structures, especially the width of wells and barriers of MQWs. For example, performance of external quantum efficiency (EQE) of LEDs is improved at high current densities with thicker wells for MQW structure. Results of temperature-dependent efficiency experiments and current-voltage (I-V) measurements will be further discussed.

**ThP16, InGaN/GaN Light Emitting Diode with R-Plane Polygonal Facet Deflectors:** Hyunggu Kim<sup>1</sup>; Min Gyu Na<sup>1</sup>; Hyuu Kyu Kim<sup>1</sup>; Hee Yun Kim<sup>1</sup>; Jae Hyoung Ryu<sup>1</sup>; Tran Viet Cuong<sup>1</sup>; Chang-Hee Hong<sup>1</sup>; <sup>1</sup>Chonbuk National University

A new concept of InGaN/GaN light emitting diodes embedded periodic deflector structure (PDE-LED) were proposed and grown on sapphire substrate with SiO<sub>2</sub> hexagonal patterned mask by using selective metal-organic chemical deposition. The artificial inverted polygonal pyramids (AIPs) were formed on masked areas and showed the {1-102} R-plane polygonal facet of 57° against {0001} c-axis, which can be used as deflector. The designed more than two hundred AIPs are periodically distributed and revealed the superior capability for enhancing the light extraction efficiency. It is because the AIPP deflector structure can provide photons multiple chances to escape from the LED side wall, contrary to rectangular conventional LED, which is confirmed by electro-luminescence optical microscope photograph inside AIPP over the (0001) surface area.

**ThP17, Integration of a Matrix Addressable Blue/Green LED Array with Multicore Imaging Fiber for Spatio-temporal Excitation in Endoscopic Biomedical Applications:** Heng Xu<sup>1</sup>; Kristina Davitt<sup>1</sup>; Yoon-Kyu Song<sup>1</sup>; Wei Dong<sup>1</sup>; Carlos Aizenmann<sup>1</sup>; Arto Nurmikko; Hyunjin Kim<sup>1</sup>; <sup>1</sup>Brown University

We have developed a micro-scale endoscopic optical image projection device, integrating an InGaN MQW two-dimensional (2D)-LED array to a multicore imaging fiber. A scalable matrix addressing scheme was used for the electrical access to individual elements in the densely packed 2D-LED array. A prototype 10×10 element array was fabricated by specialized device process flow, using deep reactive ion etching and polyimide etch-back processes for device isolation and planarization. Individual elements of the array have been operated under cw current injection up to a few kA/cm<sup>2</sup>, suggesting uncompromised performance and robustness of the device. The array was butt-coupled to a 30,000-pixel multicore image fiber to generate a

spatio-temporal pattern of light at the output end of the fiber. As application demonstration, selected illumination patterns have been projected to the retina of *Xenopus laevis* tadpoles in studies of their developing visual system, as well as optically excitable neural cells in the brain.

**ThP18, Narrow-Band Photodetection Based on M-Plane GaN:** Sandip Ghosh<sup>1</sup>; Carlos Rivera<sup>2</sup>; Jose Pau<sup>2</sup>; Elias Munoz<sup>2</sup>; Oliver Brandt<sup>3</sup>; Holger Grahm<sup>3</sup>; <sup>1</sup>Tata Institute of Fundamental Research; <sup>2</sup>Universidad Politecnica de Madrid; <sup>3</sup>Paul Drude Institute for Solid State Electronics

Rapid identification of a range of hazardous airborne biological and chemical agents requires simultaneous detection at several specific wavelengths, and consequently a set of photodetectors with very narrow band spectral responsivity. We demonstrate an ultraviolet photodetection configuration with a detection bandwidth limited to a few nanometers. It consists of a polarization-sensitive planar Schottky photodetector and a filter, both made from a strained M-plane GaN film on LiAlO<sub>2</sub>(100) substrate, grown using molecular-beam epitaxy. The optical band gap of the film depends on the orientation of the linear polarization of the incident light relative to the c-axis of GaN, which lies in the film plane. An orthogonal alignment of the c-axis of the photodetector and the filter produces a detection system with a peak responsivity at 360 nm and a bandwidth of 6 nm. Electronic-band-structure calculations show that the anisotropic in-plane strain is the crucial parameter a high responsivity and polarization contrast.

**ThP19, Ohmic Formation Mechanism of Ag(Cu) Alloy Contact on p-Type GaN:** Jun Ho Son<sup>1</sup>; Gwan Ho Jung<sup>1</sup>; Yun Goo Kim<sup>2</sup>; Changyeon Kim<sup>2</sup>; Yeo Jin Yoon<sup>2</sup>; Jong-Lam Lee<sup>1</sup>; <sup>1</sup>POSTECH; <sup>2</sup>Seoul Optodevice Co., Ltd.

Ag-based reflective ohmic contacts are widely used due to its high reflectance (>95%) and low contact resistivity. However, annealing in oxygen ambient causes Ag to be oxidized and/or agglomerated, leading to degradation in both electrical and optical properties. In this work, we present the ohmic formation mechanism of Ag(Cu) alloy contacts on p-type GaN. After annealing at 400°C for 1min in air ambient, Ag(Cu) contact showed minimum contact resistivity of ~10-6Ωcm<sup>2</sup>. However, Ag contact showed minimum contact resistivity of ~10-5Ωcm<sup>2</sup> at 300°C. SRPES results showed that the increase of metallic Ga bonds was significant in Ag(Cu) contact, resulting in lower contact resistivity than Ag contact. HRXRD revealed that Cu atoms disturb the migration of Ag atoms, preventing Ag agglomeration. Additionally, Ag(Cu) contact show good surface morphology than Ag contact. Thus, agglomeration suppression effect caused by the addition of Cu results in the good contact resistivity and smooth surface morphology.

**ThP20, Optical and Magnetic Properties of Fe-Doped GaN Magnetic Semiconductors Prepared by MOCVD Method:** Xiu Xiangqian<sup>1</sup>; Tao Zhikuo<sup>1</sup>; Xie Zili<sup>1</sup>; Han Ping<sup>1</sup>; Zhang Rong<sup>1</sup>; <sup>1</sup>Nanjing University

Fe-doped GaN thin films have been grown on c-sapphires by metal organic chemical vapor deposition. Crystalline quality and phase purity were confirmed by X-ray diffraction and Raman scattering measurements. No detectable second phases were formed during the growth. Fe-related optical transitions were observed in photoluminescence spectra. Magnetic measurements revealed the films are ferromagnetic with Curie temperature T<sub>c</sub> above room temperature. The ferromagnetism may come from carrier-mediated Fe-doped GaN diluted magnetic semiconductors or tiny iron clusters and Fe-N compounds which we have not detected.

**ThP21, Optical Properties of InGaN/GaN MQW Microdisk Arrays on GaN/Si(111) Template:** Kang Jea Lee<sup>1</sup>; Tae Su Oh<sup>1</sup>; Eun-Kyung Suh<sup>1</sup>; Kee Young Lim<sup>1</sup>; <sup>1</sup>Chonbuk National University

Specifically, total internal reflection gives rise to low loss whispering gallery modes (WGM), which propagate along the periphery of disk. Small volumes and high Q-factors of WGMs result in enhancement of optical resonance. It has been expected that GaN microdisk on Si structure can confine light strongly in microdisk cavity, because of the large discontinuity in refractive index at boundary between the cavity and surrounding air. In this work, we report the fabrication of InGaN/GaN MQW microdisk arrays on Si(111) substrates. InGaN/GaN MQWs were grown on GaN on Si(111) templates by MOCVD. The ~50 μm diameter microdisk resonators were fabricated using a combination of optical lithography and a dry etching process by ICP etcher

# Technical Program

and Si undercut etching by acid chemical solution. The evidence of WGMs in optically pumped microdisk cavities, which some interesting features such as kink spectra, have been observed at room temperature photoluminescence.

**ThP22, Performance of AlInGaN 310 nm LEDs over Laterally Overgrown AlN:** Jianping Zhang<sup>1</sup>; Rakesh Jain<sup>1</sup>; Xuhong Hu<sup>1</sup>; Yuri Bilenko<sup>1</sup>; I. Shturm<sup>1</sup>; A. Lunev<sup>1</sup>; M. Shatalov<sup>1</sup>; J. Yang<sup>1</sup>; R. Gaska<sup>1</sup>; <sup>1</sup>Sensor Electronic Technology

We report on AlInGaN 310 nm light emitting diodes (LEDs) deposited on epitaxial laterally overgrown AlN templates. High quality fully coalesced 16  $\mu\text{m}$  thick AlN template layers were overgrown over grooved AlN deposited on c-plane sapphire substrates using combination of MOCVD and Migration Enhanced MOCVD techniques. Standard lateral geometry LED devices were fabricated and flip-chip packaged onto TO-39 headers. CW output power of devices was 0.6 mW at 20 mA which is comparable to our standard 310 nm LEDs on sapphire. Initial 150 hour lifetime testing on-wafer and fully packaged devices showed that LEDs on overgrown AlN were significantly more stable than standard devices on sapphire. Additional peak at 340-350 nm appeared in the ELOG LED structure, which we attribute to the ELOG coalescent boundary defects. Detailed materials and device characterization data will be presented.

**ThP23, Photoluminescence Characteristics of GaAsSbN/GaAs (N: 0-2.5%) Single Quantum Well Structures and Light Emitting Diode:** Kalyan Nanna<sup>1</sup>; S. Iyer<sup>1</sup>; Jia Li<sup>1</sup>; W. Collis<sup>1</sup>; <sup>1</sup>North Carolina A&T State University

In this work, we present a systematic study on the variation of structural and optical properties of GaAsSbN/GaAs single quantum wells (SQWs) as a function of nitrogen concentration. These QW layers were grown by solid source molecular beam epitaxial (MBE) technique and were in-situ annealed in As ambient. A high photoluminescence (PL) peak energy reduction of 325 meV (N~1.4%) in the GaAsSbN QWs was observed with respect to the reference GaAsSb QW. The temperature dependence of the PL in these QWs exhibited S-curve behavior, a signature of localized excitons. The less pronounced S-curve in temperature dependence, smaller blue-shift in excitation dependence and more symmetric line-shape with increasing N indicate the good quality of the layers. In-situ annealing in the As ambient yielded layers of better quality even at higher N concentrations, contrary to the commonly observed behavior in the dilute nitrides. Light emitting diodes of GaAsSbN/GaAs SQW exhibited a room temperature electroluminescence (EL) peak at 1.61  $\mu\text{m}$  with an output power of 1 mW for 30 mA forward current. The diode exhibited a low turn-on voltage of ~500 mV with an abrupt reverse break-down voltage of 7.5 V. Detailed study of I-V characteristics, output power and EL spectra and its temperature dependence as a function of the forward current will be presented.

**ThP24, Quaternary InAlGaIn Quantum-Dot UV-LED Emitting at 335nm Fabricated by Anti-Surfactant Method:** Hideki Hirayama<sup>1</sup>; Sachie Fujikawa<sup>1</sup>; <sup>1</sup>RIKEN

We succeeded in the fabrication of quaternary InAlGaIn quantum dots (QDs) by using anti-surfactant method and demonstrated 335nm current injection emission of the quaternary InAlGaIn-QD ultraviolet (UV) light-emitting diodes (LEDs). The InAlGaIn-QD UV-LED was fabricated on high-quality AlN/AlGaIn buffer template directly grown on sapphire substrate by low-pressure metal-organic chemical-vapor deposition (MOCVD). Quaternary InAlGaIn-QDs were formed on the InAlGaIn buffer surface treated by silicon anti-surfactant. Self-assemble InAlGaIn QDs with the lateral size of 10-20 nm and the height of 5-8 nm were successfully grown on InAlGaIn surfaces observed from the AFM images. We observed intense photoluminescence (PL) from the InAlGaIn QDs with the wavelength at around 335nm at room temperature (RT). We obtained current injection emission from the InAlGaIn-QDs (335 nm) of the InAlGaIn-QD UV-LED under RT CW operation. The output power would be much improved with the increase of QD density and the increase of electron injection efficiency.

**ThP25, Radiative Dipole Orientation in InGaN Grown on GaN(0001):** Gerd Mueller<sup>1</sup>; Nathan Gardner<sup>1</sup>; Anneli Munkholm<sup>1</sup>; Michael Krames<sup>1</sup>; <sup>1</sup>Philips Lumileds Lighting

The distribution of radiative dipoles in active layers of c-plane grown InGaN/GaN light emitting devices (LED) strongly influences light extraction, which in turn controls the overall efficiency. The polarization of light emission from the active layer was measured in a suitable geometry using imaging polarization spectroscopy for a large variety of samples ranging from multiple quantum wells, electrically driven, to thick photo-excited pseudomorphic InGaN layers. By carefully avoiding scattered depolarized light, consistently high degrees of polarization were observed, indicating light emission from in-plane dipoles only. The generality of the finding can be explained by assuming that the near gap band structure of InGaN pseudomorphic to GaN(0001) does not allow for appreciable oscillator strength of perpendicular dipoles. As a consequence the extraction efficiency through the (0001) surface is a factor of 1.5x higher than often assumed (i.e., case of isotropic emission).

**ThP26, Stimulated Emission from Ultra-Thin In-Rich In<sub>0.7</sub>Ga<sub>0.3</sub>N/GaN Multiple Quantum Wells Grown by Metalorganic Chemical Vapor Deposition:** Hee Jin Kim<sup>1</sup>; Ho-Sang Kwack<sup>2</sup>; Sung-Hyun Park<sup>1</sup>; Suk Choi<sup>1</sup>; Keon-Hun Lee<sup>1</sup>; Yong-Hoon Cho<sup>2</sup>; Euijoon Yoon<sup>1</sup>; <sup>1</sup>Seoul National University; <sup>2</sup>Chungbuk National University

We present the results of a systematic photoluminescence (PL) study of ultra-thin In-rich In<sub>0.7</sub>Ga<sub>0.3</sub>N/GaN multiple quantum well (MQW). 10 K PL spectra were measured for a very broad range of optical excitation power from 0.1 mW up to 1 kW. Spontaneous emission at 390 nm did not shift with increasing pumping power over 7 order magnitude, indicating that there is negligible quantum confined Stark effect in ultra-thin In-rich InGaN/GaN MQW despite containing 70% indium in InGaN well. To examine the relevance of In-rich InGaN/GaN MQWs to laser applications, optically pumped stimulated emission (SE) experiments were performed at room temperature (RT) in edge emission geometry. When the pumping power density exceeds 1 MW/cm<sup>2</sup>, RT SE from the In-rich InGaN/GaN MQWs was observed at 386 nm at the high energy side of spontaneous emission at 390 nm.

**ThP27, The Effect of Sb Surfactant on the Properties of p-Type GaN:** Min-Ki Kwon<sup>1</sup>; Ja-Yeon Kim<sup>1</sup>; Chu-Young Cho<sup>1</sup>; Il-Kyu Park<sup>1</sup>; Sunwoon Kim<sup>2</sup>; Je Won Kim<sup>2</sup>; Yon-Chun Kim<sup>2</sup>; Seong-Ju Park<sup>1</sup>; <sup>1</sup>Gwangju Institute of Science and Technology; <sup>2</sup>Samsung Electro-Mechanics Company

The effect of Sb surfactant on the properties of p-GaN layer is reported. It was found that the hole concentration was increased and the sheet resistance of Mg-doped p-GaN layer with was decreased with increasing the Sb surfactant. High resolution X-ray rocking curves showed that the structural quality was improved and atomic force microscope images showed that the surface roughness of the p-GaN layer was decreased with increasing Sb surfactant. In addition, the photoluminescence (PL) peak around 450 nm related to the complex of deep donor (VN) and acceptor (MgGa) was reduced by doping Sb surfactant. The improvement of hole concentration in p-GaN layer could be attributed to the improvement of structural quality and the suppression of formation of VN-MgGa by Sb surfactant during the growth of Mg-doped p-GaN.

**ThP28, Via-Hole-Based Vertical GaN Light Emitting Diode:** Hyun Min Jung<sup>1</sup>; Gi Yeon Nam<sup>1</sup>; Byung Kyun Choi<sup>1</sup>; Tae Hee Lee<sup>1</sup>; Hyun Suk Kim<sup>1</sup>; Soo Keun Jeon<sup>1</sup>; Eun Hyun Park<sup>1</sup>; Chang Tae Kim<sup>1</sup>; Doo Jin Bak<sup>1</sup>; <sup>1</sup>EpiValley

Recently, III-nitrides have promoted great advances in LEDs. High efficiency GaN-based LEDs attract great interest for applications such as displays, signals, backlight for Liquid Crystal Display (LCD) and white-light sources. Though many approaches have been carried out to increase the external efficiency, the total light output from these LEDs is still rather low. In this study, we suggest that a vertical GaN-LED has been fabricated on a sapphire substrate with periodic via-holes formed by a laser drilling technique. N-contact metal which was deposited on the backside of sapphire substrate was directly connected with an ohmic metal of n-GaN layer through the via-holes. The via-hole-based vertical GaN-LED demonstrated an optical power improvement up to 12.5% with lower forward operating voltage

compared with a conventional GaN-LED. In addition, this vertical LED showed just 0.8% and 1.5% variation of optical power and operation voltage at the 500 hour reliability test.

## ThP: LED

**ThP29, 245-250nm AlGaIn-Based Deep Ultraviolet Light-Emitting Diodes Fabricated on High-Quality AlN Buffer on Sapphire:** *Hideki Hirayama*<sup>1</sup>; *Tomoaki Ohashi*<sup>1</sup>; *Tohru Yatabe*<sup>1</sup>; *Norihiko Kamata*<sup>2</sup>; <sup>1</sup>RIKEN; <sup>2</sup>Saitama University

We demonstrated 245-250 nm AlGaIn multi-quantum well (MQW) deep ultraviolet (UV) light-emitting diodes (LEDs) on sapphire substrates. High-quality AlN templates were used that was fabricated by using NH<sub>3</sub> pulse-flow multi-layer growth method. We achieved low threading dislocation density (TDD), crack-free AlN buffer with atomically flat-surface and with stable Ga (+c) polarity. The total thickness of AlN buffer was approximately 3.3 μm. The edge and screw dislocation density of AlGaIn layer on AlN template were 3.2×10<sup>9</sup> and 3.5×10<sup>8</sup> cm<sup>-2</sup>, respectively, observed from the cross sectional TEM image. We confirmed flat surface as step-flow mode observed from AFM images. We obtained 250 nm single-peaked emission from the LED under room temperature (RT) pulsed current injection. The maximum output power and external quantum efficiency (EQE) were approximately 20 μW, and 0.001%, respectively. We also demonstrated current injection emission of 245 nm AlGaIn-QW LED.

**ThP30, a-Plane GaN Grown by MOVPE and MBE for Optoelectronic Applications:** *Timo Aschenbrenner*<sup>1</sup>; *Karsten Goepel*<sup>1</sup>; *Carsten Kruse*<sup>1</sup>; *Stephan Figge*<sup>1</sup>; *Detlef Hommel*<sup>1</sup>; <sup>1</sup>Institute of Solid State Physics, University of Bremen

High-quality a-plane GaN layers are very attractive for use in optoelectronic devices to improve the luminescence efficiency in the green and UV spectral region compared to c-plane structures. We report on the growth of a-plane GaN on r-plane sapphire substrates either by MOVPE or MBE. HRXRD ω-scans of the GaN (11-20) reflection have been performed to quantify the structural quality of the material. For a 10 μm thick crack-free GaN layer grown by MOVPE using a two step growth a FWHM of 620 arcsec and 1340 arcsec measured in c- and m-direction, respectively, have been found. These are state of the art values for a-plane GaN grown without lateral overgrowth techniques. For a 600 nm thick GaN-MBE sample using a 20 nm AlN buffer-layer less good FWHM values of 1730 arcsec and 3520 arcsec (c- and m-direction) have been determined. We will discuss AFM, SEM and in-situ RHEED data in detail.

**ThP31, A Microstructural and Compositional Characterization of Low Resistance ITO Based Ohmic Contacts for InGaIn LEDs:** *Joon Seop Kwak*<sup>1</sup>; *K.M. Kang*<sup>1</sup>; *J. W. Seo*<sup>1</sup>; *J. M. Cho*<sup>1</sup>; *M. J. Park*<sup>1</sup>; *Y. J. Yoon*<sup>2</sup>; *S. W. Chae*<sup>2</sup>; <sup>1</sup>Sunchon National University; <sup>2</sup>Samsung Electro-Mechanics

Interfacial microstructure and elemental diffusion of Cu-doped indium oxide (CIO)/ITO ohmic contacts to p-GaN have been investigated using XTEM, XPS, Angle-resolved XPS, and their results are used to interpret the electrical properties. The CIO/ITO contacts yield contact resistivity of ~10<sup>-4</sup> Ωcm<sup>2</sup> and give transmittance higher than 95% at a wavelength of 405 nm when annealed at 630 °C for 1 min. After the 630 °C anneal, it was revealed that new multi-component oxides composed of Ga<sub>2</sub>O<sub>3</sub>-In<sub>2</sub>O<sub>3</sub> and Ga<sub>2</sub>O<sub>3</sub>-CuO were produced at the interface between the p-GaN and ITO. The formation of the new multi-component oxides having a high work function reduced the barrier height, and decreased the contact resistivity of the CIO/ITO contacts to p-GaN. In addition, the formation of the Ga-based oxides caused Ga outdiffusion, followed by the generation of Ga vacancies near the GaN surface. This increased carrier concentration near the GaN surface, and hence reduced contact resistivity.

**ThP32, A Noble Method for Current Spreading Analysis and Electrode Pattern Design in Light Emitting Diodes:** *Sungmin Hwang*<sup>1</sup>; *Jongin Shim*<sup>1</sup>; <sup>1</sup>Hanyang University

In order to analyze current spreading effects 3-dimensionally in InGaIn/GaN multiple quantum well (MQW) light emitting diode (LED), we successfully

developed a new analysis method of modeling (the) LED as 3-dimensional electrical circuit which consists of resistances and intrinsic diodes. Each circuit element was formulated by physically realizable parameters such as structural dimensions and material parameters and its value was obtained experimentally. We measured 2-dimensional light intensity distribution emitted from the surface of a fabricated device and compared with simulated one. They showed an excellently good agreement. The influences of epitaxial layers and electrode pattern geometry on device performances were investigated thoroughly by using our design tool. Based on these preliminary studies, we were able to design and fabricate high-performance LED structures with high power saturation, small power degradation after aging, and high electrostatic discharge (ESD) voltage.

**ThP33, A Novel Chip on Board LED Package Module for LCD Backlight in Car Navigation System:** *Ilku Kim*<sup>1</sup>; *Kilyoan Chung*<sup>1</sup>; *Myoung-Soo Choi*<sup>1</sup>; <sup>1</sup>Samsung Electro-Mechanics

A Novel Chip on Board LED Package Module was studied for LCD Backlight in Car Navigation System. Normally, Car-Navigation System has adopted CCFL backlight unit (BLU), but it has following some problems. So, LED BLU is one of the alternatives of CCFL BLU. But conventional type LED BLU requires more high cost and show low performance in high temperature. In this paper, we have reported a novel type of chip on board (COB) LED package. The enhanced COB module could be reduced up to 13.9 degree at 30mA compared to conventional type. As the result, COB module sample has shown the stable light-output performance after the time degradation test of 30 minutes.

**ThP34, A Novel Technique for Schottky Barrier Reduction to p-Type GaN Layers Using Kelvin Probe Force Microscopy:** *Takashi Hirotsani*<sup>1</sup>; *Tadashi Shimmura*<sup>1</sup>; *Chie Hongo*<sup>2</sup>; *Masaaki Onomura*<sup>2</sup>; <sup>1</sup>Toshiba Corporation, Corporate Manufacturing Engineering Center; <sup>2</sup>Toshiba Corporation, Semiconductor Company

Reduction of contact resistance to p-type GaN layers is important for high-reliability InGaIn/AlGaIn/GaN-based optical devices. It is effective to reduce Schottky barrier height for improving contact resistance and operation voltage. In this paper, we demonstrate the linear correlation between the surface potential difference at p-type GaN contacts and the work function of metals, using Kelvin probe force microscopy (KFM). KFM is a kind of scanning probe microscopy, and can measure the surface potential directly by a non-contact probe in the air. The surface potential difference, corresponding to Schottky barrier height, was estimated by scanning across p-type GaN surface and metal surface. We evaluated several samples of metal (Pd, Ni, Ti or Pt) formed partially on low resistance p-type GaN layers grown by low-pressure metal organic chemical vapor deposition. The mechanism of Schottky barrier height reduction and low resistance p-type electrodes will also be discussed.

**ThP35, AlN MSM and Schottky Deep UV Photodetectors:** *Rajendra Dahal*<sup>1</sup>; *Jing Li*<sup>1</sup>; *Zhaoyang Fan*<sup>1</sup>; *Mim Nakarmi*<sup>1</sup>; *Talal Tahtamouni*<sup>1</sup>; *Jingyu Lin*<sup>1</sup>; *Hongxing Jiang*<sup>1</sup>; <sup>1</sup>Kansas State University

AlN is a promising material for the development of deep ultraviolet (DUV), vacuum UV and extreme UV (EUV) detectors because of its outstanding physical properties. AlN based detectors would overcome many limitations imposed by Si technology. DUV AlN metal-semiconductor-metal (MSM) and Schottky barrier photodetectors have been demonstrated by exploiting the epitaxial growth of AlN epilayer on sapphire and n-SiC substrates, respectively. The fabricated detectors exhibited peak responsivity at 200 nm with very sharp cut off wavelength at 207 nm along with extremely low dark current, very high breakdown voltages, high responsivity and high DUV to UV/visible rejection ratio. Moreover, AlN Schottky barrier detector possesses high responsivity and very high thermal energy limited detectivity at zero bias. These outstanding features are direct attributes of the fundamental material properties and high quality of AlN epilayers. These results demonstrated that AlN epilayers are excellent materials for DUV opto-electronic device applications.

# Technical Program

**ThP36, Azimuthal Anisotropy of Light Extraction from Photonic Crystal Light-Emitting Diodes:** *Chun-Feng Lai<sup>1</sup>; Hao-Chung Kuo<sup>1</sup>; Tien-Chang Lu<sup>1</sup>; Chia-Hsin Chao<sup>2</sup>;* <sup>1</sup>National Chiao-Tung University; <sup>2</sup>Industrial Technology Research Institute

Photonic crystal (PhC) light-emitting diodes (LEDs) exhibiting anisotropic light extraction have been investigated experimentally and theoretically. Images of the anisotropy in the azimuthal direction are obtained using annular structures with triangular lattice shown in Fig. 1. Depending on the lattice constants, 6-fold symmetric patterns with varying number of petals are obtained. Fig. 2 is a diagram to illustrate the regions where patterns with different number of petals are observed. As lattice constants increases, more petals in multiple of 6 appear in the observed image. Pattern with up to 24 petals has been observed with the present setup. The formulas for the boundary of different regions have been derived and are shown in the figure. The present imaging approach provides information important for designing LED.

**ThP37, Bluish-Green Semipolar GaInN/GaN Light Emitting Diode on {1-101} GaN Side Facets:** *Thomas Wunderer<sup>1</sup>; Frank Lipski<sup>1</sup>; Joachim Hertkorn<sup>1</sup>; Peter Brückner<sup>1</sup>; Ferdinand Scholz<sup>1</sup>; Martin Feneberg<sup>1</sup>; Martin Schirra<sup>1</sup>; Klaus Thonke<sup>1</sup>; Andrey Chuvilin<sup>1</sup>; Ute Kaiser<sup>1</sup>;* <sup>1</sup>Ulm University

Bluish-green semipolar GaInN/GaN LEDs were realized on the {1-101} side facets of selectively grown GaN stripes with an on-wafer optical output power of  $240\mu\text{W} @ 20\text{mA}$  for  $\sim 500\text{nm}$  emission wavelength in electroluminescence measurements with a nearly constant efficiency for the investigated current range. Structural investigations using TEM, SEM, HRXRD and AFM have been performed and could be related to the luminescence properties in PL and CL. Similar as in planar semi- and nonpolar GaN, we observed a defect-related luminescence peak at 3.3eV which could be ascribed to stacking faults. Adequate growth conditions allowed to eliminate this class of defects in our facet LED structures. Furthermore, a higher indium incorporation of 22% for these {1-101} facets is found as compared to 14.8% for c-plane growth, what helps significantly to achieve longer wavelength emission in spite of the reduced quantum confined Stark effect in such non- and semipolar materials.

**ThP38, Carrier Dynamics of InGaN/GaN Light-Emitting Diodes with Various Doping Profiles:** *Yun-Li Li<sup>1</sup>; Yi-Ru Huang<sup>1</sup>; Yun-Chong Chang<sup>2</sup>;* <sup>1</sup>National Taiwan University; <sup>2</sup>National Cheng-Kung University

For last few years, there have been a lot of progresses on nitride based light-emitting diodes (LEDs), especially InGaN/GaN LEDs with multiple-quantum-well (MQW) structures as active region emitting visible spectrum. In this work, active region of InGaN/GaN based LEDs with various doping profiles are investigated. Barriers of MQW structures undoped or partially doped with Si are manufactured with metal-organic chemical vapor deposition (MOCVD). Photoluminescence (PL) and time-resolved photoluminescence (TRPL) experiments on these structures reveal very interesting carrier transport mechanisms with different doping profiles. For the measured samples, carrier lifetimes are reduced with increase of doping layers. This can be attributed to the stronger non-radiative recombination near the heavily doped barrier layers. At the same time, PL excitation intensity-varied experiments demonstrate reduced carrier life time with lower PL excitation intensity for partially doped samples. Measurement results will be further discussed.

**ThP39, Characterization of Plasma Damage-Free InGaN/GaN LED with Periodic Deflectors:** *Tran Cuong<sup>1</sup>; Hyung Kim<sup>1</sup>; Min Na<sup>1</sup>; Hyun Kim<sup>1</sup>; Hee Kim<sup>1</sup>; Jae Ryu<sup>1</sup>; Chang Hong<sup>1</sup>;* <sup>1</sup>Semiconductor Physics Research Center

Electrical performances of conventional InGaN/GaN LED devices are often limited by the fundamental problem of plasma damage during inductively coupled plasma process. For instance, the degradation of sidewall contamination along with rough surface morphology of n-GaN, increasing the surface recombination of the injected electron and holes might lead to deterioration of the forward and reverse voltage. Thus, in this study, a mesa-shaped LED structure was grown on n-GaN with SiO<sub>2</sub> mask pattern by using selective MOCVD to eliminate dry etching process. Use of SiO<sub>2</sub> dot pattern inside LED structure can be partially contributed to a flat surface without any edge growth effect, which usually occurred at window edge regions after selective MOCVD growth. Moreover, selective growth

on SiO<sub>2</sub> dot patterning gives inverted polygonal pyramid structures, which were responsible for the guided light deflector. Consequently, the light output intensity was increased about 20% higher than that of conventional-LEDs, while the electrical performance was compatible with those of conventional-LEDs.

**ThP40, Comparative Study of Temperature-Dependent Electroluminescence Efficiency in Blue and Green InGaN Multiple-Quantum-Well Diodes:** *Kenzo Fujiwara<sup>1</sup>; Hiroyuki Jimi<sup>1</sup>; Takayuki Inada<sup>1</sup>; Masaji Horiguchi<sup>1</sup>; Akihiro Satake<sup>1</sup>;* <sup>1</sup>Kyushu Institute of Technology

Origins of the high radiative recombination efficiency in InGaN quantum well light-emitting diodes (LEDs) under influences of high-density misfit dislocations have been receiving much attention. In this paper, the electroluminescence (EL) spectral intensity is comparatively investigated in the c-plane blue and green multiple-quantum-well (MQW) LEDs, fabricated by Nichia, over a wide temperature range ( $T=20\text{-}300\text{K}$ ) and as a function of injection current ( $I=0.01\text{-}10\text{mA}$ ). One striking result of the external quantum efficiency is that its variation pattern with temperature for a fixed current strongly depends on the In content in the active layers. The value is very sensitive to temperature and current level for the blue LED, while less sensitive for the green one. This difference observed between the blue and green MQW-LEDs indicates that the anomalous T dependence of the EL efficiency is caused by interplay of the carrier capture/escape and the internal quantum efficiency.

**ThP41, Comparison of III-Nitride Interband and Intraband Photodetectors Optimized for a Wavelength of 633nm:** *Sindy Hauguth<sup>1</sup>; Vadim Lebedev<sup>1</sup>; Oliver Ambacher<sup>1</sup>;* <sup>1</sup>Technical University Ilmenau

Transparent photodetectors for application in high precision standing wave interferometry operating at the wavelength of He-Ne-lasers (633 nm) were investigated in respect to the sensitivity and temporal response. We report on two concepts of photodetectors having a thickness of the active layers of  $\sim 20\text{nm}$ . The first detector concept is based on the intraband transition of GaN quantum well heterostructures. The second one employs thin In-rich InGaN epilayers for photocarrier generation provided by the direct band-to-band transition. The photodetectors based on the interband transitions in InGaN epilayers showed a  $>20$  times higher absorbance at 633 nm, than those photodetectors based on the intraband transition in the AlN/GaN/AlGaIn heterostructure. However, the temporal response of the latter structure is influenced by the persistence photocurrent adversely affecting performance and operating frequencies.

**ThP42, Effect of AlGaAs Cladding Layer on GaInNAs/GaAs MQW p-i-n Photodetector:** *Yung-Feng Chen<sup>1</sup>; Wei-Cheng Chen<sup>1</sup>; Ricky Chuang<sup>1</sup>; Yan-Kuin Su<sup>1</sup>; Huo-Lieh Tsai<sup>2</sup>;* <sup>1</sup>National Cheng Kung University; <sup>2</sup>Taiwan Semiconductor Manufacturing Company Ltd.

Electric properties of GaInNAs/GaAs multiple-quantum-well (MQW) p-i-n photodetector with AlGaAs cladding layer has been study. By applying a higher band gap Al<sub>0.3</sub>Ga<sub>0.7</sub>As to the photodetector, a substantial reduction in dark current was observed owing to an inherent difficulty for holes to surmount the high potential barrier between MQW and cladding layer heterojunctions under a reversed bias. Dark current obtained was as low as 4.1 pA at -3.5 V for a device with Al<sub>0.3</sub>Ga<sub>0.7</sub>As cladding layer. Photo/dark current contrast ratio obtained were  $4.2 \times 10^4$  and 11 for devices with and without Al<sub>0.3</sub>Ga<sub>0.7</sub>As cladding layer, respectively, at -3.5 V. In addition, peak responsivity of 18 mA was measured at around 1150 nm and two orders of magnitude increase in the rejection ratio was also realized at -2.0 V. We intent to demonstrate the GaInNAs/GaAs MQW p-i-n photodetector with AlGaAs cladding layer potentially could provide high photo/dark current contrast ratio and responsivity rejection ratio.

**ThP43, Effects of Sapphire Substrate Misorientation on the GaN-Based Light Emitting Diodes Grown by Metalorganic Vapor Phase Epitaxy:** *Akiko Nakamura<sup>1</sup>; Naoto Yanagita<sup>1</sup>; Toru Murata<sup>1</sup>; Katsuyuki Hoshino<sup>1</sup>; Kazuyuki Tadamoto<sup>1</sup>;* <sup>1</sup>Yamaguchi University

We have systematically investigated the influence of sapphire substrate misorientation on the structural and optical properties of GaN-based LEDs grown by MOVPE. The LED properties were found to be very sensitive to

the misorientation. We grew five samples of LEDs on sapphire substrates with various misorientation angles ( $\theta = 0.02 \sim 1.0^\circ$ ). The EL intensity increased when  $\theta$  increased to  $0.25^\circ$ . The intensity, however, decreased dramatically when  $\theta$  exceeded  $0.25^\circ$ . We also grew the samples of each layer of the LED, viz., GaN, InGaN, InGaN/GaN MQWs, and p-GaN layer. CL and PL analyses showed that the crystalline quality of InGaN (MQWs) layer became lower while that of GaN layer improved as  $\theta$  increased. In addition, the increased misorientation caused the decreased Indium composition and the Indium compositional fluctuation. Moreover, the hole concentration of p-GaN layer decreased with increasing  $\theta$ . As these results, the misorientation angle of around  $0.25^\circ$  is suitable for the LEDs.

**ThP44, Effects of the p-Electrode Reflectivity on the Extraction Efficiency of Nitride-Based Light Emitting Diodes:** *Jaehye Cho*<sup>1</sup>; Hyunsoo Kim<sup>2</sup>; Yongjo Park<sup>2</sup>; Euijoon Yoon<sup>1</sup>; <sup>1</sup>Seoul National University; <sup>2</sup>Samsung Advanced Institute of Technology

For the realization of solid-state lighting using nitride-based light emitting diodes (LEDs), the achievement of high extraction efficiency of LEDs is crucial. However, it is well known that only a small fraction of photons generated in a GaN LED can escape due to the total internal reflection at the interface between GaN and outer medium. To overcome the intrinsic limitations of the GaN LED structures and to extract more light out from the LED surface, use of high reflectivity electrode is inevitable. First, the dependency of the extraction efficiency on the p-electrode reflectivity is simulated by a point-and-shoot ray tracing method. Secondly, a few p-contact metal schemes having a different reflectance at 400 nm are fabricated, and then the light output on current injection is measured and analyzed.

**ThP45, Enhanced Light Extraction from GaN-Based Green Light-Emitting Diode with Photonic Crystal:** *Ja-Yeon Kim*<sup>1</sup>; Min-Ki Kwon<sup>1</sup>; Il-Kyu Park<sup>1</sup>; Sang Hoon Kim<sup>2</sup>; Ki-Dong Lee<sup>2</sup>; Seong-Ju Park<sup>1</sup>; <sup>1</sup>Gwangju Institute of Science and Technology; <sup>2</sup>LG Electronics Institute of Technology

Recently, the effect of two-dimensional (2D) photonic crystal (PC) has been investigated to enhance the light extraction efficiency of light-emitting diodes (LEDs). However, the effect of PC structures inside and outside photonic bandgap (PBG) on the performance of GaN-based LED has not yet been reported. We report on the GaN-based green LEDs with PC structure inside PBG (PCIG) and outside PBG (PCOG). With decreasing the photoluminescence (PL) detection angle from  $140^\circ$  to  $60^\circ$ , the enhancement of PL intensity of LED with PCIG was largely increased from 9-fold to 25-fold compared to that of LED without patterning structure, while the PL intensity of LED with PCOG was increased from 4.6 to 5.6-fold. The optical output power of green LED with PCIG was enhanced by about 2-fold compared to that of green LED with PCOG. These results suggest that the light extraction of green LED can be greatly increased by using PCIG.

**ThP46, Enhanced Light Extraction from Triangular GaN-Based Light-Emitting Diodes:** *Ja-Yeon Kim*<sup>1</sup>; Min-Ki Kwon<sup>1</sup>; Jae-Pil Kim<sup>2</sup>; Seong-Ju Park<sup>1</sup>; <sup>1</sup>Gwangju Institute of Science and Technology; <sup>2</sup>Korea Photonics Technology Institute

The improvement in light extraction efficiency of GaN based LED is considered to be crucial, and several methods have been proposed to enhance the light extraction of LEDs. However, all these studies were performed on a quadrangular (QDA) LED and other than the QDA LED have not been reported. In this study, the properties of a triangular (TRA) LED are compared with those of a conventional QDA LED. The total radiant flux from the packaged TRA LED, which was grown on patterned sapphire substrate, increased by 48% and 24% at input currents of 20 and 100 mA, respectively, compared to that of a QDA LED. In light far-field beam distribution, the light extraction in the horizontal direction of the LED was much higher than that of the QDA LED due to the enhancement of light emission from the side walls of the TRA LED.

**ThP47, Enhanced Output of GaN-Based UV light-Emitting Diode with  $Ti_3O_5/Al_2O_3$  Distributed Bragg Reflector:** *Tak Jeong*<sup>1</sup>; <sup>1</sup>Korea Photonics Technology Institute

An high reflectivity distributed bragg reflector (DBR) for ultraviolet spectrum is realized by  $Ti_3O_5/Al_2O_3$  multilayer stack. The 4 pair  $Ti_3O_5/Al_2O_3$ ,

DBR has much higher reflectivity than Ag-based omnidirectional reflector (ODR) at a wavelength of 380nm. The electric and optical properties of the DBR-LED are comparable to those LED with ITO/Ag ODR. It is experimentally shown that GaN-based UV LED with  $Ti_3O_5/Al_2O_3$  DBR showed good I-V characteristic and an enhanced optical power compared to that with Ag-based ODR due to the high reflectivity(85% at 380nm).

**ThP48, Enhancement of Light Extraction Efficiency in InGaN Based LED Using Patterned n-GaN Substrate:** *Si-Hyun Park*<sup>1</sup>; Kwang-Woo Kwon<sup>2</sup>; June Key Lee<sup>3</sup>; Sang Wan Ryu<sup>1</sup>; <sup>1</sup>Chosun University; <sup>2</sup>NINEX Company, Ltd.; <sup>3</sup>Chonnam National University

Light extraction efficiency from InGaN-based light-emitting diodes was improved (LEDs) where we patterned n-type GaN layer onto a sapphire substrate with a nano-sized SiO<sub>2</sub> columns. We performed the deposition of an indium tin oxide thin layer on SiO<sub>2</sub> layer and then wet etching, which gave rise to an oxide self-assembled clusters of a few-hundred-nm size. A subsequent SiO<sub>2</sub> etching with the oxide mask results in a SiO<sub>2</sub> columns on n-type GaN Layer. We showed the output power of the patterned n-GaN substrate (PNS) LED was increased a 1.33 time compared to that of the normal LED without n-GaN pattern when a total output power emitted in all direction from the packaging LED was measured under a current injection of 20 mA. The increase of outpour power from PNS-LED depends on the SiO<sub>2</sub> column size onto n-type GaN substrate.

**ThP49, EpiEL Provides Advanced Optical Characterization for Nitride LED Epi-Wafers:** *Max Xianyun Ma*<sup>1</sup>; <sup>1</sup>MaxMile Technologies, LLC

A virtual LED device fabrication and characterization technology, called EpiEL, has been developed to nondestructively measure LED device parameters directly on epiwafers. For nitride LED epiwafers, without any costly and time-consuming device fabrication, EpiEL can be used to not only rapidly map electro-luminescence (EL) and electrical properties of the material, but also simulate different light extraction approaches. Recent investigation indicated that most of current nitride-based LED epiwafers have a non-uniform material structure which leads to different optical observations at epitaxial and substrate sides. A possible material structure deficiency will be discussed during the presentation.

**ThP50, Estimation of Internal Quantum Efficiency in InGaN-Based Light Emitting Diodes Using Electroluminescence Decay Times:** *Shinji Saito*<sup>1</sup>; Tetsuo Narita<sup>2</sup>; Kotaro Zaima<sup>1</sup>; Koichi Tachibana<sup>1</sup>; Hajime Nagao<sup>1</sup>; Gen-ichi Hatakoshi<sup>1</sup>; Shinya Nunoue<sup>1</sup>; <sup>1</sup>Toshiba Corporation; <sup>2</sup>Nagoya University

InGaN-based Light Emitting Diodes (LEDs) have been extensively developed for fabrication of efficient solid-state lighting. Performance of LEDs is defined as the external quantum efficiency, which is the product of injection efficiency, internal quantum efficiency (IQE), and the extraction efficiency. Although the IQE could be analytically determined, few works were reported on the determination method. We investigate the IQE of InGaN-based LEDs from the semiconductor rate equation of pulse current injection. A method is presented for the IQE based on data of electroluminescence decay times measured as a function of current in the pulse injection. For the screening of built-in electric field, the pulse current was injection with bias voltage. For blue LED, the IQE was measured to be about 70%. It is found that the IQE increase with injection current, whereas the external quantum efficiency decreases at high injection.

**ThP51, Exciton Localization in GaN/AlGaIn QW and 340 nm Ultraviolet Light Emitting Diodes:** *Kean Lee*<sup>1</sup>; Peter Parbrook<sup>1</sup>; Tao Wang<sup>1</sup>; Jie Bai<sup>1</sup>; Fabio Ranalli<sup>1</sup>; Qi Wang<sup>1</sup>; Rob Airey<sup>1</sup>; Geoff Hill<sup>1</sup>; <sup>1</sup>University of Sheffield

The optical properties of GaN/AlGaIn quantum wells (QW) and 340 nm ultraviolet (UV) light emitting diodes (LEDs) have been studied by photoluminescence (PL) and electroluminescence (EL). The temperature dependent luminescence from 10 K to 400 K shows a classical 'S-shape' behaviour, attributable to exciton localization from well thickness fluctuations. The localization is found to be excitation intensity/injection current sensitive. As the injection current increases from 5 mA, the value of  $\sigma$ , indicating the degree of localization, gradually decreases from 14 meV until eventually the S-shape behaviour vanishes. We also examine the

# Technical Program

localization behaviour in both cases using a Gaussian distribution localized-state model proposed by Li et al [APL 79, 1810 (2001)] which in principle allows the emission energy at low temperatures (below 77 K) to be modelled. The role of aluminium composition in localization in the QW for deeper UV LEDs is also discussed.

**ThP52, Fabrication of GaN-Based MOS LEDs for Micro Pixels in Flat-Panel Displays:** *Tohru Honda*<sup>1</sup>; *Toshiaki Kobayashi*<sup>1</sup>; *Shigetoshi Komiyama*<sup>1</sup>; *Yoshihiro Mashiyama*<sup>1</sup>; *Masatoshi Arai*<sup>1</sup>; *Kaori Yoshioka*<sup>1</sup>; <sup>1</sup>Kogakuin University

Micro-size integrated light-emitting diodes (LEDs) that operate in the UV spectral region were fabricated using GaN layers grown on sapphire substrates by metal-organic vapor phase epitaxy (MOVPE). Schottky-type (ST) and metal-oxide-semiconductor (MOS) LEDs were realized. The near-band-edge emission of GaN was observed in the electroluminescent spectra with reversed bias under pulsed-voltage conditions. The insertion of an aluminum oxide layer in the GaN-based LED leads to an increase in electroluminescent intensity. The pseudo-heterostructure created by the thermal energy also affected the emission pattern. The refractive index in the emission area was increased with the thermal narrowing. A spotty emission pattern was observed. Here, the light was observed from the sapphire substrate side. No light output was observed from some areas such as at the edge of the device. This result indicates a reduction of light interference in each device during its electrical operation.

**ThP53, Fabrication of GaN-Based UV TF-ELDs by CS-MBE Technique and Their Application to RGB Light-Emitting Pixels:** *Masatoshi Arai*<sup>1</sup>; *Koichi Sugimoto*<sup>1</sup>; *Shinichi Egawa*<sup>1</sup>; *Tohru Honda*<sup>1</sup>; <sup>1</sup>Kogakuin University

Out-door-type large-scale flat-panel displays (FPDs) have been achieved using GaN-based LEDs. However, out-door-type small-scale (personal-use) FPDs require the development of cost-effective light-emitters for their pixels. UV GaN-based thin-film electroluminescent devices (TF-ELDs) operating were fabricated on Al substrates, whose GaN films were deposited by compound-source MBE technique. The pixels were fabricated using the GaN-based TF-ELDs combined with RGB phosphors. In this paper, the emission efficiencies of RGB phosphors in the time of the excitation by the UV TF-ELDs are discussed. Excitation efficiency was estimated by the PLE measurement of the RGB phosphors. The estimated excitation efficiency of the RGB phosphors at 370 nm were 8.3, 6.0 and 2.5%, respectively. The estimated luminance of each emitter is resulted in 3.2, 7.9 and 10.9 kcd/m<sup>2</sup>, respectively. The estimated luminance of the RGB light-emitting pixel is enough to the application for FPDs in comparison with the luminance of typical FPDs.

**ThP54, First All-HVPE Grown InGa<sub>N</sub>/InGa<sub>N</sub> MQW LED Structures for 440-510 nm:** *Alexander Syrkin*<sup>1</sup>; *Vladimir Ivantsov*<sup>1</sup>; *Oleg Kovalenkov*<sup>1</sup>; *Alexander Usikov*<sup>1</sup>; *Vladimir Dmitriev*<sup>1</sup>; *Zuzanna Liliental-Weber*<sup>2</sup>; *Meredith Reed*<sup>3</sup>; *Eric Readinger*<sup>3</sup>; *Michael Wraback*<sup>3</sup>; <sup>1</sup>TDI, Inc.; <sup>2</sup>Lawrence Berkley National Laboratory; <sup>3</sup>U.S. Army Research Laboratory

Development of alternative epitaxial technology and LED structures is extremely important for solid state lighting (SSL) progress. HVPE is known to produce low defect GaN, AlN, and AlGa<sub>N</sub> materials, however InGa<sub>N</sub> HVPE results so far have been limited. In this paper, the first InGa<sub>N</sub>-based blue (440–490 nm) and green (490–510 nm) LEDs grown by HVPE are reported. The structures are based on InGa<sub>N</sub>/InGa<sub>N</sub> multi quantum well (MQW) structures grown by HVPE. Grown InGa<sub>N</sub> MQWs and superlattices were studied by x-ray diffraction and TEM. Extended defects intersecting InGa<sub>N</sub>/InGa<sub>N</sub> structures were not found. These LED structures having “upside down structure” were grown on thick low resistive p-GaN/sapphire templates. Parameters of processed device structures will be presented. Advantages of such device geometry will be discussed. Demonstration of blue and green LEDs by HVPE technology opens a novel avenue for low defect material structures and low cost production technology for SSL application

**ThP55, Growth and Characterization of a Novel Hyperspectral Photodetector Using the III-Nitrides:** *Neeraj Tripathi*<sup>1</sup>; *James R. Grandusky*<sup>1</sup>; *Vibhu Jindal*<sup>1</sup>; *Fatemeh Shahedipour-Sandvik*<sup>1</sup>; *Douglas Bell*<sup>2</sup>; <sup>1</sup>College of Nanoscale Science and Engineering, University at Albany; <sup>2</sup>California Institute of Technology

We report on the growth and characterization of a novel tunable hyperspectral photodetector using the III-nitrides. The proposed structure consists of a stepped triangular barrier of Al(x)Ga(1-x)N multilayer with Al composition between 0% and 100% grown on a GaN/sapphire template. The Al(x)Ga(1-x)N heterostructure forms a triangular potential barrier whereby the height can be tuned by varying the applied voltage. Internal photoemission (IPE) measurements have been carried out to measure the potential barrier faced by the photoexcited carriers. A reduction in potential barrier by 0.65 eV is observed over an applied voltage of 1.3 V, confirming the tunability of detection wavelength. Current-voltage measurements and atomic force microscopy have been used to study the device structure and improve the performance. IPE, I-V and AFM results will be presented along with the principle of device operation, tunability range and device structure optimization parameters.

**ThP56, High-Speed Al(Ga)N/GaN-Based Intersubband Photodetectors at Telecommunication Wavelengths:** *Eva Monroy*<sup>1</sup>; *Fabien Guillot*<sup>1</sup>; *Esther Baumann*<sup>2</sup>; *Fabrizio Giorgetta*<sup>2</sup>; *Daniel Hofstetter*<sup>2</sup>; *Laurent Nevou*<sup>3</sup>; *Maria Tcherynecheva*<sup>3</sup>; *Francois Julien*<sup>3</sup>; *Thilo Remmele*<sup>4</sup>; *Martin Albrecht*<sup>4</sup>; <sup>1</sup>CEA-Grenoble; <sup>2</sup>University of Neuchatel; <sup>3</sup>University Paris-Sud; <sup>4</sup>Institut für Kristallzüchtung

Thanks to their large conduction band offset ( $\approx 1.8$  eV for the GaN/AlN system) and subpicosecond intersubband (ISB) scattering rates, III-nitride nanostructures are excellent candidates for ultra-high-speed unipolar devices operating at optical-fiber telecommunication wavelengths. In this work, we report the MBE growth, fabrication and characterization of Al(Ga)N/GaN-based ISB detectors for telecommunication wavelengths, around 1.55  $\mu\text{m}$ . The active region of these devices consists of Si-doped short-period GaN/Al(Ga)N superlattices. Quantum well infrared photodetectors fabricated on these samples display a spectrally-narrow photovoltaic response to TM-polarized light around 1.55  $\mu\text{m}$  at room temperature, and can be operated at frequencies up to 2.3 GHz. We have investigated the effect of the growth temperature, Si doping, barrier thickness, Al mole fraction in the barriers and number of periods on the structural and optical properties of the superlattices, and on the performance of the final devices. Results are interpreted in comparison with self-consistent simulations of the electronic structure.

**ThP57, High Brightness Near-Ultraviolet Resonant Light Emitting Diodes:** *Brian Corbett*<sup>1</sup>; *Diane Zhu*<sup>2</sup>; *Brendan Roycroft*<sup>1</sup>; *Pleun Maaskant*<sup>1</sup>; *Mahbuk Akhter*<sup>1</sup>; *Clifford McAleese*<sup>2</sup>; *Menno Kappers*<sup>2</sup>; *Colin Humphreys*<sup>2</sup>; <sup>1</sup>Tyndall National Institute; <sup>2</sup>University of Cambridge

Planar near-ultraviolet 385 nm emitting resonant LEDs containing three quantum wells have been investigated as a function of the separation between the wells and a reflective and injecting metal mirror. The extracted output power and far field of the LEDs depend on the precise positions of the wells with each well having a significant individual influence on these properties. A doubling of the output power is obtained when the wells are located around the antinode position of the standing wave while narrower far-fields are obtained with other placement of the wells. A power of 0.4 mW into a numerical aperture of 0.5 is obtained for a current of 30 mA. Calibration of the growth rate along with accurate knowledge of the material properties of the semiconductor and metal mirrors is required for controlled and enhanced emission from planar UV LEDs.

**ThP58, High Performance AlGa<sub>1-x</sub>N-Based Avalanche Photodiodes:** *Turgut Tut*<sup>1</sup>; <sup>1</sup>Bilkent University

In this work, we present the MOCVD growth, fabrication, and characterization of AlGa<sub>N</sub>-based solar-blind APDs. The avalanche gain at 68V was in excess of 1,560 with no Geiger mode breakdown. This work demonstrates the high potential of AlGa<sub>N</sub> APDs for the replacement of the PMTs for high sensitive solar blind photodetector applications.

**ThP59, High Temperature Degradation of Ohmic Contacts on p-GaN for Application in Light Emitting Diodes:** *Matteo Meneghini*<sup>1</sup>; Lorenzo Trevisanello<sup>1</sup>; Ulrich Zehnder<sup>2</sup>; Gaudenzio Meneghesso<sup>1</sup>; Enrico Zanoni<sup>1</sup>; <sup>1</sup>University of Padova; <sup>2</sup>OSRAM-OS

This paper analyzes the instabilities of ohmic contacts on p-GaN during thermal stress. The contributions of the ohmic contacts and semiconductor degradation are separated by means of the Transfer Length Method (TLM). Before stress, the I-V curves of the TLMs showed linear shape, indicating good ohmic behaviour of the contacts. Temperature treatment induced the increase of the sheet resistance of the p-GaN and the non-linearity of the characteristics of the contacts. This paper shows that the high temperature instabilities are related to the interaction between device surface and hydrogen in the PECVD-SiN passivation layer implying the decrease of the effective acceptor concentration at TLM surface, and the non-linearity of the contacts and sheet resistance increase. Degradation process was found to be reversible, after passivation removal and subsequent annealing. Finally, a technique for the deposition of passivation layers alternative to PECVD and stable at high temperature levels is proposed and demonstrated.

**ThP60, High Temperature Ohmic Contacts to p-Type GaN Using Boride and Nitride-Based Refractory Materials for Light Emitting Devices:** *Lars Voss*<sup>1</sup>; L. Stafford<sup>1</sup>; M. Hlad<sup>1</sup>; B. Gila<sup>1</sup>; C. Abernathy<sup>1</sup>; S. Pearson<sup>1</sup>; F. Ren<sup>1</sup>; I. Kravchenko<sup>1</sup>; <sup>1</sup>University of Florida

Development of p-type Ohmic contacts for GaN is of interest due to the importance of contact stability and low contact resistance for AlGaIn/InGaIn laser diodes and on light output efficiency from nitride-based light-emitting diodes (LEDs). Commonly used schemes involve high work function metals such as Ni, Pt, or Cr with an overlayer of Au. While these contacts exhibit reasonable contact resistances, their thermal stability is a concern for both device operation at elevated temperatures and during device packaging. We report on Ohmic contacts to p-GaN using families of boride and nitride based materials. Specific contact resistances in the range of  $1 \times 10^{-4}$  for Ni/Au/X/Ti/Au based contacts and  $1 \times 10^{-3}$  for X/Ti/Au, where X is the high temperature material, are observed over a wide range of anneal temperatures up to 1000°C. LEDs using these materials display much better characteristics after long periods at elevated temperatures than those with just Ni/Au.

**ThP61, Hybrid Organic/Nitride Micro-Structured Light-Emitting Diodes:** *Erdan Gu*<sup>1</sup>; Benoit Guilhabert<sup>1</sup>; David Elfstrom<sup>1</sup>; Zheng Gong<sup>1</sup>; Haoxiang Zhang<sup>1</sup>; Martin Dawson<sup>1</sup>; A. Mackintosh<sup>1</sup>; A.J.C. Kuehne<sup>1</sup>; R.A. Pethrick<sup>1</sup>; C. Belton<sup>2</sup>; D.D.C. Bradley<sup>2</sup>; <sup>1</sup>University of Strathclyde; <sup>2</sup>Imperial College London

Hybrid organic/nitride optoelectronic devices will take full advantage of the optical and electronic properties of both organic and nitride materials. The significant benefits of integrating organic optoelectronic materials such as light-emitting polymers (LEPs) with nitride light-emitting diodes (LEDs) have been identified recently. However, due to their high chemical sensitivity, fabricating polymer microstructures and integrating them with nitride LEDs present a considerable technical challenge. In this work, several approaches for fabricating organic functional polymer microstructures on AlInGaIn-based micro-structured LEDs have been developed, including self-aligned direct writing, ultraviolet laser writing and lithographic patterning. It is shown that the fabricated organic/nitride micro-structured LED devices have well defined microstructures and exhibit novel functionalities. Colour down-converted visible emission from these hybrid electroluminescent micro-structured LEDs has been achieved. These hybrid LEDs offer a promising route to development of a range of low-cost and highly efficient micro-light sources.

**ThP62, Identification of Mechanisms Responsible for High-Current Efficiency Rollover in III-Nitride Light-Emitting Diodes:** Kirill Bulashevich<sup>1</sup>; *Sergey Karpov*<sup>1</sup>; <sup>1</sup>Semiconductor Technology Research, Inc.

Most if not all of III-nitride light-emitting diodes (LEDs) suffer from the emission efficiency rollover typically observed at the current densities of  $\sim 5\text{-}50 \text{ A/cm}^2$ , which limits the high-current device performance. Using simulation, we have examined various mechanisms tentatively responsible for this effect: the electron leakage into the LED p-layers, the carrier delocalization from the In-rich regions formed in InGaIn active layers due

to compositional fluctuations, the Auger recombination in the active layers, and the LED self-heating. The electron leakage and carrier delocalization can be ruled out, as they become valuable at either much higher or much lower current densities, respectively. The Auger recombination is found to be the most probable non-thermal mechanism producing the efficiency decrease with the current density. The LED self-heating, ever increasing with current, may additionally reduce the efficiency. Possible reasons for importance of the Auger processes in wide-bandgap III-nitride materials are discussed in the paper.

**ThP63, Improved Light Extraction Efficiency of GaN-Based Light Emitting Diodes by Using Needle-Shape Indium Tin Oxide p-Contact:** *Kazuyuki Tadatomo*<sup>1</sup>; Fumio Ishida<sup>1</sup>; Kazumasa Yoshimura<sup>2</sup>; Katsuyuki Hoshino<sup>1</sup>; <sup>1</sup>Yamaguchi University; <sup>2</sup>Yamaguchi Prefectural Industrial Technology Institute

The high-efficiency GaN-based light emitting diodes (LEDs) with improved light extraction efficiency (LEE) using the needle-shape indium tin oxide (ITO) p-contact was successfully demonstrated. The needle-shape ITO p-contact was naturally grown by using electron-beam evaporation method under the precisely controlled condition. The structure of ITO p-contact varied sensitively from the planar-shape to the needle-shape with decreasing the deposition temperature and the partial oxygen pressure in the vacuum chamber. We fabricated the p-side-up GaN/sapphire LEDs with the needle-shape ITO p-contact and those with the planar-shape ITO p-contact using the same LED wafer. The external quantum efficiency (EQE) of the needle-shape ITO-LED is 1.5 times larger than that of the planar-shape ITO-LED. This improvement is attributed to the dramatic increasing of the LEE of the needle-shape ITO-LED. These results show that the optimizing shape of ITO p-contact is the key technology to increase the EQE and the LEE of ITO-LED.

**ThP64, Improvement in Light Extraction Efficiency in GaN Based LED by Nano-Scale p-GaN Roughening:** *June Lee*<sup>1</sup>; <sup>1</sup>Chonnam National University

We improved the light extraction efficiency of 380nm Ultra-Violet Light Emitting Diode (LED) by nano-size roughening of p-GaN surface. The surface roughening process is carried out by using self-assembled gold cluster as a mask. The surface roughness of p-GaN surface is controlled by p-GaN regrowth time on patterned p-GaN layer. At optimized regrowth time of p-GaN layer, that is 30 sec, LED exhibited approximately 60% increased electro-luminescence value compared to the conventional LED. Current-voltage measurement also showed that the electrical properties are considerably enhanced over those of conventional LED chip.

**ThP65, Improvement of InGaIn/GaN Top-Emitting Light-Emitting Diodes Having ZnNi/ITO p-Type Ohmic Contacts:** *S.W. Chae*<sup>1</sup>; Kyoung Chan Kim<sup>1</sup>; D. H. Kim<sup>1</sup>; S.K. Yoon<sup>2</sup>; B.W. Oh<sup>2</sup>; D.S. Kim<sup>2</sup>; H.K. Kim<sup>2</sup>; Y.M. Sung<sup>1</sup>; T.G. Kim<sup>1</sup>; <sup>1</sup>Korea University; <sup>2</sup>Samsung Electro-Mechanics Company

We report the formation of a high-transparent and low-resistant p-type GaN ohmic contact using a ZnNi/ITO (5nm/380nm) electrode scheme for high-brightness top-emitting light-emitting diodes (LEDs). Along with the ZnNi/ITO electrode, Pt/ITO (5nm/380nm), Ni/Au/ITO (2.5nm/5nm/380nm), and Ni/Au (2.5nm/5nm) electrodes on p-type GaN were prepared to compare their performance. From the measurements, the ZnNi/ITO contacts showed the best performance with a specific contact resistance of  $\sim 1.27 \times 10^{-4} \text{ cm}^2$  and a transmittance of  $\sim 90\%$  at a wavelength of 460nm. InGaIn/GaN multiple-quantum-well LEDs fabricated with the annealed ZnNi/ITO p-type electrodes gave a mean forward-bias voltage of 3.28V and a typical brightness of 11.7 mcd at 20mA. These improvements were attributed to the low light absorption coefficient of ZnNi oxides, as well as to the reduced ionization energy of the Mg acceptor, resulting from hydrogen desorption by ZnNi in the Mg-H complex during thermal annealing.

# Technical Program

**ThP66, Improvement of Near-Ultraviolet Nitride-Based Light-Emitting Diodes with Meshed p-GaN:** *H. C. Feng*<sup>1</sup>; C. M. Chen<sup>1</sup>; C. W. Kuo<sup>1</sup>; Y. K. Fu<sup>1</sup>; C. J. Tun<sup>2</sup>; C. J. Pan<sup>1</sup>; G. C. Chi<sup>1</sup>; Cheng-Huang Kuo<sup>1</sup>; <sup>1</sup>National Central University; <sup>2</sup>National Synchrotron Radiation Research Center

This investigation presents nitride-based near ultraviolet (n-UV) light emitting diodes (LEDs) with a meshed p-GaN layer. With 20 mA injection current, it was found that forward voltages were 3.33 and 3.39 V while output powers were 9.0 and 10.6 mW for the meshed indium-tin-oxide (ITO) LED and meshed p-GaN LED, respectively. The larger LED output power is attributed to increased light extraction efficiency.

**ThP67, Influence of InGaN/GaN Strained Layer Superlattice under Active Layer on the Performance of InGaN/GaN Quantum Well Light-Emitting Diodes:** *Shi Jong Leem*<sup>1</sup>; *Kyoung Chan Kim*<sup>1</sup>; Youngbo Moon<sup>2</sup>; Tae Geun Kim<sup>1</sup>; <sup>1</sup>Korea University; <sup>2</sup>Seoul National University

We investigated the performance of InGaN/GaN quantum well light-emitting diodes (LEDs) having InGaN/GaN strained layer superlattice (SLS) as a strain buffer layer for active layers. With increasing indium mole fraction of InGaN/GaN SLS, it was found that the roughness of surface was significantly reduced and the density of V-defects was gradually decreased without changing the size of V-defects. The wavelength shift was as small as 7 nm for the LEDs with  $\text{In}_{0.1}\text{Ga}_{0.9}\text{N}/\text{GaN}$  SLS while that for the LEDs with  $\text{In}_{0.02}\text{Ga}_{0.98}\text{N}/\text{GaN}$  SLS was as large as 20 nm. The reduction in the wavelength shift in the  $\text{In}_{0.1}\text{Ga}_{0.9}\text{N}/\text{GaN}$  SLS LEDs is thought to be due to the low density of V-defects as well as the reduced roughness of surface, resulting from strain relaxation and reduction of the piezoelectric field in MQW as the indium mole fraction of the InGaN/GaN SLS increases from 2 to 10%.

**ThP68, InGaN/GaN Multiple Quantum Well Blue LEDs Grown on Patterned Si Substrates with High Temperature AlN-AlGaIn Stacked Buffer Layers:** *Hu Liang*<sup>1</sup>; *Hui Wang*<sup>1</sup>; *Yong Wang*<sup>1</sup>; *Kei May Lau*<sup>1</sup>; <sup>1</sup>Photonics Technology Center, Department of Electrical and Computer Engineering, Hong Kong University of Science and Technology

Incorporation of an 500 nm  $\text{Al}_{0.3}\text{Ga}_{0.7}\text{N}$  buffer layer with high-temperature (960°C) AlN interlayers was effective in stress reduction to grow thick crack-free InGaN/GaN blue LEDs on patterned Si substrates with square islands. Compared with previously used AlN interlayer only, the HT AlN-AlGaIn stacked buffer layer not only effectively reduced the tensile stress inside devices, but also introduced less threading dislocations. LED device yield was much improved with these AlN/AlGaIn composite buffer layers. Previously, micro-cracks easily developed after thermal cycles during device processing and resulted in a very low yield, although as-grown samples were crack-free. Devices with standard Ni/Au surface emitting contacts exhibited ~1.0 mW output power at 20 mA, without Si substrate removal and packaging. With our optimized Ag-ITO contacts, LEDs on sapphire substrates emit 40% more power than Ni/Au contacts, with similar  $V_{th}$  (3.1 – 3.4V). Optimized ITO contacts and substrate transfer are being developed for better device performance.

**ThP69, Junction Temperature Analysis in Green Light Emitting Diode Dies on Sapphire and GaN Substrate:** *Jayantha Senawiratne*<sup>1</sup>; *Wei Zhao*<sup>1</sup>; *Theeradetch Detchprohm*<sup>1</sup>; *Yufeng Li*<sup>1</sup>; *Mingwei Zhu*<sup>1</sup>; *Yong Xia*<sup>1</sup>; *Arya Chatterjee*<sup>2</sup>; *Joel Plawsky*<sup>2</sup>; *Christian Wetzel*<sup>1</sup>; <sup>1</sup>Future Chips Constellation and Department of Physics, Applied Physics, and Astronomy, Rensselaer Polytechnic Institute; <sup>2</sup>Department of Chemical Engineering, Rensselaer Polytechnic Institute

We investigate pn-junction heating in 525 nm green GaInN/GaN quantum well light emitting diode (LED) dies by micro-Raman spectroscopy. Local junction temperature was assessed by the shift of the  $\text{GaN-E}_2$  (high) phonon mode. We compare dies of active area  $350 \times 350 \mu\text{m}^2$  grown on bulk GaN and sapphire substrates of different size at current densities up to 267 A/cm<sup>2</sup>. Analysis of the experiment was supported by realistic three-dimensional finite-element simulations of the thermal properties. Sapphire based LED dies reach a junction temperature as high as 240°C at a current density of 133 A/cm<sup>2</sup>, while those on bulk GaN only heat to 83°C. This corresponds to thermal resistances of 425 K/W and 63 K/W, respectively. By help of this calibration, the role of junction temperature in the spectral light output performance is identified. From the numerical simulation, dimensions and

thermal conductivity of the substrate are identified as the dominant control parameters.

**ThP70, Light Emission Enhancements of InGaN/GaN Single-Quantum-Well Light-Emitting Diodes through Surface Plasmon Coupling:** *Dong-Ming Yeh*<sup>1</sup>; *Chi-Feng Huang*<sup>1</sup>; *Tsung-Yi Tang*<sup>1</sup>; *Cheng-Yen Chen*<sup>1</sup>; *Yen-Cheng Lu*<sup>1</sup>; *C. C. Yang*<sup>1</sup>; <sup>1</sup>National Taiwan University

It has been shown that the coupling of surface plasmon (SP) with an InGaN/GaN quantum well (QW) can enhance photoluminescence (PL). In this paper, we demonstrate the SP-QW coupling effect in an InGaN/GaN single-QW light-emitting diode (LED), i.e., the enhancement of electroluminescence (EL). For the demonstration, we prepare three InGaN/GaN single-QW LEDs of the same structure except that three different metals of Ag, Al, and Au are used as the coating metals on Ni for the p-type Ohmic contacts. From the different output EL spectra of the three LEDs, one can observe the different SP-QW coupling behaviors. Such different behaviors are confirmed with the results of PL and time-resolved PL measurements. With the InGaN/GaN QW emission around 440 nm in wavelength, the Ag-coated LED shows the most significant SP-QW coupling effect, as predicted. In this LED sample, the EL spectrum is the strongest, the narrowest and the most blue-shifted.

**ThP71, Light Emitting Diodes with Wavelength-Tunable Output:** *W.N. Ng*<sup>1</sup>; *C.H. Leung*<sup>1</sup>; *P.T. Lai*<sup>1</sup>; *Hoi Wai Choi*<sup>1</sup>; <sup>1</sup>University of Hong Kong

It would be very desirable to have LEDs whose wavelengths are tunable by the user over a broad spectral range. Such devices would enable a wider range of LED-based products to be developed, including desktop-sized displays, mood-lighting, etc. We introduce the design and implementation of a broadband tunable LED, with emission wavelength ranging between 470nm and 600nm. This can be achieved through the micro-light-emitting diode strategy, where multiple individually-addressable micrometer-scaled pixels are formed on a 470 nm GaN LED. Red fluorescent microspheres for colour conversion are introduced onto designated pixels, which are interconnected. Pixels in an array emit either blue or red colour. Since the pixels are of micron-scale which are non-resolvable by the unaided human eye, the output appears optically mixed. By varying the intensity of the blue and red emitting regions by varying the bias voltages to the corresponding cathodes, the output wavelength (colour) can be continuously tuned.

**ThP72, Mechanism of GaN/AlGaIn UV LED Degradation:** *Shayla Sawyer*<sup>1</sup>; *S. Rumyanstev*<sup>1</sup>; *M. Shur*<sup>1</sup>; *X. Hu*<sup>2</sup>; *A. Sattu*<sup>2</sup>; *Yu. Bilenko*<sup>2</sup>; *I. Shturm*<sup>2</sup>; *A. Lunev*<sup>2</sup>; *J. Deng*<sup>2</sup>; *J. Zhang*<sup>2</sup>; *R. Gaska*<sup>2</sup>; <sup>1</sup>Rensselaer Polytechnic Institute; <sup>2</sup>Sensor Electronic Technology, Inc.

We report on studies of degradation of GaN/AlGaIn 280nm UV LEDs fabricated by Sensor Electronic Technology, Inc. The estimated lifetime of these tested LEDs is 500 hours, assuming an exponential decrease of the output power with time. During the aging there was no change in peak wavelength, FWHM, series resistance and low frequency noise. At high bias voltage current increased and noise decreased with aging. This experimental data showed that neither series resistance nor the multiple quantum well light emitting structure deteriorate with age. The increase of the current and decrease of the output power can be explained by the lowering of the potential barrier associated with the p contact with aging. These results will help improve the UV LED design and increase their lifetime.

**ThP73, Micron Scale Measurements of Disorder in Lattice-Matched AlInN/GaN Microcavities:** *Gabriel Christmann*<sup>1</sup>; *Dobri Simeonov*<sup>1</sup>; *Raphaël Butté*<sup>1</sup>; *Eric Feltin*<sup>1</sup>; *Jean-François Carlin*<sup>1</sup>; *Nicolas Grandjean*<sup>1</sup>; <sup>1</sup>Ecole Polytechnique Fédérale de Lausanne

We report the study of crack-free GaN microcavities (MCs) grown by metalorganic vapor phase epitaxy on c-plane sapphire substrate using two highly reflective lattice-matched AlInN/GaN distributed Bragg reflectors (DBRs) with or without InGaN/GaN quantum wells (QWs) as an active region. Using a micro-transmission setup, it is shown that these MCs exhibit a large in-plane disorder likely resulting from cavity or DBR thickness fluctuations. Although cavity modes with quality factors up to 2800 have been measured in empty MCs, their wavelength varies with position on a short length scale. Extended homogeneous areas separated by abrupt variations are observed. In addition inserting InGaN/GaN QWs brings an extra source

of disorder possibly due to their non-uniform thickness. The setup has been subsequently upgraded to allow for angular resolved measurements while keeping a micron scale resolution. This new degree of freedom led to the observation of the cavity mode quantization with angle.

**ThP74, Non-Polar a-Plane AlN/(Al)GaN Distributed Bragg Reflectors:** *Tiankai Zhu<sup>1</sup>; Amélie Dussaigne<sup>1</sup>; Gabriel Christmann<sup>1</sup>; Eric Feltrin<sup>1</sup>; Claire Pinquier<sup>1</sup>; Denis Martin<sup>1</sup>; Nicolas Grandjean<sup>1</sup>; <sup>1</sup>Ecole Polytechnique Fédérale de Lausanne*

Highly reflective a-plane AlN/GaN and AlN/Al<sub>0.1</sub>Ga<sub>0.9</sub>N distributed Bragg reflectors (DBRs) have been achieved for the first time. Samples are grown by ammonia source molecular beam epitaxy on a-plane GaN templates which are previously elaborated by hydride vapor phase epitaxy using epitaxial lateral overgrowth technique. Both DBRs use 13 periods. The room-temperature micro-reflectivity reveals that the AlN/GaN DBR is featured by a flat stopband, with a stopband width (SBW) around 35 nm. Its peak reflectivity is roughly estimated around 95%. Both the peak reflectivity and the SBW of the AlN/Al<sub>0.1</sub>Ga<sub>0.9</sub>N DBR slightly decrease, compared with the AlN/GaN one. The cross-sections of the DBR structures are characterized by scanning electron microscopy. We demonstrate that the present a-plane DBRs are of comparable optical quality to those grown on c-plane. Thus, they are promising for the fabrication of polarization-free nitride-based microcavities.

**ThP75, Novel Phosphor-Free White Light Emitting Diodes for Optimized Eye Response:** *Sucheta Ahmed<sup>1</sup>; David Lancefield<sup>1</sup>; Stephen Sweeney<sup>1</sup>; Philippe De Mierry<sup>2</sup>; Frank Tinjod<sup>2</sup>; Sébastien Chenot<sup>2</sup>; <sup>1</sup>University of Surrey; <sup>2</sup>CNRS*

We report on phosphor-free white GaN homojunction light emitting diode (LED) structures grown both with and without an additional undoped AlGaIn barrier. The electroluminescence measured from both devices exhibits yellow defect related emission. However, the incorporation of an AlGaIn barrier introduces an additional blue peak relating to the Mg doping profile. This gives rise to broadband “white” emission from the AlGaIn barrier devices. Tristimulus values (to analyse the quality of light for human vision) show that in both structures, the red and green responses increase sub-linearly with current. However, the introduction of the AlGaIn barrier causes a substantial current induced increase in the blue emission response compared with the simple homojunction. We find that the AlGaIn barrier devices also exhibit a colour rendering index of over 85 and a correlated colour temperature of 6000K. These results illustrate the importance of understanding and controlling defect-related emission for application in broadband LEDs.

**ThP76, Observation of Phonon-Assisted Stimulated Emission from Pendeo-Epitaxy GaN Stripes Grown on 6H-SiC Substrates:** *Yun-Chorng Chang<sup>1</sup>; Yun-Li Li<sup>2</sup>; Darren B. Thomson<sup>3</sup>; Robert F. Davis<sup>3</sup>; <sup>1</sup>National Cheng Kung University; <sup>2</sup>National Taiwan University; <sup>3</sup>North Carolina State University*

Phonon-assisted stimulated emission (PASE) has been demonstrated by photo-pumping GaN stripes fabricated via pendeo-epitaxy in films grown on 6H-SiC (0001) substrates. Stimulated emission with well-defined Fabry-Pérot modes located at one longitudinal optical (LO) phonon energy (90 meV) below the bandgap of GaN was observed at 77K, and the emission was transverse-electric-polarized (TE). The observed well-defined Fabry-Pérot modes and TE-polarized output verified the occurrence of PASE. An effective refractive index of 8.578 is obtained using a cavity length of 13.3 μm and mode spacing of 0.6 nm. The measured effective refractive index is significantly higher than the 2.8 value obtained from results of spectroscopic-ellipsometry, which indicates higher carrier loss occurs during stimulated emission. Results from this study provide a way to study carrier loss mechanisms during stimulated emission and pave the way for better understanding of the nature of phonon-assisted stimulated emission.

**ThP77, Optical Characteristics of Two-Dimensional Electron Gas in Undoped AlGaIn/GaN Heterostructures with a Low-Temperature AlN Interlayer:** *Ho-Sang Kwack<sup>1</sup>; Yong-Hwan Kim<sup>1</sup>; Hee Jin Kim<sup>1</sup>; Euijoon Yoon<sup>1</sup>; Yong-Hoon Cho<sup>1</sup>; <sup>1</sup>Chungbuk National University*

We have investigated the optical characteristics of two-dimensional electron gas (2DEG) in Al<sub>0.55</sub>Ga<sub>0.45</sub>N/GaN heterostructures with and without a low-

temperature AlN interlayer grown by metalorganic chemical vapor deposition. The structural and optical properties were systematically studied by means of scanning electron microscopy, temperature- and excitation power-dependent photoluminescence (PL), PL excitation, and time-resolved PL spectroscopy. A 2DEG-related PL emission (P1) clearly appeared at about 70 meV below the GaN band-edge emission for the AlGaIn/GaN structure with the low-temperature AlN interlayer. With increasing excitation power, we observed additional 2DEG-related emission peak (P2) at ~ 30 meV higher energy than P1. The carrier dynamics of these 2DEG emission peaks were investigated as a function of excitation power and temperature. The origin and carrier dynamics of these 2DEG emission peaks in AlGaIn/GaN heterostructures with and without AlN interlayer will be discussed.

**ThP78, Phosphor-Free White-Light InGaIn/GaN Quantum-Well Light-Emitting Diode of Weak Quantum-Confined Stark Effects:** *Chi-Feng Huang<sup>1</sup>; Chih-Feng Lu<sup>1</sup>; Tsung-Yi Tang<sup>1</sup>; Jeng-Jie Huang<sup>1</sup>; C. C. Yang<sup>1</sup>; <sup>1</sup>National Taiwan University*

We grew a white-light InGaIn/GaN quantum-well (QW) light-emitting diode epitaxial structure with its electroluminescence spectrum close to the ideal condition (chromaticity diagram close to (1/3, 1/3) and a color temperature around 5600 K) in Commission Internationale de l’Eclairage chromaticity based on the presrained metalorganic chemical vapor deposition technique. The prestrained growth leads to the efficient yellow emission from three InGaIn/GaN QWs of increased indium incorporation. The color mixing for white light is implemented by adding a blue-emitting QW at the top of the yellow-emitting QWs. The blue shifts of the blue and yellow spectral peaks of the generated electroluminescence spectra are only 1.67 and 8 nm, respectively, when the injection current increases from 10 to 70 mA. Such small blue shifts imply that the piezoelectric fields or the quantum-confined Stark effects in our QWs are significantly weaker than those previously reported.

**ThP79, Polychromatic Emission from Fluorescent-Microsphere-Coated LEDs:** *K.N. Hui<sup>1</sup>; W.N. Ng<sup>1</sup>; C.H. Leung<sup>1</sup>; P.T. Lai<sup>1</sup>; Hoi Wai Choi<sup>1</sup>; <sup>1</sup>University of Hong Kong*

Many on-going research efforts target the development of alternative phosphor-free white light generation, including CdSe quantum dots and multi-wavelength quantum wells. We present our solution to polychromatic light generation based on fluorescent microspheres, whose superior photo-stability and conversion efficiency make them excellent candidates as colour down-conversion agents. The incorporation of fluorescent microsphere coatings is demonstrated to fulfill the two major criteria towards an efficient white LED: (1) efficient color conversion and (2) efficient light out-coupling. We have developed a method to form large ordered arrays of microspheres based on a combination of tilting and spin-coating. With a suitable proportion of green-emitting and red-emitting fluorescent microspheres, broadband emission can readily be achieved. The overall thicknesses of the microsphere coating can be precisely controlled, giving rise to differing spectral properties. The optimal conditions give broadband white light emission with CIE coordinates of (0.24, 0.56), and an overall efficiency in excess of 70%.

**ThP80, Quantum Dots Excited InGaIn/GaN Phosphor-Free White LEDs:** *Soo-Jin Chua<sup>1</sup>; Chew Beng Soh<sup>1</sup>; Wei Liu<sup>1</sup>; Jing Hua Teng<sup>1</sup>; S.S. Ang<sup>1</sup>; S.L. Teo<sup>1</sup>; <sup>1</sup>Institute of Materials Research and Engineering*

Commercial white LEDs have been fabricated with the use of phosphors for conversion of blue or UV LED emission into white light. We report on the InGaIn/GaN based white LEDs using InGaIn quantum dots incorporated in the MQW layers. The photoluminescence spectrum of the MQWs shows a broad emission spectrum covering 460 to 700 nm. Cross-section TEM shows the existence of pyramidal shaped structures with size of 2.0 – 4.0 nm embedded in the InGaIn well. To reduce the out-diffusion of In from the InGaIn quantum dots into the well layer, the subsequent p-InGaIn layer was grown below 800°C. I-V measurement of the LEDs gives a forward voltage of 5.2 V at IF ~20mA. The chromaticity coordinate ranges from 0.28 < x, y < 0.36 with a colour temperature of ~ 6000K and can be tuned during growth by changing both the dot size and composition. PL luminescence efficiency is in excess of 50%.

# Technical Program

**ThP81, Realization of 340nm-Band High-Power InAlGaN-Based UV-LEDs by the Suppression of Electron Overflow:** *Sachie Fujikawa*<sup>1</sup>; Takayoshi Takano<sup>2</sup>; Yukihiko Kondo<sup>2</sup>; Hideki Hirayama<sup>1</sup>; <sup>1</sup>RIKEN; <sup>2</sup>Matsushita Electric Works, Ltd.

(In)AlGaIn alloys are attracting much attention as candidate materials for realizing deep ultraviolet (UV) light-emitting diodes (LEDs). In this study, we demonstrated high-power CW operations of 340nm-band InAlGaIn-based UV-LEDs by suppressing electron overflow using optimized electron injection structures. LED layer structure consisting of quaternary InAlGaIn quantum well (QW), Mg-doped InAlGaIn electron blocking layer (EBL) and Mg-doped InAlGaIn p-layers was grown on sapphire/AlN/AlGaIn template by low-pressure metal-organic chemical-vapor deposition (LP-MOCVD). The output power was dramatically improved by increasing electron blocking height and quantum well depth. Furthermore, the output power was dramatically improved by the increase of well width. These tendencies agree well with the theoretical calculations using device simulator. The maximum output power and external quantum efficiency (EQE) were 7.1mW and 0.9%, respectively, under room temperature (RT) CW operation. These results indicate that the suppression of electron overflow is quite important for the realization of high-efficiency (In)AlGaIn based UV-LEDs.

**ThP82, Remarkable Improvement of Output Power for InAlGaIn Based Ultraviolet LED by Improving the Crystal Quality of AlN/AlGaIn Templates:** *Takayoshi Takano*<sup>1</sup>; *Sachie Fujikawa*<sup>2</sup>; Yukihiko Kondo<sup>1</sup>; Hideki Hirayama<sup>2</sup>; <sup>1</sup>Matsushita Electric Works, Ltd.; <sup>2</sup>Institute Physical and Chemical Research (RIKEN)

For the realization of commercially available low-cost and high-power ultraviolet light-emitting diodes (UV-LEDs), quaternary InAlGaIn is very attractive, because highly efficient UV emission can be obtained due to In-segregation effects. We achieved remarkable improvement of output power of 340 nm-band quaternary InAlGaIn-based UV-LED and demonstrated high UV-output power by using high-quality AlN buffer templates on sapphire. Threading dislocation density for the edge type was  $1.1 \times 10^9 \text{cm}^{-2}$  observed from the cross section transmission electron microscope (TEM) image. The output power of the 340 nm-band UV-LED was increased by approximately 7 times by reducing the FWHM of (10-12) x-ray  $\omega$ -scan rocking curve (XRC) from around 800 to 510 arcsec. As a result, we achieved maximum output power of 7.1 mW under RT CW operation. From these results, we found that the crystal quality of AlN/AlGaIn templates strongly affects the output power of UV-LEDs.

**ThP83, Scanning Micro-Luminescence Spectroscopy of Commercial High-Intensity Blue InGaIn LEDs:** *Lars Reissmann*<sup>1</sup>; Jürgen Christen<sup>1</sup>; Thomas Hempel<sup>1</sup>; Tanja Mesli<sup>1</sup>; Jo Kunze<sup>1</sup>; Andreas Kaluza<sup>1</sup>; Rafael Jordan<sup>1</sup>; Hermann Oppermann<sup>1</sup>; <sup>1</sup>OvG University Magdeburg

We report on scanning micro-electroluminescence ( $\mu$ -EL) and micro-photoluminescence ( $\mu$ -PL) spectroscopy measurements on blue InGaIn-based high-power LEDs. We used LED-chips from two different manufacturers with peak wavelengths between 457-459 nm. Mounted chips were driven by DC forward currents of up to 1000 mA. The 324 nm line of a He-Cd-laser was used for PL excitation. The chip area of 1 mm<sup>2</sup> was scanned with spatial resolution of 8  $\mu\text{m}$  down to 0.5  $\mu\text{m}$  for selected areas. Both chips exhibit extraordinarily homogeneous spatial distribution of intensity and peak wavelength. The chips were subject to constant and cycling temperature treatments simulating aging processes. This resulted in massive degradation of light output power in the center of the chips. It is analyzed, whether structural defects in the semiconductor or mounting-related issues are responsible. YAG:Ce converter was applied and white LED modules with 4 chips and fluxes of up to 380 lm were fabricated.

**ThP84, Simulation and Design of InGaAsN Metal-Semiconductor-Metal Photodetectors for Long Wavelength Optical Communications:** *Shin-Li Tsai*<sup>1</sup>; Hung-Ji Lin<sup>1</sup>; Der-Yuh Lin<sup>1</sup>; Jing Yao Zheng<sup>1</sup>; <sup>1</sup>National Changhua University of Education

Optical properties of InGaAsN metal-semiconductor-metal photodetectors (MSM-PDs) with modulation-doped heterostructures have been simulated by using an APSYS simulation program. Several structure parameters such as cap layer doping concentration, cap layer thickness, spacer layer thickness

and absorption layer thickness are employed to study how these parameters change the photoresponse operating at a wavelength of 1.3  $\mu\text{m}$ . A triangular well forms by combining InGaAsN with wide gap materials such as AlGaAs. The two-dimensional electron gas (2DEG) is generated and localized at AlGaAs-InGaAsN interface so that a larger effective Schottky barrier height can be achieved to reduce the dark current. The effective Schottky barrier heights, which extracted from experimental data, were used in our simulations for the different cap layer doping concentrations. Based on the simulation results the optimized design is proposed.

**ThP85, Surface Plasmon-Enhanced Light-Emitting Diode:** *Min-Ki Kwon*<sup>1</sup>; Ja-Yeon Kim<sup>1</sup>; Baek-Hyun Kim<sup>1</sup>; Il-Kyu Park<sup>1</sup>; Chu-Young Cho<sup>1</sup>; Chisu Byeon<sup>2</sup>; Seong-Ju Park<sup>1</sup>; <sup>1</sup>Gwangju Institute of Science and Technology; <sup>2</sup>Advanced Photonics Research Institute, Gwangju Institute Science and Technology

Surface plasmons (SPs), excited on rough metallic surface by the interaction between light and metal are suggested to significantly enhance the light emission by improving the internal quantum efficiency. However, the realization of GaN based LED structure with QW-SP coupling is not yet reported. Here, we demonstrate, for the first time, SP enhanced InGaIn/GaN multiple quantum well (MQW) blue light emitting diode (LED) with an Ag nanoparticle layer inserted between n-GaN layer and MQW layer. The time resolved photoluminescence results clearly showed that the PL decay time of the blue LED with Ag nanoparticles is significantly faster than that of LED without Ag nanoparticles, indicating that spontaneous emission rate is increased with strong coupling between QW light emitters and SP of Ag nanoparticles. The optical output power of LED with Ag nanoparticles was increased by 32.2 % due to QW-SP coupling at an input current of 100 mA.

**ThP86, Temperature Dependence Intensity of 340 nm GaN/AlGaIn Ultraviolet Light-Emitting Diodes:** *Kean Lee*<sup>1</sup>; Peter Parbrook<sup>1</sup>; Tao Wang<sup>1</sup>; Jie Bai<sup>1</sup>; Fabio Ranalli<sup>1</sup>; Qi Wang<sup>1</sup>; Rob Airey<sup>1</sup>; Geoff Hill<sup>1</sup>; <sup>1</sup>University of Sheffield

The temperature dependence (10-400K) of integrated electroluminescence (EL) intensity of 340nm GaN/AlGaIn light emitting diodes is investigated and shows an anomalous 'S-shape' behaviour. No correlation between this behaviour of EL intensity and exciton localization observed in the QW is found. We attribute the presence of an electron blocking layer as being the main reason for this behaviour. Above 250K, non-radiative recombination dominates and causes the decrease of the EL intensity as the temperature increases. However, between 150K and 250K, a decrease in EL intensity as the temperature decreases is observed due to the electron blocking layer preventing hole diffusion into the QW. As the temperature further decreases towards 10K a decrease in non-radiative recombination, leads to an increase in the intensity, assuming hole tunnelling through the blocking layer.

**ThP87, The AZO:Y2O3 Transparent Contact on InGaIn/GaN MQWs LEDs:** *Li-Chi Peng*<sup>1</sup>; Wei-Chih Lai<sup>1</sup>; Cheng-Huang Kuo<sup>2</sup>; Jinn-Kong Sheu<sup>1</sup>; Shou-Jinn Chang<sup>3</sup>; <sup>1</sup>Institute of Electro-Optical Science and Engineering, National Cheng Kung University; <sup>2</sup>Department of Optics and Photonics, National Central University; <sup>3</sup>Institute of Microelectronics, National Cheng Kung University

The internal quantum efficiency and light extraction efficiency are two issues to get high efficiency LEDs. To get more light extraction efficiency the ITO transparent contact was widely used for the transparent contact of GaN based LEDs instead of Ni/Au transparent contact. ZnO based materials were also the candidates of transparent contact for the GaN based LEDs. In our study the AZO:Y were used for the transparent contact of the GaN based LEDs. The forward voltage of LEDs with AZO:Y driving at 20mA was about 3.55V and was about 0.17V higher than the LEDs with ITO. The current-voltage and power-current characteristics were shown on figure 1 and 2 respectively. The GaN based LEDs with AZO:Y has got the output power around 10% more than the GaN based LEDs with ITO.

**ThP88, Time-Resolved Electro-Luminescence Studies of InGaN Blue LEDs with Chip Size Variations:** *Shih-Wei Feng*<sup>1</sup>; Tzong-Liang Tsai<sup>2</sup>; Wen-How Lan<sup>1</sup>; C. J. Huang<sup>1</sup>; Ming-Chang Shih<sup>1</sup>; <sup>1</sup>National University of Kaohsiung; <sup>2</sup>Huga Optotech Inc.

InGaN-based light emitting diodes (LEDs) are promising candidates for applications in large-screen display, signage, and solid-state lighting. Time-resolved electro-luminescence (TREL) is a powerful tool to investigate the carrier dynamics. In this study, we will report carrier dynamics of three InGaN Blue LEDs with chip size variations by using TREL measurements. Three samples with the same structures but different chip sizes were compared. For the largest chip size sample, the EL spectrum was smaller and the delay-times (responses times) were longer than those of the other samples. It implies that the current spreading for larger chip size need more time. Rise-times and decay-times of the three samples will also be compared. In the future, carrier dynamics and luminescence mechanism will be presented in the conference.

**ThP89, Transport Properties in n-Type AlGaIn/AlN/GaN-Superlattices:** *Joachim Hertkorn*<sup>1</sup>; Peter Brückner<sup>1</sup>; Chong Gao<sup>1</sup>; Ferdinand Scholz<sup>1</sup>; <sup>1</sup>Ulm University

In order to improve the lateral conductivity in optoelectronic devices, we have investigated Si-doped AlGaIn/AlN/GaN-superlattices. As a first step we performed calculations of the band structure of AlGaIn/AlN/GaN modulation doped multi heterostructures. Based on these results we worked on optimizing the growth of low Al content ( $x_{Al} < 20\%$ ) superlattices by MOVPE. Several tens of abrupt and graded AlGaIn/AlN/GaN-layer pairs could be grown crack-free on 2  $\mu\text{m}$  thick n-GaN layers deposited on sapphire substrates with AlN nucleation. By Van-der-Pauw Hall measurements, we determined that the lateral conductivity of a 1.5  $\mu\text{m}$  thick superlattice structure is a factor of four higher than in highly n-doped bulk material with comparable thickness without compromising too much the vertical conductivity as confirmed by two step TLM-measurements. At 77 K we could demonstrate an extremely high effective mobility of 14720  $\text{cm}^2/\text{Vs}$  at  $n=8 \times 10^{17} \text{ 1/cm}^3$  ( $R=1.7 \Omega/\square$ ), a clear verification of our excellent crystal quality.

**ThP90, UV-LED Efficiency Enhancement Using Freestanding GaN Substrate:** *Markus Maier*<sup>1</sup>; Klaus Köhler<sup>1</sup>; Michael Kunzer<sup>1</sup>; Joachim Wiegert<sup>1</sup>; Shangjing Liu<sup>1</sup>; Ulrich Kaufmann<sup>1</sup>; Hans-Joachim Wagner<sup>1</sup>; <sup>1</sup>Fraunhofer Institute for Applied Solid-State Physics

Freestanding GaN-substrates with low defect density (DD) are not only the key to reduce threshold current densities and prolong lifetimes of blue laser diodes, but also enhance the output power of blue LEDs.<sup>1</sup> To study the effect of the DD on short-wavelength LEDs, we have grown LED structures by MOVPE, emitting in the 370–420 nm range, on sapphire, low dislocation templates (ULD) and freestanding GaN, with a DD ranging from  $10^9 \text{ cm}^{-2}$  to  $5 \times 10^7 \text{ cm}^{-2}$ . A clear increase in output power upon reduction of the DD is observed, being strongest for wavelengths shorter than 390 nm. Comparing the output power of LEDs on different substrates, special attention has to be paid to differences in light extraction efficiency. Though band-to-band absorption limits the use of freestanding GaN to wavelengths exceeding 380 nm, it offers the possibility to significantly enhance the light extraction via backside surface texturing. <sup>1</sup><http://compoundsemiconductor.net/articles/news/11/3/6/1>.

**ThP91, UV Emitters Grown on High Crystalline Quality AlGaIn on Sapphire:** *Kazuyoshi Iida*<sup>1</sup>; Fumiaki Mori<sup>1</sup>; Hirotaka Watanabe<sup>1</sup>; Kenichiro Takeda<sup>1</sup>; Kentaro Nagamatsu<sup>1</sup>; Motoaki Iwaya<sup>1</sup>; Satoshi Kamiyama<sup>1</sup>; Hiroshi Amano<sup>1</sup>; Isamu Akasaki<sup>1</sup>; Hisaaki Maruyama<sup>2</sup>; Takashi Takagi<sup>2</sup>; Akira Bandoh<sup>3</sup>; <sup>1</sup>Meijo University; <sup>2</sup>Ceramic Operation, Ibiden Company Limited; <sup>3</sup>Corporate R&D Center, Showa Denko K.K.

We fabricated UV-LED on 3 types of the underlying layers. All samples were grown on AlN on sapphire substrates by MOVPE. Type 1 is UV-LED on AlN template. Type 2 is ELO Al<sub>0.25</sub>Ga<sub>0.75</sub>N on grooved AlN. Type 3 is ELO Al<sub>0.25</sub>Ga<sub>0.75</sub>N on grooved Al<sub>0.25</sub>Ga<sub>0.75</sub>N on AlN template. We compared how these device performances influenced by the difference of the underlying layer. Light output intensity of UV-LED fabricated on ELO Al<sub>0.25</sub>Ga<sub>0.75</sub>N on grooved Al<sub>0.25</sub>Ga<sub>0.75</sub>N luminous intensity of this UV-LED is the stronger than that of other samples from the L-I curves. The improvement of this luminous intensity originates in a decrease in the defect in AlGaIn and control of strain.

**ThP92, Voltage Tunable Wavelength Light Emitting Diode:** *Chew Beng Soh*<sup>1</sup>; Soo Jin Chua<sup>1</sup>; Haryono Hartono<sup>1</sup>; <sup>1</sup>Institute of Materials Research and Engineering

We report on the growth and fabrication of a LED which emits light, tunable in color, ranging from red, yellow, green and cyan as the input voltage is increased. Two multiple quantum well (MQWs) structures, designated as A and B, are grown in the LEDs, with quantum dots embedded in MQWs A. The InGaIn/GaN layers are grown by MOCVD with sapphire as the substrate. A broad photoluminescence spectrum ranging from 500 nm to 700 nm is measured, which is the result of broadening attributed to the incorporation of quantum dots in the well layer of MQWs A. The emission peak at 433 nm (blue emission) is from the MQWs B. The 3D confinement in the quantum dots reduces the effective piezoelectric field effects, despite the thicker well layer of approximately 4.5 nm. To enhance the light extraction, a porous-like p-InGaIn layer is grown to form the p-contact layer.

**ThP93, Wafer-Scale Electroluminescence Studies on GaN-Based LED Structures:** *Carmen Salcianu*<sup>1</sup>; Ted Thrush<sup>1</sup>; Clifford McAleese<sup>1</sup>; Colin Humphreys<sup>1</sup>; <sup>1</sup>Cambridge University

Electroluminescence testing of LED structures is usually done at the chip level. However reliable screening of complete wafers for their optical and electrical characteristics would improve the cost effectiveness of producing LED-lamps. This paper will present wafer scale optoelectronic data, measured using both probe contacts and temporary “adherent” contacts. Although such measurements have provided a useful insight into epiwafer quality, developments are still needed both in the methodology of the characterisation technique and in the design of the grown LED structures if a reliable assay of the wafer’s device potential is to be realised. Improvements in the reproducibility of the method have resulted from better techniques for forming the n-type contact, as well as changes to the grown p-type capping layer which have improved its “contactability”. The latter was achieved using either a p-type superlattice or a highly doped p-GaN layer on top of the standard p-capping layer.

**ThP94, Well Width Dependent Luminescence Characteristics of UV-Violet Emitting GaInN QW LED Structures:** *Michael Kunzer*<sup>1</sup>; Columba Leancu<sup>1</sup>; Markus Maier<sup>1</sup>; Klaus Köhler<sup>1</sup>; Ulrich Kaufmann<sup>1</sup>; Joachim Wagner<sup>1</sup>; <sup>1</sup>Fraunhofer Institute for Applied Solid-State Physics

Temperature and excitation power dependent photoluminescence spectroscopy on GaInN UV-violet LED structures allows to separate the influence of the quantum confined stark effect (QCSE) from carrier localisation in In-induced band tail states as well as to determine the internal quantum efficiency (QE). A LED series with different quantum well widths (1–3.7nm) was grown by MOVPE on sapphire, low defect density (LDD) GaN templates and free standing GaN substrates. The photoluminescence data reveal, that the QCSE cannot be neglected even for low In-content (<10%) UV (<400nm) LED structures. Upon growth on LDD substrates, the internal QE is considerably increased for short wavelength (375–400 nm) LEDs. Furthermore, the effect of the QCSE on the current dependence of the QE has been studied by pulsed electroluminescence measurements, where a pronounced non-thermal rollover of the QE with increasing current density is observed at wavelengths >390 nm.

## ThP: Other Topics

**ThP95, Characteristics of InGaIn Designed for Photovoltaic Applications:** *Elaissa Trybus*<sup>1</sup>; Omkar Jani<sup>1</sup>; Shawn Burnham<sup>1</sup>; Jing Bai<sup>1</sup>; David Citrin<sup>1</sup>; Ian Ferguson<sup>1</sup>; Christiana Honsberg<sup>2</sup>; Myles Steiner<sup>3</sup>; W. Alan Doolittle<sup>1</sup>; <sup>1</sup>Georgia Institute of Technology; <sup>2</sup>University of Delaware; <sup>3</sup>National Renewable Energy Laboratory

This work addresses the required properties, device structures, and measured results for an InGaIn solar cell. Homojunction InGaIn solar cells with a bandgap greater than 2.0 eV are specifically targeted due to discussed cell design and material limitations. These devices are attractive because over half the available power in the solar spectrum is above 2.0 eV. Using high growth rates, InGaIn films with In compositions from 1–32% have been grown by Molecular Beam Epitaxy with negligible phase separation according to

# Technical Program

X-ray diffraction analysis, and better than 190 arcsec omega-2theta FWHM for ~0.6µm thick  $\text{In}_{0.32}\text{Ga}_{0.68}\text{N}$  film. Using measured transmission data, the absorption coefficient of InGaN at 2.4eV was calculated as  $\alpha = 2 \times 10^5 \text{ cm}^{-1}$  near the band edge. This results in the optimal solar cell thickness of ~500nm and may lead to high open circuit voltages and will also lessen the constraints on limited minority carrier lifetimes.

**ThP96, Control and Formation of Ga Nanoparticles on Polar GaN and SiC for GaN Nanostructure Growth:** *Pae Wu*<sup>1</sup>; Maria Losurdo<sup>2</sup>; Tong-Ho Kim<sup>1</sup>; Giovanni Bruno<sup>2</sup>; April Brown<sup>1</sup>; <sup>1</sup>Duke University; <sup>2</sup>Institute of Inorganic Methodologies and of Plasmas-CNR

Investigation of GaN nanostructure growth is of great import for development of nanoscale nitride semiconductor devices. GaN nanowires have been grown by the vapor-liquid-solid (VLS) growth mechanism [J. Electroceram. (2006) 17, 903–907] requiring the self-assembly of Ga droplets on the growth surface in which precursor gas is diluted before the precipitation and formation of GaN nanostructures [J. Am. Chem. Soc. (2001) 123, 2791–2798]. Through use of in situ spectroscopic ellipsometry to probe the surface plasmon resonance of Ga nanoparticles (NPs) deposited by molecular beam epitaxy onto polar GaN and SiC substrates, we demonstrate the formation and control of Ga NPs. X-ray photoelectron spectroscopy and atomic force microscopy reveal that the resultant Ga NP morphology is dependent on the SiC or GaN polarity and surface charge. The chemical and physical interaction between the SiC or GaN substrates with the Ga NPs is important for VLS GaN nanostructure growth.

**ThP97, Correlation between Chemical and Electrical Properties of P-GaN Surfaces Subjected to Halogen-Based Plasma:** *Eri Ogawa*<sup>1</sup>; Masahiro Sugimoto<sup>2</sup>; Tetsu Kachi<sup>3</sup>; Tsutomu Uesugi<sup>3</sup>; Narumasa Soejima<sup>2</sup>; Tamotsu Hashizume<sup>1</sup>; <sup>1</sup>RCIQE, Hokkaido University; <sup>2</sup>Toyota Motor Corporation; <sup>3</sup>Toyota Central R&D Laboratories, Inc

The chemical and electrical properties of the plasma-treated p-GaN surfaces were systematically characterized by X-ray photoelectron spectroscopy (XPS), I-V and C-V analyses using Schottky contacts, and Hall method. The XPS analysis showed the peak shifts of the core levels in the Ga-N bonds for the  $\text{Cl}_2$ - and  $\text{CHF}_3$ -plasma treated samples, in comparison with the as-grown sample. Moreover, the  $\text{GaCl}_x$  and  $\text{GaF}_x$  components were detected on the processed p-GaN surfaces, respectively. In the I-V characteristics between the Ni/Au electrodes evaporated on the p-GaN surfaces, a larger on-set voltage was observed for the  $\text{Cl}_2$ -plasma sample, as compared to the as-grown sample. The formation of thin  $\text{GaCl}_x$  component on p-GaN seems to enhance the Schottky barrier height. For the  $\text{CHF}_3$ -plasma sample, on the other hand, we observed the increase in resistivity of the p-GaN surface, indicating that the incorporation of F atoms into GaN may cause a compensation of holes.

**ThP98, Effects of Carbon Diffusion on Electrical and Optical Properties of N-GaN:** *Takeshi Kimura*<sup>1</sup>; Tamotsu Hashizume<sup>1</sup>; <sup>1</sup>Hokkaido University

Using  $\text{SiN}_x/\text{CN}_x$  bilayer structure prepared by electron-cyclotron-resonance assisted chemical vapor deposition, a simple process of carbon diffusion into GaN layer was developed. The thin  $\text{CN}_x$  layer with a highly carbon-rich composition can act as source for carbon diffusion. An x-ray photoelectron spectroscopy and a secondary ion mass spectrometry results showed diffusion of carbon with into GaN a depth of about 200 nm after an anneal at 1000 °C for 120 min in  $\text{N}_2$  ambient. The Photoluminescence spectra show that the deep-level-related emission was enhanced by the carbon diffusion, while no pronounced emission was observed from the shallow acceptor levels in the carbon-diffused sample. We also observed the increase in resistivity of the GaN surface after the carbon diffusion. These results indicate that the diffused carbon acts as a deep acceptor in the form of an interstitial atom or in the complex form with some defects in GaN.

**ThP99, Evolution of Surface Morphology during Crystallographic Wet Etching of N-Type GaN Using Phosphoric Acidic Solutions:** *Jae Kwan Kim*<sup>1</sup>; Taek Seung Kim<sup>1</sup>; Youngje Jo<sup>1</sup>; Han-Ki Kim<sup>2</sup>; Sang-Woo Kim<sup>2</sup>; Kyoung-Kook Kim<sup>3</sup>; Ji-Myon Lee<sup>1</sup>; <sup>1</sup>Sunchon National University; <sup>2</sup>Kumoh National Institute of Technology; <sup>3</sup>Samsung Advanced Institute of Technology

The morphology variation of the etched surface by using phosphoric acidic solution was observed by optical microscopy and atomic force microscopy. Initially, high density of hexagonal holes or pits were formed on the etched surface, with the lateral size of 20 µm or 5 µm, respectively, indicating that the crystallographic etching was occurred. However, as the etching time was increased further, the lateral size of the hexagonal holes or pits was increased, and finally, joined and merged together at the time of 100 min. This means that the etching of n-type GaN by phosphoric acidic solutions proceeded through the lateral widening and the merging of initial holes and pits. Furthermore, fundamental mechanism of initial stage of etching of n-type GaN using phosphoric acidic solutions will be reported in this presentation.

**ThP100, Fabrication and Stress Relief Modelling of GaN Based MEMS Test Structures Grown by MBE on Si(111):** *Eugenio Sillero*<sup>1</sup>; David López-Romero<sup>1</sup>; Ana Bengoechea<sup>1</sup>; Miguel Ángel Sánchez-García<sup>1</sup>; Fernando Calle<sup>1</sup>; <sup>1</sup>ISOM & DIE UPM

The fabrication of III-N MEMS and the modelling of their residual stress induced deformation is presented. GaN and AlGaIn/GaN test structures were fabricated, either with one end and both ends clamped to the Si substrate. The residual stress in the III-N layer were measured by photoluminescence and X-ray diffraction, and the stress relief induced deformation was analysed by a finite element method model. One-end-clamped structures suffer from large deformations due to the uneven stress relaxation. During micromachining, the relaxation induces large upward buckling, as measured for fabricated devices and fitted by the FEM model. Two-end-clamped structures were also studied using different topologies and under-etching lengths of the clamped region. It is concluded that the deformation of such structures may be reduced if symmetrical mechanical boundary conditions are provided, and the under-etching of the clamping region is small compared to the device dimensions.

**ThP101, Formation of Nitride Laser Cavities with Cleaved Facets on Transferred Laser Diodes on GaAs Substrates:** Wen-Chien Yu<sup>1</sup>; Shu-Mei Ye<sup>1</sup>; Feng-Ke Hsiao<sup>1</sup>; Chi-Ling Lee<sup>1</sup>; *Wei-I Lee*<sup>1</sup>; Pei-Lun Wu<sup>1</sup>; <sup>1</sup>Chiao Tung University

Smoothly cleaved facets with high reflectivities have been demonstrated on GaN laser diodes after the devices were transferred onto GaAs substrates. The GaN based laser diode structure was first fabricated by metal organic chemical vapor deposition (MOCVD) on c-plane sapphire substrates. The samples were then mounted onto thin GaAs substrates using wafer-bonding technology. Laser lift-off (LLO) technique was applied to remove the original sapphire substrate and transfer the GaN laser structure onto GaAs substrates. Since the cubic substrates have well-defined laser cavity cleavage facet, the GaN structures bonded onto the substrates also formed smooth facets after cleavage. The cleaved facets of GaN laser diodes have been characterized using atomic force microscopy (AFM) with less than 3 nm roughness. The present study demonstrated the feasibility of transferring GaN laser structures onto other more appealing substrates for formation of laser cavities.

**ThP102, Gentle Chemical Mechanical Polishing of GaN Substrates:** *Rajiv Singh*<sup>1</sup>; Arul Chakkaravarthi Arjunan<sup>2</sup>; Hung-Ta Wang<sup>1</sup>; Stephen Pearton<sup>1</sup>; Sahil Sahni<sup>1</sup>; Fan Ren<sup>1</sup>; Syamal Lahiri<sup>2</sup>; Deepika Singh<sup>2</sup>; <sup>1</sup>University of Florida; <sup>2</sup>Sinmat Inc

As GaN is chemically inert and mechanically hard, existing polishing techniques have typically employed hard particles or incompatible chemistries. Such polishing solution results in rough or damaged and scratched layers. We have developed a industrially robust and low cost chemical mechanical smoothening (CMS) process to produce atomically polished GaN substrates. Such atomically polished GaN on silicon substrates are expected to increase device yield, help development of novel device structures and enhance technical performance of GaN based devices. Our results show that the GaN surfaces can achieve atomic level smoothness and formation of a high quality surface. The rms roughness decreased from 4.1nm to less than 1Å after the

polishing process. The Schottky devices made from CMS polished substrates shows lower leakage current and large barrier height confirming the removal of the defective surface layer. The formation of such surfaces is expected to be ideal for GaN based electronic devices.

**ThP103, High-Quality Native Oxide of GaN for Surface Passivation Formed by Photo-Enhanced Electrochemical Process:** *Nanako Shiozaki*<sup>1</sup>; Fumitaro Ishikawa<sup>2</sup>; Achim Trampert<sup>2</sup>; Holger Grahn<sup>2</sup>; Tamotsu Hashizume<sup>1</sup>; <sup>1</sup>Hokkaido University; <sup>2</sup>Paul-Drude-Institut für Festkörperelektronik

This paper reports on successful oxidation of n-GaN surface using photoelectrochemical process in a mixed solution with propylene glycol and 3% tartaric acid. To oxidize the GaN surface, we first applied ramp-type bias from 0 to 3V and then constant bias at 3V under the potentiostatic control. The process with this bias form enables us to form high-quality native oxide of GaN which has thin crystalline intermediate layer at oxide/GaN interface. Photoluminescence coming from oxidized GaN surface showed 3 times higher intensity than that from un-oxidized area of the sample. The consumption of the GaN surface to form the native oxides may result in the reduction of various kinds of surface defects, leading to the drastic reduction of surface states on the oxidized GaN surfaces. This oxidation method will be useful for stability improvement of LEDs and HBTs.

**ThP104, Impact of AlN Interlayer on the Transport Properties of AlGaIn/GaN Heterostructures Grown on Silicon:** *Said Elhamri*<sup>1</sup>; W. Mitchell<sup>2</sup>; R. Berney<sup>1</sup>; M. Ahoujja<sup>1</sup>; J. Roberts<sup>2</sup>; P. Rajagopal<sup>3</sup>; J. Cook<sup>3</sup>; E. Piner<sup>3</sup>; K. Linthicum<sup>3</sup>; <sup>1</sup>University of Dayton; <sup>2</sup>Air Force Research Laboratory; <sup>3</sup>Nitronex Corporation

Hall and Shubnikov-de Haas effects measurements were performed to identify the impact of inserting a 1nm AlN interlayer between AlGaIn and GaN. The transport properties of this AlGaIn/AlN/GaN structure were compared to the conventional structure (AlGaIn/GaN). Our measurements indicate the AlN interlayer resulted in improved transport in the temperature range studied (300 K- 1.2 K). However, the impact of the AlN layer was found to be much more significant at low temperatures. The improvement is believed to be the result of reduced alloy scattering arising from a stronger confinement of the 2DEG. At 300 K the carrier density and mobility for the AlGaIn/AlN/GaN structure were roughly  $1.00 \times 10^{13} \text{ cm}^{-2}$  and  $1937 \text{ cm}^2/\text{Vs}$ . Whereas those of the conventional structure were  $8.57 \times 10^{12} \text{ cm}^{-2}$  and  $1523 \text{ cm}^2/\text{Vs}$ . Shubnikov-de Haas oscillations were observed in both samples at low T.

**ThP105, Improvement of Hydrogen Generation Efficiency Using GaN Photoelectrochemical Reaction in Electrolytes with Alcohol:** *Katsushi Fujii*<sup>1</sup>; Hitoshi Nakayama<sup>1</sup>; Keiichi Sato<sup>1</sup>; Takashi Kato<sup>1</sup>; Meoungwhan Cho<sup>1</sup>; Takafumi Yao<sup>1</sup>; <sup>1</sup>Tohoku University

Photoelectrochemical water reduction is one of the candidates for hydrogen production by solar energy. GaN is superior to many oxides like  $\text{TiO}_2$ , in terms of efficiency, since the conduction band energy is more suitable for hydrogen generation. In this report, we discussed the effect of organic addition to an electrolyte for hydrogen generation without bias. We used 1.0 mol/L NaOH as an electrolyte with and without 1.0 mol/L  $\text{CH}_3\text{OH}$  or  $\text{C}_2\text{H}_5\text{OH}$ . The current densities were almost the same at the beginning ( $0.88 \text{ mA/cm}^2$  for NaOH,  $0.99 \text{ mA/cm}^2$  for NaOH with  $\text{CH}_3\text{OH}$ ,  $0.81 \text{ mA/cm}^2$  for NaOH with  $\text{C}_2\text{H}_5\text{OH}$  under  $310 \text{ mW/cm}^2$  illumination). The photocurrent densities with alcohol decreased and almost stabilized after 200 min, while the density without alcohol decreased linearly. Hydrogen generations with alcohol were approximately double of that without alcohol where the total charges are almost the same at 300 min.

**ThP106, Improvement of the Light Output Power of GaN-Based Leds by Using Interlayered Indium Tin Oxide-Based P-Type Electrodes:** June-O Song<sup>1</sup>; Hyun-Gi Hong<sup>2</sup>; Hyeonseok Na<sup>2</sup>; *Tae-Yeon Seong*<sup>2</sup>; <sup>1</sup>National Institute for Materials Science; <sup>2</sup>Korea University

To enhance the light output of GaN-based LEDs, transparent indium tin oxide (ITO) and ZnO-based schemes have been investigated. However, single ITO single contacts showed rather poor electrical behavior because ITO has a relatively small work function (4.8eV). Thus, in this work, to improve its electrical properties, we have introduced different interlayers of

In and Sn-Ag alloy. The In/ITO and Sn-Ag/ITO contacts become ohmic with specific contact resistance of  $1.2 \times 10^{-3}$ – $4.27 \times 10^{-4} \text{ ohmcm}^2$  and transmittance of 91–95% at 460 nm when annealed at 530°C. Blue LEDs fabricated with the In and Sn-Ag/ITO contacts give forward-bias voltage of 3.31–3.42V at injection current of 20 mA. LEDs fabricated with these interlayered ITO p-type contact layers exhibit much better output power (e.g., improvement by 62–91%) at 20 mA as compared to that of LEDs with the oxidized Ni/Au contacts. Possible ohmic mechanisms are described and discussed.

**ThP107, Improvement of the Optical Performance of GaN-Based LEDs by Using Cu-Doped Indium Oxide/Sb-Doped  $\text{SnO}_2$  P-Contacts:** *Hyun-Gi Hong*<sup>1</sup>; Hyun-Seok Na<sup>1</sup>; Joon-Ho Oh<sup>1</sup>; Kang-Won Kim<sup>1</sup>; Ju-Heon Yun<sup>1</sup>; Yong-Hyun Kim<sup>1</sup>; Joon-Woo Jeon<sup>1</sup>; Yoon-Han Kim<sup>1</sup>; Tae-Yeon Seong<sup>1</sup>; <sup>1</sup>Korea University

Currently, indium tin oxide(ITO) is commonly used for p-type electrodes in GaN-based LEDs because it has high conductivity and transmittance. ITO, however, suffers from thermal instability and the exhaustion of indium. In this work, we have investigated Cu-doped indium oxide(CIO)/Sb-doped  $\text{SnO}_2$ (ATO) p-contacts to improve the optical performance of LEDs. It is shown that the CIO/ATO(250 nm) contacts become ohmic with specific contact resistance of  $2.1 \times 10^{-3} \text{ } \Omega\text{cm}^2$  and exhibit transmittance of ~81% at a wavelength of 400 nm when annealed at 630°C. Furthermore, near-UV LEDs(400 nm) with the CIO/ATO contacts show higher output power than LEDs with conventional Ni/ Au contacts. For example, LEDs with the 630°C-annealed CIO/ATO p-contacts result in improvement (by 82.4%) of the output power at 20mA compared to LEDs with Ni/ Au p-contacts. Based on XPS and AES results, possible ohmic formation mechanisms are described.

**ThP108, Nitrides for Thermoelectric Application:** *Bed Pantha*<sup>1</sup>; Rajendra Dahal<sup>1</sup>; Li Jing<sup>1</sup>; Fan Zhaoyong<sup>1</sup>; Jingyu Lin<sup>1</sup>; Hongxing Jiang<sup>1</sup>; Gernot Pomrenke<sup>2</sup>; <sup>1</sup>Kansas State University; <sup>2</sup>Air Force Office of Scientific Research

III-nitride semiconductors offer tremendous scope for the enhancement of the thermoelectric (TE) figure of merit (ZT) through the use of the bandgap engineering, alloying and nanostructure manipulation. The ZT value of a TE material can be enhanced by increasing the electrical conductivity and Seebeck coefficient and decreasing the thermal conductivity. In this study, we have employed the Hall-Effect measurement, temperature gradient method, and differential  $3\omega$  method to characterize the electrical conductivity, Seebeck coefficient, and thermal conductivity of III-nitrides. It was found that the incorporation of indium in GaN significantly reduced the thermal conductivity. Our preliminary results indicate that ZT of  $\text{In}_{0.28}\text{Ga}_{0.72}\text{N}$  alloys is comparable to that of SiGe based materials at 300 K. The development of III-nitride based TE materials may open up the possibility for monolithic integration of TE modules onto the high power electronic and optoelectronic chips for the purpose of spot cooling and thermopower generation.

**ThP109, Optimization of Ohmic Contacts to N(+)-GaN Capped AlGaIn/AlN/GaN HEMTs:** *Liang Wang*<sup>1</sup>; Fatih Mohammed<sup>1</sup>; Benedict Ofuonye<sup>1</sup>; Ilesanmi Adesida<sup>1</sup>; <sup>1</sup>University of Illinois at Urbana-Champaign

Optimization of Ti/Al/Mo/Au ohmic contacts to n+-GaN/AlGaIn/AlN/GaN heterostructures is reported. The contact performance, as obtained from I-V linearity, and contact resistance, of as-deposited and annealed contacts depends on  $\text{SiCl}_4$  plasma self-bias voltage, heat treatment condition, and Ti thickness. For the 15 nm-Ti scheme, optimum  $R_c=0.46 \text{ } \Omega\text{-mm}$  was achieved by a combination of 400 V, 1 min plasma treatment and 850°C, 30s annealing. However, untreated sample showed linear I-V curve but with  $R_c>1 \text{ } \Omega\text{-mm}$ . Doubling the Ti thickness reduced  $R_c$  and  $R_c<0.5 \text{ } \Omega\text{-mm}$  was obtained for both plasma treated and untreated samples. Optimum performance was achieved with a plasma-bias of 300 V followed by 850°C annealing. XTEM investigation indicated that 15 nm-thick Ti reacted only with the GaN cap and the AlGaIn layer remained intact. However, 30nm-thick Ti effectively thinned down both GaN cap and the top part of AlGaIn so that higher tunneling current was enabled.

# Technical Program

**ThP110, Photoelectrolysis of Water with Structured N-GaN:** *Ichitaro Waki*<sup>1</sup>; Daniel Cohen<sup>1</sup>; Rakesh Lal<sup>1</sup>; Umesh Mishra<sup>1</sup>; Steven DenBaars<sup>1</sup>; Shuji Nakamura<sup>1</sup>; <sup>1</sup>University of California, Santa Barbara

Direct water photoelectrolysis with semiconductors has attracted attention as a hydrogen production technology. Recent demonstrations of water photoelectrolysis with GaN showed the potential, but the solar-to-hydrogen conversion efficiency is not sufficient for practical use. In this study we observed more efficient direct water photoelectrolysis using a structured n-GaN photoanode and a platinum cathode without external bias. The structured n-GaN was formed by a metal stripe patterning using photolithography and a subsequent selective area regrowth. As expected, the photocurrent of the structured n-GaN was significantly enhanced in comparison with a plane n-GaN particularly at higher current densities. We attribute the enhancement to both alleviated current crowding and increased specific surface area. A gas volume analysis showed evidence of hydrogen and oxygen evolution. The origin of the photocurrent and the conversion efficiency will be discussed in detail based on water-splitting reactions and etching reactions.

**ThP111, Properties of ZnO Layers Grown by Metalorganic Chemical Vapor Deposition on GaN(0001) Templates and ZnO(0001) Substrates:** *Tommy Iye*<sup>1</sup>; Tammy Ben-Yaacov<sup>1</sup>; Hirokuni Asamizu<sup>2</sup>; Umesh Mishra<sup>1</sup>; Steven DenBaars<sup>1</sup>; James Speck<sup>1</sup>; <sup>1</sup>University of California, Santa Barbara; <sup>2</sup>Rohm Company

We study the properties of ZnO(0001) layers grown by metalorganic chemical vapor deposition on GaN(0001) templates and ZnO(0001) substrates. The layers grown homoepitaxially on ZnO substrates yield excellent results in terms of surface morphology and crystal quality. ZnO layers grown on GaN templates are smooth but exhibit pits and plateau-valley or fractal morphology with a root mean square value of 2.0 nm. The full width at half maximum of symmetric omega scans were as narrow as 288 arcsec. X-ray rocking curves recorded in skew geometry had a full width at half maximum of 936 arcsec or higher. Reciprocal space maps show that the ZnO layers grown on GaN layers are relaxed. No mismatch was detected for the layers grown homoepitaxially. Unintentionally doped ZnO layers were grown on (In,Ga)N LEDs in an attempt to use ZnO as a transparent contact.

**ThP112, Thermal Analysis of GaN Powder Formation via Reaction of Gallium Ethylenediamine Tetraacetic Acid Complexes with Ammonia:** *Yuhuai Liu*<sup>1</sup>; Shinya Koide<sup>1</sup>; Hideto Miyake<sup>1</sup>; Kazumasa Hiramatsu<sup>1</sup>; Atsushi Nakamura<sup>2</sup>; Nobuyoshi Nambu<sup>2</sup>; <sup>1</sup>Mie University; <sup>2</sup>Chubu Chelest Company, Ltd

The gallium ethylenediamine tetraacetic acid (Ga-EDTA) complexes were analyzed by thermal gravity/differential thermal analysis (TG/DTA) under ammonia gas flow to reveal the mechanism of GaN powder formation via reaction of Ga-EDTA complexes with ammonia. The results of the dynamic TG/DTA and the thermal sintering temperature/time dependence show that the precursors undergo a sharp mass loss at about 296°C due to the release of organic groups, followed by further releasing of organic groups (297 ~ 552°C), elimination of carbon and formation of GaN (552 ~ 650°C), GaN crystallization and further elimination of carbon (650 ~ 850°C), the improvement of GaN crystal quality (600 ~ 1100°C) and the initial decomposition of GaN powders. The analysis of the results indicates that proper sintering temperature for GaN powders should be approximate to 1100°C.

**ThP113, Thermal Conduction in Nitride Semiconductors and GaN-Based Device Structures:** *Alexander Balandin*<sup>1</sup>; <sup>1</sup>University of California - Riverside

Self-heating presents a major problem for the high-power density GaN-based field-effect transistors. Optimization of GaN devices requires knowledge of thermal conductivity  $K$  in GaN films and  $\text{Al}_x\text{Ga}_{1-x}\text{N}$  alloys. There is major discrepancy in the reported  $K$  values ranging from 1.30 to 2.25 W/mK at RT. The theoretically predicted maximum is  $K=4.10$  W/mK at RT. In this talk I will review our results, which explain  $K$  dependence on the defects, dislocations and alloy disorder. Our measurements were carried out using transient techniques. The theoretical analysis is based on the Callaway – Klemens and Abeles models. I will also report the electro-thermal simulations of the GaN device performance focusing on self-heating

and ambient effects. <sup>1</sup>J. Zou et al, J. Appl. Phys., 92, 2534 (2002); Appl. Phys. Lett., 79, 4316 (2001); W.L. Liu and A.A. Balandin, J. Appl. Phys., 97, 073710 (2005). <sup>2</sup>V.O. Turin and A.A. Balandin, J. Appl. Phys., 100, 054501 (2006).

# Technical Program

---

## Session KK: P-Type InN

Friday AM  
September 21, 2007

Room: 312/317  
Location: MGM Grand Hotel Conference Center

*Session Chairs:* William Schaff, Cornell University; Akihiko Yoshikawa, Chiba University

---

### 8:30 AM Invited

**KK1, P-Type InN and In-Rich InGaN:** *Joel Ager*<sup>1</sup>; <sup>1</sup>Lawrence Berkeley National Laboratory

The bandgap range of InGaN extends from the near-IR (InN, 0.65 eV) to the ultraviolet. To exploit this wide tuning range in light generation and conversion applications, pn junctions are required. The large electron affinity of InN (5.8 eV) leads to preferential formation of native donor defects, resulting in excess electron concentration in the bulk and at surfaces and interfaces, which creates difficulties for p-type doping and/or measuring of the bulk p-type activity. Capacitance voltage measurements, which deplete the n-type surface inversion layer, have been used to show that Mg is an active acceptor in InN and In-rich InGaN. Recent investigations of the properties of Mg-doped InN and InGaN will be presented, including thermopower transport measurements and photoluminescence. In collaboration with R. E. Jones, N. Miller, K. M. Yu, J. Wu, W. J. Schaff, and W. Walukiewicz.

### 9:00 AM Invited

**KK2, Electrical Properties of p-Type N-Polar InN Grown by RF-MBE:** *Daisuke Muto*<sup>1</sup>; Hiroyuki Naoi<sup>1</sup>; Shinji Fukumoto<sup>1</sup>; Kin Man Yu<sup>2</sup>; Nate Miller<sup>2</sup>; Rebecca Jones<sup>2</sup>; Joel Ager<sup>2</sup>; Eugene Haller<sup>2</sup>; Tsutomu Araki<sup>1</sup>; Yasushi Nanishi<sup>1</sup>; Wladek Walukiewicz<sup>2</sup>; <sup>1</sup>Ritsumeikan University; <sup>2</sup>Lawrence Berkeley National Laboratory

P-type N-polar InN films have been grown for the first time by RF-MBE using Mg as a dopant. The Mg content was varied by controlling the Mg cell temperature in the range of 125-140°C. Electrical properties were evaluated by electrolyte-based C-V measurements. From the  $1/C^2$ -V (Mott-Schottky) plots, it was found that Mg-doped InN grown with a Mg cell temperature of more than 130°C is p-type under a surface inversion layer. We also found that the p-type Mg-doped InN tends to have a higher net acceptor concentration as the Mg doping amount is increased. This result indicates that the p-type conductivity of InN can be controlled by changing the Mg cell temperature. This technique may be useful in the fabrication of InN-based opto-electronic devices in the future.

### 9:30 AM

**KK3, P-Type Doping of InN:** *Thomas Myers*<sup>1</sup>; Craig Swartz<sup>2</sup>; Chito Kendrick<sup>2</sup>; Phil Anderson<sup>2</sup>; Hai Lu<sup>3</sup>; Sandeep Chandril<sup>1</sup>; Y. Song<sup>2</sup>; Roger Reeves<sup>2</sup>; Steve Durbin<sup>2</sup>; William Schaff<sup>3</sup>; <sup>1</sup>West Virginia University; <sup>2</sup>University of Canterbury; <sup>3</sup>Cornell University

Of current interest is the possibility to achieve p-type conductivity in InN. The surface electron accumulation layer can mask a p-type layer's contribution to conventional Hall effect measurements. Variable magnetic field Hall measurements can be used to determine the influence of the various carriers. Temperature dependent resistivity and Hall measurements were made at magnetic fields up to 12 T on InN samples grown by molecular beam epitaxy. Quantitative mobility spectrum analysis (QMSA) and multiple-carrier fitting analyses were performed. Evidence will be presented for direct observation of p-type doping of InN in samples doped in-situ with Mg and via substrate impurity doping when growing on (111) YSZ. QMSA reveals light hole conduction in many of the samples, with one sample clearly p-type, exhibiting both heavy and light holes. At Mg concentration of  $6 \times 10^{18} \text{cm}^{-3}$ , a faint PL peak at 0.56 eV suggests an acceptor energy approximately 110 meV above the valence band.

### 9:45 AM

**KK4, Study on P-Type Dopability and Polarity Inversion in Mg-Doped In-Polar InN:** *Xinqiang Wang*<sup>1</sup>; Song-Bek Che<sup>1</sup>; Yoshihiro Ishitani<sup>1</sup>; Akihiko Yoshikawa<sup>1</sup>; <sup>1</sup>Graduate Course of Electrical and Electron Engineering, Venture Business Laboratory, InN-Project as a CREST-program of JST, Chiba University

Mg-doped InN films are grown under In-polarity regime with systematically varied Mg-beam fluxes by MBE. It is found by SIMS analysis that Mg concentration is linearly proportional to Mg-beam flux, indicating that Mg sticking coefficient is almost unity up to  $1.8 \times 10^{20} \text{cm}^{-3}$ . Electrical, crystalline and optical properties of InN films are greatly influenced by Mg-doping. With increasing Mg beam flux, electron concentration in InN decreases first by the effect of carrier compensation, and then begins to increase due to the formation of Mg-related donor-like-defects. In the partially carrier-compensated Mg-doped InN, two photoluminescence peaks are observed. The excitation power dependent PL study indicates that one emission peak is originated from free-to-acceptor emission with acceptor activation energy of about 61 meV and the other is due to the band-to-band emission. Furthermore, In-polar InN is found to be inverted to N-polar one when Mg concentration is larger than  $2.9 \times 10^{19} \text{cm}^{-3}$ .

### 10:00 AM

**KK5, Determination of the Mg Occupation-Site in MOCVD-Grown Mg-Doped InN by Using X-Ray Absorption Fine-Structure Measurements:** *Takao Miyajima*<sup>1</sup>; Shigeaki Uemura<sup>1</sup>; Yoshihiro Kudo<sup>1</sup>; Yoshinori Kitajima<sup>2</sup>; Akio Yamamoto<sup>3</sup>; <sup>1</sup>Sony Corporation; <sup>2</sup>High Energy Accelerator Research Organization; <sup>3</sup>Fukui University

InN-based devices with a p-n junction have not yet been realized because it is difficult to obtain low-resistivity p-type InN. When Mg, which is a prime candidate for a p-type dopant, is doped to InN, the conductivity has been n-type or insulating. In order to determine what prevents p-type conductivity, it is necessary to determine the Mg occupation-sites. For this, we analyzed the atomic structure around Mg atoms in Mg-doped InN by using Mg K-edge x-ray absorption fine-structure (XAFS) measurements. Our experimental data fit to the simulated data in which Mg atoms occupy the substitutional sites of In atoms. From this result, we conclude that Mg atoms essentially occupy not N atoms sites but In atoms sites, meaning that Mg atoms can act as acceptors in InN. We believe that observations of p-type conductivity are prevented by the remaining problems such as carrier compensation and electron accumulation at the surface.

### 10:15 AM

**KK6, Surface Electronic Properties of N- and P-Type InN and InGaN Alloys:** *Philip King*<sup>1</sup>; Tim Veal<sup>1</sup>; Paul Jefferson<sup>1</sup>; Hai Lu<sup>2</sup>; William Schaff<sup>2</sup>; Chris McConville<sup>1</sup>; <sup>1</sup>University of Warwick; <sup>2</sup>Cornell University

The variation of band bending as a function of composition at (0001) surfaces of undoped and Mg-doped  $\text{In}_{1-x}\text{Ga}_x\text{N}$  is investigated using x-ray photoelectron spectroscopy. Distinctly different trends in barrier height are observed for the Mg-doped compared to undoped alloys, explained in terms of Fermi-level pinning at the surface and virtual gap states. Solutions of Poisson's equation within the modified Thomas-Fermi approximation are used to model the band bending and corresponding variation of carrier concentration with depth below the surface. For undoped alloys, a transition from electron accumulation for In-rich to depletion for Ga-rich alloys occurs at  $x \approx 0.3$ , whilst for Mg-doped alloys, a transition from a surface inversion layer for In-rich to a surface hole depletion layer for Ga-rich alloys occurs at  $x \approx 0.49$ . The trend in barrier height across the composition range and calculated space-charge profiles indicate that Mg-doping induces bulk p-type conductivity across the entire composition range.

### 10:30 AM Break

# Technical Program

## Session LL: Nanostructures: Growth I

Friday AM Room: 313/316  
September 21, 2007 Location: MGM Grand Hotel Conference Center

*Session Chairs:* C. Thomas Foxon, University of Nottingham; Stephen Hersee, University of New Mexico

### 8:30 AM Invited

**LL1, Nitride Nanowires and Nanotubes:** *Peidong Yang*<sup>1</sup>; <sup>1</sup>University of California, Berkeley

Nanowires are of both fundamental and technological interest. They represent the critical components in the potential nanoscale electronic and photonic device applications.<sup>1</sup> In this talk, I will provide an overview of our recent efforts on nitride nanowire/nanotube research. Nitride nanowires can be rationally synthesized using the vapor-liquid-solid growth mechanism. By applying the epitaxial concept towards this VLS process, we can readily achieve the control over the growth direction of the nanowires.<sup>2</sup> In addition, single crystalline nitride nanotubes can be synthesized using a novel templating approach.<sup>3</sup> These one-dimensional nitride nanostructures exhibit interesting photonic properties including single nanowire lasing.<sup>4,5</sup> Their potential as photovoltaic and solid state lighting materials will also be discussed. <sup>1</sup>P. Pauzauskie, P. Yang, *Materials Today*, 9,36, 2006. <sup>2</sup>T. Kuykendall, P. J. Pauzauskie, Y. Zhang, J. Goldberger, D. Sirbully, J. Denlinger, P. Yang, *Nature Materials*, 3, 528, 2004. <sup>3</sup>J. Goldberger, R. He, H. Choi, H. Yan, P. Yang, *Nature*, 422, 599, 2003. <sup>4</sup>J. Johnson, H. J. Choi, K. P. Knutsen, R. D. Schaller, P. Yang, R. J. Saykally, *Nature Materials*, 1,101, 2002. <sup>5</sup>P. Pauzauskie, D. Sirbully, P. Yang, *Phys. Rev. Lett.* 96, 143903, 2006.

### 9:00 AM

**LL2, Fabrication of Patterned InN Nano-Columns by ECR-MBE:** *Tsutomu Araki*<sup>1</sup>; Taihei Yamaguchi<sup>1</sup>; Satoshi Harui<sup>1</sup>; Hideto Miyake<sup>2</sup>; Kazumasa Hiramatsu<sup>2</sup>; Yasushi Nanishi<sup>1</sup>; <sup>1</sup>Ritsumeikan University; <sup>2</sup>Mie University

InN-based nano-structures are very attractive for applications to long-wavelength optoelectronic devices. Recently, we have proposed a novel growth technique of position-controlled InN nano-dots on the GaN template with patterned holes prepared by using FIB. In this study, we will demonstrate successful fabrication of patterned InN nano-columns on the hole-patterned GaN templates using ECR-MBE. InN growth was carried out at 450°C for 2 hours on the GaN templates with square arrays of holes prepared by FIB. We successfully obtained the patterned InN nano-columns with a well-ordered height of ~1.5 μm and a diameter of ~200 nm. InN nano-columns showed hexagonal structures with the same in-plane orientation, indicating that InN nano-columns with [0001] growth direction were epitaxially grown on the (0001) GaN template. TEM studies also confirmed that few threading dislocations were observed in these InN nano-columns. These results indicate that this growth technique is very useful for fabricating periodic InN-based nano-structures.

### 9:15 AM

**LL3, Self-Organized Growth of Inn-Nanocolumns by MBE:** *Christian Denker*<sup>1</sup>; Florian Werner<sup>1</sup>; Joerg Malindretos<sup>1</sup>; Henning Schuhmann<sup>1</sup>; Michael Seibt<sup>1</sup>; Angela Rizzi<sup>1</sup>; Jaime Segura<sup>2</sup>; Nuria Garro<sup>2</sup>; Andres Cantarero<sup>2</sup>; <sup>1</sup>Georg-August-Universitaet Goettingen; <sup>2</sup>University of Valencia

InN-nanocolumns are an attractive system for light harvesting applications. Our aim is to investigate the growth, optical and electrical properties of nanocolumn ensembles and single objects. The samples were grown on p-Si(111) by plasma assisted MBE. Depending on the growth parameters different growth regimes for nanocolumns were identified according to their final shape: hexagonal cross-section and broadened end, rounded cross-section and tapered end. For certain growth conditions we reproducibly observe a bimodal distribution in which one type of wires shows a very high aspect ratio of 45. The early stages of nucleation have been analyzed and correlated to the final shape distribution. High-resolution TEM images

show a very good crystal quality, with features that depend on the growth mode. This fact is also reflected in photoluminescence and Raman analysis. Furthermore we will present I-V-characteristics of single nanocolumns in two- and four-point probe geometry.

### 9:30 AM

**LL4, InGaN Nanostructured Materials: Controlled Synthesis, Characterizations, and Applications:** *Olga Kryliouk*<sup>1</sup>; Josh Mangum<sup>1</sup>; Hyun Jong Park<sup>1</sup>; YongSun Won<sup>1</sup>; Tim Anderson<sup>1</sup>; Zuzanna Liliental-Weber<sup>2</sup>; <sup>1</sup>University of Florida; <sup>2</sup>Lawrence Berkeley National Laboratory

Controlled synthesis of 1D III-Nitrides creates an opportunity for their fundamental study and new applications for future electronic and photonic devices. Single-crystalline InGaN nanorods (NRs) and nanowires (NWs) were successfully grown on Al<sub>2</sub>O<sub>3</sub>, GaN, and Si substrates by non catalytic, template-free conventional metal-organic vapor phase epitaxy (MOVPE) and hydride metal-organic vapor phase epitaxy (H-MOVPE). The controlled growth of self-seeded III-Nitride nanostructured materials has been demonstrated. Complex chemical equilibrium calculations were performed for the In-Cl-H-N system considering possible reactions to determine optimum conditions for InN NR formation. It was studied thermodynamically and confirmed experimentally that InN NR growth by H-MOVPE occurs at the growth-etch transition region. Dislocation free high quality InGaN nanorods with [00.1] growth axis were deposited via solid-vapor (SV) growth mechanism. Growth parameters and optimal growth conditions were determined. Ongoing efforts in our research on InN NRs foundational applications will be presented.

### 9:45 AM

**LL5, Late News**

### 10:00 AM

**LL6, Late News**

### 10:15 AM

**LL7, Late News**

### 10:30 AM Break

## Session MM: Defects and Structural Characterization

Friday AM Room: 314/315  
September 21, 2007 Location: MGM Grand Hotel Conference Center

*Session Chairs:* Giacinta Parish, University of Western Australia; Christian Wetzel, Rensselaer Polytechnic Institute

### 8:30 AM Invited

**MM1, Atom Probe Reveals the Structure of InGaN Quantum Wells in 3D:** *Mark Galtrey*<sup>1</sup>; Rachel Oliver<sup>1</sup>; Menno Kappers<sup>1</sup>; Diane Zhu<sup>1</sup>; Clifford McAleese<sup>1</sup>; Colin Humphreys<sup>1</sup>; David Larson<sup>2</sup>; Peter Clifton<sup>2</sup>; Alfred Cerezo<sup>3</sup>; <sup>1</sup>University of Cambridge; <sup>2</sup>Imago Scientific Instruments; <sup>3</sup>University of Oxford

We have examined InGaN-based quantum well (QW) structures with the Local Electrode Atom Probe (LEAP), which gives a field of view of 150nm with direct chemical information and sub-nanometre spatial resolution in three-dimensions. We show that InGaN with a range of compositions is a random alloy, and so conclude that nm-scale In rich clusters are not essential for luminescence. We characterise the QW interfaces, and find that the upper interfaces of blue- and green-emitting QWs are more diffuse and rougher than the lower, with the difference in roughness providing a viable carrier localisation mechanism. Finally we examine a high-efficiency UV-emitting sample in which In in the barriers at the 0.1% level was thought to improve performance. However, we found In in the barriers of all our samples and so suggest that the observed discontinuities in the QWs at a ~50nm length scale are more important to performance.

# Technical Program

9:00 AM

**MM2, Effect of the Internal Electrostatic Potential on the Light Emitting Properties of InGaN Quantum Wells in Green LEDs:** *Zhihao Wu<sup>1</sup>; A. Fischer<sup>1</sup>; F. Ponce<sup>1</sup>; W. Lee<sup>2</sup>; J. H. Ryou<sup>2</sup>; J. Limb<sup>2</sup>; D. Yoo<sup>2</sup>; R. Dupuis<sup>2</sup>*; <sup>1</sup>Arizona State University; <sup>2</sup>Georgia Institute of Technology

Variations in the piezoelectric field have been observed along the growth direction in InGaN-based diodes emitting in the green region. The internal electrostatic potential distribution across the active region consisting of five InGaN quantum wells has been determined by electron holography in a transmission electron microscope. The strength of the piezoelectric field decreases along the growth direction. Its effect on light emission has been evaluated by depth profiling cathodoluminescence, where the emissions from two peaks become increasingly distinct with increasing excitation voltage. The drop in piezoelectric field strength is proposed to be related to the neutralization of piezoelectric charges by hydrogen ions which are initially abundant in the p-region and diffuse into the quantum wells during thermal annealing.

9:15 AM

**MM3, GaInN Light Emitting Diodes with Lattice-Matched AlInN/GaN Distributed Bragg Reflector on Si:** *Hiroyasu Ishikawa<sup>1</sup>; Takashi Jimbo<sup>1</sup>; Takashi Egawa<sup>1</sup>*; <sup>1</sup>Nagoya Institute of Technology

We report the impact of insertion of lattice-matched AlInN/GaN distributed Bragg reflector (DBR) on GaInN light emitting diodes (LEDs) on Si substrates. A series of the AlInN/GaN DBR LEDs with different pairs (0 to 14.5) were grown on 2-inch n-Si (111) substrates using a conventional horizontal metalorganic chemical vapor deposition method. The lattice matched AlInN/GaN DBR is superior to previous AlGaInN/AlN DBR with respect to suppression of cracking, although the crack density increases with the increase of DBR pairs. Cross sectional SEM images show that interfaces between AlInN and GaN are smoother than those of previous AlGaInN/AlN DBR. The light output power of the LED with 14.5 pairs of DBR is about 3.6-fold larger than that of LEDs without DBR. Thus, the lattice-matched AlInN/GaN DBR is effective in enhancement of performance of GaInN LEDs on Si.

9:30 AM

**MM4, V-Defect Analysis in Green and Deep Green Light Emitting Diode Structures:** *Mingwei Zhu<sup>1</sup>; Shi You<sup>1</sup>; Yuxin Wang<sup>1</sup>; Yong Xia<sup>1</sup>; Wei Zhao<sup>1</sup>; Yufeng Li<sup>1</sup>; Jayantha Senawiratne<sup>1</sup>; Zihui Zhang<sup>1</sup>; Theeradetch Detchprohm<sup>1</sup>; Christian Wetzel<sup>1</sup>*; <sup>1</sup>Rensselaer Polytechnic Institute

V-defects in the active region of GaInN/GaN light emitting diodes (LEDs) have been considered to enhance light extraction and device efficiency. For 535 - 565 nm green and deep green LEDs on c-plane sapphire, we correlate the structural morphology with electroluminescence performance. Two classes of material with active region roughness of 5 nm and 0.6 nm (RMS) are analyzed in transmission electron microscopy. In the rough material, a high density of edge-type dislocations is identified that originates within the quantum wells (QWs). They initiate V-defects that exhibit {10-11} growth facets with a second set of narrow QWs and barriers. As V-defects widen with progressive growth, the width of QW and barriers on the c-plane increases. In the smooth material, however, no V-defects can be found. QWs and barriers are highly uniform and homogenous throughout the structure. LED emission is more uniform as well and output power more than doubles.

9:45 AM

**MM5, Phase-Ordering in a-Plane InGaN Grown by Metalorganic Vapour-Phase Epitaxy:** *Kazuhide Kusakabe<sup>1</sup>; Tokuma Furuzuki<sup>1</sup>; Koji Kuramochi<sup>1</sup>; Takashi Yamazaki<sup>1</sup>; Iwao Hashimoto<sup>1</sup>; Kazuhiro Ohkawa<sup>1</sup>*; <sup>1</sup>Tokyo University of Science

Nonpolar InGaN films are attractive candidates for high-performance optical devices which emit a polarized-optical-wave or operate at a green region. We have investigated the structural characteristic of a-plane InGaN/GaN systems. In this study, an atomic-scale analysis of phase-ordering of the a-plane InGaN is discussed. The a-plane  $\text{In}_{0.09}\text{Ga}_{0.91}\text{N}$  was grown by atmospheric metalorganic vapor-phase epitaxy. Transmission electron microscope (TEM) observations revealed that the InGaN spontaneous superlattice with an IML period was formed along the [000-1] direction. In the [0001] direction, the spontaneous superlattice was not found but the lattice tilt for GaN was appeared. The atomic-resolved high-angle annular dark-field scanning TEM technique

deduced the indium compositions of InGaN superlattice as 4% and 12%. It is considered that the growth conditions used here were kinetically preference for the formation of spontaneous superlattice along the [000-1] direction. This scheme is likewise to the case of AlInGaP systems previously observed.

10:00 AM

**MM6, Analysis of Basal Plane Stacking Fault Contribution to X-Ray Rocking Curve Widths in Non-Polar GaN:** *Mel McLaurin<sup>1</sup>; Asako Hirai<sup>1</sup>; Feng Wu<sup>1</sup>; Shuji Nakamura<sup>1</sup>; James Speck<sup>1</sup>*; <sup>1</sup>University of California, Santa Barbara

Non-polar and semi-polar orientated hetero-epitaxial films of the wurtzite nitrides typically exhibit large anisotropies in X-ray rocking curve widths. Though typically used for measurements of crystal mosaic, rocking curves are also sensitive to broadening of reciprocal lattice points due to small crystal coherence lengths. We present the relationship between a predominant feature of the microstructure of non-polar and semi-polar films, basal plane stacking faults, and the anisotropic X-ray rocking curve. A variant of the Williamson-Hall analysis is used to separate the component of X-ray peak broadening due to tilt mosaic from the broadening resulting from finite coherence length in m-plane oriented GaN films. Lateral broadening of the on-axis X-ray peak due to the presence of stacking faults is found to be the dominant source of the on-axis X-ray rocking curve anisotropy in the m-plane GaN films. Implications for measurements of other orientations of the wurtzite nitrides will be discussed.

10:15 AM

**MM7, White X-Ray Microdiffraction Analysis of Defects, Strain and Tilts in a Free Standing GaN Film:** *R. Barabash<sup>1</sup>; G. Ice<sup>1</sup>; B. Haskell<sup>2</sup>; Shuji Nakamura<sup>2</sup>; J. Speck<sup>2</sup>*; <sup>1</sup>Oak Ridge National Laboratory; <sup>2</sup>University of California at Santa Barbara

We present a novel polychromatic microdiffraction (PXM) analysis of defects, strains and tilts in a free standing m-plane GaN film grown via hydride vapor phase epitaxy. The GaN film was initially grown upon a (100) gamma-LiAlO<sub>2</sub> substrate, which spontaneously separated from the film upon cooling from the 900C growth temperature. The Li concentration 2 μm from each surface according to SIMS depth profiling, was sharply different at 5x10<sup>17</sup> atoms/cc (back side) and 1x10<sup>15</sup> (epi-surface) on the two faces. Comparable oxygen doping was observed on both surfaces. Because the high-energy x-ray beam passes through the GaN film the information is obtained from the thickness of the film. PXM indicated that the lattice parameter changes more than 2% with the depth of the film. The PXM results show that the film rotates 2-3 degrees through of the film thickness. The rotations are accompanied by film buckling.

10:30 AM Break

---

## Session NN: Molecular Beam Epitaxy of Nitride Semiconductors

Friday AM  
September 21, 2007

Room: 312/317  
Location: MGM Grand Hotel Conference Center

*Session Chairs:* April Brown, Duke University; Bruno Daudin, Atomic Energy Commission/Grenoble

---

11:00 AM

**NN1, Telecom Range Intersubband Transitions in GaN/AlN Multiple Quantum Wells Grown by Ammonia Molecular Beam Epitaxy:** *Sylvain Nicolay<sup>1</sup>; Amélie Dussaigne<sup>1</sup>; Laurent Nevou<sup>2</sup>; François. H. Julien<sup>2</sup>; Nicolas Grandjean<sup>1</sup>*; <sup>1</sup>Ecole Polytechnique fédérale de Lausanne; <sup>2</sup>Action OptoGaN, IEF, Université Paris-Sud

In this work, ammonia molecular beam epitaxy (NH<sub>3</sub>-MBE) is used to achieve GaN/AlN multiple quantum wells (MQWs) operating in the Telecom range. With this aim, it is necessary to use well thickness lower than 2 nm. As a consequence, the intersubband transition (ISBT) energy is very

# Technical Program

sensitive to the QW potential shape profile. Thus, diffusion and/or surface segregation phenomena that might occur at the MQW interfaces could be critical. In order to investigate this question, several samples were fabricated with different growth temperatures ( $T_{\text{growth}}$ ) for AlN barriers. It is found that decreasing  $T_{\text{growth}}$  leads to an increase of the ISBT energy, which is consistent with a more abrupt potential profile. Interestingly, further decrease of the temperature does not lead to higher ISB absorption energy whereas the maximum experimental value ( $\approx 0.7$  eV) is much below the theoretical one. This will be discussed on the basis of strain induced interface stability.

11:15 AM

**NN2, Improved Growth Mode Diagram for Plasma-Assisted MBE Growth of (0001) GaN:** *Gregor Koblmüller*<sup>1</sup>; Sergio Fernandez-Garrido<sup>2</sup>; Enrique Calleja<sup>3</sup>; James Speck<sup>1</sup>; <sup>1</sup>University of California, Santa Barbara; <sup>2</sup>Universidad Politécnica; <sup>3</sup>E.T.S.I. Telecomunicación

Based on real-time monitoring of the crystal growth modes during the PAMBE growth of (0001) GaN, we established a universal GaN growth diagram for growth temperatures to well above 800°C. Growth mode transitions from three-dimensional islanding to two-dimensional layer-by-layer and to step-flow growth were found with increasing Ga/N ratio. The latter transition coincided with a critical Ga adlayer coverage of 1 ML on the GaN surface, corresponding to a Ga/N ratio-dependent activation energy of  $\sim 1.5$  eV. Unlike growth at low temperatures, N-rich growth conditions at very high growth temperatures were shown to follow an unexpected layer-by-layer growth mode (by the observation of RHEED intensity oscillations) while simultaneously effectively suppressing thermal decomposition. Finally, the growth modes were confirmed by atomic force microscopy of homoepitaxial GaN island nucleation studies, including correlations between surface diffusion and surface vicinity.

11:30 AM

**NN3, Closed-Loop MBE Growth of Droplet-Free GaN with Very Metal Rich Conditions Using Metal Modulated Epitaxy with Mg and In:** *Shawn Burnham*<sup>1</sup>; William Doolittle<sup>1</sup>; <sup>1</sup>Georgia Institute of Technology

Improvements to the Metal Modulated Epitaxy (MME) technique using real-time feedback for closed-loop MBE growth will be introduced, and the use of MME to examine the effects of Mg and In during droplet-regime GaN growths will be demonstrated. Improvements to the MME technique are achieved through computer controlled shutter transitions based on feedback from RHEED transients, thus creating a closed-loop control system for MBE. This allows the efficient buildup and depletion of the metal bilayer, which improves surface morphology and growth rate compared to the standard MME technique. RMS surface roughness was reduced by 41% by using this "Smart Shuttering" improvement to MME. A substantially higher peak concentration of Mg, approaching 10% atomic concentration, was achieved using the MME technique when growing thin Mg doped GaN layers. However, a negligible amount of In was incorporated into the very Ga-rich films, and increasing the In flux resulted in no appreciable change.

11:45 AM

**NN4, Plasma-Assisted MBE Growth of (11-22)-Oriented GaN/AlN Quantum Wells on m-Sapphire:** *Lise Lahourcade*<sup>1</sup>; Julien Renard<sup>1</sup>; Edith Bellet-Amalric<sup>1</sup>; Marie-Pierre Chauvat<sup>2</sup>; Pierre Ruterana<sup>2</sup>; Eva Monroy<sup>1</sup>; <sup>1</sup>CEA-Grenoble; <sup>2</sup>ENSICAEN

Polarization effects in III-nitrides can be reduced by growing along semipolar crystallographic axis. In this work we report on molecular-beam epitaxy of (11-22)-oriented AlN, GaN and GaN/AlN multi-quantum-well (MQW) structures on (1-100) m-sapphire. In a first approach, we have optimized the growth conditions of AlN. N-rich conditions and high substrate temperature make it possible to isolate the (11-22) orientation and to achieve two-dimensional AlN(11-22) layers. GaN deposited directly on m-sapphire results in (11-22)-oriented layers with (1-103)-oriented inclusions. An AlN(11-22) buffer is necessary to impose the (11-22)-orientation for the subsequent GaN layer. Best surface morphology is achieved under Ga-rich conditions, with a Ga excess of one monolayer on the GaN(11-22) surface. Applying the optimum growth conditions for two-dimensional AlN and GaN, we have synthesized GaN/AlN MQW structures. The structural quality is

supported by x-ray diffraction, and the internal electric field attenuation is confirmed by the reduction of the luminescence Stark-shift.

12:00 PM

**NN5, Molecular Dynamics of Ga Adlayers on GaN(0001):** Jared Rinehimer<sup>1</sup>; Michael Widom<sup>1</sup>; *Randall Feenstra*<sup>1</sup>; <sup>1</sup>Carnegie Mellon University

Molecular dynamics employing an embedded atom potential has been performed in an effort to deduce a structural model for the Ga adlayer(s) on GaN(0001) that agrees with low-energy electron diffraction data for this surface. Employing the same 4/3 monolayer Ga adlayer coverage as in the laterally-contracted bilayer model of Northrup et al. (PRB 61, 9932 (2000)), we use large surface unit cells (6400 atoms in the adlayer and 4800 in the substrate) with the adatoms placed initially at random surface sites. Energetically optimal structures are determined by simulated annealing and quenching. We find an optimal structure with a nearly 6x6 unit cell, having a diffraction pattern in good agreement with the experiment. As the simulation temperature is increased the adlayer is found to melt, again yielding a diffraction pattern in agreement with experiment, and at higher temperature a stable arrangement containing a fractional coverage of the adlayer is found.

12:15 PM

**NN6, A New Model Describing the Plasma-Assisted MBE Growth of GaN Thin Films:** *Theodore Moustakas*<sup>1</sup>; Anirban Bhattacharyya<sup>1</sup>; <sup>1</sup>Boston University

We propose that GaN growth under Ga-rich conditions takes place through the supersaturation of metallic Ga at the growing surface with nitrogen and subsequent crystallization from the melt onto the GaN seed. While the solubility of molecular nitrogen in Ga at usual growth temperatures of GaN is very low because the process is dissociative with a high energy barrier, the solubility in Ga of atomic nitrogen and other activated nitrogen species is expected to be relatively high. In this model the growth process of GaN is not vapor phase epitaxy but liquid phase epitaxy (LPE), driven by the constant supply of active nitrogen. Experimental evidence in support of such a model are the formation of polycrystalline GaN by exposing Ga-melt to plasma activated nitrogen, the efficient incorporation of Mg in GaN from the liquid phase (Ga+N+Mg) and the reduction of oxygen impurities due to the formation of volatile gallium oxides.

---

## Session OO: Nanostructures: Growth II

Friday AM

September 21, 2007

Room: 313/316

Location: MGM Grand Hotel Conference Center

*Session Chairs:* Kent Averett, Air Force Research Laboratory; Kris Bertness, National Institute of Standards and Technology

---

11:00 AM

**OO1, GaN Nanowires and Devices:** *Stephen Hersee*<sup>1</sup>; Xin Wang<sup>1</sup>; Alec Talin<sup>2</sup>; <sup>1</sup>University of New Mexico; <sup>2</sup>Sandia National Laboratories

This paper describes the properties and applications of GaN nanowires fabricated by MOCVD using regular MOCVD precursors with no additional catalysts. Nanowires can be grown on (0001) sapphire or SiC substrates and on (111) silicon. Massive arrays of GaN nanowires of arbitrary length can be fabricated and the position, orientation, diameter and length of each nanowire is precisely controlled. The paper will discuss the crystallographic, optical and electrical characterization of these nanowires, all of which indicate high quality GaN. Stimulated emission has been observed in optically pumped arrays and in single nanowires as short as 4.8 micrometres. The paper will also discuss preliminary heterojunction results and report our progress towards electrically pumped photonic devices. This scalable GaN nanowire process promises not only to develop revolutionary new photonic and electronic devices but also to move GaN nanowires from their current status as a laboratory curiosity into the commercial sector.

# Technical Program

11:15 AM

**OO2, Nucleation and Propagation Mechanisms for Catalyst-Free Growth of GaN Nanowires:** *Kris Bertness*<sup>1</sup>; Devin Rourke<sup>1</sup>; Alexana Roshko<sup>1</sup>; Lorelle Mansfield<sup>1</sup>; Aric Sanders<sup>1</sup>; Todd Harvey<sup>1</sup>; Norman Sanford<sup>1</sup>; <sup>1</sup>National Institute of Standards and Technology

Nucleation and propagation are shown to be distinct processes for GaN nanowire growth without catalysts in molecular beam epitaxy. Once the nanowire morphology is established, nanowire growth is relatively insensitive to starting conditions, and is driven by variations in Ga sticking coefficient with crystallographic plane under high nitrogen flux and substrate temperatures near 820°C. Nanowires therefore consistently grow with c-axis orientation and {1 -1 0 0} sidewalls. In contrast, nucleation depends strongly on the buffer layer, substrate orientation, and atomic nitrogen flux. AlN buffer layers in the range of 10 nm to 120 nm have been examined, and the density of nanowire nucleation increases with buffer layer thickness. Elimination of the AlN buffer layer produces widely varying morphologies, depending on the initial exposure conditions of the bare silicon surface to nitrogen. These differences have been exploited to pattern substrates for position control of nucleation sites.

11:30 AM

**OO3, Selective Growth of GaN Nanocolumns with Pre-Deposited Al Pattern on (111) Si by RF-Plasma Assisted Molecular Beam Epitaxy:** *Shunsuke Ishizawa*<sup>1</sup>; Hiroto Sekiguchi<sup>1</sup>; Takayuki Hoshino<sup>2</sup>; Shuichi Sugimoto<sup>2</sup>; Akihiko Kikuchi<sup>1</sup>; Katsumi Kishino<sup>1</sup>; <sup>1</sup>Sophia University and CREST, JST; <sup>2</sup>Sophia University

Emphatic selective growth technique of GaN nanocolumns using pre-deposited Al pattern on (111) Si substrate was demonstrated by RF-plasma assisted molecular beam epitaxy. The Al patterns (ex. 85 nm-diameter and 20 nm-thick dot patterns aligned in triangle lattice with 300 nm periods and wide area without Al patterns) were prepared by electron beam lithography and lift-off process. After the nitridation of Al, GaN nanocolumns were grown on them for 60 min. The spatial fluctuation of nanocolumn height was well suppressed compared with spontaneous nucleation of nanocolumns because the Al dots supply the nucleation sites. At the growth temperature higher than 966 deg., the spontaneous nucleation of GaN nanocolumns on the Si surface outside the Al patterns was completely suppressed, so the GaN nanocolumns were positioned at each Al dot. The nanocolumns with a 100 nm in diameter girdled the 85 nm Al dot patterns, consequently forming GaN nano-tube like structures.

11:45 AM

**OO4, GaN Free-Standing Nanowires by Plasma-Assisted Molecular Beam Epitaxy: Growth, Structural and Optical Properties:** *Maria Tchernycheva*<sup>1</sup>; Corinne Sartet<sup>2</sup>; George Cirlin<sup>2</sup>; Laurent Travers<sup>2</sup>; Gilles Patriarche<sup>2</sup>; Ludovic Largeau<sup>2</sup>; Olivia Mauguin<sup>2</sup>; Jean-Christophe Harmand<sup>2</sup>; Le Si Dang<sup>3</sup>; Julien Renard<sup>3</sup>; Bruno Gayral<sup>3</sup>; Laurent Nevou<sup>1</sup>; Francois Julien<sup>1</sup>; <sup>1</sup>Institut d'Electronique Fondamentale; <sup>2</sup>LPN-CNRS; <sup>3</sup>CEA-CNRS-UJF

We report on the growth, structural and optical properties of GaN free standing nanowires synthesized in catalyst-free mode on Si(111) substrate by plasma-assisted MBE. The formation of AlN nucleation islands on the substrate prior to the wire growth is shown to be an efficient way to control the nanowire density. TEM and X-ray diffraction analyses reveal wurtzite crystal structure free from stacking faults or dislocation with two orientations with respect to the substrate. The nanowire axial growth rate is shown to follow the Gibbs-Thomson law. The nucleation on the lateral facets is evidenced using thin AlN marker layers. Nanowire ensembles demonstrate a strong near band edge photoluminescence up to room temperature. Low-temperature single wire micro-photoluminescence show excitonic emission at 3.478 eV with broadening of 6-10 meV comparable to photoluminescence performed on nanowires ensemble. Optical properties along the wire axis probed by micro-cathodoluminescence are found to be uniform.

12:00 PM

**OO5, Maskless Epitaxial Overgrowth of GaN Nanocolumns:** *Kent Averett*<sup>1</sup>; Joseph Van Nostrand<sup>1</sup>; John Albrecht<sup>1</sup>; Chih-Chung Yang<sup>2</sup>; <sup>1</sup>Air Force Research Laboratory; <sup>2</sup>National Taiwan University

GaN nanocolumns (NC), demonstrating excellent crystalline quality, have been grown by molecular beam epitaxy on both silicon (111) and sapphire (0001) substrates. The growth parameters for NC formation and

density variation will be presented. An examination of photoluminescence characteristics show the columnar structures to be strain free. Additionally, SEM and TEM analysis has been performed showing the unique characteristics of each growth pattern vs. substrate, as well as confirmation of the absence of threading dislocations in the columnar structures. Epitaxial overgrowth of GaN nanocolumns has been successfully performed, by molecular beam epitaxy, showing lateral growth mode characteristics without the use of a mask, such as silicon dioxide or silicon nitride. Photoluminescence, Hall effect, and high resolution x-ray diffraction measurements demonstrate improved material quality over direct growth on sapphire. Transmission electron microscopy measurements examine the dislocation density of the overgrown material, and the results will be presented.

12:15 PM

**OO6, Growth and Optical Properties of Si- and Mg-Doped GaN Nanorods:** *Florian Furtmayr*<sup>1</sup>; Martin Vielemeyer<sup>1</sup>; Martin Stutzmann<sup>1</sup>; Martin Eickhoff<sup>1</sup>; <sup>1</sup>Technische Universität München

Self assembled GaN nanorods were fabricated by plasma assisted molecular beam epitaxy on Si(111) substrates without the use of additional catalysts. The impact of both Si- and Mg-impurities on the growth kinetics and the optical properties has been investigated. Photoluminescence measurements were performed in the temperature range of 4K to 100K. Emission from free and donor bound excitons is dominant for undoped samples, whereas the contribution of donor-acceptor recombination increases with increasing doping concentrations. In weakly Mg-doped samples emission from the acceptor bound exciton was observed. The relation between luminescence characteristics, nanorod morphology, the degree of nanorod coalescence, and the incorporation of impurities is discussed.

---

## Session PP: MOVPE Growth of InGaN Alloys for Optoelectronics

Friday AM  
September 21, 2007

Room: 314/315  
Location: MGM Grand Hotel Conference Center

*Session Chairs:* Jung Han, Yale University; Peidong Yang, University of California, Berkeley

---

11:00 AM

**PP1, Direct Observation of Uniform Optical Properties from Microphotoluminescence Mapping of InGaN Quantum Wells Grown on Slightly Misoriented GaN Substrates:** *Koichi Tachibana*<sup>1</sup>; Hajime Nago<sup>1</sup>; Shin-ya Nunoue<sup>1</sup>; <sup>1</sup>Toshiba Corporation

To realize high-performance InGaN-based laser diodes, it is very important to grow InGaN quantum wells with high crystalline quality. We have demonstrated extremely smooth surface morphology of GaN-based layers on slightly misoriented GaN (0001) substrates toward <1-100> direction. In this paper, we clearly demonstrate uniform optical properties of InGaN quantum wells on GaN substrates with misorientation toward <1-100> direction, using microphotoluminescence mapping. InGaN quantum wells were grown on some GaN (0001) substrates with misorientation angles from 0.0 to 0.4 degrees toward <1-100> direction. Microphotoluminescence mapping was investigated at room temperature. The fluctuation of peak wavelength and full width at half maximum in microphotoluminescence mapping was very small in the samples grown on GaN substrates with misorientation angles over 0.2 degrees. The average of full width at half maximum was as small as 55 meV when the misorientation angle was between 0.2 and 0.3 degrees.

11:15 AM

**PP2, Morphology Evolution of InGaN Multi-Quantum Well Structures:** *Daniel Koleske*<sup>1</sup>; Stephen Lee<sup>1</sup>; Gerald Thaler<sup>1</sup>; Mary Crawford<sup>1</sup>; Michael Coltrin<sup>1</sup>; <sup>1</sup>Sandia National Laboratories

The surface morphology evolution of InGaN multi quantum wells (MQWs) was studied as the number of QWs was increased. The MQW structures were

# Technical Program

grown using MOCVD and the InGaN QWs contained 20% indium as verified by x-ray diffraction. Single step heights were observed after the growth of an initial low temperature GaN barrier layer. After the growth of the first QW, however, we observed that the steps bunch due to the presence of indium during growth. As additional QWs are grown, only multiple step heights are observed. After the second QW growth a trench-hillock morphology develops that is oriented parallel to the step bunching direction. After 10 MQWs, the trench-hillock height difference approaches 30 Å which is the QW thickness. Neither the step bunching nor the trench-hillock morphology appears to be correlated to dislocations or V-type defects, suggesting that the step bunching drives the trench-hillock morphology evolution.

**11:30 AM**

**PP3, Temperature Stability Studies of InGaN Thin Films and Multi-Quantum Well Structures:** *Gerald Thaler<sup>1</sup>; Daniel Koleske<sup>1</sup>; Stephen Lee<sup>1</sup>; Mary Crawford<sup>1</sup>; <sup>1</sup>Sandia National Laboratories*

As the indium content is increased in InGaN quantum wells (QWs) or thin films, the maximum growth temperature that these higher indium content InGaN alloys can withstand without decomposition is dramatically reduced. Subsequent growth of GaN capping or p-type layers must be performed at reduced temperatures to maintain InGaN QW integrity. While this is a well known feature of these InGaN films, the precise thermal budget is not well documented nor the mechanisms for InGaN degradation well understood. In this study, InGaN multi-QWs and thin films have been grown using MOCVD over indium compositions of 5 to 20% and capped with GaN. After growth, each of the InGaN films was annealed under flowing N<sub>2</sub> in the MOCVD reactor to determine the kinetics of InGaN decomposition and the maximum temperature that each composition can withstand before degrading. Changes in the InGaN compositional structural integrity will be studied using x-ray diffraction.

**11:45 AM**

**PP4, Growth of Periodic Micropit InGaN-Based LED Structure on Wet-Etch Patterned Sapphire Substrate:** *Hee Yun Kim<sup>1</sup>; Tran Viet Cuong<sup>1</sup>; Hyung Gu Kim<sup>1</sup>; Hung Seob Cheong<sup>1</sup>; Jae Young Park<sup>1</sup>; Yong Seok Lee<sup>1</sup>; Chang-Hee Hong<sup>1</sup>; Eun-Kyung Suh<sup>1</sup>; <sup>1</sup>Semiconductor Physics Research Center*

In this work, periodic micropit light-emitting diode structure was grown on wet-etch patterned sapphire substrate (PSS) by metal organic chemical vapor deposition. A pyramid shape of the PSS on SiO<sub>2</sub> mask was initially fabricated by simple wet etching process. Experimental result revealed that the size as height and/or depth of pyramid shape strongly depend on the wet-etching time. After the etching process, honeycomb shape of GaN was grown on the PSS as follow: Firstly, the GaN was vertically grown on the horizontal c-plane of the PSS. After that, the horizontal c-plane of the GaN almost vanished and the honeycomb shape were formed on the inclined R-plane, where the density and distribution of the honeycomb shape could be controlled by the lateral growth mechanism of the GaN template. Our results demonstrated that under proper growth condition, periodic micropit LED structure could be fabricated on the honeycomb shape of GaN template.

**12:00 PM**

**PP5, Enhancement of Indium Incorporation in InGaN Layer through Use of a "Bedding" Layer:** *Haryono Hartono<sup>1</sup>; Chew Beng Soh<sup>2</sup>; Soo Jin Chua<sup>1</sup>; Eugene Fitzgerald<sup>3</sup>; <sup>1</sup>Singapore-MIT Alliance, National University of Singapore; <sup>2</sup>Institute of Materials Research and Engineering; <sup>3</sup>Singapore-MIT Alliance, Massachusetts Institute of Technology*

Incorporation of Indium in GaN is a compromise between quality and high Indium content as a high growth temperature is good for quality but not the latter, and vice versa. We have found a growth method to increase Indium incorporation at the same growth parameters by preparing a composite "bedding" layer consisting of InGaN and InN layers. The InGaN layer, grown at 750°C to a thickness of 40 nm on GaN/sapphire, with approximately 15% Indium mole fraction gives photoluminescence at 435 nm with FWHM of 25 nm. Next, an InN layer of approximately 75 nm is grown over it at a temperature of 580°C. A subsequent InGaN layer is grown over the InN layer under the same condition as the first. The photoluminescence of the top InGaN layer, emitting with the same intensity, is now shifted by 50 nm to 485 nm and broadened with FWHM of 75 nm.

**12:15 PM**

**PP6, Growth of InGaN Optoelectronic Structures on 150 mm Sapphire Wafers in a Planetary Reactor@:** *C. Sommerhalter<sup>1</sup>; B. Schoettker<sup>2</sup>; B. Schineller<sup>2</sup>; R. Schreiner<sup>2</sup>; J. Kaeppler<sup>2</sup>; P. Fluks<sup>3</sup>; P. Droste<sup>3</sup>; M. Heuken<sup>2</sup>; <sup>1</sup>AIXTRON Inc.; <sup>2</sup>AIXTRON AG; <sup>3</sup>CrystalQ B.V.*

One way of increasing the throughput of MOCVD to achieve cost targets for white lighting is by increasing the wafer size. The AIX 2800G4 HT MOCVD mass production tool is capable of growing either in the 42x2 inch or the 6x6 inch (150 mm) configuration. To assess the performance of the epitaxy tool five period InGaN/GaN multi-quantum-well structures on a ~3.5 μm thick GaN(:Si) buffer layer were grown. The optimization of the growth was performed on 2 inch wafers in the 42x2 inch configuration. After optimization the reactor was reconfigured to the 6x6 inch configuration by exchanging the satellite disks. The photoluminescence mapping showed a mean wavelength of 450 nm with a standard deviation of 2.48 nm without edge exclusion. The total thickness of all layers was 3.555 μm with a thickness standard deviation below 1.1% without edge exclusion. Additional results such as morphology and crystal quality will be presented.

---

## Session QQ: Special LED Session: High Efficiency Solid State Lighting: Solutions for Global Warming

Friday PM

September 21, 2007

Room: 312/313/316/317

Location: MGM Grand Hotel Conference Center

*Session Chairs:* Steven DenBaars, University of California, Santa Barbara; Andrea Hangleiter, Technical University of Braunschweig

**2:00 PM**

**QQ1, High-Power LEDs for Illumination Applications:** *Frank Steranka<sup>1</sup>; <sup>1</sup>Philips Lumileds*

As a result of recent significant increases in both the efficiency and maximum input power of high-power LEDs, they are now starting to be employed in true illumination applications. The outlook for further LED efficiency gains and the implications for future energy savings will be presented. An overview of the remaining barriers to broad adoption of LEDs in the general lighting market and the steps being taken at Philips Lumileds to address them will also be described.

**2:25 PM**

**QQ2, High Luminous Efficiency White LED Illumination:** *John Edmond<sup>1</sup>; <sup>1</sup>Cree, Inc.*

Abstract not available.

**2:50 PM**

**QQ3, High Power LEDs:** *Chung H. Lee<sup>1</sup>; <sup>1</sup>Seoul Semiconductor Company*

Abstract not available.

**3:15 PM**

**QQ4, Application of High Brightness LEDs to Automotive:** *Takashi Sato<sup>1</sup>; <sup>1</sup>Stanley Electric Company Ltd.*

Abstract not available.

**3:40 PM**

**QQ5, Crucial Issues in White LEDs for General Lighting:** *Nadarajah Narendran<sup>1</sup>; <sup>1</sup>Rensselaer Polytechnic Institute Lighting Research Center*

Abstract not available.

---

## Closing Ceremony

Friday PM

September 21, 2007

Room: 312/313/316/317

Location: MGM Grand Hotel Conference Center

## A

A. Alves, J ..... 33  
 Abe, Y ..... 58  
 Abermann, S ..... 41  
 Abernathy, C ..... 30, 101  
 Abu-Farsakh, H ..... 31  
 Acord, J ..... 38, 64  
 Adachi, S ..... 18, 76, 77  
 Adesida, I ..... 46, 49, 51, 107  
 Adivarahan, V ..... 38, 40, 84, 93  
 Afroz, S ..... 93  
 Ager, J ..... 74, 89, 93, 109  
 Aggerstam, T ..... 57  
 Agulló-Rueda, F ..... 24  
 Ahmed, S ..... 103  
 Ahn, H ..... 26  
 Ahoujja, M ..... 107  
 Aidam, R ..... 53  
 Airey, R ..... 99, 104  
 Aizawa, H ..... 45  
 Aizenmann, C ..... 95  
 Akasaka, T ..... 38  
 Akasaki, I ..... 22, 37, 38, 41, 44, 78, 82, 84, 105  
 Akazawa, M ..... 51, 68  
 Akhter, M ..... 100  
 Akimoto, K ..... 28, 47  
 Akinaga, H ..... 79  
 Akutsu, N ..... 47  
 Alarcon-Llado, E ..... 79  
 Albrecht, J ..... 24, 28, 113  
 Albrecht, M ..... 16, 22, 31, 67, 88, 100  
 Alevli, M ..... 69, 83  
 Allen, D ..... 42  
 Allerman, A ..... 33, 40  
 Al Tahtamouni, T ..... 81  
 Alves, E ..... 56, 69, 74, 93  
 Amaike, H ..... 45  
 Amanai, H ..... 41, 65  
 Amano, H ..... 22, 35, 37, 38, 41, 44, 78, 82, 84, 105  
 Ambacher, O ..... 36, 37, 39, 40, 49, 58, 70, 71, 76, 91, 98  
 An, S ..... 47, 48, 55, 58  
 Anderson, P ..... 109  
 Anderson, R ..... 87  
 Anderson, T ..... 25, 110  
 Ang, S ..... 103  
 Antcliffé, M ..... 15  
 Anzai, J ..... 56  
 Aoki, M ..... 56  
 Aoyagi, Y ..... 57, 58  
 Aoyama, A ..... 29, 30  
 Arai, M ..... 100  
 Arakawa, Y ..... 14, 17, 18  
 Araki, M ..... 85  
 Araki, T ..... 67, 69, 89, 109, 110  
 Arehart, A ..... 21  
 Arjunan, A ..... 106  
 Arslan, I ..... 87  
 Artus, L ..... 79  
 Arulkumaran, S ..... 50  
 As, D ..... 66, 75  
 Asahi, H ..... 72  
 Asai, K ..... 19  
 Asamizu, H ..... 45, 108  
 Aschenbrenner, T ..... 35, 41, 66, 97  
 Aslam, S ..... 93  
 Assali, L ..... 33

Atalay, R ..... 83  
 Avdeev, O ..... 20  
 Averett, K ..... 24, 28, 112, 113  
 Avramescu, A ..... 42  
 Azize, M ..... 18, 46

## B

Babic, D ..... 36  
 Back, S ..... 54, 94  
 Baek, J ..... 27, 56, 71  
 Baghdadli, T ..... 78  
 Baharin, A ..... 94  
 Bai, J ..... 27, 99, 104, 105  
 Bak, D ..... 96  
 Baksht, T ..... 46  
 Balachander, K ..... 53  
 Balakrishnan, K ..... 40  
 Balandin, A ..... 108  
 Baldassarri, G ..... 14  
 Banas, M ..... 92  
 Bandalo, V ..... 39  
 Bando, A ..... 78, 82  
 Bandoh, A ..... 22, 37, 41, 105  
 Barabash, R ..... 111  
 Baranwal, V ..... 68  
 Barash, I ..... 20  
 Barber, Z ..... 64  
 Bardoux, R ..... 43  
 Bardwell, J ..... 53  
 Baribeau, J ..... 53  
 Barlage, D ..... 59  
 Barnard, J ..... 28  
 Baron, N ..... 18, 46  
 Bartel, T ..... 17, 27  
 Basile, A ..... 42  
 Baski, A ..... 28  
 Bastek, B ..... 19, 44, 77, 82  
 Basu, A ..... 46, 49  
 Baumann, E ..... 100  
 Baumberg, J ..... 14  
 Baur, B ..... 39, 40  
 Baur, J ..... 14  
 Bay, H ..... 57  
 Bechstedt, F ..... 75  
 Beckers, M ..... 74  
 Bedoya-Pinto, A ..... 52, 63  
 Beechem, T ..... 36  
 Behmenburg, H ..... 62  
 Bell, D ..... 100  
 Bellet-Amalric, E ..... 112  
 Belousov, M ..... 91  
 Belton, C ..... 101  
 Ben-Yaacov, T ..... 108  
 Bengoechea, A ..... 76, 106  
 Bensaoula, A ..... 52  
 Bergman, P ..... 18, 22  
 Berney, R ..... 107  
 Bertagnolli, E ..... 41  
 Bertelli, M ..... 69  
 Bertness, K ..... 24, 59, 87, 90, 112, 113  
 Bertoni, C ..... 69  
 Bertram, F ..... 19, 44, 63, 77, 82  
 Bethke, J ..... 85  
 Bhat, R ..... 42  
 Bhattacharyya, A ..... 112  
 Bickermann, M ..... 20  
 Bigenwald, P ..... 33  
 Bilenko, Y ..... 35, 93, 96, 102

Billingsley, D ..... 51, 53  
 Bimberg, D ..... 17  
 Bird, T ..... 72  
 Birner, S ..... 37  
 Biswas, R ..... 70  
 Blaesing, J ..... 49, 57, 63  
 Blanchard, P ..... 24, 59, 90  
 Bläsing, J ..... 63, 73, 76  
 Bockowski, M ..... 20  
 Boettinger, W ..... 32  
 Bogart, K ..... 92  
 Bogdanov, M ..... 20, 32  
 Bonanni, A ..... 18, 85  
 Bonanno, P ..... 27  
 Bondokov, R ..... 92  
 Boney, C ..... 52  
 Borasio, M ..... 30  
 Borghs, G ..... 28, 42, 53, 55  
 Borisov, B ..... 24  
 Böttcher, K ..... 19  
 Bougrioua, Z ..... 62, 82  
 Boulay, S ..... 50  
 Boutros, K ..... 15  
 Bowen, R ..... 15  
 Bradley, D ..... 101  
 Braña, A ..... 46  
 Brandt, O ..... 82, 95  
 Brar, B ..... 15  
 Braun, H ..... 42, 61  
 Bremers, H ..... 22  
 Bretagne, T ..... 43  
 Brimont, C ..... 77  
 Briot, O ..... 16  
 Bronner, W ..... 13  
 Brooksby, J ..... 88  
 Brown, A ..... 37, 83, 106, 111  
 Brown, D ..... 85  
 Brückner, K ..... 37  
 Brückner, P ..... 27, 80, 81, 98, 105  
 Brüderl, G ..... 42  
 Brünighoff, S ..... 14, 61  
 Brunner, F ..... 30, 73, 80  
 Bruno, G ..... 31, 37, 83, 106  
 Buchheim, C ..... 37  
 Budagosky, J ..... 44  
 Buegler, M ..... 80  
 Bühlmann, H ..... 87  
 Bulashevich, K ..... 32, 67, 101  
 Bunin, G ..... 46  
 Burnham, S ..... 51, 105, 112  
 Burton, B ..... 24  
 Butté, R ..... 14, 43, 66, 87, 91, 102  
 Buyanova, I ..... 77  
 Byeon, C ..... 104

## C

Cai, Z ..... 27  
 Calle, F ..... 46, 106  
 Calleja, E ..... 24, 76, 91, 112  
 Calleja, J ..... 24, 74, 76  
 Calleja Pardo, E ..... 43  
 Champion, R ..... 14, 23  
 Cantarero, A ..... 44, 110  
 Cantarero Sáez, A ..... 90  
 Cao, Y ..... 15, 47, 48  
 Capizzi, M ..... 83  
 Carlin, J ..... 14, 36, 41, 47, 48, 66, 74, 87, 91, 102  
 Castiglia, A ..... 14

# Index

Catellani, A.....	69	Chou, W.....	75	Dang, L.....	113
Cerezo, A.....	110	Chow, D.....	15	Danilchyk, A.....	43
Cha, O.....	78	Chow, P.....	48, 53	Darakchieva, V.....	19, 70, 74
Chae, S.....	61, 97, 101	Chow, S.....	80	Dartsch, H.....	35, 41, 66
Chambard, G.....	30	Chow, T.....	48	Das, J.....	42
Chandolu, A.....	72	Chow, W.....	33	Das Bakshi, S.....	28
Chandra, M.....	36	Christen, J.....	19, 43, 44, 49, 57, 63, 73, 76, 77, 82, 104	da Silva Jr., E.....	78
Chandrasekaran, R.....	62	Christensen, N.....	70, 90	Datta, R.....	65
Chandrashekar, M.....	68	Christmann, G.....	14, 66, 102, 103	Daudin, B.....	16, 28, 44, 111
Chandril, S.....	109	Christopoulos, S.....	14	Daumiller, I.....	49
Chang, C.....	72	Chu, C.....	61	David, A.....	66, 94
Chang, E.....	57	Chu, J.....	61, 73	Davis, R.....	103
Chang, J.....	31	Chu, R.....	13, 15, 17	Davitt, K.....	95
Chang, P.....	72	Chu, W.....	53, 59	Davydov, A.....	25, 30, 32, 71, 76
Chang, S.....	58, 80, 104	Chua, C.....	45, 93	Davydov, V.....	69
Chang, W.....	75	Chua, S.....	56, 61, 64, 69, 74, 80, 103, 105, 114	Dawson, M.....	101
Chang, Y.....	21, 30, 98, 103	Chuang, C.....	26	Dawson, P.....	65
Chao, C.....	98	Chuang, R.....	98	DeCuir, Jr., E.....	66
Chapman, P.....	49	Chung, J.....	42, 50	Deen, D.....	15, 48
Chassagne, T.....	18	Chung, K.....	97	Degroote, S.....	28, 42, 53, 55
Chatterjee, A.....	102	Chung, R.....	65, 84	De Jaeger, J.....	50
Chauvat, M.....	112	Chung, T.....	71	del Alamo, J.....	39
Che, S.....	51, 71, 86, 109	Chuvilin, A.....	80, 98	De Mierry, P.....	103
Chee How, L.....	50	Cico, K.....	41, 48	DenBaars, S.....	12, 13, 15, 21, 32, 44, 45, 59, 64, 65, 84, 85, 108, 114
Chemekova, T.....	20	Cimalla, V.....	37, 58, 71, 76, 91	Deng, J.....	35, 49, 50, 93, 102
Chen, C.....	25, 55, 81, 90, 102	Cirlin, G.....	113	Denker, C.....	90, 110
Chen, G.....	51	Citrin, D.....	105	Derenge, M.....	22, 67
Chen, H.....	68, 90	Clafin, B.....	22	Derluyn, J.....	42, 53
Chen, K.....	33, 54, 55, 89, 90	Clifton, P.....	90, 91, 110	Detchprohm, T.....	45, 61, 81, 102, 111
Chen, L.....	90	Clos, R.....	31	Deveaud, B.....	88
Chen, M.....	25, 59	Cobb, C.....	85	Dickey, E.....	38, 64
Chen, N.....	72	Cobet, C.....	90	Dietl, T.....	18
Chen, P.....	80	Coffie, R.....	17	Dietz, N.....	69, 83
Chen, Q.....	25, 53, 59	Cohen, D.....	42, 84, 108	Diez, A.....	49, 57, 63
Chen, R.....	90	Collazo, R.....	58, 85	Dikme, Y.....	43, 47, 57, 62, 78
Chen, W.....	75, 77, 98	Collis, W.....	96	Dillon, T.....	27
Chen, X.....	64, 74, 83	Colocci, M.....	91	Dimitriev, V.....	93
Chen, Y.....	24, 25, 28, 70, 98	Coltrin, M.....	85, 113	Dimitropoulos, C.....	83
Chen, Z.....	32	Contreras, O.....	55	Ding, Y.....	51
Cheng, A.....	54	Contreras Solorio, D.....	32	Disalvo, F.....	68
Cheng, C.....	61	Cook, J.....	107	Dmitriev, V.....	30, 32, 71, 100
Cheng, H.....	61	Corbett, B.....	100	Dmowski, L.....	70, 73
Cheng, K.....	42, 53, 55	Cordier, Y.....	18, 35, 46, 50	Doan, T.....	61
Cheng, Y.....	53	Corfdir, P.....	88	Donahue, M.....	37
Chenot, S.....	18, 46, 50, 103	Corrion, A.....	13, 17, 21	Dong, W.....	95
Cheong, H.....	54, 78, 114	Crawford, M.....	33, 92, 113, 114	Doolittle, W.....	31, 51, 53, 105, 112
Chern, G.....	86	Crégut, O.....	77	Dorsaz, J.....	14, 87
Cherns, D.....	23, 71	Creighton, J.....	87	Dräger, A.....	42
Chhajed, S.....	61	Cros, A.....	44	Droste, P.....	114
Chi, G.....	54, 102	Cross, J.....	27	Du, D.....	56
Chi, T.....	26, 30, 31	Cross, K.....	85, 92	Dunne, G.....	40
Chichibu, S.....	12, 19, 21, 45, 62, 84, 87, 88, 91	Crozat, P.....	67	Dupuis, R.....	17, 40, 67, 111
Chikalova-Luzina, O.....	69	Cuerdo, R.....	46	Durbin, S.....	109
Chikyow, T.....	56	Cullis, A.....	27	Durkaya, G.....	83
Chinone, T.....	79	Cuong, T.....	95, 98, 114	Dussaighe, A.....	43, 53, 82, 103, 111
Cho, C.....	59, 96, 104	Cusco, R.....	79		
Cho, H.....	31, 47, 48, 88	Czernecki, R.....	73		
Cho, J.....	54, 61, 97, 99			<b>E</b>	
Cho, M.....	15, 20, 31, 107			Eastman, L.....	36, 39, 64, 74, 83
Cho, Y.....	54, 94, 96, 103			Ecke, G.....	71, 76
Choe, H.....	19, 20, 24, 25, 26, 59			Eddy, C.....	76
Choi, B.....	96			Edmond, J.....	114
Choi, H.....	25, 47, 102, 103			Edwards, P.....	93
Choi, M.....	97			Egami, S.....	39
Choi, S.....	71, 83, 96			Egawa, S.....	100
Choi, W.....	54			Egawa, T.....	111
Choi, Y.....	39, 66, 80			Eichler, C.....	14
Chor, E.....	46, 47			Eickelkamp, M.....	47, 57
Chou, M.....	53, 55, 62				

## D

d' Eurydice, M.....	78
Dabiran, A.....	48, 53
Dadgar, A.....	31, 43, 49, 55, 57, 63, 73, 76, 82
Dahal, R.....	97, 107
Dai, Q.....	54
Dalmau, R.....	58, 85
Dammann, M.....	13
Dang, C.....	94

## E

Eastman, L.....	36, 39, 64, 74, 83
Ecke, G.....	71, 76
Eddy, C.....	76
Edmond, J.....	114
Edwards, P.....	93
Egami, S.....	39
Egawa, S.....	100
Egawa, T.....	111
Eichler, C.....	14
Eickelkamp, M.....	47, 57

# Index

- Eickhoff, M ..... 37, 39, 40, 113  
 Ejeckam, F ..... 36  
 Elder, K ..... 83  
 Elfstrom, D ..... 101  
 Elhamri, S ..... 68, 107  
 Emiroglu, D ..... 22  
 Emura, S ..... 72  
 Endoh, A ..... 49  
 Epelbaum, B ..... 20  
 Eri, T ..... 13  
 Esser, N ..... 90  
 Evans, K ..... 16, 22  
 Evans-Freeman, J ..... 22  
 Evstratov, I ..... 32  
 Ewing, D ..... 22
- F**
- Fahy, S ..... 74  
 Faili, F ..... 36  
 Faleev, N ..... 27  
 Falta, J ..... 27  
 Fan, F ..... 61  
 Fan, Z ..... 97  
 Fang, Z ..... 22  
 Fareed, R ..... 29, 38, 40, 84  
 Farjami Shayesteh, S ..... 34  
 Farrell, R ..... 84  
 Feduniewicz-Zmuda, A ..... 12  
 Feenstra, R ..... 85, 112  
 Feezell, D ..... 84  
 Fehlberg, T ..... 90  
 Felbinger, J ..... 36  
 Fellows, N ..... 44, 45, 65  
 Feltin, E ..... 14, 36, 47, 66, 87, 88, 91, 102, 103  
 Feneberg, M ..... 38, 75, 80, 81, 98  
 Feng, H ..... 102  
 Feng, S ..... 33, 105  
 Feng, Z ..... 25  
 Fenwick, W ..... 70, 83  
 Ferguson, I ..... 23, 25, 70, 83, 105  
 Fernandez-Garrido, S ..... 112  
 Fichtenbaum, N ..... 15, 85, 94  
 Fieger, M ..... 47, 57  
 Figge, S ..... 22, 35, 41, 66, 97  
 Filip, O ..... 20  
 Fini, P ..... 44  
 Fischer, A ..... 111  
 Fitzgerald, E ..... 114  
 Flanigan, P ..... 74  
 Flissikowski, T ..... 82  
 Fluks, P ..... 114  
 Follstaedt, D ..... 92  
 Fornari, R ..... 16, 19, 22  
 Forsberg, U ..... 55  
 Founta, S ..... 28  
 Fox, A ..... 48  
 Foxon, C ..... 14, 110  
 Foxon, T ..... 23  
 Francis, D ..... 36  
 Franke, A ..... 44, 82  
 Franssen, G ..... 73, 88, 90  
 Franz, D ..... 93  
 Frauenheim, T ..... 23  
 Freitas, J ..... 63  
 Fröhlich, K ..... 41, 48  
 Fu, D ..... 76  
 Fu, Y ..... 54, 102  
 Fuchs, F ..... 75
- Fuhrmann, D ..... 22, 42  
 Fujii, K ..... 64, 107  
 Fujii, T ..... 38  
 Fujikawa, S ..... 35, 96, 104  
 Fujimura, I ..... 18  
 Fujioka, H ..... 29, 30, 41, 65, 72  
 Fujishima, T ..... 69  
 Fujita, T ..... 79  
 Fujito, K ..... 18, 44, 65, 84  
 Fujiwara, K ..... 45, 98  
 Fujiwara, M ..... 71  
 Fukui, K ..... 73, 79  
 Fukui, T ..... 27  
 Fukumoto, S ..... 89, 109  
 Fukuyama, H ..... 29  
 Funato, M ..... 42, 45, 61, 65  
 Fuoss, P ..... 83  
 Furtmayr, F ..... 113  
 Furukawa, Y ..... 73, 74  
 Furuta, K ..... 79  
 Furuzuki, T ..... 111  
 Fuutagawa, N ..... 92
- G**
- Gadanez, A ..... 57, 63, 76  
 Galitsyn, Y ..... 52  
 Gallardo, E ..... 24, 74, 76  
 Gallart, M ..... 77  
 Gallinat, C ..... 63, 70, 86, 89, 90  
 Galtrey, M ..... 91, 110  
 Ganière, J ..... 88  
 Gao, C ..... 105  
 Gao, R ..... 82  
 Gao, Y ..... 21  
 Gaquiere, C ..... 36, 50  
 Garcia, M ..... 37  
 Garcia, R ..... 20, 72  
 García, R ..... 71  
 García-Cristóbal, A ..... 44  
 Gardner, N ..... 96  
 Gargallo-Caballero, R ..... 74  
 Garrett, G ..... 24, 45, 92, 93  
 Garro, N ..... 110  
 Garro Martínez, N ..... 90  
 Gaska, R ..... 21, 35, 49, 50, 68, 77, 78, 93, 96, 102  
 Gautier, S ..... 57, 78, 79  
 Gayral, B ..... 113  
 Ge, W ..... 89  
 Gebinoga, M ..... 40  
 Geok Ing, N ..... 50  
 Georgakilas, A ..... 73, 90  
 George, S ..... 24  
 Gerger, A ..... 30  
 Germain, M ..... 42, 53, 55  
 Gerstl, S ..... 91  
 Gerstmann, U ..... 23, 33  
 Gherasoiu, I ..... 72  
 Ghosh, S ..... 95  
 Giangregorio, M ..... 37, 83  
 Gibb, S ..... 36  
 Giesen, C ..... 62  
 Gil, B ..... 16, 33, 35, 43  
 Gila, B ..... 30, 101  
 Gilliot, P ..... 77  
 Giorgetta, F ..... 100  
 Giuliani, F ..... 16  
 Gobsch, G ..... 75  
 Goepel, K ..... 97
- Goetz, W ..... 12  
 Gogova, D ..... 19, 22  
 Goldhahn, R ..... 37, 75, 90  
 Golka, S ..... 48, 58, 67  
 Gomar-Nadal, E ..... 76  
 Gomyou, A ..... 67  
 Gong, Z ..... 101  
 Gonschorek, M ..... 36, 41, 47  
 González, D ..... 71  
 Gorczyca, I ..... 70, 73, 90  
 Gossard, A ..... 63  
 Goto, H ..... 15, 20  
 Goto, Y ..... 29, 30  
 Gott, A ..... 23  
 Gotthold, D ..... 72  
 Govorkov, A ..... 53  
 Graham, S ..... 36  
 Grahm, H ..... 44, 82, 95, 107  
 Grandal, J ..... 24, 76, 91  
 Grandjean, N ..... 14, 16, 19, 36, 41, 43, 47, 48, 53, 66, 74, 82, 87, 88, 91, 102, 103, 111  
 Grandusky, J ..... 26, 32, 100  
 Gray, J ..... 87  
 Green, D ..... 36  
 Gregusova, D ..... 48  
 Grenko, J ..... 16  
 Griffiths, I ..... 23  
 Grundy, A ..... 14  
 Grzanka, S ..... 73  
 Grzegory, I ..... 12, 73, 88  
 Gu, E ..... 101  
 Guan, B ..... 93  
 Guehne, T ..... 62, 82  
 Guilhabert, B ..... 101  
 Guillet, T ..... 43  
 Guillot, F ..... 67, 87, 100  
 Guo, Y ..... 31  
 Gupta, S ..... 23, 70  
 Gurary, A ..... 91  
 Gurioli, M ..... 91  
 Gurskii, A ..... 43  
 Gutowski, J ..... 17, 35, 66  
 Guzmán, A ..... 74  
 Gwo, S ..... 26, 69
- H**
- Ha, J ..... 15, 20, 47, 48  
 Ha, L ..... 21, 23  
 Haberer, E ..... 59  
 Habocek, U ..... 80  
 Hagihara, K ..... 29  
 Hahn, S ..... 47  
 Hahn, B ..... 14  
 Hahn, C ..... 47  
 Hakomori, A ..... 29  
 Haldar, P ..... 26  
 Haller, E ..... 74, 89, 93, 109  
 Halsall, M ..... 92  
 Han, I ..... 21  
 Han, J ..... 56, 87, 113  
 Han, K ..... 73  
 Han, M ..... 70, 77  
 Han, P ..... 24, 54  
 Han, Y ..... 61, 80  
 Hanada, T ..... 31  
 Hane, K ..... 51  
 Hang, D ..... 55  
 Hangleiter, A ..... 22, 42, 114

# Index

Hanser, A	16	Hoel, V	50	Lida, K	105
Hanser, D	22, 61	Hoffbauer, M	74	Ikeda, N	38, 39
Hao, D	64, 74, 83	Hoffmann, A	17, 69, 80, 82	Iliopoulos, E	73, 90
Hara, K	59	Hoffmann, L	22	Im, H	77, 88
Hara, N	41	Hofmann, T	70	Im, I	31
Harboeck, U	82	Hofstetter, D	100	Imade, M	13, 19, 21
Hardtdegen, H	48	Hollander, J	65	Imai, K	46
Harmand, J	113	Holm, R	76	Imanishi, K	41
Harris, J	33	Holtz, M	24, 72	Imura, M	22, 41
Harrison, P	92	Holtz, P	59	Inada, T	98
Hartmann, C	16	Hommel, D	17, 22, 27, 35, 41, 42, 66, 97	Inoue, K	69
Hartono, H	69, 105, 114	Homoth, J	69	Inoue, S	29, 30
Harui, S	110	Honda, T	100	Inoue, T	75, 83
Harvey, T	113	Honda, Y	47, 62, 81	Inoue, Y	29
Hasegawa, F	23, 49	Hönerlage, B	77	Inushima, T	70
Hasegawa, H	51, 68	Hong, C	78, 95, 98, 114	Ishida, A	29
Hasegawa, S	72	Hong, H	107	Ishida, F	101
Hashimoto, A	51, 52, 56, 83, 86	Hong, S	15	Ishiguro, O	38
Hashimoto, I	111	Hong, Y	55, 77	Ishiguro, T	18, 77
Hashimoto, N	86	Hongo, C	97	Ishii, T	25
Hashimoto, P	15	Honsberg, C	105	Ishikawa, F	107
Hashizume, T	39, 42, 69, 106, 107	Hooper, S	35	Ishikawa, H	111
Haskell, B	15, 44, 111	Horie, H	41, 65	Ishitani, Y	51, 71, 86, 109
Hata, M	47	Horiguchi, M	98	Ishizawa, S	25, 87, 113
Hatakenaka, S	74	Horio, K	67	Ito, M	36
Hatakoshi, G	99	Hoshi, T	21	Ito, R	51
Hauguth, S	70, 98	Hoshino, K	18, 77, 85, 98, 101	Itoh, K	38, 73
Haupt, C	37, 49, 58	Hoshino, T	113	Ivanov, I	55
Hawkridge, M	23, 71	Houchin, Y	86	Ivanov, S	71
Hayakawa, T	84	Hourahine, B	23, 93	Ivantsov, V	30, 100
Hayashi, E	38	Howgate, J	39	Ive, T	108
Hayashi, K	61	Hsiao, C	59	Iwahashi, Y	75
Hayashi, M	84	Hsiao, F	26, 106	Iwaki, Y	64
He, X	70	Hsiao, Y	57	Iwao, K	51, 52
Heffernan, J	35	Hsu, L	93	Iwaya, M	22, 37, 38, 41, 44, 78, 82, 84, 105
Heidelberger, G	48	Hsu, M	30, 53	Iyer, S	96
Heimann, P	20	Hsueh, T	58, 80	Iza, M	45, 66, 94
Hein, M	37	Hu, E	59, 66, 94		
Heinle, U	49	Hu, F	51	<b>J</b>	
Helava, H	20	Hu, M	15	Jadwisieniczak, W	80
Hemmingsson, C	22	Hu, X	35, 49, 50, 93, 96, 102	Jahn, U	43
Hempel, T	49, 57, 63, 73, 76, 104	Huang, C	24, 102, 103, 105	Jahnke, F	66
Henderson, W	51, 53	Huang, H	26, 30, 31, 53	Jain, A	64
Hennig, C	19	Huang, J	24, 28, 103	Jain, R	21, 96
Henry, R	76	Huang, S	76	Jang, D	68
Hepper, D	36	Huang, W	48, 57	Jang, J	27
Herlufsen, S	17	Huang, Y	80, 95, 98	Jang, L	56
Hernandez, S	79	Huebschman, B	49	Jani, O	105
Hernandez Cocolletzi, H	32	Hui, K	103	Jansen, R	43, 47, 57, 78
Hersee, S	110, 112	Hultman, L	16, 74	Janzén, E	55
Hertkorn, J	38, 98, 105	Humphreys, C	12, 22, 26, 28, 35, 64, 65, 100, 105, 110	Jean, J	19, 20, 24, 25, 26, 59
Hertog, B	48	Hums, C	63, 76	Jefferson, P	109
Heuken, M	15, 16, 43, 47, 57, 62, 73, 78, 114	Hung, A	49	Jegert, G	37
Hierro, A	74	Hurni, C	66	Jelev-Vlaev, S	32
Higo, M	70	Hwang, B	77, 88	Jeliazkov, S	71
Hijikata, Y	75, 83	Hwang, E	86	Jena, D	15, 47, 48, 51, 86, 87
Hikosaka, T	62, 81	Hwang, S	61, 97	Jeon, C	61
Hill, G	99, 104	Hylton, N	65	Jeon, D	94
Hinoki, A	67, 69	Hyun, S	47, 48	Jeon, H	76
Hiraga, K	29			Jeon, J	107
Hirai, A	44, 64, 111	<b>I</b>		Jeon, S	27, 96
Hiramatsu, K	25, 40, 56, 79, 108, 110	Ibanez, J	79	Jeon, Y	54, 71
Hirano, S	75, 83	Ice, G	111	Jeong, H	78
Hirata, G	72, 75	Ichihara, J	45	Jeong, M	78
Hirayama, H	29, 35, 37, 79, 96, 97, 104	Ichinokura, H	14	Jeong, T	99
Hiromura, Y	72	Ide, T	47, 68	Jetter, M	30, 44
Hirotsani, T	97	Iida, D	44, 84	Jhin, J	29
Hizikata, Y	75			Jia, Z	44
Hlad, M	30, 101				

# Index

Jiang, F	83	Katayama, R	53, 71, 75, 92	Klochikhin, A	69
Jiang, H	74, 81, 97, 107	Kato, K	38, 87	Knafo, Y	46
Jiang, R	24, 54	Kato, N	41, 79, 80	Knauer, A	30, 73, 80
Jiang, Z	25	Kato, T	107	Kneissl, M	33, 39, 57, 73, 77, 80
Jimbo, T	111	Katona, T	35, 38, 40, 84, 93	Knoke, I	80
Jimenez, J	79	Kauer, M	35	Ko, G	61
Jimi, H	98	Kaufmann, U	105	Ko, T	82
Jin, D	36	Kawai, H	75	Kobatake, H	29
Jindal, V	26, 32, 100	Kawakami, Y	42, 45, 61, 65	Kobayashi, A	30, 41, 65
Jing, L	107	Kawamura, F	13, 19, 21	Kobayashi, G	87
Jmerik, V	71	Kawanishi, H	23, 49	Kobayashi, T	100
Jo, Y	106	Kawano, S	30, 72	Kobayashi, Y	38
Joblot, S	50	Kawano, T	17	Koblmueller, G	17, 66, 70, 86, 89, 90, 112
Joh, J	39	Kawasaki, K	57	Kocan, M	94
Johnson, M	16, 59	Kawashima, T	44, 84	Kodama, M	38
Johnson, N	45, 93	Kaya, S	38	Koh, E	21
Johnston, C	28, 65	Kazimirov, A	27	Köhler, K	105
Jönen, H	22	Ke, W	75	Kohn, E	36
Jones, H	93	Keller, S	15, 32, 85, 94	Kohno, M	71
Jones, K	22, 49, 67	Kendrick, C	109	Koide, S	108
Jones, R	74, 89, 93, 109	Kent, A	14	Kojima, K	42, 65
Jordan, R	104	Khachapuridze, A	12, 73	Koleske, D	63, 85, 92, 113, 114
Joshin, K	41	Khan, A	29, 35, 38, 40, 84, 93	Kominami, H	59
Ju, J	56	Khan, N	74	Komissarova, T	71
Julien, F	67, 87, 91, 100, 111, 113	Khan, T	48	Komiyama, S	100
Jung, G	95	Kharchenko, A	85	Komoda, H	59
Jung, H	96	Kheirodin, N	67	Kondo, Y	35, 104
Jung, T	25	Khokhlov, D	71	Kondou, T	61
Justo, J	33	Khongphetsak, S	23	Kondratyev, A	54
<b>K</b>		Khurgin, J	51	Koo, H	95
Kachi, T	38, 106	Kiecana, M	18	Kordos, P	48
Kaeding, J	21	Kiefer, R	13	Kosaka, K	19, 67, 69
Kaeppler, J	16, 114	Kikawa, J	67, 69	Kotani, J	39, 42
Kaiser, U	80, 98	Kikkawa, T	17, 41	Koudymov, A	50
Kajikawa, M	79	Kikuchi, A	25, 87, 113	Koukitu, A	14, 16, 72
Kajitani, R	57	Kim, B	104	Kovalenkov, O	30, 71, 93, 100
Kakanakova, A	55	Kim, C	19, 20, 24, 25, 26, 59, 80, 95, 96	Koyama, T	19, 21
Kakanakova-Georgieva, A	55	Kim, D	49, 51, 54, 95, 101	Kozlovsky, V	78
Kako, S	17	Kim, E	21, 23, 76, 81	Kral, K	32
Kalden, J	17	Kim, H	23, 26, 61, 71, 94, 95, 96, 98, 99, 101, 103, 106, 114	Krames, M	45, 96
Kalisch, H	43, 47, 57, 78	Kim, I	97	Kravchenko, I	101
Kaluza, A	104	Kim, J	21, 23, 54, 59, 61, 63, 94, 95, 96, 99, 104, 106	Krein, P	49
Kamata, N	29, 37, 79, 97	Kim, K	31, 44, 47, 48, 49, 59, 64, 101, 102, 106, 107	Krischok, S	70
Kambayashi, H	39	Kim, S	51, 96, 99, 106	Krishnan, B	37, 38, 62, 84
Kamber, D	13	Kim, T	37, 83, 101, 102, 106	Krost, A	31, 43, 49, 55, 57, 61, 63, 73, 76, 82
Kamimura, J	25	Kim, Y	26, 54, 55, 61, 94, 95, 96, 103, 107	Krtschil, A	49, 63, 73
Kaminska, A	73, 90	Kimura, N	46	Krukowski, S	73
Kamiya, S	67, 69	Kimura, S	72	Kruse, C	35, 66, 97
Kamiyama, S	22, 37, 38, 41, 44, 78, 82, 84, 105	Kimura, T	32, 106	Kryliouk, O	23, 25, 93, 110
Kamler, G	12	Kindel, C	17	Krysko, M	12, 73, 88
Kamo, Y	89	King, P	109	Ku, P	25
Kamoshita, T	72	Kingkeo, K	49	Ku, Y	26
Kanamura, M	41	Kirste, L	53	Kuball, M	14, 36, 40, 67
Kane, M	23, 25, 70	Kirste, R	69, 80, 82	Kubota, M	45, 62
Kanechika, M	38	Kisel, O	63	Kubota, Y	14
Kaneta, A	65, 88	Kishimoto, S	36, 41	Kuboya, S	75
Kang, H	23, 83	Kishino, K	25, 66, 87, 113	Kudo, Y	92, 109
Kang, K	97	Kisielowski, C	27	Kudymov, A	49
Kang, S	26	Kitajima, N	14	Kuehne, A	101
Kang, T	76, 77, 88	Kitajima, Y	109	Kulik, A	20
Kanjilal, D	68	Kitamori, K	46	Kumagai, Y	14, 16, 72
Kaplun, J	46	Kitamura, T	79	Kumar, S	68
Kappers, M	12, 22, 26, 28, 64, 65, 100, 110	Kitano, Y	13, 19, 21	Kumar, V	46, 49, 51
Karpov, S	20, 32, 67, 101	Kitaoka, Y	13, 19, 21	Kunii, T	89
Kasai, S	39	Kittler, G	40	Kunugi, S	56
Kasamatsu, Y	84	Kiyomi, K	18	Kunze, J	104
Kataoka, T	53, 71			Kunze, M	49
				Kunzer, M	53, 105
				Kuo, C	54, 80, 102, 104

# Index

Kuo, H	82, 94, 98
Kuokstis, E	77
Kups, T	71
Kurai, S	27
Kuramochi, K	111
Kuramoto, M	14
Kurdoghlian, A	15
Kurihara, K	73
Kuroda, M	41
Kurouchi, M	67, 73
Kuryatkov, V	24
Kusakabe, K	64, 111
Kuzmik, J	41, 48
Kwack, H	54, 96, 103
Kwak, J	97
Kwon, K	99
Kwon, M	59, 94, 96, 99, 104
Kwon, S	56, 71

## L

Lagoudakis, P	14
Lahiri, S	106
Lahourcade, L	112
Lai, C	81, 98
Lai, E	87
Lai, K	16
Lai, P	25, 102, 103
Lai, W	54, 58, 80, 104
Lal, R	108
Lampert, W	37
Lan, W	105
Lancefield, D	103
Landis, G	68
Largeau, L	113
Larson, D	91, 110
Larsson, M	59
Laski, J	72, 75
Latifi, K	83
Lau, K	37, 55, 89, 102
Laubsch, A	42
Laügt, S	82
Lay, T	81
Lazic, S	24, 74, 76
Leancu, C	105
Lebedev, V	70, 71, 76, 98
LeBlanc, H	42
Leconte, S	58
Lee, C	50, 106, 114
Lee, D	21, 55, 80
Lee, G	54
Lee, H	15, 20, 47, 48, 69
Lee, I	56
Lee, J	47, 48, 49, 70, 76, 95, 99, 101, 106
Lee, K	27, 31, 95, 96, 99, 104
Lee, M	31, 68, 75
Lee, S	15, 19, 20, 24, 25, 26, 31, 56, 59, 76, 79, 85, 92, 113, 114
Lee, T	96
Lee, U	22
Lee, W	17, 26, 30, 54, 106, 111
Lee, Y	23, 114
Leem, S	102
Lefebvre, P	43
Leite Alves, H	33
Lell, A	14, 61
Leroux, M	82, 91
Leszczynski, M	73
Leung, C	25, 102, 103

Levin, I	27
Leys, M	42, 53, 55
Li, B	89
Li, D	56
Li, G	68
Li, J	38, 96, 97
Li, N	25
Li, Q	87
Li, T	18, 57, 85
Li, Y	21, 45, 61, 81, 95, 98, 102, 103, 111
Lian, C	46
Liang, H	102
Liang, J	79
Lieten, R	28
Liliental-Weber, Z	23, 25, 74, 93, 100, 110
Lim, J	94
Lim, K	95
Limb, J	40, 67, 111
Lin, D	26, 72, 104
Lin, E	81
Lin, F	80
Lin, G	68
Lin, H	26, 69, 75, 104
Lin, J	74, 81, 97, 107
Lin, K	57
Lin, S	25
Lin, T	73
Lin, Y	59
Linkohr, S	40
Linthicum, K	12, 35, 107
Lipski, F	81, 98
Lischka, K	66, 75, 85
Liu, C	23, 47, 58
Liu, J	17
Liu, K	21, 77, 78
Liu, L	61
Liu, P	26, 30, 31
Liu, R	28
Liu, S	105
Liu, T	24
Liu, W	54, 61, 69, 92, 103
Liu, Y	108
Liu, Z	33, 50
Lobanova, A	56
Lohmeyer, H	17, 35, 66
Look, D	22
López-Romero, D	106
Lordi, V	33
Lorenz, A	42
Lorenz, K	56, 93
Lorenz, P	70
Lorenzini, P	50
Losurdo, M	31, 37, 83, 86, 106
Lozano, J	71
Lozykowski, H	80
Lu, C	103
Lu, H	69, 70, 73, 90, 109
Lu, J	68
Lu, T	82, 98
Lu, W	46
Lu, Y	102
Lucznik, B	12, 73, 88
Luebbers, B	40
Luna, E	24, 76
Lundin, W	54
Lundskog, A	55
Lunev, A	35, 93, 96, 102
Lupu, A	67
Lutgen, S	14, 42

Lüth, H	48
Lutsenko, E	30, 43

## M

Ma, M	99
Maaskant, P	100
Machado, W	33
Machhadani, H	67
Machleidt, T	91
Mackintosh, A	101
Madrigal-Melchor, J	32
Mahadik, N	76
Mai, D	52, 63
Maier, M	105
Makarov, Y	20, 67
Makimoto, T	38
Makiyama, K	41
Malindretos, J	52, 63, 90, 110
Manasreh, M	66
Mangum, J	23, 25, 93, 110
Manning, I	38
Mansfield, L	24, 59, 113
Mansurov, V	52, 59
Marcinkevicius, S	78
Marcon, D	42
Mariette, H	28
Markov, A	53
Maroldt, S	49, 58
Marso, M	48
Martin, D	19, 53, 82, 103
Martin, J	78
Martin, R	79, 92, 93
Martin, T	36, 40, 67
Martinez, O	79
Maruyama, H	41, 78, 82, 105
Mashiyama, Y	100
Mashkov, V	58
Massies, J	18, 50, 91
Mastro, M	76
Masuda, M	38, 39
Masuda, N	40
Masui, H	44, 45
Mates, T	52, 84, 85
Matioli, E	94
Matocha, K	40
Matsui, K	86
Matsui, T	49
Matsumoto, K	85
Matsuoka, T	32, 67
Mattei, S	87
Matthews, K	64, 74, 83
Mauder, C	47, 57, 78
Mauguin, O	113
Mauri, F	33
McAleese, C	22, 28, 65, 91, 100, 105, 110
McCarthy, L	94
McConville, C	109
McGroddy, K	94
McKittrick, J	72
McKittrick, J	75
McLaurin, M	44, 62, 64, 84, 111
Medjdoub, F	36
Mei, J	28, 29, 88
Meignien, L	67
Meissner, E	80
Meneghesso, G	101
Meneghini, M	101
Menendez, J	77

# Index

Menozzi, R	94	Murakawa, K	23	Niermann, T	52
Meshi, L	23	Murata, T	98	Niikura, E	23
Mesli, T	104	Murotani, H	78, 79, 80, 82	Niiyama, Y	39
Metzner, S	44	Murthy, M	76	Nikiforov, A	71, 84
Meyer, T	61	Muto, D	89, 109	Nikishin, S	24, 72
Miao, Z	76	Myers, T	83, 109	Nikitin, A	52, 59
Michler, P	30, 44			Nishikawa, N	47
Mickevicius, J	77	<b>N</b>		Nishizawa, Y	72
Micovic, M	12, 15	Na, H	107	Nishizuka, K	65
Miczek, M	69	Na, M	95, 98	Niyamakom, P	57
Miguel-Sánchez, J	74	Nagahama, S	42	Noculak, A	47
Miko	93	Nagai, T	84	Noda, M	89
Mikulla, M	13	Nagai, Y	56, 83	Noguchi, N	29
Miller, N	74, 89, 109	Nagalyuk, S	20	Noh, D	26
Milosavljevic, I	15	Nagamatsu, K	82, 105	Noh, M	80
Mimura, T	49	Nagao, S	18, 41, 65	Noh, T	54
Mimura, Y	51	Nagashima, T	16	Noltmeyer, M	82
Minegishi, T	31	Nagata, S	20	Noma, R	73
Mishima, T	13	Nagata, T	56	Nomura, T	38, 39
Mishra, K	72, 75	Nago, H	99, 113	Noro, T	22
Mishra, U	12, 13, 15, 17, 21, 32, 52, 85, 94, 108	Nakagawa, N	79	Northrup, J	44
Misra, P	52, 82	Nakagawa, S	29	Novak, J	48
Missert, N	92	Nakajima, A	67	Novikov, S	14, 23
Mita, S	58, 85	Nakajima, F	75	Nunna, K	96
Mitamura, K	72	Nakamura, A	98, 108	Nunoue, S	99, 113
Mitchel, W	22, 68, 107	Nakamura, F	36	Nurmikko, A	94, 95
Mitome, M	28	Nakamura, K	29		
Miura, A	84	Nakamura, N	79	<b>O</b>	
Miyachi, T	27	Nakamura, S	12, 13, 21, 32, 38, 44, 45, 59, 64, 65, 84, 94, 108, 111	O'Donnell, K	79, 92, 93
Miyajima, T	92, 109	Nakamura, T	53, 71	O'Malley, S	27
Miyake, H	25, 40, 56, 79, 108, 110	Nakanishi, Y	59, 74	O'Steen, M	72
Miyoshi, N	13	Nakano, T	29, 30	Obata, T	14
Mizerov, A	71	Nakao, M	67	Ofuonye, B	107
Mizue, C	69	Nakarmi, M	97	Ogawa, E	106
Mizuno, K	38	Nakashima, S	79	Oh, B	101
Mizuno, S	67	Nakayama, H	107	Oh, J	107
Mizutani, T	36, 41	Nakayama, M	89	Oh, M	94
Mochizuki, T	18	Nam, G	96	Oh, T	19, 20, 24, 25, 26, 59, 95
Mohammed, F	107	Nambu, N	108	Ohashi, T	29, 37, 79, 97
Mokhov, E	20	Namita, H	18	Ohba, R	72
Monemar, B	18, 19, 22, 74, 78, 91	Namkoong, G	31	Ohira, S	30
Monroy, E	16, 37, 58, 67, 87, 100, 112	Nanishi, Y	39, 67, 69, 73, 89, 109, 110	Ohkawa, K	64, 111
Mont, F	54	Nanjo, T	58	Ohki, T	41
Montes, M	74	Naoe, S	79	Ohshima, T	75
Moon, P	71	Naoi, H	89, 109	Ohta, H	39, 45, 62, 84
Moon, Y	102	Napierala, C	75	Ohta, J	29, 30, 41, 65, 72
Morales, F	71	Napierala, J	42	Ohta, M	14
Moram, M	64	Narendran, N	114	Oishi, S	51, 75
Morgan, K	92	Narita, T	99	Oishi, T	58
Mori, F	105	Narukawa, Y	45, 61, 65	Okada, H	74, 75
Mori, T	59	Nause, J	25	Okada, N	22, 41, 78, 82
Mori, Y	13, 19, 21	Navarro-Quezada, A	18, 85	Okamoto, K	29, 30, 45, 62, 84
Morkoç, H	28	Nega, R	38	Okamoto, N	41
Morret, M	16	Nener, B	90, 94	Oku, T	89
Motegi, N	67	Nepal, N	74	Okumura, H	47, 52, 79
Motogaito, A	25	Netzel, C	42, 57	Oliver, R	12, 22, 26, 28, 110
Motsnyi, V	55	Neubert, B	27	Omiya, H	28, 65
Moustakas, T	62, 84, 112	Neugebauer, J	31	Onabe, K	40, 53, 71, 75, 92
Mouti, A	14	Nevou, L	67, 87, 91, 100, 111, 113	Ono, W	75
Mudryi, A	30	Newman, S	13	Onomura, M	97
Mueller, G	96	Ng, G	50	Onuma, T	19, 45
Mukai, T	28, 42, 45, 61, 65	Ng, W	25, 102, 103	Oogi, Y	59
Müller, S	13, 53	Ni, X	28	Oota, H	18
Munkholm, A	83, 96	Nicolay, S	91, 111	Oppermann, H	104
Munoz, E	95	Nie, C	24	Orihara, M	75, 83
Muñoz, E	46, 74	Nielsenschütz, F	37, 58, 70	Orito, F	13
Murai, A	12	Nielsenschütz, M	91	Ort, P	40
Murakami, H	14, 16, 72			Ortenberg, L	46

# Index

Oshima, M ..... 72  
 Oshima, Y ..... 13  
 Osinsky, A ..... 48, 53  
 Ostermaier, C ..... 47, 48  
 Otake, H ..... 39, 79  
 Ougazzaden, A ..... 57, 70, 78, 79  
 Ould Saad Hamady, S ..... 78

## P

Pala, N ..... 49, 50  
 Palacios, T ..... 42, 50, 87  
 Pan, C ..... 26, 54, 102  
 Pandey, A ..... 68  
 Paniagua, A ..... 15  
 Pantha, B ..... 107  
 Parbrook, P ..... 27, 45, 92, 99, 104  
 Parekh, A ..... 91  
 Parish, G ..... 90, 94, 110  
 Park, C ..... 76, 77, 88  
 Park, D ..... 54  
 Park, E ..... 23, 25, 96  
 Park, H ..... 110  
 Park, I ..... 59, 94, 96, 99, 104  
 Park, J ..... 31, 54, 80, 95, 114  
 Park, K ..... 54  
 Park, M ..... 97  
 Park, S ..... 31, 59, 71, 84, 94, 96, 99, 104  
 Park, Y ..... 71, 77, 88, 99  
 Paschos, O ..... 26  
 Paskov, P ..... 18, 22, 78  
 Pastor, D ..... 79  
 Patriarche, G ..... 113  
 Pau, J ..... 95  
 Pavlovskii, V ..... 43  
 Pearton, S ..... 30, 53, 101, 106  
 Pei, Y ..... 15  
 Peng, H ..... 72  
 Peng, L ..... 81, 104  
 Perea-Lopez, N ..... 72, 75  
 Perlin, P ..... 12, 73, 88  
 Peter, M ..... 14  
 Pethrick, R ..... 101  
 Petrov, I ..... 31  
 Petrova, E ..... 53  
 Pettinari, G ..... 83  
 Piner, E ..... 107  
 Ping, H ..... 57, 95  
 Pinos, A ..... 78  
 Pinquier, C ..... 53, 82, 103  
 Piskorska-Hommel, E ..... 27  
 Plawsky, J ..... 102  
 Plesiewicz, J ..... 70, 73  
 Ploog, K ..... 12  
 Plotnikov, D ..... 71  
 Poblentz, C ..... 13, 15, 17, 21, 88  
 Pogany, D ..... 41, 48  
 Polimeni, A ..... 83  
 Polyakov, A ..... 30, 53  
 Pomeroy, J ..... 36, 40, 67  
 Pomrenke, G ..... 107  
 Ponce, F ..... 20, 28, 29, 65, 72, 88, 92, 111  
 Pophristic, M ..... 39  
 Porowski, S ..... 12, 73, 88  
 Portail, M ..... 18, 50  
 Poweleit, C ..... 77  
 Pozina, G ..... 22  
 Pozzovivo, G ..... 41, 48, 67  
 Prather, D ..... 27

Preble, E ..... 22  
 Pribble, B ..... 13, 15  
 Prinz, G ..... 38, 80  
 Pritchett, D ..... 51, 53  
 Protzmann, H ..... 73  
 Pugel, D ..... 93  
 Py, M ..... 36, 47

## Q

Qadri, S ..... 76  
 Qin, Z ..... 70, 73, 76  
 Quast, M ..... 18, 85  
 Quay, R ..... 13  
 Queren, D ..... 42  
 Quinn, W ..... 91

## R

Rahimzadeh Khoshroo, L ..... 47, 57, 78  
 Rajagopal, P ..... 107  
 Rakel, M ..... 90  
 Ramm, M ..... 20  
 Ranalli, F ..... 99, 104  
 Rao, M ..... 76  
 Raukas, M ..... 72, 75  
 Raynolds, J ..... 32  
 Raynor, B ..... 13  
 Razeghi, M ..... 70  
 Readinger, E ..... 86, 93, 100  
 Recht, F ..... 13, 15, 17, 94  
 Redwing, J ..... 38, 64, 83  
 Reed, M ..... 40, 45, 93, 100  
 Reeves, R ..... 109  
 Reiherzer, J ..... 68  
 Reißmann, L ..... 17, 43, 104  
 Remmele, T ..... 67, 88, 100  
 Ren, F ..... 101, 106  
 Renard, J ..... 112, 113  
 Rice, A ..... 58, 85  
 Richter, E ..... 19  
 Riedel, G ..... 36  
 Righi, M ..... 69  
 Rinehimer, J ..... 112  
 Ringel, S ..... 21, 38  
 Ristic, J ..... 43, 88, 91  
 Rivera, C ..... 95  
 Rizzi, A ..... 41, 52, 63, 69, 90, 110  
 Roberts, J ..... 107  
 Robins, L ..... 22, 24  
 Rodrigues, S ..... 78  
 Rodríguez-Vargas, I ..... 32  
 Roeckerath, M ..... 48  
 Roenkov, A ..... 20  
 Roever, M ..... 63  
 Roger, D ..... 70  
 Rogers, C ..... 87  
 Rolfe, S ..... 53  
 Rong, Z ..... 57, 95  
 Rosales, A ..... 85  
 Roshko, A ..... 24, 113  
 Rossberg, M ..... 22  
 Rossow, U ..... 22, 42  
 Rost, H ..... 19, 22  
 Rourke, D ..... 59, 113  
 Rowland, L ..... 63  
 Roycroft, B ..... 100  
 Ruffenach, S ..... 16  
 Ruiz, F ..... 55

Rumbolz, C ..... 14  
 Rumyanstev, S ..... 102  
 Ruterana, P ..... 30, 112  
 Ryabova, L ..... 71  
 Ryou, J ..... 12, 17, 40, 67, 111  
 Ryu, J ..... 95, 98  
 Ryu, S ..... 99

## S

Sahni, S ..... 106  
 Saida, J ..... 81  
 Saito, H ..... 45, 86  
 Saito, M ..... 44, 64, 65, 84  
 Saito, S ..... 99  
 Saito, T ..... 79, 80  
 Sakai, T ..... 79  
 Sakamoto, K ..... 87  
 Sakamoto, T ..... 61  
 Sakuma, Y ..... 56  
 Sakurai, T ..... 47  
 Sakuta, H ..... 27  
 Salcianu, C ..... 105  
 Salvestrini, J ..... 57  
 Sampath, A ..... 24, 92, 93  
 Sánchez-García, M ..... 24, 76, 91, 106  
 Sanders, A ..... 24, 59, 113  
 Sanford, N ..... 24, 32, 59, 87, 90, 113  
 Sanna, S ..... 23  
 Sano, M ..... 61  
 Sanorpim, S ..... 75  
 Sar, A ..... 50  
 Sarney, W ..... 24  
 Sartel, C ..... 113  
 Sasaki, T ..... 13, 19, 21  
 Satake, A ..... 45, 98  
 Sato, H ..... 44  
 Sato, K ..... 107  
 Sato, S ..... 41, 75  
 Sato, T ..... 114  
 Sattu, A ..... 35, 93, 102  
 Sauer, R ..... 38, 80, 81  
 Sawada, T ..... 46  
 Sawahata, J ..... 28  
 Sawaki, N ..... 62, 81  
 Sawicki, M ..... 18  
 Sawyer, S ..... 102  
 Sazawa, H ..... 47, 52  
 Scarpulla, M ..... 63  
 Schaake, C ..... 85  
 Schaefer, J ..... 70  
 Schaff, W ..... 64, 68, 69, 70, 72, 73, 74, 83, 89, 90, 93, 109  
 Schenk, D ..... 42  
 Schenk, T ..... 30  
 Schillgalies, M ..... 14, 42  
 Schineller, B ..... 16, 43, 114  
 Schirra, M ..... 80, 81, 98  
 Schlager, J ..... 24, 90  
 Schley, P ..... 75  
 Schmidt, M ..... 44, 59, 64, 84  
 Schmidt, S ..... 20  
 Schmidt, T ..... 27  
 Schmitz, A ..... 15  
 Schoettker, B ..... 114  
 Scholz, D ..... 61  
 Scholz, F ..... 12, 27, 38, 80, 81, 98, 105  
 Schörmann, J ..... 66, 75  
 Schowalter, L ..... 68, 92

# Index

Schreiner, R.....	114	Simeonov, D.....	43, 87, 91, 102	Sugimoto, K.....	100
Schrenk, W.....	48	Simin, G.....	49, 50	Sugimoto, M.....	38, 106
Schubert, E.....	54, 61, 92	Simms, R.....	67	Sugimoto, S.....	113
Schubert, M.....	61, 70	Singh, D.....	106	Sugimura, H.....	22, 37, 41
Schuette, M.....	46	Singh, R.....	106	Sugita, K.....	56, 83
Schuhmann, H.....	110	Sinitsyn, M.....	54	Sugiura, S.....	41
Schulz, O.....	49	Sipahi, G.....	78	Suh, C.....	13, 17
Schulze, F.....	31, 43, 63	Sirenko, A.....	27	Suh, E.....	78, 90, 95, 114
Schwarz, U.....	18, 42, 61	Sitar, Z.....	58, 85	Suita, M.....	58
Scolfaro, L.....	33, 78	Sitter, H.....	85	Sumii, T.....	41
Sebald, K.....	17, 35, 66	Sizov, D.....	42	Sumiya, S.....	19
Sedhain, A.....	74, 81	Sizov, V.....	30	Sumner, J.....	26, 28
Segal, A.....	20, 54	Skierbiszewski, C.....	12	Sun, Q.....	56
Seguin, R.....	17	Smart, J.....	54, 92	Sun, W.....	35
Segura, J.....	110	Smeeton, T.....	35	Sun, X.....	55
Segura Ruiz, J.....	90	Smirnov, A.....	69	Sundaesan, S.....	30, 71, 76
Seibt, M.....	52, 110	Smirnov, M.....	69	Sung, Y.....	101
Seitz, C.....	16	Smirnov, N.....	30, 53	Suski, T.....	12, 13, 70, 73, 88, 90
Sekiguchi, H.....	87, 113	Smith, D.....	28, 62	Suzuki, A.....	67, 69
Sellers, I.....	91	Smith, H.....	22	Suzuki, K.....	46
Semenov, A.....	71	Snyder, D.....	38	Suzuki, T.....	51
Semond, F.....	43, 50, 91	Soejima, K.....	45	Svane, A.....	70, 90
Senawiratne, J.....	45, 61, 81, 102, 111	Soejima, N.....	38, 106	Swartz, C.....	109
Seo, H.....	31, 49, 59	Soh, C.....	69, 74, 103, 105, 114	Sweeney, S.....	103
Seo, J.....	28, 97	Sohn, Y.....	19, 20, 24, 25, 26, 59	Syrkin, A.....	30, 71, 100
Seong, T.....	66, 107	Sommerhalter, C.....	114	Syvajarvi, M.....	16, 63
Shah, P.....	22, 49, 67	Son, J.....	61, 95		
Shahedipour-Sandvik, F.....	26, 32, 100	Son, M.....	88	<b>T</b>	
Shapiro, A.....	32	Sonderegger, S.....	88	Tachibana, K.....	99, 113
Shapovalova, L.....	30, 93	Sone, C.....	61	Tackeuchi, A.....	79
Sharma, R.....	21	Song, D.....	24, 72	Tadatomo, K.....	77, 85, 98, 101
Shatalov, M.....	35, 93, 96	Song, H.....	95	Taguchi, T.....	27, 79, 80
Shealy, J.....	36	Song, J.....	107	Tahtamouni, T.....	97
Shen, B.....	70, 73, 76	Song, Y.....	94, 95, 109	Tai, N.....	25
Shen, H.....	24, 45, 86, 92, 93	Sota, T.....	19	Tajima, J.....	14
Shen, L.....	13, 15, 17	Soukhoveev, V.....	30, 32, 71	Tajima, M.....	39, 42
Shen, S.....	17, 40, 67	Specht, P.....	27	Takada, K.....	16
Shen, X.....	52	Speck, J.....	13, 15, 17, 21, 44, 52, 59, 62, 63, 64, 65, 66, 70, 84, 85, 86, 89, 90, 94, 108, 111, 112	Takagi, T.....	22, 41, 78, 82, 105
Sheng, T.....	57	Spencer, M.....	39, 68	Takahashi, K.....	46
Sherliker, B.....	92	Srinivanson, S.....	28	Takahashi, S.....	75
Sherwin, M.....	92	Srinivasan, S.....	65	Takano, F.....	79
Sheu, J.....	21, 58, 80, 104	Srolovitz, D.....	56	Takano, T.....	35, 104
Shi, J.....	39, 68	Stadelmann, P.....	14	Takasu, H.....	39, 45, 84
Shi, L.....	77	Stafford, L.....	101	Takeda, K.....	105
Shiao, W.....	24, 28	Stanton, N.....	14	Takeda, S.....	23
Shibata, M.....	13	Starikov, D.....	52	Takeuchi, H.....	89
Shibata, T.....	19	Stauss, P.....	14	Takeuchi, M.....	36, 57, 58
Shields, P.....	23	Steiner, M.....	105	Talalaev, R.....	54, 56
Shih, M.....	105	Steinmetz, E.....	30	Talbot, J.....	72, 75
Shikata, G.....	75, 83	Steins, R.....	48	Taliercio, T.....	43
Shim, J.....	97	Steins, W.....	39	Talin, A.....	87, 112
Shimada, T.....	67	Stephan, R.....	37	Tamboli, A.....	59
Shimizu, M.....	47	Stephenson, G.....	83	Tamulaitis, G.....	77
Shimmura, T.....	97	Stepp, D.....	22	Tan, L.....	47, 92
Shimojo, T.....	75	Steranka, F.....	114	Tanabe, T.....	84
Shinohara, K.....	15	Stevens, M.....	65	Tanaka, H.....	89
Shiozaki, N.....	107	Stokker-Cheregi, F.....	91	Tanaka, J.....	87
Shirahama, T.....	89	Stoklas, R.....	48	Tanaka, M.....	19
Shon, Y.....	23, 76	Strasser, G.....	41, 48, 58, 67	Tanaka, T.....	41, 84
Shturm, I.....	93, 96, 102	Strauss, U.....	14, 42, 61	Tang, C.....	70
Shubina, T.....	18, 71	Streiffer, S.....	83	Tang, H.....	53, 87
Shur, M.....	21, 49, 50, 77, 78, 102	Strittmatter, A.....	17	Tang, N.....	70, 73, 76
Siche, D.....	19, 22	Stutzmann, M.....	36, 37, 39, 113	Tang, T.....	24, 28, 102, 103
Siebert, M.....	27	Su, Y.....	54, 98	Tang, Y.....	70
Siekacz, M.....	12	Subramaniam, A.....	50	Tanikawa, T.....	62
Sijmus, B.....	55	Suchocki, A.....	73, 90	Tanner, S.....	87
Sillero, E.....	106	Sugawara, M.....	21	Tanpo, M.....	13, 21
Sim, S.....	69, 74			Tao, J.....	72, 75
Simbrunner, C.....	18, 85				

# Index

Tarasuk, N	43	Ueno, K	41, 65	Wei, S	32
Tautz, S	14	Uesugi, T	38, 106	Weidemann, O	37
Tchernycheva, M	67, 87, 100, 113	Ulbrich, R	69	Weimann, G	13
Teisseyre, H	12	Umana-Membreno, G	90, 94	Weisbuch, C	18, 66, 94
Teng, J	103	Umeno, K	73	Weise, F	40
Teo, S	103	Uren, M	36, 40, 67	Wenderoth, M	69
Teppe, F	35	Usikov, A	30, 71, 93, 100	Weng, X	38, 64
Terada, Y	92	Usui, A	18, 19, 22	Werder, D	87
Tessarek, C	17, 35			Werner, C	90
Teweldeberhan, A	74	<b>V</b>		Werner, F	90, 110
Thaler, G	85, 92, 113, 114	Valencia, A	25	Wernicke, T	57, 77
Thapa, S	38	van der Laak, N	12	Wetzel, C	45, 61, 81, 92, 102, 110, 111
Thomas, A	20, 72	Van Hove, M	42	Weyers, M	19, 30, 57, 73, 77, 80
Thomidis, C	84	Van Nostrand, J	113	Wheeler, V	16
Thompson, C	83	Vantsov, V	71	Widom, M	112
Thompson, D	12	Vaudin, M	24	Wiegert, J	105
Thomsen, C	80	Veal, T	86, 89, 109	Wieneke, M	57, 73, 82
Thomson, D	103	Veis, M	29	Wierer, J	66
Thonke, K	38, 75, 80, 81, 98	Veit, P	73	Wiersig, J	66
Thrush, T	35, 105	Veksler, D	78	Willadsen, P	15
Tian, F	46	Vembu, B	36	Willemann, M	48
Tian, Y	76	Vennégués, P	28, 50, 62, 65	Williamson, T	74
Tilak, V	40, 41	Vescan, A	47, 57	Winnacker, A	20
Ting, S	91	Vetury, R	36	Witte, H	63, 73
Tinjod, F	103	Vielemeyer, M	113	Woitok, J	57, 78
Toda, Y	18, 76, 77	Vinattieri, A	91	Wollweber, J	16
Togashi, R	14, 72	Vispute, R	76	Wolter, S	37
Tokuda, Y	58	Viveiros, E	49	Won, Y	110
Tonisch, K	37, 49, 58	Vodakov, Y	20	Wong, M	52
Toropov, A	18	Volkova, A	30	Wong, W	15
Tottereau, O	18	Voss, L	30, 101	Wowchak, A	48, 53
Touati, S	50			Wraback, M	24, 40, 43, 45, 86, 92, 93, 100
Trampert, A	24, 76, 107	<b>W</b>		Wu, F	17, 44, 62, 64, 65, 84, 85, 111
Tran, C	61	Wagner, H	105	Wu, H	81
Tränkle, G	19	Wagner, J	105	Wu, J	55, 74, 89
Travers, L	113	Wakaba, M	67	Wu, P	26, 106
Trevisanello, L	101	Wakahara, A	73, 74, 75	Wu, S	54, 58
Trimarchi, G	33	Wakamiya, Y	49	Wu, Y	13
Tripathi, N	26, 32, 100	Waki, I	108	Wu, Z	65, 92, 111
Tripathy, S	69, 74	Walsh, A	32	Wunderer, T	27, 80, 81, 98
Tronc, P	52	Walter, A	14		
Trybus, E	105	Waltereit, P	13, 53, 62	<b>X</b>	
Tsai, C	25	Walukiewicz, W	74, 89, 93, 109	Xi, J	42
Tsai, H	98	Wang, C	55, 71, 76	Xia, Y	45, 61, 81, 92, 102, 111
Tsai, M	59	Wang, G	87	Xiang, N	80
Tsai, S	104	Wang, H	102, 106	Xiangqian, X	57, 95
Tsai, T	25, 105	Wang, J	89	Xiao, D	42
Tsai, W	75	Wang, K	25, 47, 86, 93	Xie, J	48
Tsatsulnikov, A	54	Wang, L	25, 53, 107	Xie, Z	24, 54
Tsay, J	26, 30, 31, 81, 82	Wang, M	76	Xing, H	15, 46, 48
Tsifotidis, T	44	Wang, Q	60, 99, 104	Xiu, H	28, 35
Tsuchiya, T	67, 69	Wang, R	83	Xiu, X	24, 54
Tu, C	77	Wang, S	25, 81, 82	Xu, F	70, 76
Tu, L	25, 30, 53, 59, 68	Wang, T	27, 56, 60, 81, 82, 92, 99, 104	Xu, H	95
Tu, T	75	Wang, W	23	Xu, J	76
Tu, Y	59	Wang, X	25, 71, 77, 86, 109, 112	Xu, S	72
Tun, C	54, 102	Wang, Y	55, 64, 102, 111	Xu, T	50, 84
Tungare, M	26, 32	Wang, Z	70		
Tut, T	100	Warde, E	67	<b>Y</b>	
Tyagi, A	65, 84	Wasserbauer, J	36	Yablonskii, G	43, 78
		Watababe, K	13	Yagi, S	47
<b>U</b>		Watanabe, H	105	Yaguchi, H	63, 75, 83, 92
Ueda, H	38	Watanabe, I	49	Yakimova, R	16, 63
Ueda, M	45, 61, 65	Watson, I	56, 79, 92, 93	Yakovlev, E	54, 56
Ueda, T	41	Way, C	55	Yamada, N	19, 21
Uedono, A	19, 21	Wegener, D	40	Yamada, T	61, 67, 69
Uehara, T	56	Wegscheider, M	18, 85	Yamada, Y	52, 78, 79, 80, 82
Uemura, S	92, 109				

Yamaguchi, A.....	64, 81
Yamaguchi, D.....	93
Yamaguchi, H.....	62
Yamaguchi, K.....	64
Yamaguchi, M.....	62, 81
Yamaguchi, T.....	17, 27, 110
Yamamoto, A.....	51, 52, 56, 73, 83, 86, 109
Yamamoto, Y.....	89
Yamashita, Y.....	49
Yamazaki, T.....	111
Yanagawa, T.....	73
Yanagita, N.....	98
Yang, C.....	24, 28, 102, 103, 113
Yang, J.....	21, 35, 49, 50, 96
Yang, P.....	110, 113
Yang, Y.....	90
Yang, Z.....	49, 50, 73, 76
Yano, Y.....	47
Yao, T.....	15, 20, 31, 107
Yatabe, T.....	79, 97
Yazdi, G.....	16, 63
Ye, S.....	106
Yeh, D.....	102
Yeh, J.....	25
Yeh, R.....	31
Yehuda, I.....	46
Yen, H.....	94
Yen, J.....	61
Yen, W.....	80
Yi, G.....	55, 58
Yim, J.....	89
Yonezu, H.....	73, 74
Yoo, D.....	40, 67, 111
Yoo, K.....	88
Yoon, E.....	23, 54, 65, 71, 96, 99, 103
Yoon, S.....	101
Yoon, Y.....	95, 97
Yoshida, S.....	38, 39, 75, 83
Yoshida, T.....	13
Yoshikawa, A.....	51, 71, 86, 109
Yoshimura, K.....	101
Yoshimura, M.....	13, 19, 21
Yoshioka, K.....	100
You, S.....	81, 111
Young, E.....	64, 84
Yu, H.....	25
Yu, K.....	74, 89, 93, 109
Yu, W.....	106
Yugova, T.....	53
Yun, J.....	107

## Z

Zah, C.....	42
Zaima, K.....	99
Zang, K.....	64
Zanoni, E.....	101
Zavarin, E.....	54
Zehnder, U.....	101
Zeng, H.....	26
Zenneck, J.....	52
Zettler, T.....	30
Zhang, B.....	38, 84, 93
Zhang, G.....	70, 73, 76
Zhang, H.....	101
Zhang, J.....	21, 35, 77, 78, 93, 96, 102
Zhang, Q.....	94
Zhang, R.....	24, 54
Zhang, W.....	47, 57

Zhang, Y.....	17, 28, 40, 64, 67
Zhang, Z.....	70, 111
Zhao, L.....	62
Zhao, W.....	45, 61, 81, 102, 111
Zhao, X.....	42, 50
Zhao, Y.....	51
Zhaoyong, F.....	107
Zheleva, T.....	22, 67
Zheng, J.....	26, 104
Zheng, Y.....	24, 54
Zhi Hong, L.....	50
Zhikuo, T.....	95
Zhong, H.....	45, 65, 84
Zhou, H.....	56
Zhou, L.....	28, 62
Zhou, W.....	73
Zhou, Y.....	72
Zhu, D.....	91, 100, 110
Zhu, M.....	45, 61, 81, 102, 111
Zhu, T.....	19, 53, 82, 103
Zhuravlev, K.....	52, 59
Zielinski, M.....	18
ZiLi, X.....	57
Zili, X.....	95
Zimmermann, T.....	15, 48
Zunger, A.....	33

# Join TMS today and receive membership through 2008!

*As your professional partner for career advancement, TMS offers you technical information and networking opportunities specific to your field.*

## Enjoy these benefits for the remainder of 2007 and all of 2008:

- **Free** print and electronic subscription to *JOM*, the monthly technical journal exploring the traditional, innovative and revolutionary issues in the minerals, metals and materials fields
- **Free** downloads from Materials Technology@TMS, a new Web site that allows you to network, share knowledge and utilize resources in technology-specific communities online
- **Free** access to TMS e-Library, powered by Knovel®, with databases, online engineering reference books and analytical tools
- **Discounts** on the *Journal of Electronic Materials*, and *Metallurgical and Materials Transactions A and B*
- **Discounts** on publications and conference fees
- **Networking** opportunities with fellow members and colleagues from around the globe
- **Members-only** access to the TMS network of professionals through the searchable online membership directory
- **Special privilege** at the online TMS Career Center

## To begin enjoying these benefits:

Complete an application at the TMS registration desk and pay your \$105 annual dues. You may also join online at [www.tms.org/Society/membership.html](http://www.tms.org/Society/membership.html) for instant access.

For more information, visit [www.tms.org](http://www.tms.org), e-mail [membership@tms.org](mailto:membership@tms.org) or call (800) 759-4TMS, ext 259.

# TMS

Your Professional Partner for Career Advancement

LEARN • NETWORK • ADVANCE

[www.tms.org](http://www.tms.org)

# Program-at-a-Glance

Room	312/313/ 316/317	313/316	314/315	312/317	318/319	Prefunction Area
<b>SUNDAY</b>						Registration 2:00-7:00 PM Welcoming Reception 5:00-7:00 PM
	Opening Ceremony and Plenary Session	Session A: LED and Laser I	Session B: Microwave Devices I	Session C: Bulk Growth and HVPE I		Registration 7:00 AM-5:00 PM
<b>MONDAY</b>		Session D: LED and Laser II  Session G: Quantum Dots: Growth	Session E: Microwave Devices II  Session H: Epitaxial Growth for Electronic Devices	Session F: Bulk Growth and HVPE II  Session I: Optical Characterization of Bulk Materials and Microcavities	Exhibition 3:00-7:00 PM	Poster Session I 5:30-7:00 PM
		Session J: Deep UV LEDs and Lasers  Session M: MOVPE Growth of AlGaIn Alloys I	Session K: Microwave Devices III  Session N: High Voltage and Advanced Device Structures I	Session L: Sensors and Characterization I  Session O: Sensors and Characterization II	Exhibition 9:30 AM-12:00 PM	Registration 7:00 AM-5:00 PM
<b>TUESDAY</b>		Session Q: High Voltage and Advanced Device Structures II  Session T: Nonpolar and Semipolar Materials and Devices I	Session P: MOVPE Growth of AlGaIn Alloys II  Session S: Quantum Dots: Characterization Rump Session I	Session R: Optical Characterization of Lasers  Session U: Optical Characterization of LEDs Rump Session II	Exhibition 3:00-7:00 PM	Poster Session II 5:30-7:00 PM
		Session V: Solid State Lighting and LEDs  Session Y: Optical and Structural Characterization and Related Topics	Session W: Nonpolar and Semipolar Materials and Devices II  Session Z: Nonpolar and Semipolar Materials and Devices III	Session X: Growth of Novel Nitride Semiconductors  Session AA: Optoelectronic Devices	Exhibition 9:30 AM-12:00 PM	Registration 7:00 AM-1:00 PM
<b>WEDNESDAY</b>						Poster Session III 1:30-2:30 PM
		Session CC: Nonpolar and Semipolar Materials and Devices IV  Session FF: Nanostructures: Devices	Session DD: Engineered Properties of GaN by MOVPE Growth  Session GG: Optical and Structural Characterization I	Session BB: InN Growth  Session EE: InN Heterostructures and Quantum Wells	Exhibition 9:30 AM-12:00 PM	Registration 7:00 AM-5:00 PM
<b>THURSDAY</b>		Session JJ: Optical Characterization of Alloys and MQWs	Session II: Nanostructures: Characterization	Session HH: InN: Surface and Electronic Properties		Poster Session IV 5:00-6:00 PM
		Session LL: Nanostructures: Growth I  Session OO: Nanostructures: Growth II	Session MM: Defects and Structural Characterization  Session PP: MOVPE Growth of InGaIn Alloys for Optoelectronics	Session KK: P-Type InN  Session NN: Molecular Beam Epitaxy of Nitride Semiconductors		Registration 7:00-11:00 AM
<b>FRIDAY</b>						
	Session QQ: Special LED Session: High Efficiency Solid State Lighting: Solutions for Global Warming Closing Ceremony					